Vol. 174, August 1, 1985
Complete in one issue

ISSN 0003-2670

ANALYTICA CHIMICA ACTA

International journal devoted to all branches of analytical chemistry

ELSEVIER

ANALYTICA CHIMICA ACTA

International journal devoted to all branches of analytical chemistry
Revue internationale consacrée à tous les domaines de la chimie analytique
Internationale Zeitschrift für alle Gebiete der analytischen Chemie

PUBLICATION SCHEDULE FOR 1985

	J	F	M	A	M	J	J	A	S	O	N	D
Analytica Chimica Acta	167	168	169	170/1 170/2	171	172	173	174	175	176	177	178

Scope. *Analytica Chimica Acta* publishes original papers, short communications, and reviews dealing with ever aspect of modern chemical analysis both fundamental and applied.

Submission of Papers. Manuscripts (three copies) should be submitted as designated below for rapid and efficier handling:

Papers from the Americas to: Professor Harry L. Pardue, Department of Chemistry, Purdue University, West Lafayette IN 47907, U.S.A.

Papers from all other countries to: Dr. A. M. G. Macdonald, Department of Chemistry, The University, P.O. Box 36 Birmingham B15 2TT, England. Papers dealing particularly with computer techniques to: Professor J. T. Cler Universität Bern, Pharmazeutisches Institut, Baltzerstrasse 5, CH-3012 Bern, Switzerland.

Submission of an article is understood to imply that the article is original and unpublished and is not being considere for publication elsewhere. Upon acceptance of an article by the journal, authors will be asked to transfer the copyrigh of the article to the publisher. This transfer will ensure the widest possible dissemination of information.

Information for Authors. Papers in English, French and German are published. There are no page charge Manuscripts should conform in layout and style to the papers published in this Volume. Authors should consul Vol. 170 for detailed information. Reprints of this information are available from the Editors or from: Elsevier Editoria Services Ltd., Mayfield House, 256 Banbury Road, Oxford OX2 7DH (Great Britain).

Reprints. Fifty reprints will be supplied free of charge. Additional reprints (minimum 100) can be ordered. An orde form containing price quotations will be sent to the authors together with the proofs of their article.

Advertisements. Advertisement rates are available from the publisher.

Subscriptions. Subscriptions should be sent to: Elsevier Science Publishers B.V., Journals Department, P.O. Bo 211, 1000 AE Amsterdam, The Netherlands. Tel: 5803 911, Telex: 18582.

Publication. *Analytica Chimica Acta* appears in 12 volumes in 1985. The subscription for 1985 (Vols. 167–178) i Dfl. 2400.00 plus Dfl. 264.00 (p.p.h.) (total approx. US $986.70). All earlier volumes (Vols. 1–166) except Vols. 2 and 28 are available at Dfl. 215.00 (US $79.60), plus Dfl. 15.00 (US $5.60) p.p.h., per volume.

Our p.p.h. (postage, packing and handling) charge includes surface delivery of all issues, except to subscribers in th U.S.A., Canada, Japan, Australia, New Zealand, P.R. China, India, Israel, South Africa, Malaysia, Singapore, Soutl Korea, Taiwan, Pakistan, Hong Kong and Brazil who receive all issues by air delivery (S.A.L. — Surface Air Lifted) a no extra cost. For the rest of the world, airmail and S.A.L. charges are available upon request.

Claims for issues not received should be made within three months of publication of the issues. If not they cannot b honoured free of charge.

For further information, or a free sample copy of this or any other Elsevier Science Publishers journal, readers in th U.S.A. and Canada can contact the following address: Elsevier Science Publishing Co. Inc., Journal Informatio Center, 52 Vanderbilt Avenue, New York, NY 10017, U.S.A., Tel: (212) 916-1250.

ANALYTICA CHIMICA ACTA
VOL. 174 (1985)

ANALYTICA CHIMICA ACTA

International journal devoted to all branches of analytical chemistry

ELSEVIER Amsterdam–Oxford–New York–Tokyo

Anal. Chim. Acta, Vol. 174 (1985)

0003-2670/85/$03

Printed in The Netherlands

Analytica Chimica Acta, 174 (1985) 1—26
Elsevier Science Publishers B.V., Amsterdam — Printed in The Netherlands

AN EXTENSION OF THE MULTIVARIATE COMPONENT-RESOLUTION METHOD TO THREE COMPONENTS

ODD S. BORGEN[a] and BRUCE R. KOWALSKI*

Laboratory for Chemometrics BG-10, University of Washington, Seattle, Washington 98195 (U.S.A.)

(Received 7th January 1985)

SUMMARY

The extension of the multivariate curve resolution theory presented is based on the minimum assumptions of non-negativity of sensor responses and non-negativity of quantities of components, as given by Lawton and Sylvestre. The theory is explicitly given for three components, while the algorithms developed may potentially be extended to the more general *n*-component case. The analytical solution to the problem of defining the physically permitted regions for the sensor responses ("spectra") or quantity profiles of pure components is given. Implementations of the algorithms developed are used for finding the permitted ranges of the pure component spectra from mixture spectra. Extensions of the minimal assumption theory are suggested.

The resolution of multicomponent mixtures is a general problem in chemistry. Depending on the nature of the sample and the available chemical instrumentation, several data-processing approaches are available. Each approach has its own requirements as well as limitations. When multidimensional chemical data are available, multivariate statistical analysis can be applied. These data are available when the concentrations of the components can be varied by some method and multichannel spectral or other sensor responses can be obtained as a function of the relative amounts of the individual components.

Perhaps the commonest, but not the only, case occurs when a chromatograph is coupled to a spectrometer and multichannel spectral data are obtained as a function of time. The concentrations of the various sample components change as the components elute from the column, hopefully separated to some degree from each other. When a single-component elution profile is sampled by the spectrometer, the observed spectra, standardized to unit area, are all the same except for noise in the spectral intensities. When two or more components, not well separated in time, elute from the column, the spectra recorded are those of varying mixtures of the pure spectra of the components. When this occurs, and the pure component spectra are not

---

[a]Permanent address: Laboratory for Physical Chemistry, The University of Trondheim, The Norwegian Institute of Technology, N-7034 Trondheim-NTH, Norway.

0003-2670/85/$03.30

available, the problem of resolving the number of components, their pure spectra and their relative amounts eluting within a selected time period, can be approached by a number of methods stemming from principal component analysis.

A direct solution for the two-component case, to the limit of instrumental resolution, was developed by Lawton and Sylvestre [1] and later extended by and applied to gas chromatography/mass spectrometry (g.c./m.s.) and gas chromatography/ultraviolet-visible spectrophotometry (g.c./u.v.-vis.) data by Kowalski and coworkers [2—4] and others, e.g., Gilbert et al. [5]. While a generalization of this method to the multicomponent case has been hinted at by all these authors, no direct solution based on minimal assumptions has been forwarded. The form of the solution for a particular three-component case has been shown by Ohta [6].

Lately, several investigators have approached the multicomponent resolution problem from several different angles. Chen and Hwang [7] have used a polar coordinate mapping of the permitted regions of factor space on the assumption of positive spectral densities for the resolution of two (and with less success three) components from g.c./m.s. data. The method has been extended and applied to liquid chromatography/ultraviolet-visible spectrophotometry (l.c./u.v.-vis.) data by Vandeginste [8]. Martens and coworkers [9, 10] have approached the determination of the spectra of pure components in near-infrared (i.r.) measurements by extrapolation of the observed spectra, applying non-negativity constraints. Still another approach has been used for selecting approximations to the spectra of the pure components for target analysis by Knorr and Futrell [11] and later Malinowski [12], while Gemperline [13] has applied a uniqueness target-vector search approach to the component resolution of chromatograms. In a recent article, Meister [14] combines the non-negative response constraint with an heuristic approach to the determination of reasonable approximations to the spectra of pure components. This method is expected to be most suitable when the system is fairly well resolved. A valuable treatment of the influence of experimental errors is given.

In the present paper, the multicomponent resolution problem has been treated on the assumption that both the components and corresponding sensitivities of the chemical sensors (e.g., their pure spectra) are initially unknown, and the minimum number of physical constraints is applied. A detailed analysis of the determination of the regions of possible solutions will be given for three components. The resulting algorithms may be generalized to multicomponent systems. This is, however, beyond the scope of the present article.

The term "component resolution" is preferred rather than "curve resolution" because of the multivariate approach, and the intended chemical applications. Because the subject of this article is mainly the extension of the theory of component resolution to three-component systems, some of the features of the method have been illustrated by using simulated data,

experimental applications being left to later studies. Finally, a simple application of an added "continuity constraint" is demonstrated.

THEORY

A natural starting point for an extension to multicomponent systems is the theoretical background for the curve resolution method previously introduced by Lawton and Sylvestre [1]. However, several changes of notation will be made, applying symbols with chemical associations. The results derived in the following sections are completely general within the constraints to be defined.

The matrices

$\mathbf{R}$ (NSA × NSE)
$\mathbf{N}$ (NSA × NCO)
$\mathbf{S}$ (NCO × NSE)

are introduced. Their elements represent r_{ik}, the response of sensor k to sample i, n_{ij}, the quantity of component j in sample i, and s_{jk}, the sensitivity of sensor k to component j (i.e., response of sensor k to the pure component j). The integers NSA, NSE and NCO denote the number of samples, sensors and components, respectively. Assume the existence of an experimental set of observations organized as a response matrix $\mathbf{R}$ (NSA × NSE) where the responses of NSE sensors have been recorded for NSA samples. Here the row $\mathbf{r}_i^T$ of $\mathbf{R}$ is the response vector for sample i, the column $\mathbf{n}_j$ of $\mathbf{N}$ is the quantity vector for component j, and the row $\mathbf{s}_k^T$ is the sensitivity vector for component k. The vectors ($\mathbf{s}_k^T$; $k = 1..\text{NCO}$) form a basis for the row vector space containing the response vectors.

It is further assumed that a linear model of the form

$$\hat{\mathbf{R}}\ (\text{NSA} \times \text{NSE}) = \hat{\mathbf{N}}\ (\text{NSA} \times \text{NCO})\ \hat{\mathbf{S}}\ (\text{NCO} \times \text{NSE}) \tag{1}$$

where the residual $\mathbf{D} = \mathbf{R} - \hat{\mathbf{R}}$ is minimized for a given NCO, gives a satisfactory fit to the model. Here, $\hat{\mathbf{N}}$ and $\hat{\mathbf{S}}$ represent the quantities and sensitivities for the real chemical components. A solution to Eqn. 1 can be obtained by applying one of the well established methods of "classical" factor analysis [15] or principal component analysis [16]. The determination of the number of components is by itself a non-trivial problem to which approaches have been made, e.g. by cross-validation [17, 18]. Such a solution will be of the form

$$\hat{\mathbf{R}} = \tilde{\mathbf{N}}\ \tilde{\mathbf{S}} \tag{2}$$

where $\tilde{\mathbf{s}}_k^T$, the orthonormal eigenvectors of the principal components, again will span the R^{NCO}-space of the response vectors. However, except by the most improbable accident, $\tilde{\mathbf{N}}$ and $\tilde{\mathbf{S}}$ will not be identical to $\hat{\mathbf{N}}$ and $\hat{\mathbf{S}}$, representing the physical quantities. This follows from the fact that any

solution

$$\hat{R} = (\tilde{N}\,T)\,(T^{-1}\,\tilde{S}) \qquad (3)$$

where T (NCO × NCO) is any non-singular matrix, is valid. One of the difficulties with principal component analysis applied to chemical problems [15] is precisely the determination of T. However, as $\hat{S}$ is formed by a linear transformation of $\tilde{S}$, the eigenvectors span the vector space containing both response and sensitivity vectors.

As a matter of convenience, often in the following the equivalent "column eigenvector space" spanned by ($\tilde{s}_k$; k = 1 . . NCO) will be applied rather than the "row eigenvector space" of Eqn. 2 spanned by ($\tilde{s}_k^T$; k = 1 . . NCO). In this space, all response and sensitivity vectors will also be expressed as column vectors. For simplicity of notation, the superscript in the vector symbol is also dropped in the following development, writing s_k rather than $\tilde{s}_k$.

Before using the model of Eqn. 2 for further data analysis, one should very carefully inspect the residual matrix D for indications of general bad fit of the model, outliers, or rows or columns of R with low information content. For reasons that will become obvious, negative elements in $\hat{R}$ must also be avoided. They will originate from noise or offsets in the observations.

Finally, it is often found to be an advantage to deal with the response matrix R′ = R—A, referred to the averages of the responses rather than the origin. The columns of A contain the average values of the responses of the corresponding sensors. The following sections have been based on responses referred to the origin, however.

Physical constraints

To this point, no assumptions have been made except that a linear model will fit the observations with satisfactory accuracy. Three assumptions are now introduced based on the physical origin of the observations, similar to those originally used by Lawton and Sylvestre [1]. Thus, first, for many experimental methods the sensitivities of all sensors to all components will be non-negative. In fact, the requirement is rather that all responses are in the same direction from some arbitrary origin, the direction being set positive. Second, the quantities of the chemical components are all non-negative. Often the relative amounts of the components, ranging from 0 to 1 will be preferred. And third, under these conditions all responses must be non-negative.

These assumptions lead to the following two constraints which allow a full or partial resolution of the components, i.e., limiting the possible values of quantity and sensitivity vectors for a given response matrix.

First constraint

Under the given assumptions, the elements of any physically realizable response vector, both those actually observed, the sensitivity vectors, and those corresponding to any possible mixture of the components must have non-negative elements for all sensors. Any vector v in column eigenvector-

space can be expressed by

$$\mathbf{v} = \sum_{j=1}^{NCO} d_j \cdot \mathbf{s}_j \tag{4}$$

The possible response vectors will be limited to those that satisfy

$$v_k = \sum_{j=1}^{NCO} d_j \cdot s_{kj} = d_1 \cdot s_{k1} + \sum_{j=2}^{NCO} d_j \cdot s_{kj} \geqslant 0 \; (k = 1..\mathrm{NSE}) \tag{5}$$

The components of the first eigenvector $\mathbf{s}_1$, corresponding to the largest eigenvalue of the principal component solution, will always be positive (or, if negative, the signs of all elements may arbitrarily be changed as this causes no violation of the orthonormality properties of the eigenvectors). By introducing $f_{kj} = s_{kj}/s_{k1}$, where $f_{k1} = 1$, into Eqn. 5, the inequalities are still valid:

$$d_1 + \sum_{j=2}^{NCO} d_j \cdot f_{kj} \geqslant 0 \; (k = 1..\mathrm{NSE}) \tag{6}$$

A standardization of all vectors in column eigenvector space is now done so that for a vector v

$$\sum_{k=1}^{NSE} w_k \cdot v_k = 1 \tag{7}$$

The weighting factors, w_k, allow for different weights of the sensor responses derived from quantities such as the variances of the observations, distance between observations in spectra, etc.

The eigenvectors are normalized to unit length by

$$|\mathbf{s}_j|^2 = \sum_{k=1}^{NSE} (s_{kj})^2 = 1 \; (j = 1..\mathrm{NCO}) \tag{8}$$

during the principal component analysis, and the sum of components of the eigenvectors, $c_j = \Sigma_{k=1}^{NSE} w_k \cdot s_{kj}$, is introduced. Any standardized vector will be constrained to the hyperplane

$$\sum_{j=1}^{NCO} c_j \cdot d_j = c_1 \cdot d_1 + \sum_{j=2}^{NCO} c_j \cdot d_j = 1 \tag{9}$$

in eigenvector space.

Solving for the vector component d_1 along $\mathbf{s}_1$ yields

$$d_1 = (1/c_1) \left[1 - \sum_{j=2}^{NCO} c_j \cdot d_j\right] \tag{10}$$

Other standardization schemes also exist, of course. It is, for example, possible to normalize all vectors to unit length. The vectors will thus be located on a sphere in eigenvector space. The standardization of Eqn. 7, which will presently lead to a set of linear limiting equations, is preferred here.

Equations 6 and 10 are now combined ($c_1 > 0$ as $s_{k1} > 0$ for all k, i.e., all sensors), leading to the important set of constraint inequalities

$$1 + \sum_{j=2}^{NCO} (c_1 \cdot f_{kj} - c_j) \cdot d_j \geqslant 0 \; (k = 1 \ldots NSE) \tag{11}$$

one for each sensor. These are, under the given assumptions, general and combine the non-negativity and standardization conditions, reducing the dimensionality of the resolution problem from NCO to (NCO −1).

In the R^{NCO-1} "standardization" space, the origin (i.e., the zero vector) must be permitted as Eqn. 11 is satisfied by ($d_j = 0$; $j = 2$. NCO). The boundaries of the permitted region of R^{NCO-1} space are thus defined by the subset of the hyperplanes

$$1 + \sum_{j=2}^{NCO} (c_1 \cdot f_{kj} - c_j) \cdot d_j = 1 + \sum_{j=2}^{NCO} (a_{kj} \cdot d_j) = 0 \tag{12}$$

where $a_{kj} = (c_1 \cdot f_{kj} - c_j)$ located nearest the origin. This permitted region will be a hyperpolyhedron in R^{NCO-1} space. For a practical implementation of Eqn. 12, it may be convenient to rescale eigenvector space by defining $c_j = 1$ ($j = 1 \ldots NCO$), i.e., to rescale the eigenvectors. This leads to a simpler version of Eqn. 12:

$$1 + \sum_{j=2}^{NCO} (f'_{kj} - 1) \cdot d_j = 1 + \sum_{j=2}^{NCO} a'_{kj} \cdot d_j = 0 \tag{13}$$

where f'_{kj} and thereby a'_{kj} have to be recalculated from the new basic vectors.

The general formulation of the first constraint is thus an exercise in hyperspace geometry. Any physically possible vector in R^{NCO-1} space must be located on a surface of, or within, the convex hyperpolyhedron (in the following called FIRPOL) surrounding the origin.

Second constraint

On the assumption of non-negative quantities of the components, it follows that any response vector must be located on or within a simplex in R^{NCO-1} "standardization-space", the vertices of which are the component sensitivity vectors. Any mixture of the pure components, which must be present in non-negative quantities, will have a response vector located within or on the faces of the simplex.

[For convenience the term "vector" is used for the vectors themselves and their termination points in the standardization hyperplane. A simplex (as in simplex optimization) is any geometric figure delimited by $n + 1$ points in n-dimensional space. In this paper a simplex will always be non-degenerate, i.e., spanning (utilizing) the full dimensionality of the space. The term, ON the simplex, indicates a location on one of the (hyper)planes connecting the points, while WITHIN the simplex indicates a location within the volume of (hyper)space delimited by the (hyper)planes.]

Combined constraints

The sensitivity vectors must be located in the region of "standardization"-space delimited by the hyperpolyhedron, FIRPOL, (including its surfaces). The sensitivity vectors form the vertices of a simplex which must enclose the response vectors, or rather, the convex hyperpolyhedron (in the following called INNPOL) inscribing all the observed response vectors.

So far, a generally applicable component resolution theory based on the original Lawton and Sylvestre [1] curve-resolution with some extensions has been developed. The theory is complete for the given physical constraints. It remains, however, to implement a method for determining the possible solutions for the sensitivity vectors and quantity vectors. This will be done explicitly for two and three components in later sections.

The transposed solution

Attention has been focused on "sensitivity eigenvector space", spanned by NCO eigenvectors, which contains the component sensitivity vectors and response vectors. These vectors have as elements the responses of all sensors for a given sample. In many cases, however, the primary interest is in the quantity vectors of the components, i.e., the quantities of a component in all samples. The transposed observation matrix, $\underline{\mathbf{R}} = \mathbf{R}^{\mathrm{T}}$, can be modelled by

$$\hat{\underline{\mathbf{R}}}\,(\mathrm{NSE} \times \mathrm{NSA}) = \hat{\underline{\mathbf{S}}}\,(\mathrm{NSE} \times \mathrm{NCO}) \cdot \hat{\underline{\mathbf{N}}}\,(\mathrm{NCO} \times \mathrm{NSA}) \qquad (14)$$

This time, however, a "quantity eigenvector-space" is obtained, spanned by quantity row vectors $\hat{\underline{\mathbf{n}}}_k^{\mathrm{T}}$ $(1 \times \mathrm{NSA})$ having as elements the quantities of component k in all samples. The response row vectors $\underline{\mathbf{r}}_i^{\mathrm{T}}$ $(1 \times \mathrm{NSA})$ of this space will contain as elements the responses of sensor i for all samples. Non-negativity constraints will apply as before, but standardization will take place by summing the vector elements over all samples. The resulting possible quantity vectors will be constrained analogously to the sensitivity vector in "sensitivity eigenvector-space".

Transformation constraints

From Eqns. 2 and 3 it follows that $\hat{\mathbf{N}} = \tilde{\mathbf{N}} \cdot \mathbf{T}$ and $\hat{\mathbf{S}} = \mathbf{T}^{-1} \cdot \tilde{\mathbf{S}}$, where $\mathbf{T}$ and $\mathbf{T}^{-1}$ is the specific pair of mutually inverse transformation matrices connecting $\tilde{\mathbf{N}}$ and $\tilde{\mathbf{S}}$ with $\hat{\mathbf{N}}$ and $\hat{\mathbf{S}}$. From the assumptions, all elements of $\hat{\mathbf{N}}$ and $\hat{\mathbf{S}}$ must be non-negative, thus constraining the possible values of $\mathbf{T}$ to those which transform the known $\tilde{\mathbf{N}}$ into $\hat{\mathbf{N}}$ having non-negative elements, while $\mathbf{T}^{-1}$ transforms the known $\tilde{\mathbf{S}}$ into $\hat{\mathbf{S}}$ with non-negative elements, retaining the reciprocity relation between $\mathbf{T}$ and $\mathbf{T}^{-1}$.

LIMITING CONDITIONS

The limiting conditions for two components

Before the discussion of systems with more than two components, the original self-modeling curve-resolution method of Lawton and Sylvestre [1] is reviewed within the framework of this paper.

The first constraint conditions, corresponding to the limiting hyperplanes of Eqn. 12, reduce to points on a line, i.e.,

$1 + a_{j2}\ d_2 = 0; d_2 = -1/a_{j2}\ (j = 1\ ..\ \mathrm{NSE})$

when NCO = 2. All limit points with negative a_{j2} will have positive d_2 coordinates. The second constraint conditions will correspond to the highest positive and the lowest negative response vectors. This is illustrated in Fig. 1. The correspondence between this figure and the line containing the segments AI and AII in Fig. 2 of the paper by Lawton and Sylvestre [1] is noted.

Several studies applying the theory of Lawton and Sylvestre to two-component systems have been made over the last ten years [2—5] and this subject is not discussed further.

The limiting conditions for three components

The three-component case has the advantage of ease of visualizing the results, while introducing new features. The standardization hyperplane reduces to a plane which contains all possible response and sensitivity vectors. The theory leading to the permitted regions for the sensitivity vectors can in fact be deduced from geometrical considerations, as will be shown below. No previous attempt seems to have been made to solve three-component systems by using the minimal-assumption component resolution theory, except for the previously reported investigation by Ohta [6], this being a purely numerical mapping of the constraints.

In this section, only the theory leading to resolution of the sensitivity vectors (or quantity vectors) for the pure components will be discussed. The examples shown have been included more for illustration of the theory than for complete realism. The simulations appearing in this article are

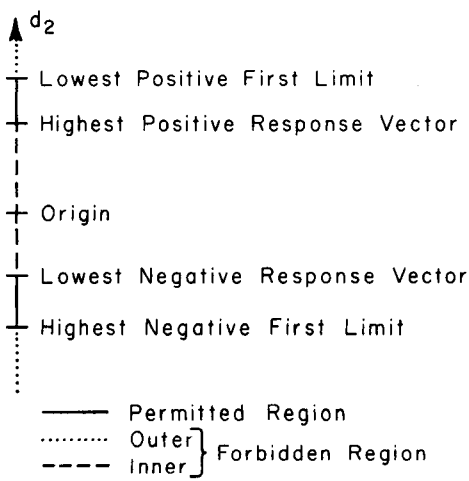

Fig. 1. Constraints for the two-component case.

described in the Appendix. The actual computations were done on the VAX 11/780 computer system of the Chemistry Department, University of Washington. The computer programs and details of algorithms applied are described elsewhere [19].

The first constraint, FIRPOL

The limiting hyperplanes of Eqn. 12 reduce to lines for three components, i.e.,

$$1 + a_{j2}\, d_2 + a_{j3}\, d_3 = 0 \quad (j = 1 \ldots \mathrm{NSE})$$

when NCO = 3. FIRPOL, the hyperpolyhedron delimiting the region of physically realizable response vectors from the first constraint condition, will in this case be a convex polygon defined by these lines, containing the origin. Several algorithms have been applied to the problem of defining FIRPOL from the intersecting limiting lines, of which some are particularly suited for generalization to the multicomponent problem. It should be possible to solve the multiple inequalities by linear programming but this has not been attempted. Here, more direct methods were preferred for keeping track of the positions of the vertices and edges of FIRPOL, in consideration of the bookkeeping necessary in higher-dimensional spaces.

First, the limiting lines defining FIRPOL for three simulated systems are shown. FIRPOL is clearly outlined by the limiting lines. Only the members of sets of parallel limiting lines closest to the origin are shown, as well as other limiting lines located near the origin. Simulation, SIM1, of intermediate resolution is shown in Fig. 2. Several of the limiting lines do not contribute to the definition of FIRPOL; SIM2 in Fig. 3 is identical to SIM1 except for a larger applied noise component. The limiting lines are shifted by an appreciable amount from their positions in SIM1, as would be expected. The eigenvector space is distorted. Comparison of the coordinates of the

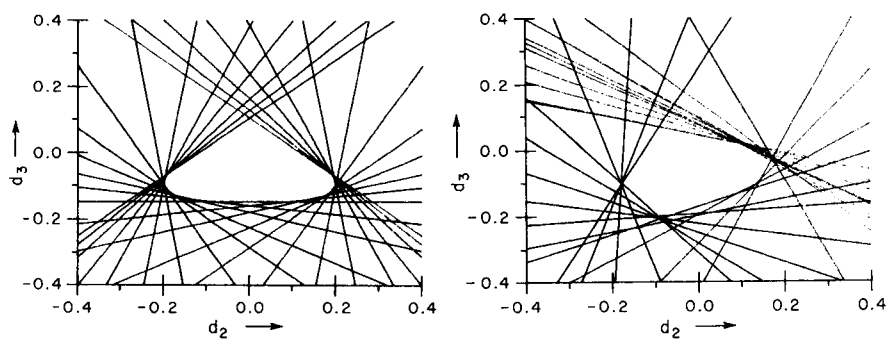

Fig. 2. Limiting lines in a region of standardization space near the origin outlining FIRPOL for simulated data set SIM1 (moderate resolution, no noise).

Fig. 3. Limiting lines in a region of standardization space near the origin outlining FIRPOL for simulated data set SIM2 (moderate resolution, noise applied).

sensitivity vectors obtained from SIM1 and SIM2, gives an estimated "RMS coordinate noise" of 1.5%, which is appreciably smaller than the applied noise in SIM2 (see Appendix). A well resolved system, SIM5, shows a completely triangular FIRPOL (Fig. 4).

The second constraint; some general considerations

A detailed discussion of the theoretical background for locating the possible (permitted) regions for the three sensitivity vectors (i.e., response vectors for the pure components) is now presented. These must be vertices of simplexes (triangles) enclosing INNPOL and located within or on the edges of FIRPOL.

Given a vertex p1 in Fig. 5, the possible locations of the second vertex will be delimited by the positive (i.e., counter-clockwise to INNPOL) tangent p1-a-*q*1 to INNPOL intersecting FIRPOL in q1. The possible locations of the third vertex will be delimited by the negative (i.e., clockwise to INNPOL) tangent p1-c-r1 to INNPOL intersecting FIRPOL in *r*1. As the simplex must enclose INNPOL, two further restrictions apply: (1) the second vertex cannot be located outside the shaded region II delimited by the tangents p1-a and r1-b; (2) the third vertex cannot be located outside the region III delimited by the tangents p1-c and q1-c. For the vertex p1, a family of sensitivity simplexes is permitted with one vector in p1 and the other two in the regions II and III, respectively. It must be emphasized, however, that no pair of vectors in these regions may be members of a simplex. The choice of a point in II or III will further restrict the location of the remaining vertex.

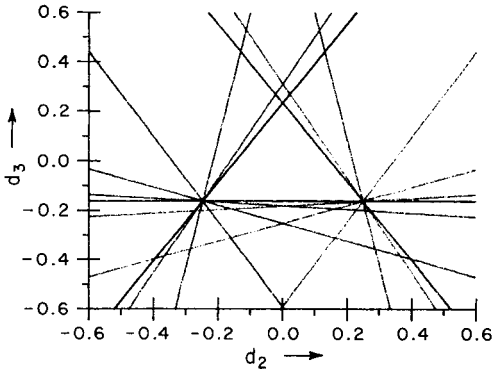

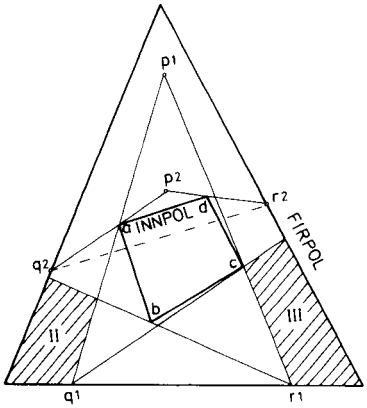

Fig. 4. Limiting lines in a region of standardization space near the origin outlining FIRPOL for simulated data set SIM5 (well resolved).

Fig. 5. Permitted simplexes with one vertex in p1 must have the two other vertices in regions II and III. No permitted simplex with a vertex in p2.

Now consider another point p2 in Fig. 5. No sensitivity vector simplex enclosing INNPOL is possible, as the line connecting q2 and r2 (the intersections of the tangents p2-a and p2-d with FIRPOL) passes through INNPOL.

This provides one obvious criterion for testing whether a given point p*i* may be a vertex of a simplex enclosing INNPOL, or not: find the tangents p*i*-g*i* and p*i*-h*i*, where g*i* and h*i* now represent the vertices of INNPOL through which the positive and negative tangents pass; then locate the intersections q*i* and r*i* of the tangents with FIRPOL. If the line q*i*-r*i* does not intersect INNPOL, p*i* is a possible location for a sensitivity vector.

The tangent algorithm

As the next step, a systematic method is derived for finding the regions of FIRPOL where a sensitivity vector can be located, and the forbidden regions between them (or the one permitted and the one forbidden region, if such is the case). It is, of course, completely possible to make a systematic search through a sufficiently fine grid of points in FIRPOL for permitted regions. This would be unnecessarily time-consuming, and gives little new insight.

Consider any tangent to INNPOL, e.g., q1-b-r1 in Fig. 6. By constructing a negative tangent from q1 through the corner a of INNPOL and a positive tangent from r1 through d, it is found that in this case a simplex q1, r1, p1 is permitted (i.e., these points may be the locations of sensitivity vectors). It is now of fundamental importance that p*i* is the vertex located closest to

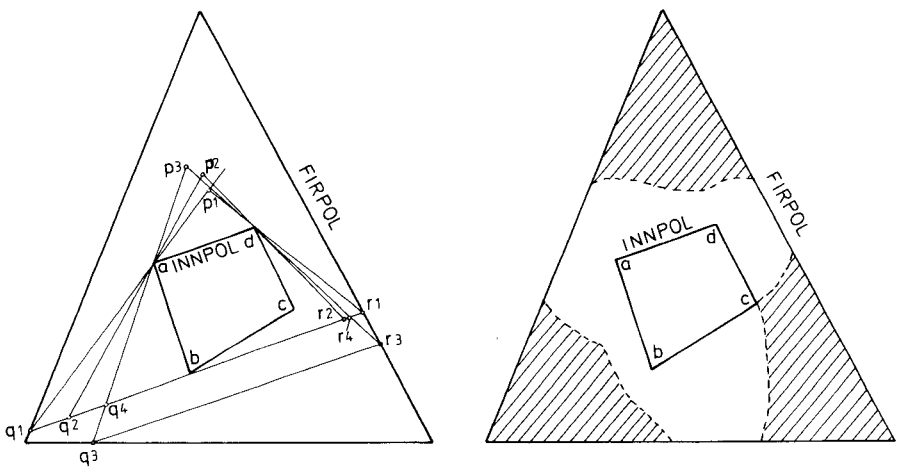

Fig. 6. On all simplexes enclosing INNPOL with two vertices on a given tangent to INNPOL or on any line parallel with this tangent, p1 will be the third vertex nearest to the tangent.

Fig. 7. Permitted regions for sensitivity vectors determined by the tangent algorithm (shaded).

the given tangent of any simplex including INNPOL with the two other vertices located within or on FIRPOL on the tangent or on any line parallel to it but further away from INNPOL. This latter fact follows from the convexity of FIRPOL. Simplexes resulting from some point pairs illustrating this principle are shown in Fig. 6 as q2, r2, p2; q3, r3, p3; q4, r4, p3.

When the tangent sweeps around INNPOL, the points p*i* will map out the border between the possible and forbidden locations for simplex vertices under the above conditions. When p*i* falls outside FIRPOL, no permitted sensitivity vector can exist for that tangent. When p*i* is located within or on FIRPOL, it defines the border between permitted and forbidden sensitivity vector regions.

This provides the means for a systematic search for the inner limit of the region of permitted locations for sensitivity vectors. It may also happen that the point of intersection is located on the side of the first tangent opposite to INNPOL. This will, in general, yield non-permissible solutions as the resulting simplexes do not enclose INNPOL. The intersections will also be located outside FIRPOL or, in the limit, on a vertex of FIRPOL.

Figure 7 shows the result of applying this tangent algorithm to the example from the two previous figures. The points p*i* falling outside FIRPOL are without interest for this problem and have not been shown. The tangent algorithm as described above is still a numerical method as the limiting points have to be computed for a suitable number of tangents. It will, however, be shown that the tangent method in fact yields exact analytical solutions to the problem.

Exact solutions for the permitted regions; the limiting function

For the same example, with the vertices of INNPOL denoted a, b, c, d as before, the symbols A, B, C are used for the edges of FIRPOL and AB, BC, CA for its vertices as in Fig. 8. (Note that although the theory is derived in terms of this specific example, the results have completely general applicability.) Again, construction of an arbitrary tangent T2 to INNPOL intersects FIRPOL in q and r. Proceeding as before, the negative tangent q-a (T1) and the positive tangent r-c (T3) are constructed. Again a point of intersection p results. It is noted that p is the intersection of two lines, T1 and T3, defined by the point pairs q, a and r, c where a and c are vertices of INNPOL. The points p and q are defined by the intersections of tangent T2 with the edges A and B of FIRPOL. It is a simple matter to express the coordinates of p from the given quantities. The vertices a, b, c of INNPOL and edges A, B of FIRPOL are fixed while the orientation of tangent T1 (as defined by some suitable parameter) is the independent variable determining the locations of the dependent variables q, r and finally p.

Thus there is an exact but unwieldy equation for the location of p. This particular equation has only local validity. While the orientation of the tangent T2 varies, it is seen that a finite family of equations of this form exists where each equation defines p over a limited range. The generating

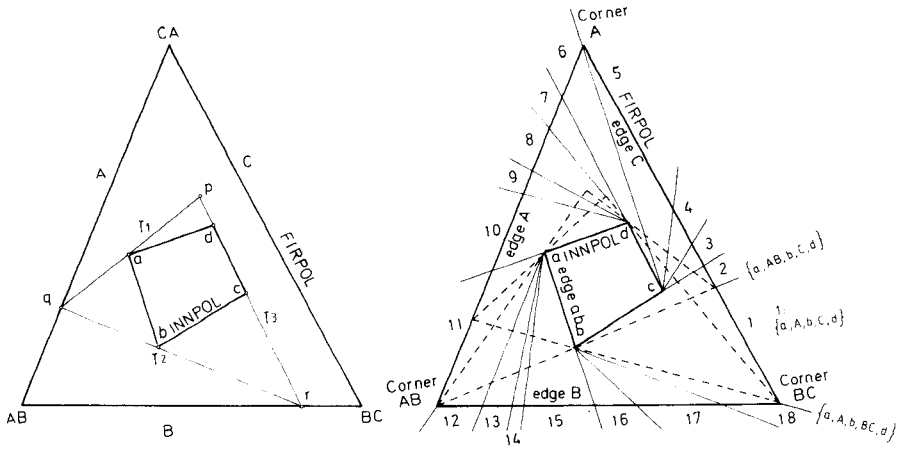

Fig. 8. Notation for edges and corners of FIRPOL and INNPOL. The simplex shown is of type {a, A, b, B, cd} (see text).

Fig. 9. The 18 limiting equations for this example are indicated by the locations of the generating tangents bordering their domains. Region 1 with simplexes of type {a, A, b, C, d} is bordered by the generating tangents {a, A, b, BC, d} and {a, AB, b, C, d}. The limiting equations correspond to simplexes of types:
1 {a, A, b, C, d}; 2 {a, B, b, C, d}; 3 {a, B, c, C, d}; 4 {b, B, c, C, d}; 5 {b, B, c, C, a}; 6 {b, B, c, A, a}; 7 {b, B, d, A, a}; 8 {b, C, d, A, a}; 9 {c, C, d, A, a}; 10 {c, C, d, A, b}; 11 {c, C, a, A, b}; 12 {c, C, a, B, b}; 13 {c, C, a, B, c}; 14 {c, A, a, B, c}; 15 {d, A, a, B, c}; 16 {d, A, b, B, c}; 17 {a, A, b, B, c}; 18 {a, A, b, B, d}.

tangent, T2, passes successively through all the corners of INNPOL, intersecting in turn the edges and vertices of FIRPOL and finally defines p by tangents through varying vertices of INNPOL. One thus has to keep track of the range of validity of each partial equation. This is a nontrivial, although well defined problem of bookkeeping. Even in the simple example given, a great number of ranges will exist.

A limit-defining simplex can be denoted by: {⟨tangent point of T1 on INNPOL⟩, ⟨edge of FIRPOL intersected in q⟩, ⟨tangent point of T2 on INNPOL⟩, ⟨edge of FIRPOL intersected in r⟩, ⟨tangent point of T3 on INNPOL⟩}.

Points will be symbolized by lower case letters; lines by capital letters. Two letter symbols indicate either a tangent along an edge of INNPOL or a line passing through the intersection of two edges of FIRPOL. The simplex in Fig. 8 is thus: {a, A, b, B, cd}. The symbol cd shows that in this case the tangent T3 passes through an edge of INNPOL with vertices c and d. Figure 9 shows the distinct ranges of limiting equations for this simple example.

The complete numeric computation of the limiting function using the tangent algorithm for all possible orientations of the tangent will thus require a lot of bookkeeping, but is simple in principle. It would be conven-

ient, however, to be able to eliminate the forbidden regions in which the intersection point falls outside FIRPOL in advance. This is the subject of the next section.

Equations have now been derived, describing the limiting function for the permitted regions of the sensitivity vectors where the intersection point falls on or within FIRPOL. These regions represent the maximum information attainable through use of the component resolution theory without introduction of further constraints. They can also be interpreted as the minimum regions of allowable solutions possible under the given assumptions.

THE SIMPLEX ROTATION ALGORITHM

Further considerations of the properties of sensitivity vectors lead to a very efficient procedure for eliminating the major part of the forbidden regions. For reasonably resolved systems, the procedure also leads to an excellent approximation to the permitted regions.

Starting with a point on an edge of FIRPOL, one constructs tangents to INNPOL in either the positive or negative directions: (1) from the starting point construct a tangent; (2) from the intersection of this tangent with FIRPOL construct another tangent; (3) finally, from the intersection of the second tangent with FIRPOL, construct a third tangent to INNPOL. This will intersect the first tangent, forming a closed simplex around INNPOL. As shown in Fig. 10, there are three types of such simplexes: (a) the vertices of sensitivity vector simplexes closed on the edges of FIRPOL, the limiting case; (b) the vertices of sensitivity vector simplexes closed within FIRPOL; (c) simplexes which are not closed within or on FIRPOL, the vertices of which cannot be sensitivity vectors.

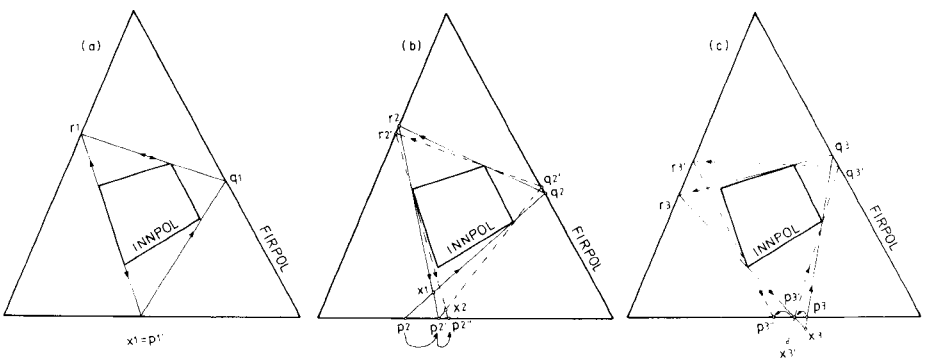

Fig. 10. Simplex rotation. All edges of the simplexes are tangents to INNPOL while the first two vertices are located on edges of FIRPOL. (a) All vertices on edges of FIRPOL (limiting simplex); invariant to rotation in either direction. (b) Rotating positive simplexes starting in a permitted point on an edge of FIRPOL. (c) Rotating positive simplexes starting in a forbidden point on an edge of FIRPOL.

A simplex formed from positive (negative) tangents in this way will be called a positive (negative) simplex. Consider the point p1 in Fig. 10(a) located on an edge of FIRPOL. The positive simplex starting in p1 has the vertices q1, r1, x1, where the point of closure x1 coincides with p1. Placing p1 in this unique position results in one, and only one, possible sensitivity vector simplex starting in the point. Note that an identical negative simplex starts in p1. Constructing a positive simplex from another point p2 in Fig. 10(b) results in the simplex q2, r2, x2. This is a permitted sensitivity simplex as all its vertices are located on or within FIRPOL. A family of sensitivity vector simplexes whose edges are not necessarily tangents to INNPOL can be constructed starting in p2.

An extended simplex is defined as consisting of the edges and extensions of edges of a simplex. Thus p2 and p2′ in Fig. 10(b) are points on the extended simplex corresponding to the simplex q2, r2, x2. Figure 10(b) further shows a very important result. When a starting point is chosen which results in a positive sensitivity vector simplex, the point p2′ on the extended simplex located on FIRPOL will be in a positive direction from the starting point, p2. The point, p2′, will itself be located on the extended simplex and therefore be the location of a permitted sensitivity vector. Conversely, constructing the negative simplex x2, r2, q2 and starting with a permitted sensitivity vector p2′, results in the extended simplex point p2. This is also a permitted sensitivity vector, but now located in the negative direction from the starting point along the edge of FIRPOL. Continuing this reasoning, when starting from a point which is a permitted sensitivity vector, one generates a series of permitted positive simplexes; the starting points, p2 followed by p2′, p2″ etc., (themselves extended simplex points on the edge of FIRPOL of the preceding simplex) will move along the edge of FIRPOL, always in the positive direction. Or, starting in a permitted point and generating negative simplexes will produce a succession of points which will move in the negative direction along the edge of FIRPOL.

Finally in Fig. 10(c), starting with a point p3, a positive simplex q3, r3, x3 is constructed which is not closed on or within FIRPOL. The starting point p3 and intersecting point p3′ are both forbidden locations for a sensitivity vector. Thus, starting with a forbidden point, one obtains a forbidden intersection point located in the negative direction along the edge of FIRPOL. A negative simplex will yield a forbidden intersection point in the positive direction on FIRPOL.

The following conclusions can be made. Starting with a permitted point on FIRPOL and constructing a positive (negative) simplex provides another permitted point located in the positive (negative) direction on FIRPOL. Starting with a forbidden point on FIRPOL and constructing a positive (negative) simplex yields a forbidden point located in the negative (positive) direction on FIRPOL. Starting with a point on a limiting simplex, the same point will result regardless of the mode of rotation of the simplex. An iterative procedure for locating limiting simplexes has thus been developed.

Starting with a permitted or forbidden point, one will move (by choice in the positive or negative direction) to convergence on a limiting simplex. Any point on FIRPOL will be a possible starting point. If no limiting simplex exists, i.e., all points on FIRPOL are either permitted or forbidden, one will eventually move around FIRPOL, passing the original starting point. This gives a definite criterion for the non-existence of any limiting simplex.

The case for which all points on the edges of FIRPOL are forbidden is trivial as no possible solution exists. The case for which all edges of FIRPOL are permitted will be treated in some greater detail in a later section. From actual experience with numerous simulated chemical systems, the convergence properties of this simplex rotation algorithm are excellent, as convergence to any reasonable numerical accuracy will be reached (if at all) within a few iteration cycles (simplexes), typically 3—6. For a discussion of the practical difficulty of formulating analytical convergence criteria, a recent report can be consulted [20].

A useful procedure will be to start in any point, rotating first in the positive direction, then in the negative direction until the limiting simplexes have been found. In the improbable event of choosing a point of a limiting simplex by accident, another point must be selected for the second iteration. If there is doubt whether a section of the edge of FIRPOL contains permitted points or not, it is simple to construct the points of intersection with FIRPOL of a positive and a negative tangent to INNPOL from any point in the section and to test for intersection of INNPOL by their connecting line. Alternatively, a positive or negative simplex can be constructed from the point to test for closure within or on FIRPOL. In Fig. 11 are shown the two limiting simplexes derived for the previous example.

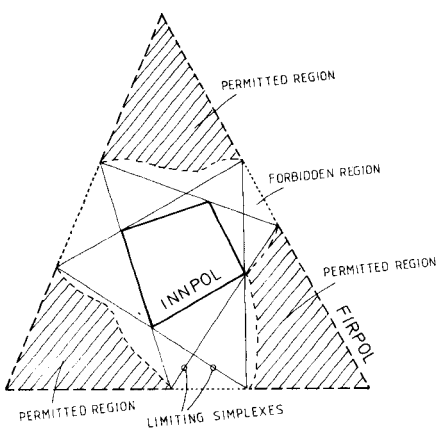

Fig. 11. Limiting simplexes determined by the rotating simplex method for the example used in Fig. 7.

TENTATIVE AND PERMITTED REGIONS

This section considers in some more detail the case in which two limiting simplexes exist. The three actual permitted regions for sensitivity vectors found by the tangent algorithm are shown beside the limiting simplexes in Fig. 11. It appears that the polygonal regions defined by the edges of FIRPOL and those of the limiting simplexes enclose the three permitted regions. Even in this example, having very large permitted regions and consequently low resolution of the components, these polygons (the tentative regions) are rather good approximations to the actually permitted regions. The permitted regions can never exceed the tentative regions.

Inspection of Fig. 12(a) shows that the edges of the simplexes themselves are not permitted, only their vertices on FIRPOL. Before the tangent algorithm is applied to perform an exact (or rather, as accurate as desired) mapping of the permitted regions, simplex rotation should be used to eliminate forbidden regions. As shown in Fig. 12(b), only tangents between T1 and T1′ need be applied for region I; only tangents between T2 and T2′ need be applied for region II; and only tangents between T3 and T3′ need be applied for region III. These range-defining tangents are all edges of the limiting simplexes. All other tangents outside these ranges will result in simplexes which are not closed within or on FIRPOL. In this way, the amount of computation can be reduced greatly.

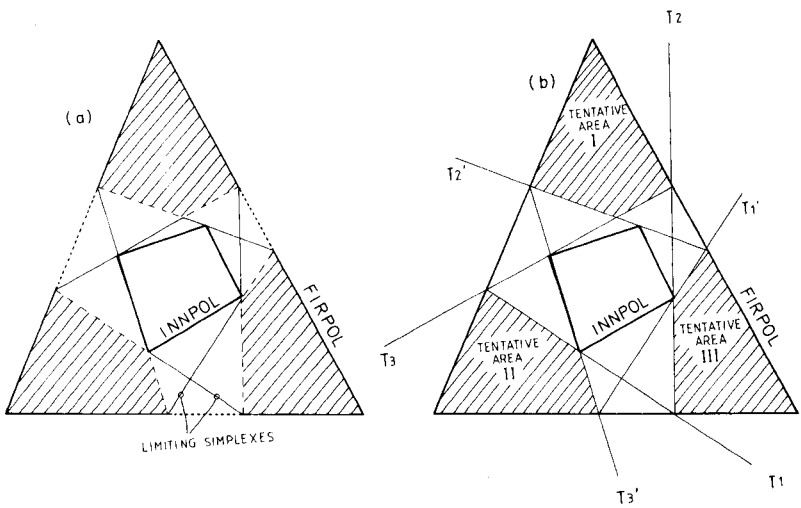

Fig. 12. Permitted and tentative regions. (a) Tentative regions determined by the rotating tangent method; the sections of the edges of FIRPOL delimited by the limiting simplexes (solid lines) are always permitted, while the edges of the limiting simplexes themselves are forbidden. (b) For determining the permitted regions, which are subregions of the tentative regions, only generating tangents between T1 and T1′, T2 and T2′, T3 and T3′ need be considered.

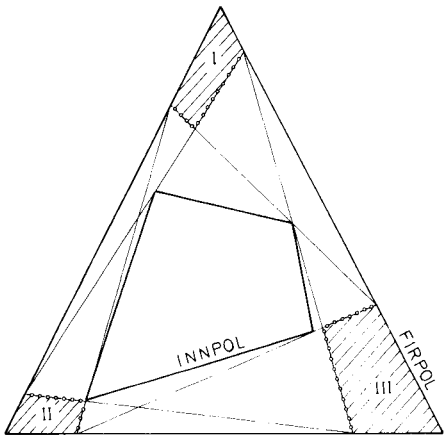

Fig. 13. For a sufficiently well resolved system, tentative and permitted regions (open circles) nearly coincide.

The earlier examples were chosen with very low component resolution in order to emphasize the differences between possible and tentative regions. For a system with somewhat better resolution as shown in Fig. 13, one finds that the tentative regions calculated by simplex rotation and the permitted regions calculated by the tangent algorithm practically coincide. For fairly well resolved systems, one can expect that the tentative regions will be excellent approximations to the permitted regions. This can easily be verified for selected points near the limiting simplexes by applying any of the now familiar methods.

Simplifications when all edges of FIRPOL are permitted

When all points on the edges of FIRPOL are permitted, the border between the permitted and forbidden region may be found by systematic application of the tangent algorithm. Some simplification may be possible when one or several vertices of INNPOL are permitted locations.

In another example, it can be seen from Fig. 14(a) that the vertex *a* of INNPOL is a forbidden point for any tangent while *b* will be permitted for tangents between (and including) T*b* and T*b'*. By similar reasoning, vertices *c* and *d* will be permitted points for tangents in the ranges T*c*—T*c'* and T*d*—T*d'*. With the tangent algorithm, only the tangents ranging between T*b'* and T*c*, T*c'* and T*d*, and T*d'* and T*b* need to be searched. The resulting permitted region for this example is shown in Fig. 14(b). In this way an appreciable amount of computation can be eliminated.

The interpretation of "permitted regions"

It must be emphasized at this point what is meant by the phrase "permitted region". It is not possible to form a (potential) sensitivity vector simplex from any combination of points in the permitted regions. Only the

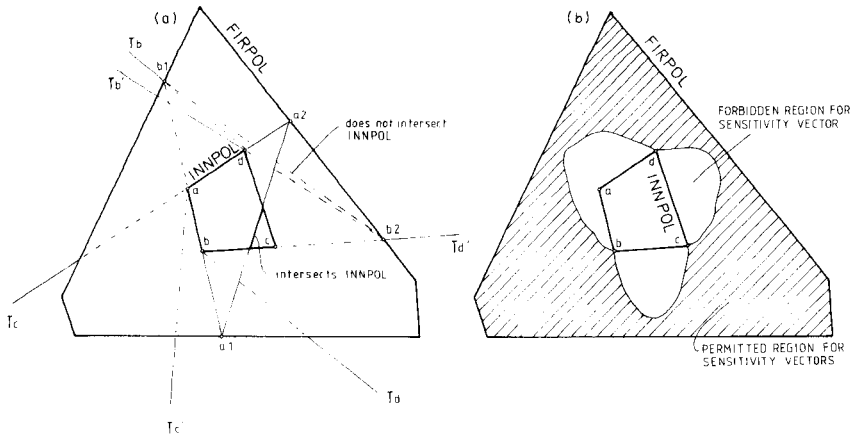

Fig. 14. A low-resolution case with a single permitted region. (a) Some vertices of INNPOL may be permitted positions, here b, c and d; this is easily seen from the simplexes originating in vertex a (solid) through a, b, a1, a2, d, in vertex b (broken lines) through b, c, b2, b1, a, and correspondingly from c and d (not shown). (b) The permitted regions found by the tangent method; here all generating tangents between Tc and Tc', Td and Td', Tb and Tb' in Fig. 15(a) can be disregarded, as they only give the permitted points identical to vertices *c*, *d* and *b* of INNPOL.

first (potential) sensitivity vector can be picked at random in any of the regions. The possible regions for the second sensitivity vector will be limited when the first vector has been selected or otherwise obtained. Further, when two sensitivity vectors have been selected, the remaining freedom of choice for the final vector will be even more limited. These restrictions are illustrated in Fig. 15. Figure 15(a) shows the permitted regions I, II, III resulting from a resolution study. Choosing one sensitivity vector in region I constrains the choice of the second vector to the reduced regions of Fig. 15(b). The choice of two vectors which must be mutually permissible further constrains the possible region for the final vector as in Fig. 15(c). Even when only one continuous permitted region exists (no convergence of the rotating simplex algorithm) the same rules apply to selection of sensitivity vector simplexes.

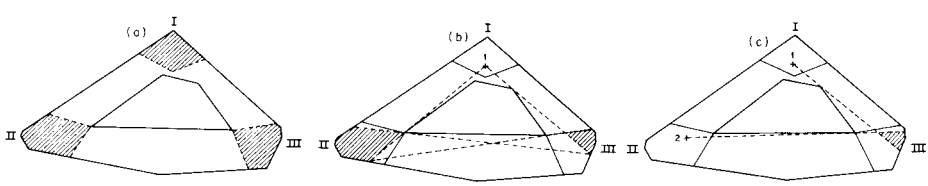

Fig. 15. Restrictions on the locations of sensitivity vectors, given three separate permitted regions. (a) The first sensitivity vector may be located anywhere in the permitted regions I, II and III. (b) Permitted subregions II and III when a vector 1 in region I has been selected. (c) Permitted subregion III when two mutually permissible vectors 1 in region I and 2 in region III have been selected.

It is important to note that any triplet of sensitivity vectors chosen within the above limitations only defines a potential sensitivity vector simplex. The component resolution theory as derived here cannot decide between the potential simplexes, and thus the real sensitivity vectors of the three pure components. The component resolution theory by itself is limited to yielding information about the possible regions within the limitations stated in this section.

For a more complete resolution of the components, other methods or extensions of the fundamental theory must be pursued. The most direct approach is extended data collection when possible, following a strategy indicated in the later section on the importance of sensors and samples. A potentially useful approach may be evaluation of points within the permitted regions by target vector analysis. This may be an alternative to the recent methods of choosing a set of orthogonal target vectors by Malinowski [12] or target vector scan by Gemperline [13]. Information about the experimental method, such as the "composition continuity constraint" of chromatographic methods, can also yield added resolution as shown in a subsequent section on application of supplementary information.

It may be noted here that when a triplet of sensitivity vectors has been chosen, these are only known in the standardized form. Their absolute values can be obtained by using the fact that all the response vectors with known real values can now be expressed by the sensitivity vectors.

The importance of samples and sensors on the limiting conditions

The detailed analysis of the influence of experimental uncertainty on the permitted regions is not pursued here. Both FIRPOL and INNPOL, and thus the final result, will depend on the accuracy of the response matrix. Experimental uncertainty was taken into account in the derivation of the first constraint by Meister [14].

However, the simulations show that for certain systems, several of the limiting lines will not contribute to the definition of FIRPOL; similarly, some of the observed response vectors may fall inside INNPOL and thus have no influence on the shape of this polygon and the following definition of the permitted regions for the sensitivity vectors.

Any high-quality experimental response vector will contribute to the improvement of the signal-to-noise ratio, the definition of the eigenvectors, and indirectly to the shape of FIRPOL, INNPOL and the permitted regions. The data points associated with these samples and sensors may be of minor importance for definition of the permitted regions. However, the calculations supply information which may be used to plan for supplementary data collection. The properties of limiting lines which will add to the definition of FIRPOL will be known, while added samples should have response sensors which increase the size of INNPOL. Finally, the resulting permitted regions will critically depend on both the sensitivity and quantity resolution of the data, and thus on optimal experimental design.

SIMULATED CHEMICAL SYSTEMS

In order to show the shapes of FIRPOL, INNPOL and the limiting simplexes for a more realistic chemical system, Fig. 16 is presented in which these polygons are graphed for the simulated system called SIM1.

Figure 17 shows response vectors, sensitivity vectors, and the permitted regions for the sensitivity vectors for the five simulated chromatograms. (The tentative regions are shown for ease of presentation, but these are quite good estimates of the permitted regions.) As the data are simulated, it is possible to show the locations of the sensitivity vectors, the targets of a real investigation. A comparison of SIM1 with SIM2—4 clearly illustrates the effects of noise, reduced component resolution, and presence of a minor component on the relative sizes of the permitted regions. SIM5 is very well resolved. The permitted regions coincide with the known sensitivity vectors. The simple simulation, SIM6, is included to show the effect of transposing the data matrix. The data matrix of SIM6 was processed in the same way as for the SIM1—5, yielding the permitted regions for the sensitivity vectors in the sensitivity eigenvector space (Fig. 17F). Transposing the data matrix before processing instead yields the permitted regions for the quantity vectors (Eqn. 14), directly giving the possible quantity vectors for the components in Fig. 18. In the sense of multicomponent resolution, this system is not resolved because the permitted regions are of finite size. It is known, however, that the pure sensitivity vectors have been measured for samples 1, 2, 3. These are located in the inner end of the permitted sensitivity vector regions of Fig. 17F. The corresponding quantity vectors in Fig. 18 that are not well determined by the "measurements" are located at the outer ends of the permitted regions in "quantity vector space". This is in complete accord with the observations made in the investigation on two-component systems referred to earlier.

Application of supplementary information

As can be seen from the preceding three-component examples, the basic physical constraints do not by themselves provide complete resolution

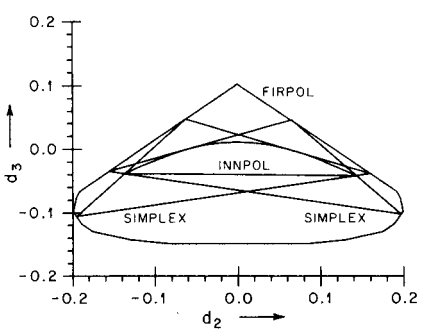

Fig. 16. FIRPOL, INNPOL and limiting simplexes for simulated data set SIM1.

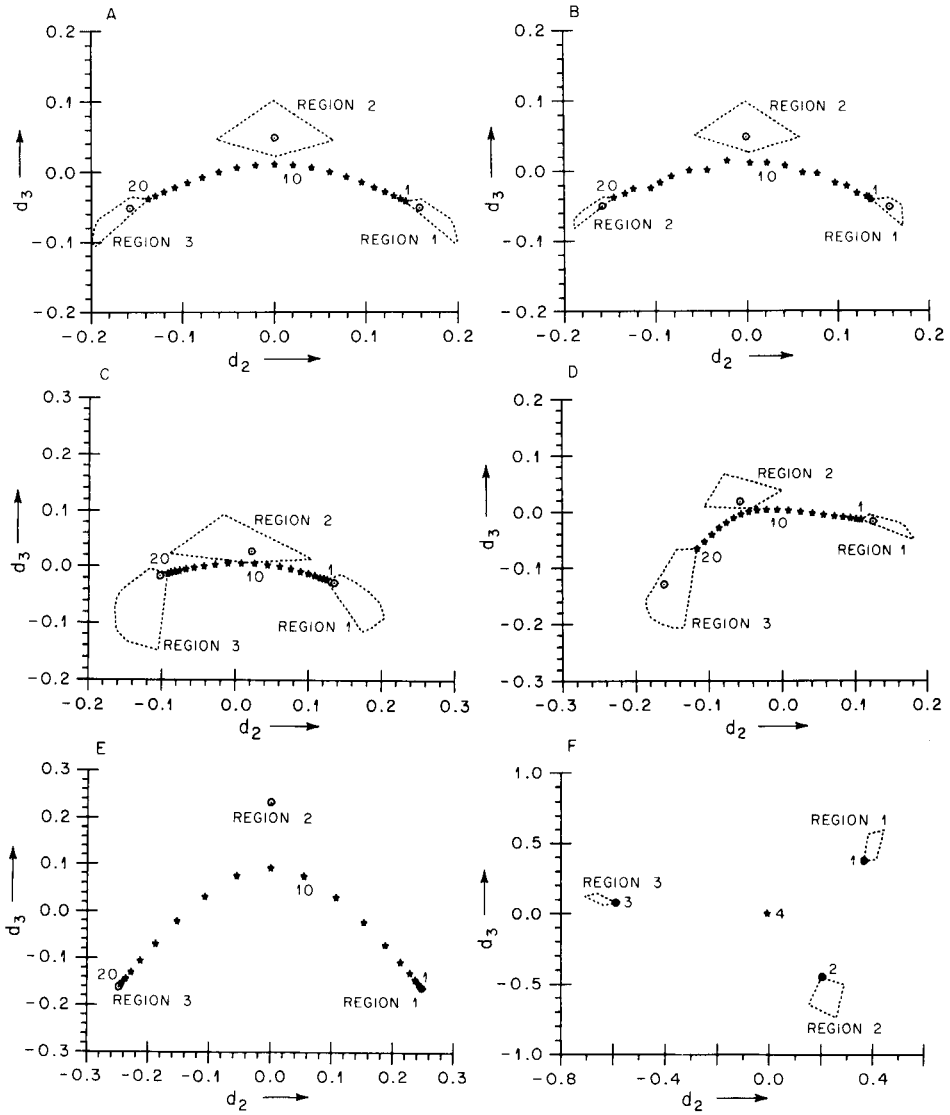

Fig. 17. Response vectors (⋆), sensitivity vectors (○) and permitted regions for simulated data sets: (A) SIM1; (B) SIM2; (C) SIM3; (D) SIM4; (E) SIM5; (F) SIM6.

except in favorable cases. This is also well known from earlier studies. No assumptions have been made about the actual measurement technique and, although it is not a main subject of this article, it is shown that introduction of such information may yield greatly enhanced resolution.

For measurements on systems with smoothly varying quantities (an additional "continuity constraint") of the components, such as chromatographic measurements, typical patterns as shown in the examples are

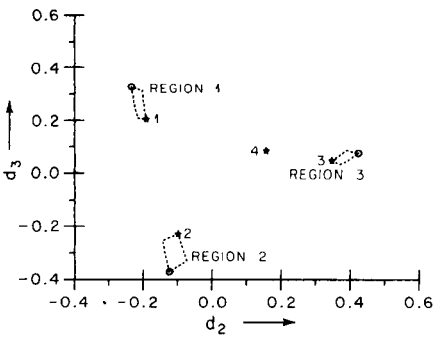

Fig. 18. Based on the transposed response matrix of the simulated data set SIM6, the permitted regions for the quantity vectors are shown in "quantity standardization space". Symbols: (○) quantity vector; (★) response vector.

obtained. Usually, the first and last samples will be composed mainly of a single component, and the response vectors corresponding to these samples will converge towards their respective sensitivity vectors. Near-coincidence of several response vectors may indicate an approximation to a sensitivity vector.

In several of the simulations, tangents through a number of the first and the last response vectors will give the approximate loci of two of the sensitivity vectors and the approximate location of the last one. This is illustreated for SIM4 in Fig. 19. Although this is not the most favorable example,

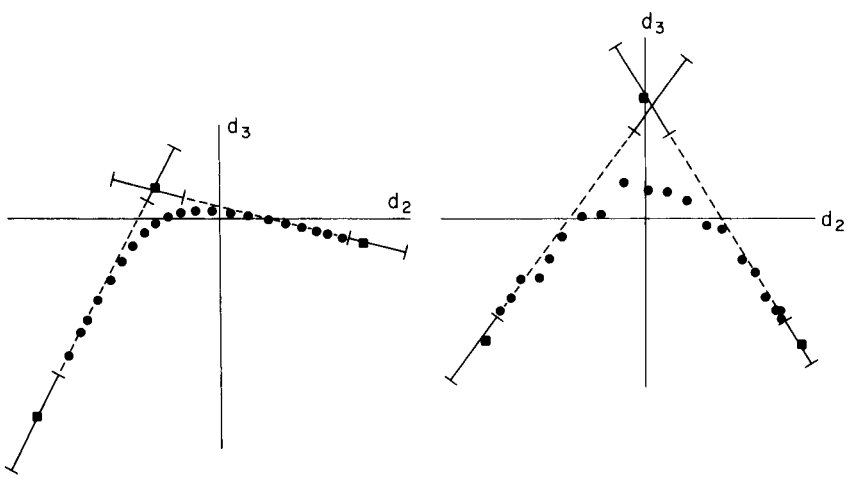

Fig. 19. For chromatography-type data, one sensitivity vector is located while the two others are constrained to line segments through the two permitted regions by extrapolated tangents through the first and last response vectors. (Simulated data set SIM4.)

Fig. 20. For chromatography-type data, location of the sensitivity vectors somewhat inferior to that of Fig. 19 is possible in the presence of heavy experimental noise. (Simulated data set SIM2.)

the locations of two of the sensitivity vectors are limited to line segments within the permitted regions. The third sensitivity vector is well located. When a large amount of noise is present, all locations become more uncertain. Figure 20 shows that even for the high noise simulation (SIM2) quite good approximations to the correct sensitivity vectors result when a reasonable tangent fit is made.

More than three components

Although the algorithms described for three components can be applied to the higher-dimensional problem of more than three components, the practical generalization of the necessary algorithms is not a trivial problem. The general algorithms for FIRPOL and INNPOL are reasonably simple to implement, but the location of permitted regions will require very efficient programming in the multicomponent case. This effort is proceeding.

One of the authors (OSB) expresses his gratitude to the University of Trondheim, Norwegian Institute of Technology, for granting leave of absence, and to the Royal Norwegian Council for Scientific and Industrial Research for granting a research fellowship. This research was supported in part by the U.S. Department of Energy.

APPENDIX

Simulated chemical systems

Several studies have been done with data from simulated three-component chemical systems which have varying component resolution. Some of these are used as examples in this paper. The simulated data were generated by a program [19] which computes response matrices from user-specified parameters of quantity and sensitivity. There are several options for noise generation.

The sensitivity and quantity vectors used in the simulations are shown in Figs. A1 and A2 and Table A2, as listed in Table A1. The SIM1—SIM5 all represent simulated chromatograms with 20 samples and 25 sensors where the total response as given by a quantity-sensitive sensor would be a somewhat wide and unresolved peak.

The relative amounts of the components are 1:1:1 except for SIM4 where the ratios are 5:5:1. Also, the quantity vectors of SIM5 are somewhat narrower than those of the other simulations, for enhanced resolution. Simulations SIM1 and SIM3 show the effect

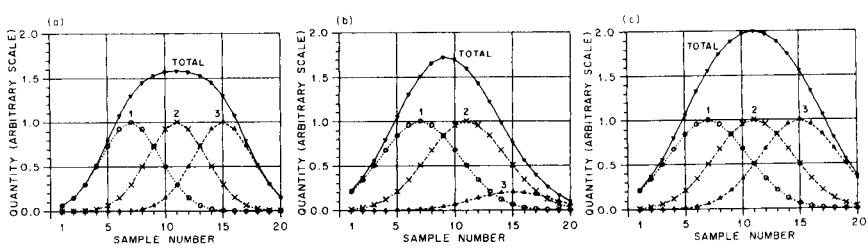

Fig. A1. Quantity vectors used in simulations: (a) SIM1, SIM2 and SIM3; (b) SIM4; (c) SIM5.

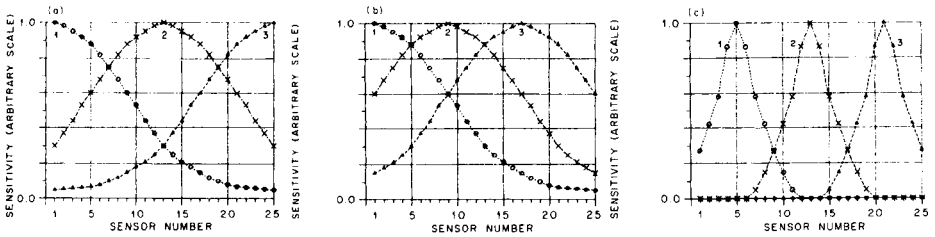

Fig. A2. Sensitivity vectors used in simulations: (a) SIM1, SIM2 and SIM4; (b) SIM3; (c) SIM5.

TABLE A1

Quantity and sensitivity data for simulations

Data set	Quantity vector	Sensitivity vector	No. of samples	No. of sensors	Noise applied
SIM1	Fig. A1(a)	Fig. A2(a)	20	25	no
SIM2	Fig. A1(a)	Fig. A2(a)	20	25	yes
SIM3	Fig. A1(a)	Fig. A2(b)	20	25	no
SIM4	Fig. A1(b)	Fig. A2(a)	20	25	no
SIM5	Fig. A1(c)	Fig. A2(c)	20	25	no
SIM6	Table A2	Table A2	4	4	no

TABLE A2

Relative sensitivities and quantities for SIM6

Component no.	Sensitivity of sensor no.				Quantity of sample no.			
	1	2	3	4	1	2	3	4
1	1.0	0.2	0.1	0.05	1.0	0.0	0.0	1.0
2	0.2	1.0	0.05	0.1	0.0	1.0	0.0	1.0
3	0.05	0.1	0.2	1.0	0.0	0.0	1.0	1.0

of varying sensitivity resolution of the components, and SIM1 and SIM4 show the effect of varying relative amounts of the components.

Simulations SIM1 and SIM2 show the effect of noise added to noise-free data; SIM2 is identical to SIM1 except for an applied noise component generated as a normally distributed random number with variance = $(0.005)^2\ (R\text{max})^2 + (0.05)^2\ (R\text{max})\ R$, where R is the response and Rmax is the maximum response.

The total responses for SIM1 and SIM2 are shown in Figs. A3 and A4 as typical examples of data used in these studies. Here, SIM5 represents a well resolved system and SIM6 is a simple system with few samples and sensors.

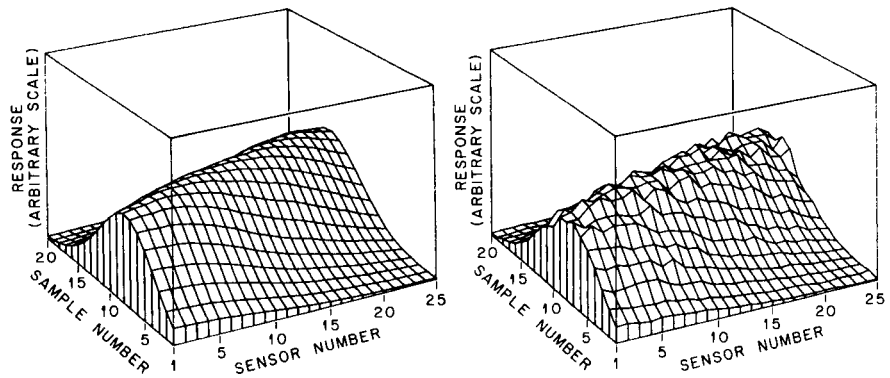

Fig. A3. Responses for simulation SIM1, no noise.

Fig. A4. Responses for simulation SIM2, noise added to SIM1.

REFERENCES

1 W. H. Lawton and E. A. Sylvestre, Technometrics, 13 (1971) 617.
2 M. A. Sharaf and B. R. Kowalski, Anal. Chem., 53 (1981) 518.
3 M. A. Sharaf and B. R. Kowalski, Anal. Chem., 54 (1982) 1291.
4 D. W. Osten and B. R. Kowalski, Anal. Chem., 56 (1984) 991.
5 R. A. Gilbert, J. A. Llewellyn, W. E. Swartz and J. W. Palmer, Appl. Spectrosc., 36 (1982) 428.
6 N. Ohta, Anal. Chem., 45 (1973) 553.
7 Jie-Hsung Chen and Lian-Pin Hwang, Anal. Chim. Acta, 133 (1981) 271.
8 B. G. M. Vandeginste, Pure and Appl. Chem., 55 (1983) 2007.
9 H. Martens, Anal. Chim. Acta, 112 (1979) 423.
10 E. Spjøtvoll, H. Martens and R. Volden, Technometrics, 24 (1982) 173.
11 F. J. Knorr and J. H. Futrell, Anal. Chem., 51 (1979) 1236.
12 E. R. Malinowski, Anal. Chim. Acta, 134 (1982) 129.
13 P. J. Gemperline, J. Chem. Inf. Comput. Sci., 24 (1984) 206.
14 A. Meister, Anal. Chim. Acta, 161 (1984) 149.
15 E. R. Malinowski and D. G. Howery, Wiley-Interscience, New York, 1980.
16 H. Martens and H. Russwurm Jr. (Eds.), Applied Science Publ., London, 1983.
17 S. Wold, Technometrics, 20 (1978) 397.
18 H. T. Eastment and W. J. Krzanowski, Technometrics, 24 (1982) 73.
19 O. S. Borgen and B. R. Kowalski, Technical Reports 111—113, Laboratory of Physical Chemistry, University of Trondheim, Norwegian Institute of Technology, 1984—5.
20 O. S. Borgen and B. R. Kowalski, Technical Report 114, Laboratory of Physical Chemistry, University of Trondheim, Norwegian Institute of Technology, 1985.

Analytica Chimica Acta, 174 (1985) 27—40
Elsevier Science Publishers B.V., Amsterdam — Printed in The Netherlands

A KALMAN FILTER FOR CALIBRATION, EVALUATION OF UNKNOWN SAMPLES AND QUALITY CONTROL IN DRIFTING SYSTEMS
Part 4. Flow Injection Analysis

P. C. THIJSSEN*, L. T. M. PROP and G. KATEMAN

University of Nijmegen, Faculty of Science, Department of Analytical Chemistry, Toernooiveld, 6525 ED Nijmegen (The Netherlands)

H. C. SMIT

University of Amsterdam, Laboratory for Analytical Chemistry, Amsterdam (The Netherlands)

(Received 21st February 1985)

SUMMARY

The application of state estimation in flow injection analysis is described. The linear calibration graphs normally provided often suffer from drifting parameters. The entire system is based on a set of algorithms for prediction, filtering, smoothing, evaluation, control and optimization. Selection and verification of the calibration model and the noise covariances used are investigated. The experimental results demonstrate the applicability of the calibration system in practice as a simple intelligent analyzer. The spectrophotometric determination of chloride in aqueous samples serves as the example.

Flow injection analysis is a fast, reliable and versatile routine method for the determination of many chemical constituents in unknown samples. The method is based on the injection of a small volume of sample into a continuously flowing stream. The moving aliquot may be treated consecutively with reagents, diluted, incubated, dialyzed, extracted, etc. The final product is led through an appropriate detector to generate a peak-shaped signal, directed towards a recorder or computer. Unknown samples are evaluated by using calibration graphs prepared from concentration standards with use of the height, width or area of the measured peaks. In conjunction with a computer the operation of the system is easy to automate, e.g., control of a sample changer, switching of the injection valve, stopped flow, channel switching and recording of the signal are simple. Data-processing techniques facilitate peak computations (height, width, area, baseline, etc.), drift correction and linear regression [1—5].

The present paper describes the application of state estimation in flow injection analysis. This method allows the on-line correction for drift on the calibration graph. The entire calibration system furnishes a set of algorithms for prediction, filtering, evaluation, control, optimization and smoothing

[6—8]. In practice, problems arise because of the selection of the peak-preprocessing procedure, of the calibration model and of the numerical values for the noise covariances used. A related topic investigates the verification of the performance of the implemented calibration system. This is illustrated by means of automated flow injection analysis for the determination of chloride in aqueous samples.

THEORY

Many methods for chemical analysis are based on the construction of a regression function from known standards of which unknown samples are evaluated. For calibration, the linear relationship $z = ac + b$ is commonly employed; z and c correspond to the measurement and the concentration, respectively and slope a and intercept b are parameters. For this type of modelling, the least-squares approach provides a proper solution. The parameters of the model are estimated from the measurements and the concentrations of the calibration standards. The evaluation of unknown samples is performed by the reverse formulation $c = (z - b)/a$ [9—11].

As a major source of error in practical situations, the straightforward calibration model may be inadequate. Modifications can be made, for example, with the terms c^2, $1/c$, $\log(c)$ or 10^c. In a similar way, extension to a higher-order model is obtained. The conventional least-squares method still holds for the estimation procedure. A different approach has to be considered when drift is present in the calibration graph. Each parameter is extended in order to describe the time-dependent drifting behaviour. This results in a separated set of equations: a state equation that models the dynamics in time and a measurement equation that describes the calibration model. For a drifting first-order calibration graph, the following state-space model (Eqn. 8 [8]) can be applied:

$$\begin{pmatrix} a(k) \\ b(k) \\ \alpha(k) \\ \beta(k) \end{pmatrix} = \begin{pmatrix} 1 & 0 & 1 & 0 \\ 0 & 1 & 0 & 1 \\ 0 & 0 & 1 & 0 \\ 0 & 0 & 0 & 1 \end{pmatrix} \begin{pmatrix} a(k-1) \\ b(k-1) \\ \alpha(k-1) \\ \beta(k-1) \end{pmatrix} + \mathbf{w}(k-1)$$

$$z(k) = (c, 1, 0, 0) \begin{pmatrix} a(k) \\ b(k) \\ \alpha(k) \\ \beta(k) \end{pmatrix} + v(k)$$

Here, the state refers to slope a and intercept b, each extended by an extra parameter, α and β, respectively. Modifications or extensions to alternative calibration models with or without drift can be made in a similar fashion. A particular time is denoted by the index k, $v(k)$ is the measurement noise on the signal and $\mathbf{w}(k)$ denotes the system noise describing random variations in the state. The system noise and measurement noise are assumed to be white

with zero means and covariances $Q(k-1)$ and $R(k)$, respectively. The state-space model described in this way is directly applicable to the field of state estimation. By using the concentrations and measurements of the calibration standards, the state is estimated on-line by the Kalman filter. For the evaluation of unknown samples, the associated measurement and predicted state are used. The quality performance of the system is controlled on-line by comparison with a predefined criterion. The decision to re-calibrate is followed by optimization of the concentration standards available. Afterwards, the quality of the evaluated results can be improved by smoothing the stored estimates of the Kalman filter. An interesting feature of the proposed state-space model is that it may be applied when there is uncertainty about the presence of drift. When there is no drift in a parameter, this quantity in the state has an actual value of zero. State estimation will produce relatively small numerical values for this quantity, which is in general not statistically different from zero. A disadvantage of the model extension to account for drift is the increase in the number of calibrations required.

The entire system with algorithms for prediction, filtering, smoothing, evaluation, control and optimization is summarized in Table 1. Specific

TABLE 1

The calibration system

Model	$\mathbf{x}_k = F(k, k-1)\mathbf{x}_{k-1} + \mathbf{w}_{k-1}$
	$z_k = \mathbf{h}_k^t \mathbf{x}_k + v_k$
Prediction	$\hat{\mathbf{x}}_{k/k-1} = F(k, k-1)\hat{\mathbf{x}}_{k-1/k-1}$
	$P_{k/k-1} = F(k, k-1)P_{k-1/k-1}F^t(k, k-1) + Q_{k-1}$
Filtering	$\hat{\mathbf{x}}_{k/k} = \hat{\mathbf{x}}_{k/k-1} + \mathbf{k}_k[z_k - \mathbf{h}_k^t \hat{\mathbf{x}}_{k/k-1}]$
	$P_{k/k} = P_{k/k-1} - \mathbf{k}_k \mathbf{h}_k^t P_{k/k-1}$
	$\mathbf{k}_k = P_{k/k-1}\mathbf{h}_k[\mathbf{h}_k^t P_{k/k-1}\mathbf{h}_k + R_k]^{-1}$
Smoothing	$\hat{\mathbf{x}}_{k/N} = \hat{\mathbf{x}}_{k/k} + A_k[\hat{\mathbf{x}}_{k+1/N} - \hat{\mathbf{x}}_{k+1/k}]$
	$P_{k/N} = P_{k/k} + A_k[P_{k+1/N} - P_{k+1/k}]A_k^t$
	$A_k = P_{k/k}F^t(k+1, k)P_{k+1/k}^{-1}$
Optimization	Maximize $\mathbf{h}_k^t P_{k/k-1}\mathbf{h}_k / R_k$
Evaluation	$\hat{c} \leftarrow z_k - \mathbf{h}_k^t \hat{\mathbf{x}}_{k/l} = 0$
	$c, \bar{c} \leftarrow [z_k - \mathbf{h}_k^t \hat{\mathbf{x}}_{k/l}]^2 - F(1, \infty)[\mathbf{h}_k^t P_{k/l}\mathbf{h}_k + R_k] = 0$
Control	Maximize $N(\%) = [(c - \underline{c})/c, (\bar{c} - c)/c] \times 100\%$
	$N_{\max} \geq N_{\text{crit}} \rightarrow$ calibrate
	$N_{\max} < N_{\text{crit}} \rightarrow$ assessment
Verification	$\chi^2(k-n) = \sum_{i=1}^{k} [z_i - \mathbf{h}_i^t \hat{\mathbf{x}}_{i/l}]^2 / [\mathbf{h}_i^t P_{i/l}\mathbf{h}_i + R_i]$
Selection	$F(k_1, k_2) = \chi_1^2(k_1)/k_1 \; k_2/\chi_2^2(k_2)$

descriptions of the various equations have been given [6—8]. Some additional features are incorporated in the calibration system. First, the verification and selection of the peak-preprocessing procedure, the calibration model and the numerical values of the noise covariances. For this purpose, the computed χ^2 values and F values based on the innovations (filtering) and residuals (smoothing) are compared with their critical limits; χ^2 statistics are employed as a two-sided test with a preset confidence level and given degrees of freedom. Modelling errors may cause excessive χ^2 values that may also result from the use of insufficient noise covariances. Alternatively, too low χ^2 values may be associated with the implementation of higher noise covariances as required. As a consequence, the imprecision of the evaluated results used in the quality-control procedure will also be exaggerated. Based on a preset confidence level, the F-test checks one-sided whether two independent χ^2 values each with its degrees of freedom, are statistically different or not. In addition, the autocorrelation function of the standardized innovations or residuals may be used for selection and verification.

Equations for the evaluation of the result and its confidence interval are given in state-space notation. The formulation follows from a Bayesian approach and holds generally for any calibration graph with or without incorporation of drift. The presented equations are iteratively solved by means of a bisection procedure. In order to compute the confidence interval, the bisection is initiated twice each time with the previously evaluated result as one of its starting values. In this way, one obtains the evaluated result and its lower and upper confidence limits. The confidence interval thus found is generally asymmetric around the evaluated result. If no solution exists, the bisection iterates to very bad values. For a given confidence level, the Fisher value $F(1, k - n)$ equals the square of the Student t statistic, $t^2(k - n)$. In the special case of a priori known noise covariances, the critical constant simplifies to $F(1, \infty)$, i.e., for a 95% confidence level the numerical value 3.84 (= 1.96^2) should be used. An alternative term frequently presented in elementary statistics textbooks is the critical constant $rF(r, k - n)$. The difference results from the request for a simultaneous confidence interval in a multidimensional space. The projection of the estimate by the regression function to a particular point produces a scalar, thus for inverse regression, a one-dimensional formulation is required [12, 13].

EXPERIMENTAL

In order to demonstrate the applicability of the calculations, an automated flow injection system was used for the determination of chloride in aqueous samples [14]. The well-established chemical reaction is based on the metathesis of thiocyanate in mercury(II) thiocyanate by chloride in the presence of iron(III); an iron thiocyanate complex is formed, which is measured spectrophotometrically at 470 nm [15]. The hardware of the automated analyzer (Fig. 1) consists of a computer-controlled injection valve and a sample changer

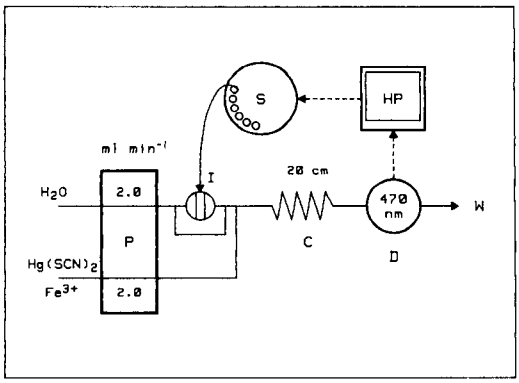

Fig. 1. The flow-injection system for the determination of chloride with mercury(II) thiocyanate and iron(III): P, peristaltic pump; S, sample changer; I, injection valve; W, waste; C, reaction coil; D, photometric device at 470 nm; HP, interfaced computer.

provided with a turntable (40 cups). The signal is sampled 600 times during 24 s with a photometric device (0—1 V with a resolution of 3 decimal digits). The time required for stepping the disk, moving the sampler arm and aspiration of the sample into the injection loop (100 μl) inclusive of data processing and plotting of the peak is about 16 s. This means that a total time of 40 s is required for each sample (i.e., 90 samples/hour can be processed). The height and area of the peaks with or without baseline correction are computed and used as the measurements in the estimation and evaluation procedure [16].

Some experiments were done in the following order (see Fig. 2): (1) standards of 2 and 10 mg l^{-1} were repeatedly injected 50 times (Fig. 2a); (2) standards of 2, 4, 6, 8 and 10 mg l^{-1} were injected 20 times (Fig. 2b); (3) standards (10, 8, 6, 4, 2 mg l^{-1}) and unknown samples (6 mg l^{-1}) placed at fixed positions in the time sequence (Fig. 2c); (4) standards (10, 8, 6, 4, 2 mg l^{-1}) and unknown samples of varying concentration (4—8 mg l^{-1}) were processed by the on-line system (Fig. 2d). For case 4, the five calibration standards were placed twice on the turntable disk, at positions 1—5 and positions 21—25 with 30 unknown samples in between. In order to facilitate the on-line operation of the calibration system, some modifications to the experimental setup were made. Measuring the peak signal (24 s), aspiration of the sample (16 s) and data processing (8 s) must be done separately. Because of the manipulation of the turntable disk of the sample changer, timing of the system has to be scheduled at equal intervals. Therefore, a time unit of 1 min was used. When no peak was found within the time scheduled, the disk was moved more than four steps ahead and then waited for next time unit. Additionally, the calibration standards were placed from high to low values with respect to the direction of the turntable disk to minimize the total analysis time. In this way, a sample frequency of about 50—60 h^{-1} was obtained for case 4.

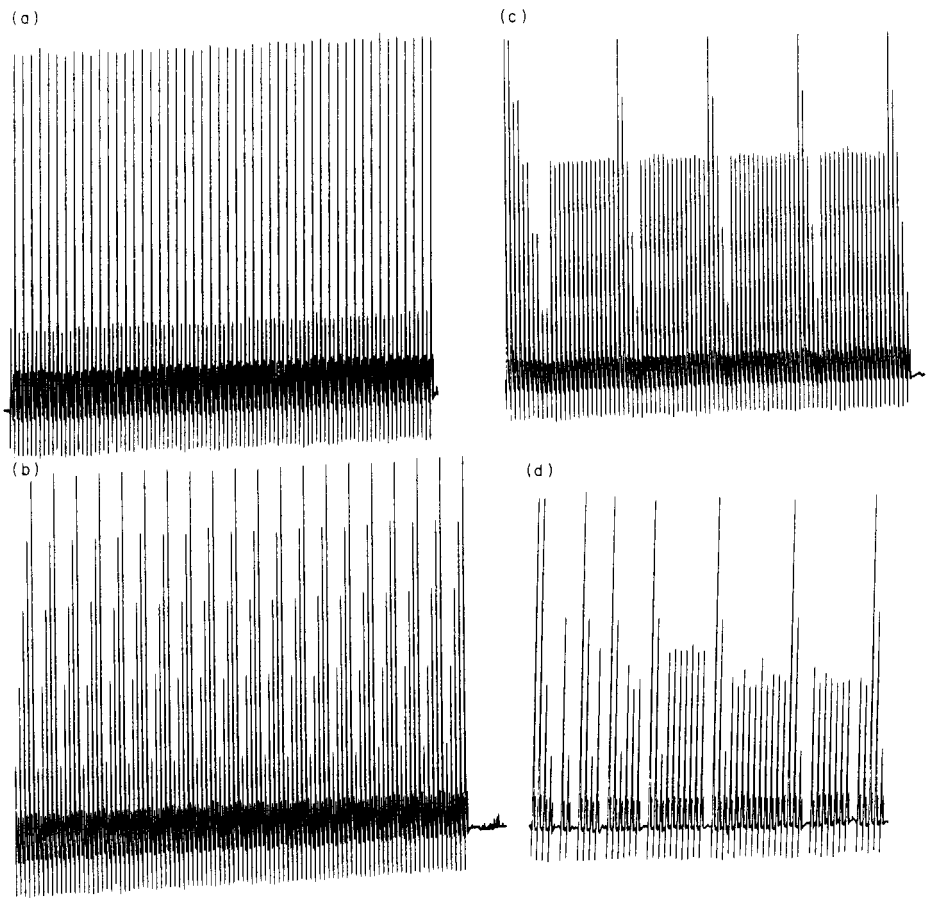

Fig. 2. Flow-injection peaks for chloride: (a) repeated standards of 2 and 10 mg l^{-1}; (b) repeated standards of 2, 4, 6, 8 and 10 mg l^{-1}; (c) standards and repeated unknown samples (each 6 mg l^{-1}) at fixed positions in the sequence; (d) chloride standards and unknown samples (variable concentration) by the on-line system. Sample throughput: (a—c) 90 h^{-1}; (d) 60 h^{-1}.

RESULTS

In the first experiment, 2 and 10 mg l^{-1} chloride standards were injected repeatedly, to establish the numerical values of the noise covariances and to avoid modelling errors from a non-linear calibration graph. Figure 2(a) shows that a high measurement noise is present and that the drift pertains mainly to the baseline. The height and area of the measured peaks were computed with and without baseline correction. A drifting first-order calibration graph was used for state estimation with the Kalman filter and fixed interval smoother. The χ^2 values in Table 2 were obtained with numerical values for the measurement noise variance of $R = 15 \times 10^{-6}$ and for the system noise covariances

TABLE 2

χ^2 values for the flow-injection peaks of Fig. 2(a, b) used by the Kalman filter (KF) and by the fixed-interval smoother (SM) with the peak height (H), baseline-corrected peak height (HB), the peak integral (I) and the corrected peak integral (IB) as measurements[a]

		H	HB	I/300	IB/300
Fig. 2(a)	KF	99.3/105.3	122.5/165.7	107.6/97.7	650.1/727.2
1st order	SM	91.6/95.9	114.2/153.2	97.6/81.1	608.3/663.4
Fig. 2(b)	KF	618.8[b]/705.3	662.7/918.1	134.9/145.3	797.2/1321.6
1st order	SM	578.7/661.1	620.1/857.7	122.0/134.4	744.2/1225.9
Fig. 2(b)	KF	69.8[b]/86.4	67.5/133.6	61.0/85.4	395.4/638.9
2nd order	SM	62.0/75.2	59.3/112.7	53.8/74.1	354.4/537.8

F values, drifting first/second-order calibration graph	1.70—10.46
F values, baseline-corrected/uncorrected peak heights	0.95—1.60
F values, baseline-corrected/uncorrected peak areas	5.90—9.12
F values, Kalman filter/fixed-interval smoother	1.07—1.20

[a]First-order calibration graph: $R = 15 \times 10^{-6}$, $Q_{33} = Q_{44} = 10^{-10}$, $\chi^2(96)_{0.025} = 70.8$, $\chi^2(96)_{0.975} = 125.0$, $F(96, 96)_{0.95} = 1.40$. Second-order calibration graph: $R = 15 \times 10^{-6}$, $Q_{44} = Q_{55} = Q_{66} = 10^{-10}$, $\chi^2(94)_{0.025} = 69.1$, $\chi^2(94)_{0.975} = 122.7$, $F(94, 94)_{0.45} = 1.41$.
[b]Autocorrelation function shown in Fig. 3.

of $Q_{33} = Q_{44} = 10^{-10}$. They offer a good description of the measurements performance. However, the baseline-corrected areas do not agree well. Extension of the experimental design to repeated injections of 2, 4, 6, 8 and 10 mg l^{-1} showed errors for every kind of peak processing when a drifting first-order calibration graph (4-parameter state, $\times 1$—$\times 4$) was used. Extension of the model to a drifting second-order calibration graph (6-parameter state, $\times 1$—$\times 6$) produced a significant decrease of the χ^2 values as indicated by the range of the F values found. Here, the noise covariances $Q_{44} = Q_{55} = Q_{66} = 10^{-10}$ and $R = 15 \times 10^{-6}$ were used. Examples of autocorrelation functions of the standardized innovations in Fig. 3 demonstrate the effect of better modelling of the behaviour of the systems. For the standardized residuals of the smoother, the autocorrelation behaviour is identical. Similar results are found for the other peak characteristics. Another conclusion from Table 2 is that the baseline-correction procedure should be omitted as a data pre-processing procedure. The corrected peak areas always deviate significantly, while the corrected peak heights sometimes produce bad χ^2 values. When the baseline correction is omitted, there is no significant difference between the use of peak heights and peak areas. For further experimentation the uncorrected peak heights were used. Fixed-interval smoothing yields no significant improvements in the estimation. Care has to be taken in withdrawing the smoothing procedure, however, because it can affect the evaluated results of the unknowns (see below). Although the final χ^2 values are somewhat low with respect to their critical values, the same noise covariances were used for the next experiment.

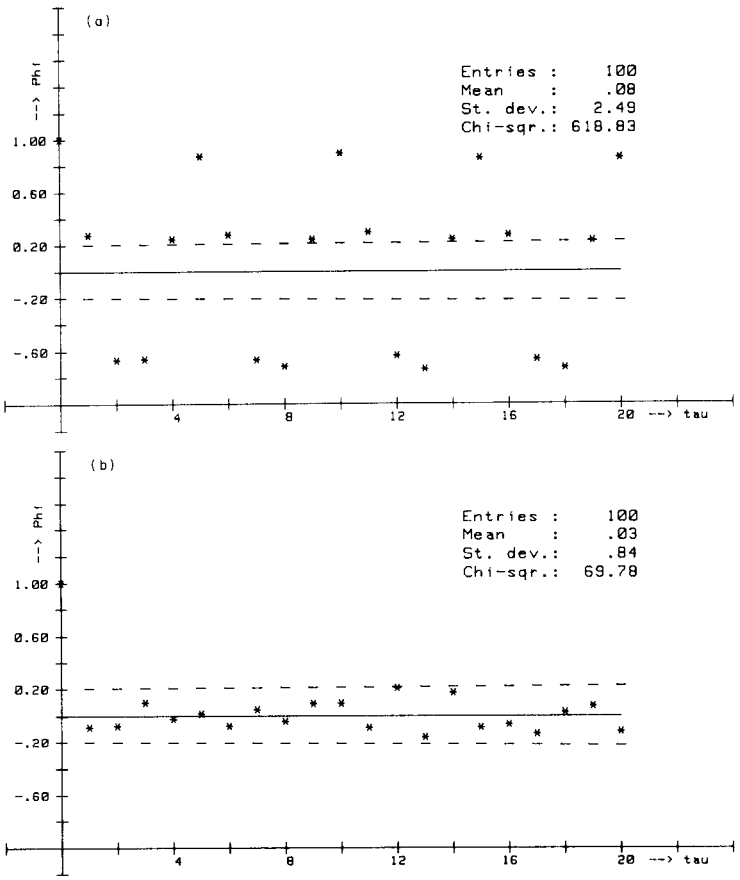

Fig. 3. Results for the uncorrected peak heights of Fig. 2(b). Autocorrelation function of the standardized innovations by the Kalman filter: (a) with a drifting first-order calibration graph; (b) with a drifting second-order calibration graph.

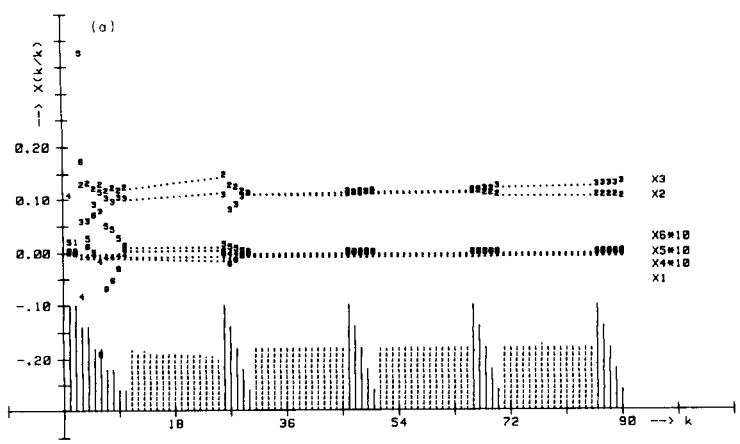

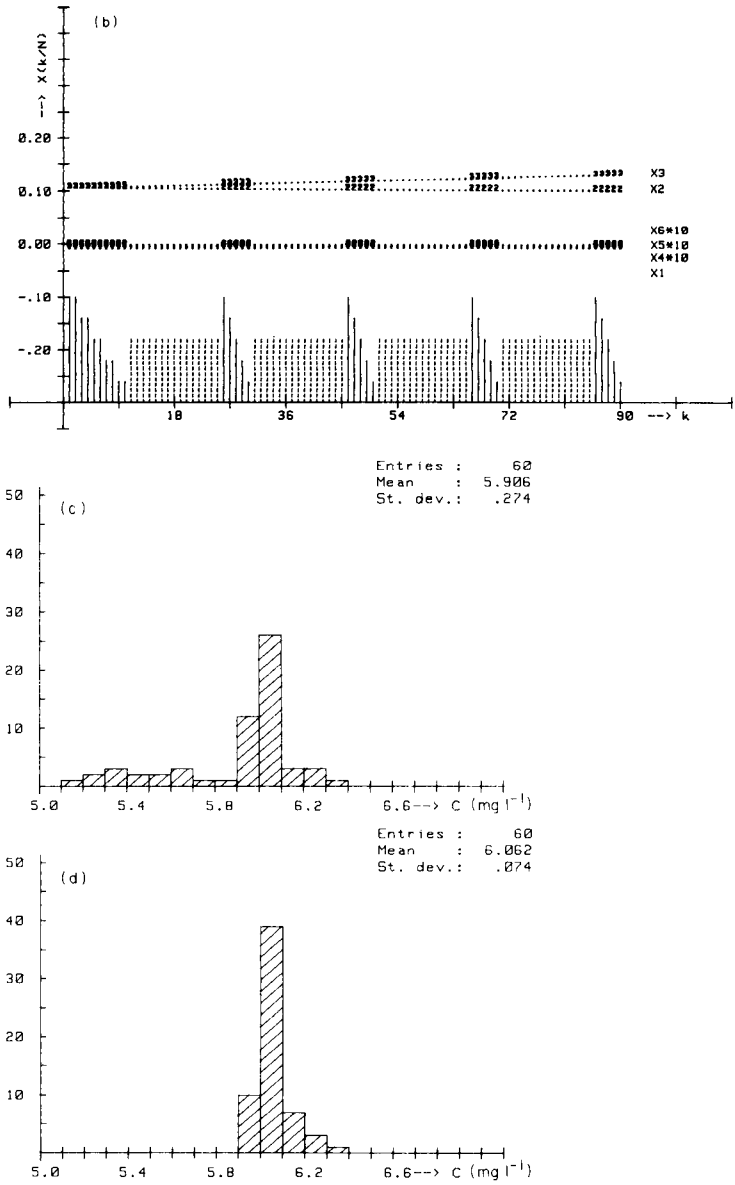

Fig. 4. Results for the uncorrected peak heights of Fig. 2(c). A drifting second-order calibration graph is used with the system noise covariances $Q_{44} = Q_{55} = Q_{66} = 10^{-10}$ and the measurement noise variance $R = 15 \times 10^{-6}$. (a) The state and concentrations used by the Kalman filter: (—) points 1—6 used for calibration; (---) evaluation with unmarked data points. (b) The state and concentrations used by the smoother; symbols as for (a). (c) The evaluated results obtained by the Kalman filter. (d) The evaluated results obtained by the smoother.

TABLE 3

Results for the flow-injection system based on the uncorrected peak heights of Fig. 2(c, d) with the Kalman filter (KF) and smoother (SM)[a]

		χ^2	Mean (mg l^{-1})	Variance
Fig. 2(c)	KF	12.6	5.906	0.0750
	SM	8.1	6.062	0.0054
	F value	1.56	—	13.89[b]
Fig. 2(d)	KF	5.0	—	—
	SM	4.0	—	—
	F value	1.25	—	—

[a]Second-order calibration graph: $R = 15 \times 10^{-6}$, $Q_{44} = Q_{55} = Q_{66} = 10^{-10}$, $\chi^2(24)_{0.025} = 12.4$, $\chi^2(24)_{0.975} = 39.4$, $F(24, 24)_{0.95} = 1.98$; $\chi^2(18)_{0.025} = 8.2$, $\chi^2(18)_{0.975} = 31.5$, $F(18, 18)_{0.95} = 2.22$.
[b]Here, $F(k1, k2) = s^2_{KF}/s^2_{SM}$ and $F(59, 59)_{0.95} = 1.54$.

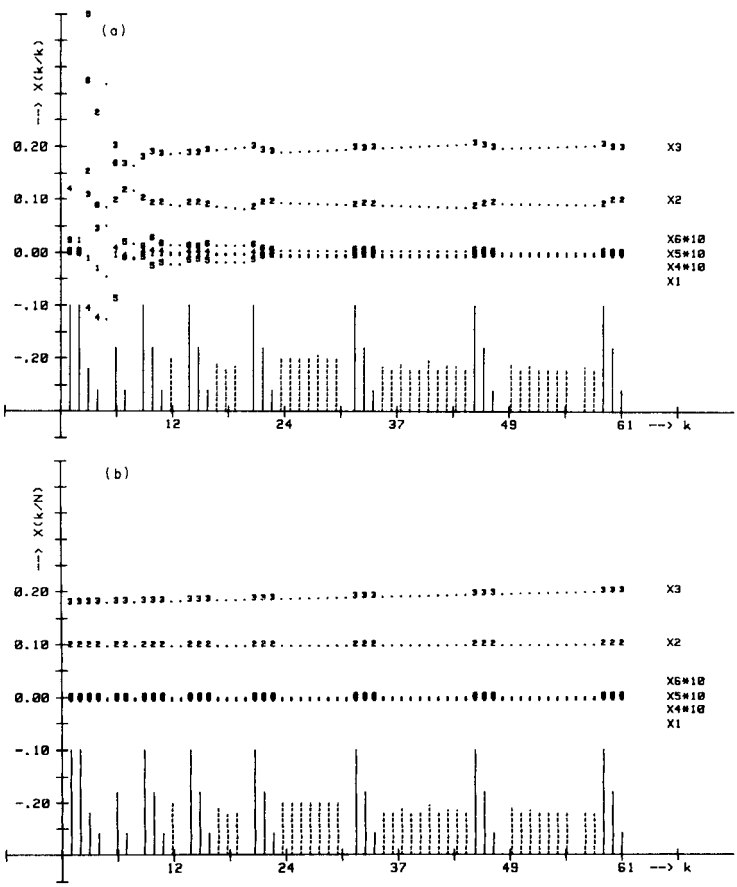

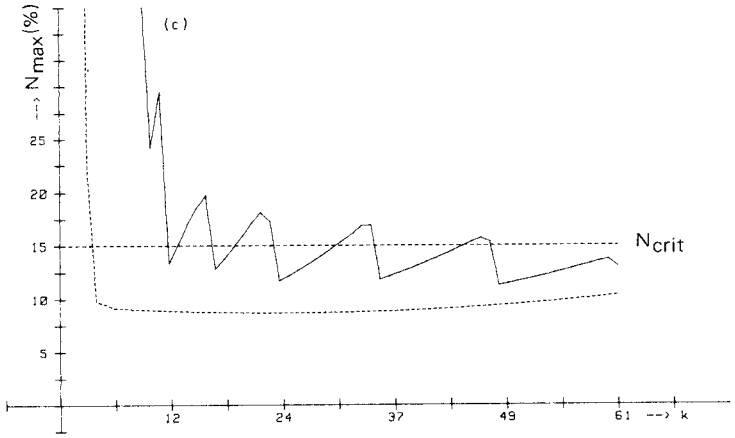
(c)
--> Nmax(%)
25
20
15
10
5
Ncrit
12
24
37
49
61 --> k

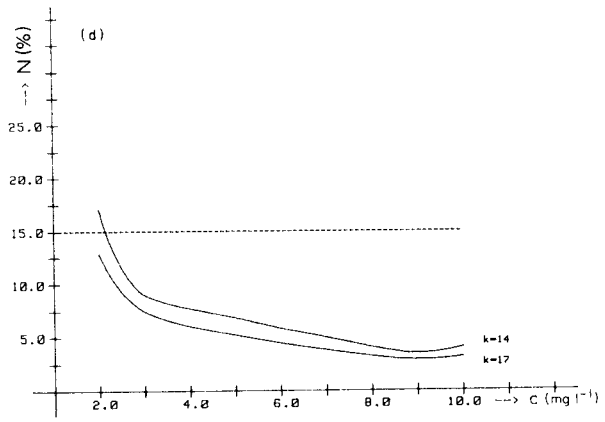
(d)
--> N(%)
25.0
20.0
15.0
10.0
5.0
k=14
k=17
2.0
4.0
6.0
8.0
10.0 --> C (mg l-1)

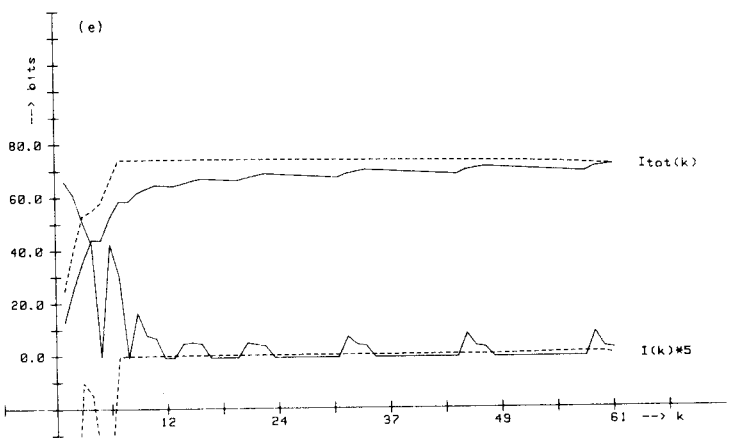
(e)
--> bits
80.0
60.0
40.0
20.0
0.0
Itot(k)
I(k)*5
12
24
37
49
61 --> k

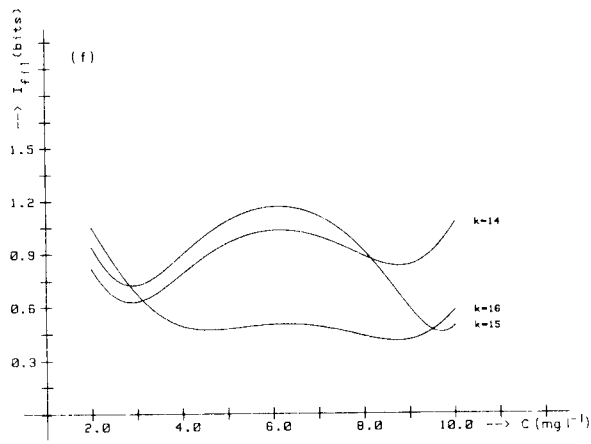

Fig. 5. Results for the on-line calibration system with use of the uncorrected peak heights (Fig. 2d), a drifting second-order calibration graph with the noise covariances $Q_{44} = Q_{55} = Q_{66} = 10^{-10}$ and $R = 15 \times 10^{-6}$, a critical imprecision $N_{crit} = 15\%$, and calibration standards of 10, 8, 6, 4 and 2 mg l^{-1}. (a) The state and concentrations employed by the Kalman filter: (—) points 1—6 used for calibration; (---) evaluation with unmarked data points. (b) The state and concentrations employed by the smoother; symbols as for (a). (c) The resulting maximal imprecision N_{max} in the sequence: (—) Kalman filter; (---) smoother. (d) The imprecision $N(\%)$ for varying concentration for $k = 14$ (upper curve) and $k = 17$ (lower curve). (d) The resulting information yield I and I_{tot} in the sequence: (—) Kalman filter; (---) smoother. (f) The information, I_{fil}, for varying concentrations at $k = 14$, $k = 16$ and $k = 15$ (top to bottom at right-hand side).

Figure 2(c) shows the output for a normal flow-injection system, in which calibration standards and a series of identical unknowns are placed at fixed positions in the sequence. The uncorrected peak heights and concentration values of the calibrations were used for estimation. The state of the drifting second-order calibration graph estimated on-line by the Kalman filter is depicted in Fig. 4(a). Hereafter, the on-line estimates were improved by the fixed-interval smoother; Fig. 4(b) clearly demonstrates the effect of smoothing on the estimation performance. The results evaluated for the identical samples (6 mg l^{-1} chloride) processed by the Kalman filter and smoother are shown as histograms in Fig. 4(c, d). Table 3 shows that a significant F value (s^2_{KF}/s^2_{SM}) of 13.89 is found, i.e., a variance reduction $VR = (1 - 1/F) \times 100\%$ of 93% is found for the evaluated results, although the χ^2 value is not significantly decreased by smoothing. When the Kalman filter does not operate quite accurately, the smoother will reduce its adverse effects on the evaluated results. Therefore, smoothing is recommended as a powerful tool in the calibration system.

Implementation of the entire calibration system with use of prediction, filtering, evaluation, control, optimization and smoothing is now described. For on-line operation of the system, the uncorrected peak heights, a drifting second-order calibration graph with numerical values of $Q_{44} = Q_{55} = Q_{66} =$

10^{-10}, $R = 15 \times 10^{-6}$ for the noise covariances, a critical imprecision N_{crit} = 15%, and five calibration standards 10, 8, 6, 4, 2 mg l^{-1} are processed. If the preset criterion, N_{crit}, is exceeded by the maximal imprecision, N_{max}, calibration of the flow-injection system is initiated. Hereafter follows the decision on which of the calibration standards available gives the optimal performance for estimation. The system has the freedom to control its behaviour completely, except at the end of a run when it is forced to recalibrate. In the given example (Fig. 2d), 30 unknown samples on the turntable disk have to be analyzed. The concentrations of the standards, the measurements and the evaluated results of the unknowns are marked in the computer by their position on the turntable disk. After about 9—12 calibrations, the system starts to process the unknowns and recalibrates regularly. A total of 24 calibration standards and 7 waiting times are required to finish the run. The estimated state is shown in the time sequence for the Kalman filter in Fig. 5(a) and for the smoother in Fig. 5(b). The conclusions are similar to the previous conclusions, but here variable unknowns are used in the range 4—8 mg l^{-1} chloride. Figure 5(c) shows the maximal imprecision, N_{max}, controlled on-line by the Kalman-filter, to be less than 15%. It is improved by the smoother to about 10%. The entire imprecision function for the concentration is shown in Fig. 5(d) at $k = 14$ when the preset criterion is exceeded and at $k = 17$ when it is not exceeded. The information yield, I and I_{tot}, gained by the system is shown in Fig. 5(e, f). Each time the system calibrates, a positive information yield is found. The quality-control procedure forces the total information of the system to remain above a fixed level and it is improved moderately by the smoother. For some indices k, the entire information function such as used by the optimization procedure is depicted in Fig. 5(f). From a theoretical point of view, the extremes and the centre are the best positions in a second-order calibration graph. In the time sequence, the combinations 10, 6 and 2 mg l^{-1} are always used in the given order for calibration purposes.

For the given example in flow injection analysis, the numerical values of the noise covariances were $Q_{44} = Q_{55} = Q_{66} = 10^{-10}$ and $R = 15 \times 10^{-6}$. The system noise has only a minor effect on the quality performance of the system. This is partly explained by slowly varying effects such as changes in the flow pressure, room temperature, reagent concentration, aging of the optical fibers, etc. The high measurement noise present can be accounted for by various random effects such as the reproducibility of the sample cups, the injection of the sample, transport of the aliquot, detector noise etc. The first effect, i.e., the sample cups, has the main effect on the quality performance. Current experimentation shows that better reproducible treatment of the sample cups decreases the measurement noise variance R significantly to about 5×10^{-6}.

Conclusions

The application of state estimation in flow injection analysis has been investigated. Some results for the determination of chloride in aqueous samples are given as an example. In practice, the peak pre-processing proce-

dure, the calibration model and the numerical values of the noise covariances to be implemented are of importance. They are selected and verified by means of the χ^2 and F values based on the innovations and residuals and compared with their critical limits. The model is shown to be a second-order calibration graph with drift on each parameter. A baseline correction procedure used for the peak-shaped signals produces significant deviations. Inaccurate results obtained by the Kalman filter can be reduced adequately by the smoother.

The experimental results demonstrate the applicability of the entire calibration system in practice. The noise covariances are found by off-line matching of the χ^2 values obtained. Alternatively, adaptation of the covariances of system noise and measurement noise can be done on-line by the calibration system. This complex topic will be treated separately.

This work was supported by The Netherlands Research Organisation Z.W.O.

REFERENCES

1 J. Růžička and E. H. Hansen, Flow Injection Analysis, Wiley, New York, 1981.
2 D. Betteridge, Anal. Chem., 50 (1978) 832A.
3 J. Růžička and E. H. Hansen, Anal. Chim. Acta, 114 (1980) 3.
4 C. B. Ranger, Anal. Chem., 53 (1981) 21A.
5 B. Rocks and C. Riley, Clin. Chem., 28 (1982) 409.
6 P. C. Thijssen, S. M. Wolfrum, G. Kateman and H. C. Smit, Anal. Chim. Acta, 156 (1984) 87.
7 P. C. Thijssen, Anal. Chim. Acta, 162 (1984) 253.
8 P. C. Thijssen, G. Kateman and H. C. Smit, Anal. Chim. Acta, 173 (1985) 265.
9 D. G. Mitchell, W. N. Mills, J. S. Garden and M. Zoleb, Anal. Chem., 49 (1977) 1655.
10 J. S. Garden, D. G. Mitchell and W. N. Mills, Anal. Chem., 52 (1980) 2310.
11 S. N. Deming and S. L. Morgan, Clin. Chem., 25 (1979) 840.
12 R. G. Miller, Simultaneous Statistical Interference, McGraw-Hill, New York, 1966.
13 S. Zacks, Parametric Statistical Interference, Pergamon Press, Oxford, 1981.
14 L. T. M. Prop, P. C. Thijssen and L. G. G. van Dongen, Talanta, 32 (1985) 230.
15 E. H. Hansen and J. Růžička, J. Chem. Educ., 56 (1979) 677.
16 W. G. Boyle and D. P. Ryan, Computer programs in BASIC language for graphite-furnace atomic absorption using the methods of additions, Microinfo, Alton, Hants, England, 1979.

Analytica Chimica Acta, 174 (1985) 41—51
Elsevier Science Publishers B.V., Amsterdam — Printed in The Netherlands

SIMULTANEOUS DETERMINATION OF FIVE DIFFERENT FOOD PROTEINS BY HIGH-PERFORMANCE LIQUID CHROMATOGRAPHY AND PARTIAL LEAST-SQUARES MULTIVARIATE CALIBRATION

WALTER LINDBERG* and JERKER ÖHMAN

Department of Analytical Chemistry, Institute of Chemistry, University of Umeå, S-90 187 Umeå (Sweden)

SVANTE WOLD

Research Group for Chemometrics, University of Umeå, S-90 187 Umeå (Sweden)

HARALD MARTENS

Norwegian Food Research Institute, P.O. Box 50, N-1432 Ås-NLH (Norway)

(Received 10th December 1984)

SUMMARY

A method is described for the simultaneous determination of food proteins originating from different raw food materials. The proteins are hydrolysed to amino acids which are labelled with dansyl chloride and finally separated by reversed-phase high-performance liquid chromatography. Partial least-squares multivariate calibration is used to resolve and quantify the overlapping amino-acid patterns. The method enables muscle protein, collagen, soy protein (both texturate and isolate), casein and milk protein to be quantified in both heated and raw samples from the same calibration set. The accuracies for the raw and heated samples averaged 3% and 6% relative total protein content, respectively.

The accurate and rapid determination of muscle protein and protein extenders in foods is of importance for quality control because both the price and the nutritional quality are ruled by the food composition. Numerous methods exist for each protein source. However, to improve accuracy and master possible interferences, there is a need for further development.

In the determination of food proteins, the first problem is to find conditions of measurement which give the best possible representation of the chemical composition. This representation should ideally give a unique data pattern for each protein source. In the ideal case, each pattern should also show small within-source variations and be insensitive to varying manufacturing conditions. If the pattern of a given source (e.g., soy protein) does vary between batches (e.g., different soy varieties) or with manufacturing conditions (different ways of preparing the protein: extraction, texturation, etc.), then the data analysis must be modified. This requires that the within-source variations must be at least systematic so that they can be modelled mathematically. These systematic variations must also be such that the patterns of the different types of protein sources can be distinguished.

0003-2670/85/$03.30

Among the extenders, soy protein and collagen are the commonest. Collagen is usually determined from the content of hydroxyproline, an amino acid unique to this protein. For soy protein, electrophoresis [1] and enzyme-linked immunoassays [2] seem to be the most promising techniques. The electrophoretic method is unable to detect insoluble proteins such as textured soy protein. Quantification of more or less overlapping electrophoretic bands is another problem with the method. The immunoassay may be more promising. Meat protein is usually determined from its protein-bound 3-methylhistidine content; this amino acid provides fair selectivity for muscle protein even though it occurs in rather low concentration. For quantification, chromatographic separations are used [3]. This may be a good method when only muscle protein content is of interest. None of these methods allows accurate determination of many different protein sources at the same time.

In a recent paper, the possibility of determining several types of protein in a sample was outlined; high-performance liquid chromatography (h.p.l.c.) was used in combination with partial least-squares regression [4]. This approach was intended to take advantage of the multivariate character of a chromatogram and to use the information from all the peaks (amino acids). In earlier work of this type [5, 6], a conventional ion-exchange amino-acid analyzer was used in combination with multiple regression. Although the sample preparation remains time-consuming (protein hydrolysis, amino acid derivatization), chromatographic measurements are faster than in the previous methods. Partial least-squares methods are also better suited for calibration problems than multiple regression.

The choice of amino acids as indicators is advantageous in that they are the smallest protein units and so least prone to undergo changes on processing. Another advantage is that it should be comparatively easy to get good recoveries in sample work-up. The number of major amino acids is limited to about 17 and standard substances are also available, which has obvious advantages. Difficulties arise from the fact that all proteins contain all the 17 major amino acids, although in varying amounts. None of the major amino acids is particular to any of the protein sources. Among the minor amino acids, only hydroxyproline in collagen and *N*-methylhistidine in muscle protein are available at present as selective indicators. This means that multivariate data analysis must be used to resolve the mutually overlapping amino-acid patterns by combining the amino acids mathematically.

This paper is concerned with the feasibility of using the partial least-squares (PLS) method to determine simultaneously different proteins often found in processed food samples from their chromatographic amino-acid pattern. Samples of ground beef were prepared according to standard procedures and mixed with different amounts of common meat extenders such as collagen, different qualities of soy, casein and dried milk. These samples were then divided into two parts, where one half was heated while the other half was untreated. The samples were then hydrolysed, derivatized with dansyl chloride and analysed by reversed-phase high-performance liquid chromatography

(h.p.l.c.). Test samples were also prepared and analysed under similar conditions in order to investigate the potential of the method. These collected data were then processed with respect to possible differences between heated and raw samples, and calibration models were calculated in order to investigate the accuracy of the prediction for the samples in the test set.

MULTIVARIATE MODELLING

The concepts of partial least-squares regression and calibration has been thoroughly described elsewhere [7—9]; therefore, this discussion is limited to its application for proteins in foods. Multivariate approaches to determinations of proteins in mixtures from amino acids have traditionally been based on the so-called direct curve resolution of the chromatographic amino-acid pattern of a food product [5, 6]. In this data analysis, the amino-acid pattern of the product is described as a combination of the patterns of the different protein sources in their pure form, plus some measurement noise in the amino-acid data of the product:

product pattern = conc. (1) × pattern of source (1) + conc. (2) × pattern of source (2) + . . . measurement errors (I)

Based on data for amino-acid patterns from each of the protein sources (1, 2 . . .) analyzed separately, one calculates the combination of protein source concentrations, conc. (1), conc. (2),. . . , that most resembles the pattern of the unknown food product, i.e., the apparent measurement errors of all the 17 amino acids are minimized in the least-squares sense (multiple linear regression, MLR). Otto and Wegscheider [10] recently compared MLR and PLS and found that PLS in some cases gave 25 times lower prediction errors than MLR. The superiority of PLS was particularly pronounced for substances where the spectrum suffered overlap over the whole spectral range. In the present data set, a comparison for soy protein showed on average 10% lower prediction errors with PLS than with MLR.

The earlier way of modelling protein mixtures [5, 6] is associated with some significant shortcomings. Direct curve resolution requires that all the major constituents (protein sources) are included in the model, and that the pattern of each source is invariant and precisely known. If these requirements are not met, then the lack-of-fit residuals termed "measurement errors" in the above expression for the product pattern also include other types of errors (model errors), and the resulting constituent concentrations will be systematically wrong.

In this paper, a newer regression technique, partial least-squares (PLS) regression, is used in order to alleviate some of the problems involved in the direct curve resolution. The PLS technique is based on indirect calibration: amino-acid data from a set of products with known concentrations of the most interesting protein sources are used to build a statistical model of the amino-acid variations in that type of product. Once calibrated, the model

estimates the concentrations of these protein sources in unknown products from their amino-acid pattern.

The following paragraphs list some problems in direct curve resolution that the PLS regression reduces or eliminates.

Unidentified protein sources in the calibration set. If a protein source is present in significant amounts in a calibration set, without being calibrated for in the direct curve resolution model, then the contributions of this source to the product pattern may seriously degrade the model. For instance, if soy protein is present but not included in the calibration model, then soy protein will be interpreted as muscle protein, because soy and muscle protein resemble each other in amino-acid pattern.

In PLS calibration, it is not necessary explicitly to calibrate for all proteins in a calibration set. The only necessity is that proteins which may be present in future samples are also represented in the calibration set. In PLS regression, each protein source will give rise to a mathematical "factor", and the number of factors then corresponds to the number of distinguishable protein sources present in the calibration set. If not modelled explicitly, the effect of such unidentified proteins can still be eliminated in PLS regression, provided that these unidentified proteins vary from sample to sample in the set of calibration products. Neither their amino-acid patterns nor their concentrations need be known in these calibration products; it is enough that they vary in concentration. The PLS program will then report just that it has found an extra type of systematic variation in the amino-acid data of the calibration samples, and will remember this extra factor for the modelling of future unknown food products. Thus PLS regression can compensate for unidentified systematic errors.

The amino-acid pattern of a protein source is not constant. In addition to being represented in the calibration set, the direct curve resolution also requires that the amino-acid pattern of every protein source in the model is precisely known. This means that none of the protein sources can have a variable amino-acid composition. For instance, soy protein cannot be allowed to vary with the degree of extraction or processing. If soy isolate has an amino-acid pattern slightly different from soy flour, owing to selective extraction of only water-soluble proteins, then the direct curve resolution may mistakenly regard the two types of soy protein differently and give erroneous concentration results. Again, in PLS regression most such variabilities can be compensated for automatically, provided that the different qualities of each protein source are represented in the food products used for calibration. The PLS method just finds and remembers an extra factor of amino-acid variability.

Interaction and nonlinearity. The amino-acid data of the food products always contain some measurement uncertainty, and this is allowed for in the conventional model for curve resolution (model I). Problems occur, however, if the amino-acid data of pure protein constituents do not properly represent the contributions of these protein sources to data in a real food product. This

may be so because the food ingredients interact during protein hydrolysis, chromatographic separation or peak integration. Such model errors lead to systematic errors in the determination of protein source concentrations if direct curve resolution is used. Indirect calibration methods based on amino-acid data from real food products with known protein concentrations avoid this model problem, because each protein is modelled in its natural environment, i.e., where future samples are to be analyzed.

EXPERIMENTAL

Apparatus and chemicals

The liquid chromatographic system consisted of two Constametric-III pumps and a Spectromonitor-III ultraviolet detector (LDC) operated at 250 nm. For eluent mixing, a home-made gradient mixer consisting of a Swagelok tee (0.0625 in.) and a 10-cm stainless steel capillary tube (0.0625/0.03 in.) filled with glass beads of 0.5-mm diameter. The column (150 mm long, 4 mm i.d.) was packed with Hypersil C18 (Shandon). For data evaluation, an 128K IBM-PC microcomputer was used with the SIMCA-3B program package. (The package is available from Sepanova AB, Östrandsvägen 14, S-12243 Enskede, or Principal Data Components, 2505 Shepard Blvd., Columbia, Missouri 65201).

Acetonitrile (HPLC grade; Rathburns) and dansyl amino acids (Sigma) were used.

Procedure

The chromatographic conditions were as follows: pump A was used for acetonitrile/water (15:85, v/v) with 0.03 M phosphate buffer at pH 7.5; pump B was used for acetonitrile/water (35:65). The gradient was changed linearly over a period of 25 min with a final delay of 4 min before returning to the initial conditions.

For calibration, a batch of ground meat was prepared. Different meat extenders were added to samples taken from this batch. The calibration set was generated so as to contain the commonest meat extenders at appropriate concentration intervals (Table 1). Each sample was then divided into two and one part was heat-treated. Two sets with identical composition but different pretreatment were thus obtained. A test set with samples of a similar range in composition was prepared simultaneously and treated in the same way.

Both the calibration and the test set were hydrolysed with 6 M hydrochloric acid for 22 h at 383 K at a concentration of 2 mg of protein per ml of acid. The samples were subsequently filtered and evaporated under a nitrogen atmosphere. Finally the residues were diluted to appropriate concentrations with 0.04 M lithium carbonate buffer (adjusted to pH 9.5 with hydrochloric acid). The hydrolysates were labeled by using dansyl chloride dissolved in acetonitrile (6.1 mg ml^{-1}) with an acetonitrile/water ratio of 1:3. The samples were allowed to stand overnight or until the yellow colour had

TABLE 1

Relative protein composition of calibration samples (%, w/w)

Sample	Muscle	Collagen	Soya	Casein	Whey
1	96.3	3.7	0	0	0
2	85.5	3.3	11.2	0	0
3	69.3	2.7	28.0	0	0
4	76.6	3.0	0	20.4	0
5	85.5	14.5	0	0	0
6	76.6	23.4	0	0	0
7	80.5	3.2	0	13.2	3.1
8	68.4	2.6	0	23.5	5.5
9	97.3	2.1	0	0	0
10	65.6	2.6	18.2	11.0	2.6

disappeared. The solution was diluted so that the acetonitrile concentration would not exceed the initial acetonitrile concentration in the eluent in order to obtain good performance for the early eluting peaks.

RESULTS AND DISCUSSION

The separation of the amino acids is seen in Fig. 1. They were each assigned by comparison with retention times of standard dansyl amino acids. In the hydrolysis, tryptophan is destroyed, cysteine is oxidized to cysteic acid, and asparagine and glutamine react with water and thereby appear as acids. Lysine,

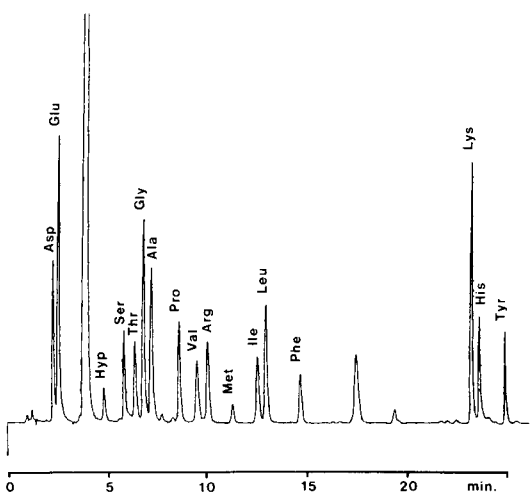

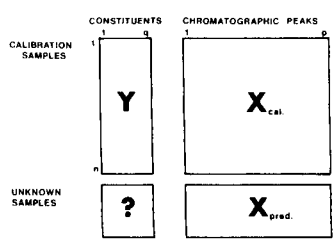

Fig. 1. Separation of dansyl amino acids. For chromatographic conditions, see Experimental.

Fig. 2. Organization of data in multivariate calibration.

histidine and tyrosine are di-dansylated which is reflected in their longer retention times.

The dansylation reaction was chosen primarily because it is possible also to detect the secondary amino acids, which is particularly useful in the determination of collagen. Other reasons were the stability of the derivative, which allows time flexibility if many samples are to be processed, and the simple derivatization procedure. No attempts were made to identify the other minor peaks because they contributed little to the PLS model. Consequently, these peaks were excluded and the calibration was made only with the identified peaks.

For the data analysis, the areas of all identified peaks except tyrosine were used as X-variables. Tyrosine was omitted because its retention time fluctuated and so its area was uncertain. The corresponding food protein concentrations were used as Y-variables. Thus, for n samples two matrices are formed, and their interrelationship is to be calculated (Fig. 2). The model can then be used to analyze samples of unknown composition from their amino-acid pattern. Because the relative proportion of the food proteins was the relevant quantity, each chromatogram was normalized to 100. Normalization was also advantageous because dilution errors would not affect the data.

Initially, the principal components of the X-matrix were calculated, in order to get an overview of the data structure. Separate models with 3 principal components were calculated for both raw and heated samples and the distances of every sample from each class model were plotted against each other (Fig. 3) [11, 12]. Two partially overlapping groups, which coincided

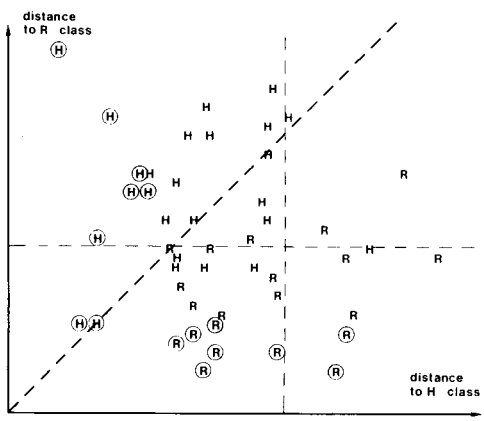

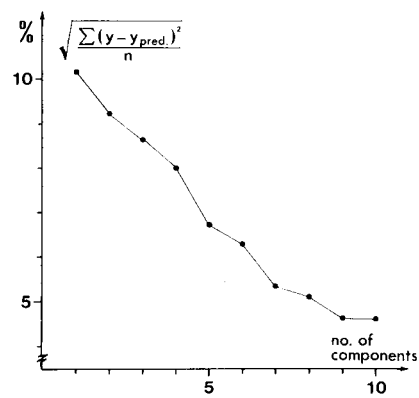

Fig. 3. Class distance plots for raw and heated samples. The dashed horizontal and vertical lines indicate 95% confidence limits and the line at 45° indicates equal class distance. The circled samples were used for calculation of each class model and all samples were then classified to both models.

Fig. 4. Residual standard deviation for different numbers of components from the test set of the joint calibration (Table 2).

with the raw and heated samples, respectively, was observed. From the confidence limits, however, it is seen that various samples lie within the limits of both classes, which indicates only minor differences between raw and heat-treated samples. Therefore, it remained uncertain whether the class separation originated from the heating or only reflected a temporal variation in the hydrolysis. This effect was also too small to be visually recognized in the chromatograms.

In order to investigate the implications of this finding, PLS calibrations were done both on each class separately and on the joint calibration set (Table 2). In the case for which the classes were treated separately, the calibration sets consisted of the samples shown in Table 1 plus two replicates, altogether 12 samples. The calibration model obtained was then used for prediction of the independent samples of the test set. The optimum number of PLS components was evaluated by calculating the residual standard deviation of the test samples after incorporating each calibrating factor and selecting the number which gave the smallest residual. This is exemplified in Fig. 4. For the separate calibrations on raw and heated samples, the optimum number was 6; when the raw and heated samples were considered as one class, the optimum number was 9. This indicates non-linearity and/or interaction between the protein constituents, because the number of components is higher than the number of constituents.

In the case of separate class calibration (Table 2), the concentrations of collagen and casein are adequately predicted and thus it is clearly seen whether or not those proteins have been added. Muscle and soy are predicted with a lower accuracy and in some samples are not easily distinguished, which is seen as a positive prediction error for muscle followed by a negative error for soya and vice versa. This is caused by the close similarity in amino-acid composition. For casein and collagen, however, the compositions differ, which simplifies the identification and quantification of these constituents. Thus it is confirmed that the uniqueness of the amino-acid pattern strongly affects the possibility of achieving accurate predictions. The results given for raw and heated samples in Table 2A and B, however, suffer somewhat from the rather small calibration set, which affects the precision of the estimated parameters in the calibration model.

In the calibration where the heated and raw ground-beef samples were considered as one class, the calibration set consisted of 41 samples (Table 2C, D). The increased number of calibration samples is beneficial because the precision of the estimated parameters will increase, provided that the two classes have the same general tendencies. This set also consisted of the samples listed in Table 1 plus replicates. In the joint calibration, the features previously found can still be detected but the errors are generally smaller. Even the presence of whey can be indicated although the problem and so the experimental design was not formulated primarily for that purpose. These results mean that the small qualitative difference found between heated and raw samples in the principal components analysis does not have any significant

TABLE 2

Predictions of samples calibrated on raw and heated samples and when raw and heated samples were considered as one class (%, w/w)

Sample no.	Muscle			Collagen			Soya			Casein			Whey			Dissimilarity[a] factor
	true	pred.	error	true	pred.	error	true	pred.	error	true	pred.	error	true	pred.	error	
A. *Raw samples*[a]																
1	68.8	68.9	−0.1	2.7	5.3	−2.6	28.5	20.5	8.0	0	3.0	−3.0	0	2.3	−2.3	2.9
2	96.8	99.6	−2.8	3.2	1.8	1.3	0	−5.1	5.1	0	1.9	−1.9	0	1.8	−1.8	2.0
3	63.2	64.4	−1.2	19.6	14.9	4.7	17.2	17.4	−0.2	0	2.6	−2.6	0	0.7	−0.7	0.7
4	72.8	64.3	8.5	2.8	−1.7	4.5	9.6	17.7	−8.1	12.0	14.5	−2.5	2.8	5.1	−2.3	1.3
5	76.6	66.8	9.8	3.0	2.8	0.2	0	4.6	−4.6	20.4	22.0	−1.6	0	3.8	−3.8	0.6
6	80.5	75.2	5.3	3.1	2.5	0.6	0	11.3	−11.3	13.3	9.9	3.4	3.1	1.1	2.0	1.3
7	85.5	84.3	1.2	14.5	14.4	0.1	0	5.2	−5.2	0	−2.4	2.4	0	−1.5	1.5	0.8
1b	68.8	69.5	−0.7	2.7	5.6	−2.9	28.5	23.8	4.7	0	1.1	−1.1	0	0.0	0	1.2
B. *Heated samples*[a]																
1	68.8	78.2	−9.4	2.7	8.2	−5.5	28.5	14.4	14.1	0	−0.4	0.4	0	−0.3	0.3	0.8
2	96.8	83.4	13.4	3.2	0.5	2.6	0	14.1	−14.6	0	1.9	−1.9	0	0.1	−0.1	2.3
3	63.2	66.9	−3.7	19.6	11.7	7.9	17.2	17.5	−0.3	0	4.0	−4.0	0	0.0	0	2.1
4	72.8	81.6	−8.8	2.8	0.2	2.6	9.6	2.0	7.6	12.0	12.8	−0.8	2.8	3.5	−0.7	2.8
5	76.6	79.5	−2.9	3.0	4.3	−1.3	0	1.6	1.6	20.4	13.2	7.2	0	1.5	−1.5	2.2
6	80.5	85.9	−5.4	3.2	2.4	0.7	0	−0.1	0.1	13.3	9.3	4.0	3.1	2.6	0.5	1.3
7	85.5	88.3	−2.8	14.5	11.6	2.9	0	−2.7	2.7	0	4.2	−4.2	0	−1.4	1.4	2.7
1b	68.8	77.4	−8.6	2.7	9.1	−6.4	28.5	8.4	20.1	0	5.3	−5.3	0	−0.2	0.2	3.9
C. *Raw samples with raw and heated samples considered as one class*[b]																
1	68.8	67.2	1.6	2.7	6.3	−3.6	28.5	31.2	−2.7	0	−2.5	2.5	0	−2.0	2.0	3.8
2	96.8	90.3	6.5	3.2	2.4	0.8	0	6.1	−6.1	0	0.8	−0.8	0	0.3	−0.3	0.7
3	63.2	66.3	−3.1	19.6	16.0	3.6	17.2	16.4	0.8	0	1.1	−1.1	0	0.4	−0.4	0.7
4	72.8	68.5	4.3	2.8	−1.4	4.2	9.6	15.9	−6.3	12.0	13.5	−1.5	2.8	3.4	−0.6	1.1
5	96.3	94.4	1.9	3.8	4.1	−0.3	0	4.2	−4.2	0	−2.4	2.4	0	−0.2	0.2	1.0
6	76.0	74.8	1.2	3.0	4.7	−1.7	21.0	22.8	−1.8	0	−2.7	2.7	0	0.4	−0.4	1.5
1a	68.8	61.8	7.0	2.7	1.6	1.1	28.5	32.3	−3.8	0	3.2	−3.2	0	1.7	−1.7	1.3
1b	68.8	57.2	11.6	2.7	10.4	−7.7	28.5	41.0	−12.5	0	−8.2	8.2	0	0.5	−0.5	2.7
1c	68.8	66.7	2.1	2.7	1.7	1.0	28.5	29.6	−1.1	0	1.4	−1.4	0	0.6	−0.6	1.5
2a	96.8	97.9	−1.1	3.2	0.2	3.0	0	2.2	−2.2	0	−0.4	0.4	0	0.0	0	1.7
3a	63.2	65.5	−2.3	19.6	17.7	1.9	17.2	13.8	3.4	0	1.9	−1.9	0	1.2	−1.2	0.6
D. *Heated samples with raw and heated samples considered as one class*[b]																
1	68.8	69.7	−0.9	2.7	7.2	−4.5	28.5	24.9	3.6	0	−2.0	2.0	0	0.2	−0.2	0.9
2	96.8	87.2	9.2	3.2	2.7	0.5	0	10.3	−10.3	0	−0.7	0.7	0	0.3	−0.3	2.2
3	63.2	67.0	−3.8	19.6	15.0	4.6	17.2	14.7	2.5	0	1.8	−1.8	0	1.4	−1.4	1.6
4	72.8	74.4	−1.6	2.8	−2.1	4.9	9.6	12.6	−3.0	12.0	12.5	−0.5	2.8	2.6	0.2	1.0
5	96.3	80.7	15.6	3.8	10.2	−6.4	0	11.4	−11.4	0	−2.0	2.0	0	−0.3	0.3	0.3
6	76.0	61.2	15.4	3.0	6.7	−3.7	21 0	32.1	−11.1	0	−0.5	0.5	0	0.6	−0.6	3.2
2a	96.8	97.1	−0.3	3.2	1.5	1.7	0	−2.9	2.9	0	3.3	−3.3	0	0.8	−0.8	1.7

[a] Dissimilarity factor calculated as (residual variance of sample)/(residual variance of calibration set); F-statistic 95%; 9.45 d.f.; 2.10.
[b] Dissimilarity factor calculated as (residual variance of sample)/(residual variance of calibration set); F-statistics 95%; 6.131 d.f.; 2.15.

influence on the accuracy of the predictions. However, heating seems to affect the precision; the residuals are larger for heated samples, regardless of the calibration method (Table 3).

In this kind of multivariate modelling, it is also possible to calculate the distance between the sample and the calibration model. This measure can be used to test the reliability of the prediction for a particular sample. The test variable is the quotient between sample variance and the residual variance of the calibration set and can thus be tested by the F-test if normal distribution is assumed for the residuals. The degrees of freedom for the sample are the number of variables (p) minus the number of extracted components (a), and those for the calibration set are $(n - a - 1)(p - a)$. In the Y-block, the number of degrees of freedom is obtained analogously to multiple regression, i.e., each constituent in the Y-block will lose one degree of freedom for each extracted component. This is so because only the loading vector of the Y-block is used when the Y-residuals are calculated (see earlier algorithm [9]).

Like all statistical tests, this test is built on a probability assumption, i.e., a defined risk of misjudgement. Still, the measure can provide useful information concerning the appropriateness of a model in analyzing a sample and will consequently reflect the reliability of the result. For brevity, this discussion is limited to Table 2C, D. All these samples are regarded as belonging to one class and should therefore lie within the limits in, e.g., 95% of cases. They do so, except for a few cases in which high dissimilarity factors are obtained. These high values indicate unreliability, and perhaps originate from unsuccessful hydrolysis, derivatization, chromatographic or computational failure. Examples are seen for raw sample 1b and heated sample 6, for which high dissimilarity factors are accompanied by large errors in the predictions. However, there is always a risk of misjudgement because of the statistical test. This is seen for raw sample 1 and heated sample 5; in the first case a correct measurement is rejected, whereas in the second case an erroneous result is accepted. Rejection of a correct measurement is, however, often not very serious; it will usually lead to repeat analysis of the sample. This kind of test should be efficient in quality-control applications, where the number of samples is seldom a limiting factor.

TABLE 3

Residual standard deviations of the predictions for the different calibration sets in Table 2 (%, w/w)

Calibration set	$[\Sigma(y - y_{pred.})^2/n]^{1/2}$					
	Muscle	Collagen	Soya	Casein	Whey	Total
A	5.1	2.7	6.6	2.4	2.1	4.2
B	7.7	4.4	10.4	4.1	0.8	6.4
C	3.6	2.5	3.7	2.0	1.0	2.8
D	9.4	4.8	8.3	3.3	0.7	6.2

Conclusion

The method described allows a simultaneous determination of several proteins in food. The method demands that all major amino-acid sources and other types of variations are included in the calibration set. This is achieved by calibrating against representative foodstuffs of similar composition. The accuracy of the determination depends on the uniqueness of each amino-acid pattern and the precision in the measurements. The method seems to be relatively little influenced by heating of the sample; the accuracy for raw samples is about 3% and that for heated samples is about 6%. These samples were analysed during a two-month period so that the drift must be regarded as low.

In order to explore further the potential of the method, work should be directed to analyzing more samples of different origins and treatments. Closer examination of the precision of each variable would also be beneficial, because improved weighting of the variables could thus be accomplished.

Financial support from Norske Meieriers Salgssentral, Oslo, is gratefully acknowledged.

REFERENCES

1 D. J. Armstrong, S. H. Richert and S. H. Riemann, J. Food Technol., 17 (1982) 327.
2 C. H. S. Hitchcock, F. J. Bailey, A. A. Crimes, D. A. G. Dean and P. J. Davies, J. Sci. Food Agric., 32 (1981) 157.
3 D. Jones, D. Shorley and C. Hitchcock, J. Sci. Food Agric., 33 (1982) 677.
4 W. Lindberg, J. Öhman, S. Wold and H. Martens, Anal. Chim. Acta, 171 (1985) 1.
5 B. Lindquist, J. Östgren and I. Lindberg, Z. Lebensm. Unters. Forsch., 159 (1975) 15.
6 H. Martens, K. I. Hildrum, A. Bakker, S. Å. Jensen, P. Lea, B. Eskeland, E. Vold and H. Russwurm, 26th European Meeting of Meat Research Workers, Colorado Springs, 1980, Vol. 1, 1980, p. 146.
7 H. Martens and S. Å. Jensen, in J. Holas and J. Kratchovil (Eds.), 7th World Cereal and Bread Congress, Prague, June 1982, Elsevier, Amsterdam, 1983.
8 H. Martens and T. Naes, Multivariate Calibration by Data Compression, Report from Norwegian Food Research Institute, Aas-NLH, Norway, 1984.
9 W. Lindberg, S. Å. Persson and S. Wold, Anal. Chem., 55 (1983) 643.
10 M. Otto and W. Wegscheider, Anal. Chem., 57 (1985) 63.
11 S. Wold, Pattern Recognition, 8 (1976) 127.
12 K. V. Mardia, J. T. Kent and J. M. Bibby, Multivariate Analysis, Academic Press, New York, 1979.

Analytica Chimica Acta, 174 (1985) 53—60
Elsevier Science Publishers B.V., Amsterdam — Printed in The Netherlands

PREDICTING RETENTION DATA IN GAS-LIQUID CHROMATOGRAPHY BY MULTIVARIATE ANALYSIS

R. FELLOUS*, L. LIZZANI-CUVELIER and R. LUFT

Laboratoire de Chimie Organique, Institut Polytechnique Méditerranéen, Université de Nice, Parc Valrose, F-06034 Nice Cedex (France)

(Received 20th November 1984)

SUMMARY

Satisfactory reproduction of the retention data matrix in the case of a series of monosubstituted benzenes and a series of aliphatic substances proves the general character of the prediction equation

$$x_{Q_i,\,\Phi_j} = a_{Q_i} x_{ST1,\,\Phi_j} + b_{Q_i} x_{ST2,\,\Phi_j} + c_{Q_i} x_{ST3,\,\Phi_j} + d_{Q_i} x_{ST4,\,\Phi_j}$$

where $x_{Q_i,\,\Phi_j}$ are the retention data x of unknown solute Q_i on phase Φ_j; a_{Q_i}, b_{Q_i}, c_{Q_i} and d_{Q_i} are regression coefficients which to some extent account for forces of orientation, charge transfer and association; and $x_{ST_i,\,\Phi_j}$ are independent variables representing the retention data of the four compounds of the standard set of substances on a given phase Φ_j. These four compounds are selected by diverse methods of multivariate analysis. The predicted values show very satisfactory agreement with the observed values.

A three-dimensional multiparametric model has been described for estimating the retention data of a substance Q on a stationary phase Φ_j in gas-liquid chromatography (g.l.c.) [1]. This model is based on the results of principal components analysis (BMDP-P4M-18.1 procedure) [2], applied to the retention data of a population of 17 monosubstituted benzenes, measured over 21 stationary phases. This factor analysis leads to a series of principal components (pattern) and associated scores for each case; its final aim is to transform the statistical factors into real ones, expressed in a physicochemical sense. To this end, earlier studies gave convincing results with a series of 26 alcohols [3], another with a series of 25 aliphatic hydrocarbons [4] and a third with 18 ether oxides [5]. In each of these populations, the only differences between substances within a series appear in the skeleton of the alkyl group and thus it is not surprising that relations exist between principal components and physical properties such as boiling point, molecular refraction, etc. The results are not satisfactory when factor analysis is applied to heterogeneous sets of data [6, 7]. Nevertheless, analysis of the g.l.c. retention data of 17 monosubstituted benzenes on 21 stationary phases, has been shown [8] to lead to acceptable relationships.

In a continuation of that work, solvent/solute interactions are investigated here. The aim was to identify two data sets, one relative to stationary phases

0003-2670/85/$03.30

and another to substances, that would allow a satisfactory description of global solvent/solute interactions in gas-liquid chromatography. It was shown previously [8] that the best choice of a standard set of stationary phases for multivariate analysis would be SE-30, OV-210 and DEGS. The selection of a standard set of substances is the target of the present work.

DATA SET

Retention data on which this work is based are given in Table 1.

SELECTION AND CLASSIFICATION OF SUBSTANCES

Cluster analysis (BMDP-P1M-17.1 procedure [2]) was used. When applied to logarithms of adjusted retention times, cluster analysis, based on measures of similarity and linkage rules, leads to parallel results if the measures of similarity represent the value of the correlation coefficient or the angular distance between two variables.

Figure 1 indicates that the examined monosubstituted benzenes are distributed among two sets. Set I groups compounds where the bond between the benzene ring and the substituent Z is characterized by weak polarizability. The substituents pertaining to this set (CF_3, CH_3, F, H) show the smallest retention times for every stationary phases. Set II is divided in two groups 1 and 2, each of which is also separated in two parts a and b. Group II-1 includes those compounds with p-π electron-donating substituents (OCH_3, SH, Br, Cl, I), the only exception being methyl benzoate. Group II-2a contains compounds with π-π electron-acceptor substituents (CHO, NO_2, $COCH_3$, CN). Group II-2b consists of substances with substituents which undergo strong hydrogen bonding (type III of Pimentel's [9] classification).

The standard set of substances was selected with the aid of three techniques: (a) factor analysis by diagonalization of the covariance matrix (BMDP-P4M-18.1 procedure [2]); (b) stepwise regression leading to successive eliminations of the substances bearing the least information (BMDP-P2R-13.2 procedure [2]); (c) stepwise discriminant analysis providing a classification based on decreasing discriminating power, which in the present case gave the sequence OH > $COCH_3$ > I > NH_2 (BMDP-P7M-18.4 procedure [2]). The results of these different analyses are grouped in Table 2.

Before the standard set of substances was selected, all compounds which had short retention times on all stationary phases were discarded because of poor precision. All these compounds were in group I. Among the remaining substances, those which best described the factorial axes were benzonitrile (ST1), iodobenzene (ST2), methoxybenzene (ST3) and phenol (ST4). These four substances, ST1—ST4, constitute the standard set of substances. It is obvious that the present results are conditioned by the combination of substances and of stationary phases and that these results could vary if the number and mixture of the items in the lists of substances and phases were changed.

TABLE 1

Logarithms of adjusted retention times, log t', of monosubstituted benzenes

Z_t[a]	Apiezon L	SE-30	DC-200	PMPE-5R	Apiezon H	OV-17	Ucon 50-HB 2000	Ucon LB-550X	OV-210	OV-225	NPGS
H	0.9906	0.6180	0.8170	0.6218	0.9476	0.8100	0.9868	0.7482	0.4298	0.6907	0.6207
CF_3	0.9912	0.7324	0.9542	0.5798	0.9243	0.8195	1.033	0.8195	0.6628	0.7324	0.7324
CH_3	1.322	0.8921	1.121	0.9243	1.225	1.057	1.225	1.000	0.6628	0.9243	0.8921
OCH_3	1.611	1.107	1.369	1.391	1.563	1.491	1.702	1.418	1.057	1.384	1.405
Br	1.754	1.188	1.444	1.459	1.697	1.563	1.762	1.483	1.090	1.422	1.431
Cl	1.524	1.017	1.250	1.193	1.459	1.342	1.539	1.250	0.9243	1.193	1.210
F	1.033	0.7324	0.9243	0.6812	0.9542	0.8195	1.057	0.8062	0.5563	0.7482	0.7324
I	2.038	1.401	1.659	1.781	1.993	1.835	2.033	1.757	1.274	1.699	1.690
CHO	1.728	1.225	1.477	1.653	1.751	1.676	1.957	1.655	1.405	1.701	1.716
SH	1.812	1.236	1.494	1.606	1.769	1.665	1.930	1.615	1.158	1.582	1.611
$COOCH_3$	1.974	1.453	1.720	1.868	1.987	1.895	2.146	1.870	1.519	1.833	1.850
CN	1.736	1.270	1.511	1.728	1.808	1.756	2.075	1.768	1.571	1.844	1.831
$COCH_3$	1.940	1.422	1.676	1.892	1.988	1.888	2.162	1.874	1.617	1.920	1.921
NH_2	1.737	1.241	1.489	1.708	1.742	1.716	2.182	1.820	1.305	1.823	1.933
NO_2	2.006	1.477	1.726	1.991	2.046	1.971	2.281	1.981	1.744	2.048	2.045
CH_2OH	1.831	1.350	1.591	1.826	1.869	1.806	2.380	2.018	1.387	1.947	2.078
OH	1.627	1.193	1.441	1.617	1.629	1.635	2.507	2.068	1.204	1.953	2.166

Z	Carbowax 20M	XF-1150	FFAP	PDEAS	DEGA	DEGS	EGS	DEGSEB	QF1	DCL5X
H	0.0523	0.738	0.9857	0.6876	0.936	0.4771	0.5211	1.101	0.7251	−0.2565
CF_3	0.0414	0.7356	1.033	0.6128	0.8921	0.4771	0.5051	1.072	0.8921	0.0792
CH_3	0.2304	0.9263	1.225	0.8865	1.114	0.7782	0.7482	1.283	0.9243	0.0792
OCH_3	0.7404	1.438	1.739	1.400	1.641	1.338	1.310	1.769	1.230	0.5563
Br	0.7993	1.451	1.791	1.461	1.665	1.334	1.283	1.826	1.270	0.6021
Cl	0.4914	1.231	1.556	1.179	1.425	1.100	1.054	1.587	1.246	0.3424
F	0.0414	0.7952	1.093	0.7404	0.9542	0.6628	0.6232	1.114	0.8195	0.0000
I	1.076	1.699	2.075	1.757	1.952	1.617	1.556	2.119	1.447	0.8195
CHO	1.076	1.843	2.069	1.773	1.976	1.708	1.672	2.056	1.571	0.9138
SH	1.004	1.657	2.017	1.698	1.889	1.563	1.521	2.015	1.338	0.6233
$COOCH_3$	1.185	1.887	2.192	1.842	2.121	1.809	1.787	2.236	1.672	1.009
CN	1.223	2.008	2.195	1.894	2.104	1.834	1.797	2.175	1.723	1.057
$COCH_3$	1.267	2.039	2.252	1.957	2.199	1.906	1.888	2.285	1.768	1.121
NH_2	1.332	2.046	2.354	1.999	2.251	1.996	1.968	2.285	1.477	0.8195
NO_2	1.430	2.177	2.404	2.126	2.338	2.052	2.038	2.413	1.897	1.250
CH_2OH	1.498	2.157	2.520	2.130	2.408	2.138	2.107	2.442	1.539	0.9542
OH	1.650	2.239	2.686	2.288	2.487	2.231	2.178	2.516	1.369	0.7782

[a]The substituent on the benzene ring.

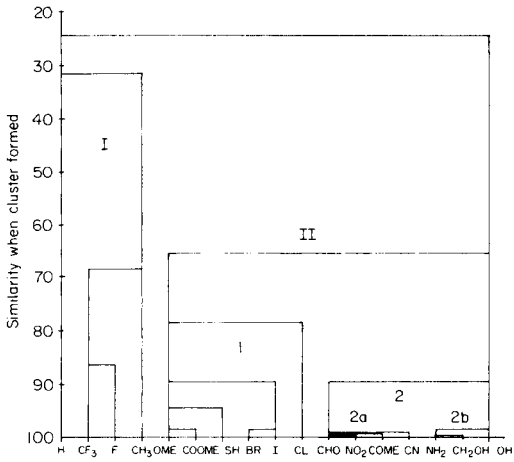

Fig. 1. Tree printed over correlation matrix clustering by maximum distance method for monosubstituted benzenes.

ELABORATION OF A MODEL FOR THE PREDICTION OF RETENTION DATA

With the aid of the standard set of substances, a multiparametric equation was developed that should allow the prediction of retention data for any unknown compound Q_i:

$$x_{Q_i,\ \Phi_j} = a_{Q_i} x_{ST1,\ \Phi_j} + b_{Q_i} x_{ST2,\ \Phi_j} + c_{Q_i} x_{ST3,\ \Phi_j} + d_{Q_i} x_{ST4,\ \Phi_j} \quad (1)$$

In this relationship, $x_{Q_i,\ \Phi_j}$ are dependent variables representing the retention data of solutes Q_i on a stationary phase Φ_j; a_{Q_i}, b_{Q_i}, c_{Q_i} and d_{Q_i} are the regression coefficients; $x_{ST1,\ \Phi_j}$, $x_{ST2,\ \Phi_j}$, $x_{ST3,\ \Phi_j}$ and $x_{ST4,\ \Phi_j}$ are independent variables representing the retention data of the standard substances ST1, ST2, ST3, ST4 on a stationary phase Φ_j.

Equation 1 was tested with the aid of 13 × 21 retention data sets (13 monosubstituted benzenes measured on 21 stationary phases). The predicted

TABLE 2

Classification of data on the monosubstituted benzenes by the three techniques

Classes	Numerical taxonomic aggregation	Factor analysis		Stepwise regression	Stepwise discriminant analysis
		Factor axis	Factor plane		
I	CF_3, F, CH_3, H	—	CH_3	CF_3	
II-1	OMe, COOMe, SH, Br, I, Cl	I, OMe	COOMe	I	I
II-2a	CHO, NO_2, COMe, CN	CN	COMe	CN	COMe
II-2b	NH_2, CH_2OH, OH	OH	OH	OH	OH, NH_2

TABLE 3

Detailed values for acetophenone by application of the multiparametric relationship

Φ_j	log t' Obs.	log t' Predicted	Δ[a]	σ_e[b]	Error[c] (%)
Apiezon L	1.9395	1.9427	−0.0032	0.012	0.2
SE-30	1.4216	1.3991	0.0225	0.007	1.6
DC-200	1.6758	1.6504	0.0253	0.008	1.6
PMPE-5R	1.8921	1.8766	0.0155	0.008	0.8
Apiezon H	1.9877	1.9970	−0.0093	0.010	0.5
OV-17	1.8876	1.9027	−0.0151	0.008	0.8
Ucon 50-HB-2000	2.1620	2.1786	−0.0167	0.008	0.8
Ucon LB550X	1.8739	1.8756	−0.0017	0.006	0.1
OV-210	1.6170	1.6226	−0.0056	0.013	0.3
OV-225	1.9201	1.9315	−0.0114	0.005	0.6
NPGS	1.9212	1.9026	0.0186	0.006	0.9
Carbowax 20M	1.2672	1.2774	−0.0102	0.016	0.8
XF-1150	2.0392	2.0515	−0.0123	0.009	0.6
FFAP	2.2524	2.2847	−0.0324	0.008	1.4
PDEAS	1.9566	1.9788	−0.0222	0.088	1.1
DEGA	2.1987	2.1853	0.0133	0.007	0.6
DEGS	1.9063	1.8855	0.0209	0.007	1
EGS	1.8876	1.8369	0.0507	0.007	2.7
DEGSeb	2.2847	2.2870	−0.0023	0.007	0.1
QF_1	1.7679	1.7833	−0.0154	0.013	0.9
DCL-5X	1.1206	1.1082	0.0124	0.014	1.1

[a]Log t' (observed) minus log t' (predicted). [b]Standard error of estimate. [c]Δ/log t' (measured).

TABLE 4

Application of the multiparametric relationship for the prediction of retention data of monosubstituted benzenes

Z_i[a]	a_{Z_i}	b_{Z_i}	c_{Z_i}	d_{Z_i}	r[b]	σ_e[c]
H	−0.7097	−1.1868	2.9113	−0.0270[d]	0.9946	0.086
CF_3	−0.1844[d]	−1.2533	2.6682	−0.2574	0.9948	0.088
CH_3	−0.5001	−0.5499	2.1806	−0.1317	0.9981	0.047
Br	−0.0787	0.3941	0.7082	−0.0384	0.9999	0.016
Cl	−0.1188[d]	−0.4839	1.8060	−0.1314	0.9995	0.042
F	−0.4018	−1.1872	2.6777	−0.1048[d]	0.9980	0.056
CHO	0.6762	0.0588[d]	0.2529	0.0083[d]	0.9999	0.012
SH	−0.0674[d]	0.4076	0.5329	0.1433	0.9999	0.021
$COOCH_3$	0.5500	0.5393	0.0238[d]	−0.0556[d]	0.9999	0.031
$COCH_3$	0.8790	0.3947	−0.1915[d]	−0.0486	0.9999	0.022
NH_2	0.3164	0.0440	0.2190	0.4490	0.9999	0.034
NO_2	1.0864	0.4912	−0.5399	−0.0134[d]	0.9999	0.023
CH_2OH	0.3218	0.3594	−0.1900[d]	0.5284	0.9999	0.030

[a]The substituent on the benzene ring. [b]Multiple correlation coefficient. [c]Standard error of estimate. [d]Fischer's test > 2%.

values were obtained for the substituents H, CF_3, CH_3, Br, Cl, F, CHO, SH, $COOCH_3$, $COCH_3$, NH_2, NO_2, CH_2OH by use of a transformed Eqn. 1:

$$\log t'_{Z_i,\ \Phi_j} = a_{Z_i} \log t'_{CN,\ \Phi_j} + b_{Z_i} \log t'_{I,\ \Phi_j} + c_{Z_i} \log t'_{OMe,\ \Phi_j} + d_{Z_i} \log t'_{OH,\ \Phi_j}$$

where subscript Z_i represents the substituent on the benzene ring. The results were compared with the observed values and fitted in an acceptable manner, as illustrated in the case of acetophenone (Table 3). In the case of the retention data of the 12 other compounds, the concordance between observed and predicted values was also very satisfactory; thus mean regression coefficients were obtained (Table 4).

Definition of a prediction model for non-benzene substances

To check the applicability of the general Eqn. 1 in the case of non-aromatic substances, the g.l.c. data published by Rohrschneider [10] were

TABLE 5

Detailed values for acetone by application of the multiparametric relationship

Φ_j	I obs.[a]	I predicted	Δ[b]	σ_e[c]	Error[d] (%)
Squalane	422	410.9	11.1	6.30	3
DC-200	472	462.6	9.4	5.78	2
Apiezon L	450	439.6	10.4	7.42	2
Diethylhexyl sebacate	546	546.9	−0.9	4.68	0.2
Celanese ester NR-9	558	554.1	3.9	4.26	0.7
Di-isodecyl phthalate	572	584.3	−12.3	4.40	2
DC-710	593	596.0	−3.0	7.38	0.5
QF1	740	746.5	−6.5	11.76	0.9
Polypropylene glycol	599	596.0	3.0	6.26	0.5
Acetyltributyl citrate	647	662.4	−15.4	5.96	2
Tricresyl phosphate	691	693.0	−2.0	4.07	0.2
PMPE	661	643.5	17.5	8.06	3
Marlophene 87	692	693.5	−1.5	4.85	0.2
Polypropylene sebacate	689	692.2	−3.2	3.73	0.5
Marlophene 814	733	749.5	−16.5	4.26	2
NPGS	827	813.0	14.0	5.70	2
XF-1150	887	899.0	−12.0	5.47	1
Carbowax 20M	824	857.9	−33.9	5.81	4
Carbowax 4000	833	853.7	−20.7	6.39	2
Reoplex 400	885	885.2	−0.2	5.61	0.2
DEGS	1071	1051.5	19.5	6.20	2
Ethylene glycol cyanoethylether	1149	1141.4	7.6	7.35	0.7
1,2,3-Triscyano-2-ethoxypropane	1247	1222.4	24.6	7.75	2

[a]Kovats index. [b]$I_{obs.} - I_{pred.}$ [c]Standard error of estimate. [d]Δ/I (measured).

TABLE 6

Application of the multiparametric relationship for the prediction of retention indices of Rohrschneider's data

Q_i	a_{Q_i}	b_{Q_i}	c_{Q_i}	d_{Q_i}	r[b]	σ_e[c]
Thiophene	−0.0158[d]	0.8504	0.3524[d]	0.0882	0.9999	7.8
Nitroethane	0.7397	−0.6974	1.2023	0.0596	0.9999	6.6
Acetone	0.7292	−0.9092	1.3066	−0.1693[d]	0.9998	15.1
Phenylacetylene	−0.2703	0.6533[d]	0.8696	0.4319	0.9999	17.9
Styrene	−0.2283	0.1475[d]	1.7023	0.059[d]	0.9999	11.5
Toluene	−0.2167	−0.0119[d]	1.6620	0.0055[d]	0.9999	0.5
Cyclohexane	−0.6896	−0.6576[d]	2.6150	−0.0528[d]	0.9998	14.5
2,4-Dimethylpentane	−0.9954	−2.2603	4.2764	0.1522[d]	0.9994	23.5
Pyridine	0.1955[d]	0.1977[d]	0.8046[d]	0.2622[d]	0.9998	24.1
Nitromethane	0.7723	−0.1478[d]	0.2100[d]	0.3416	0.9999	9.7
Butan-2-one	0.5382	−1.1679	1.9485	−0.1766[d]	0.9998	13.7
Benzene	−0.0716[d]	0.3023[d]	1.0054	0.0120[d]	0.9999	9.3
Cyclopentanol	−0.3017	−0.2414[d]	1.2488	0.9016	0.9999	9.9
t-Butanol	−0.1683	−1.1448	1.6327	0.7981	0.9999	9.2
Allylic alcohol	−0.0906	0.1853	0.0789	1.1838	0.9999	8.7
Isopropanol	−0.1289	−0.6165	0.8697	0.9519	0.9999	4.3
n-Propanol	−0.172	−0.347	0.681	1.035	0.9999	5.7
Chloroform	−0.351	0.460[d]	0.526[d]	0.609	0.9998	16.7
Crotonaldehyde	0.615	−0.755	1.558	−0.152[d]	0.9999	10.6
Propanal	0.547	−0.620	1.166	−0.144[d]	0.9999	11.4
n-Butylacetate	−0.015[d]	−1.516	3.101	−0.067[d]	0.9999	13.4
Dioxane	0.352	0.103[d]	0.918	−0.048[d]	0.9998	21.2
n-Dibutyl ether	−0.898	−1.961	4.363	0.110[d]	0.9998	17.6
CCl_4	−0.464	0.238[d]	1.348	0.114[d]	0.9999	9.8
$C_2F_2Cl_4$	−0.653	−1.054	2.785	0.246[d]	0.9998	19.2
2-Ethyl-1-hexene	−0.9635	−1.798	4.090	0.1193[d]	0.9998	20.0

[b–d]See Table 4.

subjected to the same mathematical analyses as the above data series. In particular, principal component analysis showed that the factorial space was best described by using the data for acetonitrile (ST1′), methyl iodide (ST2′), ethyl bromide (ST3′) and ethanol (ST4′). Each of the ST1′, ST2′ and ST4′ defines one of the three successive factorial axes; ST3′ is located near the centre of gravity of the factorial planes 1, 2 and 2, 3. A quick examination of these results showed that in the ST1′, ST2′, ST3′ and ST4′ series, the functional groups are the same or pertain to the same cluster (ST3 = ROMe, ST3′ = RBr) as in the ST1, ST2, ST3 and ST4 series. By introducing the ST1′, ST2′, ST3′ and ST4′ standards into Eqn. 1 the retention indices of any substances Q_i on a stationary phase Φ_j are easily predicted:

$$I_{Q_i,\,\Phi_j} = a_{Q_i} I_{\text{acetonitrile},\,\Phi_j} + b_{Q_i} I_{\text{MeI},\,\Phi_j} + c_{Q_i} I_{\text{EtBr},\,\Phi_j} + d_{Q_i} I_{\text{EtOH},\,\Phi_j}$$

As before, this equation was tested with a series of products and phases (26 × 23 data sets); the results were compared with the observed series

and fitted in an acceptable manner, as illustrated in the case of acetone (Table 5). Table 6 displays the mean regression coefficients obtained from Rohrschneider's data.

REFERENCES

1 R. Fellous, D. Lafaye de Micheaux, L. Lizzani-Cuvelier and R. Luft, J. Chromatogr., 248 (1982) 35.
2 W. J. Dixon, BMDP Statistical Software, UCLA Press, Berkeley, CA, 1981.
3 P. H. Weiner, C. J. Dack and D. C. Howery, J. Chromatogr., 69 (1972) 249.
4 D. G. Howery, Anal. Chem., 46 (1974) 829.
5 R. B. Selzer and D. G. Howery, J. Chromatogr., 115 (1975) 139.
6 P. H. Weiner and D. G. Howery, Anal. Chem., 44 (1972) 1189.
7 D. G. Howery, P. H. Weiner and J. S. Blinder, J. Chromatogr. Sci., 12 (1974) 366.
8 R. Fellous, D. Lafaye de Micheaux, L. Lizzani-Cuvelier and R. Luft, Anal. Chim. Acta, 154 (1983) 191.
9 S. N. Vinogradov and R. H. Linnell, Hydrogen Bonding, Van Nostrand-Reinhold, New York, 1971.
10 L. Rohrschneider, J. Chromatogr., 22 (1966) 6.

Analytica Chimica Acta, 174 (1985) 61—69
Elsevier Science Publishers B.V., Amsterdam — Printed in The Netherlands

COMPUTER-BASED SYSTEM FOR CORRELATING MOLECULAR STRUCTURES WITH MASS SPECTRAL DATA

MARSHALL M. SIEGEL

American Cyanamid Company, Medical Research Division, Lederle Laboratories, Pearl River, NY 10965 (U.S.A.)

(Received 14th February 1985)

SUMMARY

Algorithms are described for correlating a proposed molecular structure with a mass spectrum. All molecular substructures of a proposed structure are determined which have the same masses as the fragment ions. The most likely fragment ion structures are those molecular substructures formed with the fewest number of bond cleavages in the proposed structure. The algorithms, which incorporate methods for handling rearrangement and adduct ions, utilize either nominal or exact data originating from any ionization method. The algorithms are demonstrated using the mass spectra of a substituted azetidinyl ketone and the macrolide antibiotic avermectin A_{1a}.

Mass-spectral data systems have been designed for the correlation and elucidation of chemical structures of unknown compounds by relating through some algorithms the observed mass spectrum to a molecular structure. Two techniques commonly used are [1—3]: (1) library search algorithms in which the library spectra are matched against the mass spectrum of the unknown, and (2) interpretative methods in which a mass spectrum is interpreted according to mass spectral rules to generate the unknown structure. An example of the library search method is probability based matching (PBM) [4] developed by McLafferty and co-workers. Examples of interpretative methods are the DENDRAL method [5] developed by Lederberg and co-workers and the self-training interpretive and retrieval system (STIRS) [4] developed by McLafferty and co-workers. In many instances, however, instead of the structure being totally unknown, a structure for the substance is proposed and the consistency or inconsistency of that structure has to be established from mass spectral data.

This paper demonstrates a simple utilitarian computer-aided structure correlation/elucidation scheme in which the masses of the observed ions in a mass spectrum are correlated with the masses of molecular substructures which were generated from a proposed molecular structure. The proposed scheme is independent of the ionization mode and is applicable to either nominal or exact mass data.

Mass spectral interpretation can be simplistically described as a bookkeep-

0003-2670/85/$03.30

ing method for correlating the mass and charge of molecular substructures with ions observed in the mass spectrum. Focusing on the bookkeeping necessary to predict the molecular substructure masses, the following statements can be made. First, any fragment ion consists of a molecular substructure which could be predicted by finding the most logical of the molecular substructures consistent with the mass of the fragment ion. Second, the most logical molecular substructure among the possible molecular substructures is generally that substructure which is generated with the fewest number of bond cleavages from the proposed molecular structure. In general for complex molecules, only four or fewer bond cleavages of the molecular structure are likely to produce the molecular substructures.

THE ALGORITHMS

The most practical way to implement the above two statements about substructure masses is to consider the proposed structure as constructed from a set of bound molecular subunits which do not undergo further fragmentation. These subunits are called superatoms [5]. Examples of superatoms are the smallest units of a molecule containing only single bonds excluding hydrogen ($-CH_3$, $-CH_2-$, $-\overset{|}{C}H-$, $-O-$, $-NH-$) and units of a molecule with double or triple bonds or conjugated bond systems ($-CH=CH-$, $-C\equiv C-$, $-CH=CH-CH=CH-$, $-\overset{|}{C}=O$, phenyl, pyridyl, $-C\equiv N$, etc.). The mass of every fragment ion observed in the mass spectrum can be expressed as a combination of superatoms of equal mass which are all bound together as a single subset of the proposed molecular structure. The most logical subset of superatoms to describe each of the fragment ions is that subset requiring the fewest superatom bond cleavages of the proposed structure.

The algorithms necessary to implement the above method must identify all the combinations of the superatom masses equal to the observed fragment ion masses. (These combinations are called superatom subsets.) Included in these computations must be provisions for the occurrence of rearrangement processes, viz., proton rearrangements (losses and gains), neutral molecule losses and adduct ion formation. The algorithms must find those superatom subsets in which all the superatoms are bound together as a substructure of the proposed molecular structure and must compute the number of superatom bond cleavages necessary to create each of the substructures from the proposed structure.

Combination calculations

The algorithm used to compute all of the combinations of superatoms of a given nominal (or exact) mass is similar to those used to compute elemental compositions from exact mass data [6, 7]. Instead of computing the exact masses from all the combinations of exact elemental masses, nominal (or exact) masses are computed from all of the combinations of the superatom

nominal (or exact) masses. Two classes of superatoms are included in the algorithm. One class consists of those superatoms which are part of the molecular structure and the second class consists of those superatoms necessary to describe rearrangement processes in the mass spectrum. This latter class of superatoms is considered as unbonded superatoms because they can be found anywhere in the structure. Each of the unbonded superatoms when lost from a submolecular structure, e.g., losses of H, H_2O, CH_3OH, CH_3CO_2H, etc., is assigned a negative mass while each of the superatom adducts to the molecular substructure, e.g., proton transfers, adducts of NH_4^+, Na^+, thioglycerol, etc., is assigned a positive mass. (Adduct ions are commonly observed in chemical-ionization, fast atom-bombardment and field-desorption mass spectra.) If the mass of an unbonded superatom lost is identical to the mass of any superatom in the set, a number of degenerate subsets of superatoms of the same mass will be computed. The algorithm provides for the suppression of these degenerate sets. For example, if superatoms for a proton lost and a proton gained are considered in one computation, no loss or gain of a proton is degenerate with a gain and a loss of a proton. The latter superatom set is suppressed.

Structure calculations

The molecular structure is input into the algorithm as a series of superatoms of known mass together with a look-up table consisting of all the superatom bond pairs making up the molecule. The algorithm for determining whether superatoms in a subset are all bound together works as follows. One superatom in the subset is chosen and all superatoms bound to it are determined by comparison with the bond-pair look-up table. This list of superatoms is compared to the subset of superatoms. If no superatoms in the subset are found in the list, the superatom subset has a discontinuity and all the superatoms are not bound together. If, however, superatoms in the subset are found in the list, these superatoms are flagged. Again, all of the superatoms bound to the flagged superatoms are listed and compared to the superatom subset. All previously unflagged superatoms found in the list are now flagged. This process continues until the number of flagged superatoms equals the number of superatoms in the subset. If this condition is (or is not) met, all of the superatoms in the subset are (or are not) bound together.

The number of superatom bond cleavages for a given substructure is simply computed by counting all the bond pairs in which only one superatom member of the pair is present in the substructure. Unbonded rearrangement superatoms are not counted in this algorithm.

APPLICATION OF THE ALGORITHM FOR CORRELATING MOLECULAR STRUCTURES WITH MASS SPECTRAL DATA

Substituted azetidinyl ketone

This application of the algorithms illustrates the interpretation of an electron-impact mass spectrum of a simple molecule. The mass spectral data

TABLE 1

Superatom combinations satisfying the mass spectral data for substituted azetidinyl ketone (1, 2)

Fragment ion[a] (*m/z*)	Number of superatom combinations satisfying proposed structure	Best fit of superatoms to proposed structure												Number of superatom bond cleavages
		Superatom names:												
		P1	P2	C0	C1	C2	N1	C3	Me	P3	TB	H1	H2	
		Superatom masses:												
		77	76	28	12	13	14	14	15	77	57	1	−1	
		Number of superatoms present												
383	1	1	1	1	1	1	1	1	1	1	1	0	0	0
368	2	1	1	1	1	1	1	1	0	1	1	1	1	1
367	1	1	1	1	1	1	1	1	0	1	1	0	1	1
366	0													
327	1	1	1	1	1	1	1	1	1	1	0	1	0	1
326	1	1	1	1	1	1	1	1	1	1	0	0	0	1
243	0													
222	4	1	1	1	1	0	0	1	1	0	0	0	0	2
221	8	1	1	1	1	0	0	1	1	0	0	0	1	2
182	1	1	1	1	0	0	0	0	0	0	0	1	0	1
181	1	1	1	1	0	0	0	0	0	0	0	0	0	1
167	0													
160	3	0	0	0	0	1	1	0	0	1	1	0	1	2
153	2	1	1	0	0	0	0	0	0	0	0	0	0	1
152	2	1	1	0	0	0	0	0	0	0	0	0	1	1
151	0													
149	0													
147	0													
146	3	0	0	0	1	1	1	1	1	1	0	1	0	2
131	6	0	0	0	1	1	1	1	0	1	0	1	0	3
106	0													
105	2	0	1	1	0	0	0	0	0	0	0	1	0	2
104	2	0	1	1	0	0	0	0	0	0	0	0	0	2
91	1	0	0	0	0	1	0	0	0	1	0	1	0	2
77	3	1	0	0	0	0	0	0	0	0	0	0	0	1
		0	0	0	0	0	0	0	0	1	0	0	0	1
76	3	1	0	0	0	0	0	0	0	0	0	0	1	1
		0	0	0	0	0	0	0	0	1	0	0	1	1
70	2	0	0	0	0	0	1	0	0	0	1	0	1	2
69	4	0	0	0	1	1	1	1	1	0	0	1	0	3
		0	0	1	1	0	0	1	1	0	0	0	0	3
57	1	0	0	0	0	0	0	0	0	0	1	0	0	1

[a]See ref. 8.

for 4-biphenylyl *trans*-1-*tert*-butyl-3-methyl-2-phenyl-3-azetidinyl ketone (1) was obtained from the EPA/NIH Mass Spectral Data Base [8]. The structure drawn as superatoms is illustrated as structure (2). Table 1 lists the observed nominal mass fragment ions, the total number of possible fits of the superatom masses to the fragment ion mass (with the constraint that all the superatoms in the substructure are bound together), and, the most likely fragment ion structure (based on the criteria of the fewest number of superatom cleavages from the proposed structure). Data are listed in a format similar to the computer print-out. The most significant fragment ions are illustrated

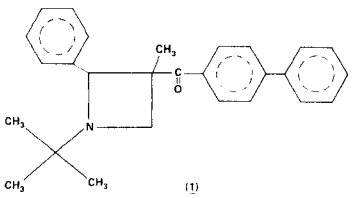

(1)

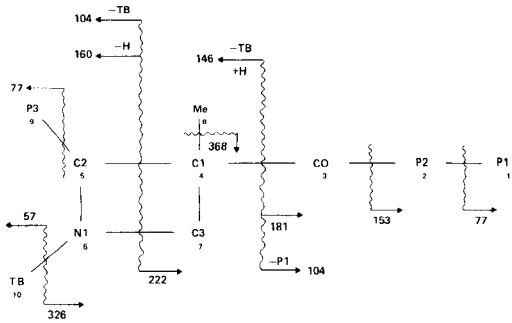

(2)

together with the superatom structure (**2**). It is noted in Table 1 that some ions appear to originate either as contaminants, e.g., phthalate ions at *m/z* 149, 167, or as impurities/unusual rearrangements, e.g., ions at 243, 366. The major fragment ions, however, are consistent with the proposed structure.

Avermectin A_{1a}

Avermectins, members of the macrolide class of antibiotics, are potent anthelmintic agents. Their structures have been elucidated by x-ray [9], nuclear magnetic resonance [10] and mass spectral [10] techniques. The electron-impact mass spectral data for avermectin A_{1a} have been published as well as the proposed structures for the fragment ions [10]. The application of the above-described algorithms for a very complex molecular structure is now illustrated and the computer-generated results are compared with those of the published data.

The proposed structure for avermectin A_{1a} (**3**) and the structure drawn as superatoms (**4**) are illustrated below. The wavy lines drawn through the bonds

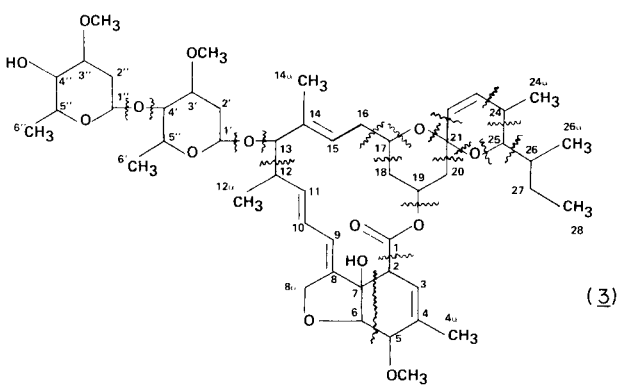

(3)

TABLE 2

Input data for mass spectral correlation program for avermectin A_{1a}: superatoms and bond look-up table

Superatom number or bond number	Superatom name	Superatom exact mass	Superatom elemental composition	Superatom bonds (Superatom no.—Superatom no.)	
1	S1	145.0865	$C_7H_{13}O_3$	1	2
2	O1	15.9949	O_1	2	3
3	S2	128.0837	$C_7H_{12}O_2$	3	4
4	O2	15.9949	O_1	4	5
5	C1	67.0548	C_5H_7	5	6
6	C2	151.0759	$C_9H_{11}O_2$	5	10
7	C3	97.0653	$C_6H_9O_1$	6	7
8	CT	43.9898	CO_2	7	8
9	C4	41.0391	C_3H_5	8	9
10	C5	13.0078	CH	9	10
11	O3	15.9949	O_1	9	12
12	C6	12.0000	C	10	11
13	C7	26.0156	C_2H_2	11	12
14	C9	28.0313	C_2H_4	12	13
15	CN	13.0078	CH	13	14
16	O4	15.9949	O_1	14	15
17	TR	57.0704	C_4H_9	15	16
18	WA	−18.0105	H_2O	16	12
19	H1	1.0078	H	15	17
20	H2	−1.0078	H		

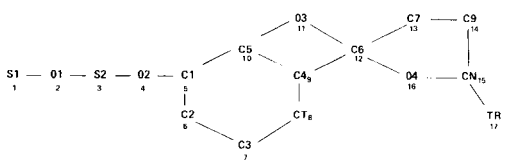

(4)

of the avermectin A_{1a} structure (3) bracket the atoms which constitute the superatoms illustrated in the superatom structure (4). Table 2 lists the names and numbers for the superatoms, their corresponding exact masses, elemental compositions and the list of bond connectivities for the corresponding superatoms in terms of their superatom numbers. Only twenty superatoms were chosen to permit the computer (PDP DEC-10) to operate in the interactive mode. The computer processing time became lengthy when more than twenty superatoms were computed. Under those conditions, batch operation was more practical. When the superatoms were chosen, it was assumed that the sugar moieties and the allylic conjugated aliphatic system remained intact and did not undergo fragmentation. Three unbonded structures were included as superatoms, viz., proton and water losses from the substructures and a proton gain to the substructures. Hence, 17 bonded superatoms with 19 superatom

bond pairs were necessary to describe the avermectin A_{1a} structure and 3 unbonded superatoms were necessary for the rearrangement processes.

The number of superatom combinations with and without satisfying the structural relationship are compared for both nominal and exact mass data in Table 3. There is a great reduction in the number of possible combinations which satisfy the required structural relationship in the latter case. There are about five times more nominal mass combinations than exact mass combinations satisfying the structural relationship. However, the most glaring result of the calculations is that the most likely structures predicted in both the nominal and exact mass calculations are identical to the published structures for fragments a, c, f, h, m, n, o, q and r. Besides the prediction of the published structures in the exact and nominal mass modes for ions d and k, several degenerate structures were predicted as well in the nominal mass mode. The predicted structures for ions b and f', for which only nominal mass data were available, are identical to the published structures. The structure for ion p is predicted correctly when an unbonded methanol loss superatom is considered as the twenty-first superatom. The program did not predict the published structures for fragment ions s, t and u because they are fragment ions of the sugar moieties which were considered as one superatom. Clearly, if the number of superatoms is increased, there is a greater likelihood in predicting correct structures. The price paid is simply a greater processing time for the computer and additional possible structures from which to choose the most likely fragment ion structure.

CONCLUSIONS

Algorithms are proposed for predicting fragment ion structures by correlating a proposed structure with the masses of the ions observed in a mass spectrum. Little knowledge of mass fragmentation mechanisms is necessary because a mass bookkeeping method is used which is restricted by the proposed structure. Judicious choice of the superatoms making up the structure is perhaps the only technical ability necessary for using the algorithms effectively. If there is doubt about which superatoms to choose, then the more chosen, the more likely the correct substructure will be chosen. The number of possible molecular substructures predicted is very few and in most cases the substructure generated with the fewest number of bond cleavages in the proposed structure is the correct one. If degenerate substructures are predicted, a judicious choice of the most likely structure is often possible.

The schemes presented in this paper are applicable to the rationalization of the fragmentation structures of large molecules, which eliminates tedious manual bookkeeping exercises and to the discovery of mass spectral substructure correlations among compounds within a structural class. They are also useful for automated spectrum/structure correlation for chemists inexperienced in mass spectral interpretation and for automatic scanning of

TABLE 3

The number of superatom combinations having a nominal or exact mass within experimental e

Structure assignment[a]	M^+	a	b	c	d	f	f′	h
Experimental exact mass[a] (daltons)	886.5072	742.4229	598	580.3406	456.2886	305.2120	289	221.1
Number of superatom combinations[d]								
(A) Nominal mass results								
No structural constraints	1	335	1078	1242	1921	1567	1305	924
Structure relationship for the fragment ion is satisfied	1	11	17	19	31	22	24	18
Structure relationship satisfied for (0), (1), (2), (3), (4) superatom bond cleavages	(0) 1	(1) 1 (4) 1	(1) 1 (3) 1	(1) 2[e] (3) 3	(3) 6	(1) 1[f] (3) 2	(1) 1 (3) 2	(2) 1 (4) 5
(B) Exact mass results[h]								
No structural constraints	1	128	—[i]	136	392	393	—[i]	267
Structure relationship for the fragment ion is satisfied	1	4	—[i]	7	1	1	—[i]	5
Structure relationship satisfied for (0), (1), (2), (3), (4) superatom bond cleavages	(0) 1	(1) 1	—[i]	(1) 2[e] (3) 2	(3) 1	(3) 1	—[i]	(2) 1

[a]See original paper [10] for data. [b]In the original paper [10], ion s (t) is related to q (r) by computed, the number of correlations for ion s (t) increases by the numbers of correlation u is a fragment ion of the superatom S1. [d]Underlines indicate that the computer-generated re additional correlations needed when an additional superatom equivalent to the loss of 32.0 proposed by the computer algorithm. The alternative structure suggested is a loss of H_2(sistent with sugars [S1 + O1 + S2 + O2] but exact mass data are inconsistent with this struct used for calculation ± 15 mmu or 15 ppm whichever is greater. [i]No high-resolution exact r

mass spectral data bases to evaluate the quality of the spectra and identify logical and illogical peaks.

The FORTRAN listings for the algorithms are available from the author.

The constructive comments of Raymond E. Carhart, Kevin Haraki, Steven Greenhouse and Rudolf Francel in developing the algorithms and for preparing the manuscript are greatly appreciated.

REFERENCES

1 J. R. Chapman, Computers in Mass Spectrometry, Academic Press, London, 1978, Ch. 5 and 7.
2 F. W. McLafferty and R. Venkataraghaven, in M. L. Gross (Ed.), High-Performance Mass Spectrometry: Chemical Applications, Symposium Series 70, American Chemical Society, Washington, DC, 1978, p. 310.
3 R. E. Carhart and D. H. Smith, in M. L. Gross (Ed.), High-Performance Mass Spectrometry: Chemical Applications, Symposium Series 70, American Chemical Society, Washington, DC, 1978, p. 325.

ıe measured mass for avermectin A_{1a}

	m	n	o	p	q	r	s[b]	t[b]	u[c]
1587	169.1226	111.0446	275.1292	257.1382	145.0867	127.0754	113.0604	95.0496	87.0444
	526	291	1239	937 [1305]	200	302	260	214	101
	7	9	18	9 [24]	8	10	6	15	1
	(2) 1 (4) 2	(2) 1[g] (3) 1 (4) 1	(2) 1 (4) 4	(4) 2 [(1)] 1 [(3)] 2	(1) 1 (2) 2	(1) 1 (2) 3 (4) 2	(2) 1 (4) 3	(2) 1 (3) 1 (4) 5	(2) 1
	113	131	287	273 [343]	76	103	100	108	28
	2	6	12	1 [1]	5	6	2	10	0
	(2) 1 (4) 1	(3) 1 (4) 1	(2) 1 (4) 4	(4) 1 [(1)] 1	(1) 1 (2) 2	(1) 1 (2) 3	(4) 2	(3) 1 (4) 4	0

of a methanol molecule. When an additional superatom equivalent to the loss of CH_3OH is). [c]No correct correlation for ion u was observed because the proposed structure [10] for uivalent to the proposed structure in original paper. Numbers in square brackets indicate the ons (CH_3OH) was computed. [e]The proposed structure for ion c [10] and an alternative is ons 7 and 8 and cleavage of the sugars at carbon 13 with a proton loss from carbon 12. [f]Con- + H — H_2O] is the proposed structure, but is an illogical fragment. [h]Experimental errors are available.

4 F. W. McLafferty, Interpretation of Mass Spectra, 3rd edn., University Science Books, Mill Valley, CA, 1980, Ch. 10.

5 R. K. Lindsay, B. G. Buchanan, E. A. Feigenbaum and J. Lederberg, Applications of Artificial Intelligence for Organic Chemistry: The DENDRAL Project, McGraw-Hill, New York, 1980.

6 S. R. Shrader, Introductory Mass Spectrometry, Allyn and Bacon, Boston, 1971, Appendix C.

7 R. A. Miller and F. J. Kohl, Computer Programs for the Interpretation of Low-Resolution Mass Spectra: Program for Calculation of Molecular Isotopic Distribution and Program for Assignment of Molecular Formulas, National Aeronautics and Space Administration, Washington, DC, 1977, NASA Technical Memorandum X-3564.

8 S. R. Heller and G. W. A. Milne, EPA/NIH Mass Spectral Data Base, Supplement 1, 1980, U.S. Department of Commerce, Washington, DC, 1980, p. 5037.

9 J. P. Springer, B. H. Arison, J. M. Hirshfield and K. Hoogsteen, J. Am. Chem. Soc., 103 (1981) 4221.

10 G. Albers-Schonberg, B. H. Arison, J. C. Chabala, A. W. Douglas, P. Eskola, M. H. Fisher, A. Lusi, H. Mrozik, J. L. Smith and R. L. Tolman, J. Am. Chem. Soc., 103 (1981) 4216.

Analytica Chimica Acta, 174 (1985) 71—82
Elsevier Science Publishers B.V., Amsterdam — Printed in The Netherlands

COMPUTERIZED DYNAMIC VOLTAMMETRIC DETECTION IN HIGH-PERFORMANCE LIQUID CHROMATOGRAPHY
Part 1. On-line Cyclic Voltammetry of the Antineoplastic Agents Etoposide and Teniposide

H. H. J. L. PLOEGMAKERS* and M. J. M. MERTENS

Pharmaceutical Laboratory, State University of Utrecht, Catharijnesingel 60, 3511 GH Utrecht (The Netherlands)

W. J. VAN OORT

Licentec, Churchilllaan 11, 3527 GV Utrecht (The Netherlands)

(Received 23rd January 1985)

SUMMARY

An automatic, reliable, dynamic oxidative electrochemical detection system is described for on-line determination of electro-active compounds in effluents from high-performance liquid chromatographic systems. Detection can be done at constant potential or by using potential scans. The system consists of easily obtainable commercial hardware, combined with commonly available chromatographic apparatus. Special attention is given to automatic component detection, data storage in a Ramdisk, noise filtering, automatic half-wave potential calculation and a high-resolution paper copy of the voltammograms. The system is tested for Etoposide (VP 16-213) and Teniposide (VM 26).

High-performance liquid chromatography (h.p.l.c.) is one of the most powerful techniques in pharmaceutical analysis for the separation of less volatile compounds. For on-line detection, many methods are available, based on different physicochemical principles; during the last decade, electrochemical detection (e.c.d.) has been developed as a sensitive method, applicable for particular groups of compounds. The introduction of the glassy carbon electrode in electrochemical detection has simplified analysis for many organic and inorganic compounds on a routine basis. The combination of a deaerated flow stream and some kind of mercury electrode allows the determination of numerous compounds [1], but in practice more experience and insight is needed for routine, on-line determinations with mercury electrodes than with carbon electrodes.

In general, both modes of electrochemical detection can offer high sensitivity for suitable compounds. Selectivity depends on the structure of the compound(s) to be determined and of the interfering compounds in the sample. It can be influenced by selection of the measuring potential, but the most powerful qualitative part of the l.c./e.c.d. combination is still a well-optimized high-pressure chromatography column. When the separation

0003-2670/85/$03.30

power of the column is not high enough or when more qualitative information is needed, more sophisticated detection methods such as scanning—ultraviolet and mass spectrometric methods are required. With electrochemical detectors, if only minute amounts of sample are available, which prevents taking fractions of the eluent stream for off-line processing, methods are needed that produce more information about the compounds during their residence time in the detector compared with known methods such as constant-potential electrochemical detection.

Several electro-active drugs, like surprisingly many of the anticancer agents, are of particular interest for electrochemical investigations, because they need (enzymatic) oxidation or reduction for activation in vivo. The final active species in vivo is usually not the previously administered compound. The properties of the metabolites are of importance to elucidate the disposition and working pattern of the drugs. However, only minor amounts of sample (if any) are normally available from patients. In such situations, on-line electrochemical detection that offers more information than just the established concentration is again desirable. The result of such methods can be, for example, a compound-specific curve providing more information about the electrochemical properties of that particular compound [2, 3].

A flexible computerized combination of a liquid chromatographic system with a relatively easily-controlled detection system, provided with fast data-handling devices, can offer such information. The application of computerized on-line data handling can also contribute to lower systematic blank values, which are a standard problem in electrochemical detection whether in the dynamic or in the static mode. At high sensitivity levels, the method itself generates high capacity and base-line currents, exponentially varying with higher negative or positive potentials and dependent on experimental conditions. Attempts have been made to solve this problem, e.g., by using dual cells [4], but computerization can provide more elegant and practical solutions for routine analysis.

Various attempts have been reported to subtract blank solution currents from Faradaic currents [5—7] and to run on-line voltammetric determinations [8—11]. The computer systems described by these authors had random access memories (RAM) varying from 512 byte to 64 kbytes. Depending on the required resolution in potential and peak currents (1 or 2 bytes per measurement), one scan could consume 500—4000 bytes. Less favourable properties of these systems were the relatively low speeds of data storage (floppy disk) and data transport and the few options available to control the systems.

One aim of the present investigation was to use cheap and commercially available components, to enable pharmaceutical analysts without computer skills to combine the hardware described with existing and widely used electrochemical apparatus. After DA and AD converters have been combined with normal electrochemical equipment, the potentiostat can be controlled by a simple microcomputer to produce cyclic voltammetric curves, etc. The

automatic detection system presented is equipped with 320 kbytes of RAM memory. It stores data only when a compound enters the detector, performs parabolic noise filtering, calculates the half-wave potential when used in the d.c. mode and allows a hard-copy of the voltammograms to be made by a digital plotter afterwards.

The anticancer agent Etoposide (VP 16-213) was selected as a model compound, because it is a highly toxic drug that needs to be activated enzymatically by metabolism, probably through an oxidative process, and of which relatively little is known. Its electrochemical oxidative behaviour in vitro was described in detail recently [12]. For the determination of levels in blood plasma, selective and sensitive methods of analysis are available, based on separation systems for the drug and endogeneous compounds. In this paper, this compound is determined by electrochemical detection, on-line with h.p.l.c.; the method is based on the liquid chromatographic systems and the electrochemical detector developed by Holthuis et al. [13].

EXPERIMENTAL

Hardware requirements

The heart of the on-line data-acquisition system (Fig. 1) is a Basis 108 computer which is compatible with Apple-II. This computer has 128 kbytes of RAM, and is equipped with two 125-K Apple floppy-disk drives. This computer is combined with an Axlon 320-K Ramdisk, a 12-bit, 16-channel Digilog A/D converter, a 12-bit D/A converter (made by coupling a CCS-7720 parallel interface and an Analog Devices AD-DAC80 D/A converter), a CCS model 7424 real-time clock, an Itoh 8510 parallel printer with screen-

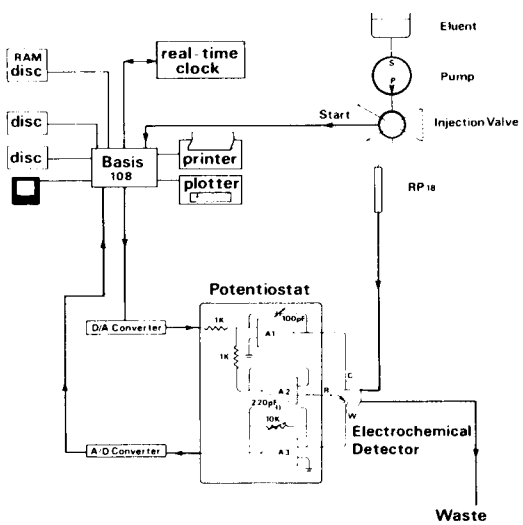

Fig. 1. Schematic diagram of the chromatographic, electrochemical and computer hardware system.

dump facility (Kronemuis APL-13 graphic printer interface), a Hewlett-Packard 7470A serial plotter and a Kipp and Zonen BD-40 *Y-t* recorder.

The computer system is connected to a Metrohm 641-VA detector and a homemade, electrochemical detector with central injection [13]. The cell consists of a glassy carbon working electrode (GCE; diameter 3 mm; Metrohm EA-286/1) placed in the centre of a platinum ring auxiliary electrode (10 mm i.d., 13 mm o.d.). The distance between the glassy carbon electrode and the jet can be adjusted by a micrometer on which the electrode is mounted. The effluent stream is directed perpendicularly to the surface of the glassy carbon electrode. An Ag/AgCl reference electrode with a Vycor glass-tipped jacket is placed close to the working and the auxiliary electrode. The diameter of the outlet jet for the effluent from the chromatographic system is 0.11 mm. The cell is submerged in a vessel containing the mobile phase.

The chromatographic system consists of a 510 solvent delivery system, a U6K septumless injector (both from Waters Associates) and a RP18 LiChrosorb analytical column (30 cm × 3.9 mm i.d.; 10 μm). The injector has a switch which is connected to the game-connector of the computer by means of a 74LS00 flip-flop debouncer.

Chemicals and samples

Etoposide (VP-16-213) and Teniposide (VM-26) were kindly supplied by Bristol Myers, The Netherlands. For the determination of Etoposide and Teniposide in pure solutions, the compounds were dissolved in methanol (p.a., Merck) to give concentrations of 0.5155 and 0.6268 mg ml^{-1}, respectively. The injection volume was 25 μl.

The mobile phase consists of methanol/0.020 M phosphate pH 7 buffer (55:45, w/w).

Software

The software consists of five programs written in Applesoft-BASIC, and several auxiliary programs written in 6502 machine language (Table 1). The software is available on disk from the authors at cost price.

The HPLC program runs a standard h.p.l.c./e.c.d. at constant potential. It controls the chromatographic system, investigates how many components are present in the mixture and establishes the retention times of these substances. The PARAMETER program allows the operator to enter parameters such as initial voltage, voltage range and scan speed for cyclic voltammetry; it converts these parameters to microprocessor-readable formats.

To provide insight into the time scale of the programs, an example of a calculation is presented. Given a voltage range of 1000 mV, the range is divided into 1000/(5000/4096) = 819 steps of 1.22 mV each. Given a scan rate of 1 V/3 s, this means that 1 step will take about 3.66 ms. After the potential has been changed, there is a delay of 2.67 ms. After the A/D conversion, which takes 0.03 ms, about 1 ms will remain to execute the machine-language routines and an additional delay is involved, which is necessary to synchro-

TABLE 1

Description of the functions of the programs

Language	Program name	Function
Applesoft BASIC	HPLC	H.p.l.c./e.c.d. at constant potential
Applesoft BASIC	PARAMETER	Parameters for cyclic voltammetry
6502 Assembly	BLANK	Measurements of blank solution
6502 Assembly	CLOCK	To reset and to start real-time clock
6502 Assembly	DUMMY	To stabilize GCE
6502 Assembly	THRESHOLD	Detection of passage of a compound through the detector
6502 Assembly	DETERMINATION	To run a cyclic voltammogram of a compound
Applesoft BASIC	PLOTTER	Display of voltammograms on screen and production of a paper copy
Applesoft BASIC	CALCULATION	To filter data and to calculate $E_{1/2}$
Applesoft BASIC	STATISTICS	To calculate standard deviation

nize all types of scans. After a cyclic voltammogram of the blank solution (mobile phase) has been done, the operator can enter a threshold value. From this threshold and the stored blank measurements, the program calculates the ultimate threshold values and stores these values into the memory.

The switch in the chromatographic injector is connected to the game-connector of the computer. The CLOCK program watches the value of address 49249 ($C061 hexadecimal) of the game-connector. A change in this value from 255 ($FF hexadecimal) to 127 ($7F hexadecimal) indicates that an injection has been made. Then the real-time clock is reset and the computer jumps to the DUMMY program to stabilize the GCE. After the working electrode has stabilized, the THRESHOLD program is run. This program compares the measurements obtained at certain potentials with the corresponding threshold values stored in the memory, automatically and on-line. If the current value passes the threshold value stored in the memory, the scan is completed and the DETERMINATION subroutine is executed. After the measuring scan has been completed, the data (including the retention time) are transferred to the Ramdisk and the computer jumps back to the THRESHOLD program.

If the analysis time is over, or the Ramdisk memory is full (which happens after 68 scans), the data are transferred from the Ramdisk memory to a floppy disk and the PLOTTER program for selection and plot is run. After the cyclic voltammograms have been displayed and hard copies of the most suitable scans have been made by the PLOTTER program, the CALCULATION program is run. This program contains a filter section, a first-derivative section and a drawing/calculating section. It calculates automatically the

inflection point of the cyclic voltammogram (see below for explanation of the curve shape) from its first derivative, and then the program establishes the beginning and end of each peak in the voltammetric derivative curve. From both points, the normal voltammetric curve is extrapolated in a horizontal direction. A line through the inflection point is also drawn. From the point of intersection of that line and the upper extrapolated line, a perpendicular line is drawn. The distance between the points of intersection of the perpendicular and the two extrapolated lines is divided into two equal parts. Through the middle, a line parallel to the lower extrapolated line is constructed. The point of intersection of that line and the voltammetric curve is calculated, giving the half-wave potential.

RESULTS AND DISCUSSION

H.p.l.c./e.c.d. at constant potential

Comparison of the described digital system in the constant-potential mode with a l.c./e.c.d. system equipped with a *Y-t* recorder showed that the systems were equivalent to each other in terms of stability, reproducibility and sensitivity. Figure 2 shows a chromatogram with electrochemical detection at constant potential obtained from the digital system described. The retention times of Etoposide and Teniposide are 4.5 and 7.0 min, respectively.

H.p.l.c./e.c.d. in the cyclic voltammetric mode

During preliminary measurements with the digital system in the cyclic voltammetric mode, various problems arose, which are inherent to the use of (micro)computers. These problems will be discussed successively.

Current spikes caused by the D/A converter. Each time the THRESHOLD program was run, the computer jumped to the DETERMINATION program even when no compound passed the detector. The program functioned

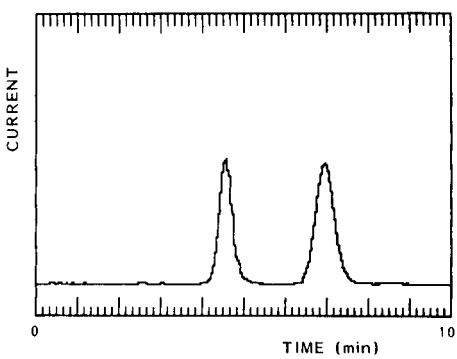

Fig. 2. Chromatogram of Etoposide (VP 16-213) and Teniposide (VM 26) with retention times of 4.5 min and 7.0 min, respectively. Conditions: current range, 0.5 μA full scale; 13 μg and 15 μg injected, respectively; mobile phase, methanol/0.020 M phosphate buffer pH 7 (55:45 w/w); LiChrosorb RP-18 column; 1 ml min^{-1} flow rate; potential, +800 mV vs. Ag/AgCl (3 M KCl).

properly only when the threshold value was very high (>2200 mV). It became clear that peaks in the pilot voltage were being generated by the D/A converter. The D/A converter receives its data from two addresses; whenever the D/A output has to be changed, first the low-byte address content is transferred to the converter and then the high-byte address content. Between these changes, the converter output suffers a glitch (an undefined value). The solution to this problem consists of inserting two 8-bit latches (74LS373) between the 6821 peripheral interface adapter (PIA) and the inputs to the D/A converter. The two bytes are placed successively into the latches and are transferred simultaneously to the converter by triggering the enable input of the 74LS373 by a TTL output of the game connector.

Noise filtering. The filtering of random noise is a problem for many analytical methods. Application of passive or active low-pass filters has disadvantages such as over- or under-critical damping. The methods presented here offer the possibility of filtering and checking the remaining noise level as often as needed. There are several filter possibilities [14]. The moving average technique has the disadvantage that each measurement in sets of ten contribute equally to the result. The symmetrical triangular function has the advantage of weighting of measurements within sets, but the symmetrical parabolic function is still better. In the actual scan, although eight measurements were averaged at each potential and although the A/D converter is equipped with a low-pass filter, the noise level is still too high to obtain a smoothed first derivative (Fig. 3a) and normal voltammetric curve. The filter, applied in this investigation, is a so-called 11-point symmetrical parabolic filter [15]; here, parabolic means that successive measurements around a particular measurement are multiplied by the respective coefficients 0.074, 0.111, 0.182, 0.333, 0.666, 1.00, 0.666, 0.333, 0.182, 0.111, 0.074. The calculations are similar to the triangular filter, the sum of the multiplications being divided by the sum of the coefficients.

The advantage of this method compared with the symmetrical triangular filter is that the curves conserve their original form, because there is less contribution to the result from points some distance away from the measured point. Figure 3(a—d) shows the effect of the symmetrical parabolic filter on the voltammetric curve and its first derivative after the program has been applied 0, 1, 2 and 3 times. Because the program simply uses a two-dimensional array, it is applicable for all kinds of slow and fast measurements.

Hysteresis of the glassy carbon electrode. Originally, when a compound was detected during the THRESHOLD program, the computer jumped immediately to the DETERMINATION subroutine. In practice, however, the glassy carbon electrode was not fast enough to follow these potential changes; this resulted in large, short-term capacity currents. In the final system, the scan is not interrupted but continued until the initial voltage has been achieved. At this moment, the computer jumps to the DETERMINATION program and produces the definite cyclic voltammogram.

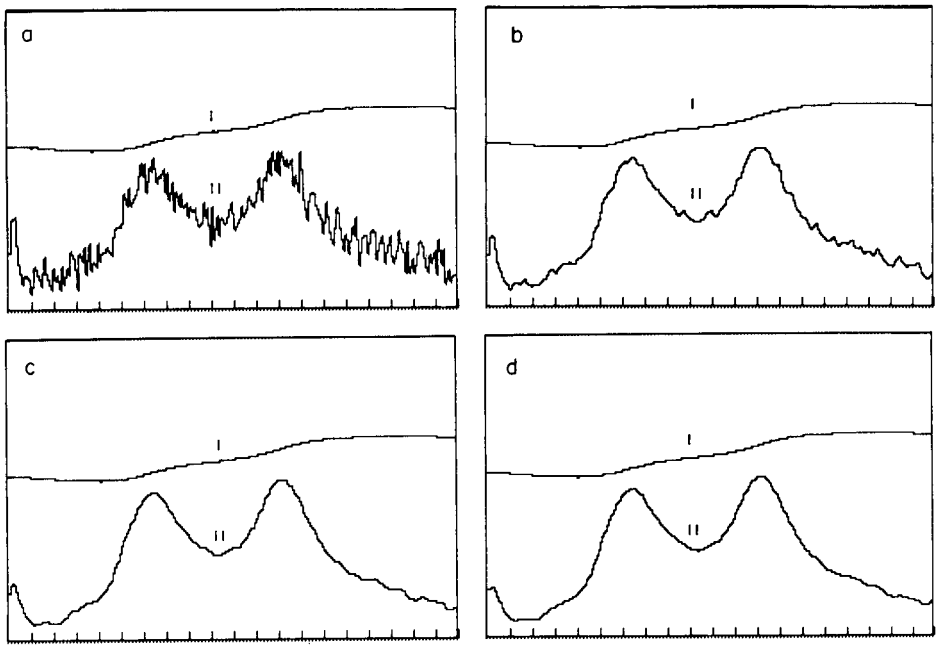

Fig. 3. The influence of repetitive parabolic filtering on d.c. curves (I) and first derivative curves (II) of an on-line linear-sweep voltammogram of 13 μg of Etoposide (VP 16-213): (a) filtered; (b) filtered 1×; (c) filtered 2×; (d) filtered 3×.

Similar problems can exist in the first scan; in this case, the DUMMY program is run to stabilize the GCE.

The voltammetric curve

One of the striking differences between cyclic voltammograms obtained with the dynamic electrochemical system and those obtained with a static system, is the wave form. On-line oxidative voltammograms do not show peaks, but have forms closely resembling d.c. waves as shown in Fig. 4(a, b). These waves are due to the continuous transport of electro-active material towards the working electrode by the flow stream. Accordingly, the diffusion layer is not exhausted in this time scale and no peaks appear, in contrast to batch-wise voltammetry at solid electrodes.

The geometry of the working electrode in the detector cell greatly improves the problem of contamination by adsorbing lipophilic compounds [13]. This was proved by the high reproducibility obtained for a large series of successive injections.

In on-line linear-sweep voltammetry at the GCE, Etoposide and Teniposide show two oxidative waves. For Etoposide, the first wave appears at 333 mV (n = 5, s.d. = 2 mV) and the second at 660 mV (n = 5, s.d. = 2 mV). For Teniposide, the first wave appears at 278 mV (n = 5, s.d. = 4 mV) and the second at 565 mV (n = 5, s.d. = 6 mV). All potentials were measured at pH 7

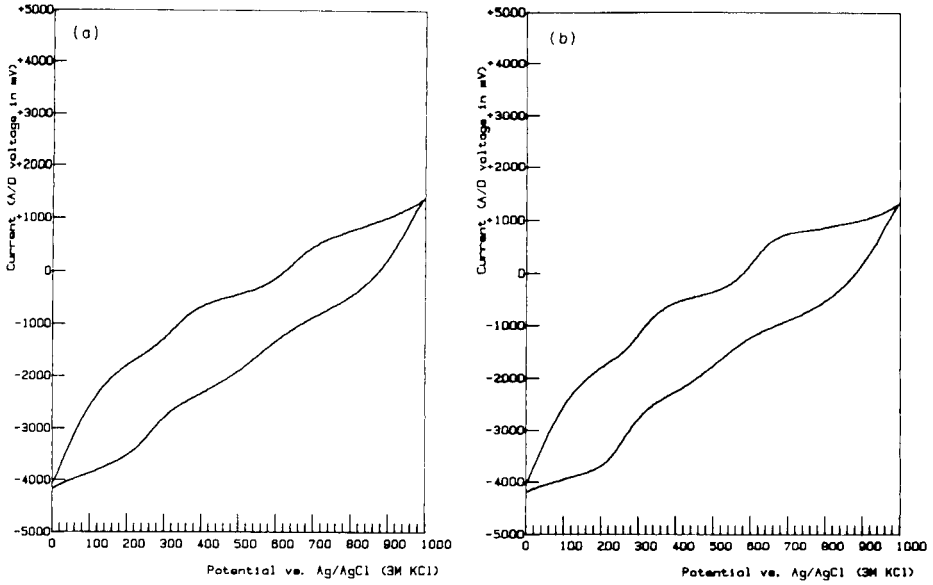

Fig. 4. On-line cyclic voltammograms: (a) 13 μg of Etoposide (VP 16-213); (b) 15 μg of Teniposide (VM 26). Conditions: current range 0.5 μA (×9/10), flow rate 1 ml min^{-1}, scan speed 300 mV s^{-1}.

in a 0.020 M phosphate buffer vs. an Ag/AgCl (3M KCl) electrode. Because there is probably no Nernstian equilibrium in flow systems, the term "$E_{1/2}$" is used here to distinguish it from the conventional half-wave potential, $E_{1/2}$, in classical d.c. polarography. In batch systems, two peaks are observed in solutions of Etoposide of the same pH with the same buffer at the same electrodes (E_{p1} = +370 mV, E_{p2} = +690 mV). This voltammetric activity is caused by oxidation of the phenolic hydroxyl group, which proved to be a two-step, two-electron process in the medium pH range [12].

Under normal h.p.l.c. conditions (flow rate 1 ml min^{-1}), the compound is present in the detector cell for 60 s. The intention of the dynamic electrochemical detection is to obtain appropriate qualitative information about the compound and to give certainty about the number of components in a chromatographic peak. For this purpose, it is necessary to scan at least six times during those sixty seconds (twice on the rising slope, twice at the top and twice on the descending slope). To obtain a fair resolution between the voltammetric waves, the rise of the potential during each program cycle has to be small. Because of this limitation, such a cycle may not take more than several milliseconds. Based on these conditions, the time scale does not allow a wait of 3.6 ms after each step (in contrast to differential pulse voltammetry, which allows delays of 33 ms) until the capacity current has decreased. This involves intrinsic high capacity currents (blank values) under these circumstances.

"Half-wave potential" calculations

Table 2 shows a comparison between the manual "$E_{1/2}$" estimation and the results of the off-line CALCULATION program. Because the program is written in BASIC and the filter section applies 2-dimensional arrays, the calculation takes 5 min. It is clear that the CALCULATION program performs satisfactorily.

Comparison with the batch method

Comparison with respect to scan speed, sensitivity and reproducibility, between this computerized h.p.l.c. system, the classical batch-wise voltammetry system and computerized batch-wise voltammetry shows that there are several differences. In the classical system, the XY recorder is coupled directly to the voltage-ramp generator of the polarograph; the scan speed is limited to about 500 mV s^{-1} by the mechanical possibilities of the recorder. In computerized systems, the data are stored during the scan; after the scan, the data are recalled from memory and plotted at any required rate. The limitation in this method is the speed of the machine-language program (3000 mV s^{-1}), and the limitations of fast scans at solid electrodes, which are generally hampered by large residual capacity currents.

Because the batch mode and the h.p.l.c. mode are so different, it is hard to compare the sensitivities of the several methods. In all cases, however, the sensitivity is limited by the capacity current: in the normal batch mode, the offset of the polarograph and the recorder may be inadequate; in computerized systems, the A/D converter will be overloaded and all measurements will be equal, i.e., 4095 ($FFF Hex). The concentration limit and the absolute mass limit have not so far been optimized but are about 4×10^{-5} mol l^{-1} and 10 μg, respectively. Although a computerized automatic scanning detector in a flow system is probably more prone to error than a batch system, the stan-

TABLE 2

Calculations of "$E_{1/2}$" of Etoposide (13 μg) and Teniposide (15 μg) at pH 7, from 5 successive injections. Chromatographic system: methanol/0.020 M phosphate buffer pH 7 (55:45, w/w) at 1 ml min^{-1} with a LiChrosorb RP18 column (N 4.4% = 3950)

"$E_{1/2}$" for Etoposide (mV vs. Ag/AgCl/3M KCl)				"$E_{1/2}$" for Teniposide (mV vs. Ag/AgCl/3M KCl)			
Calculated by computer		Manually constructed		Calculated by computer		Manually constructed	
Wave 1	Wave 2	Wave 1	Wave 2	Wave 1	Wave 2	Wave 1	Wave 2
334	656	325	650	276	559	300	560
334	661	335	660	281	559	285	560
334	661	335	665	285	568	290	570
329	661	330	660	276	573	285	570
334	661	335	660	276	568	280	570

dard deviation of the "$E_{1/2}$" calculations in the flow system is in the range 0.2—0.6% whereas that for the batch system was 0.2%.

Any A/D converter induces noise, thus the noise level in computerized measurements is always higher than in analog systems, even when an analog low-pass filter is used. Application of a digital filter program and an averaging technique, however, reduced the noise considerably. This makes the computerized system superior to the analog system in this respect. Only the computerized system can measure automatically, store the measured data and subtract blank solution measurements, and handle data. The limitations of the system are the input range of the A/D converter (—5 V → +5 V) and the amplitude of the capacity current.

Conclusions

The preliminary low-cost system described in this paper, although not yet optimized for all parameters, has several promising properties compared with systems described earlier [5—11]. The h.p.l.c. system with electrochemical detection at constant potential shows similar sensitivity and reproducibility as earlier analogous systems. In the present system with dynamic electrochemical detection, there are some new and attractive features. The system monitors the input signal on screen continuously, thus avoiding the need for an oscilloscope. The automatic detection system, insensitive to noise smaller than a preset threshold value, makes it possible to scan for 20 min (or longer) over a potential range of 1000 mV with increments of 1.22 mV, without storing any unwanted data. If a compound has been detected during its residence in the detector cell, usually 9 scans are run and stored; in this way, it should be possible to detect whether the peak consists of one or more components.

The use of the Ramdisk makes it possible to store 68 scans, each of which is accompanied by its retention time and can have the blank subtracted. Because transfer of data, and storage in the Ramdisk is programmed in machine language, there is no delay between scans. This is the main advantage over floppy-disk storage systems. The PLOTTER program provides a high-resolution paper copy.

Because all curves are transferred from the Ramdisk to a floppy disk, the CALCULATION program offers the possibility of calculating automatically the "half-wave potential" at any time (e.g., at night). This program also makes it possible to filter and to examine the remaining noise level, as many times as required.

The system has been optimized for reliability, ease of operation, simplicity, speed and data-storage volume; less attention has been paid to sensitivity and the most favourable pilot voltage. Of course, some parameters need further investigation, e.g., the large capacity current can overload the potentiostat and the analog/digital converter at increased sensitivity. It may be reduced by using smaller glassy carbon electrodes [16], lower scan rates, higher flow rates, etc. These features and several practical applications in pharmaceutical analysis are now under investigation.

We thank Prof. Dr. W. E. van der Linden and Dr. M. T. Bos (Technical University of Twente), Dr. J. J. M. Holthuis (Pharmaceutical Laboratory, State University of Utrecht) and Mr. H. Erkelens (Analytical Chemical Laboratory, State University of Utrecht) for their constructive contributions and advice.

REFERENCES

1 W. Kemula, in P. Zuman and I. M. Kolthoff (Eds.), Progress in Polarography, Interscience, New York, 1962, Vol. 2, 397.
2 J. Wang and H. D. Dewald, Anal. Chim. Acta, 153 (1983) 325.
3 N. Thørgersen, J. Janata and J. Růžička, Anal. Chem., 55 (1983) 1986.
4 A. M. Bond, in Modern Polarographic Methods in Analytical Chemistry, Marcel Dekker, New York, 1980, 157.
5 R. Samuelsson, J. O'Dea and J. Osteryoung, Anal. Chem., 52 (1980) 2215.
6 W. Lowry Caudill, A. G. Ewing, S. Jones and R. M. Wightman, Anal. Chem., 55 (1983) 1877.
7 T. A. Last, Anal. Chem., 55 (1983) 1509.
8 J. E. Anderson, A. M. Bond, I. D. Heritage, R. D. Jones and G. G. Wallace, Anal. Chem., 54 (1982) 1702.
9 A. M. Bond and R. D. Jones, Anal. Chim. Acta, 152 (1983) 13.
10 A. M. Bond and G. G. Wallace, Anal. Chem., 55 (1983) 718.
11 P. A. Reardon, G. E. O'Brien and P. E. Sturrock, Anal. Chim. Acta, 162 (1984) 175.
12 J. J. M. Holthuis, P. Zuman, F. M. G. M. Römkens, J. Renema and W. J. van Oort, J. Electroanal. Chem. Interfacial Electrochem., 000 (1985) 000.
13 J. J. M. Holthuis, F. M. G. M. Römkens, H. M. Pinedo and W. J. van Oort, J. Pharm. Biomed. Anal., 1 (1983) 89.
14 A. Savitzky and M. J. E. Golay, Anal. Chem., 36 (1964) 1627.
15 J. A. Titus, C. A. Titus and D. G. Larsen, TRS-80 Interfacing, Howard W. Sams, Indianapolis, 1981.
16 L. A. Knecht, E. J. Guthrie and J. W. Jorgenson, Anal. Chem., 56 (1984) 479.

Analytica Chimica Acta, 174 (1985) 83—94
Elsevier Science Publishers B.V., Amsterdam — Printed in The Netherlands

LANGMUIR—BLODGETT FILM CHARACTERISTICS AND PHOSPHOLIPID MEMBRANE ION CONDUCTION
Part 1. Modification by Cholesterol and Oxidized Derivatives

U. J. KRULL, MICHAEL THOMPSON*, E. T. VANDENBERG and H. E. WONG

Department of Chemistry, University of Toronto, 80 St. George Street, Toronto, Ontario M5S 1A1 (Canada)

(Received 12th February 1985)

SUMMARY

The energy barrier to inorganic ion conduction through bilayer lipid membranes (BLM) is investigated as a function of molecular packing and dipolar potential characteristics. Arrhenius energy barrier information is derived from temperature-dependent electrochemical experiments with phosphatidyl choline/steroid BLM. The steroids studied at 0.65 mole fraction in phospholipid were 5-cholesten-3β-ol, 5,7-cholestadien-3β-ol, 5-cholesten-3β,7α-diol, 5α-cholestan-3β,5α,6β-triol, 5α-cholestan-5α,6α-epoxy-3β-ol, 5-cholesten-3β-ol-7-one and 5α-cholestan-3-one. Correlation of the barrier magnitude with molecular packing characteristics, obtained by collecting monolayer data from a Langmuir—Blodgett trough, indicates that the BLM ion current is almost completely controlled by molecular density. The sensitivity of the energy barrier as a function of molecular packing is as great as 0.1 eV for a 0.01-nm^2 adjustment.

Mechanisms of inorganic ion conduction through natural and artificial cell membranes have been the subject of intense research for many years. In biological systems, the two major routes for membrane ion conduction appear to be facilitated transport by complexation of ions in mobile hydrophobic carrier molecules, or fixed pores or channels. Such protein or polypeptide-based pathways are apparently often coupled in natural systems with selective "gating" molecules, resulting in chemically moderated ion-transport systems suitable for control of many distinct biochemical processes. An interesting feature of artificial membranes employed as models of natural structures, such as the bilayer lipid membrane (BLM), is that significant ion conduction can be established under physiological conditions in the absence of proteinaceous membrane-modifying structures. This feature is significant in the understanding of natural ion-conductive processes, but more importantly, selective "gating" molecules can be used for control of BLM ion current, indicating potential for development of a novel form of electrochemically-based biosensor [1].

The premise of operation of natural sensory membranes begins with a chemoreceptive-selective binding event at the surface, which causes increased ion conduction through the membrane. The BLM has been investigated as a

0003-2670/85/$03.30

selective biochemical transducer by incorporation of "receptor" proteins into the BLM structure. Selective binding systems which have proved capable of generating analytical signals as an increased transmembrane ion current include enzyme-substrate, antibody-antigen-complement, lectin-saccharide and hormone-receptor complementary pairs [1, 2]. The development of a useful transducer requires an understanding of the mechanism of signal generation, which in this case is associated with parameters such as membrane-external aqueous ion concentration and applied potentials external to the membrane, and the fluidity, thickness, dielectric constant, formal surface charge and surface dipolar potentials of the membrane.

Apparently two physical parameters, described herein as the dipolar potential and fluidity/packing characteristics, are the major features responsible for transmembrane ion-current moderation. The BLM consists of closely-packed ordered lipid molecules which contain dipolar species responsible for a net molecular dipole moment. An anisotropic membrane organization results in the creation of planes of dipolar charge, which act as electrostatic fields controlling transmembrane ion current, and represents a static situation which can be perturbed to generate analytical signals. In the absence of formal surface-charge action, alteration of dipolar potential by the receptor-stimulant complex, through lipid headgroup perturbation, receptor-complex contributions and/or dipole realignment, offers a possible mechanism for signal generation. This mechanism can be associated entirely with reduction of the electrical potential energy barrier to ion current in the absence of formal transmembrane pores or ion-carrier complexes. A second feature expected to be significant for control of ion current is related to the physical/chemical potential energy barrier referred to as molecular fluidity/packing. In this case transmembrane diffusion of ions in the absence of protein-based conduction mechanisms is intimately associated with the interactions of lipid molecules. The relative significance of the two major physical parameters must be established in order to develop transducers based on selective receptor-stimulant complexation.

The total potential energy barrier to BLM ion current can be estimated experimentally from electrochemical current dependence on temperature, resulting in a measurement of the Arrhenius energy barrier [3]. Additional information about intermolecular association in the form of the average molecular area at known surface pressure can be established by use of Langmuir—Blodgett thin-film trough compression techniques. This work correlates these two experimental methods and demonstrates that there is a very sensitive relationship between molecular packing and the Arrhenius energy barrier, indicating important ramifications for interpretation of natural receptor and anaesthetic activity, and development of BLM transducers.

EXPERIMENTAL

Materials and equipment

The phospholipid used was lyophilized egg phosphatidyl choline (PC; Avanti Biochemicals, Birmingham, AL). The steroids used were 5-cholesten-3β-ol, 5,7-cholestadien-3β-ol, 5-cholesten-3β,7α-diol, 5α-cholestan-3β,5α,6β-triol, 5α-cholestan-5α,6α-epoxy-3β-ol, 5-cholesten-3β-ol-7-one, and 5α-cholestan-3-one (Research Plus, Bayonne, NJ). Methylation of phosphatidyl choline for capillary gas chromatography involved the use of sodium methoxide freshly prepared from sodium in dry methanol. All other chemicals were of reagent-grade quality.

The BLM support housing consisted of two clamped identical perspex half-cells separated by a thin teflon sheet (0.1 mm thick) containing a circular aperture (1 mm diameter) in which the BLM was formed. An external +25 mV d.c. potential was applied across the membrane between two Ag/AgCl reference electrodes (Orion Research) extended with agar salt bridges. The external circuitry consisted of a power supply and a microprocessor-controlled multichannel digital electrometer (Keithley System 1, Keithley Instruments) for data acquisition. The solution cell and sensitive electronic equipment were isolated in a grounded Faraday cage. An infrared heat source provides elevated temperatures, as required.

A high-resolution capillary gas chromatograph was used to determine the extent of phosphatidyl choline/steroid oxidation to ensure the invariability of the membrane chemistry. A Durabond fused silica column (30 m × 0.25 mm i.d.) with a 0.25-μm DB-1 coating and a practical efficiency of 10^5 plates (J and W Scientific, Rancho Cordova, CA) was used with a standard flame ionization detector.

The Langmuir—Blodgett thin-film trough used was a Lauda film balance Type 1974 (Sybron-Brinkmann, Toronto, Canada).

Procedures

The mixture used for BLM formation consisted of 20 mg of phosphatidyl choline and 20 mg of steroid in 1 ml of dry n-decane. The mixture was introduced into the aperture between the two solution compartments containing 0.1 M potassium chloride by means of a fine sable hair brush. Membrane formation occurred spontaneously and was monitored by surface optical reflectivity and electrical properties. After stabilization, the infrared source was activated and the transmembrane current was measured as a function of temperature. The temperature range investigated was 21—35°C, increased at ca. 0.5°C min^{-1}. All BLM-forming solutions were investigated at least four times to establish reproducibility.

All phosphatidyl choline/steroid solutions in hydrocarbon were analyzed by capillary gas chromatography after base-catalyzed lipid transmethylation before being used in trough and electrochemical experiments. Samples containing 1—10 mg of phosphatidyl choline and steroid were treated for

15 min at room temperature with a solution of 1 ml of freshly prepared 0.5 M sodium methoxide and 1 ml of dry benzene. The mixtures were extracted with 3 ml of diethyl ether, which was washed twice with 3 ml of 1 M sodium chloride, dried and concentrated before injection into the chromatograph. Temperature programming allowed separation of lipid methylate and all steroids [4].

For the trough experiments, approximately 2 mg of phosphatidyl choline and 2 mg of steroid were dissolved in 5 ml of hexane. If the preparation of homogeneous solutions was difficult (as for the diol and triol steroids), little chloroform was added as secondary solvent. After ultrasound treatment to ensure homogeneous dispersion, about 100 μl of solution was slowly added to the pure water or 0.1 M KCl subphase in the trough from a syringe. At least ten minutes then elapsed to ensure complete removal of the volatile solvent before compression experiments were initiated. Compression was done slowly to allow proper intermolecular equilibration on the aqueous surface. The system was calibrated so that the output directly provided average molecular area and pressure data. Each sample solution was investigated for compression characteristics at least four times to establish reproducibility. Experiments at elevated temperature utilized the internal circulating system provided in the Lauda instrument, and an external pump assembly.

RESULTS AND DISCUSSION

Remarkable alterations of residual ion current through BLM were observed as a result of phospholipid/cholesterol oxidation (Fig. 1). The two major zones of the membrane affected by the oxidation process are the surface

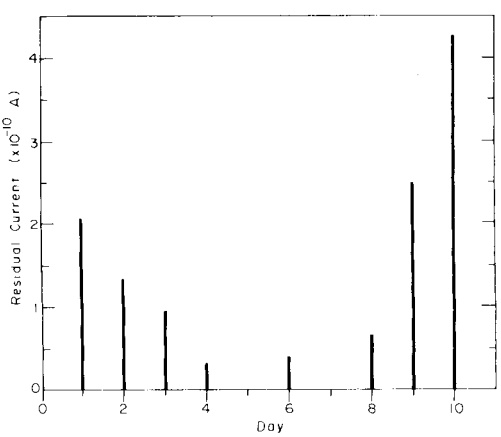

Fig. 1. Relationship of BLM ion current to age of PC/cholesterol BLM-forming mixture in decane.

headgroup zone, because of oxidation of the steroid nucleus, and the hydrocarbon zone, because of the injection of polar sites at the unsaturated positions of the acyl chains of phosphatidyl choline. These effects will combine dipolar modification, caused by increased average molecular polarity, with reduced packing and increased fluidity, arising from internal polar repulsion in the membrane.

These results indicated the need to isolate the influence of the steroid from any effects associated with phospholipid oxidation. In this respect, the doping of phosphatidyl choline membranes with cholesterol and its autooxidation products offers a useful means for internal modification of membrane parameters such as surface dipole potential and molecular packing [5—10]. In the present work, the various steroids (Fig. 2) were incorporated to identical 0.65 mole fractions in phosphatidyl choline BLM for electrochemical estimation of the energy barrier to ion conduction. Experiments were done at various temperatures and the Arrhenius equation $I_T = I_0 \exp(-eQ/kT)$, where I represents ion current, e is standard charge, Q the potential energy barrier and kT the usual Boltzman factor, was applied. The values obtained are given in Table 1. All curves used in the analysis had to be linear over at least four celsius degrees before data were considered acceptable, but most plots showed substantially better characteristics over the small temperature range investigated (22—32°C). The range of standard deviations is wide for the measured potentials in Table 1. The major causes of these variations are discrepancies of thickness and area of individual BLM; these parameters are not readily controlled in the membrane formation technique. The chemistry of the lipid steroid moieties was carefully monitored with capillary gas chromatography to ensure that species variability was not a significant source of error.

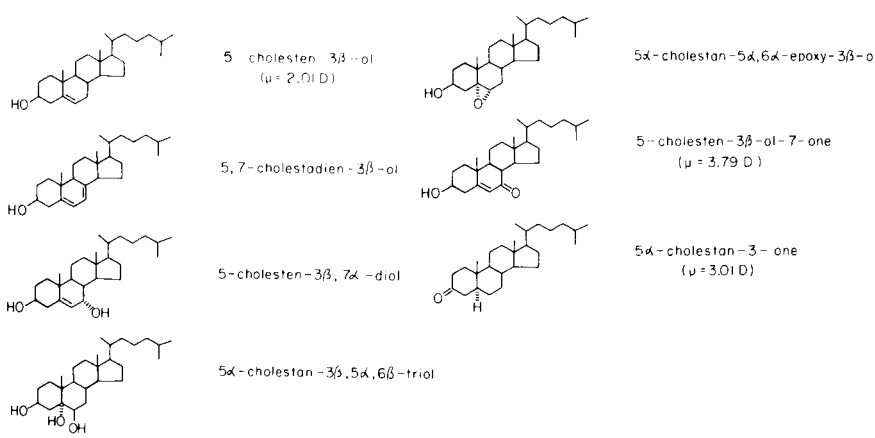

Fig. 2. Structures of the steroids employed for monolayer/bilayer experiments. The significance of the dipole moments is explained in the text.

TABLE 1

Arrhenius potential energy barrier from phosphatidyl choline/steroid BLM electrochemistry

BLM steroid	Barrier (eV)	BLM steroid	Barrier (eV)
5-Cholesten-3β-ol (cholesterol)	1.18 ± 0.03	5α-Cholestan-5α,6α-epoxy-3β-ol (epoxy)	0.35 ± 0.04
5,7-Cholestadien-3β-ol (diene)	0.80 ± 0.25	5-Cholesten-3β-ol-7-one (7-one)	0.63 ± 0.04
5-Cholesten-3β,7α-diol (diol)	irreproducible	5α-Cholestan-3-one (3-one)	0.19 ± 0.02
5α-Cholestan-3β,5α,6β-triol (triol)	0.49 ± 0.16		

Table 1 shows clearly that there is a significant variation in the potential energy barrier for the steroids studied. In view of the 1000-meV range between extremes, and the contribution expected from the electrostatic dipolar field of some 600 meV, it is apparent that the steroid molecules influence some important parameter other than the dipole potential at the membrane surface.

Because molecular fluidity/packing characteristics represent a second physical feature of importance in controlling transmembrane ion current in BLM, a correlation of changes in molecular packing with the steroids was attempted. The representative compression curves for various phosphatidyl choline/steroid mixtures shown in Fig. 3 demonstrate the conventionally-designated zones of loose association, partial condensation, complete condensation and collapse. The variability in the shapes of pressure/area isotherms is not completely understood, though it is accepted that the observed trends are representative of intermolecular packing characteristics which result in profiles reflecting the existence of phase transitions as discontinuities [11—14]. Information can be derived from the isotherms by observation of the collapse pressure (i.e., the maximum compression pressure withstood by the monolayer). Until the collapse point is reached under compression, lipid molecules are stabilized by hydrophobic acyl chain interactions and electrostatic interactions in the headgroup zone. At the collapse point, molecular repulsion supersedes attractive forces, creating an energetically unfavourable situation, and lipids slip out of the plane of the monolayer resulting in multilayer and island production. The collapse pressures listed in Table 2, which summarizes the data in Fig. 3, were measured at the inflection point preceding the maximum pressure attained for the complete condensation curve.

The molecular area measured at the collapse pressure is significant because it represents the smallest average area that a molecule in a monolayer can occupy. However, overcompression of a monolayer is possible because

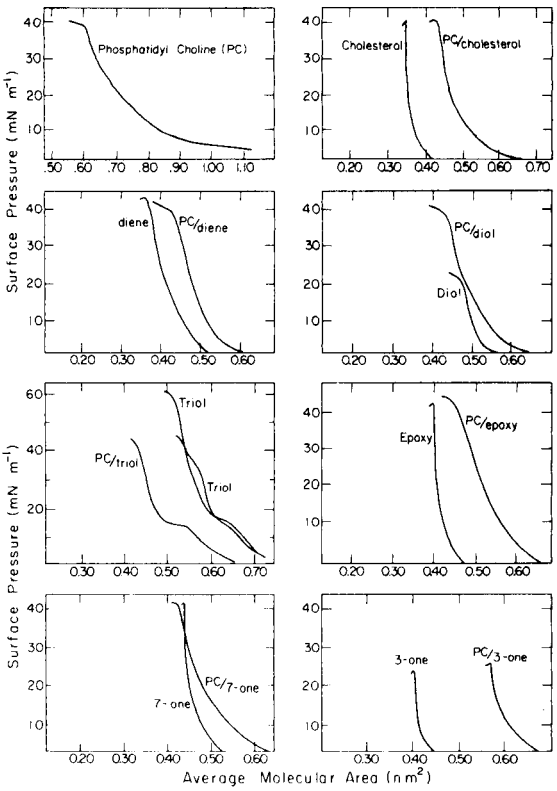

Fig. 3. Pressure/area isotherms collected for steroid and phosphatidyl choline/steroid mixtures over water at 21 ± 1°C. All PC/steroid mixtures contained equal weights of PC and steroid. Abbreviations are as listed in Table 1.

collapse is very sensitive to defects in the organized monolayer [11]. Particularly for very pure lipids which have no defects suitable for initiating monolayer disruption, the compression curves may develop a pressure maximum after the collapse is initiated because of subsequent relaxation processes. The above results indicate that cholesterol was the only lipid to generate a significant pressure maximum, though the other steroids exhibited slight pressure drops after collapse. The phosphatidyl choline/steroid curves all reached a plateau of pressure, discounting the likelihood that overcompression had occurred. To eliminate the possibility of extracting incorrect results from the non-equilibrium situation existing at the collapse point, data were also collected at 16 and 32 mN m^{-1} (Table 2). The results were reproducible for any one series of compression curves obtained from a particular phosphatidyl choline/steroid solution (standard deviations 0.01—0.015 nm^2). However, some experiments yielded substantial variation in results obtained for different phosphatidyl choline/steroid solutions which were prepared in apparently identical fashion. This phenomenon, which may

TABLE 2

Summary of monolayer results for steroid and PC/steroid films

Monolayer	Collapse pressure ($mN\ m^{-1}$)	Molecular area (nm^2) at various pressures		
		Collapse	32 $mN\ m^{-1}$	16 $mN\ m^{-1}$
Cholesterol	41.2 ± 1.9	0.367 ± 0.003	0.376 ± 0.001	0.392 ± 0.002
PC/cholesterol	43.0 ± 0.7	0.456 ± 0.010	0.472 ± 0.009	0.497 ± 0.006
Diene	44.5 ± 1.1	0.360 ± 0.020	0.371 ± 0.020	0.424 ± 0.010
PC/diene	41.6 ± 1.5	0.401 ± 0.055	0.430 ± 0.057	0.485 ± 0.048
Diol	20.1 ± 0.9	0.484 ± 0.001	—	0.492 ± 0.002
PC/diol	43.0 ± 0.7	0.410 ± 0.007	0.451 ± 0.008	0.566 ± 0.018
Triol	43.2 ± 1.8	0.447 ± 0.011	0.500 ± 0.004	0.583 ± 0.050
PC/triol	43.9 ± 2.2	0.411 ± 0.015	0.451 ± 0.018	0.539 ± 0.005
Epoxy	46.1 ± 0.7	0.389 ± 0.002	0.397 ± 0.001	0.408 ± 0.001
PC/epoxy	44.1 ± 0.6	0.446 ± 0.020	0.468 ± 0.017	0.523 ± 0.034
7-One	43.2 ± 1.3	0.427 ± 0.013	0.437 ± 0.014	0.467 ± 0.009
PC/7-one	44.6 ± 0.7	0.410 ± 0.008	0.435 ± 0.010	0.491 ± 0.014
3-One	23.9 ± 0.6	0.415 ± 0.023	—	0.427 ± 0.023
PC/3-one	26.2 ± 1.5	0.528 ± 0.028	—	0.569 ± 0.025
Phosphatidyl choline	43.1 ± 0.6	0.617 ± 0.045	0.707 ± 0.062	0.868 ± 0.053

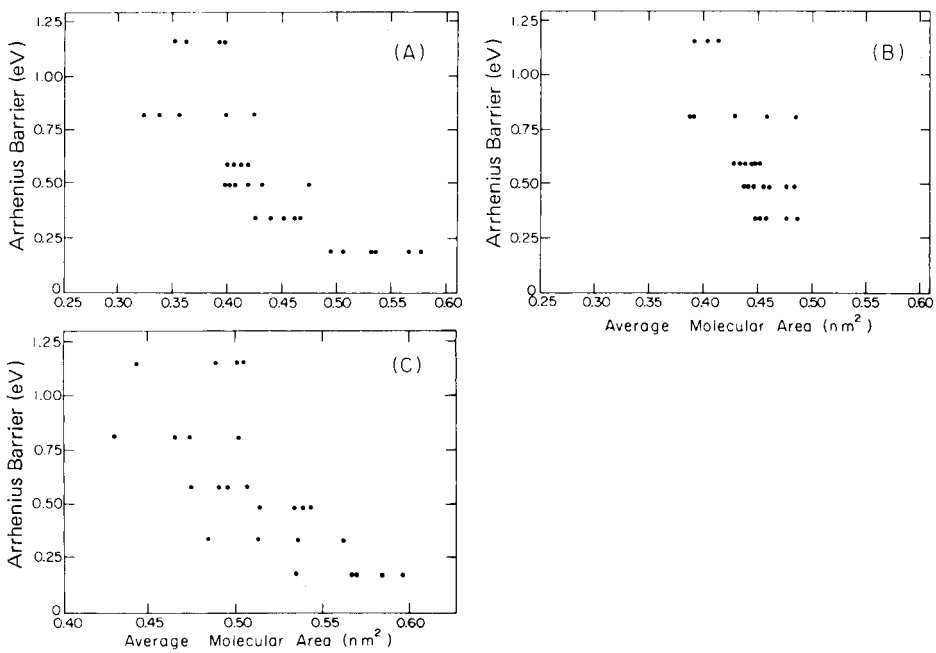

Fig. 4. Correlation of monolayer average molecular areas (in nm^2) with the Arrhenius potentials (in eV) derived from BLM experiments: (A) molecular area determined at the monolayer collapse point; (B) molecular area determined at 32 $mN\ m^{-1}$; (C) molecular area determined at 16 $mN\ m^{-1}$. Each data point represents the mean value of a minimum of four BLM electrochemical results.

be caused by impurities associated with oxidation, has been noted before in compression experiments, even for pure phosphatidyl choline [15].

A correlation of the electrochemical results and the monolayer trough work (Fig. 4) shows that a direct relationship exists between average molecular area and Arrhenius energy barrier, although deviations occur at low area because of finite molecular size, and at maximum area because of membrane dissociation. The maximum sensitivity in energy barrier of the membrane to variations in molecular area was observed to be as high as 0.1 eV for 0.01 nm^2. There are two potential sources of concern regarding the validity of these results. First, electrolyte was used in all electrochemical experiments whereas a pure water subphase was used in the trough; replacement of the water in the trough with electrolyte altered the shape of the compression curve in the molecular loose-association zone, but left the maximum compression point unchanged. Secondly, it can be argued that the basic premise for the electrochemical experiments is false because the temperature ramp not only provides Arrhenius data but may also induce concurrent fluidity/packing alterations. The problem must be evaluated from the standpoint of the relative magnitude of such an effect which is of the order of 0.01 nm^2 for a 4°C change in the 22—28°C range normally used for Arrhenius potential energy calculations.

The factors responsible for the enhancement or reduction of molecular interactions and, consequently, the variation in average molecular area can be discussed in terms of the structural characteristics of the molecules shown in Fig. 2. The consensus of opinion regarding cholesterol action on phosphatidyl choline membranes is that a condensation effect is prevalent, resulting from a steroid-induced restriction of the mobility of the acyl chain of phosphatidyl choline [5—10]. The steroid structure required to produce this effect is optimized by the presence of the 3-hydroxyl group, the planar nucleus and the side-chain [16]. It is apparent from this work that the spatial distribution of the ring system and the potential for hydrogen bonding or other electrostatic effects are critical factors controlling molecular interactions.

The collapse pressures of most of the phosphatidyl choline/steroid mixtures were similar, though that for the PC/3-one combination was much smaller. This contrast was also apparent for the pure 3-one collapse pressure, indicating substantially reduced stabilization compared to that for the other steroids. The major difference between the 3-one and the other molecules is the replacement of the 3-hydroxy group with a carbonyl moiety. It has been determined that the hydroxyl group can participate in hydrogen bonding and is known to bind at the carbonyl sites in phospholipid matrices [17, 18]. Apparently the absence of such a stabilizing effect, coupled with the electrostatic repulsion expected when carbonyls are brought into close proximity in compression experiments, results in the reduced collapse pressure. With respect to molecular packing, the steroids would be expected to exhibit facilitated alignment in the absence of puckered rings, or rings with many protruding functional groups. The data given in Table 2 are

consistent with the concept, and indicate that the planar 5,7-diene and cholesterol have minimum areas, whereas molecules of greater substitution such as the diol and triol species result in maximum area. Because the polar area of the steroids examined here is much smaller than that for the hydrocarbon, these molecules probably occupy a conical volume, with one apex at the polar group, which is swept out as rotation occurs on an axis perpendicular to the air/water interface [19]. Minor alterations of the polar groups on a volume basis should not have a tremendous influence on the measured molecular area. However, a substantial difference between the 3-one species and cholesterol has been observed and is consistent with previous observation of other 3-ketosteroids [19]. The latter may not be in a perpendicular rotational orientation and may therefore sweep out larger volumes [19], though it is not obvious why such a distortion should predominate, and electrostatic repulsion should probably be considered. Furthermore, recent experiments suggest that water may be present in the hydrophobic zone of BLM under certain conditions [20]; this water may be involved in electrostatic shielding of polar moieties such as the carbonyls of the 7-one and 3-one, or the epoxy residue, when these are present in hydrophobic environments. This would result in a physical expansion of a monolayer and would decrease the effective width of the non-polar zone in BLM. The reverse situation could occur if increased compression forced water molecules from the binding sites. Under these conditions, the molecular area at the collapse pressure should only be a function of dynamic steroid shape and electrostatic repulsion.

The influence of hydrogen bonding is clearly demonstrated by contrasting the average molecular area of the steroids with the phosphatidyl choline/steroid mixtures. The order of size between the two series is inconsistent, implying that chemical bonding effects must override simple packing considerations. At high compression, only the PC/3-one had identical measured and calculated (based on independent average measurements for PC and 3-one) areas, as expected for a steroid incapable of extensive hydrogen bonding.

The correlation of BLM ion current with average molecular area indicates that it is the interstitial spaces between lipid molecules, which are related to the bent acyl chains in unsaturated phospholipids and the rotation of these molecules, that control transmembrane ion permeation [19, 21]. In this respect, a matter for concern is the applicability of monolayer data to BLM results. Previous investigations have indicated discrepancies between the two systems [22]. However, objections are largely overcome by considering the following features of this work: (a) collapse areas and individual molecular areas at chosen pressures were used, rather than interpretation of the entire compression curve; (b) only one phospholipid was used for all experiments; (c) only relative trends rather than absolute data values are considered. Moreover, it is generally accepted that monolayers are useful models for bilayer systems [23], especially at pressures of about 30 mN m^{-1} as used in the present work [23, 24].

The influence of surface dipolar potential on BLM ion current must be included in investigations of steroids of substantially different dipole moments. Certainly, this potential can moderate ion current [25], though this feature may be much less significant than packing considerations. Calculations indicate [11] that the surface dipolar potential difference between PC/cholesterol and PC/3-one membranes on a first approximation should be small for the respective steroid parameter values of 2 debye [26], 0.37 nm^2 for cholesterol and 3 debye [27], 0.54 nm^2 for the 3-one. The large difference between the BLM Arrhenius barriers for these two systems implies that most of the energy barrier results from molecular packing constraints on ion transport. Because contributions to the dipolar potential are dependent on dipole moment, density and angular inclination [2], and may originate from the steroids, phosphatidyl choline and bound water [2], the above analysis is clearly not conclusive.

Conclusions

The significance of the above findings is substantial from the standpoint of transducer design. The results indicate that a transducer suitable for selective organic sensing can be based on receptor physics which control local intermolecular packing. This can be adjusted by conformational changes of the receptor molecule, exposing or shielding polar residues which affect local molecular packing of adjacent molecules. Substantial local changes in dipolar potential might align other dipolar species through dipole-dipole and dipole-induced dipole interactions in the electrostatic field, resulting in possible changes in fluidity/packing [28]. Chemical "amplification" may be possible by inducing reduction in the dipolar potential field through receptor activity, and concurrently coupling with a physical/chemical potential energy reduction dominated by fluidity increases. Further probing of ion transport moderation by molecular fluidity/dipolar potential, and defect structures in the BLM hydrocarbon zone, will be described in the following paper.

We thank the Natural Science and Engineering Research Council of Canada and the Ministry of the Environment, Province of Ontario, for support of this work. We are indebted to A. Arya for technical assistance.

REFERENCES

1 G. Eisenman (Ed.), Membranes, Vol. 2, M. Dekker, New York, 1972.
2 M. Thompson, U. J. Krull and L. I. Bendell-Young, Proc. Int. Meet. Chemical Sensors, Fukuoka, Japan, Elsevier-Kodansha, 1983, p. 576.
3 G. L. Jendrasiak and J. H. Hasty, Biochim. Biophys. Acta, 348 (1974) 45.
4 U. J. Krull, M. Thompson and A. Arya, Talanta, 31 (1984) 489.
5 R. Benz and D. Cros, Biochim. Biophys. Acta, 506 (1978) 265.
6 S. A. Simon, T. J. McIntosh and R. Latorre, Science, 216 (1982) 65.
7 P. R. Cullis, B. de Kruyff and R. E. Richards, Biochim. Biophys. Acta, 426 (1976) 433.
8 P. L. Yeagle, W. C. Hutton, C. Huang and R. B. Martin, Biochemistry, 16 (1977) 4344.

9 M. F. Brown and J. Seelig, Biochemistry, 17 (1978) 381.
10 M. J. Karnovsky, A. M. Kleinfeld, R. L. Hoover and R. D. Klausner, J. Cell Biol., 94 (1982) 1.
11 G. L. Gaines, Insoluble Monolayers at Liquid-Gas Interfaces, Interscience, New York, 1966, p. 177.
12 M. C. Phillips and D. Chapman, Biochim. Biophys. Acta, 163 (1968) 301.
13 L. W. Horn and N. L. Gershfeld, Biophys. J., 18 (1977) 301.
14 J. F. Baret, H. Hasmony, J. L. Firpo, J. J. Dupin and M. Dupeyrant, Chem. Phys. Lipids, 30 (1982) 177.
15 J. M. Smaby, A. Hermetter, P. C. Schmid, F. Paltauf and H. Brockman, Biochemistry, 22 (1983) 5808.
16 R. A. Demel and B. de Kruyff, Biochim. Biophys. Acta, 457 (1976) 109.
17 N. P. Franks, J. Mol. Biol., 100 (1976) 345, 359.
18 L. S. Ramsammy, V. P. S. Chanhan, L. L. Box and H. Brockerhoff, Biochem. Biophys. Res. Commun., 118 (1984) 743.
19 J. Gallay and B. de Kruyff, FEBS Lett., 143 (1982) 133.
20 I. M. Campbell and A. B. Pawagi, Can. J. Biochem., 60 (1982) 593.
21 R. Benz and P. Läuger, Biochim. Biophys. Acta, 468 (1977) 245.
22 L. J. Lis, M. McAlister, N. Fuller, R. P. Rand and V. A. Parsegian, Biophys. J., 37 (1982) 667.
23 N. L. Gershfeld and K. Tanija, Nature (London), 279 (1979) 708.
24 A. Blume, Biochim. Biophys. Acta, 557 (1979) 32.
25 M. Thompson, U. J. Krull, L. I. Bendell-Young, I. Lundström and C. Nylander, Anal. Chim. Acta, 173 (1985) 129.
26 A. L. McClellan, Tables of Experimental Dipole Moments, W. H. Freeman and Company, San Francisco, 1963.
27 W. D. Kumler and G. M. Fohlen, J. Am. Chem. Soc., 67 (1945) 437.
28 E. Neumann, in G. Milazzo (Ed.), Principles of Electric Field Effects in Biological Systems: Topics in Bioelectrochemistry and Bioenergetics, Vol. 4, Wiley, New York, 1981.

Analytica Chimica Acta, 174 (1985) 95—102
Elsevier Science Publishers B.V., Amsterdam — Printed in The Netherlands

LANGMUIR—BLODGETT FILM CHARACTERISTICS AND PHOSPHOLIPID MEMBRANE ION CONDUCTION
Part 2. Ethylenic Acyl Chain Oxidation

U. J. KRULL, MICHAEL THOMPSON*, B. WINSBORROW and H. E. WONG

Department of Chemistry, University of Toronto, 80 St. George Street, Toronto, Ontario M5S 1A1 (Canada)

(Received 12th February 1985)

SUMMARY

The influence of polar moieties located in the non-polar hydrocarbon zone in bilayer lipid membranes on ion conduction is described. Natural egg-derived phosphatidyl choline combined with cholesterol produces membranes containing several ethylenic residues in the hydrocarbon interior. Catalytic oxidation of these residues by ultraviolet radiation provides a significant density of permanently-bound polar species within the membrane. The extent of such oxidation is correlated with the Arrhenius energy barrier to ion conduction for bilayer membranes and molecular packing characteristics obtained from Langmuir—Blodgett monolayer compression experiments. The results confirm that membrane ion current is almost entirely controlled by molecular packing.

Inorganic ion transport through bilayer lipid membranes (BLM) can be substantial even in the absence of protein-based conductive pathways. If external variables such as temperature, electrolyte concentration and hydrostatic pressure are constant, then the within-membrane energy barrier to ion conduction is governed principally by electrostatic and steric factors. The former are associated with ion binding to the membrane surface, the magnitude of the transmembrane dipolar potential originating from the anisotropic alignment of polar lipid headgroups at each membrane-aqueous solution interface [1], and within-membrane non-polar terms [2]. Steric effects which are related to lateral and axial lipid motion in the membrane, can be adjusted at the membrane surface by the choice of the lipid molecule and/or by intermolecular electrostatic binding/repulsion characteristics [3]. Ions must penetrate the hydrophobic interior of the BLM in an electrical conduction process, thus it is also of interest to probe the effects of chemical alterations in this environment. The membranes used here are formed from structural lipids such as cholesterol and phosphatidyl choline. The latter can be chosen to contain a number of unsaturation sites in the available acyl chains, which by use of selective chemical reactions provide a degree of control of the chemistry of the membrane hydrocarbon interior. Of particular importance to ion conduction is the presence of polar species in the non-polar zone, because introduction of fixed polar sites should both perturb

0003-2670/85/$03.30

acyl chain packing characteristics and afford permanent low-energy binding sites to the ions traversing the hydrocarbon zone. These effects can be studied by controlled oxidation of unsaturated ethylenic residues in the acyl chains of phosphatidyl choline.

In the previous paper [3], which described work with various steroids, Langmuir—Blodgett monolayer experiments and measurement of the total energy barrier to ion conduction by the Arrhenius equation [4] indicated that the relationship between average molecular area and potential barrier has a sensitivity of up to 0.1 eV/0.01 nm^2. The minimum area occupied by any molecule in the BLM can be envisaged as the maximum area of the base of a cone generated by rotational motion of the molecule around an axis perpendicular to the plane of the membrane [5]. This can be altered by changing molecular configuration or by intermolecular electrostatic effects. The present paper is concerned with the relative importance of electrostatic and steric influences on BLM ion current.

EXPERIMENTAL

Materials and methods were described in detail in Part 1 [3]. Oxidized phosphatidyl choline was prepared from egg-derived phosphatidyl choline (Avanti Biochemicals) by irradiation at 254 nm of a 2% (w/v) solution in dry n-decane at room temperature under air. After oxidation, cholesterol was added to the same weight concentration as for the phosphatidyl choline. This solution was stored in the dark under nitrogen at —5°C to avoid further lipid oxidation.

RESULTS AND DISCUSSION

The unoxidized acyl chains present in the lipid were identified by capillary gas chromatography (c.g.c.) in their methyl ester form after a base-catalyzed transmethylation [6]. The quantitative separation shown in Fig. 1 demonstrates the simultaneous measurement of phosphatidyl choline and cholesterol. The observed phosphatidyl choline chain methylate signals represent unoxidized material, and any reduction of individual peak area is proportional to the extent of oxidation. In order to obtain a reasonable representative estimate of the degree of oxidation, the signal for linoleate (C-18:2) was chosen as a standard; this choice is somewhat arbitrary, but linoleate has the advantage of being the most abundant poly-unsaturate available in this analysis, which insures good susceptibility to oxidation [7] and a good signal-to-noise ratio for quantitative purposes. All results based on this standard refer to the area observed for the C-18:2 methylate as a percentage of the total area calculated for all unoxidized acyl chain methylates.

The expected distribution of the acyl chains available in egg-derived phosphatidyl choline are summarized in Table 1, which also lists the results

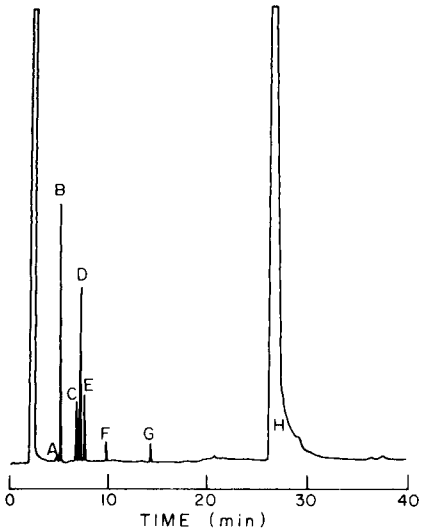

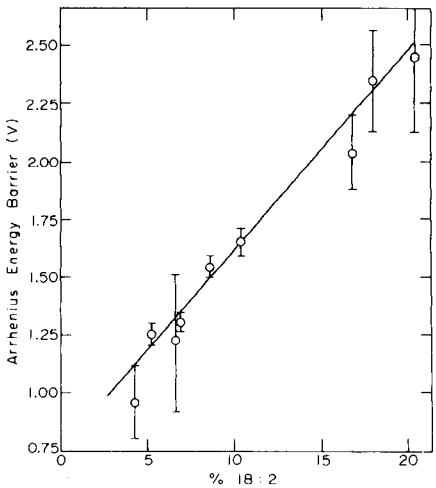

Fig. 1. Capillary gas chromatogram. The initial attenuation factor was 16, reduced to 2 after 8 min, and 1 after 12 min. Compound identification: (A) 16:1, (B) 16:0 (methylate), (C) 18:2, (D) 18:1, (E) 18:0, (F) 20:4, (G) 22:6, (H) cholesterol. See text and Table 1 for explanation.

Fig. 2. Correlation of the oxidation of the olefinic acyl chains, measured as relative percent signal for 18:2 compared to the total signal for all methylates, and the Arrhenius energy barrier for transmembrane ion conduction derived from BLM ion current/ temperature dependence.

TABLE 1

Summary of phosphatidyl choline hydrocarbon distribution

Acyl chain designation	Composition (%)	
	Specified	Measured by c.g.c.
16:0	33.0	32.5 ± 1.0
16:1	2.1	2.5 ± 0.5
18:0	15.4	16.4 ± 0.9
18:1	31.7	31.3 ± 1.0
18:2	17.8	18.8 ± 1.0
20:4	4.3	3.5 ± 0.5
22:6	1.7	1.0 ± 0.3

[a]Product specifications, 1984, Avanti Biochemicals Inc.

obtained from the c.g.c. method described above. The purpose of this work was to investigate only the effects of alteration of the chemistry in the membrane interior, thus the concurrent steroid determination was very useful and offered a simple method to guarantee a purity of about 95%

cholesterol, and reproducible distribution of small quantities of oxidized steroid. This eliminates membrane surface effects which might have appeared because of uncontrolled steroid oxidation. For correlation with electrochemical or monolayer experiments, all gas chromatography was completed immediately after the other experimentation.

The planar BLM used in this work were quite stable and remained intact for up to several hours, developing ion currents characteristically in the picoampère range. The ion currents measured for these BLM were often ten-fold less than those observed for membranes formed from unoxidized phosphatidyl choline doped with steroids [3]. Membrane thinning lasted for at least 10 min and significant current drift ceased before experiments were initiated. Data were collected for the temperature range 22—30°C, and only BLM which showed a linear relationship between measured ion current and the inverse of the absolute temperature for an interval of at least 4°C were compiled in calculations. To insure reasonable statistics, at least four Arrhenius energy barrier determinations were averaged to produce the results expressed in Table 2. Also summarized in this table are the results of the oxidation determinations and monolayer compression experiments. The results indicate a large range of Arrhenius energy barriers, from a maximum of 2.5 eV in unoxidized membranes to 0.95 eV for considerable oxidation. The values are entirely consistent with the measured degree of oxidation as illustrated in Fig. 2 (correlation coefficient 0.99), though they are substantially greater than those previously observed for the steroid studies [3].

As oxidation occurs at the ethylenic residues of the acyl chains of phosphatidyl choline, polar moieties evolve which alter the membrane packing characteristics. This is readily apparent as demonstrated by the linearity of the molecular area/oxidation curves in Fig. 3 (correlation coefficient 0.9). Controversy has arisen as to the compression pressure which can yield a realistic measure of average molecular area. For a very pure lipid, overcom-

TABLE 2

Summary of electrochemical and monolayer experimental data

PC oxidation: C-18:2 percentage of total acyl chain signal	Arrhenius energy barrier (eV)	Molecular area (nm^2) at collapse pressure	Molecular area (nm^2) at 16 mN m^{-1}
19.9	2.46 ± 0.30	0.396 ± 0.004	0.500 ± 0.004
17.8	2.35 ± 0.25		
16.7	2.03 ± 0.15	0.400 ± 0.011	0.442 ± 0.010
10.3	1.63 ± 0.03	0.473 ± 0.005	0.534 ± 0.010
8.6	1.54 ± 0.06		
6.9	1.30 ± 0.04	0.514 ± 0.012	0.589 ± 0.011
6.4	1.22 ± 0.28	0.468 ± 0.006	0.553 ± 0.005
5.2	1.25 ± 0.06		
4.3	0.94 ± 0.18	0.546 ± 0.10	0.620 ± 0.011

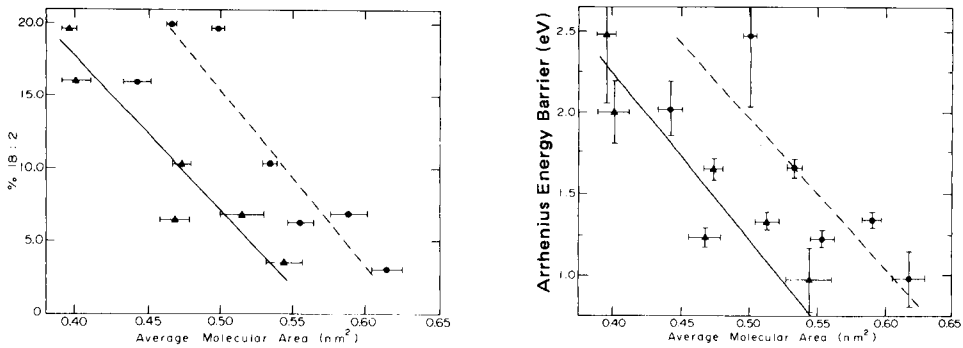

Fig. 3. Relationship between the relative degree of oxidation of olefinic acyl chains and the average molecular area evaluated by monolayer compression experiments: (—, ▲) at the collapse pressure; (---, ●) at 16 mN m^{-1}.

Fig. 4. Relationship between the average molecular area of the oxidized phosphatidyl choline, evaluated from monolayer experiments at the collapse pressure (—, ▲) and at 16 mN m^{-1} (---, ●), and Arrhenius energy barrier results derived from the temperature dependence of the BLM ion current.

pression can result from absence of the defect required to initiate film collapse [8]. Great care is therefore needed in using molecular area measurements obtained at the collapse pressure, and generally areas measured at 15 mN m^{-1} were considered to represent reasonably ideal values measured under equilibrium conditions [8]. With respect to potential sources of error, there was no evidence of phase transitions over the range of temperature examined. Furthermore, there was little susceptibility to the presence of 0.1 M KCl in the trough sub-phase, and no evidence of overcompression at the collapse point. The latter observation is confirmed by the similarity of the molecular area/oxidation curves shown in Fig. 3 for data obtained at the collapse pressure and at 16 mN m^{-1}, and by the fact that compression curves do not exhibit maxima after film collapse [3]. Though direct measurements of pressures in the type of BLM used here are not available, a reasonable approximation indicates a value of 30 mN m^{-1} [9].

Of particular significance to BLM ion conduction are the results correlating the Arrhenius energy barrier to the average molecular area (Fig. 4). The points are scattered, but the general trends are consistent with the data observed for steroid experiments [3]. The correlation coefficient for the line based on the average molecular area data at the collapse pressure is about 0.92, and again an increase in molecular area causes a decrease in the energy barrier to transmembrane ion conduction. The slopes of the lines in Fig. 4 again demonstrate a remarkable sensitivity for the energy barrier/molecular packing relation, 0.1 eV for only 0.01 nm^2 alteration.

The acyl chain chemistry used, summarized in Table 1, indicates that a substantial number density of ethylenic residues exists in the BLM hydrocarbon interior. The probability of any one acyl chain containing at least one

double bond is approximately 55%, while the probability of finding more than one ethylenic linkage in a chain containing unsaturates is about 40%, implying substantial opportunity for oxidation. The natural stereochemistry of the ethylenic residues is generally the *cis* configuration, and divinyl methane-type linkages are found in such polyethylenic chains [10—12], thus substantial perturbations in internal membrane order must be present [13]. This apparently acts as one source of reduction of energy barrier to ion conduction, because dynamic internal packing disorder provides transient interstitial spaces between molecules suitable for ion entrapment and ultimate transport. The proposed mechanism for oxidation of ethylenic acyl chains is a free radical autoxidation catalyzed by ultraviolet radiation in the presence of molecular oxygen [10—12]. Reaction initiation involves proton extraction resulting in the formation of a resonance-stabilized free radical. Further reaction for a diene compound such as C-18:2 occurs by addition of molecular oxygen, and termination follows when an intermolecular proton-transfer occurs. This final step produces another free-radical intermediate which continues the above process. Polyolefinic reaction can become much more complicated and, once the radical has been formed by proton extraction, can generally proceed via three distinct routes [12] to form conjugated hydroperoxides which slowly go on to form many oxidized species including alcohols, aldehydes, ketones and carboxylic acids. Unsaturated lipid hydrocarbon chains can readily undergo such processes at normal ambient room conditions. Oxidation reactivity is dependent on the degree of unsaturation [7]. These problems impose limitations on analysis of the extent and exact type of oxidation in lipid preparations, thus the simpler approach based on the global reduction of a known reactive ethylenic chain concentration was used here as a relative measure of oxidation.

In terms of BLM membranes, the key feature of the oxidation reactions described above is that they promote injection of polar groups into the hydrocarbon interior of the BLM. This has an obvious effect on internal chain packing order as shown by the relationship of increasing average molecular area with increasing oxidation in Fig. 3. This is the result of both the physical size of the polar moieties on the acyl chains, as well as intermolecular electrostatic repulsions which are expected for interactions of polar and non-polar acyl chains. The introduction of polar species into the hydrocarbon zone of BLM has some other interesting facets. The polar moieties would act as low-potential energy sites suitable for electrostatic binding of ions, affording a low-energy pathway through the membrane based on a "jumping" mechanism of ion movement across such sites. This effect should increase as oxidation increases, because the probability of continuous alignment of appropriate electrostatic binding sites would increase. Further, the lipid molecules in BLM experience substantial lateral motion [14], thus clusters of polar groups held by hydrogen bonding or electrostatic forces may form in the membrane interior, which could create polar

ion-conductive pathways similar to formal channels in the non-polar zone. Yet the linearity shown in Fig. 2 suggests that the "jumping" mechanism is not important in reduction of the ion-transport energy barrier under the oxidation conditions normally encountered in BLM; even in cases of substantial oxidation, as measured by the percentage concentration of C-18:2 at approximately 4%, about 80% of all acyl chains present contain no polar functional groups. That a jumping mechanism plays an insignificant role is also supported by the relationship between the Arrhenius barrier and the average molecular area (Fig. 4); the sensitivity of the Arrhenius barrier to molecular packing is very similar to that observed for steroid-modified BLM [3].

CONCLUSIONS

The purpose of this work was to identify some of the major physical parameters available in BLM which could be adjusted to generate substantial changes in transmembrane ion current. The results described above, taken in conjunction with the previous steroid-modified BLM results [3], have identified three features that seem to be of fundamental significance to future selective-membrane development: (1) electrochemical signals based on alterations of transmembrane ion current are predominantly controlled by molecular packing and order parameters; (2) the sensitivity of the transmembrane energy barrier to variations in average molecular area is very large, attaining a value of about 0.1 eV for a change of only 0.01 nm^2; (3) the influence of steroids on the magnitude of the measured Arrhenius barrier is much greater than that of the oxidized phosphatidyl choline, indicating that membrane surface chemistry could play a predominant role in controlling ion current.

An ideal selective receptor designed to control a BLM ion current should be located in the surface volume of the membrane, and should operate mechanically by substantially perturbing the internal order of the underlying membrane on binding to the stimulant. Coupling this perturbation with a concurrent change in surface dipolar potential induced by the binding event [1] would produce a synergic signal amplification.

We thank the Natural Sciences and Engineering Research Council of Canada and the Ministry of the Environment, Province of Ontario, for support of this work.

REFERENCES

1 M. Thompson and U. J. Krull, Anal. Chim. Acta, 147 (1983) 1.
2 I. Lundström and C. Nylander, J. Theor. Biol., 88 (1981) 671.
3 U. J. Krull, M. Thompson, E. T. Vandenberg and H. E. Wong, Anal. Chim. Acta, 174 (1985) 83.
4 G. L. Jendrasiak and J. H. Hasty, Biochim. Biophys. Acta, 348 (1974) 45.

5 M. Kates and A. Kuksis (Eds.), Membrane Fluidity, Humana Press, Clifton, NJ, 1980, part I.
6 U. J. Krull, M. Thompson and A. Arya, Talanta, 31 (1984) 489.
7 R. T. Holman, Prog. Chem. Fats Other Lipids, 9 (1966) 3.
8 G. L. Gaines, in Insoluble Monolayers at Liquid—Gas Interfaces, Interscience, New York, 1966, p. 177.
9 A. Blume, Biochim. Biophys. Acta, 557 (1979) 32.
10 N. Porter, L. Lehman, B. Weber and K. Smith, J. Am. Chem. Soc., 103 (1981) 6447.
11 H. Weenen and N. Porter, J. Am. Chem. Soc., 104 (1982) 5216.
12 N. Porter, R. Wolf and H. Weenen, Lipids, 15 (1979) 167.
13 R. Benz and P. Läuger, Biochim. Biophys. Acta, 468 (1977) 245.
14 W. W. Webb, L. S. Barak, D. W. Tank and E. S. Wu, Biochem. Soc. Symp., 46 (1981) 191.

Analytica Chimica Acta, 174 (1985) 103—113
Elsevier Science Publishers B.V., Amsterdam — Printed in The Netherlands

DETERMINATION OF PSEUDOURIDINE AT SUBMICROMOLAR CONCENTRATIONS BY CATHODIC STRIPPING VOLTAMMETRY AT A MERCURY ELECTRODE

EMIL PALEČEK

Institute of Biophysics, Czechoslovak Academy of Sciences, Kralovpolska 135, 612 65 Brno (Czechoslovakia)

(Received 4th January 1985)

SUMMARY

Pseudouridine (5-ribosyluracil), uridine (*N*,1-ribosyluracil), deoxyuridine (*N*,1-deoxyribosyluracil) and uracil are investigated by means of d.c. polarography and by differential and normal pulse polarography. Pseudouridine, which is known to be a cancer marker, yields anodic polarographic currents in the pH range 7—11, whereas uridine and deoxyuridine are inactive under the same conditions. The polarographic response of pseudouridine obtained is due to the formation of a sparingly soluble mercury compound. Pseudouridine can be determined by differential pulse polarography in the concentration range $2—6 \times 10^{-6}$ M and by differential-pulse cathodic stripping voltammetry at concentrations two orders of magnitude lower. Small excesses of uridine, deoxyuridine or proteins do not interfere with the determination.

The ability of nucleic acid bases to yield anodic polarographic currents arising from the formation of a sparingly soluble mercury compound was discovered almost thirty years ago [1, 2]. This phenomenon has recently been utilized in the determination of these substances at submicromolar concentrations by means of cathodic stripping voltammetry [3—7]. Anodic polarographic currents are also produced by the usual purine nucleosides and nucleotides [5], while the pyrimidine analogues are inactive [3, 8]. It might be expected that the reason for the inactivity of the usual pyrimidine nucleosides is substitution of the pyrimidine ring at N1 (Fig. 1). The inactivity of these substances may, however, be due to the presence of a bulky sugar residue in the molecule (irrespective of the position at which it is bound). To resolve this question, a uridine isomer, pseudouridine (Fig. 1), in which the ribose residue is bound to C5, was investigated.

Pseudouridine is one of the unusual nucleosides contained in transfer ribonucleic acid (tRNA) [9]. The determination of pseudouridine has recently attracted much attention, as this substance is excreted by cancer patients [10—15]. Levels of pseudouridine excretion in the urine of cancer patients correlate with disease activity; monitoring of these levels has successfully been applied for diagnostic and prognostic evaluations in various kinds of malignant diseases.

0003-2670/85/$03.30

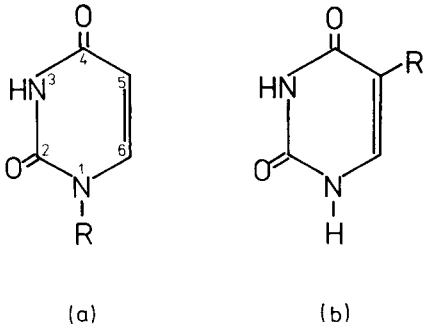

Fig. 1. Uracil and its nucleosides: (a) R = H, uracil; R = ribose, uridine; R = deoxyribose, deoxyuridine; (b) R = ribose, pseudouridine.

In this paper, it is shown that, unlike uridine (Fig. 1) and deoxyuridine, pseudouridine produces anodic polarographic currents conditioned by the formation of a sparingly soluble mercury compound. Pseudouridine can be determined by differential-pulse cathodic stripping voltammetry (d.p.c.s.v.) at submicromolar concentrations even in the presence of an excess of uridine, deoxyuridine and proteins.

EXPERIMENTAL

Chemicals and instrumentation

Uracil, uridine, deoxyuridine and pseudouridine were produced by Calbiochem. All other reagents were of analytical grade. The supporting electrolytes used were 0.05 M borax, borate or carbonate buffers.

Polarographic and voltammetric measurements were made with an EG and G PARC 174A polarographic analyzer with an Omnigraphic Model 9002A *X-Y* recorder. A three-electrode system was used, including a mercury-drop working electrode, platinum wire as the auxiliary electrode and a saturated calomel (K77) reference electrode, connected to the analyzed solution via a K65 bridge tube filled with background electrolyte. A PARC K62 polarographic cell bottom combined with the K66 polarographic cell top was used as the electrochemical cell.

General methods

The volume of the solution analyzed was usually 2 ml. The conventional dropping mercury electrode (DME) or a Model 303 stationary mercury-drop electrode (SMDE) was used as the mercury-working electrode. Other conditions were as in previous papers [4, 8]. The conventional DME had a drop time of t = 5.6 s with open circuit in 0.05 M borax with a mercury column height of 35 cm.

Stripping voltammetric measurements were done with a hanging mercury-drop electrode (HMDE; Metrohm E410) as the working electrode. Instrum-

ent settings for differential-pulse cathodic stripping voltammetry (unless otherwise stated) were: scan rate 5 mV s^{-1}, modulation amplitude 50 mV, pulses applied at 0.5-s intervals, deposition time (with stirring) 60 s (unless otherwise stated) plus a 20-s quiescent period, HMDE 4 divisions (area 0.022 cm^2). All measurements were done at room temperature (25°C). The solutions were deoxygenated by passing a slow stream of oxygen-free nitrogen through them for 10 min and, during the measurements, over their surface.

RESULTS

Polarography

Pseudouridine at a concentration of 1×10^{-4} M was examined in a medium of 0.05 M borax (pH 9.2), already used with success in studying bases of nucleic acids [1, 8]. Under these conditions, pseudouridine gave an anodic peak in differential pulse polarography (d.p.p.) (Fig. 2a) at a potential about 10 mV more negative than the uracil peak (Fig. 2c). Under the same conditions, uridine and deoxyuridine gave only small inflections (Fig. 2b) and shifted the potential of mercury dissolution (background) to more negative values.

The height of the d.c. polarographic wave of pseudouridine (Fig. 2a) was

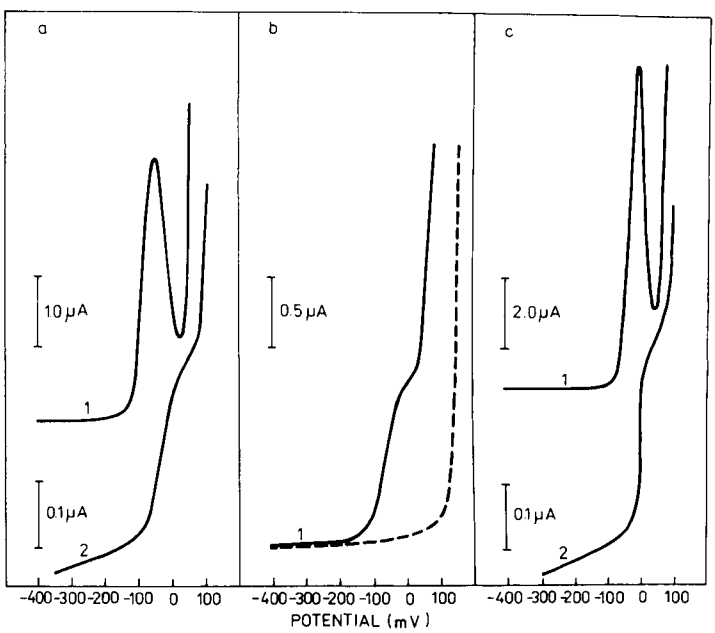

Fig. 2. Polarograms of uracil and its ribosides: (a) 50 μM pseudouridine; (b) 100 μM uridine; (c) 50 μM uracil. Curves: (1) d.p.p., pulse amplitude 50 mV, scan rate 2 mV s^{-1}; (2) d.c. polarography, DME. (----) background electrolyte. Electrolyte: 0.05 M borax (pH 9.2).

only a little less than that of uracil (Fig. 2c) at equimolar concentrations, which indicates approximately the same consumption of electrons in the electrode process of both substances. On the basis of a comparison of wave heights of uracil and veronal, Manoušek and Zuman [1] assumed the release of one electron in the uracil electrode process. These authors, however, considered the electrode process of veronal to be a single-electron one, whereas later work [16, 17] indicates the consumption of two electrons.

Dependence on pH. The d.p.p. behaviour of 42.5 μM uridine and pseudouridine was studied in the pH range 7—12; in this pH range, uridine was either quite inactive or gave only a small inflection, as at pH 9.2 (Fig. 2b). The height of the d.p.p. peak of pseudouridine was almost independent of pH in the range of pH 9—11 (Fig. 3). At pH values below 8.9, the height of the peak increased sharply with decrease in pH, reaching its maximum value at around pH 7.7. Normal pulse polarography (n.p.p.) also showed the polarographic curves to increase in height sharply in this pH range (Figs. 3 and 4). In contrast, the height of the d.c. polarographic (d.c.p.) curve was practically independent of pH in the same range (Fig. 3). The potentials of

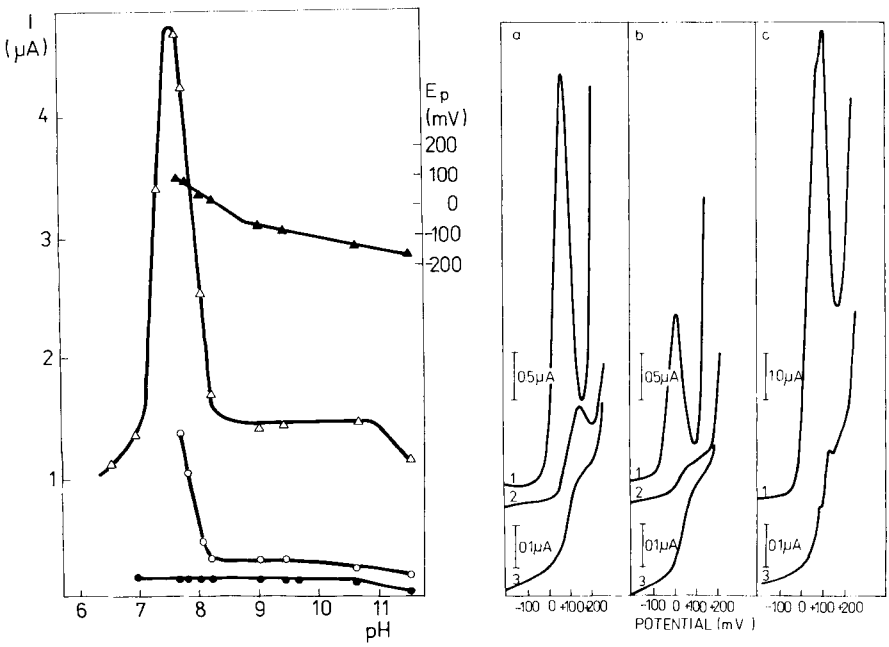

Fig. 3. Dependence of d.p.p., n.p.p. and d.c.p. signals of pseudouridine on pH: (△) d.p.p. peak height; (○) n.p.p. wave height; (●) d.c.p. wave height. (▲) d.p.p. peak potential (E_p). 42.5 μM pseudouridine in 0.05 M borate buffer. Other conditions as in Fig. 2.

Fig. 4. Polarograms of pseudouridine in 0.05 M borate buffer: (a) pH 7.8; (b) pH 8.2; (c) pH 7.8. Curves: (1) d.p.p.; (2) n.p.p.; (3) d.c.p. Pseudouridine concentration: (a,b) 42.5 μM; (c) 0.2 mM. Other conditions as in Fig. 2.

the d.p.p. peaks and the half-wave potential of the n.p. and d.c.p. curves shifted to more negative values with increasing pH, similarly as with uracil [9], suggesting the involvement of an ionized species in the electrode process.

The difference between the d.c. and the pulse polarographic behaviour of pseudouridine in the pH range 7—8 is probably conditioned by the adsorption of reactant on the electrode, which greatly affects its pulse polarographic behaviour [18—20]. This is also suggested by the shape of the n.p.p. wave (Fig. 4), where in this pH range a maximum appeared [18, 21], while at higher pH its shape corresponded to the usual polarographic wave. At higher concentrations of pseudouridine (from about 1×10^{-4} M), the shapes of the d.c.p. and the d.p.p. curves were deformed because of adsorption phenomena both at pH 7—8 (Fig. 4) and pH 9.2 (not shown). Similar deformations have already been observed in uracil curves [1, 8].

Dependence on pseudouridine concentration. The height of the d.p.p. peak was linearly dependent on pseudouridine concentration in the range 2—60 μM (not shown). The potential of the peak remained practically unchanged with increasing pseudouridine concentration in this range. At concentrations above 80 μM, the height of the peak was not dependent on pseudouridine concentration or fell with increasing concentration. D.c. polarography gave a similar picture of dependence on concentration, beginning at 5 μM pseudouridine. Under the same conditions, the height of the n.p.p. wave grew with concentration even at concentrations higher than 80 μM. Dependence on the pseudouridine concentration studied at pH 7.8 and 9.2 was of similar character, the limit of pseudouridine detection, however, being about twice as high at pH 9.2 compared with pH 7.8.

Formation of a sparingly soluble mercury compound. On the basis of analogy with uracil, it can be expected that the anodic peak of pseudouridine depends on the formation of a sparingly soluble compound with the mercury electrode. To test this assumption, inverse (or reverse) pulse polarography (i.p.p.) [22] was applied to solutions of ascorbic acid (which is oxidized at the electrode [23]), uracil (which forms a sparingly soluble compound with the mercury electrode, and pseudouridine. The i.p.p. curve of uracil had the shape of a maximum, while the i.p.p. curve of ascorbic acid had the usual polarographic wave shape (Fig. 5). The height of the i.p.p. wave of ascorbic acid did not depend on the initial potential (E_i) (Fig. 6a), while the height of the uracil wave rose steeply with a shift to more positive potential. The i.p.p. behaviour of pseudouridine (Figs. 5, 6) corresponds to the behaviour of uracil. The height of the n.p.p. curve of all three substances was independent of E_i (Fig. 6) and of the drop time (not shown) of the SMDE (in the case of the SMDE, the mercury drop forms within 50 ms and its surface is constant throughout the life of the drop). The height of the i.p.p. curves of uracil and pseudouridine increased sharply with drop time (the height of peaks of the two substances during the drop time $t = 5$ s was about ten times higher than at $t = 0.5$ s), whereas the height of the ascorbic

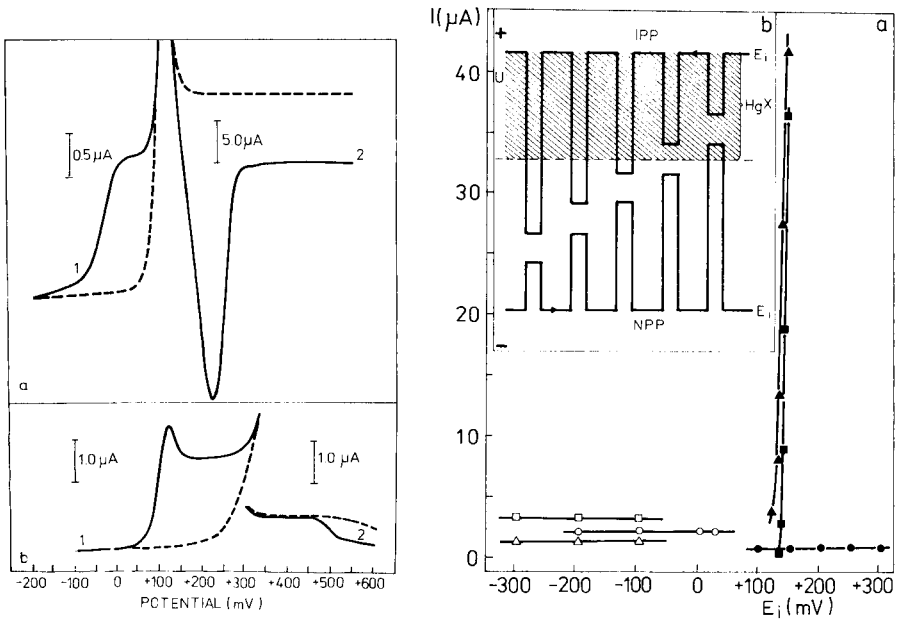

Fig. 5. Polarograms of pseudouridine and ascorbic acid: (1) n.p.p.; (2) i.p.p.; (---) background electrolyte. (a) 0.1 mM pseudouridine in 0.05 M borax, pH 9.2; (b) 0.1 mM ascorbic acid in 0.05 M sodium acetate, pH 4.5.

Fig. 6. Dependence of the currents obtained in n.p.p. (open symbols) and i.p.p. (filled symbols) on the initial potential (E_i): (●, ○) 0.1 mM ascorbic acid in 0.05 M sodium acetate, pH 4.5; (△, ▲) 0.1 mM pseudouridine; (□, ■) 0.1 mM uracil in 0.05 M borax, pH 9.2. (b) Schematic diagram of the potential waveforms used for normal pulse polarography (n.p.p.) and inverse (reverse) pulse polarography (i.p.p.). In n.p.p., the initial potential (E_i) is held at a value more negative than that of the anodic n.p.p. wave and voltage pulses are scanned towards positive potentials. In i.p.p., E_i is held at the potential of the n.p.p. wave (at which the compound with mercury, HgX, may be formed) and voltage pulses are scanned towards negative potentials.

acid wave fell with time. The results of these experiments show that in the case of uracil and pseudouridine, a compound is formed and accumulated at the positively charged electrode; during the scan to negative potentials, this compound is reduced. It can therefore be concluded that pseudouridine, like uracil, reacts with the mercury electrode to form a sparingly soluble compound.

The results of i.p.p. measurements of uracil and pseudouridine solutions (Fig. 6) also indicate that this method could be used to determine substances forming sparingly soluble compounds with the mercury electrode (whether a mercury-drop electrode or a stationary mercury electrode). The fact that a compound with mercury is generated in the period preceding the application of the pulse might be exploited to increase the sensitivity of the determination.

Cathodic stripping voltammetry

The ability of pseudouridine to form a sparingly soluble compound with the mercury of the electrode makes pseudouridine potentially detectable by cathodic stripping voltammetry (c.s.v.) [5, 22]. For c.s.v., pseudouridine was first accumulated at the electrode at the potential (deposition potential, E_d), where it formed a compound with mercury (deposition). The compound was then stripped by scanning to negative potentials (by either linear-sweep or differential-pulse voltammetry, d.p.c.s.v.), and a peak attributed to reduction of the mercury bound in the compound appeared (Fig. 7). Comparison of linear-sweep voltammetry and d.p.c.s.v. showed better sensitivity in d.p.c.s.v. The height of the d.p.c.s.v. peaks was directly proportional to the pulse amplitude in the range 5—50 mV. Further measurements were done by the d.p.c.s.v. method and a pulse amplitude of 50 or 25 mV. The d.p.c.s.v. measurements of pseudouridine were studied in relation to E_d, deposition time, pH and other conditions. Similarly to the behaviour of nucleic acid bases, the peak height of pseudouridine depended strongly on E_d (Fig. 8) with an optimum close to 0.25 V; no changes in the peak potential in dependence on E_d were observed (in the potential range investigated). The height of the d.p.c.s.v. peak depended on pH in a manner similar to that

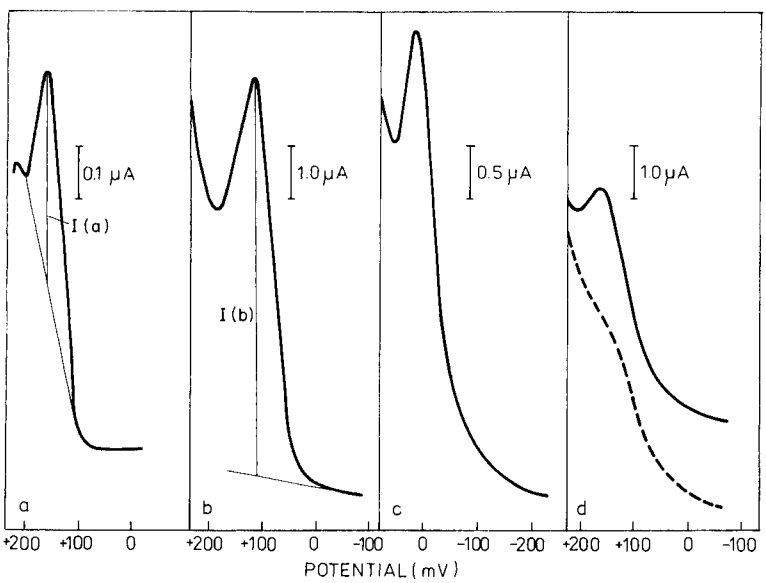

Fig. 7. Cathodic stripping voltammograms of pseudouridine: (a, b) 2.9×10^{-7} M pseudouridine in 0.05 M sodium borate/boric acid, pH 7.8, with 60-s deposition time (t_d); (c) 5.1×10^{-7} M pseudouridine in 0.05 M borax, pH 9.2, t_d = 45 s; (d) 5×10^{-8} M pseudouridine in 0.05 M sodium borate/boric acid, pH 7.8, t_d = 180 s, (----) background electrolyte. (a) Linear-sweep voltammetry, scan rate 200 mV s^{-1}; (b—d) d.p.c.s.v., HMDE, pulse amplitude 50 mV, scan rate 5 mV s^{-1}. See later text for explanation of peak-height measurement.

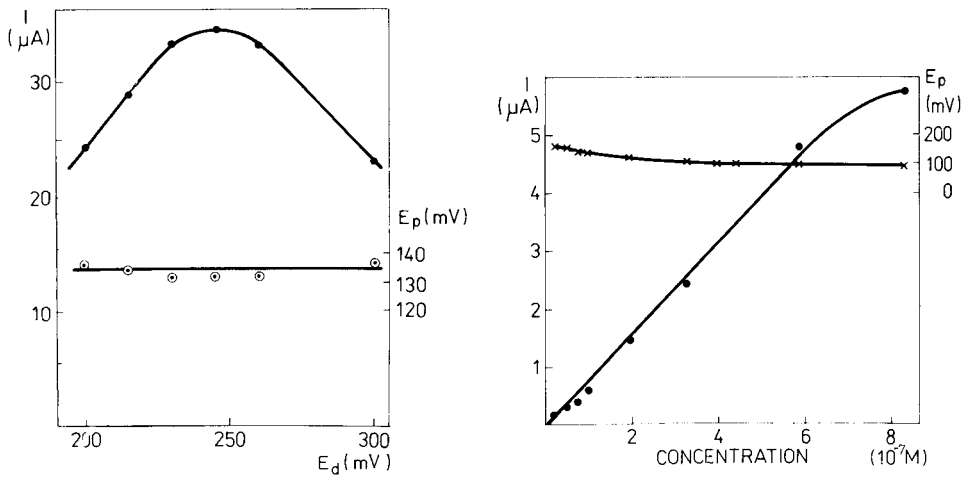

Fig. 8. Dependence of the potential (E_p) and height (I) of the d.p.c.s.v. peak of pseudouridine on the deposition potential (E_d): (○) peak potential; (●) peak height. Conditions: 0.2 μM pseudouridine in 0.05 M borate buffer pH 7.8, waiting time 30 s; other conditions as in Fig. 7.

Fig. 9. Dependence of height (I) and potential (E_p) of the d.p.c.s.v. peak on pseudouridine concentration: (●) peak height; (×) peak potential. Conditions: waiting time 60 s, pH 7.8; other conditions as in Fig. 7.

obtained by means of d.p.p. (Fig. 3), with a maximum around pH 7.7.

For measurements above the concentration of 1×10^{-7} M, borax, borate and carbonate buffers in the pH range 7.7—10.5 could be used. The lowest limit of detection was found in 0.05 M sodium borate/boric acid at pH 7.8. In this medium, the height of the d.p.c.s.v. peak depended linearly on concentration of pseudouridine in the range 5×10^{-8}—6×10^{-7} M (Fig. 9), at a deposition time of 60 s. The potential of the peak shifted with increasing pseudouridine concentration towards more negative values. At a pseudouridine concentration of 6×10^{-8} M, the height of the peak was linearly dependent on the deposition time in the range 30—180 s.

Determination of pseudouridine in the presence of an excess of uridine and other compounds

In body fluids, pseudouridine is accompanied by various substances, including its isomer uridine. Separation of pseudouridine from uridine is difficult and a direct determination of pseudouridine in the presence of uridine would be useful.

Differential pulse polarography. Pseudouridine (4.2×10^{-5} M) in 0.05 M borate, pH 7.8, can be determined by means of d.p.p. with a relative standard deviation of ±2% (n = 10). Under these conditions, the effects of an excess of uridine, deoxyuridine, lysozyme or bovine serum albumin on the pseudouridine peak height were tested. Equimolar concentrations of

uridine or deoxyuridine had almost no effect on the pseudouridine peaks. At higher concentrations of these nucleosides, the peak became deformed, mainly because of the shift of background to more negative potentials (Fig. 2b). A three-fold amount of uridine resulted in a decrease of the pseudouridine peak height by 40% when the peak was measured in the usual way (I(a), Fig. 7) and by 3% when its height was measured as shown for I(b) (Fig. 7). A five-fold amount of deoxyuridine did not affect the pseudouridine peak height, whereas a 25-fold amount of deoxyuridine caused a decrease of 35% in the pseudouridine peak measured as for I(a), but practically no change in the peak height measured as for I(b). With the 25-fold amount of uridine, reliable measurement of the pseudouridine peak height was impossible. A 4.2-fold amount of lysozyme resulted in a decrease in the pseudouridine peak by 5% and a shift in the peak potential to more positive values by 5 mV; a ten-fold amount of bovine serum albumin decreased the peak by 44% measured as for I(a) or 14% measured as for I(b).

Differential-pulse cathodic stripping voltammetry. Pseudouridine (4.5×10^{-7} M, 0.11 μg ml^{-1}) in 0.05 M borate, pH 7.8 (deposition time 60 s) was determined by d.p.c.s.v. with a relative standard deviation of $\pm 2.6\%$ ($n = 10$). As in the case of d.p.p., the presence of an excess of uridine resulted in a deformation of the pseudouridine peak; a ten-fold amount of uridine decreased the pseudouridine peak (under the same conditions) by 20% when measured as for I(a) (Fig. 7) or 8% measured as for I(b). A 25-fold amount of deoxyuridine, however, had practically no effect on the pseudouridine peak height. The higher capacity of uridine to deform the pseudouridine peak is due at least in part to the presence of impurities in the preparation, as the uridine fraction from h.p.l.c. deformed the pseudouridine peak (in both the d.p.c.s.v. and d.p.p. modes) to a substantially lesser extent. The presence of albumin at concentrations up to 0.4 μg ml^{-1} did not influence the pseudouridine peak height; at 1.1 μg ml^{-1} the peak increased by 4% and at 2.4 μg ml^{-1} by 26%, measured as for I(a). The analytical consequence of these results is that for determination of pseudouridine in the presence of a substantial amount of the above-mentioned substances, the method of standard addition is to be recommended. The peak height vs. concentration plots were linear over moderate ranges, so that standard additions must be selected carefully.

DISCUSSION

It has been shown above that pseudouridine gives anodic polarographic currents (Fig. 2) governed by the formation of a sparingly soluble compound with mercury, similarly to uracil (Figs. 1, 2, 5, 6) [1, 8]. Uridine and deoxyuridine are inactive under these conditions (Fig. 2). These results indicate that the cause of the inactivity of these substances is not the presence of a bulky sugar residue in its molecule, but substitution at N1.

In bulk aqueous solution, uracil and uridine did not interact with mer-

cury(II) chloride up to the addition of a 5-fold amount of the salt. Uridine/$HgCl_2$ interaction has been observed under different experimental conditions with a 32-fold excess of mercury(II) chloride. Binding of methylmercury to N3 of both uracil and uridine has been detected [24—26]. Thus the mere application of these data cannot explain the polarographic behaviour of uracil and its nucleosides or reveal the nature of the compound of uracil and pseudouridine formed at the mercury electrode. The interaction of derivatives of barbituric acid (which differs from uracil only in the presence of an extra oxygen at C6) with a mercury electrode has been studied in detail [16, 17]. It is assumed that polymeric complexes of barbiturates are formed, where two mercury atoms are bound to N1 and N3 [27—29]. If binding of methylmercury(I) to N3 of the uracil [26] and the results contained in this work are taken into account, it seems probable that the formation of a compound of uracil or pseudouridine on the electrode involves binding of the mercury to N1 and N3. The inactivity of uridine and deoxyuridine observed (i.e., their inability under the given conditions to produce an anodic d.p.p. peak) does not eliminate the possibility of a reaction of these substances with the mercury of the electrode. But if these substances form a compound with the mercury, it is apparently formed at more positive potentials than in the case of pseudouridine and uracil, as indicated by the inflection in the d.p.p. curve (Fig. 2), and the mercury probably does not bind to N1.

It has recently been shown [11—15] that cancer patients excrete elevated levels of pseudouridine and of some modified nucleosides in their urine. These nucleosides (usually called cancer markers) do not originate from cell death but rather from a very high turnover of tRNA in tumour tissue [11]. The determination of these substances offers a measure of the effect of therapy on the course of the disease and may provide early cancer diagnosis. High levels of pseudouridine have been observed in various types of cancer, including mesothelioma [15], where other means of diagnosis can be very difficult and painful.

Practical analysis for these substances is possible by reversed-phase h.p.l.c. with ultraviolet absorption detection combined with an affinity gel isolation technique [10]; the method was used to determine various guanine nucleosides as well as pseudouridine. Previous work [5] and some preliminary measurements with derivatives of guanosine suggest that these substances could be quantified electrochemically. The electrochemical activity of pseudouridine demonstrated above suggests the possibility of determining pseudouridine in the urine of cancer patients after h.p.l.c. separation with a polarographic detector operating in the anodic mode. The general principle of utilizing the property of uric acid and related substances to form insoluble compounds with mercury has recently been described [30]. The application of the i.p.p. mode (with a sufficiently long drop time) might increase the sensitivity of detection. Another possibility would be to apply d.p.p. or c.s.v. directly for the determination of pseudouridine in the affinity gel fraction containing only pyrimidine nucleosides [10]; purine nucleosides

can be eliminated by heating the sample in a strong acid prior to its application to the affinity gel.

The author thanks Jan Paleček for preliminary work and Mrs. Irena Postbieglová for skillful technical assistance.

REFERENCES

1 O. Manoušek and P. Zuman, Chem. Listy, 49 (1955) 668.
2 E. Paleček, Naturwissenschaften, 45 (1958) 186; Collect. Czech. Chem. Commun., 25 (1960) 2283.
3 E. Paleček and F. Jelen, Collect. Czech. Chem. Commun., 45 (1980) 3472.
4 E. Paleček, Anal. Biochem., 108 (1980) 128.
5 E. Paleček, Anal. Lett., 13 (1980) 331.
6 E. Paleček, F. Jelen, Mac Anh Hung and J. Lasovský, Bioelectrochem. Bioenerg., 8 (1981) 621.
7 E. Paleček, J. Osteryoung and R. A. Osteryoung, Anal. Chem., 54 (1982) 1389.
8 E. Paleček, F. Jelen and O. Manoušek, Collect. Czech. Chem. Commun., 45 (1980) 3460.
9 W. E. Cohn, J. Biol. Chem., 235 (1960) 1488.
10 C. W. Gehrke, K. C. Kuo, G. E. Davis, R. D. Suits, T. P. Waalkes and E. Borek, J. Chromatogr., 150 (1978) 455.
11 J. Spear, C. W. Gehrke, K. C. Kuo, T. P. Waalkes and E. Borek, Cancer, 44 (1979) 2120.
12 C. W. Gehrke, K. C. Kuo, T. P. Waalkes and E. Borek, Cancer Res., 39 (1979) 1151.
13 R. W. Trewyn, R. Glaser, D. R. Kelly, D. G. Jackson, W. P. Graham and C. E. Speicher, Cancer, 49 (1982) 2513.
14 D. A. Heldman, M. R. Grever, C. E. Speicher and R. W. Trewyn, J. Lab. Clin. Med., 101 (1983) 783.
15 E. Borek, O. K. Scharma and T. P. Waalkes, in G. Nass (Ed.), Modified Nucleosides and Cancer, Springer-Verlag, Heidelberg, 1983, p. 301. (Other papers in this text are also relevant.)
16 R. D. Armstrong, M. Fleschmann and J. W. Oldfield, Trans. Farad. Soc., 65 (1969).
17 M. Fleischmann, K. Manandhar and D. Plefcher, J. Electroanal. Chem., 98 (1979) 241.
18 G. C. Barker and J. A. Bolzan, Fresenius Z. Anal. Chem., 216 (1966) 215.
19 F. C. Anson, J. B. Flanagan, K. Takahashi and A. Yamada, J. Electroanal. Chem. Interfacial Electrochem., 67 (1976) 253.
20 J. B. Flanagan, K. Takahashi and F. C. Anson, J. Electroanal. Chem., 81 (1977) 261.
21 G. Wollf and H. W. Nürnberg, Z. Anal. Chem., 216 (1969) 169.
22 J. Osteryoung and E. Kirowa-Eisner, Anal. Chem., 52 (1980) 62.
23 J. Kůta and E. Paleček, in G. Milazzo (Ed.), Topics in Bioelectrochemistry and Bioenergetics, Vol. 5, Wiley, London, 1983, p. 1.
24 R. C. Lord and G. J. Thomas, Biochim. Biophys. Acta, 142 (1967) 1.
25 G. L. Eichhorn and P. Clark, J. Am. Chem. Soc., 85 (1963) 4020.
26 S. Mansy, T. E. Wood, J. C. Sprowles and R. S. Tobias, J. Am. Chem. Soc., 96 (1974) 1762.
27 C. O. Björling, A. Berggren and B. Nygard, Acta Chem. Scand., 16 (1962) 1481.
28 R. D. Armstrong and E. Barr, J. Electroanal. Chem., 20 (1969) 173.
29 K. Kunimatsu and R. Parsons, J. Electroanal. Chem., 100 (1979) 335.
30 F. Palmisano, E. Desinomi and P. G. Zambonin, J. Chromatogr., 306 (1984) 205.

Analytica Chimica Acta, 174 (1985) 115—122
Elsevier Science Publishers B.V., Amsterdam — Printed in The Netherlands

HETEROGENEOUS SAMPLES IN FLOW-INJECTION SYSTEMS
Part 1. Whole Blood

JEFFREY J. HARROW and JIŘÍ JANATA*
Department of Bioengineering, University of Utah, Salt Lake City, Utah 84112 (U.S.A.)
(Received 20th March 1985)

SUMMARY

It is shown that the direct analysis of heterogeneous samples by non-steady state flow methods is associated with error because of undefined dilution and dispersion. This problem is examined theoretically and confirmed experimentally on determinations of pH and CO_2 in whole blood. It is also shown that microbubbles attached to the surface of a microelectrode or CHEMFET can substantially reduce the precision of the results.

Although flow-injection systems are well established for the analysis of homogeneous solutions, the analysis of heterogeneous mixtures, such as whole blood, presents problems. The central assumption of flow injection analysis (f.i.a.) is that the dispersion of the sample is constant and reproducible, so that calibrating solutions and unknown samples are treated in the same way. However, blood cells are "designed" teleologically to be very efficient stirring elements [1]; i.e., their tumbling action in a shear flow field greatly increases the transport of oxygen to the capillary wall [2]. The consequence of this factor for the present purpose is that in unsegmented flow systems such as f.i.a., whole blood specimens are dispersed differently than are homogeneous calibrating solutions. In non-steady-state flow systems, this would represent a source of error. To our knowledge this problem has not been adequately addressed in the literature. In this first paper of a series, it is shown that the presence of red blood cells (RBC) can lead to two types of error: one is related to the hydrodynamic effect of the red blood cells on the dispersion, and the other to the effect of the heterogeneity of the sample on the dilution. The occurrence of other sources of error such as viscosity and bubbles, which can be controlled to some extent by the design of the manifold, is also discussed. A second paper deals with the solutions to these problems. It is shown that, in principle, complete elimination of all of these problems for whole blood is not possible in non-steady state systems such as f.i.a.

THEORY

Symbols used in this treatment are summarized in Table 1. The error arising from the dilution of a heterogeneous sample can be derived as follows. In

TABLE 1

List of symbols

C_a	Concentration of added standard
C_f	Final concentration
C_{max}	Concentration of the peak at its maximum
C_0	Sample concentration
D	Dispersion
D_{eff}	Effective dispersion
h	Hematocrit, or fraction of volume of sample which is cellular
n_a	Number of moles of added standard
n_0	Number of moles in sample
V_0	Sample volume

standard terminology [3], the dispersion D is the ratio of the concentration in the sample to the concentration in the peak at its maximum: $D = C_0/C_{max}$. Another way of looking at this is that the volume element of fluid which occurs at the peak maximum has been mixed with $D - 1$ volumes of carrier. To see this, a sample, which initially has volume V_0, concentration, C_0, and moles, n_0, may be considered. By adding $(D - 1)V_0$ volumes of carrier, the final concentration, C_f, becomes

$$C_f = n_0/[V_0 + (D - 1)V_0]$$

or

$$C_f = n_0/V_0D \tag{1}$$

Because $n_0/V_0 = C_0$, Eqn. 1 becomes $C_f = C_0/D$, thus $C_f = C_{max}$.

For a sample that is heterogeneous, the case is different, because the dilution of the aqueous phase and the total volume cannot be equal. For example, it can be seen (Fig. 1) that for a sample which is 50% of particulate by volume, a two-fold increase of total volume results in a three-fold increase of the volume of aqueous phase. An expression for this effect can be developed. The initial sample volume, V_0, consists of a fraction of particulates, hV_0, and a fraction of solution, $(1 - h)V_0$, where $0 \leqslant h \leqslant 1$ (typically 10–50%). The number of moles of the analyte in the liquid phase is then

$$n_0 = C_0(1 - h)V_0 \tag{2}$$

and the added volume will still be $(D - 1)V_0$. If the hydrodynamic behavior of the flow-injection system is assumed to be the same for a heterogeneous sample as for a homogeneous sample (which is true in the range of low flow rates) and if no exchange of the analyte occurs between the two phases, the final concentration will be

$$C_f = n_0/[(1 - h)V_0 + (D - 1)V_0] \tag{3}$$

Substituting for n_0 from Eqn. 2, this becomes

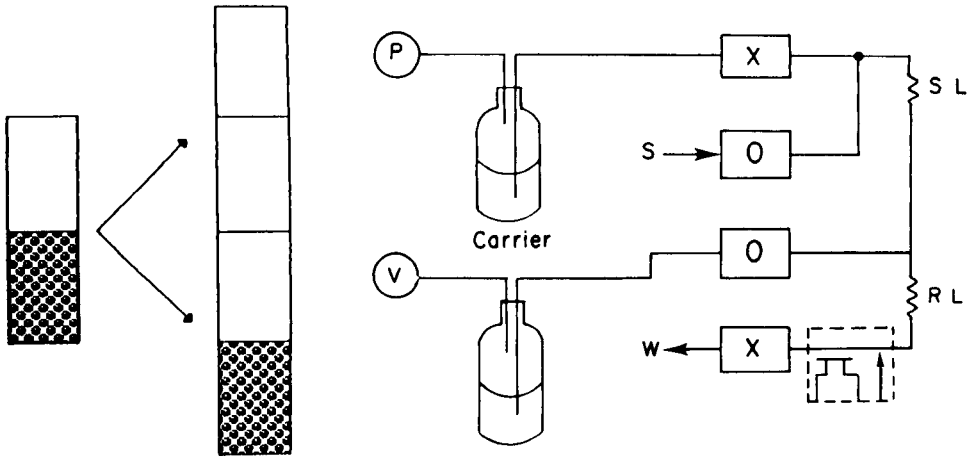

Fig. 1. The origin of the dilution error in heterogeneous samples. In the example shown, $D = 2$, and $h = 50\%$, thus $D_{eff} = 3$.

Fig. 2. Schematic diagram of the four-valve manifold and pH flow cell. Valves marked X are closed; valves marked O are open. Sample S is aspirated by vacuum, V, into the sample loop, SL. When the valves switch states, the carrier propels the sample through the reactor length, RL, past the CHEMFET detector and on to waste, W.

$$C_f = [C_0(1-h)V_0]/[(1-h)V_0 + (D-1)V_0] \quad (4)$$

Dividing by V_0 gives

$$C_f = [C_0(1-h)]/(D-h) \quad (5)$$

Thus,

$$D_{eff} = C_0/C_f = (D-h)/(1-h) \quad (6)$$

The effective dispersion is therefore a function of the hematocrit, just because of dilution considerations. In order to appreciate the magnitude of this effect, a medium-dispersion flow-injection manifold with dispersion equal to 5 may be considered. If a blood sample of hematocrit 40%, which is normal for a healthy male, is injected, it will have an effective dispersion of 7.7, if the assumptions of the model are valid (similar hydrodynamics and no exchange of analyte with the cells). This would result in an error greater than 50%.

EXPERIMENTAL

The CHEMFET detector, injection valve mechanism, reagent bottles, etc., were mounted on a breadboard (28 cm × 28 cm × 25 cm). Instead of a conventional rotary injection valve, a system of four solenoid valves was used for injection [4]. Interconnecting tubing was 0.5 mm inner diameter.

Measurements of pH

The manifold shown in Fig. 2 was used for the pH determinations. The sample loop was 25-cm (50 μl) coiled with a 1-cm diameter, and the reactor was a straight 75-cm segment. Initially, Freon was used for propulsion. The carrier solution was 0.140 M sodium chloride buffered with 0.02 M 3-(*N*-morpholino)propanesulfonic acid (MOPS), with pH adjusted to 6.7 by addition of sodium hydroxide. The sample solutions were based on the carrier solution, with pH adjusted to 7.4 by addition of sodium hydroxide. The viscosity of the samples was increased to approximately that of plasma (relative viscosity 1.67—2.35) and whole blood (3.8—5.7) by the addition of polyacrylamide. The resulting viscosity was measured with a capillary viscometer. Samples were prepared with a relative viscosity of 2.5 (referred to as V2) and 4.9 (referred to as V4). The pH 7.4 solution without any added polyacrylamide is referred to as V1. To make a protein-free red blood cell (RBC) suspension, washed cells were obtained from one-day-old citrated sheep blood by five repetitions of the cycle of centrifugation, decanting and resuspension in two volumes of V1, resulting in a suspension of pH 7.4, hematocrit 33%, referred to as B.

The peaks were recorded on a strip-chart recorder for graphical evaluation. Flow rates were adjusted by varying the gas pressure over the range of 0.05—0.8 bar, resulting in flow rates of 0.25—2 ml min^{-1}. At each flow rate, samples of V1, V2, V4, and B (all pH 7.4) were injected, along with a sample of V1 adjusted to pH 7.2. Conversion of the data from peak heights to pH units was done by linear interpolation, with the two injections of V1 (pH 7.4 and 7.2) serving as standards.

Measurements of pCO_2

Two slightly different methods were compared for the determination of carbon dioxide. These experiments were done one year apart, and the differences between them reflect the advances made in f.i.a. technology in this period. In the first experiment, a rotary injection valve was used with the gas-exchange cell available then [5]. The sample loop was 25 cm (50 μl). The carrier stream was 0.14 M sodium chloride buffered with 0.02 M MOPS, adjusted to pH 7.4. The acceptor stream was 0.10 M sodium sulfate, 0.4 mM in sodium hydrogencarbonate. The gas exchanger was home-made and consisted of a sandwich of microporous teflon tape between two acrylic blocks which were grooved to form two planar, complementary fluid channels of 4 cm × 2 mm × 0.2 mm.

To make protein-free RBC suspensions of known pCO_2, washed erythrocytes were obtained from one-day-old sheep blood by five repetitions of the cycle of centrifugation, decanting, and resuspension in two volumes of an isotonic pCO_2 buffer. The pCO_2 buffer consisted of 45 mM sodium chloride, 75 mM disodium hydrogenphosphate and 12 mM sodium hydrogencarbonate, adjusted to pH 7.40. The washed cells were suspended in an equal volume of this buffer, and aliquots of this suspension were further diluted to give sus-

pensions with hematocrits ranging from 2 to 30%. These were injected into the manifold, where both carrier and acceptor streams flowed continuously at a rate of 1 ml min^{-1} (driving pressure 0.5 bar). The actual pCO_2 of the solutions was assayed simultaneously by using an IL-813 blood gas analyzer (Instrumentation Laboratories, Lexington, MA), and the volume fraction of red cells (hematocrit) was determined by capillary centrifugation.

A year later, the four-valve solenoid injection system was used instead of a rotary injection valve. The gas-exchanger cell was built as described by Andisheh et al. [6]. It is based on a 5 × 1 × 1-cm PVC block, to which are applied multiple layers of adhesive-backed Kapton tape in which patterns have been cut to define the flow channels. A pH electrode is incorporated into the PVC block flush with the surface, using a PVC-based ion-selective membrane. Located 1 cm downstream from this electrode is a similarly built reference electrode. The first layer adjacent to the surface of the block is the tape layer which defines the flow path of the acceptor stream; next is the teflon membrane, then the tape layer for the donor (carrier) stream, then a sealing layer. The teflon layer does not extend the complete length of the two flow channels, but extends only as far as is necessary to cover the two electrodes. Consequently, the two channels join downstream of the electrodes, which equalizes the pressure across the gas-exchange membrane.

The flow conditions used were as specified by Andisheh et al. [6] and different from those used in the first method in that the acceptor stream did not flow continuously. After the sample loop had been loaded, its contents were injected into the carrier stream, which carried the sample over the teflon membrane while the acceptor stream was stationary. After a fixed period from the time of injection (10 s), the acceptor stream was turned on.

The samples and solutions were prepared in the same manner as in the first experiment, except that the acceptor stream was 0.14 M sodium chloride, 0.4 mM in sodium hydrogencarbonate. The experiments were controlled by an Apple II^+ personal computer.

RESULTS

Measurements of pH

Table 2 contains the peak heights of the standard solutions (pH 7.4 and 7.2), and of the test solutions which were all nominally pH 7.4, but with cells (B) or with viscosity 2 (V2) or 4 (V4) at six flow rates in the range 0.25—2.0 ml min^{-1}. The actual peak heights observed are listed in the columns headed *O*. The columns headed E show the expected peak heights of the test solutions, calculated from their pH values measured statically, based on the response of the system to the standard solutions. The ratios of the observed responses to the expected responses in the columns headed *O*/E, represent the influence of the matrix on the dispersion (*D*). The effective dispersion is obviously a function of both the matrix and of the flow rate. If

TABLE 2

Comparison of peak heights for pH measurements with different flow rates and viscosities. (See text for detail.)

Flow rate (ml min^{-1})	Peak height (arbitrary units)													
	Standards		Test solutions											
	7.4[a]	7.2[b]	V2[c]				V4[d]				B[e]			
			O	E	*O*/E	ΔpH	*O*	E	*O*/E	ΔpH	*O*	E	*O*/E	ΔpH
0.25	30.2	22.8	35.0	29.8	1.2	0.11	36.0	30.6	1.2	0.13	45.1	29.3	1.5	0.34
0.5	24.0	17.7	30.0	23.6	1.3	0.16	31.0	24.4	1.3	0.19	59.0	23.3	2.5	0.94
0.75	21.6	15.8	30.1	21.3	1.4	0.25	33.7	21.9	1.5	0.35	67.7	20.9	3.2	1.35
1.0	20.8	15.6	28.0	20.5	1.4	0.24	38.3	21.1	1.8	0.57	70.7	20.2	3.5	1.63
1.5	17.4	13.0	42.9	17.1	2.5	0.99	20.8	17.7	1.2	0.13	55.5	16.9	3.3	1.47
2.0	17.5	12.5	19.2	17.2	1.1	0.06	44.0	17.8	2.5	0.90	35.5	16.9	2.1	0.61

(a—e) pH measured statically: [a]7.39, viscosity 1; [b]7.22, viscosity 1, [c]7.38, viscosity 2; [d]7.40, viscosity 4; [e]7.37, blood cell suspension, hematocrit 33%.

this effect is ignored, and if a pH value is calculated from the response of the system to the standard solutions without any correction, an error will result. The columns headed ΔpH represent this error, i.e., the difference between the true pH, measured statically, and the calculated pH based on the calibration obtained from the standard solutions.

Figure 3 shows the peak symmetry [7] as a function of flow rate. In addition the peak half width increased with viscosity and decreased with cellularity. The data show that for all samples, peak symmetry declines and the pH error tends to increase with increasing flow rate. At all flow rates, V1 has the best symmetry, V2 and V4 have lower values, and B has the worst.

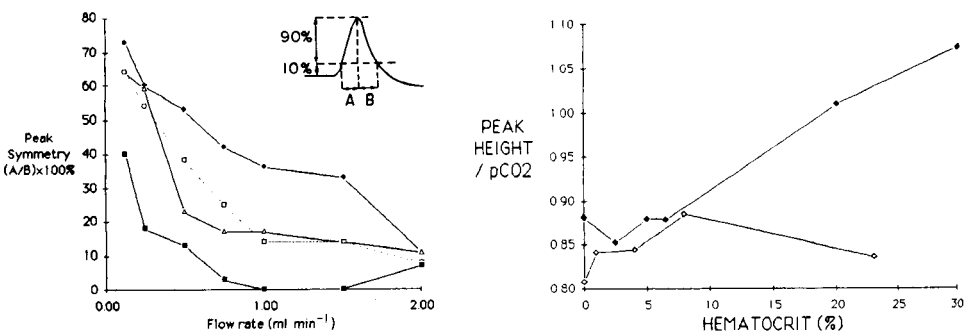

Fig. 3. Dependence of peak symmetry (A/B) on flow rate for samples of different viscosity and cell content. Samples: (•) V1; (△) V2; (□) V4; (■) B. For composition of samples, see text.

Fig. 4. Dependence of transfer function (peak height/pCO_2 in torr) on hematocrit for two different flow cells: (•) cell 1 with pCO_2 = 30; (○) cell 2 with pCO_2 = 60.

Measurements of pCO_2

In the first experiment, the pCO_2 of the suspensions, as measured by the IL-813, varied from 31 to 35 mmHg, and the hematocrit from 0 to 31%. In the second experiment, pCO_2 ranged from 58 to 68, and the hematocrit ranged from 0 to 23%. For each sample, the transfer function of the flow-injection system was calculated by dividing the peak height, in arbitrary units, by the measured pCO_2. Figure 4 shows the dependence of this transfer function as a function of the hematocrit for the two different manifolds; in the first experiment, increasing the hematocrit caused a larger transfer of CO_2 across the membrane, resulting in a change in the transfer function by approximately 40%, whereas in the second experiment, the transfer function was more constant, maintaining its value (±5%).

An inadvertent injection of a sample which contains an air bubble produces an oddly-shaped high peak; tiny bubbles can then become attached to the sensor surface causing distortion of subsequent peaks. The effect is, of course, random. It can be greatly reduced by using helium instead of Freon as the propellant gas. With helium, the best-case relative standard deviation of the peaks was 0.3%.

DISCUSSION

In f.i.a., the shape of the peak produced by the detector is a complicated function of many variables, including the sample volume, sample viscosity, reactor volume and geometry, flow rate, tubing diameter, detector response and geometry. Conditions which favor increased radial mixing decrease sample dispersion in the axial direction, resulting in higher and more symmetric peaks. Methods of increasing radial mixing include packing the reactor tube with beads, or coiling it to induce secondary flow. An excellent theoretical discussion of this phenomenon for aqueous solutions, with experimental data for various reactor types, is available [8].

A change of viscosity or introduction of RBC will also increase radial mixing. In other words, the dispersion is no longer constant, but is a function of the viscosity and cell content of the sample.

The same theory predicts that RBC will increase mass transport across a membrane, and the first experiment on carbon dioxide confirms this. The second experiment shows that by reducing the volume of the flow cell and by keeping the acceptor stream static, this effect is reduced. This may be explained by considering the boundary layer on the blood side of the membrane as a variable resistance, the value of which is a function of the hematocrit. When both streams flow, changes in the boundary-layer resistance will significantly change the amount of mass transport. If only the blood stream flows, the limiting resistance in the system is the resistance on the acceptor side, where diffusion occurs without the benefit of convective assistance.

The practical consequence of this is that by proper design of the system, it is possible to minimize the influence of increased stirring by red cells.

The bubble experiments show that although bubble effects can be minimized by proper degassing and by using helium as the propellant, it is impossible to eliminate them completely, and when a bubble appears, it will change the dispersion for a period of time extending beyond its passage through the system. Small surface detectors, such as microelectrodes and CHEMFETs, are particularly prone to this type of disturbance.

Both the bubble experiments and the viscosity/blood-cell experiments have a serious implication for non-steady-state flow analysis of whole blood. It is impossible to achieve accuracy by calibrating the system with aqueous standards and then make determinations on heterogeneous samples if the dispersion changes in an unknown manner, as will happen if a bubble is passed, or if neither the viscosity nor the hematocrit of the sample are known beforehand. These errors can be minimized, if not completely eliminated, by proper design of the manifold and the detector. However, the dilution error is fundamental and cannot be eliminated without prior knowledge of the hematocrit value. It is interesting to note that if the distance between the detector and the point of injection is minimized, the dispersion approaches unity, in which case the viscosity and hematocrit effect disappear altogether [6]. In that case, however, the flow-injection system operates essentially in a steady-state mode ($D = 1$), and the power to do chemistry by controlled mixing of sample with reagents is largely lost.

This work was partly supported by the NIGMS Grant number 22952. We also acknowledge the encouragement and support of our colleagues at Critikon Inc. One of us (J. J. H.) thanks Professor W. J. Kolff and the Institute for Biomedical Engineering for financial support during this work.

REFERENCES

1 H. Brenner and D. W. Cardiff, J. Coll. Interface Sci., 47 (1974) 199.
2 W. E. Stuart and J. P. Sorenson, Trans. Soc. Rheol., 16 (1972) 1.
3 J. Růžička and E. H. Hansen, Flow Injection Analysis, Wiley, New York, 1981.
4 J. J. Harrow and J. Janata, Anal. Chem., 55 (1983) 2461.
5 J. Růžička and E. H. Hansen, Anal. Chim. Acta, 134 (1982) 55.
6 L. Andisheh, N. J. Ho, J. Kratochvil, J. E. Moore, J. Růžička, L. Spritzer and B. Thompson, Proc. Int. Symp. Ion Select. Elect. Physiol. Med., Burg Rabenstein, W. Germany, August, 1983.
7 J. P. Foley and J. G. Dorsey, Anal. Chem., 55 (1983) 730.
8 J. M. Reijn, W. E. van der Linden and H. Poppe, Anal. Chim. Acta, 126 (1981) 1.

Analytica Chimica Acta, 174 (1985) 123—132
Elsevier Science Publishers B.V., Amsterdam — Printed in The Netherlands

HETEROGENEOUS SAMPLES IN FLOW-INJECTION SYSTEMS
Part 2. Standard Addition

JEFFREY J. HARROW AND JIŘÍ JANATA*
Department of Bioengineering, University of Utah, Salt Lake City, Utah 84112 (U.S.A.)
(Received 20th March 1985)

SUMMARY

It is shown that the effect of undefined dispersion in flow injection analysis (f.i.a.) of heterogeneous samples can be eliminated by the method of standard addition. This is a significant improvement over the direct calibration method. However, because f.i.a. is basically a precise dilution method, the initial free volume of the sample (e.g., total volume minus hematocrit, for whole blood) must be known in order to produce accurate results for such samples. The Gran plot technique is adapted for f.i.a. and it is shown that the dispersion, D, can be obtained from these experiments.

The method of standard addition is often used to overcome effects caused by the difference between the matrix of the sample and that of the standard solution. The principal requirement for this method to be applicable is that the response of the system be linear [1]. In order to meet this requirement various linearization procedures, including the Gran plot technique [2] for potentiometric electrodes, have been devised.

Traditionally, analysis of blood samples is done on the serum. With the advent of ion-selective electrodes, direct measurement of electrolytes on whole blood is possible by static measurement techniques. Several manufacturers offer instruments that will quantify two or more analytes in samples of heparinized whole blood. To conduct chemical manipulations, some sort of flow system must be used, which necessitates accounting for the rheological properties of blood. Flow injection analysis (f.i.a.) has been used to determine electrolytes in whole blood [3]; the flow conditions reported were such that pseudo-steady-state conditions were used, i.e., the sample loop was bigger than the reactor, resulting in a flat peak ($D = 1$). In this way, the flow-injection apparatus was used merely to present the sample to the detector and to wash it out.

Two groups have reported on the use of standard addition in conjunction with f.i.a. Israel and Barnes [4] used a method for atomic absorption spectrometry, which they called standard addition; the analyte was pumped continuously through the carrier stream into the nebulizer in order to obtain a steady-state absorbance signal. Discrete volumes of standard were injected into the analyte stream, resulting in transient absorbances, which were

positive when the concentrations of the standard were higher than the concentration of the analyte, and negative when the standard concentrations were lower. It does not solve all problems found in the analysis of whole blood, as it too is affected by changes in dispersion caused by matrix effects. Technology for true standard addition has been introduced by another group, who first used two linked sliding injection valves to dilute the sample first, and later to sample part of its dispersed tail for injection into a second system [5]. By this process, accurate 1:1000 dilutions were obtained. In a later paper [6], they used the double sliding valve to make a system with two identical injectors, for the sample and for the standard, which come together in a merging zone. By injecting different standards with the same sample, the coefficients of the general standard addition method can be determined. Parameters included a 500-μl sample size and a 70-cm mixing coil, which gave a flat peak, i.e., it was a steady-state method. These systems could not be used for multiple standard additions because of the incomplete overlap between the sample and the standard [7]. Instead, a system was used in which a concentrated standard was injected into a long reactor and its tail was sampled. By varying the time of sampling, the concentration of the standard was chosen. The diluted standard was then mixed with the injected sample in a two-line system with merging zones.

GENERAL CONSIDERATIONS

Standard addition techniques

In the method of standard addition, the response, r, of the sensor is assumed to be a linear function of the concentration, C, of the analyte. By adding a known amount, n_A, of standard A, which produces incremental response, Δr, the slope of the response, $\Delta r/n_A$, can be evaluated, and from that, the initial concentration can be calculated by the formula

$$C = r/\Delta r V_0/n_A = r n_A/\Delta r V_0 \quad (1)$$

By adding a fifth valve (valve 3 in Fig. 1) to the system described in the earlier paper [1], any of the addition techniques which were described in the

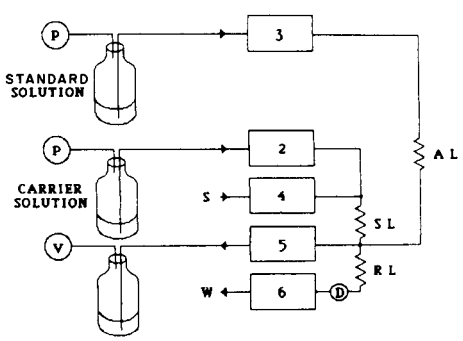

Fig. 1. Five-valve system used for standard addition: D, detector; P, pressure; V, vacuum; S, sample; W, waste; SL, sample loop; RL, reactor loop; AL, addition loop.

introduction can be implemented. Also, methods which could not be done by commutating valves, such as chopping of the sample by the standard, can be done with the solenoid valves merely by changing the computer-control software.

There are two basic schemes for designing a method for standard addition in f.i.a. In the first, one tries to utilize a single injection of sample, to which is added a standard appropriately timed so that two peaks result, one predominantly sample, and the other sample plus standard. In the other approach, multiple injections of sample are necessary. In each injection, a different amount of standard is added, and each injection results in a single peak.

The possibility of doing standard addition on a single injection is initially more appealing, as it promises shorter analysis times with less consumption of sample. However, it will be shown that this method has limitations which prevent its general applicability to the problem of difficult matrices.

Method of standard addition on a single injection

In this method, the sample, S, is injected and at some later time, t_i, the standard addition stream, A, (comprising the standard) is delivered for a period of time t_A. By varying t_i, double peaks can be generated (Fig. 2). These curves were obtained experimentally using the manifold of Fig. 1, with the experimental parameters given in the figure legend.

The amount of added standard is established from the formula

$$n_A = C_A Q_A t_A \qquad (2)$$

where n_A is the number of moles of added standard, C_A is the concentration of the added standard, and Q_A is the flow rate of the standard. To avoid dilution of sample, Q_A should be small compared to the flow rate of the carrier stream, Q_C, and t_A should be short compared to the sample injection time in order to prevent unnecessary peak broadening. These two constraints imply that C_A must be large, i.e., the addition should be a brief pulse of concentrated standard. The product of C_A, Q_A, and t_A, which is the amount of standard added, should be comparable to the amount of the sample.

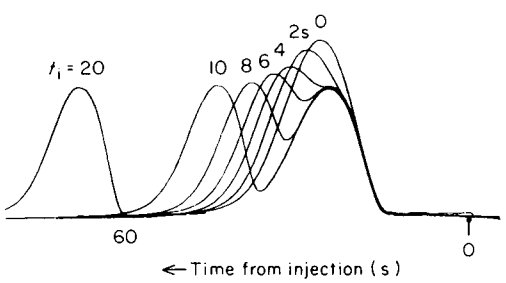

Fig. 2. Experimental peaks obtained by varying the delay time t_i. The first sample of 75 µl of 0.140 M NaCl/4 mM KCl was injected at $t = 0$ and the subsequent additions were made at times t_i as shown in the figure. The carrier was 0.140 M NaCl/0.5 mM KCl at a flow rate of 1.0 ml min^{-1}. The standard stream was 0.140 M NaCl/10 mM KCl flowing at 0.2 ml min^{-1}. The detector used was a potassium-ion CHEMFET flow cell [3].

If t_i is large compared to the peak width of the system, then the two peaks will be independent, without any region of mixing between the sample and the standard. This would not be standard addition, as the method of standard addition requires such mixing. It would be a way to calibrate the system with each injection for samples of similar matrix to the standard. This would address the problem of sensor gain drift, such as would be caused by adherent bubbles, but not the problem of differences in the dispersion during transport caused by matrix effects. If t_i is small compared to the peak width, then the two peaks will fuse into one and be unresolvable. Thus, to maximize mixing of the sample and standard, t_i should be as small as possible so that two peaks are still resolvable.

By using the tanks-in-series model, this situation has been computer-simulated. The computed curves closely resemble the experimental results (Fig. 3).

The curve which represents the case for which the peaks are as close together as possible and still distinguishable is divided into the concentration contributions from the first injection (the sample) and the second (the standard). It can be seen that at the peak maxima, there is very little overlap between sample and standard, i.e., because of the Gaussian shape of the peaks, the peaks must merge into one before there is any substantial degree of mixing.

It is tempting to try to put narrow peaks on a broader peak. However, this cannot be done if the standard is introduced at the same point as the sample because the width of a peak in f.i.a. is primarily determined by the transport process [8]. For the standard plus sample to undergo the same dispersive process as the sample alone, the standard must be introduced at the same point as the sample, which means that the peak widths will be similar, as in the simulation. Adding standard at a different point from the sample can be

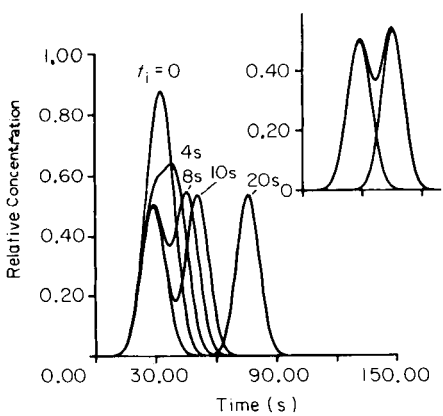

Fig. 3. Computer simulation of the variation of t_i. Conditions: 20 tanks; 30-s residence time; 0.5-s sample injection time; 0.05-s standard addition time. The numbers of moles injected are equal. The insert shows the simulated individual contributions resulting from the two injections at t_i = 10 s.

useful for determinations such as buffer capacity as long as the dispersion of the sample remains constant. However, this does not help in the problem of accurate determinations on heterogeneous samples such as whole blood, when the dispersion is unknown.

It is concluded that in order to achieve true standard additions, the standard must be introduced at the same point as the sample, and that the peaks must overlap to the point that they become unresolvable. Thus the method of standard addition cannot be done on a single injection.

Method of standard addition with multiple additions

In this method (Fig. 4), the sample is first injected without any addition of standard. After the first injection is completed, the sample loop is loaded a second time. Before the sample is injected, standard is added to the reactor loop at the junction of the sample loop and the reactor loop. Then, the sample and the standard are injected. As these two closely adjacent zones travel towards the detector, mixing occurs, so that by the time of their arrival to the detector, the two will have merged completely. By varying the duration of standard addition, t_A, the amount of added standard is controlled. As in the previous section, the standard should be concentrated, so that a brief pulse can be used. In this case, the reason for the brevity is that if the pulse is too long, then merging of the standard with the sample will be incomplete. Fortunately, this is an easy condition to meet.

Gran plot

The Gran plot technique [2] has been used to linearize the response of logarithmic detectors. The response of a potentiometric electrode, such as CHEMFET, is

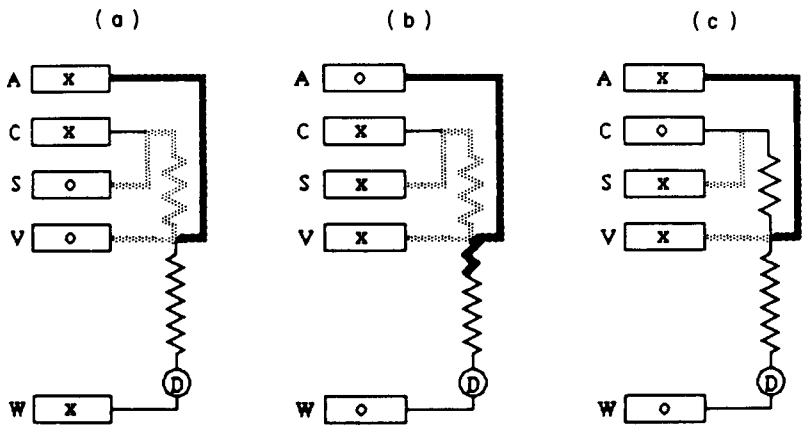

Fig. 4. Sequence used in the standard addition technique: (a) after loading, before addition; (b) after addition, before injection; (c) after injection. C, carrier solution; A, standard solution; other symbols correspond to those in Fig. 1; x and o mean that the valve marked is closed and open, respectively.

$$E = E^0 + S \log(n_0/V_0) \quad (3)$$

where S is the slope of the response. When volume, V_A, containing n_A moles of the analyte is added to sample (step 2, Fig. 4), the overall concentration, C, is $C = (n_0 + n_A)/(V_0 + V_A)$. As the sample and added standard travel to the detector, the added volume is $V_0 = (D - 1)V_0$ and the number of moles added is $n_0 = (D - 1)V_0C_0$. Thus the final potential after dispersion is

$$E' = E^0 + S \log[(Q_A t_A C_A + V_0 C_0 D)/(Q_A t_A + V_0 D)] \quad (4)$$

Equation 3 can be subtracted from Eqn. 4. Taking exponentials and rearrangement gives

$$10^{\Delta E/S} = \Omega = 1 + Q_A t_A (C_A - C_0)/C_0(Q_A t_A + V_0 D) \quad (5)$$

For a small volume of added standard and/or a large D, $Q_A t_A = V_A \ll V_0 D$ and Ω becomes a linear function of t_A

$$\Omega = 1 + Q_A t_A (C_A - C_0)/V_0 C_0 D \quad (6)$$

Under those conditions, the dispersion of the system can be evaluated from the slope of the plot of Ω against t_A and the initial (unknown) concentration of the sample, C_0, can be calculated from the intercept of the plot with the time axis ($\Omega = 0$, t_A^0), for which

$$C_0 = Q_A C_A t_A^0/(Q_A t_A^0 - V_0 D) \quad (7)$$

EXPERIMENTAL

Determination of potassium ion concentration

The feasibility of the Gran plot technique was first demonstrated with homogeneous solutions. The carrier was 0.14 M sodium chloride spiked with 0.5 mM potassium chloride. The standard was 0.14 M NaCl/20 mM KCl. The samples were 0.14 M sodium chloride, with 2, 4, 6 or 8 mM potassium chloride (referred to as **K2**, **K4**, **K6**, and **K8**). Helium propulsion was used. The sample loop was 100 μl (50 cm) and the reactor loop was a 75-cm coil. The flow rate of the carrier, Q_0, was 1 ml min^{-1}, and that of the standard was 0.2 ml min^{-1}. The potassium ion-selective electrode flow cell [3] was used.

The sequence of valve activation was as follows (see Fig. 4). First, the sample loop was loaded, by opening the valves to sample, S, and vacuum, V. After a period of 10 s, these valves were closed. Then the valve to waste, W, was opened. The valve to the standard, A, was opened for 1, 2, 4 or 8 s, and then closed. Finally, the valve to the carrier, C, was opened for 30 s. The results are shown in Fig. 5 in which D is a parameter. The departure of these plots from linearity for higher values of t_A indicates that Eqn. 6 is no longer valid.

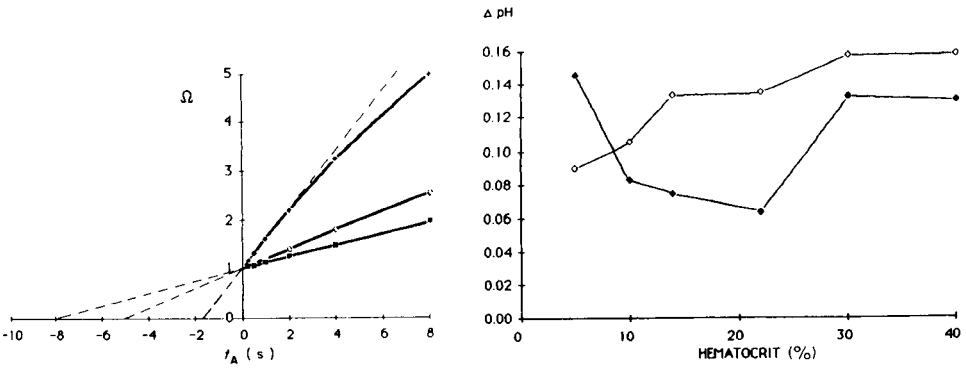

Fig. 5. The Gran plot for a flow-injection arrangement. The initial concentration of the sample, 0.5 mM K^+; Q_A = 0.2 ml min^{-1}; V_0 = 100 μl; C_A = 20 mM K^+. D: (•) 1; (○) 3; (▪) 5.

Fig. 6. pH error, ΔpH, caused by the hematocrit in a flow-injection system: (•) standard addition; (○) direct.

Determination of pH

The determination of pH by standard addition does not require the linearization of the signal as used above. A pH CHEMFET sensor was substituted for the potassium sensor, otherwise the manifold was the same. The carrier was 0.14 M NaCl/20 mM Na_2HPO_4/20 mM Tris buffer, adjusted to pH 7.14. From the carrier, solutions of pH 7.44 and 7.69 were made by addition of sodium hydroxide. Washed blood cells were prepared as before, using the pH 7.69 buffered saline solution. Samples of different hematocrits were prepared by mixing the washed blood cells with the pH 7.69 solution. The standard was 0.01 M hydrochloric acid. The carrier flow rate was 1 ml min^{-1}, and the standard flow rate was 0.2 ml min^{-1}. The sample loop was 100 μl, and the reactor coil was 75 cm of 0.5 mm i.d. tubing.

The system was calibrated by injections of the 7.40 and 7.69 buffers. Then, each of the samples was injected three times without standard, and three times with standard added for 4 s, which is equivalent to 13 μl or 130 nmol of acid.

The pH was determined by the direct method, using linear interpolation between the standards, and by the method of standard addition. The pH of the samples was also determined simultaneously by the IL-813 blood gas analyzer, and the actual hematocrit by capillary centrifugation.

The hematocrit value of the samples ranged from 5% to 40%. Their pH, as measured by the IL-813, varied from 7.63 to 7.40, depending on the hematocrit, becoming more acidic with greater hematocrit value. The difference between the pH as measured by the IL-813, and the pH determined by the two flow-injection methods is called ΔpH. The results are plotted in Fig. 6 as a function of the red blood cell (RBC) volume fraction (hematocrit) of

the samples. The graph shows that except for one data point, the method of standard addition yields results which were closer to the IL-813 than the direct method. However, the presence of hematocrit still introduces unacceptably high absolute error.

DISCUSSION

The effect of a heterogeneous sample on the standard addition technique can be examined as follows. If n_A mol of standard is added to the sample containing n_0 mol of analyte, then the resulting concentration after dispersion, C_{fA}, is

$$C_{fA} = [C_0(1-h)V_0 + n_A]/[(1-h)V_0 + (D-1)V_0] \quad (8)$$

where h is the hematocrit. Dividing by V_0 gives

$$C_{fA} = [C_0(1-h) + n_A/V_0]/(D-h) \quad (9)$$

The response to the added amount, n_A, is

$$\Delta r = K(C_{fA} - C_f) = Kn_A/V_0(D-h) \quad (10)$$

where K is a proportionality constant. Substitution of Eqn. 1 into Eqn. 10 and rearrangement gives

$$C = C_0(1-h)/V_0 = n_0/V_0 \quad (11)$$

In this equation, the D term disappears, confirming the expectation that the method of standard addition should be insensitive to differences of dispersion, be they caused by the hydrodynamics of the red cells, or by viscosity or even by bubbles adherent to the walls of the flow cell. But because the nonparticulate volume of the sample is unknown without prior knowledge of the volume fraction of cells (the hematocrit), the concentration cannot be determined by this measurement technique, only the total number of moles.

Thus, because of the unknown volume of distribution of analyte, the method of standard addition cannot be used to determine concentration directly. It can provide a technique for measurement which does not rely on the assumption of constant dispersion, but it determines total moles, not concentration. The same is true for the Gran plot technique as can be seen from Eqn. 6, which for a heterogeneous sample becomes

$$C_0 = Q_A t_A^0 C_A/[Q_A t_A^0 - (1-h)V_0 D] \quad (12)$$

from which the C_0 cannot be evaluated without prior knowledge of h.

Conclusions

The method of standard addition can be done by using the solenoid valve system, and this method measures pH in blood cell suspensions with an accuracy somewhat better than a direct measurement of peak height without standard addition. However, the dependence of this technique on knowledge

of the red-cell volume fraction (hematocrit) presents a fundamental problem for non-steady-state flow systems. A critical analysis of the process shows that the method actually determines the number of moles of sample in the free volume. Because this volume is unknown and it is being diluted (for $D > 1$), the method cannot give accurate determinations of concentration in heterogeneous samples. In homogeneous samples, the method of standard addition in f.i.a. provides a means of determination which does not assume a constant dispersion and can be used with both linear and logarithmic detectors. Thus, it can be useful as a robust method which would not be affected by changes in dispersion, such as those caused by bubbles or by viscosity.

This work was partially supported by the NIGMS Grant, Number 22952. One of us (J. J. H.) thanks Professor W. J. Kolff and the Institute for Biomedical Engineering for financial support. We also thank Dr. J. M. Reijn, University of Amsterdam, for computer simulation and our colleagues at Critikon Inc., for making their CHEMFET flow cells available.

NOTE ADDED IN PROOF

Gran plot in f.i.a. In the original paper the concentration of analyte in the carrier stream has been ignored which has resulted in a propagating error in Eqns. 3—7 and Eqn. 12. The correct derivation is given below.

The potential of an electrode in dispersed (D) sample of the initial concentration C_0 is

$$E = E^0 + S \log [n_0 + (D - 1)V_0C_0]/[V_0 + (D - 1)V_0] \quad (1)$$

where $(D - 1)V_0$ is the volume added due to dispersion and C_0 is the concentration of the analyte in the carrier stream. When volume of the standard addition solution V_A containing n_A moles of analyte is added the final potential after dispersion is

$$E' = E_0 + S \log [n_0 + n_A + (D - 1)V_0C_0]/[V_0D + V_A] \quad (2)$$

Equation 1 is subtracted from Eqn. 2 and the result is exponentiated yielding

$$10^{(E-E')/S} = \Omega = [V_0C_0 + (D - 1)V_0C_0 + Q_A t_A C_A]\, V_0D/(V_0D + Q_A t_A)\, [V_0C_0 + (D - t)V_0C_0] \quad (3)$$

Because $D \geqslant 1$ and V_A is small compared to V_0, $(Q_A t_A \ll V_0D)$,

$$\Omega = 1 + Q_A t_A C_A/[V_0C_0 + (D - 1)V_0C_0] \quad (4)$$

For $\Omega = 0$, $t_A{}^0$,

$$C_0 = -[Q_A t_A{}^0 C_A + (D - 1)V_0C_0]/V_0 \quad (5)$$

In the presence of hematocrit (volume fraction h) Eqn. 5 becomes:

$$C_0 = -[Q_A t_A{}^0 C_A + (D - 1)(1 - h)V_0C_0]/(1 - h)V_0 \quad (6)$$

REFERENCES

1 B. E. H. Saxberg and B. R. Kowalski, Anal. Chem., 56 (1979) 1031.
2 J. Buffle, N. Parthasarathy and D. Monnier, Chimia, 25 (1971) 223.
3 L. Andisheh, N. J. Ho, J. Kratochvil, J. E. Moore, J. Růžička, L. Spritzer and B. Thompson, Int. Symp. Ion Sel. Electr. Physiol. Med., Burg Rabenstein, West Germany, August, 1983.
4 Y. Israel and R. M. Barnes, Anal. Chem., 56 (1984) 1118.
5 B. F. Reis, A. O. Jacintho, J. Mortatti, F. J. Krug, E. A. G. Zagatto, H. Bergamin and L. C. R. Passenda, Anal. Chim. Acta, 123 (1981) 221.
6 E. A. G. Zagatto, A. O. Jacintho, F. J. Krug, B. F. Reis, R. E. Bruns and M. C. U. Araujo, Anal. Chim. Acta, 145 (1983) 169.
7 M. F. Gine, B. F. Reis, E. A. G. Zagatto, F. J. Krug and A. O. Jacintho, Anal. Chim. Acta, 155 (1983) 131.
8 J. M. Reijn, H. Poppe and W. E. Van der Linden, Anal. Chem., 56 (1984) 943.

Analytica Chimica Acta, 174 (1985) 133—139
Elsevier Science Publishers B.V., Amsterdam — Printed in The Netherlands

DETERMINATION OF MIXED POLYNUCLEAR AROMATIC HYDROCARBONS IN THE VAPOR PHASE BY LASER-INDUCED FLUORESCENCE SPECTROMETRY

D. L. PETERSON and F. E. LYTLE*

Department of Chemistry, Purdue University, West Lafayette, Indiana 47907 (U.S.A.)

N. M. LAURENDEAU

Flame Diagnostics Laboratory, School of Mechanical Engineering, Purdue University, West Lafayette, Indiana 47907 (U.S.A.)

(Received 4th March 1985)

SUMMARY

Laser-induced fluorescence spectrometry is shown to be a viable technique for quantifying polynuclear aromatic hydrocarbons (PAH) in the vapor phase. Mixtures of anthracene, fluoranthene, and phenanthrene were analyzed in a vapor cell at temperatures ranging from 50° to 90°C. The individual concentrations of PAH's in these mixtures were calculated by a least-squares matrix technique and were accurate to within 3—5% at levels of about 5×10^{12}—3×10^{15} molecules cm^{-3}.

Laser-induced fluorescence spectrometry (l.i.f.s.) is being developed as a non-intrusive method for determining concentrations of species such as polynuclear aromatic hydrocarbons (PAH's) in combustion sources. These compounds are known to be formed in flames and their possible role in soot formation has been discussed in numerous reviews [1—7]. Laser Raman and fluorescence techniques can provide in-situ, spatially resolved, dynamic measurements of flame species [8—10]; hence, they are of interest in combustion diagnostics.

Laser-induced fluorescence spectrometry has long been used to detect PAH's at the sub-part-per-trillion level in fluid solutions [11]. More recently, Whitaker and Bushaw [12] reported detection of pyrene at the $\mu g\ l^{-1}$ level in the vapor phase. By injecting PAH's into the post-reaction zone of an ethylene/air flame, Coe and Steinfeld [13] obtained emission spectra of pyrene and fluoranthene at flame temperatures. The spectra were slightly broadened by the elevated temperatures but remained indicative of the species injected. Further work by Coe et al. [14, 15] examined individual excitation and emission spectra of pyrene, fluoranthene, and acenaphthalene under flame conditions.

Jandris and Force [16] examined the linearity of the fluorescence signal versus concentration for anthracene and fluoranthene as vapors. Plots of log

0003-2670/85/$03.30

(fluorescence intensity X temperature) vs. 1/temperature were linear over five orders of magnitude for anthracene, and over four orders of magnitude for fluoranthene. The 1.9-cm pathlength vapor cell was kept at a pressure of 3 torr. These authors also suggested that a mixture of anthracene and fluoranthrene could be quantitatively resolved by using bandpass filters for emission wavelength selectivity and time discrimination based on lifetime differences.

In this paper, the gas-phase fluorescence intensities of anthracene, fluoranthene, and phenanthrene were monitored directly in a heated, 1-atm. pressure cell by l.i.f.s. Linear plots of fluorescence intensity versus number density (molecules cm^{-3}) were recorded at five emission wavelengths for each PAH. These plots were used to generate a system of overdetermined linear equations which were then used to quantify mixtures of the same three PAH's. The calculated values were correct within 5.2% for anthracene, 0.98% for fluoranthene, and 2.9% for phenthanrene.

EXPERIMENTAL

Instrumentation and chemicals

The apparatus is shown in Fig. 1. The excitation source was a Molectron DL18 dye laser pumped by the second harmonic (532 nm) of a Molectron MY34 Nd:YAG laser. The laser pulse had a 3-ns temporal bandwidth (FWHM) and a repetition rate of 10 Hz. The dye laser output was frequency-doubled, producing typical pulse energies of 0.8—1.4 mJ at the excitation

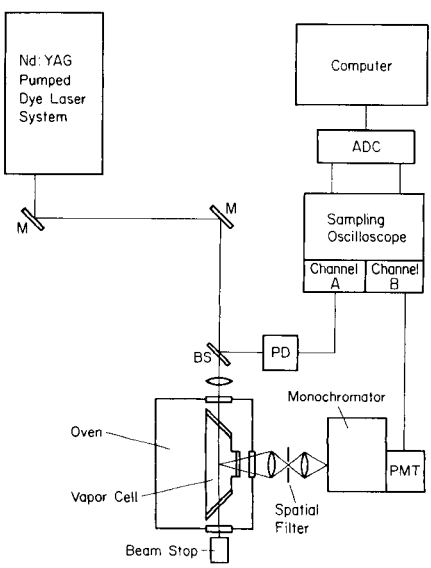

Fig. 1. Apparatus: BS, 4% beam splitter; M, u.v. coated dielectric total reflectors; PD, photodiode; PMT, photomuliplier; ADC, analog/digital converter. Components are described further in the text.

wavelength of 282 nm. The laser dye was rhodamine 6G (Eastman Kodak Co.) which was used as received.

A 250-cm focal length quartz lens was used to focus the laser radiation into the vapor cell. The resultant fluorescence signal was collected and focused onto the entrance slit of a 1/4-m Schoeffel GM-252 monochromator by using a dual lens/spatial filter arrangement. A slit width of 0.3 mm was chosen to produce a bandpass of 2 nm. The resultant probe volume and average laser power density were approximately 0.04 cm^3 and 90 mW cm^{-2}, respectively. A fast-wired RCA 1P28B photomultiplier was used to detect the output of the monochromator [17]. The signal produced by the photomultiplier was processed by a Textronix (7S14) 350-ps sampling oscilloscope and digitized by a microcomputer-controlled analog/digital converter. The microcomputer also provided stepper motor control of the monochromator.

Prior to reaching the fluorescence cell, a portion of the laser beam was picked off with a quartz plate, attenuated with a neutral density filter, and detected with a Texas Instruments TIED-56 photodiode. The signal from the photodiode was also processed by the sampling oscilloscope and microcomputer for use as a peak power monitor.

The fluorescence cell consisted of a pyrex tube (2.54-cm diameter) with quartz windows. The windows in line with the excitation laser beam were placed at Brewster's angle to minimize stray reflections. The cell had a 12-cm path length which further reduced interferences from the cell windows. A small removable nipple at the bottom of the cell held the solid PAH's and an opening on the side of the cell provided connections to a vacuum pump and nitrogen for pressure and atmospheric control. The cell was placed in a convection oven with quartz optical access ports. The temperature stability of the oven was $\pm 1°C$.

The PAH's, obtained commercially, were used as received: anthracene (Aldrich, 99+%), fluoranthene (Aldrich, 98+%), and phenanthrene (Aldrich, 98+%). The emission spectra of these PAH's in the vapor phase were compared to reference spectra of pure compounds in the liquid phase and were found to be essentially free of fluorescing impurities.

Procedures

The PAH's tended to adhere to the walls of the cell thus making a lengthy cleaning procedure necessary prior to each run. The cell was rinsed with ethanol, soaked in a nitric/sulfuric acid solution for 24 h, and then rerinsed several times with ethanol. The cell was then positioned in the oven, heated to 150° C and pumped down for 1 h to minimize background fluorescence.

While the cell was cooling, the collection optics were adjusted to maximize the Rayleigh scattering signal. This daily adjustment corrected for any changes in the cell position. Once the cell had cooled to room temperature, the cell nipple was removed and filled with an excess of a single PAH. The nipple was replaced and the cell flushed three times with nitrogen. Vapor-phase mixtures were created by mixing together excesses of solid PAH's and placing

them in the cell nipple. Throughout the experiment, the total pressure in the cell was maintained at 1 atm., with over 99% of this pressure accounted for by the nitrogen diluent.

With the cell at 22°C, background measurements were recorded. The background levels were high because of scattering off the cell walls. At the lower limit of the linear range (50°C), the background was approximately 5% of the maximum fluorescence signal. The cell was then heated (50—90°C) to provide a range of concentrations of vapor-phase PAH's. The fluorescence intensities were averaged over 1200 laser pulses and were corrected for both laser power and background.

At each temperature, purity checks were obtained by recording spectra of the individual PAH's over the 350—500-nm range. However, for the generation of calibration curves, the fluorescence intensities were monitored at only five emission wavelengths: 360, 370, 390, 400, and 460 nm. This allowed more extensive signal averaging for a given period of time.

The vapor pressures of the PAH's over the temperature interval were calculated by using the Antoine equation $\log P = A - B/(C + T)$. This equation is suitable for pressures ranging from 0.015 to 2 atm. The constants A, B, and C used for calculating the vapor pressures of anthracene, fluoranthene, and phenanthrene were obtained from API monographs [18, 19]. The concentrations of the PAH's were then calculated by using the vapor pressure and the ideal gas law.

RESULTS AND DISCUSSION

The vapor-phase spectra of anthracene, fluoranthene, and phenanthrene were the same as those reported for the PAH's in cyclohexane [20]. No spectral shift or hot bands were observed for temperatures ranging from 50° to 90°C. The monitored emission wavelengths were chosen to correspond to significant peaks in the emission spectra: 360, 370, and 390 nm for phenanthrene, 390 and 400 nm for anthracene, and 460 nm for fluoranthrene. The relative fluorescence intensities of each compound normalized to a concentration of 1×10^{14} molecules cm^{-3} are given in Table 1.

TABLE 1

Normalized fluorescence intensity for 1×10^{14} molecules cm^{-3} at different emission wavelengths

PAH	Normalized fluorescence intensity				
	360 nm	370 nm	390 nm	400 nm	460 nm
Anthracene	0.21	0.56	0.68	0.68	0.36
Fluoranthene	0.21	0.24	0.36	0.51	1.0
Phenanthrene	0.14	0.036	0.027	0.0088	—[a]

[a]No observable signal over background level.

The linear dynamic range, slope, intercept, and standard deviations of the slope and intercept of plots for fluorescence (intensity/laser power) versus number density (molecules cm^{-3}) for the five emission wavelengths of each PAH are given in Table 2. Each calibration consists of data taken on three or more days and has been corrected for both laser power and background fluctuations. The lower limit of the linear range is dictated by the operating range of the oven and the upper limit is a consequence of the long pathlength of the cell. The linear ranges, however, are sufficient to demonstrate the quantitation of a mixture of the three PAH's.

As expected, the steepest slope of the calibration for each PAH corresponds to the peak of the respective emission spectrum. All the intercepts are low positive numbers with the exception of the plots for phenanthrene at emission wavelengths of 370, 390, and 400 nm. The intercepts of these calibration curves, although negative, are close to zero. The slopes and intercepts of the calibration plots were used to construct a system of over-determined linear equations.

The fluorescence intensities of mixtures of anthracene, fluoranthene, and phenanthrene were measured at the five emission wavelengths. These data were combined with the calibration results for single compounds and the individual concentrations of each PAH were computed by least-squares matrix calculations. The results are given in Table 3. The sum of the squares of the residuals was $\leqslant 0.0001$ for all the mixtures, therefore, the three-component

TABLE 2

Summary of calibration parameters

Compound	λ_{em}	Slope[a]	Intercept[a]
Anthracene[b]	360	5.46×10^{-15} (6.39×10^{-16})	0.308 (0.040)
	370	1.66×10^{-14} (2.31×10^{-15})	0.668 (0.146)
	390	2.20×10^{-14} (9.59×10^{-16})	0.618 (0.068)
	400	2.46×10^{-14} (8.27×10^{-16})	0.350 (0.058)
	460	1.27×10^{-14} (6.30×10^{-16})	0.221 (0.045)
Fluoranthene[c]	360	5.35×10^{-15} (2.28×10^{-16})	0.327 (0.069)
	370	6.38×10^{-15} (1.68×10^{-16})	0.348 (0.051)
	390	9.77×10^{-15} (3.31×10^{-16})	0.552 (0.092)
	400	1.37×10^{-14} (4.57×10^{-16})	0.774 (0.139)
	460	3.64×10^{-14} (8.03×10^{-16})	0.426 (0.205)
Phenanthrene[d]	360	1.51×10^{-15} (4.60×10^{-17})	0.422 (0.053)
	370	2.29×10^{-15} (2.81×10^{-17})	0.080 (0.032)
	390	1.43×10^{-15} (3.25×10^{-17})	0.032 (0.037)
	400	7.86×10^{-16} (2.09×10^{-17})	0.042 (0.022)
	460	5.21×10^{-16} (2.41×10^{-17})	0.553 (0.028)

[a]With standard deviation in parentheses. [b]Linear range 5×10^{12}—2×10^{14} molecules cm^{-3}. [c]Linear range 1×10^{13}—7×10^{14} molecules cm^{-3}. [d]Linear range 5×10^{13}—2×10^{15} molecules cm^{-3}.

TABLE 3

Results of analysis of mixtures[a]

Temp. (°C)	Actual number densities (10^{13} molecules cm^{-3})			Calculated number densities (10^{13} molecules cm^{-3})			Standard errors (10^{13} molecules cm^{-3})		
	Anth	Fluor	Phen	Anth	Fluor	Phen	Anth	Fluor	Phen
50	0.438	1.42	7.82	0.461	1.41	7.60	0.169	0.136	0.532
55	0.817	2.42	13.0	0.809	2.39	13.1	0.144	0.116	0.453
65	2.63	6.63	34.1	2.60	6.63	34.1	0.150	0.121	0.471
73	6.23	14.1	70.1	6.23	14.1	69.8	0.104	0.084	0.329
85	20.6	41.0	192	20.6	41.0	192	0.223	0.179	0.701
90	32.8	62.4	285	32.8	62.4	285	0.198	0.160	0.625

[a]Anth = anthracene, Fluor = fluoranthene, Phen = phenanthrene.

linear model was assumed to be valid. The greatest errors in the calculated values for the individual PAH's are 5.2% for anthracene, 0.98% for fluoranthene, and 2.9% for phenanthrene. Over most of the linear range, the calculated value is correct to within 1%. At temperatures exceeding 90°C, the concentrations of the PAH's are high enough to give detectable non-linear absorption effects.

These results demonstrate that a three-component mixture of vapor-phase PAH's can be quantified by laser-induced fluorescence spectrometry. Some of the problems encountered with the static vapor cell should be eliminated by using a burner, because the flowing system will prevent the accumulation of PAH's on the walls, which will, in turn, reduce scattering from the walls and windows. Further investigations will include two-photon excitation studies and measurements in flame environments. The two-photon excitation studies are of particular interest because of the potential reduction in background levels.

We thank Mr. Paul Ludington for his initial work on the experimental equipment. This research was supported by the Department of Energy Office of Basic Energy Sciences, Contract No. DE-ACO2-78ERO4939.

REFERENCES

1 B. B. Chakraborty and R. Long, Combust. Flame, 12 (1968) 226.
2 M. L. Lee and K. D. Bartle, in D. C. Siegla and G. W. Smith (Eds.), Particulate Carbon Formation During Combustion, Plenum Press, New York, 1980, p. 91.
3 H. F. Calcote, Combust. Flame, 42 (1981) 215.
4 B. S. Haynes and H. Gg. Wagner, Prog. Energy Combust. Sci., 7 (1981) 229.
5 J. P. Longwell, 19th Symposium (International) on Combustion, The Combustion Institute, Pittsburgh, Pennsylvania, 1982, p. 1339.
6 K. H. Homann, Formation of Large Molecules, Particulates, and Ions in Premixed Hydrocarbon Flames; Progress and Unresolved Questions, 20th Symposium (International) on Combustion, Ann Arbor, Michigan, 1984.

7 J. D. Bittner and J. B. Howard, in D. C. Siegla and G. W. Smith (Eds.), Particulate Carbon Formation During Combustion, Plenum Press, New York, 1980, p. 109.
8 A. C. Eckbreth, P. A. Bonczyk and J. F. Verdieck, Prog. Energy Combust. Sci., 5 (1979) 253.
9 D. R. Crosley (Ed.), Laser Probes for Combustion Chemistry, ACS Symposium Series, No. 134, American Chemical Society, Washington, D.C., 1980.
10 A. D'Allessio, in D. C. Siegla and G. W. Smith (Eds.), Particulate Carbon Formation During Combustion, Plenum Press, New York, 1980, p. 207.
11 J. H. Richardson and M. E. Ando, Anal. Chem., 49 (1977) 955.
12 T. J. Whitaker and B. A. Bushaw, J. Phys. Chem., 85 (1981) 2180.
13 D. S. Coe and J. I. Steinfeld, in D. R. Crosley, (Ed.), Laser Probes for Combustion Chemistry, ACS Symposium Series No. 134, American Chemical Society, Washington, D.C., 1980, p. 159.
14 D. S. Coe and J. I. Steinfeld, Chem. Phys. Lett., 76 (1980) 485.
15 D. S. Coe, B. S. Haynes and J. I. Steinfeld, Combust. Flame, 43 (1981) 211.
16 L. J. Jandris and R. K. Force, Anal. Chim. Acta, 151 (1983) 19.
17 J. M. Harris, F. E. Lytle and T. C. McCain, Anal. Chem., 48 (1976) 2095.
18 A. P. Kudchadker, Anthracene and Phenanthrene, API Monograph Series, American Petroleum Institute Publication 708, 1979.
19 A. P. Kudchadker, S. A. Kudchadker, R. C. Wilhoit and S. K. Gupta, Acenaphthalene, Fluorene, and Fluoranthene, API Monograph Series, American Petroleum Institute Publication 715, 1981.
20 J. B. Berlman, Handbook of Fluorescence Spectra of Aromatic Molecules, Academic Press, New York, 1971.

Analytica Chimica Acta, 174 (1985) 141—149
Elsevier Science Publishers B.V., Amsterdam — Printed in The Netherlands

THE SYNTHESIS AND ANALYTICAL CAPABILITIES OF CHROMOGENIC AZA-12-CROWN-4 AS A SELECTIVE REAGENT FOR LITHIUM ION

K. SASAKI[a] and G. PACEY
Department of Chemistry, Miami University, Oxford, OH 45056 (U.S.A.)
(Received 31st January 1985)

SUMMARY

The synthesis and analytical capabilities of a new chromogenic crown ether, 1-(2-hydroxy-5-nitrobenzyl)-1-aza-4,7,10-trioxacyclododecane, chromogenic aza-12-crown-4. Constants found for this aza-12-crown-4 were pK_{a1} = 5.77, pK_{a2} = 10.31, pK_{ex} (Li) = 10.18, and pK_{ex} (Na) = 12.50. The calibration curve obtained for the extraction-spectrophotometric procedure was linear from 0.3 to 2 $\mu g\ ml^{-1}$. The imprecision of the measurement was calculated from the mean value of the standard deviations of triplicate samples over the linear range and was less than 5%. Results for the determination of lithium in blood serum and urine exhibited good agreement with atomic absorption data.

Selective reagents which permit the isolation of a particular ion from a complex matrix or mixture of ions are of interest to many chemists. When the matrix in question includes two or more alkali metals cations, it is often difficult to isolate one alkali metal ion from the mixture without interference from the others. With respect to biological systems, such as blood serum which contains a relatively large amount of sodium ion, a reagent having the ability to extract lithium ion selectively (and quantitatively) in the presence of sodium ion is of interest for biochemical assays.

The ability of crown ethers to extract alkali and alkaline earth metal ions selectively was recognized by Pedersen [1]. Nonetheless, there has been little successful work in utilizing these compounds for analytical purposes (other than in ion-selective electrodes) until quite recently [2—8]. Crown ether reagents which can be used for the spectrophotometric determination of mg l^{-1} concentrations of potassium ion in the presence of higher concentrations of sodium ion have most frequently been reported.

The background for this work was the crown ether *N*-(2-hydroxy-5-nitrobenzyl)-aza-15-crown-5 which was reported to be an extractant for lithium ion [9]. Although this compound was efficient for extracting lithium ion ($-\log K_{ex}$ (LiL) = 9.15), the extraction efficiency of the reagent for sodium

[a]Present address: Department of Chemistry, Faculty of Science, Nagoya University, Nagoya 464, Japan.

0003-2670/85/$03.30

ion was of the same order of magnitude (—log K_{ex} (NaL) = 9.76), thus the selectivity was poor.

Another compound of interest is cryptand [2.1.1] [8], which extracts lithium ions more selectively and more efficiently than the previous chromogenic aza-15-crown-5 reagent. However, not only is cryptand [2.1.1] difficult to synthesize, but the cryptand also requires an ion-pairing reagent, in this case resazurin, in order to exhibit sensitivity to lithium. The [2.1.1] cryptand by itself is not selective for lithium ions.

This paper describes the synthesis and analytical capabilities of a new chromogenic crown ether, 1-(2-hydroxy-5-nitrobenzyl)-1-aza-4,7,10-trioxacyclododecane, essentially chromogenic aza-12-crown-4.

EXPERIMENTAL

Syntheses

The chromogenic aza-12-crown-4 was synthesized by the following reaction scheme:

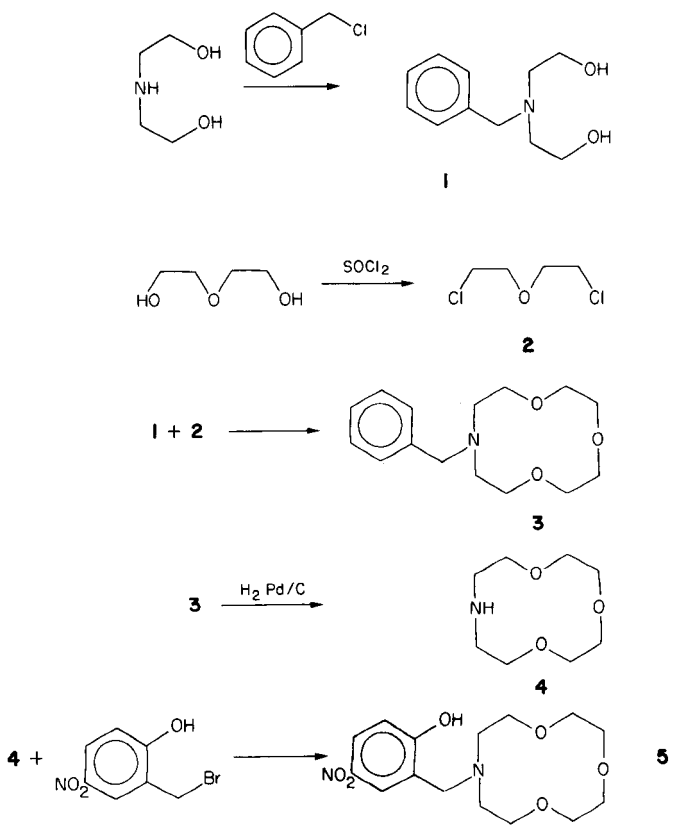

Preparation of 3-benzyl-1,5-diol-3-azapentane (1). Benzyl chloride (158 g, 1.25 mol) was stirred, with a water bath for cooling, while diethanolamine (126 g, 1.2 mol) was gradually added. The temperature of the reaction mixture was kept below 70°C until it became homogeneous and heat-release stopped. It was then kept at 70°C for ⩾1 h, left to cool, and added to 200 ml of 1 M hydrochloric acid. The aqueous solution was washed with four 100-ml portions of chloroform. To the aqueous solution, 300 ml of 5 M sodium hydroxide was added, with water-bath cooling, in order to isolate the oily product. The oil layer was mixed with 300 ml of chloroform, washed with 100 ml of water and dried over anhydrous magnesium sulphate. The chloroform solution was evaporated to dryness. The pure compound 1 was obtained as a light-yellow oil. [Yield 67%. ^{1}H-n.m.r. ($CDCl_3$): δ 2.50—2.68 (t, 4H, N—CH_2), δ 3.2 (br, 2H, OH), δ 3.41—3.60 (t, 4H, O—CH_2); δ 3.60, (s, 2H, Ar—CH_2), δ 7.10 (s, 5H, Ar—H).]

Preparation of 1,5-dichloro-3-oxapentane (2). In a procedure similar to that described by Pedersen [1], diethylene glycol was chlorinated with thionyl chloride in the presence of pyridine in benzene. The product was purified by vacuum distillation (0.7 Torr, 40°C—0.25 Torr, 35°C). [Yield 69%. ^{1}H-n.m.r. ($CDCl_3$): δ 3.4—3.9 (m, 8H).]

Preparation of 1-benzyl-1-aza-4,7,10-trioxacyclododecane (3). The cyclization of the diol (1) with the dichloride (2) was done under the template effect of lithium ions in a highly diluted solution as suggested by Miyasaki et al. [10]. A 1.6-l portion of t-butyl alcohol was refluxed together with lithium metal (6.2 g, 0.9 mol) with stirring for 2 h. Diol 1 (58.5 g, 0.3 mol) dissolved in 50 ml of t-butyl alcohol was added to the reaction mixture and refluxing was continued for an additional 2 h. Dichloride 2 (42.9 g, 0.3 mol) and lithium bromide (26 g, 0.3 mol) were added to the reaction vessel and the heterogeneous mixture was refluxed for 10 days to ensure reaction. The alcohol solvent was evaporated by rotary evaporation. Water (250 ml) was added to the residue to dissolve the inorganic salts and a reddish-brown oil was isolated. The oil layer was mixed with 60 ml of chloroform, washed with three 30-ml portions of 1 M sodium hydroxide, and slowly mixed with 100 ml of 5 M hydrochloric acid while room temperature was maintained by water cooling. Thereafter, the aqueous layer was washed with three 50-ml portions of chloroform, and 80 ml of 4 M sodium hydroxide was added slowly to a cooled vessel containing the aqueous solution to isolate the oil. The cooled mixture was extracted with chloroform, the organic layer was dried over anhydrous magnesium sulphate and evaporated to dryness under vacuum. The pure compound 3 was obtained by vacuum distillation (0.027 Torr, 112°C—0.04 Torr, 123°C). [Yield 63%. ^{1}H-n.m.r. ($CDCl_3$): δ 2.5—2.75 (m, 4H, N—CH_2), δ 3.35—3.65 (m, 14H, 0—CH_2, Ar—CH_2), δ 7.10 (s, 5H, Ar—H).]

Preparation of 1-aza-4,7,10-trioxacyclododecane (4). Compound 3 (45.1 g, 0.17 mol), ethanol (7 g), and 10% palladium on carbon (0.5 g) were shaken in a hydrogen atmosphere at 50 psi. Shaking was continued until the pressure

became constant. After the palladium/carbon had been filtered off, the solvent was evaporated. The pure compound 4 was sublimed from the residue with gentle heating on a water bath (75—77°C; crude material melted at this temperature). The sublimate formed white needles and was hygroscopic. [Yield 60%. ^{1}H-n.m.r. (D_2O): δ 2.53—2.70 (t, 4H, N—CH_2), δ 3.5—3.75 (m, 12H, O—CH_2), no signal at 7.1 (Ar—H of benzyl group, possible contaminant).]

Preparation of 1-(2-oxy-5-nitrobenzyl)-1-hydro-1-aza-4,7,10-trioxacyclododecane (5). The aza-crown 4 (1.05 g, 0.0060 mol), freshly distilled tetrahydrofuran (THF; 50 ml), and potassium hydroxide pellets (0.8 g, 0.014 mol) were placed in a flask. A solution of 2-hydroxy-5-nitrobenzyl bromide (1.40 g, 0.0060 mol) in THF was added with vigorous stirring, which was continued for 14 h. Bright yellow and white powders were produced, and the potassium hydroxide pellets were completely consumed. After evaporation of the solvent, the residue was dissolved into water (20 ml), and 6 M hydrochloric acid (about 2.2 ml) was added dropwise until the solution turned colorless or pale yellow (diprotonated form). The solution was extracted with chloroform while 5 M potassium hydroxide was added dropwise to convert the diprotonated compound to the monoprotonated dipolar ion (5), which was easily extracted into chloroform. The addition of potassium hydroxide and shaking for extraction were continued until no increase in the color intensity of the aqueous layer was observed. The aqueous layer was extracted with two 20-ml portions of chloroform. All the chloroform solutions were combined, washed with four 20-ml portions of water, filtered through dry filter paper and evaporated to dryness. The residue was dissolved in water, filtered and evaporated to dryness in order to remove water-insoluble impurities. The pure compound 5 was obtained by dissolution of the residue into chloroform and evaporation to dryness in vacuum with heating (80—90°C). Compound 5 (bright yellow) crystallized slowly from a glassy solid. [Yield 93%; m.p. 98.5°C. ^{1}H-n.m.r. ($CDCl_3$): δ 2.6—2.8 (m, 4H, N—CH_2), δ 3.5—3.8 (m, 14H, O—CH_2, Ar—CH_2), δ 6.62—6.77 (d, 1H, Ar—H), δ 7.72—8.02 (m, 2H, Ar—H). Found: 55.3% C, 7.0% H, 8.5% N. Calcd. for $C_{15}H_{22}O_6N_2$: 55.2% C, 6.8% H, 8.6% N.]

Determination of acidity constants, K_{a1} *and* K_{a2}

An aqueous solution (50 ml) containing the crown ether reagent (8.70×10^{-5} M), hydrochloric acid (6×10^{-4} M), and cesium chloride (0.1 M) was titrated with potassium hydroxide (0.1 M below pH 12, or 1 M above pH 12); a Metrohm automatic titrator (Dosimat E535 equipped with Potentiograph E536) was used. The titration was interrupted at every 0.3—1.5 pH increase for measurement of the absorption spectrum of the solution. A 3—4-ml portion of the solution was removed to a cuvette, the spectrum was recorded on a Hewlett-Packard 8450A spectrophotometer, and the solution was returned to the titration vessel with a pipet. The spectrum was corrected for dilution.

Liquid-liquid extraction of solutions containing lithium ion

Into each of a series of nine 50-ml round-bottomed flasks was placed 5 ml of chloroform and 5 ml of an aqueous solution containing the aza-12-crown-4 reagent (6.7×10^{-4} M = 22 μg ml^{-1}), potassium hydroxide (0.1 M), and lithium chloride solutions to give lithium concentrations of 5×10^{-5}—4×10^{-4} M in the aqueous layer (0.35—2.8 μg ml^{-1} lithium). Each of the flasks was shaken for 20 min and left standing for more than 10 min at room temperature (20 ± 2°C). Absorbance of the organic layer was measured at 400 nm with the 8450A spectrophotometer.

Effect of sodium ion. The effect of sodium ion in the extraction system was determined in a procedure similar to that used for lithium ion. Solutions were prepared in six round-bottomed flasks to contain 5 ml of chloroform and 5 ml of an aqueous solution containing aza-12-crown-4 reagent (6.7×10^{-4} M), potassium hydroxide (0.1 M), lithium chloride (1×10^{-4} M; 0.694 μg ml^{-1}) and sodium chloride (1×10^{-3}—5×10^{-3} M; 23—115 μg ml^{-1}). After the mixture had been shaken, the absorbance of the organic layer was measured at 400 nm.

Procedure for urine and blood samples

It is necessary to remove proteins from samples to avoid emulsions during the extraction process. Place 3.0 ml of serum or 1.0 ml of urine and water (3 ml for serum or 11 ml for urine) in a centrifuge tube, mix well and heat in a boiling water bath for 15 min. Centrifuge for 10 min. Transfer a 2.0-ml aliquot of the sample solution to a stoppered centrifuge tube to which has been added 2.0 ml of the crown ether solution (1×10^{-3} M), 1 ml of 1 M potassium hydroxide, and enough water to dilute the sample to 10 ml. Mix well and shake for 10 min with 10 ml of organic solvent. After phase separation, measure the absorbance of the organic phase at 400 nm against a chloroform blank.

RESULTS AND DISCUSSION

Determination of acidity constants

Before the data obtained from the experiments used to determine the acidity constants K_{a1} and K_{a2} can be interpreted, the equilibria of the extraction system must be defined. The equilibria for the chromogenic aza-12-crown-4 reagent in an aqueous solution are shown in Fig. 1; the constants are defined as follows:

$$K_{a1} = [HL]\ [H^+]/[HLH^+]; K_{a2} = [L^-]\ [H^+]/[HL]; K_{ML} = [ML]/[L^-]\ [M^+]$$

where K_{a1} and K_{a2} are the acidity constants, and K_{ML} is the complex formation constant. By assuming no significant complex formation, the absorbance, A, at any wavelength, and the total concentration of the reagent $[HL]_t$ are written as

$$A = \epsilon_{HLH^+}[HLH^+] + \epsilon_{HL}[HL] + \epsilon_{L^-}[L^-]; [HL]_t = [HLH^+] + [HL] + [L^-]$$

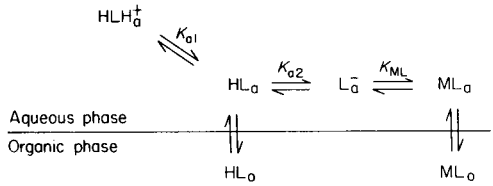

Fig. 1. The chemical equilibrium for this extraction system. HLH^+ is the chromogenic aza-12-crown-4 with both the ring nitrogen and the phenolic oxygen protonated. HL is the chromogenic aza-12-crown-4 with the hydroxy group deprotonated but the ring nitrogen still protonated. L^- is the chromogenic aza-12-crown-4 with both ring nitrogen and hydroxy group deprotonated ML is the chromogenic aza-12-crown-4 L^- species complexed with a metal ion.

where ϵ is molar absorptivity. The acidity constants can then be rewritten as

$$-\log K_{a1} = \mathrm{pH} - \log (\epsilon_{HLH^+} [HL]_t - A)/(A - \epsilon_{HL} [HL]_t) \quad (1)$$

$$-\log K_{a2} = \mathrm{pH} - \log (\epsilon_{HL} [HL]_t - A)/(A - \epsilon_{L^-} [HL]_t) \quad (2)$$

because it can be assumed that $[HL]_t \gg [L^-]$ for K_{a1} and $[HL]_t \gg [HLH^+]$ for K_{a2}. The fact that the spectra obtained from the titration described above exhibit two distinct isosbestic points (342.8 nm and 401.4 nm), depending on pH, confirmed that $[L^-]$ or $[HLH^+]$ can be neglected as compared with $[HL]_t$ in a certain pH region; thus $[HL]_t$ is much greater than $[L^-]$ at pH $\leqslant$6.6 (Eqn. 1 is valid), and $[HL]_t$ is much greater than $[HLH^+]$ at pH $\leqslant$9.7 (Eqn. 2 is valid).

At pH $\leqslant$6.6, the absorbance decreasing to the isosbestic point at 401.4 nm reflects the decay of HLH^+ and the growth of HL, so that these absorbance data can be used for the evaluation of $-\log K_{a1}$ from Eqn. 1. At pH $\geqslant$ 9.7, the absorbance deviating from the isosbestic point at 342.8 nm reflects the decay of HL and the growth of L^-, so that these absorbance data can be used for the evaluation of $-\log K_{a2}$ from Eqn. 2. In Eqns. 1 and 2, because $[H^+]$ is known experimentally, and because $\epsilon_{HL} [HL]_t$ can be obtained as the average value of absorbances at each isosbestic point, the only unknown parameters are $\epsilon_{HLH^+} [HL]_t$ and $\epsilon_{L^-} [HL]_t$, which can be adjusted to give constant values for $-\log K_{a1}$ and $-\log K_{a2}$, respectively, by applying the observed absorbance sets to the equations.

Table 1 lists the constants found for the chromogenic aza-12-crown-4 reagent as well as the reported values for the previously reported crown ether, *N*-(2-hydroxy-5-nitrobenzyl)-aza-15-crown-5 [9]. The value of $-\log K_{a1}$ for the aza-12-crown-4 reagent agrees reasonably well with that reported for the aza-15-crown-5 reagent. However, the higher value of $-\log K_{a2}$ for the aza-12-crown-4 compound indicates that the proton of the reagent of the present compound is more tightly bound to the nitrogen atom and that complex formation is enhanced at pH $>$10.3.

TABLE 1

Acidity constants, K_{a1} and K_{a2}, and extraction constant, K_{ex} (ML)

	$-\log K_{a1}$	$-\log K_{a2}$	$-\log K_{ex}$ (LiL)		$-\log K_{ex}$ (NaL)	
			0.1 M KOH	0.05 M KOH	0.1 M KOH	0.05 M KOH
Chromogenic aza-12-crown-4	5.77[a]	10.31[a]	10.18[b]	10.23[b]	12.50[b]	12.49[b]
Chromogenic aza-15-crown-5[c]	5.79[d]	9.69[d]	9.15[e]		9.76[e]	

[a] μ = 0.1 (CsCl). [b] Solvent, chloroform. [c] From [9]. [d] μ = 0.1 [$(CH_3)_4NCl$)]. [e] Solvent, 1,2-dichloroethane; pH unspecified.

Determination of extraction constant, K_{ex}

The extraction equilibria illustrated in Fig. 1 can be described by

$$K_{ex} = [ML_o]\,[H_w^+]/[HL_o]\,[M_w^+]$$

where subscripts o and w indicate the organic and aqueous phases, respectively. The following equations are then valid:

$$[HL]_t = [HL_o] + [ML_o] + [L_w^-] + [HL_w] + [ML_w]$$

$$[M^+]_t = [M_w^+] + [ML_w] + [ML_o]$$

$$E = A_o/[HL_o] + [ML_o] = (\epsilon_{HL_o}\,[HL_o] + \epsilon_{ML_o}\,[ML_o])/([HL_o] + [ML_o]) \quad (3)$$

where $[M^+]_t$ denotes a total alkali metal concentration. By assuming $[L_w^-] \gg [HL_w] + [ML_w]$, and $[M^+]_t \gg [HL]_t$, then $[HL]_t = [HL_o] + [ML_o] + [L_w^-]$ and $[M^+]_t = [M_w^+]$. Combining these equations with the definition of K_{ex} and Eqn. 3 gives

$$1/(E - E^\circ) = ([H^+]_w/K_{ex}\,\Delta\epsilon) \cdot \{(1/[M]_t) + (1/\Delta\epsilon)\} \quad (4)$$

and

$$E = A_o/\{[HL]_t - (A_w/\epsilon_{L_w^-})\} \quad (5)$$

where $\Delta\epsilon = \epsilon_{ML_o} - \epsilon_{HL_o}$, and E° denotes the E value in the absence of the metal ion in the system ($E^\circ = \epsilon_{HL_o}$). Equation 4 shows that the plot of $1/(E - E^\circ)$ against $1/[M]_t$ gives a straight line and that K_{ex} can be calculated from the slope, the intercept, and the pH value. The absorbance at the 401.4 nm isosbestic point gives $\epsilon_{L_w^-}$, so that the values of E and E°, which are necessary for the plot, can be obtained experimentally.

The partition equilibrium system was studied in a similar manner. The concentrations $[HL]_t$, $[M^+]_t$, and $[OH^-]$ were 5.35×10^{-5} M, 4×10^{-3}—2 M (as chloride), and 10^{-2}—10^{-1} M (as potassium hydroxide), respectively. Chloroform was used as the solvent.

The plots of data obtained for the determination of K_{ex} according to Eqn. 4 were straight lines for the lithium and sodium ion systems. Table 1

shows the $-\log K_{ex}$ values obtained from the plots together with that reported for the aza-15-crown-5 compound. The $-\log K_{ex}$ value for lithium did not exhibit significant dependence on the hydroxide concentration used.

To confirm the important assumption that $[L_w^-] \gg [HL_w] + [ML_w]$, Eqn. 3 (the left equation) was used for the evaluation of E instead of Eqn. 5, which was derived from Eqn. 3 under that assumption. The extraction constants obtained were compared with those obtained by using Eqn. 5. When Eqn. 3 was applied, the species HL_o and ML_o in the organic layer were extracted into 0.1 M hydrochloric acid as HLH^+, and the concentration of HLH^+ was determined spectrophotometrically and equated to $[HL_o] + [ML_o]$ in Eqn. 3. The extraction constants obtained in this way were $-\log K_{ex}$ (LiL) = 10.25, and $-\log K_{ex}$ (NaL) = 12.47, which agreed well with those obtained with the values generated with the assumption (Table 1).

When compared with the aza-15-crown-5 compound, the value of K_{ex} (LiL) for the aza-12-crown-4 reagent is smaller by a factor of ten. However, the ratio of K_{ex} (LiL) to K_{ex} (NaL) for the chromogenic aza-12-crown-4 is much greater than that for the aza-15-crown-5; thus, the selectivity of the present reagent for lithium ions in the presence of sodium ions is much higher than for the aza-15-crown-5.

Extraction conditions

Three solvents, chloroform, 1,2-dichloroethane and dichloromethane were compared, with potassium or sodium hydroxide to control pH. With 0.01 M hydroxide, no significant sensitivity or interference differences were observed between either the cations of the buffers or between the organic solvents. At 0.1 M hydroxide, however, large differences were observed both between the cations and between the organic solvents. Potassium hydroxide gave higher sensitivity in both chloroform and dichloromethane than sodium hydroxide, but not in 1,2-dichloroethane. Dichloromethane exhibited the highest sensitivity when used with potassium hydroxide, but was subject to increased interference by sodium ions. The combination of dichloromethane and sodium hydroxide allowed most of the reagent to pass into the organic layer and, as a result, the absorbance could not be measured. The results show that the optimum combination of high sensitivity, low interference, low blank absorption, and stability after extraction were achieved in a system with 0.1 M potassium hydroxide and chloroform.

Various other organic solvents were tested as organic media with 0.01 M potassium hydroxide solutions. Nitromethane and 10% nitromethane in chloroform extracted most of the reagent species into the organic phase, so that no response of the reagent to lithium or sodium ion was observed. Methylisobutyl ketone showed only slight extraction of the metal complex. No extraction occurred into benzene, carbon tetrachloride, chlorobenzene, or trichlorethylene. Although triethylamine (1 M chloroform) was examined as an organic buffer, the response to lithium ions was smaller and the response to sodium ions was larger than in the $KOH/CHCl_3$ system. A combina-

TABLE 2

Determination of lithium ion in blood serum or urine with chromogenic aza-12-crown-4[a]

Blood Serum		Urine	
Atomic absorption	Present method	Atomic absorption	Present method
3.5	3.4	10.5	10.4
7.0	6.8	14.0	14.0
10.5	10.3	21.0	20.8
		42.0	40.7

[a]Mean of triplicate determinations. All numbers are $\mu g\ ml^{-1}$.

tion of the amine (1 M in chloroform) and 0.1 M sodium hydroxide as buffer gave an intermediate response to lithium ions, and the response was not stable.

Analytical capabilities of the chromogenic aza-12-crown-4 reagent

A calibration curve was obtained with a linear portion from 0.3 to 2 $\mu g\ ml^{-1}$, which can be expressed as $C_{Li} = 3.00\,A \pm 0.05$, where C_{Li} and A denote the concentration of lithium ($\mu g\ ml^{-1}$) and the net absorbance at 400 nm, respectively. The imprecision of the measurement was $<5\%$, calculated from the mean value of the standard deviations of triplicate samples over the linear range. The error seemed to be mainly caused by the instability of the absorbance after the separation of the organic layer. The stability was improved, with slight loss of sensitivity and slight increase in interference, by the addition of a small amount of t-butanol (2% v/v) to the chloroform, but the blank absorbance increased by a factor of 1.6.

A 30-fold excess of sodium relative to lithium resulted in an 8% increase in absorbance.

Results for lithium in blood serum and urine are shown in Table 2. The concentration of the crown ether was lower than that used to determine physical constants because the sensitivity was too high for Li^+ concentrations in these samples. The results were in good agreement with results obtained with atomic absorption spectrometry.

REFERENCES

1 C. J. Pedersen, J. Am. Chem. Soc., 89 (1967) 7017.
2 M. Takagi, H. Nakamura and K. Ueno, Anal. Lett., 10(13) (1977) 1115.
3 H. Nakamura, M. Takagi and K. Ueno, Talanta, 26 (1978) 921.
4 H. Nakamura, M. Takagi and K. Ueno, Anal. Chem., 52 (1980) 1668.
5 G. Pacey and B. Bubnis, Anal. Lett., 13(12) (1980) 1085.
6 G. Pacey and B. Bubnis, Analyst, 100 (1981) 636.
7 B. P. Bubnis, J. L. Steger, Y. P. Wu, L. A. Meyer and G. E. Pacey, Anal. Chim. Acta, 139 (1982) 307.
8 Y. P. Wu and G. E. Pacey, Anal. Chim. Acta, 162 (1984) 285.
9 H. Nakamura, H. Sakka, M. Takagi and K. Ueno, Chem. Lett., (1981) 1305.
10 T. Miyasaki, S. Yanagida, A. Itoh and M. Okahara, Bull. Chem. Soc. Jpn., 55 (1982) 2005.

Analytica Chimica Acta, 174 (1985) 151—161
Elsevier Science Publishers B.V., Amsterdam — Printed in The Netherlands

A SOLID-STATE CHEMILUMINESCENCE DETECTOR FOR HYDROGEN PEROXIDE BASED ON AN IMMOBILIZED LUMINOPHORE
Application to Rain Water

P. VAN ZOONEN, D. A. KAMMINGA, C. GOOIJER*, N. H. VELTHORST and R. W. FREI

Department of General and Analytical Chemistry, Free University, De Boelelaan 1083, 1081 HV Amsterdam (The Netherlands)

G. GÜBITZ

Institut für Pharmazeutische Chemie, Universität Graz, A-8010 Graz (Austria)

(Received 8th February 1985)

SUMMARY

The construction and functioning of a chemiluminescence detector for hydrogen peroxide is described. It is based on peroxyoxalate chemiluminescence and consists of a two-bed reactor packed with solid trichlorophenyloxalate (TCPO) and 3-aminofluoranthene immobilized on controlled pore glass beads. Optimal conditions (pH, solvent, TCPO purity) for flow-independent operation are discussed. Samples can be injected into a moving stream or directly into the monitor with a syringe so as to provide a manually operated field monitor. The detection limit is 1.5×10^{-8} M, and calibration graphs are linear over six orders of magnitude. The r.s.d. for the manual monitoring mode is ±3% for 17 $\mu g\ l^{-1}$ hydrogen peroxide. A sample throughput of 100 h^{-1} is possible in the flow injection mode, and 40 samples h^{-1} for manual injection.

There are two main reasons for the development of a hydrogen peroxide detector. First, investigations regarding acid rain require the availability of a hydrogen peroxide field monitor. Secondly, its coupling to reaction detectors (which produce hydrogen peroxide) in high-performance liquid chromatography (h.p.l.c.) and flow injection analyses (f.i.a.) is promising.

The acidity of rain and cloudwater is determined by the amount of sulphur oxides and nitrogen oxides released into the atmosphere and subsequently dissolved in the water. Hydrogen peroxide is believed to be one of the key reactants in the decomposition cycle of the sulphur oxides. This is supported both by laboratory experiments and field measurements [1—4]. The normal hydrogen peroxide concentrations in rain water vary from less than 1 $\mu g\ l^{-1}$ (3×10^{-8} M) in polluted areas to more than 1 $\mu g\ ml^{-1}$ (3×10^{-5} M) in relatively clean areas [1, 2]. A significant problem connected with the quantitation of hydrogen peroxide is that very dilute aqueous peroxide samples are unstable. That is why field monitoring is essential.

Many photochemical and enzymatic reactions are known to yield hydrogen

peroxide. Hence, in principle, a hydrogen peroxide monitor will be more useful in flow dynamic systems if it is coupled to such reaction systems. The detection system described here has already been applied to effluents from a photochemical reactor [5].

Detection is based on peroxyoxalate chemiluminescence, which requires three reactants, hydrogen peroxide, bis-(2,4,6)-trichlorophenyloxalate (TCPO) and a luminophore. In a previous paper a detector was described in which TCPO was used as a bed reactor [6]. In the present study, the solid-state reactor principle has been extended by immobilizing the luminophore, which enables the system to be significantly simplified. The luminophore chosen is 3-aminofluoranthene, which is known to be one of the most efficient luminophores in peroxyoxalate chemiluminescence. Detection limits in the low femtomole range were reported for the aminopolyaromatic hydrocarbons [7, 8]. The 3-aminofluoranthene was immobilized on controlled pore glass (c.p.g.) beads and packed into a flow cell, mounted close to a photomultiplier tube. A number of reactor designs will be discussed, together with the experimental conditions. The results of hydrogen peroxide standard addition experiments on rain-water samples will also be presented.

EXPERIMENTAL

Chemicals and apparatus

The TCPO was prepared as described by Mohan and Turro [9] and recrystallized three times from benzene (Uvasol, Merck). The product was kept under reduced pressure for several hours to evaporate it to dryness and to remove traces of trichlorophenol. Trizma base (reagent-grade; Sigma) was recrystallized twice from ethanol and the pH was adjusted with nitric acid. Acetonitrile (h.p.l.c. grade; Baker, Deventer, The Netherlands) was purified on an alumina column as described before [6]. Analyzed-grade acetone (Baker) was also purified on alumina; h.p.l.c. grade methanol was used as received. The preparation of the immobilized aminofluoranthene was as described elsewhere [10].

The cell design is shown in Fig. 1. This cell can be mounted into an Oriel 3075 miniature sample compartment (Oriel Corporation, Stamford, CT, U.S.A.) which is attached to an Oriel 77781 photomultiplier housing. The photomultiplier tube was operated at 500—800 V by an Oriel 7070 photomultiplier detection system. In the flow-injection measurements a Kontron

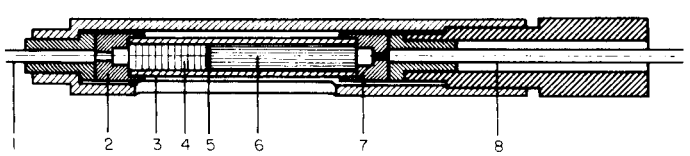

Fig. 1. Design of the packed flow cell in the two-layer mode: (1) inlet capillary; (2) inlet cap with frit; (3) quartz tube; (4) TCPO layer; (5) frit; (6) luminophore layer; (7) outlet cap with frit; (8) outlet capillary.

410 h.p.l.c. pump (Kontron, Zürich, Switzerland) and a Rheodyne 7120 injection valve equipped with a teflon injection loop were used. All connecting capillaries were 0.4 mm inner diameter teflon.

Procedures

The flow-injection measurements were made as previously described [6]. Manual injections were made by putting a Valco-fill port fitting on the inlet capillary of the cell. A solution for injection was prepared by mixing the sample with the organic solvent and the buffer. These injections were done with a Hamilton 1001 gas-tight syringe.

RESULTS AND DISCUSSION

The application of a hydrogen peroxide detector as a field monitor requires not only that the system is simple but also that it is flow-independent, i.e., the signal is independent of the flow rate of the mobile phase. If the latter condition is fulfilled, direct sample introduction by manual injection with a syringe will be possible, so that a pumpless monitoring system can be used. Such a flow independence would also be advantageous for f.i.a. and h.p.l.c. detection systems as it eliminates the noise arising from pump pulsations.

Several optimization parameters were discussed previously [6] with attention confined to the quantitation of hydrogen peroxide in acetonitrile/water mixtures. The present results obtained with the immobilized luminophore lead to similar optimized conditions. An important advantage of the new system is freedom in choosing the best solvents as limitations are not imposed by the low solubility of the luminophore. Another advantage of immobilization is that very little or no luminophore is consumed, whereas in the previous set-up it had to be added continuously to the carrier phase. In the case of 3-aminofluoranthene, which is rather toxic, immobilization provides greater safety in its application.

Immobilization procedure

Immobilization of 3-aminofluoranthene was first attempted by using a simple procedure for binding amines to cellulose [11, 12]; this involves the use of cyanuric chloride to create a binding site on the support. However, a drastic change in the spectroscopic properties of the luminophore occurred when it was coupled to the support. A hypsochromic shift of more than 50 nm was observed for the excitation and emission maxima. Similar observations were made for glass beads or silica gel when the same immobilization procedure was used. This change in spectroscopic properties resulted in lower chemiluminescence intensities. For this reason, the procedure described by Gübitz et al. [10] for immobilization of 3-aminofluoranthene on c.p.g. was used. This procedure involved binding with 3-glycidoxypropyltrimethoxysilane, which gives a fairly long inert spacer-arm, which hardly interacts with

the aromatic luminophore. Glass beads were chosen for their excellent mechanical stability and good transparency to visible radiation.

Reactor design

Figure 2 shows four experimental configurations for the application of peroxyoxalate chemiluminescence for hydrogen peroxide detection: manifold A is the conventional one and configuration B with the solid-state TCPO reactor is as described previously [6]; C and D show systems with the immobilized fluorophore. In C, the TCPO reactor was the same as in B but in D TCPO and immobilized 3-aminofluoranthene were packed together in the reactor.

Comparison of configurations C and D shows that the former has a greater capacity for TCPO so that an average reactor lifetime of more than 8 h can readily be achieved, whereas for D only ca. 3 h continuous operation time is possible at flow rates of 1 ml min^{-1} without excessive band-broadening caused by voids appearing in the TCPO layer. A disadvantage of C is that the signal depends on the flow rate, because of the time lag between the reaction of hydrogen peroxide with TCPO in the first reactor, and the actual excitation step in the second reactor. During this interval some of the intermediate formed in the first reactor decomposes, and the amount decomposed before it reaches the second reactor depends on the flow rate. Furthermore, the two reactors in C provide greater band-broadening and a higher back-pressure than in D.

Two different packings for the combined reactor system in D were studied, a bed with luminophore and TCPO homogeneously mixed, and a two-layer bed (Fig. 1). The homogeneously mixed bed is inconvenient because the

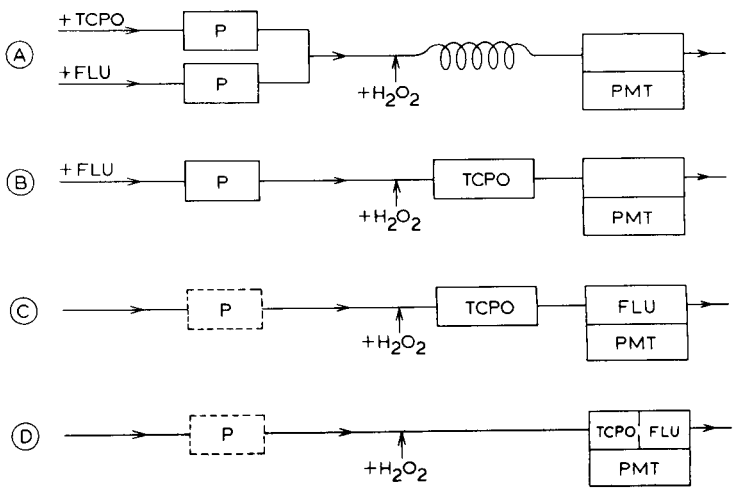

Fig. 2. Detector configurations investigated: (A) conventional system; (B) system with solid-state TCPO reactor; (C) system with separate solid-state TCPO and immobilized luminophore reactors; (D) mixed reactor system (FLU indicates the luminophore, P the pump).

reactor cannot easily be repacked with TCPO when it becomes depleted, for only TCPO is consumed during use. The two-layer reactor can easily be repacked with TCPO when voids appear in the TCPO layer. The signal-to-noise ratio of the two-layer reactor is slightly worse than that of the homogeneously mixed bed reactor. However, the difference is no more than 10% so the two-layer system is generally more favourable.

The two-layer bed reactor should be equipped with an inlet frit, and with a frit placed between the TCPO and the luminophore layer. The former is necessary to spread the flow evenly over the whole reactor. If it is omitted, shorter useful lifetimes are observed, because of channel formation in the TCPO layer; and an inhomogeneous flow pattern will cause variable chemiluminescence intensity in different parts of the reactor, so that irreproducible re-installation will influence the signal. The frit between the TCPO and the luminophore layer makes it possible to replace the TCPO in the reactor easily.

The dimensions of the reactor cell were not very critical; quartz tubing of 3-mm inner diameter with a length of 27 mm was used. The ratio of material in the two layers did not strongly influence the reactor characteristics, so a ratio of TCPO to 3-aminofluoranthene of 1.0:2.0 was used.

Reactor performance

The flow characteristics of configurations B, C and D are compared in Fig. 3, which shows the dependence of the peak height on the injection

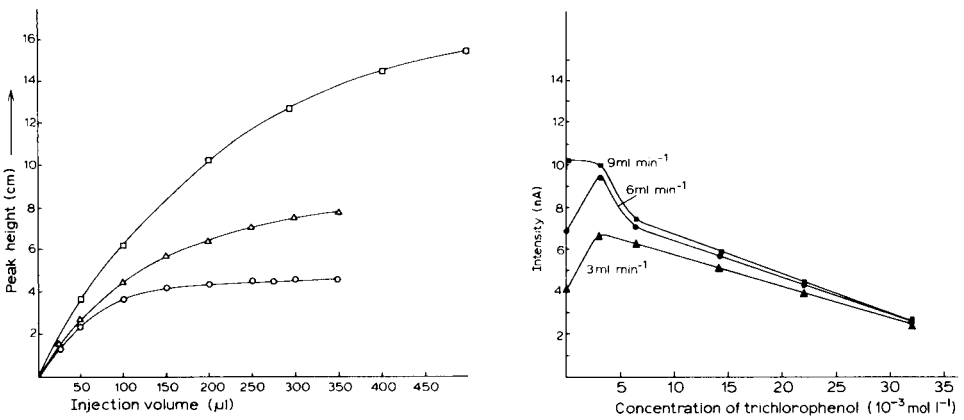

Fig. 3. Plots of injection volume vs. peak height for three of the configurations: (□) without immobilized luminophore, configuration B; (△) with immobilized luminophore and separate solid-state TCPO reactor, configuration C; (○) two-layer reactor, configuration D. (It is emphasized that the ordinate does not give information on the signal-to-noise ratio because the measurements were done with different photomultiplier tubes).

Fig. 4. Dependence of intensity on trichlorophenol concentration with 80% methanol/20% Tris buffer, pH 8 as the mobile phase. Flow rate: (▲) 3 ml min^{-1}; (●) 6 ml min^{-1}; (■) 9 ml min^{-1}.

volume. As can be seen, manifold D gives maximum peak height at a small injection volume (ca. 150 μl), indicating that immobilization of the luminophore leads to improved flow characteristics. This can be attributed to the decreased dead volume of the packed flow-cell and to localization of the actual excitation reaction in the flow-cell, so that no band-broadening is caused by detection of chemiluminescence occurring in the inlet and outlet capillaries.

No loss in performance of the immobilized 3-aminofluoranthene was observed over a period of one month.

Choice of solvent

As mentioned before, there are no solubility limitations in choosing a solvent when an immobilized fluorophore is used. Several organic solvent/water mixtures were examined with solvents which are commonly used in h.p.l.c. Tetrahydrofuran, acetonitrile, methanol and acetone were studied. All experiments were done with 20% Tris buffer and 80% organic solvent. A higher water content will result in lower sensitivity, probably because of hydrolysis of TCPO, a non-chemiluminescent side-reaction which becomes more important at higher water contents.

Tetrahydrofuran was unsuitable; it gave a very high background, presumably because of peroxide formation. Acetone and acetonitrile were very suitable. When methanol was used, the performance of the system varied strongly with the purity of the TCPO batch used. This gave a bad day-to-day reproducibility, and in addition the signal became flow-dependent for system D. This flow-dependence varied from one TCPO batch to another. Given these observations for methanol, more attention had to be paid to the production and purification of TCPO. It appears that recrystallized TCPO always contains traces of trichlorophenol (TCP), which is a precursor in the synthesis of TCPO. Removal of TCP by sublimation led to a large increase of the flow dependence of the chemiluminescence. Furthermore, with these purified TCPO batches, flow rates higher than 5 ml min^{-1} were necessary to reach detection limits in the low $\mu g\ l^{-1}$ range, and very low chemiluminescence intensities were observed in these methanolic solutions. This low chemiluminescence intensity is probably caused by a non-chemiluminescence side-reaction of TCPO which only takes place in methanol and competes with the actual chemiluminescent reaction of TCPO and hydrogen peroxide. If the rate of this side-reaction is greater than the rate of the reaction between TCPO and hydrogen peroxide, a flow dependence will be introduced because TCPO is consumed before it reaches the immobilized fluorophore. A similar anomalous behaviour of methanolic mobile phases in peroxyoxalate chemiluminescence was reported by Weinberger [13].

As TCP is the major degradation product of TCPO, the addition of TCP may influence such a side-reaction. If this is correct it would be possible to apply methanol as a solvent providing that during the reaction a reproducible TCP concentration is maintained, so that the side-reactions of TCPO can be

controlled. This is confirmed by the data shown in Fig. 4 where the interrelationships of intensity, flow rate and TCP concentration are shown. Essentially flow-independent conditions will be found for TCP concentrations larger than about 0.02 mol l^{-1}.

Apparently in acetonitrile and acetone, these side-reactions play a minor rôle. In these solvents, no effect of TCP content on the signal was observed under the same experimental conditions.

Effect of pH and water content

The rôle of Tris buffer in acetonitrile/water mixtures was investigated previously for configuration B [6]. There was no significant effect of the pH on the signal between pH 7.5 and 10. For acetone and acetonitrile in configurations C and D this was also found to be true. For methanol, the flow-dependence of the signal, which was very strong when purified TCPO was used, could be controlled to some extent by adjusting the pH of the aqueous buffer. In pH 9.5 buffer an increase in flow rate from 1.0 to 2.0 ml min^{-1} doubled the signal, whereas at pH 7.5 an increase of only 20% was observed.

For all the systems investigated, the chemiluminescence intensity increases strongly with a decrease of the water content, in line with the results reported previously [6]. Detailed experiments on the peroxyoxalate reaction in media with high water contents [14] showed that the strong dependence of the signal on the solvent/water ratio caused severe irreproducibility if the sample plug and the carrier stream did not mix to give a homogeneous solution before entering the reactor. Unfortunately, such mixing is difficult to achieve and therefore, in the present experiments, the sample was adjusted to have the same composition as the carrier stream before being injected into the flow system.

Flow-injection measurements on standard solutions

The peak height was directly proportional to the hydrogen peroxide concentration over a large linear range. The log-log calibration plot was linear with a slope of 1.0 from the detection limit up to at least 10^{-2} M ($r = 0.9999$, 15 points). Each new reactor should be calibrated before use, because the slopes of the normal calibration graphs differ from reactor to reactor within a range of ±10% from the mean value. This is probably due to irreproducibility in the packing procedure of the reactor.

The reproducibility of the method was tested by ten replicate injections of 5×10^{-7} M (17 μg l^{-1}) hydrogen peroxide. The relative standard deviation (r.s.d.) was 2.4%. The detection limit was 1.5×10^{-8} M (0.5 μg l^{-1}) corresponding to a signal-to-noise ratio of 3. The flow system could handle 100 samples h^{-1}.

Analysis of real samples

Figure 5 shows an example of standard addition of hydrogen peroxide to a rain-water sample, followed by flow injection measurements. The results of

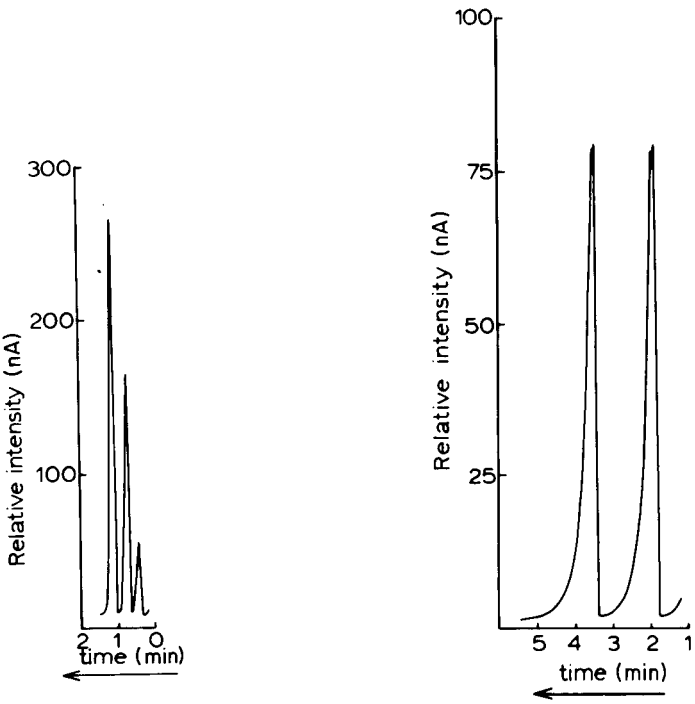

Fig. 5. Responses from rain water with 25 μg l^{-1} H_2O_2 added, with standard additions of 75 and 125 μg H_2O_2 l^{-1}.

Fig. 6. Signal obtained from two manual injections of 30 μg l^{-1} H_2O_2.

several standard addition experiments on samples taken by the KEMA Institute (Arnhem, The Netherlands) are shown in Table 1. Two different reactors of the same design were utilized. The aim of this experiment was to investigate the sensitivity of the method to matrix effects. As can be seen from Table 1, all samples gave straight standard addition plots with slopes very similar to that of the calibration graph for the reactor used. The additions were in the range 10 μg l^{-1}—2 μg ml^{-1} (3×10^{-7}—6×10^{-5} M). The measurements were done immediately after spiking the sample, because hydrogen peroxide was unstable, especially in the upper part of the concentration range investigated. This series of measurements is part of a larger set of measurements which are being made to compare this method with the copper-catalyzed luminol system used by KEMA [16] which will be reported later. In this series, hydrogen peroxide was detected in only two of the samples, 5 μg l^{-1} (15—16:10:84) and 8 μg l^{-1} (16—19:10:84). The reason for this is probably that the samples were two months old when analyzed.

TABLE 1

Data on standard addition to rain water samples

Sample	Slope ($nA/\mu g\ l^{-1}$)	Correlation coefficient	Standard deviation[a] ($\mu g\ l^{-1}$)	No of results
8—9:10:84	8.29	0.9999	1.0	8
9—10:10:84	8.24	0.9998	3.0	16
13—16:10:84	8.26	0.9998	4.0	14
18—19:10:84	8.59	0.9998	2.0	14
19—22:10:84	8.92	0.9995	3.2	14
22—23:10:84	8.01	0.9992	3.5	14
Calibration plot[b]	8.21	0.9999	1.0	8
Calibration plot[c]	8.19	0.9998	2.1	10
Calibration plot[d]	6.84	0.9999	1.1	8
24—25:10:84	6.87	0.9999	2.1	12
25—26:10:84	6.69	0.9998	1.5	14
15—16:10:84	6.23	0.9998	2.0	14
16—19:10:84	7.01	0.9988	3.2	14

[a]Calculated from the residual quadratic sum [15]. [b]Before first series of measurements. [c]After first series of measurements. [d]New reactor used for the last 4 measurements.

Manual injections

Because hydrogen peroxide solutions are unstable in the concentration range investigated, it is obvious that a need exists for simple field monitors to permit on-site analyses of samples. The feasibility of a monitor operated with manual injection of samples, without carrier stream or pumping system, was therefore investigated. Manual injections were made by mixing a sample of water with the appropriate organic solvent and adding a small amount of concentrated Tris buffer; 1 ml of this mixture was forced through the two-layer cell D with a syringe. A typical trace obtained is shown in Fig. 6; the signal reaches a maximum value rather rapidly, and the peak height obtained is a measure of the hydrogen peroxide concentration. At the end of the manual injection, when the flow is stopped, the signal decreases. With this 1-ml sample, there is no need for a wash step to clean the cell for the next sample. As can be seen from Fig. 3, 1 ml is such an excessive volume that the sample itself performs the wash step and only in the first part of the trace can the influence of the previous sample be observed.

Such manual injections show a blank signal because the background cannot be observed continuously as in the flow-injection mode. The limit of detection of this method depends therefore on the standard deviation of the blank; here, the limit of detection is defined as the concentration which corresponds to the signal of the blank plus 3 times the standard deviation of the blank. In this way, typical limits of detection of 4×10^{-8} M ($1.3\ \mu g\ l^{-1}$) were obtained. The system can handle 40 samples h^{-1}. The r.s.d. for 10 replicate injections

of 5×10^{-7} M hydrogen peroxide was 3.0%. It is essential to have a flow-independent system for acceptable performance of such a manual-injection monitor. The present system showed no variation when the time for injection of 1 ml of sample mixture was varied between 5 and 30 s (from 12 to 0.5 ml min^{-1}).

Conclusions

The solid-state reactor based on solid TCPO and 3-aminofluoranthene immobilized on glass beads and packed in a two-layer bed permits rapid and simple analyses for hydrogen peroxide in aqueous samples. The method is adaptable for field measurements because under appropriate conditions the chemiluminescence signal is flow-independent, and manual injection becomes feasible. The limit of detection for hydrogen peroxide is low enough for real samples to be analyzed. A linear calibration range of several orders of magnitude was observed.

Preliminary investigations show that the performance of the system is comparable to that of the copper-catalyzed luminol chemiluminescence system used by KEMA [16]. The chemical properties of both systems are very different, however, and the luminol system, for example, is sensitive to the presence of some metal ions. The systems will therefore show different interferences when applied to real samples.

The development of a cheap hydrogen peroxide field monitor based on manual injection and a battery-operated photomultiplier tube is currently underway. Simultaneously the potential of such a monitor for detection in h.p.l.c. and f.i.a. via coupling with photochemical and enzymatic reactions which produce hydrogen peroxide is being explored.

We thank Dr. Römer and Mr. Veltkamp from N.V. KEMA for putting the rain-water samples at our disposal. This work was supported by the Dutch Foundation for Technical Sciences, Grant no. 12-20-46/79-0 VCH 11.0137.

REFERENCES

1 S. A. Penkett, B. M. R. Jones, K. A. Brice and A. E. J. Eggleton, Atmos. Environ., 13 (1979) 123.
2 D. Klockow and P. Jacob, in W. Jaeschke and V. Mohnen (Eds.), The Chemistry of Multiphase Atmospheric Systems, Springer Verlag, Berlin-Heidelberg, 1984.
3 L. R. Martin and D. E. Damschen, Atmos. Environ., 15 (1981) 1615.
4 S. M. Kunen and A. L. Lazrus, J. Geophys. Res., 88 (1983) 3671.
5 J. R. Poulson and J. W. Birks, unpublished results.
6 P. van Zoonen, D. A. Kamminga, C. Gooijer, N. H. Velthorst and R. W. Frei, Anal. Chim. Acta, 167 (1985) 249.
7 K. W. Sigvardson and J. W. Birks, Anal. Chem., 55 (1983) 432.
8 K. W. Sigvardson, J. M. Kennish and J. W. Birks, Anal. Chem., 56 (1984) 1096.
9 A. G. Mohan and M. J. Turro, J. Chem. Educ., 51 (1974) 528.
10 G. Gübitz, P. van Zoonen, C. Gooijer, N. H. Velthorst and R. W. Frei, Anal. Chem., 57 (1985) in press.

11 L. A. Saari and W. R. Seitz, Anal. Chem., 54 (1982) 821.
12 G. Kay and E. M. Crook, Nature, 216 (1967) 514.
13 R. Weinberger, J. Chromatogr., 314 (1984) 155.
14 M. L. Grayeski and W. R. Seitz, Anal. Biochem., 136 (1984) 277.
15 R. D. Lark, B. R. Craven and R. L. Bosworth, The Handling of Chemical Data, Pergamon Press, Oxford, 1968, pp. 140—144.
16 F. G. Römer, A. A. Veltkamp and P. van Galen, Contribution to the 3rd European Symposium on Physico-chemical Behaviour of Atmospheric Pollutants, Varese, Italy, 1984.

Analytica Chimica Acta, 174 (1985) 163—172
Elsevier Science Publishers B.V., Amsterdam — Printed in The Netherlands

DETERMINATION OF TECHNETIUM BASED ON QUENCHING OF THE FLUORESCENCE OF SOME ORGANIC COMPOUNDS, WITH APPLICATION TO VEGETATION

F. GRASES,* G. FAR and J. G. MARCH

Department of Analytical Chemistry, Faculty of Sciences, University of Palma de Mallorca, 07071-Palma de Mallorca (Spain)

(Received 14 February 1985)

SUMMARY

Technetium is an effective quencher of the fluorescence produced by 2,5-diphenyloxazole (PPO), 1,4-bis(4-methyl-5-phenyl-2-oxazolyl)benzene (POPOP) and 2,2′-pyridil [1,2-dioxo-1,2-bis(2-pyridyl)ethane]. Spectrofluorimetric procedures for 0.01—12 μg Tc ml^{-1} with PPO and 0.1—12 μg ml^{-1} with 2,2′-pyridil, and a spectrophotometric method for 1—15 μg ml^{-1} are described. The distribution of technetium in vegetation is measured by applying the PPO method.

The most widely used method for determining technetium involves counting the 0.292-MeV β-ray of ^{99}Tc [1—4]; excellent separation and purification of ^{99}Tc from all other β-contaminants is required. Neutron activation analysis also yields high sensitivity, but the procedure for separating and purifying the technetium prior to activation is laborious and time-consuming, and very fast post-activation chemical separations are needed to remove interferents which have half-lives close to that of ^{100}Tc (15.8 s) [5, 6]. Recently a mass spectrometric technique has been developed for the determination of ^{99}Tc; it provides a low detection limit, of about 1×10^{-12} g (0.02 pCi) or less. However, this method also requires expensive and sophisticated instrumentation, as well as extensive chemical separation and purification steps to remove interferents from ^{99}Ru and ^{97}Mo [7, 8]. The recent production of appreciable quantities of technetium from nuclear power plants and nuclear fuel reprocessing has created considerable interest in the development of simple and sensitive nonradiochemical methods of analysis that could be used to supplement the radiochemical procedures. It is necessary to consider that ^{99}Tc is a potential toxic pollutant [8—11]. However, few methods have been described so far for technetium determinations by means of non-radiochemical processes [12—15].

Although technetium was first obtained in 1937, until recently the amount available has been very small. For this reason, the chemistry of this element is still not very well known [16—18]. In this paper, interactions between technetium and various fluorescent organic compounds are studied

0003-2670/85/$03.30

with the aim of extending knowledge about the behaviour of this element in solution. As a result, new methods for its fluorimetric and spectrophotometric determination have been developed, and the distribution of ^{99m}Tc in vegetation has been studied.

EXPERIMENTAL

Reagents, solutions and apparatus

Stock solutions of 4.3×10^{-6} M 2,5-diphenyloxazole (PPO), 4.3×10^{-6} M 1,4-bis(4-methyl-5-phenyl-2-oxazolyl)benzene (POPOP) (Sigma Chemical Co.) and 1.6×10^{-3} M 2,2′-pyridil [1,2-dioxo-1,2-bis(2-pyridyl)ethane] (Ega chemie) were prepared in ethanol. A 1.8×10^{-2} M tin(II) chloride solution in 0.16 M hydrochloric acid was used with 2,2′-pyridil and a 0.1 M tin(II) chloride solution in 6 M hydrochloric acid was used with PPO. Technetium-99m, dissolved as ammonium pertechnetate (119.0 μg Tc ml^{-1}) was supplied by Amersham/Searle Corp. (Arlington Heights, IL).

A Perkin-Elmer LS-5 spectrofluorimeter and a Perkin-Elmer 552 spectrophotometer, with 1.0-cm cells, were used.

Procedures

Fluorimetric or spectrophotometric determination of technetium with 2,2′-pyridil. In a 1.5 × 16-cm test tube, place 2 ml of the 1.6×10^{-3} M 2,2′-pyridil solution (recently prepared) and the volume of technetium(VII) solution necessary for the final concentration of technetium to be between 0.1 and 12 μg ml^{-1} for the fluorimetric determination of between 1 and 15 μg ml^{-1} for the spectrophotometric determination. Add 0.3 ml of 0.16 M hydrochloric acid and 0.1 ml of 0.018 M tin(II) chloride in 0.16 M hydrochloric acid. Make the total final volume 5 ml, by addition, if necessary, of water prior to addition of the acid. Mix thoroughly and warm the solution for 10 min at 65°C. Measure the fluorescence intensity (λ_{ex} = 369 nm, λ_{em} = 469 nm) or the absorbance (at 360 nm) against a reagent blank, after cooling to room temperature.

Fluorimetric determination of technetium with PPO. In a 1.5 × 16-cm test tube, place 1.5 ml of the 4.3×10^{-6} M PPO solution, the volume of technetium(VII) solution necessary for the final concentration of the technetium to be 0.01—12 μg ml^{-1}, 3 ml of 4.0 M hydrochloric acid and 0.1 ml of 0.1 M tin(II) chloride in 6 M hydrochloric acid. Make the total final volume 5 ml as above. Mix thoroughly and measure the fluorescence intensity (λ_{ex} = 315 nm, λ_{em} = 411 nm).

Preparation of vegetation samples. Phaseolus vulgaris was used as the sample. The plants were sown in a layer of vermiculite and were germinated in a culture chamber at 20°C with a nutritive solution of the composition indicated in Table 1. After germination, one series of plants was watered with the same nutritive solution and another series was fed with a solution of the same composition that also contained 0.7 mg l^{-1} technetium(VII). The

TABLE 1

Composition of the nutritive solution (pH 5)

Salt	Conc. (mg l^{-1})	Salt	Conc. (mg l^{-1})	Salt	Conc. (mg l^{-1})
KNO_3	505	H_3BO_3	1.43	$CoCl_2 \cdot 4H_2O$	0.10
$Ca(NO_3)_2$	820	$MnSO_4 \cdot H_2O$	1.02	$Na_2MoO_4 \cdot 2H_2O$	0.05
$NaH_2PO_4 \cdot 2H_2O$	203	$ZnSO_4 \cdot 7H_2O$	0.22	EDDHA-Fe[a]	3.33
$MgSO_4 \cdot 7H_2O$	370	$CuSO_4 \cdot 5H_2O$	0.08		

[a]EDDHA is ethylenediaminedihydroxyacetate.

total time from planting to harvesting was 35 days. Afterwards, the plants were separated into root, stem and leaves, and were dried at 105°C to constant weight. A 0.5-g portion of dried sample was wet-ashed to complete decomposition of organic material with nitric/perchloric/sulphuric acids (10:1:1 by volume). The solution was evaporated to eliminate nitric and perchloric acids, and allowed to cool. The solution was filtered, and water added to give a volume of 10 ml.

RESULTS AND DISCUSSION

Quenching by technetium of the fluorescence of PPO and POPOP

Possible interactions between technetium and 2,5-diphenyloxazole (PPO) and 1,4-bis(4-methyl-5-phenyl-2-oxazolyl)benzene (POPOP) were investigated. The technetium(VII) and the reagent were mixed in the presence or absence of a reducing agent ($SnCl_2$) at different pH values, and the change of fluorescence was observed. In all cases, the fluorescence of the reagents was quenched. However, maximum quenching was obtained when tin(II) chloride was present (Fig. 1a) and in a strongly acidic medium (Fig. 1b). When an adequate PPO concentration was used for a given quantity of technetium, more effective quenching was obtained than when the same POPOP concentration was used. Quenching of the fluorescence of such reagents (λ_{ex} = 315 nm, λ_{em} = 411 nm) is a consequence of the intense paramagnetism of the technetium ions. Quenching cannot be attributed to the formation of a complex between technetium(IV) and PPO or POPOP, because quenching occurs to the same extent if reduction of technetium(VII) by tin(II) is done in the presence of these reagents (in which case complex formation can occur directly) or in their absence, the reagent being added later (in which case, technetium dioxide and anionic chloride complexes of technetium are formed, which will react with PPO or POPOP only slowly).

The Stern-Volmer constant [19] was evaluated (Fig. 2) as 2.5×10^4 M^{-1}. As can be seen, when the temperature is increased, the slope of the curve also increases; this confirms that the quenching is dynamic [19]. The greater

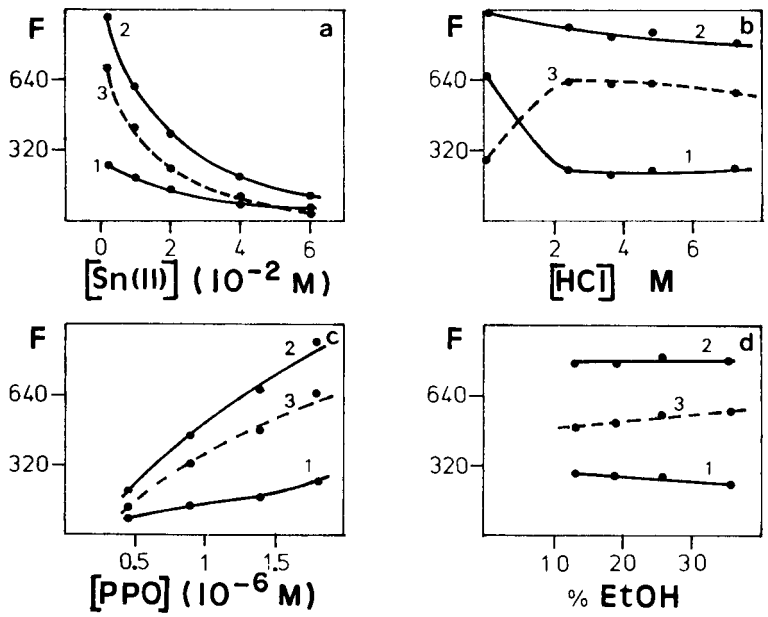

Fig. 1. Effect of variables on the fluorescence of the Tc-PPO system (λ_{ex} = 315 nm, λ_{em} = 411 nm). Curves: (1) 11.9 μg mol^{-1} technetium(VII) present; (2) reagent blank; (3) difference between (1) and (2). (a) Influence of Sn(II) concentration (1.8 × 10^{-6} M PPO, 7.1 M HCl, 20% ethanol); (b) influence of HCl concentration (1.4 × 10^{-6} M PPO, 2 × 10^{-3} M Sn(II), 30% ethanol); (c) influence of PPO concentration (7.1 M HCl, 2 × 10^{-2} M Sn(II), 20% ethanol); (d) ifnluence of ethanol concentration (1.8 × 10^{-6} M PPO, 2 × 10^{-3} M Sn(II), 7.1 M HCl).

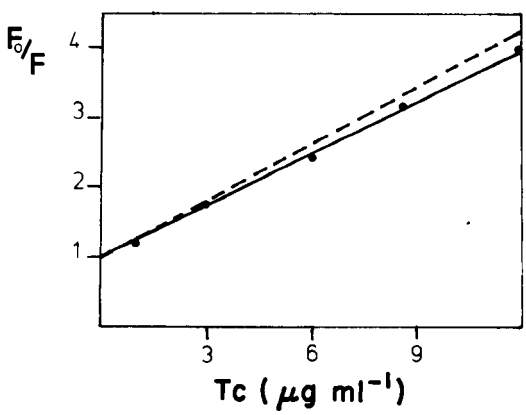

Fig. 2. Stern—Volmer plots: (—) at 20°C, (---) at 65°C. (2 × 10^{-3} M Sn(II), 2.4 M HCl, 1.3 × 10^{-6} M PPO, 30% ethanol.)

quenching of technetium on PPO can be attributed to the fact that PPO has a greater quantum efficiency that POPOP.

Maximum quenching is obtained in the presence of tin(II) chloride. This indicates that technetium in a reduced form is a more effective quencher that pertechnetate. Maximum fluorescence was obtained for a final concentration of 2×10^{-3} M tin(II) chloride, which was chosen for further work. As shown in Fig. 1(b), the acidity of the medium slightly affects the fluorescence of PPO, but at hydrochloric acid concentrations below 2.4 M the quenching effect is much less. Thus the optimum hydrochloric acid concentration was chosen as 2.4 M. Quenching can therefore be attributed to the presence of anionic chloride complexes of technetium.

The effect of PPO concentration is shown in Fig. 1(c). As can be seen, good sensitivity was obtained at a final concentration of 1.3×10^{-6} M and this was chosen for the determination of technetium. The ethanol concentration has little effect on the fluorescence measurements (Fig. 1d); consequently, for further work the concentration chosen was 30% (v/v).

Effect of technetium on the 2,2'-pyridil/tin(II) system

When a recently prepared ethanolic 2,2'-pyridil solution is mixed with sufficient tin(II) chloride in acidic media, a pale yellow species is formed on warming that exhibits an intense blue fluorescence (λ_{ex} = 369 nm, λ_{em} = 469 nm). With increasing tin(II) concentrations, the yellow colour becomes more intense but the blue fluorescence abruptly decreases. Presumably complexation takes place after reduction of keto groups to hydroxyl groups [20]:

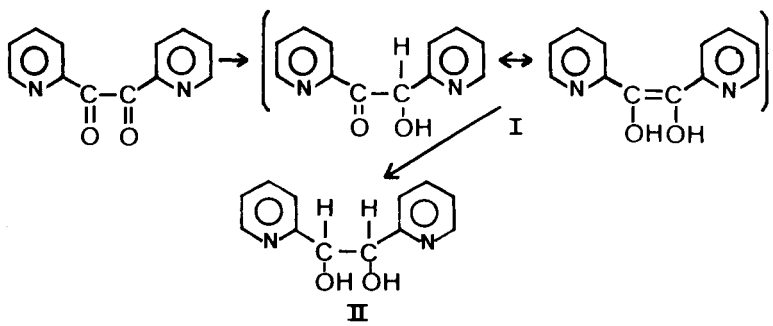

Compound I exhibits greatest rigidity and planarity and consequently will be the most fluorescent. Formation of compound II implies a decrease in fluorescence as a consequence of the loss of rigidity and planarity. In the presence of traces of technetium, the fluorescence is greatly quenched and the solution becomes intensely yellow-brown ($\epsilon = 3.8 \times 10^3$ l mol^{-1} cm^{-1} at 360 nm). Quenching of the fluorescence in the presence of technetium and the development of this colour depends on the acidity, ethanol concentration, tin(II) concentration, 2,2'-pyridil concentration and time of warming. The effects of these five variables were therefore studied. The effect of

warming time is shown in Fig. 3(a); the fluorescence of the blank and of the technetium sample continuously increased. The difference in intensity between the two solutions reached a maximum after 10 min and then decreased. It is interesting to note that the maximum difference in fluorescence occurs at the same time at which the maximum difference in absorbance is achieved.

As shown in Fig. 3(b), decreasing acidity decreases the fluorescence and absorbance of the samples. This is because the product exhibits maximum fluorescence in acidic media and because an acidic medium is necessary for its formation. Moreover, the maximum differences of fluorescence or absorbance occur at the same acidity (10^{-2} M). The fluorescence obtained when the acidic 2,2′-pyridil solution is warmed in the presence of tin(II) chloride depends markedly on the concentration. Both maximum fluorescence and maximum absorbance were obtained at a final concentration of 3.5×10^{-4} M; this concentration was therefore chosen for further work. Above this concentration, the fluorescence abruptly decreased, probably because of the higher reducing strength of the medium.

The effect of the 2,2′-pyridil concentration is shown in Fig. 3(c). As can

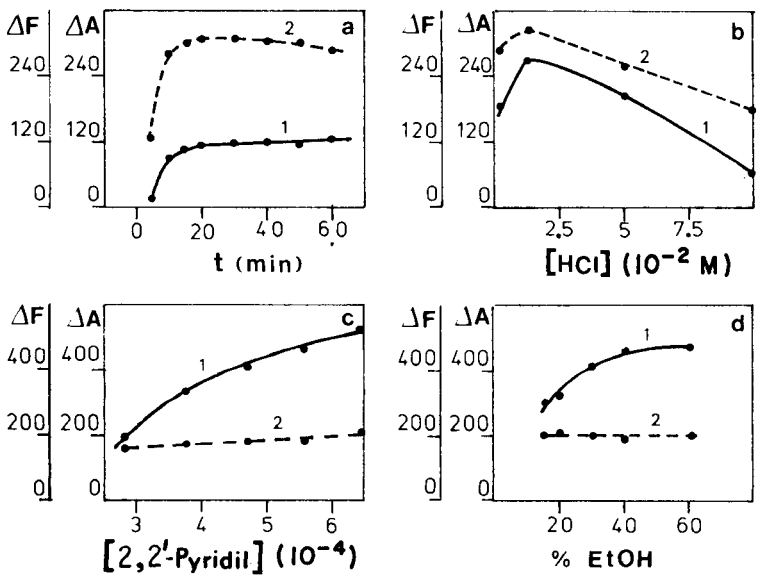

Fig. 3. Effect of variables on the fluorescence (λ_{ex} = 369 nm, λ_{em} = 469 nm) and absorbance (λ = 410 nm) of the Tc/tin(II)/2,2′-pyridil system. Curves: (1) difference of fluorescence between technetium sample (11.9 μg ml^{-1}) and reagent blank; (2) difference of absorbance between technetium sample (11.9 μg ml^{-1}) and reagent blank. (a) Influence of heating time (9.4×10^{-4} M 2,2′-pyridil, 30% ethanol, 0.02 M Sn(II), 0.1 M HCl); (b) influence of HCl concentration (4.7×10^{-4} M 2,2′-pyridil, 30% ethanol, 1×10^{-3} M Sn(II), heating time 10 min); (c) influence of 2,2′-pyridil concentration (30% ethanol, 0.01 M HCl, 3.5×10^{-4} Sn(II), heating time 10 min); (d) influence of ethanol concentration (7.5×10^{-4} M 2,2′-pyridil, 0.01 M HCl, 3.5×10^{-4} M Sn(II), heating time 10 min).

be seen, maximum difference of fluorescence and absorbance over the blank was obtained for a final concentration of 6.6×10^{-4} M. Changes in the ethanol concentration had little effect on the absorbance measurements but a more important effect on the fluorescence (Fig. 3d). For further work the concentration chosen was 40% (v/v), because it was the smallest concentration that gave maximum sensitivity.

Maximum quenching of the fluorescence by technetium corresponds to maximum absorbance of the solution. This absorbance must correspond to the formation of a complex between reduced technetium and the fluorescent product that results from reduction of the diketone. Maximum complex formation therefore corresponds to maximum quenching.

Characteristics of the analytical methods

The fluorescence was measured at the maximum excitation and emission wavelengths (λ_{ex} = 315 nm, λ_{em} = 411 nm for PPO and λ_{ex} = 369 nm, λ_{em} = 469 nm for 2,2′-pyridil) for different amounts of technetium under the experimental conditions in which quenching is a maximum. The absorbance was measured at 360 nm for different amounts of technetium under the optimum conditions. There were linear relationships between the decrease of fluorescence intensity or absorbance and the technetium concentration in the ranges shown in Table 2.

The selectivity of the spectrofluorimetric and spectrophotometric methods was tested by measuring the fluorescence and absorbance in the presence of several foreign ions under the recommended conditions. The maximum tolerable concentrations of several ions in the spectrofluorimetric determination of technetium by use of PPO are given in Table 3; U(VI), Re(VII), Mo(VI) and W(VI), elements that frequently accompany technetium, cause only slight interference. In spectrofluorimetric determination of technetium by use of 2,2′-pyridil, Mo(VI), Fe(III), Al, Cu(II), Hg(II) and V(V) cause important perturbations which can be attributed to these ions reacting with the reduced reagent in a similar manner to technetium. As can be seen in Table 3, the selectivity of the spectrophotometric method based on this diketone is similar to that of the fluorimetric method except that aluminium does not interfere.

TABLE 2

Characteristics of the analytical methods

Reagent	Technique	Linear range (μg ml^{-1})	R.s.d.[a] (%)
PPO	Spectrofluorimetry	0.01—1 1—12	1.6
2,2′-pyridil	Spectrofluorimetry	0.1—1 1—12	2.0
2,2′-pyridil	Spectrophotometry	1—15	1.8

[a]Relative standard deviation for 11 determinations (95% confidence) of 1.0 μg Tc ml^{-1}.

TABLE 3

Maximum tolerable concentrations of foreign ions in the determination of technetium(VII) (1.0 $\mu g\ ml^{-1}$)

Tolerance limit ($\mu g\ ml^{-1}$)	Foreign ion
Fluorimetry with PPO[a]	
100	Ca, Mg, Sr, Ba, Zn, Mn(II), Ni, Co(II), Cr(III), Fe(III), V(V), Re(VII), Cl^-, NO_3^-, SO_4^{2-}
50	Al, Hg(II)
20	Cu(II), U(VI)
10	Mo(VI), W(VI)
Fluorimetry with 2,2'-pyridil[b]	
50	Ca, Mg, Sr, Ba, Zn, Mn(II), Co(II), Ni, Cr(III), Re(VII), U(VI), Cl^-, SO_4^{2-}, NO_3^-
10	W(VI)
1	Al, Cu(II), Hg(II), V(V)
0.2	Fe(III), Mo(VI)
Spectrophotometry with 2,2'-pyridil[b]	
50	Ca, Mg, Sr, Ba, Al, Cr(III), Re(VII), Cl^-, SO_4^{2-}, NO_3^-
20	Ni, Zn, Mn(II)
10	Hg(II), Co(II), U(VI)
2	Cu(II), W(VI)
0.2	Mo(VI)
<0.2	Fe(III), V(V)

[a—c]Tolerable amounts are those giving errors of: [a]$\leqslant$1.6%, [b]$\leqslant$2.0%, [c]$\leqslant$1.8%.

It is important to emphasize that in all cases interference of cations can easily be avoided by separation of technetium as pertechnetate by ion-exchange chromatography. Other adequate methods of separating technetium from interfering anions are also available [21]. Obviously, the presence of high concentrations of oxidants must be avoided because they would react with the tin(II).

Applications

There has recently been considerable interest in measuring the environmental concentrations and distributions of technetium. For this reason, the distribution of technetium in plants (*Phaseolus vulgaris*) that had been fed with a synthetic solution (Table 1) containing technetium, was studied and compared with results on similar plants grown in the same way but without technetium. The presence of technetium dramatically stunted the growth of these plants.

The spectrofluorimetric PPO procedure was applied to the determination of technetium in vegetation. This procedure cannot be applied directly with the usual calibration because some products of the mineralization interfere

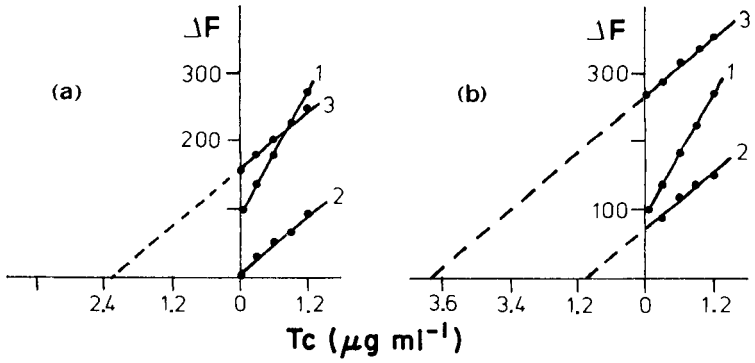

Fig. 4. Application of the standard addition method to the determination of technetium in vegetation: (a) plant leaves; (b) plant stalks. Curves: (1) calibration plot in absence of matrix; (2) plot obtained by standard addition to reference material (plants fed without technetium); (3) plot obtained by addition to a sample of vegetation fed with technetium.

slightly, but the quenching is still proportional to the concentration of technetium added (Fig. 4). Therefore technetium can be determined by use of the standard addition method. The results obtained (mean of 3 determinations) were 110 μg Tc g^{-1} of dried leaves and 140 μg g^{-1} of dried stems but no technetium was detected in the roots.

Financial support by CAICYT (Grand No. 2060-83) is gratefully acknowledged.

REFERENCES

1 N. W. Golchert and J. Sedled, Anal. Chem., 41 (1969) 669.
2 F. O. Hoffman, J. W. Huckabee, D. M. Lucas, C. T. Garter, T. G. Scott, R. L. Walker, P. S. Gouge and C. V. Holmes, Sampling of technetium-99 in vegetation and soils in the vicinity of operating gaseous diffusion facilities, Oak Ridge Natl. Lab. Rep., ORNL/TM-7386, 1980.
3 J. H. Kaye, J. A. Merrill, R. R. Kinnison, M. S. Rapids and N. E. Ballou, Anal. Chem., 54 (1982) 1158.
4 N. Y. Chu and J. Feldstein, Talanta, 31 (1984) 809.
5 G. Boyd and Q. Larson, J. Phys. Chem., 60 (1956) 707.
6 S. Foti, E. Delucchi and V. Akamian, Anal. Chim. Acta, 60 (1972) 261, 269.
7 T. J. Anderson and R. L. Walker, Anal. Chem., 52 (1980) 709.
8 J. H. Kaye, M. S. Rapids and N. E. Ballou, Proc. Third Int. Conf. on Nuclear Methods in Environmental and Energy Research, Columbia, MO, CONF-771072, 1977, pp. 211—224.
9 F. O. Hoffman, C. T. Garten, J. W. Huckabee and D. Lucas, J. Environ. Qual., 11 (1982) 134.
10 F. O. Hoffman, Environmental behaviour of technetium in soil and vegetation: implications for radiological impact assessment, Oak Ridge Natl. Lab. Rep., ORNL-5856, 1982.
11 F. O. Hoffman, C. T. Garten, D. M. Lucas and J. W. Huckabee, Environ. Sci. Technol., 16 (1982) 214.

12 J. H. Kaye and N. E. Ballou, Anal. Chem., 50 (1978) 2076.
13 K. Schwochau, Top. Curr. Chem., 96 (1981) 110.
14 A. F. Kuzina, Radiokhimiya, 21 (1979) 178.
15 F. Grases, J. G. March, F. Mata and A. Peñafiel, Anal. Chim. Acta, 166 (1984) 71.
16 A. J. Jones and A. Davison, Int. J. Appl. Radiat. Isot., 33 (1982) 867.
17 A. Davison and A. J. Jones, Int. J. Appl. Radiat. Isot., 33 (1982) 875.
18 K. Schwochau, Radiochim. Acta, 32 (1983) 139.
19 J. R. Lakowicz, Principles of Fluorescence Spectroscopy, Plenum Press, New York, 1983.
20 E. Muller and O. Bayer, Methoden der Organischem Chemie, Georg Thieme Verlag, Stuttgart, 1981.
21 F. J. Miller and P. F. Thomason, Anal. Chem., 32 (1960) 1429.

Analytica Chimica Acta, 174 (1985) 173—182
Elsevier Science Publishers B.V., Amsterdam — Printed in The Netherlands

FACTORS INFLUENCING THE FREE OXYGEN CONTENT IN AN ELECTROTHERMAL ATOMIZER

A. B. VOLYNSKY*, E. M. SEDYKH and B. YA. SPIVAKOV

V. I. Vernadsky Institute of Geochemistry and Analytical Chemistry of the USSR Academy of Sciences, Moscow, V-334 (U.S.S.R.)

I. HAVEZOV

Institute of General and Inorganic Chemistry of the Bulgarian Academy of Sciences, Sofia, 1040 (Bulgaria)

(Received 19th June 1984)

SUMMARY

A considerable decrease in the partial pressure of free oxygen in the gas phase within a graphite atomizer during atomization with the use of ascorbic acid as a matrix modifier was proved by using the method suggested by L'vov and Ryabchuk. A similar change in the gas-phase composition was observed in graphite tubes treated with compounds of refractory metals. A mechanism for this oxygen binding is suggested. It is shown that the sensitivity of the determination of tin is improved by decreasing the free oxygen content of the gas phase.

In electrothermal atomic absorption spectrometry, much attention is given to problems concerning the elimination of matrix interferences and to improving detection limits. In this connection, the use of chemical methods of separation and preconcentration as well as matrix modifiers has recently gained popularity. Ascorbic acid and other water-soluble organic substances as well as inorganic salts have been used as matrix modifiers [1—4]. The action of ascorbic acid is usually attributed to amorphous carbon which is formed as a result of thermal decomposition of the modifier. This carbon affects the processes both in the condensed and the gas phase within an electrothermal atomizer [1, 5]. Different organic solvents and chelating agents may also serve as sources of amorphous carbon in a graphite furnace [6, 7].

It is known that graphite tubes treated with compounds of refractory metals (La, Mo, Zr, W, etc., the so-called modified graphite tubes), have considerable advantages over conventional tubes [8—15]. The effect of carbide coatings on analyte determination in a graphite furnace is usually explained by processes occurring on the surface of the furnace. For example, it is supposed for modified graphite tubes that the atomized fraction of elements showing a tendency to form stable carbides increases because of suppression of carbide formation [8, 12, 15—18]. The decreased matrix

interferences in modified furnaces [15, 19—21] are at least partially caused by better wetting of the furnace surface. This leads to less interference from analyte occlusion [22].

There is no common opinion about the effect of modification on the chemical activity of the graphite atomizer surface. Some authors believe that refractory metal carbides are more active reductants than graphite [8, 23]. Others [12, 18, 22, 24] think that the treatment of graphite furnaces with refractory metal compounds results in a decreased activity of the atomizer surface because of blocking of active graphite sites. Better resistance to oxidation owing to fewer active sites results in a prolonged life for the graphite tube [24]. The decreased reactivity of the furnace surface provides a longer lifetime when used for the analysis of samples containing strong oxidizing agents and high concentrations of acids [15, 25].

The mechanisms of processes occurring in modified graphite furnaces, therefore, have not been studied sufficiently. It has been established that carbide coatings obtained by treatment of graphite tubes with zirconium, tungsten or molybdenum solutions do not form a compact layer on the atomizer surface and therefore do not prevent completely any contact between the sample and the graphite [11]. Thus, slower carbide formation is not the only factor responsible for better sensitivity in modified graphite furnaces for elements forming stable carbides. The increase in the atomized function of such elements may also be connected with prevention of oxide formation. It is known that carbide-forming elements form very stable oxygen compounds. For example, the dissociation energy is 783 kJ/mol^{-1} for SiO (428 kJ mol^{-1} for SiC), 700 kJ mol^{-1} for YO and 779 kJ mol^{-1} for CeO (445 kJ mol^{-1} for CeC) [26]. Prevention of oxide formation is probably the main reason for the better sensitivity of determinations in modified graphite furnaces for elements which do not form stable carbides but do form relatively stable oxides (tin [9], selenium [27], arsenic [11] and lead [22]).

It was found in the work described here that the use of ascorbic acid and modified graphite furnaces leads to a decrease in the partial pressure of free oxygen, $P(O_2)$, within the electrothermal atomizer. The reasons for the prolonged lifetime of modified tubes are considered. It is shown that a change in the sensitivity of tin determination in aqueous solutions and organic extracts may largely be dependent on a change in the value of $P(O_2)$ if the heating rate and the inert gas flow rate are varied during atomization.

EXPERIMENTAL

Apparatus

The Perkin-Elmer atomic absorption spectrometer, model 603, used was connected to an HGA-76B graphite atomizer and a Perkin-Elmer 056 recorder. A deuterium background corrector was used. Argon containing no more than 7×10^{-4}% oxygen was used as purge gas. Perkin-Elmer graphite tubes both with and without pyrolytic graphite coatings were tested. The

tubes were treated with a sodium tungstate solution as described previously [9]. To coat the tubes with zirconium carbide, their inner surface was covered by a thin layer of 10 mg of zirconium dioxide as an aqueous suspension and dried and processed by heating the atomizer according to a given program [13]. A hollow-cathode lamp was used for tin determination and an electrodeless discharge lamp for oxygen, both at 224.6 nm with a bandwidth of 0.2 nm. Sample volumes of 20 and 40 μl were injected for tin and oxygen, without and with a graphite platform, respectively. Peak heights were measured. The heating parameters for tin determination and indirect oxygen determination are listed in Table 1. Graphite tubes were weighed on a WA-33 balance (Model PRL-T-A13, Poland).

Reagents

All the reagents used were of analytical grade. Methyl isobutyl ketone (MIBK) was distilled before use. The stock solution of tin was prepared by dissolving tin metal (100 mg) in 2.5 ml of a (1 + 3) mixture of hydrochloric and nitric acids and by adding subsequently 3 M nitric acid to give a final volume of 100 ml. Working solutions of tin in 0.5 M nitric acid were prepared immediately before use. Working solutions prepared in 0.5 M hydrochloric acid were stable for at least 2 weeks.

Organic extracts were prepared by shaking a solution of tin in 6.9 M hydrochloric acid with MIBK or with 0.1 M tri-n-octylamine (TOA) in MIBK (the equilibration time was 20 min and the ratio of the volumes was 1:1). The concentration of tin in the aqueous phase at equilibrium was determined, and its value was used for calculating the tin content of an extract (with allowance for the change in the volumes of the phases during extraction).

Estimation of changes in the free oxygen content of the gas phase in the atomizer

L'vov and Ryabchuk [28] have shown that the calibration graph for tin deviates from linearity under certain conditions of tin determination (an

TABLE 1

Heating parameters

	Tin			Oxygen		
	Time (s)	Temp. (°C)	Heating rate (°C s^{-1})	Time (s)	Temp. (°C)	Heating rate (°C s^{-1})
Drying	20	110	50	40	150	20
Ashing	20	800	200	25	800	80
				2	1250	600
Atomization	6	2600[a]	600	2	2200	20

[a]Gas-stop during atomization.

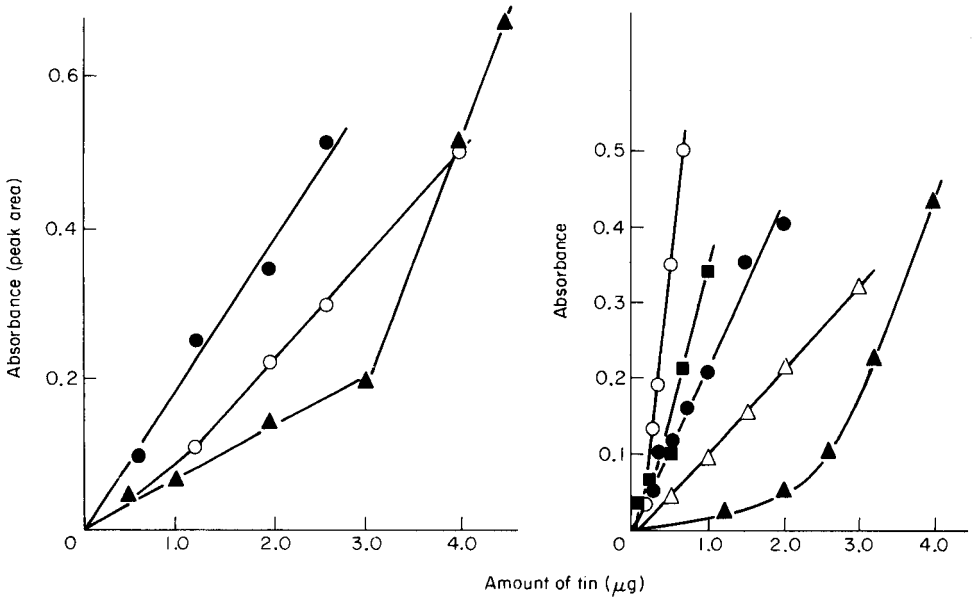

Fig. 1. Calibration graphs for tin in pyrolytically-coated graphite furnaces in the presence of: (●) 5% ascorbic acid solution; (○) 1% ascorbic acid; (▲) no ascorbic acid.

Fig. 2. Influence of graphite tube material on calibration graphs for tin: (▲, ○) tube with pyrolytic coating; (△, ●, ■) porous graphite tube; (●, ○) tube treated with Na_2WO_4 solution; (■) tube treated with ZrO_2 suspension.

example is shown in Fig. 1). By extrapolating the linear portion of the calibration graph to the intersection with the abscissa the value of m_i (the "inert" quantity of tin) proportional to $P(O_2)$ in the atomizer can be found. Essential differences in the optimum conditions for indirect determination of oxygen from the conditions of determination of other elements (fast heating rates, gas-stop or miniflow during atomization) are the main drawback of using this method for oxygen determination. That is why only a qualitative estimation of the change in the gas phase composition during atomization was made.

To eliminate the effect of surface processes in the graphite tube on the results, the nitric acid solution of tin was placed onto a pyrolytic graphite platform, and the central part of the analytical zone in the atomizer was limited by two graphite disks having a central hole 2.8 mm in diameter [28]. The disks, 2 mm thick, were placed near the graphite furnace windows. In the case of tin determination in the presence of a modifier, 20 μl of aqueous solutions of ascorbic acid of different concentrations were placed on the platform and dried. Integrated signal measurements were used in this case because of changes in peak shapes. Temperature program parameters for the determination of oxygen are summarized in Table 1.

Measurements of graphite tube weight

For tin determination, three graphite tubes without pyrolytic graphite coatings from the same batch were tested. One was treated with a solution of sodium tungstate. In a second tube, determinations were done in the presence of 50 μl of carbon tetrachloride (the drying time was doubled). In order to obtain a more pronounced effect for processes occurring during atomization, the ashing time was decreased to 5 s. Determinations were done in a full flow of inert gas. Graphite tubes were weighed after each 10 determinations.

RESULTS

Change in the free oxygen content in the atomizer

It was found that the values of m_i, which are proportional to $P(O_2)$, decrease with increasing ascorbic acid concentration (Fig. 1, Table 2). The values of m_i also decrease when changing from pyrolytic graphite-coated tubes to porous graphite tubes and further in tubes treated with tungsten and zirconium compounds (Fig. 2, Table 2).

Weight and thickness changes of graphite tubes

The data obtained show the graphite losses from both inner and outer atomizer surfaces during use. The largest weight losses were observed for graphite tubes treated with sodium tungstate (Fig. 3). It should be noted that a decrease in the ashing time adversely affected the precision of the results. The worst precision was observed for tin determination in the presence of carbon tetrachloride. That is why data on tin determination under such conditions are not plotted in Fig. 4, which presents the analytical signals as a function of the operating lifetime of the graphite tubes. A comparison of curves 1 and 2 in Fig. 4 testifies to the advantage of tubes with carbide coatings for tin determination.

Figure 5 illustrates sectional views of graphite tubes without pyrolytic graphite coatings after more than 100 determinations. The most intensive

TABLE 2

Values of m_i (proportional to $P(O_2)$) in treated and untreated pyrolytic and porous graphite tubes

Tube	Pyrolytic graphite				Porous graphite		
Treatment	None			Na_2WO_4	None	Na_2WO_4	ZrO_2
m_i (μg)	2.4	0.4[a]	0.0[b]	0.12	0.15	−0.07	0.0
S.d. (μg)	0.5[c]	0.3[c]	0.9[c]	0.04[d]	0.09[d]	0.19[d]	0.2[d]

[a] 1% ascorbic acid solution added. [b] 5% ascorbic acid solution added. [c] Standard deviation for 5 integrations. [d] Standard deviation for 5 peak-height measurements.

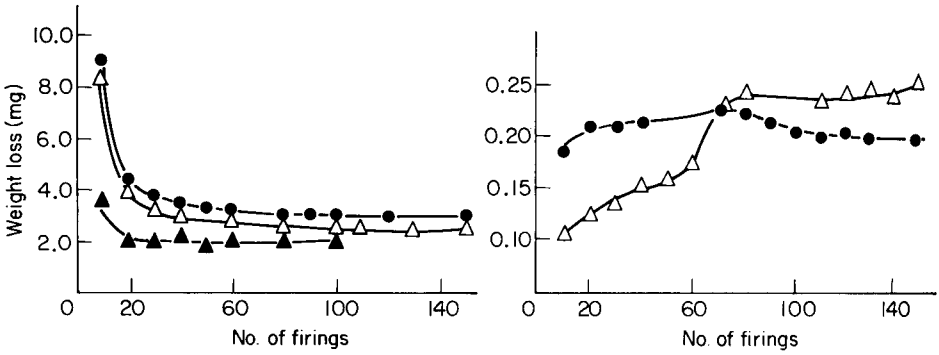

Fig. 3. Weight change of porous graphite tubes as a function of the number of firings in the determination of tin in 0.5 M HCl. (△) Initial weight of tube 1.0627 g, 0.2 μg Sn. (•) Tube treated with Na_2WO_4; initial weight 1.0370 g, weight after treatment 1.0395 g, 20 ng Sn. (▲) In the presence of CCl_4; initial weight of tube 1.0580 g, 0.6 μg Sn.

Fig. 4. Influence of number of firings on peak-height absorbance obtained for tin: (△) porous graphite tube, 0.2 μg Sn; (•) tube treated with Na_2WO_4, 20 ng Sn.

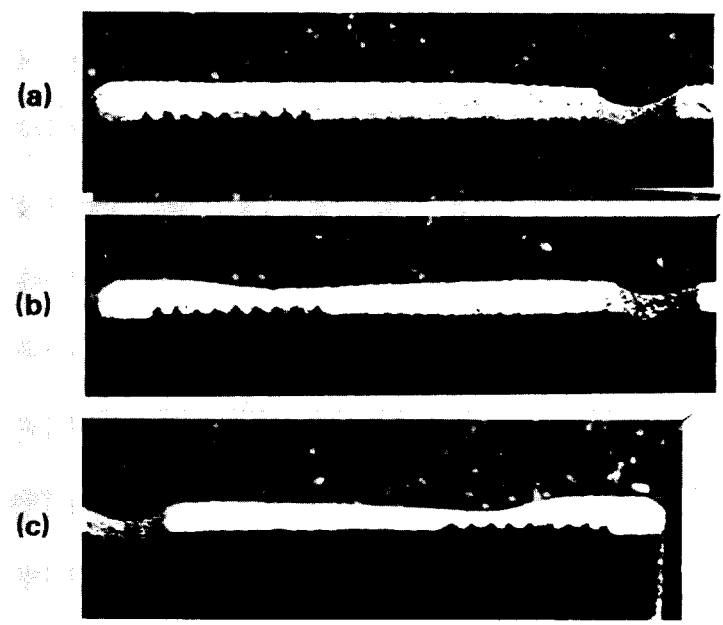

Fig. 5. Sections of used porous graphite tubes: (a) conventional tube; (b) tube treated with Na_2WO_4; (c) tube treated with ZrO_2.

burn-out of graphite from the conventional tube is observed in the middle section. For the tungsten- and zirconium-treated tubes, the places with the most noticeable burn-out are shifted towards the ends of the tubes.

Effect of other parameters on tin determination

As seen from the data listed in Table 3, the dependence of the tin signal on the heating rate during atomization exhibits a maximum The decrease in the tin signal during ramp heating may be eliminated either by ashing in the gas-stop mode or by using an additional ashing stage (800°C for 2 s, gas-stop mode). The effect caused by the additional ashing stage sharply diminishes in the presence of ascorbic acid. The largest increase in the tin signal in the presence of ascorbic acid and with the use of the additional ashing stage was observed for graphite tubes with pyrolytic graphite coating (Table 3).

TABLE 3

Effect of heating rate on the peak height signal from 0.15 $\mu g\ ml^{-1}$ tin in 0.5 M HNO_3

Surface material	Heating rate during atomization ($°C\ s^{-1}$)	Presence of 5% ascorbic acid	Signal[a]	
			1	2
Porous graphite	1400	—	0.25	0.49
		+	0.41	0.55
	600	—	0.51	0.51
		+	0.59	0.60
Pyrolytic graphite	1400	—	0.03	0.28
		+	0.27	0.47
	600	—	0.20	0.31
		+	0.47	0.47
	400	—	0.23	0.21
		+	0.53	0.52
	180	+	—	0.42

[a] Signal after 1 and 2 ashing stages.

TABLE 4

Amounts of tin (ng) giving an absorbance of 0.100

Conditions	Gas-stop			Full flow		
	0.5 M HCl	MIBK	0.1 M TOA in MIBK	0.5 M HCl	MIBK	0.1 M TOA in MIBK
Porous graphite	0.60	0.67	0.87	71	45	63
Porous graphite, 5% ascorbic acid	0.54	0.59	0.59	59	38	48
Porous graphite treated with Na_2WO_4	0.58	0.77	1.24	14.3	11.8	15.4
Graphite with pyrolytic coating	1.38	1.46	1.48	>4000	200	400

Table 4 shows the effects of a modifier (ascorbic acid) and of the surface material on the determination of tin in aqueous solutions and organic extracts. As can be seen, when the gas-stop mode is used during atomization the absorbance from aqueous solutions of tin is only slightly larger than that of tin-containing extracts. For full gas flow during atomization, the tin signals considerably decrease for all the solutions studied, the largest decrease being observed for graphite tubes with a pyrolytic graphite coating. In this mode the tin signals are higher for extracts than for aqueous solutions. The signals may differ by more than two orders of magnitude when 0.5 M hydrochloric acid solutions of tin are injected into tubes having different coatings.

DISCUSSION

The data obtained indicate that, depending on the conditions, the free oxygen content in graphite tubes varies over a wide range. In passing from the graphite tube with a pyrolytic graphite coating to the porous graphite tube and then to a determination in the presence of ascorbic acid, a decrease in the value of $P(O_2)$ in the gas phase is observed. This decrease is caused by the different ability of the amorphous carbon formed by thermal decomposition of ascorbic acid and the different types of graphite to react with oxygen [29]. A considerable effect on the reaction rate of carbon with oxygen is also produced by a sharp increase in the surface area on passing from pyrolytic graphite to porous graphite and then to amorphous carbon.

The observed decrease in the tin signal when ramp heating is used during atomization (Table 3) is due to the change in the gas composition. In this heating mode, the amount of oxygen bound by the atomizer graphite before the appearance of free tin atoms decreases. Stopping the inert gas flow during ashing leads to a decrease in the oxygen content, which favours tin atomization. A similar effect is produced by ascorbic acid (Table 3). The reaction of oxygen with the products of destruction of the organic matrix results in a greater absorbance for organic extracts of tin than for aqueous solutions in the case of the full gas flow during atomization (Table 4).

A considerable increase in tin signals in graphite tubes treated with a sodium tungstate solution, particularly in full gas flow mode during atomization (Table 4), is also connected with a decrease in $P(O_2)$ (Table 2). The decrease is due to the catalytic action of compounds of heavy metals on the oxidation of carbon by oxygen [30]. It is known that carbides of tungsten, molybdenum, zirconium and other refractory metals are easily oxidized at $\geqslant$1000°C [31]. The oxidation rate sharply increases with increasing sample dispersion [32]. Thus, at high temperatures, carbides of refractory metals may serve as oxygen carriers [30]. The metal oxide or oxycarbide formed [33] is converted to the carbide as a result of interaction with the atomizer graphite. The possibility of interaction between the carbide coating on the furnace and the oxygen impurity in the inert gas was first indicated by Vickrey et al. [10].

The data obtained from measurements of the graphite tube weight also testify to the acceleration of the interaction between the atomizer graphite and oxygen impurity in the presence of tungsten compounds (Fig. 3). Also, the chlorine formed during thermal decomposition of carbon tetrachloride inhibits the oxidation of graphite [34], leading to a decrease in the graphite tube weight loss. The rise in the stability of the graphite tube at high temperatures produced by treatment with halogen-containing compounds has been reported previously [35].

It is known that a carbide coating prolongs the lifetime of graphite tubes [12—14]. However, weight losses for such tubes may be greater than for tubes without coatings (Fig. 3). The graphite burning-out geometry is the reason for this apparent contradiction. Conventional graphite tubes burn out primarily in the central part (Fig. 5a) where the temperature is at a maximum [36] and, consequently, the reaction rate of graphite with oxygen is also at a maximum [34]. The burning-out of the central part of the tube leads to its rapid failure. For graphite tubes coated with carbides of refractory metals, the interaction between oxygen and graphite takes place at lower temperatures [30]. Therefore, the removal of oxygen from the purge gas begins at the instant it reaches the atomizer surface (Fig. 5b, c). Thus, argon from which oxygen has been removed is supplied to the central part of the graphite tube, resulting in a prolonged life for the tube. Moreover, a decrease in the wall thickness at the tube ends allows a more nearly isothermal environment in the furnace [36].

Thus, the chemical activity of the surface increases with the use of ascorbic acid and in graphite tubes treated with refractory metal compounds. This results in a lower concentration of free oxygen in the gas phase in the furnace during atomization. Such a change promotes more complete atomization of tin and other elements forming relatively stable oxides [11, 13, 22, 27] and probably of carbide-forming elements [8, 14, 17, 18]. The lifetimes of modified graphite furnaces are longer because such furnaces lose material from the ends, rather than the middle.

REFERENCES

1 J. G. T. Regan and J. Warren, Analyst, 101 (1976) 220.
2 E. M. Sedykh, Yu. I. Belyaev and E. V. Sorokina, Zh. Anal. Khim., 35 (1980) 2348.
3 L. N. Sukhoveeva, G. G. Butrimenko and B. Ya. Spivakov, Zh. Anal. Khim., 35 (1980) 649.
4 A. B. Volynsky, E. M. Sedykh, B. Ya. Spivakov and Yu. A. Zolotov, Zh. Anal. Khim., 38 (1983) 435.
5 E. M. Sedykh, Yu. I. Belyaev and P. I. Ozegov, Zh. Anal. Khim., 34 (1979) 1984.
6 J. Komárek, D. Kolčava and L. Sommer, Collect. Czech. Chem. Commun., 45 (1980) 3313.
7 K. Ohta and M. Suzuki, Anal. Chim. Acta, 108 (1979) 69.
8 G. Müller-Vogt and W. Wendl, Anal. Chem., 53 (1981) 651.
9 H. Fritzsche, W. Wegscheider, G. Knapp and H. M. Ortner, Talanta, 26 (1979) 219.
10 T. M. Vickrey, G. V. Harrison, G. J. Ramelov and J. C. Carver, Anal. Lett., A13 (1980) 781.

11 T. M. Vickrey, G. V. Harrison and G. J. Ramelov, Anal. Chem., 53, (1981) 1573.
12 J. Takahashi, T. Kitahara, N. Hirabayashi, K. Sato, K. Yoshida, H. Haragushi and K. Fuwa, Bunseki Kagaku, 30 (1981) 90.
13 I. Havezov, E. Russeva and N. Jordanov, Fresenius Z. Anal. Chem., 296 (1979) 125.
14 Gui-wen Zhao, Shou-xin Wang, Ming-yang Zhu and Kaoru Sakai, Bunseki Kagaku, 32 (1983) 164.
15 I. Havezov and E. Russeva, in Abstr. Pap. X Jubilee Natl. Conf. Atom. Spectrosc., Veliko Turnovo, Bulgaria, 1982.
16 P. Lagas, Anal. Chim. Acta, 98 (1978) 261.
17 J. H. Runnels, R. Merryfield and H. B. Fisher, Anal. Chem., 47, (1975) 1258.
18 H. S. Wahab and C. L. Chakrabarti, Spectrochim. Acta, Part B, 36 (1981) 463.
19 W. Slavin and D. C. Manning, Anal. Chem., 51 (1979) 261.
20 J. E. Poldoski, Anal. Chem., 52 (1980) 1147.
21 D. J. Hodges and D. Skelding, Analyst, 108 (1983) 813.
22 M. P. Bertenshaw, D. Gelsthorpe and K. C. Wheatstone, Analyst, 107 (1982) 163.
23 Gao Ying-qi and Ni Zhe-ming, Acta Chim. Sin., 40 (1982) 1021.
24 S. G. Salmon and J. A. Holcombe, Anal. Chem., 54 (1982) 630.
25 G. Severin, E. Schumacher and F. Umland, Fresenius Z. Anal. Chem., 311 (1982) 201.
26 K. S. Krasnov (Ed.), Molecular Constants of Inorganic Substances, Khimia, Leningrad, 1979 (in Russian).
27 T. M. Vickrey and M. S. Buren, Anal. Lett., 13A (1980) 1465.
28 B. V. L'vov and G. N. Ryabchuk, Spectrochim. Acta, Part B, 37 (1982) 673.
29 W. R. Smith and M. H. Polley, J. Phys. Chem., 60 (1956) 689.
30 D. W. McKee, in P. L. Walker and P. A. Thrower (Eds.), Chemistry and Physics of Carbon (Vol. 16), M. Dekker, New York, 1981, pp. 1—118.
31 R. F. Voitovich, The Oxidation of Carbides and Nitrides, Naukova Dumka, Kiev, 1981 (in Russian).
32 R. F. Voitovich and A. A. Pugach, The Oxidation of High Melting Point Substances, Metallurgiya, Moscow, 1978, p. 28 (in Russian).
33 S. I. Alyamovsky, Yu. G. Zainulin and G. P. Shveikin, Oxycarbides and Oxynitrides of IVA and VA subgroup metals, Nauka, Moscow, 1981 (in Russian).
34 R. J. Day, P. L. Walker and C. C. Wright, Industrial Carbon and Graphite, Soc. Chem. Ind., London, 1958, pp. 348—370.
35 W. Slavin and D. C. Manning, in Abstr. Pap. Pittsburgh Conf. Anal. Chem. Appl. Spectrosc., Atlantic City, U.S.A., 1981, p. 225.
36 W. Slavin, S. A. Myers and D. C. Manning, Anal. Chim. Acta, 117 (1980) 267.

Analytica Chimica Acta, 174 (1985) 183—189
Elsevier Science Publishers B.V., Amsterdam — Printed in The Netherlands

DETERMINATION OF CADMIUM BY SUCTION-FLOW LIQUID-LIQUID EXTRACTION COMBINED WITH INDUCTIVELY-COUPLED PLASMA ATOMIC EMISSION SPECTROMETRY

TAKAHIRO KUMAMARU*, YOKO NITTA, FUMIO NAKATA and HIROSHI MATSUO

Department of Environmental Science, Faculty of Integrated Arts and Sciences, Hiroshima University, 1-1-89 Higashisenda-machi, Naka-ku, Hiroshima 730 (Japan)

MASAHIKO IKEDA

Engineering Department, Nippon Jarrell-Ash Co. Ltd., 28 Joshungamae-cho, Shimotoba, Fushimi-ku, Kyoto 612 (Japan)

(Received 11th February 1985)

SUMMARY

The flow manifold described permits suction-flow liquid-liquid extraction of cadmium in a discrete aqueous sample as its diethyldithiocarbamate into carbon tetrachloride. The organic extract is fed into the nebulizer of an inductively-coupled plasma atomic emission spectrometer by a peristaltic pump. An increase in sensitivity of ca. 250-fold is achieved in comparison with direct aspiration of the aqueous solution. The sampling frequency is 20 h^{-1} and the consumption of carbon tetrachloride and 5% (w/v) sodium diethyldithiocarbamate solution are each 0.6 ml min^{-1}. The 3σ detection limit is 0.4 ng ml^{-1} cadmium, and the calibration is linear up to 300 ng ml^{-1}. The relative standard deviation for 10 replicate measurements is 1.5% for 50 ng ml^{-1} cadmium. The flow interferences observed can be decreased or eliminated by the addition of citrate to the buffer solution. Results of analysis of some certified biological reference materials are given.

In trace metal determinations by inductively-coupled plasma atomic emission spectrometry (i.c.p.a.e.s.), liquid-liquid extraction is one of the most preferred techniques for sample pretreatment [1—3]. The extraction serves the dual purposes of concentration of the metals of interest and their separation from an interfering matrix. The degree of concentration depends on the ratio of aqueous and organic phase volumes or their flow rates. The matrix separation greatly decreases any background signal caused by concomitants.

In this paper, a new system is proposed, specifically designed for on-line extraction by use of the suction-flow method coupled with i.c.p.a.e.s. The teflon suction sampling cup which was used for hydride generation atomic absorption spectrometry [4—7] is applied with a continuous liquid-liquid extraction system as an alternative sample introduction procedure for the determination of cadmium in discrete samples. This suction-cup sampling system is very simple to operate and it is easy to change the sample size according to the concentration of the analyte. Also its use permits a less

0003-2670/85/$03.30

expensive device than a sample injection valve in flow injection analysis. In the discrete suction/flow extraction system, continuous feeding of the organic extract to a nebulizer was easily achieved by direct coupling with the extraction system and i.c.p. emission spectrometer. The organic extract was transported to the nebulizer without significant loss. The flow rate of each reagent should be as small as possible for practical convenience. The limiting factors of the extraction/i.c.p.a.e.s. system were investigated to obtain maximum sensitivity for cadmium, and the technique is applied to the analysis of some biological samples.

EXPERIMENTAL

Reagents

All the reagents used were of analytical-reagent grade. Pure water (Miniclear Model DC-610 system, Organo, Tokyo) was used. A solution of chelating agent (5% w/v) was freshly prepared by dissolving sodium diethyldithiocarbamate (DDTC) in water and filtering through No. 2 filter paper before use. An acetate buffer solution (2 M, pH 6.2) was prepared by mixing sodium acetate solution and acetic acid, and filtering through No. 2 filter paper. Carbon tetrachloride was used without further purification. A 1000 μg ml^{-1} stock solution was prepared by dissolving 0.500 g of cadmium metal in dilute nitric acid and diluting to 500 ml with water. Solutions of suitable concentrations were prepared by dilution.

Apparatus

Kyoto Koken Model UOP-1S (Kyoto, Japan) and Nippon Jarrell-Ash Model ICAP 575 (Kyoto, Japan) inductively-coupled plasma atomic emission spectrometers were used. The flow system comprised a 6-channel, variable-speed peristaltic pump (Nippon Jarrell-Ash, Kyoto), a PTFE suction cup [4], a phase separator (polypropylene), a PTFE extraction coil and T-joints. The other parts of the flow system were made of 1 mm i.d. PTFE tubing. The assembly is shown in Fig. 1. To obtain a high concentration ratio with the lowest possible total flow rate of reagents, the inner diameters of the pump tubing for DDTC, carbon tetrachloride and sample were 0.8 mm, 0.8 mm and 3.2 mm, respectively. The pump tubing used for carbon tetrachloride and the DDTC solution was renewed each day. The phase separator was specially designed to decrease response time with its low dead volume and to improve the reproducibility of separation with a rectangular teflon membrane (Florinate FG Filter; Millipore, Bedford, U.S.A.) using long axes for the flowing stream, as shown in Fig. 2. The separator groove for the segmented flow stream had a relatively large volume (180 μl), while the recipient groove volume was 60 μl. A needle valve for keeping slight positive pressure on the waste-port side facilitated quantitative recovery of the organic extract, which was introduced into a concentric nebulizer. Thus the organic phase was separated smoothly from the segmented flow stream of organic and aqueous solutions.

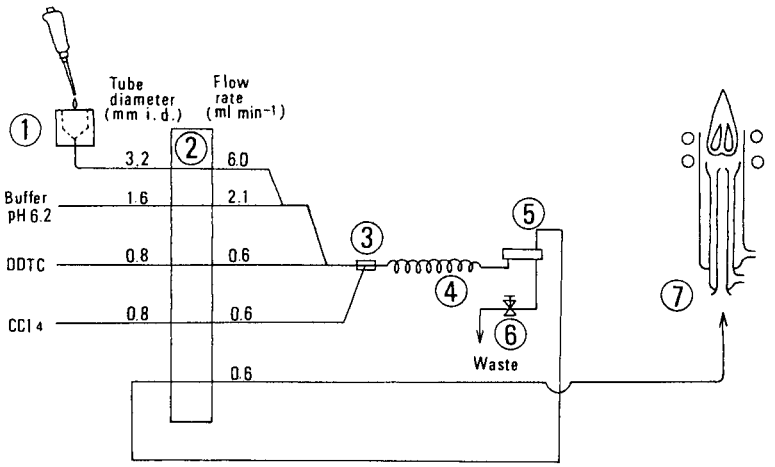

Fig. 1. Flow diagram for extraction of cadmium with DDTC into carbon tetrachloride: (1) teflon suction cup; (2) peristaltic pump; (3) segmentor; (4) extraction coil; (5) phase separator; (6) needle valve; (7) i.c.p.

Two-vessel digestion bombs [8] were used for the dissolution of samples. Each bomb consisted of a teflon PFA (perfluoroalkylvinyl ether) Tuf-Tainer vial (Pierce Chemical, Rockford, U.S.A.) of 7-ml capacity, a 23-ml PTFE vessel and a stainless steel jacket (San'ai Science, Nagoya, Japan).

Procedure for cadmium determination

A sample solution, usually 5 ml, was added to the suction cup from a Pipetman P-5000 (Gilson International). As shown in Fig. 1, the sample was sucked into the buffer line, mixed with the DDTC solution, and with carbon tetrachloride in the segmentor. The segmented solution was carried into the extraction coil and the phase separator. The organic extract was introduced by the peristaltic pump into the nebulizer of the plasma spectrometer. The transient emission signal was recorded on a strip-chart recorder, and the peak height was measured. The optimum operating conditions are shown in Table 1.

The emission peak appeared within 150 s of sample introduction. A standard cadmium solution containing cadmium alone was always added before and after each interfering test solution or a practical sample to check the change of sensitivity.

Sample digestion procedure [8]

Weigh the sample (ca. 300 mg dry weight) in a PFA vial and add 3 ml of nitric acid. Close the cap of the vial tightly and put the vial into the PTFE vessel. Add 1 ml of water, cover with the PTFE lid and insert the vessel into the stainless steel jacket. Fasten the steel cap tightly. Heat the bomb in an air oven at 90°C for 2 h, increase the temperature to 140°C and keep it for 4 h

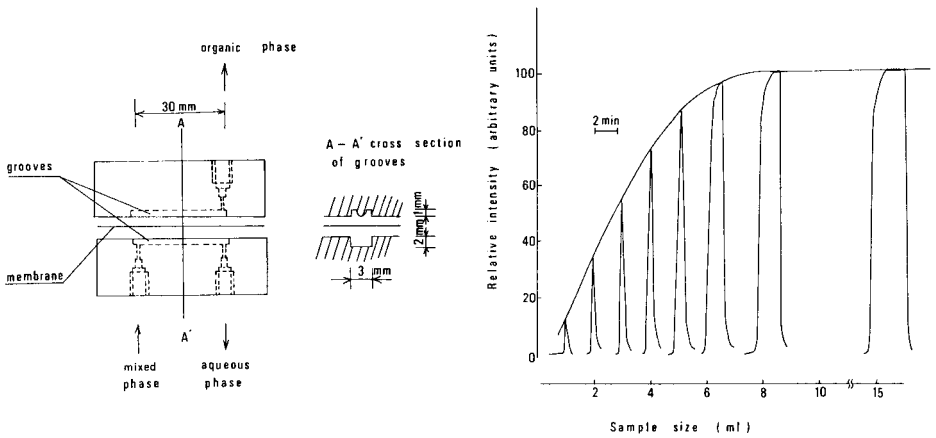

Fig. 2. Construction of a phase separator showing the top and bottom membrane holders and the teflon membrane.

Fig. 3. Recorder tracings obtained with various sample volumes (50 ng ml^{-1} cadmium; time constant 10 s).

at that temperature. After the bomb has cooled overnight, open the cap and expel the gas inside the PTFE vessel. Take out the vial and open the cap slowly. Place the vial on a hot plate and evaporate the contents to ca. 0.3 ml at 130—140°C. Add 0.5 ml of perchloric acid and heat to white fumes. Add 0.6 ml of a (1 + 5 v/v) 3 M sulphuric acid/nitric acid and evaporate to near dryness. Dilute to 6 g with water. Prepare a blank solution by the same procedure. Determine cadmium by using 2.5 ml of the digest solutions for each measurement.

TABLE 1

Recommended operating conditions

Plasma system		*Suction-flow extraction*	
R.f. power	2.0 kW	Sample size	5 ml
Outer gas (argon)	12 l min^{-1}	Pumping speed	Control 4
Intermediate gas (argon)	1.0 l min^{-1}	Sample	6 ml min^{-1}
Nebulizer gas (argon)	0.3 l min^{-1}	Buffer	2.1 ml min^{-1}
Observation height	11 mm above load coil	DDTC	0.6 ml min^{-1}
Photomultiplier voltage	800 V	Carbon tetrachloride	0.6 ml min^{-1}
Response	10 s time constant	Extraction coil	4 m long, 1 mm i.d.
Analysis line	214.438 nm (Cd II)	Phase separator	
		Groove size	2 × 30 × 1 mm (top piece)
			3 × 30 × 2 mm (bottom piece)
		Teflon membrane	10 × 40 mm, pore size 0.2 μm

RESULTS AND DISCUSSION

Optimization of conditions

The volume of sample taken in the suction cup was varied by using the volume-adjustable pipette. Figure 3 shows several typical signals obtained with different volumes (1—15 ml) of a 50 ng ml^{-1} cadmium solution at a fixed pumping speed (control 4) and a time constant for the electronic circuit of 10 s. The peak height was proportional to the volume added up to about 6 ml and thereafter was constant. A 5-ml sample plug showed ca. 80% of the plateau intensity. This volume seems to be a good compromise between high sensitivity and the practical requirements of high sampling frequency and low reagent consumption.

Variation of the time constant of the electronics circuit had no appreciable effect on the intensity provided that it was in the range 3—10 s. However, the signal became noisy at the smaller time constants. Best reproducibility was obtained at 10 s.

The effects of pumping speed and length of extraction coil were investigated. The results are shown in Fig. 4. Flow rate controls 3 and 4 gave the highest signals for extraction coils of all lengths tested. The sensitivity was almost proportional to the length of the extraction coil up to 2 m, as the extraction efficiency increased. Coils more than 3 m long gave maximum constant intensity. To ensure extraction equilibrium, a 4-m long extraction coil and a flow rate control of 4 were used subsequently.

The effect of the membrane pore size in the phase separator was examined in the range 0.2—10 μm. When the pore size was less than 1 μm, the organic

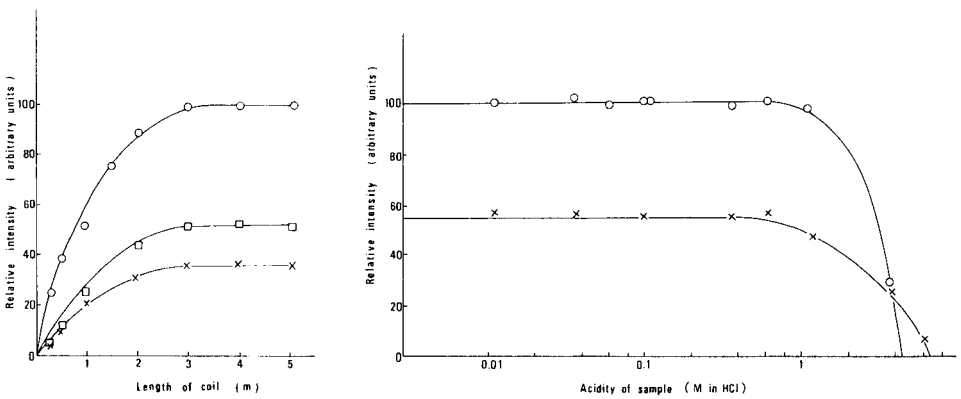

Fig. 4. Effect of pumping speed and length of extraction coil on the emission intensity of cadmium. Pumping speeds: (○) as in Table 1; (□) Control 8, sample 16 ml min^{-1}, buffer 5.5 ml min^{-1}, DDTC 1.8 ml min^{-1}, carbon tetrachloride 1.8 ml min^{-1}; (×) Control 10, sample 21.5 ml min^{-1}, buffer 13.4 ml min^{-1}, DDTC 2.2 ml min^{-1}, carbon tetrachloride 2.2 ml min^{-1}.

Fig. 5. Effect of sample acidity and buffer flow rate on the emission signal from a 50 ng ml^{-1} cadmium solution: (○) 2.1 ml min^{-1}, 1.6 mm i.d. tubing; (×) 9.4 ml min^{-1}, 4.0 mm i.d. tubing.

extract was completely separated and gave constant intensity. The efficiency of the phase separation also depended on the structure of separator. The recommended device, made in the laboratory, is shown in Fig. 2.

The DDTC/cadmium complex was confirmed to be quantitatively extracted into carbon tetrachloride in the pH range 5—13; a 2 M pH 6.2 acetate buffer solution was used throughout.

Effects of sample acidity and flow rate of the buffer were investigated. As Fig. 5 shows, the sample acidity should be less than ca. 0.6 M; 1.6-mm i.d. tubing with flow rate 2.1 ml min^{-1} for the buffer solution gave higher intensity than 4.0-mm i.d. tubing with 9.4 ml min^{-1}. The decrease in sensitivity with the wider tube might be due to decreased extraction efficiency caused by shorter residence time in the reaction coil.

The concentration of DDTC was not found to be critical above 0.05%, and signals were essentially constant above 1%. However, 5% (w/v) DDTC tended to give less signal fluctuation, and therefore was used in the recommended procedure.

Sensitivity and precision

Under the operating conditions summarized in Table 1, a linear calibration graph was obtained for up to 300 ng ml^{-1} cadmium. The 3σ detection limit [9] was 0.4 ng ml^{-1}. The sensitivity and detection limit were much improved, being ca. 250- and 80-times higher, respectively, than those obtained by direct aspiration of an aqueous solution. These improvements are attributed not only to the preconcentration of cadmium by extraction, but also to the enhancement effect of carbon tetrachloride [10]. The relative standard deviation for 10 replicate measurements was 1.5% for 50 ng ml^{-1} cadmium and the sample throughput was 20 h^{-1}.

Interferences

The interferences of large amounts of alkali and alkaline earth metals and most anions can be avoided by the extraction. As listed in Table 2, most cations and anions did not interfere when present in 1000-fold amounts with

TABLE 2

Maximum permissible amounts of foreign ions for cadmium determination (results within 10% error)[a]

Ion	Max. permissible wt. ratio (Ion/Cd)	
Mn^{2+}	150	700[b]
Co^{2+}	110	270[b]
Ni^{2+}	150	$\geqslant$1000[b]

[a]The following species were tolerated at a 1000:1 ratio: Na^+, K^+, NH_4^+, Mg^{2+}, Ca^{2+}, Cr^{3+}, Cr(VI), Fe^{3+}, Cu^{2+}, Zn^{2+}, Ag^+, Pt(IV), Hg^{2+}, Al^{3+}, Pb^{2+}, Sb(III), NO_3^-, SiO_3^{2-}, SO_4^{2-}, Cl^- (50 ng ml^{-1} cadmium, 5 ml of sample). [b]10% citrate added to 2 M acetate buffer.

TABLE 3

Determination of cadmium in certified biological reference materials

Sample	Cadmium found[a] ($\mu g\ g^{-1}$)	Certified value ($\mu g\ g^{-1}$)
Orchard leaves (N.B.S. SRM 1571)	0.13 ± 0.01	0.11
Pepperbush (N.I.E.S. CRM No. 1)	6.2 ± 0.1	6.7 ± 0.5
Mussel (N.I.E.S. CRM No. 6)	0.79 ± 0.02	0.82 ± 0.03

[a]Mean ± av. dev., 2 results.

respect to cadmium. Significant interferences were encountered only from manganese(II), cobalt(II) and nickel; the maximum permissible amounts of these species were 150-, 110- and 150-fold, respectively. The interferences from these ions, especially nickel and manganese could be greatly decreased by the use of an acetate/ammonium citrate buffer, because of the masking action of citrate.

Application to the determination of cadmium in biological samples

The accuracy of the present method was established by analyzing certified reference materials. In particular, three types of biological samples were analyzed, Orchard Leaves (N.B.S., U.S. Department of Commerce) and Pepperbush and Mussel (National Institute for Environmental Studies, Environmental Agency of Japan).

The results obtained after decomposition of the samples as described above are shown in Table 3. The data are in good agreement with the certified values.

REFERENCES

1 J. M. Motooka, E. L. Mosier, S. J. Sutley and J. G. Viets, Appl. Spectrosc., 33 (1979) 456.
2 A. Miyazaki, A. Kimura, K. Bansho and Y. Umezaki, Anal. Chim. Acta, 144 (1982) 213.
3 R. V. Whiteley Jr. and R. M. Merrill, Fresenius Z. Anal. Chem., 311 (1982) 7.
4 M. Ikeda, F. Nakata, H. Matsuo and T. Kumamaru, Bunseki Kagaku, 33 (1984) 416.
5 T. Kumamaru, F. Nakata, S. Hara, H. Matsuo and M. Kiboku, Bunseki Kagaku, 33 (1984) 624.
6 M. Ikeda, Anal. Chim. Acta, 167 (1985) 289.
7 M. Ikeda, Anal. Chim. Acta, 170 (1985) 217.
8 K. Okamoto and K. Fuwa, Anal. Chem., 56 (1984) 1758.
9 IUPAC, Anal. Chem., 48 (1976) 2294.
10 T. Kumamaru, H. Matsuo and Y. Yamamoto, The 1984 International Chemical Congress of Pacific Basin Societies, Honolulu, December 1984, Abst. No. 01I05.

Analytica Chimica Acta, 174 (1985) 191—201
Elsevier Science Publishers B.V., Amsterdam — Printed in The Netherlands

EFFECT OF DROPLET SIZE ON THE PHOSPHINE DEPRESSION OF CALCIUM ATOMIC EMISSION SIGNALS IN FLAME SPECTROMETRY

GARY L. LONG[a] and CHARLES B. BOSS*

Department of Chemistry, North Carolina State University, Raleigh, NC 27650 (U.S.A.)

(Received 29th November 1984)

SUMMARY

The effect of the droplet size on the magnitude of the phosphine depression of calcium signals is discussed. The droplet size governs the time required for droplet desolvation in the flame. It is during the desolvation process that the combustion products of phosphine, PO_x, diffuse into the droplet and form a refractory compound with the analyte. The longer the desolvating droplet resides in the PO_x-contaminated flame, the more severe the depression. A uniform droplet generator, a pneumatic nebulizer spray chamber system, and a glass-frit nebulizer spray chamber system were the sample introduction systems studied. Droplet sizes of (55 μm, 0.5—10 μm (2 μm mean), and <0.1—2 μm (0.1 μm mean) were produced by these systems, respectively, and depressions of the calcium signals of 57%, 55%, and 4% were noted. These results suggest that the phosphine depression on calcium signals may be alleviated by using a glass-frit nebulizer (or modifying a commercial nebulizer) to remove droplets greater than 2 μm in diameter.

Phosphine, PH_3, is a normal contaminant in acetylene. The presence of phosphine in the contamination range of 20—500 $\mu l\ l^{-1}$ of acetylene has been shown to depress the atomic emission signals of alkaline earth metals in air/acetylene flames [1, 2]. In addition to understanding the mechanism of depression, the characterization of this depression is of importance because phosphine contamination levels may abruptly change in an acetylene tank while the tank is being used, thus affecting the accuracy of measurement.

In their diagnostic work, Long and Boss [1, 2] found the depression to result from a condensed-phase vaporization interference, whereby the combustion products of phosphine, PO_x, diffuse into the desolvating droplet to form a refractory Ca—PO_x compound [1, 2]. This depression has been observed to be similar in nature to the well-known Ca^{2+}/phosphate depression [3] in that depressing effects of phosphate and phosphine on calcium signals have been shown to be additive. This behavior is thought to indicate that a similar calcium/phosphorus oxide compound is formed [1]. Also, phosphate-releasing agents, such as lanthanum ions, reduce the magnitude of the Ca^{2+}/phosphine depression [1]. However, it is important to state clearly

[a]Present address: Department of Chemistry, Virginia Polytechnic Institute and State University, Blacksburg, Virginia 24061, U.S.A.

the believed difference between these depressions; the Ca^{2+}/phosphate depression is the result of a condensed-phase reaction occurring in the analyte matrix, while the Ca^{2+}/phosphine depression is the result of a reaction occurring in the flame between the condensed-phase analyte and vapor-phase PO_x species.

Because this reaction is thought to be diffusion-controlled, a well-characterized flame and a stable method of uniform droplet introduction, such as the droplet generator [2], were used in a diagnostic study of this depression. With such a system, the data obtained from observation of measured sized droplets in phosphine-free and phosphine-contaminated flame allowed the effect of droplet size on the depression to be noted and a theoretical model of the depression to be developed. These observations showed that the magnitude of the phosphine depression on calcium signals is dependent on the size of the droplet. The droplet size governs the time required for the droplet to undergo desolvation in the flame, larger droplets requiring longer desolvation times. These longer desolvation times permit a greater mass of PO_x to diffuse into each droplet and remove the analyte in the formation of a refractory compound. With the use of these measured, sized droplets, one can equate the loss in analyte signals to the mass of analyte consumed in this reaction. This loss has been confirmed by the mathematical model, based on Fick's laws of diffusion [4], which relates the mass consumed to the three-halves power of desolvation time of the droplet. The calculated masses from the equations were found to be in good agreement with the experimentally observed masses.

Although the depression has been well-characterized for the droplet generator system, this system is not capable of producing droplets less than 40 μm in diameter and injecting them into the flame. This inability hampers the study of droplet size effect on the Ca^{2+}/phosphine depression because the droplets produced by the droplet generator are an order of magnitude larger than those produced by commercial pneumatic nebulizers. Therefore, in order to observe the effect of smaller sized droplets on the depression, other, well-characterized, sample introduction systems must be used.

In this paper, the effect of droplet size on the Ca^{2+}/phosphine depression is studied through the use of three different sample introduction techniques. Each of these systems produces droplets with a different mean droplet diameter. By comparing the differences in the magnitude of the depression for each system, a better understanding of droplet size effects on calcium determinations in phosphine-contaminated flames can be obtained. The depression is then explored with a pneumatic nebulizer. This system, which has been previously characterized for phosphine work [1], produces droplets ranging from as small as 0.5 μm to as large as 10 μm, with a mean droplet diameter of 2 μm [5, 6]. The third system to be compared is a glass-frit nebulizer. The design of this nebulizer has been described by Layman and Lichte [7], and is capable of producing very small droplets having a range of droplet sizes from 0.1 μm (94% of the mass) to 5 μm, with a mean diameter

of 0.1 μm. This particular system allows the effect of very small droplets on the Ca^{2+}/phosphine depression to be observed.

The equations developed are used to predict the depressing effect of phosphine on calcium signals from the droplet generator. However, predictions for the pneumatic nebulizer and the glass-frit nebulizer cannot be made accurately because the mathematical model is based on uniform sized droplets that are sufficiently separated in the flame so that a droplet does not shield another droplet from the diffusing PO_x species. This model is also based on the assumption that the droplets are not exposed to phosphine before they enter the flame. Both assumptions are invalid for a conventional burner-nebulizer. Nevertheless, a comparison of the magnitude of the depression from each system will allow a more complete understanding of the role of droplet size in the Ca^{2+}/phosphine depression.

EXPERIMENTAL

Reagents

All chemicals used were analytical-reagent grade and water was deionized. The Ca^{2+} stock solution was 0.260 M (10,000 mg l^{-1} Ca^{2+}) prepared from calcium carbonate in 3 M hydrochloric acid. Solutions were diluted to obtain the desired concentrations.

Purified-grade acetylene (Airco, Grade 2.6) and commercial-grade acetylene (Air Products) were used. The phosphine concentrations of these fuels were found to be 19 μl l^{-1} of fuel for the purified-grade and 260 μl l^{-1} for the commercial-grade acetylene. The procedure for this determination has been described [8]. The compressed air and the phosphine/helium standard mixture (5210 μl l^{-1}) were obtained from Air Products.

Instrumentation

In all measurements, a stoichiometric air/acetylene flame was used. The air and acetylene flow rates were adjusted to 6.7 and 1.8 l min^{-1}, respectively, so that data obtained from these systems can be meaningfully compared. A two-stage liquid scrubber was used to reduce the phosphine concentration of the purified-grade acetylene to below 0.1 μl l^{-1}.

The instrumental setup for the droplet generator consisted of the generator hardware, a round capillary burner, a monochromator, and the detection electronics, all of which have been previously described [2]. An Instrumentation Laboratory atomic spectrometer (Model 351) was fitted with a Model J nebulizer and a short-path nitrous oxide/acetylene burner head [1]. The burner was rotated 90° from the absorption position so that the emission could be best observed.

The glass-frit nebulizer was constructed following the design of Layman and Lichte [7] from a 20-mm fine-grade porous glass frit (Corning 32592-045). The analyte solution was delivered to the frit from a syringe pump (Sage Instruments Model 351) fitted with a 5-ml glass syringe. A stainless

steel needle (18 gauge) was attached to the syringe and inserted into a 30-cm length of 1-mm i.d. hard plastic tubing. The remaining end of the tubing was clipped at a 45° angle and glued into the lower glass arm of the frit. This angle was necessary to assure an even distribution of the analyte solution onto the surface of the frit. A delivery rate of 35 μl min^{-1} was used. The back-pressure above the frit was maintained at 15 psi with compressed air. The wash solution was introduced into the upper chamber of the frit through plastic tubing inserted into the upper glass arm, after which a hand-operated screw drive was attached to a 20-ml plastic syringe. Approximately 2 ml of the wash solution (0.1 M hydrochloric acid) were needed to wash the frit of analyte solution. The aerosol was introduced into the drain port of a locally-constructed spray chamber by using a 15-cm piece of 8-mm i.d. Tygon tubing. The round capillary burner was used to provide a stiff laminar flame for the emission studies [9].

To produce the desired level of phosphine contamination, the 0.0521% phosphine/helium standard mixture was metered into the fuel flow. By measuring the flow rates, one can then calculate the contamination level. This apparatus was fully described in earlier [8], and the same method was used for the droplet generator and the glass-frit nebulizer. However, contamination levels for the IL-351 were produced in a different manner. Rather than disturbing the fuel line plumbing in this instrument, a welding-grade acetylene was used to provide phosphine contamination. The particular cylinder of acetylene used was found by flame photometry [8] to have a phosphine level of 260 μl l^{-1}.

Data collection and display

Flame profiles of calcium emission (at 422.7 nm) were collected under the control of an Ohio Scientific 2C-4P microcomputer. The specific interfaces and programs used to collect the data and store the profiles on disk have been documented [10]. Among the interfaces used were an analog-to-digital converter, a stepper motor controller, a parallel *I/O* port for BCD transfer, and a digital-to-analog converter. With these interfaces and their respective programs, 100—250 data points could be collected in a flame profile. By obtaining digital profiles of the blank and analyte, with and without phosphine, the effect of phosphine on the calcium signal as a function of height can be studied.

The data obtained from flame emission profiles were plotted as background-corrected relative emission intensities. Plots were constructed with a Houston Instruments X-Y recorder. Data presented within each figure were obtained under nearly identical experimental conditions. Because the detection systems used were not calibrated to alleviate long-term drift in sensitivity, no attempt was made to present a consistent intensity scale from one figure to the next. On each figure, the intensity scale has been adjusted to illustrate the relative magnitudes and shapes of the signals.

RESULTS AND DISCUSSION

The magnitude of the Ca^{2+}/phosphine depression is dependent on the time required for a droplet to desolvate in a phosphine-contaminated flame. During desolvation, a droplet acquires PO_x, which rapidly reacts with analyte to form a refractory compound. The inability of the flame to break down this compound into free atoms results in a diminished analyte signal.

The effect of droplet size on calcium signals in various phosphine-contaminated flames may best be illustrated by constructing flame emission profiles of the analyte signals. By scanning the signal intensity over the same range of flame observation heights for these systems, the effect of the different mean droplet diameters on the depression can be observed. With these data, the magnitude of the depressions can then be compared to the relative desolvation times of these droplets. For systems that produce non-uniform sized droplets, the effect of the droplet size distribution on the depression can also be observed by noting the differences in the shapes of the flame profiles obtained in phosphine-free and phosphine-contaminated flames.

Droplet generator

The effect of large droplets on the phosphine depression of calcium signals can be seen in Fig. 1. These data were obtained by injecting 55-μm droplets

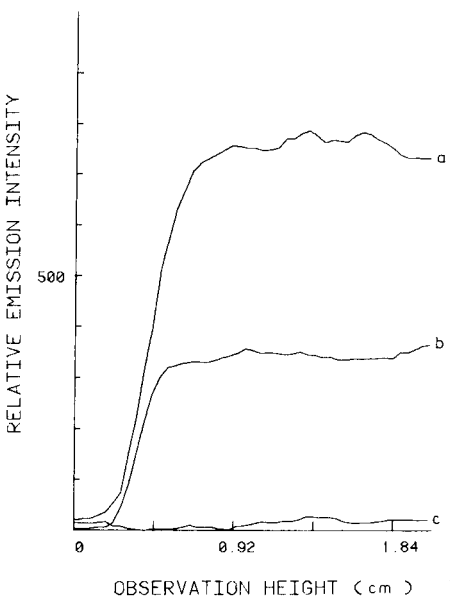

Fig. 1. Flame profiles of calcium emission from a 0.62 mM Ca^{2+} solution in various flames using 55-μm droplets produced by the droplet generator: (a) PH_3-free acetylene; (b) PH_3 present at 126 $\mu l\ l^{-1}$; (c) PH_3 present at 285 $\mu l\ l^{-1}$.

of a 0.62 mM calcium solution at a rate of 1900 drops per second into various phosphine-contaminated flames. Curve *a* is the flame emission profile obtained with a phosphine free fuel, i.e., the purified-grade acetylene scrubbed to reduce the phosphine concentration to less than 0.1 μl l^{-1}. When the calcium solution was introduced into flames containing increasing amounts of phosphine, a significant reduction, or even elimination, of the emission intensity occurred (curves *b* and *c*, Fig. 1). Clearly, under the conditions of curve *c*, most of the analyte is removed as a refractory compound. From the lack of signal intensity at the higher observation heights, the refractory compound does not vaporize and dissociate into vapor-phase atoms.

The effect of these levels of phosphine contamination on the calcium signals from 55-μm droplets can also be calculated by using equations developed for the droplet generator [11]. In the equation

$$D_o^2 - D_f^2 = kt \tag{1}$$

D_o is the original droplet diameter, D_f is the final dry particle diameter, and k is the desolvation rate [11]. For calcium particles D_f was found to be <0.3 μm for 80-μm droplets containing 100 μg ml^{-1} calcium [12]. Because $D_o^2 \gg D_f^2$, an accurate value of D_f need not be known and is assumed to be zero in these calculations. The desolvation rate was experimentally evaluated as 3.8×10^5 μm^2 s^{-1} for aqueous solutions in a stoichiometric air/acetylene flame [13]. From Eqn. 1, the desolvation time for a 55-μm droplet in an air/acetylene flame is calculated to be 8.0×10^{-3} s. The moles of analyte removed in the formation of a refractory compound for this desolvation time can be calculated from the equation [2]

$$M = 2\pi k D C_b R^{-1} t^{3/2} [k^{-1/2} + (\pi D)^{-1/2}] \tag{2}$$

in which M represents the moles of calcium, k is the desolvation rate, D is the diffusion coefficient of the PO_x species (measured to be 0.80 cm^2 s^{-1}), C_b is the bulk concentration of the PO_x species in the flame (1×10^{-10} mol cm^{-1} PO_x for 285 μl of phosphine per l of fuel, and 5×10^{-11} mol cm^{-1} PO_x for 126 μl of phosphine per l of fuel), R is the stoichiometric ratio of the reaction between the P and Ca species (0.3 from the Ca^{2+}/phosphate depression), and t is the desolvation time calculated from Eqn. 1. For a 55-μm droplet in a flame containing phosphine at 285 μl l^{-1} of fuel, approximately 3.2 pg of calcium should be used in the formation of a refractory compound. The 55-μm droplets from the 0.62 mM Ca^{2+} solution only contain 2.2 pg of calcium. Hence, all the calcium should be bound as a refractory compound. This calculated result agrees with the observed data (curve *c*, Fig. 1); there was no significant analyte emission at any observation height. For phosphine at 126 μl l^{-1}, approximately 1.4 pg of calcium should be needed, leaving 0.8 pg of calcium unbound. Hence, 64% of the analyte should be bound as a refractory compound. The data in curve *b* indicate that 57% of the calcium atoms react with PO_x to form a refractory compound for this level of phosphine contamination. The agreement between these percentages

indicates that these equations may be used to model the depressing effects of phosphine on calcium signals as long as a stable system is used to introduce the droplets into the flame.

These observed data and calculations also indicate that the phosphine depression of calcium signals for large droplets at these levels of phosphine is quite severe. For droplets requiring such large desolvation times, enough PO_x may diffuse into the droplet so as to result in all the analyte being bound. To reduce these depressing effects, smaller droplet sizes should be used.

Pneumatic nebulizer

The pneumatic nebulizer is the most commonly used sample introduction system in flame atomic spectrometry. It produces a wide range of droplet sizes. In this study, an Instrumentation Laboratory Model J nebulizer was used. This nebulizer produces droplets ranging from 0.5 μm to >10 μm, with a mean droplet diameter of 2 μm [5]. Approximately 51% of these droplets are >10 μm. However, the cutoff diameter, d_c, for this spray chamber is 4.4 μm [6]. Although the nebulizer produces small droplets, the inability of the nebulizer to produce uniform droplets complicates the study of the Ca^{2+}/phosphine depression.

The effect of phosphine contamination on calcium signals with this nebulizer is illustrated in Fig. 2A. Changing the phosphine-free fuel to commercial-grade acetylene with a phosphine level of 260 μl l^{-1} results in only a 55% depression of the analyte signal. Because a smaller mean size droplet is produced by this nebulizer, a shorter desolvation time is required for the droplets. For the average 2-μm droplet, approximately 1.1×10^{-5} s is needed for desolvation to be complete. In this shorter time period, a lesser amount of PO_x should diffuse into the desolvating droplet, leading to a smaller percentage of the analyte being removed as a refractory compound. If Eqn. 2 is invoked for this 2-μm droplet in the fuel containing 260 μl l^{-1} phosphine ($C_b = 9.6 \times 10^{-11}$ mol cm^{-3}), approximately 1.5×10^{-16} g of calcium should be consumed. However, each 2-μm droplet contains only 1.0×10^{-16} g of calcium. This discrepancy points out a possible problem with the mathematical model. If C_b is not constant throughout the flame, the model will fail to predict the magnitude of the depression. The model requires C_b to be known and constant during droplet desolvation. In reality, C_b may vary in the flame depending on the degree of combustion of the flammable phosphine. Therefore, if the droplet partially desolvates before phosphine combustion is complete, the observed depression will be less than that predicted by the diffusion-based model.

This effect of incomplete phosphine combustion may be partially supported by the difference in the slopes of curves a and b in Fig. 2A. The reduction in the slope was earlier reported to be caused by a decrease in the free atom supply rate [1]. More probably, the decrease is the result of the different desolvation times required for the various sizes of droplets which are produced by this nebulizer and the possible difference in the PO_x bulk

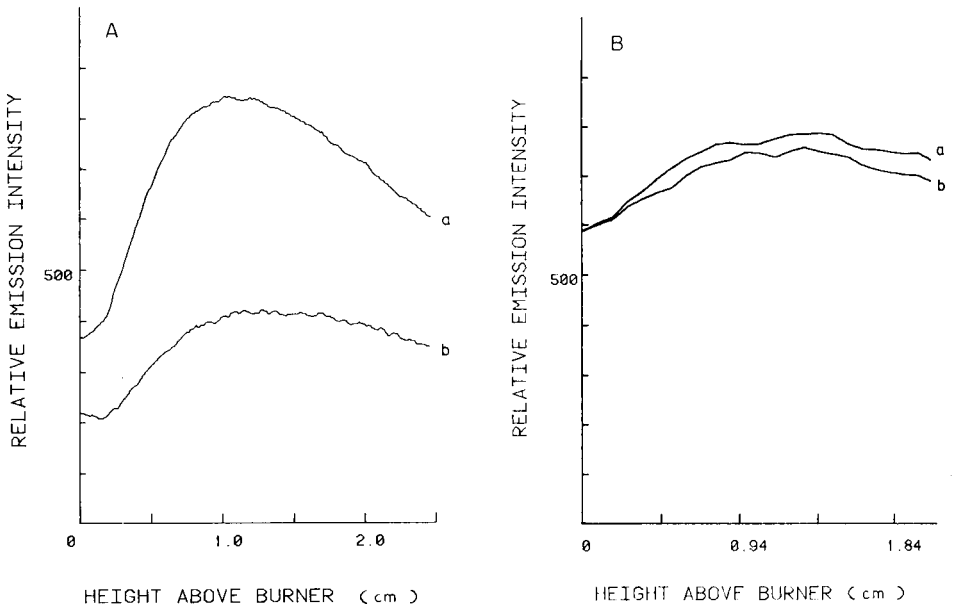

Fig. 2. Flame profiles of calcium emission from a 0.62 mM Ca^{2+} solution: (A) from droplets produced by the pneumatic nebulizer (mean droplet diameter 2 μm); (B) from droplets produced by the pneumatic nebulizer (mean droplet diameter 0.1 μm). Profiles: (a) phosphine-free acetylene; (b) phosphine present at 260 $\mu l\ l^{-1}$ of acetylene for A and at 285 $\mu l\ l^{-1}$ for B.

concentration, C_b, in the flame. The smaller droplets have a considerably shorter desolvation time than the larger droplets. This difference in size would then affect the amount of PO_x that would diffuse into the droplet by limiting the desolvation time and causing the droplet to be completely desolvated before a stable PO_x bulk concentration has been established. It is possible that a stable PO_x bulk concentration is only established much higher in the flame, possibly at 2 cm and higher. It is for this reason that the model may fit the droplet generator data accurately only when the analyte signal is observed from 5 to 10 cm when the droplet has been injected into the flame near the top of the burner.

Therefore, in comparing the effect of desolvation times of the droplets on the depression, two factors must be taken into account: shorter desolvation times permit less PO_x to diffuse into the droplet, and extremely short desolvation times may result in the droplet being sufficiently desolvated before a stable PO_x bulk concentration is established in the flame. In Fig. 2A, the depression of the signal from the smaller droplets can be seen at low observation heights near the surface of the burner above the primary reaction zone. At the 0.00-cm observation height, a significant analyte signal is shown (curve *a*). Such an emission can occur only from the smaller droplets, which

rapidly desolvate and vaporize in the flame. When the fuel containing 260 μl l^{-1} phosphine is used, a 40% depression of the emission signal occurs at this observation height (curve *b*). The signal depression becomes greater in magnitude with increasing observation height. At the 1.00-cm position, a 55% depression of the signal is observed for the phosphine-contaminated fuel. Although the signal at this height is the summation of signals from the various stages of vaporization, the greater portion of this signal is caused by the analyte which is contained in the larger droplets. Thus, small differences in the diameter of the droplets produced by a pneumatic nebulizer can significantly affect the depression of calcium signals in phosphine-contaminated flames.

Glass-frit nebulizer

The effect of very small droplets on the Ca^{2+}/phosphine depression was studied with a glass-frit nebulizer. This nebulizer is capable of producing droplets from <0.1 μm to 2 μm diameter, with the distribution being heavily skewed (94% of the mass) toward the smaller droplets, and the mean droplet diameter being 0.1 μm. Although a desolvation time of 2.6×10^{-8} s could be calculated from Eqn. 1, this heat-transfer desolvation equation cannot be rigorously applied to such small spheres [13]. The desolvation time, if any, for these droplets will be extremely short. The short desolvation time would then serve to limit severely the obtainable PO_x concentration in the desolvating droplet.

The flame emission profile from a standard calcium solution with this nebulizer and a phosphine-free fuel is shown in Fig. 2B (curve *a*). The initial slope of the curve is significantly less than the slopes of the profiles obtained with the other sample introduction systems, because of the extremely short desolvation time required for the 0.1 μm droplets. These droplets desolvate almost instantaneously and vaporize on being introduced into the flame. This large signal is observed just above the primary reaction zone at zero height above the burner top. At greater heights, the analyte signal increases, partly because of the analyte contained in the larger droplets which make up 4% of the total mass of the droplets produced by the nebulizer and which require a longer desolvation time in the flame. Also, the rise in the emission signal is caused, in part, by a small increase in the temperature of the flame in the first centimeter above the burner.

The effect of phosphine on calcium signals from these droplets is shown in curve *b*, Fig. 2B. Unlike the previous sample introduction systems, the phosphine contamination only causes a 4% depression in the analyte signal at 1.00 cm above the burner. For 0.1-μm droplets, Eqn. 2 would predict that 1.9×10^{-20} g of calcium is consumed from an available 1.3×10^{-20} g. The depression, however, is observed to decrease with lower observation heights. Just above the primary reaction zone at the 0.00-cm position, there is no depression of the analyte signal. The signal at this position is exclusively caused by the analyte contained in the small droplets. This observation

TABLE 1

Effect of droplet size on the phosphine depression of calcium signals[a]

Mean droplet diameter (μm)	Residence time (s)	PH_3 level ($\mu l\, l^{-1}$)	Depression (%)
55	8.0×10^{-3}	285	100
55	8.0×10^{-3}	126	57
2	1.1×10^{-5}	260	55
0.1	2.6×10^{-8}	285	4

[a]Calcium concentration is 0.62 mM. All observations are made at the 1.00-cm position.

would support the hypothesis that desolvation of the droplet was complete before an appreciable PO_x bulk concentration could be established in the flame, thus preventing PO_x from diffusing into the droplet. Only with the larger droplets, which require a longer desolvation time, is the PO_x bulk concentration great enough that the PO_x species can diffuse into the droplet and consume a significant portion of the analyte in the formation of a refractory compound. However, these droplets make up a small fraction of the droplets produced from the glass-frit nebulizer. Because of this skewed distribution toward smaller droplet sizes, the total depressing effect of phosphine on calcium signals is minimal with this nebulizer.

Conclusion

Through the comparison of the three sample introduction systems, the effect of droplet size of <0.1—5 μm, 0.5—10 μm, and 55 μm in diameter on the phosphine depression of calcium signals is studied. The results of these experiments are summarized in Table 1. The mean droplet sizes, desolvation times for these droplets, and the percent depressions are also listed.

Although none of these systems eliminates the depressing effect of phosphine, the small droplets from the glass-frit nebulizer produce the lowest depression (4%). This small depression is attributed to the small percentage of the total mass of analyte that is contained in the larger droplets (2—5 μm). These results suggest that by using a glass-frit nebulizer or modifying commercial nebulizers with flow spoilers [6] to eliminate droplets over 2 μm in diameter, the sensitivity for calcium, and probably strontium and barium in phosphine-contaminated flames can be greatly improved.

REFERENCES

1 G. L. Long and C. B. Boss, Anal. Chem., 54 (1982) 624.
2 G. L. Long and C. B. Boss, Anal. Chem., 54 (1982) 2496.
3 C. Th. J. Alkemade and M. H. Voorhuis, Fresenius Z. Anal. Chem., 163 (1958) 91.
4 H. S. Carslaw and J. C. Jaeger, Conduction of Heat of Solids, Clarendon Press, Oxford, England, 2nd edn, 1959.
5 M. S. Cresser and R. F. Browner, Appl. Spectrosc., 34 (1980) 364.

6 D. D. Smith and R. F. Browner, Anal. Chem., 56 (1984) 2702.
7 L. R. Layman and F. E. Lichte, Anal. Chem., 54 (1982) 638.
8 G. L. Long and C. B. Boss, Anal. Chem., 53 (1981) 2363.
9 K. M. Aldous, R. F. Browner, R. M. Dagnall and T. S. West, Anal. Chem., 42 (1970) 939.
10 G. L. Long, Ph.D. Dissertation, North Carolina State University, Raleigh, NC, 1982.
11 N. C. Clampitt and G. M. Hieftje, Anal. Chem., 44 (1972) 1211.
12 C. B. Boss, Ph.D. Dissertation, Indiana University, Bloomington, IN, 1977.
13 N. C. Clampitt, Ph.D. Dissertation, Indiana University, Bloomington, IN, 1974.

Analytica Chimica Acta, 174 (1985) 203—210
Elsevier Science Publishers B.V., Amsterdam — Printed in The Netherlands

SCREENING FOR SELECTED TOXIC ELEMENTS IN URINE BY SEQUENTIAL-SCANNING INDUCTIVELY-COUPLED PLASMA ATOMIC EMISSION SPECTROMETRY

MARY M. KIMBERLY* and DANIEL C. PASCHAL

Clinical Chemistry Division, Center for Environmental Health, Centers for Disease Control, Public Health Service, U.S. Department of Health and Human Services, Atlanta, Georgia 30333 (U.S.A.)

(Received 11th April 1985)

SUMMARY

A rapid screening method for nine elements (Se, As, Cr, Zn, Cd, Pb, Ni, Mn, and Cu) in human urine is described. A sequential-scanning inductively-coupled plasma atomic emission spectrometer, incorporating a cross-flow nebulizer, was used. Internal standardization with yttrium compensated for the differences between the aqueous calibration standards and the undiluted urine specimens. Accuracy was evaluated with aqueous (NBS SRM 1643a, EPA 378-13, and EPA 476-3) and urine (NBS SRM 2670 and Fisher Urichem Level II) reference and control materials. Detection limits for the system were evaluated from analyses of normal urine materials found to contain low levels of the elements investigated.

Determining toxic levels of priority inorganic pollutants in urine is an important part of any emergency screening scheme. Investigators have reported the results of several studies in which they sought to determine normal levels of trace metals in human urine by inductively-coupled plasma atomic emission spectroscopy (i.c.p./a.e.s). Haas et al. [1] investigated the use of simultaneous i.c.p./a.e.s. methods incorporating an ultrasonic nebulizer for multi-element determinations in urine. They found that detection limits for many of the elements investigated prohibited quantification of trace levels. Barnes and Genna [2] used preconcentration on chelating resins to overcome this problem. Their method, however, is time-consuming and requires large volumes of samples.

In the case of exposure to one or several toxic elements, the levels of metal excreted in the urine are often higher than the detection limits in this matrix. Table 1 lists the normal and toxic levels of several elements in urine [3, 4]. On the basis of detection limits observed by Haas et al. [1], it should be possible to develop a screening method for urine that would detect exposure to toxic levels of these metals.

The i.c.p. technique is suitable for toxic element screening. It is rapid compared to other atomic spectrometric methods such as graphite-furnace atomic absorption spectrometry. When a cross-flow nebulizer is used, the

0003-2670/85/$03.30

TABLE 1

Normal and toxic levels of some elements in urine[a]

Element	Normal (ng ml^{-1})	Toxic (ng ml^{-1})	Element	Normal (ng ml^{-1})	Toxic (ng ml^{-1})
Se	34	100	Pb	40	150
As	80	174	Ni	4.5	100
Cr	4—5	40—50	Mn	<1—10	<10—260
Zn	500	700	Cu	20	79
Cd	0.1—0.2	5			

[a]Compiled from Friberg et al. [3] and Baselt [4].

relatively high dissolved solids in urine (approximately 1% NaCl) can be accommodated [5]. Thus, lengthy sample preparation, including dilution, extraction, or preconcentration, is eliminated. Less than 25 ml of urine is required to screen for nine elements (Se, As, Cr, Zn, Cd, Pb, Ni, Mn, and Cu); all but manganese are listed as Environmental Protection Agency (EPA) High Priority Pollutants [6, 7]. Sequential-scanning i.c.p. systems provide the additional advantage of flexibility in the selection of wavelengths that are both sensitive and interference-free.

Aqueous solutions and urine specimens are nebulized and introduced into the plasma with significantly different efficiencies. This is a consequence of the varying dissolved solids content of these two types of matrices [8, 9]. When the specimens are analyzed by using a calibration curve established with aqueous standards, inaccurate results are obtained because the emission intensities observed for the atomic or ionic transitions do not correctly reflect the analyte concentrations. Matrix-matching is one technique that can be used to compensate for this discrepancy. Urine specimens are, however, highly variable in their matrix compositions. The use of an average or "normal" type of matrix for calibration standards would not adequately improve accuracy for all specimens.

The theory and practice of internal standardization with the type of instrumentation used in this work have been described [8, 10]. Briefly, internal standardization compensates for differences in nebulization and solution transport by an intensity-ratio procedure. Use of an internal standard eliminates the need to match exactly the matrix composition of the calibration standards to that of the samples.

The rapid urinary screening procedure reported here includes cross-flow nebulization, yttrium internal standardization, and sequential-scanning i.c.p./a.e.s. Five elements can be quantified per minute and toxic levels of the nine elements investigated can be detected.

EXPERIMENTAL

Instrumentation

A Perkin-Elmer ICP-6000 system was used in this study. The operating conditions for the spectrophotometer and torch are recorded in Table 2. The system is controlled by a Model 7500 laboratory computer which aided in developing the method and in acquiring and storing the data.

The wavelengths were chosen from published wavelength tables [11]. The most sensitive emission lines were the first investigated. A less sensitive line was necessary only for arsenic; the As 193.696-nm line has a major carbon interference from the matrix at 193.091 nm. After wavelengths had been selected, background correction points were chosen by consideration of the standards, blank, and urine matrices. This was done with the graphics capability of the 7500 computer. In this mode, the spectra of the various matrices could be compared. Background intervals were selected that would compensate accurately for baseline shifts and sloping baselines [12]. Integration times were selected on the basis of the sensitivity of the individual emission lines. The wavelengths, background correction intervals, and integration times selected are listed in Table 3. For wavelengths below 200 nm, the optical path between the plasma and the photomultiplier tube was purged with nitrogen. The torch extension was used at all times [13].

TABLE 2

Operating conditions for the ICP-6000 system

Slit setting	0.02 nm (low)	Plasma gas flow	12 l min^{-1}
Read delay	25 s	Auxiliary gas flow	0 l min^{-1}
Replicates	3	Nebulizer gas pressure	30 psi
		Plasma viewing height	15 mm
		Forward power	1.25 kW
		Reflected power	<5 W

TABLE 3

Wavelengths, background correction, and integration times

Element	Wavelength (nm)	Background corr. (nm)	Integration time (s)
Se	196.026	±0.23	2
As	197.197	±0.10	2
Cr	205.552	±0.16	1
Zn	213.856	±0.10	1
Cd	214.438	−0.32, +0.18	2
Pb	220.353	±0.14	2
Ni	232.003	±0.18	2
Mn	257.610	−0.27	1
Cu	324.754	+0.19	1

Reagents and calibration standards

The concentrated stock solutions (1000 mg l^{-1}) of the elements were Instra-Analyzed atomic spectral standards (J. T. Baker). Yttrium (1000 mg l^{-1}), the internal standard, was obtained from Aldrich. Redistilled nitric acid (G. Frederick Smith Chemical Company) was used and water was from a Millipore Milli-Q water purification system.

Multi-element master standard solutions were prepared from the concentrated stock solutions. The calibration standards were prepared by diluting these solutions. All the working standards and blanks were acidified to 1% with nitric acid, and they contained 10 mg l^{-1} yttrium.

Pipetting was done with volumetric pipets or calibrated Eppendorf microliter pipets equipped with Ranin RT-200 or RT-20 disposable tips. The latter pipets were calibrated by weighing aliquots of Milli-Q water dispensed from them at room temperature. Five measurements were made to evaluate the average pipet volume. All volumetric glassware was acid-cleaned before being used.

Reference materials and samples

National Bureau of Standards' Standard Reference Material (SRM) 2670 (normal and elevated levels of toxic elements in urine) and Fisher Urine Chemistry Control Level II (lot number 485-024, expiration date February 1, 1986) were used as reference materials. These materials were purchased in freeze-dried form and were reconstituted with 1% nitric acid. The elevated-level SRM is certified for As, Cd, Cr, Cu, Pb, and Se; tentative values are available for manganese and nickel. The normal level SRM is certified only for copper and selenium; tentative values for the other elements (except zinc) are available. The Fisher Level II material has target values for As, Cu, Pb, and Zn.

Urine was collected from healthy laboratory workers, pooled, and acidified to 1% with nitric acid. The pool was dispensed by 10-ml aliquots into Corning 15-ml polyethylene tubes and frozen at −20°C. The urine was thawed as needed. This pool was used as a "normal" urine from which the detection limits for this experimental system were evaluated.

An EPA Water Supply Control Sample (378-13) and an EPA Water Pollution Quality Control Check Sample (476-3), as well as NBS SRM 1643a (trace elements in water), were used as aqueous reference materials. Each of these substances has target values for, or is certified for, several of the elements investigated. The EPA water specimens were prepared from concentrates according to the directions supplied. The final acid concentration was 0.15%. The NBS SRM 1643a did not require reconstitution; its acid content is approximately 3%.

The urine and water materials were prepared in acid-cleaned volumetric flasks containing an appropriate volume of 1000 mg l^{-1} yttrium to yield a final concentration of 10 mg l^{-1}.

RESULTS AND DISCUSSION

Nitrogen purge

The optical path was purged with nitrogen for the use of wavelengths below 200 nm. Formerly, purge or vacuum had been recommended as necessary only below 190 nm [14]. As Fig. 1 shows, however, the arsenic 197.197-nm and the selenium 196.026-nm lines have significant baseline structure in an aqueous matrix, which is greatly reduced when the optical path is purged with nitrogen. The torch extension alone does not eliminate this structure. Similar spectra were obtained, under the same conditions, for a urine matrix containing these $\mu g\ ml^{-1}$ levels of arsenic and selenium. At the low concentration levels encountered for these elements in urine, the baseline structure is a more important consideration than at higher concentrations. Background correction points are more confidently chosen when this structure is minimized.

Results for reference materials

The results for the water reference and control materials are recorded in Table 4. The values for most of the elements are within the expected range. Exceptions are cadmium and selenium. The results for cadmium tended to be lower than expected even when the concentration is well above the detection limit, as in 476-3. The concentration of selenium in all specimens is below the detection limit for this element in water. The standard deviations for arsenic, lead, and selenium are quite large for some of the materials. This is due, in part, to the low emission intensities of the wavelengths used for those elements.

The results for the urine reference materials are recorded in Table 5. With the exception of zinc in Level II, all concentrations obtained by the proposed method are well within the control ranges. The result obtained here for zinc is high; contamination of the material is a very likely explanation for this observation. The levels of nickel and manganese in the SRM 2670 are not certified by the National Bureau of Standards. The concentrations

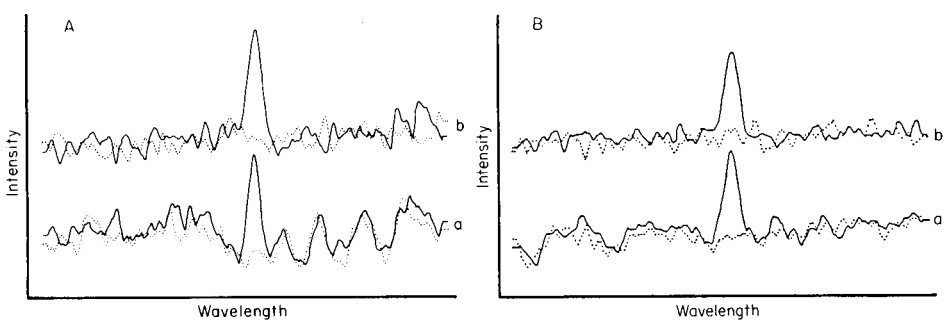

Fig. 1. Spectra for aqueous 1000 ng ml^{-1} arsenic solution (—) and blank solutions (- - -) around the arsenic 197.197-nm emission line: (a) with torch extension only; (b) with the optical path purged with nitrogen. Same for selenium at 196.026 nm.

TABLE 4

Results for water reference materials[a]

Element	Element concentration (ng ml^{-1})					
	SRM 1643a		EPA 378-13		EPA 476-3	
	True	Found[b]	True	Found[c]	True	Found[d]
Se	11 ± 1	35 (39.5)	7.6	ND	16	ND
As	76 ± 7	72 (61.6)	43	36 (63.7)	61	73 (36.0)
Cr	17 ± 2	20 (4.2)	46	46 (4.9)	65	62 (4.5)
Zn	72 ± 4	61 (4.2)	—	—	26	23 (5.6)
Cd	10 ± 1	9 (1.4)	4.6	3.2 (2.4)	27	23 (1.6)
Pb	27 ± 1	30 (38.0)	45	43 (19.2)	113	130 (56.9)
Ni	55 ± 3	62 (17.7)	—	—	96	83 (11.8)
Mn	31 ± 2	28 (2.4)	—	—	47	41 (9.4)
Cu	18 ± 2	21 (10.5)	—	—	37	37 (9.2)

[a]Standard deviation was calculated from all values in all runs, e.g., 3 replicates with 4 runs = 12 measurements (n = 12). Standard deviations are given in parentheses. ND means not detected. [b]n = 12. [c]n = 9 or 12. [d]n = 15 or 18.

TABLE 5

Results for urine reference materials[a]

Element	Element concentration (ng ml^{-1})					
	SRM 2670 (normal)		SRM 2670 (elevated)		Fisher Level II	
	True	Found[b]	True	Found[c]	True	Found[d]
Se	30 ± 8	37 (30.6)	460 ± 30	475 (36.1)		
As	[15]	62 (35.6)	480 ± 100	504 (63.1)	217 ± 46	258 (25.3)
Cr	[13]	10 (3.3)	85 ± 6	75 (3.2)		
Zn	—	—	—	—	2300 ± 600	3182 (174)
Cd	[0.4]	ND	88 ± 3	85 (3.8)		
Pb	[<20]	ND	109 ± 4	94 (19.8)	172 ± 85	159 (21.3)
Ni	[70]	61 (13.2)	[300]	257 (25.3)		
Mn	[30]	24 (2.8)	[330]	310 (6.2)		
Cu	130 ± 20	135 (12.0)	370 ± 30	359 (12.2)	243 ± 40	249 (9.8)

[a]See Table 4. Values in square brackets are information values assigned by NBS. [b]n = 9. [c]n = 15, 18 or 21. [d]n = 15.

for these two elements determined in this work are low compared with the information target values. The results are, however, in reasonable agreement with the value assigned by NBS and could be within the true limits, once the material has been certified for these elements.

The results obtained here for the normal-level SRM 2670 are reasonable, considering that there are no certified values for As, Cr, Cd, Pb, Ni, and Mn and that the information values are at or below the detection limits for As, Cr, Cd, and Pb in urine.

Detection limits

Detection limits were calculated from measurements made with the pooled "normal" urine and with the normal-level SRM. The values reported in Table 6 are averages of five estimates of the detection limit. These were calculated as follows. Five runs of the "normal" urine pool and three runs of the normal-level SRM were done. In each run, the measurements were done in triplicate. From each run, an average concentration and standard deviation of the three measurements were determined. The standard deviations were averaged, and the result was multiplied by 3 to obtain an estimate of the detection limit [15].

These normal urine materials approximate matrix blanks. Some of the elements to be screened, particularly As, Pb, Cu, Zn, and Se, will be present. With the exception of zinc (which has a normal level of approximately 360 ng ml^{-1}), these levels are at or below the levels detectable in urine. Therefore, such materials can be used to evaluate a reliable estimate of detection limits in urine. Also included in Table 6 are the detection limits found by Haas et al. [1] for their simultaneous i.c.p. system and the aqueous detection limits calculated by Winge et al. [11].

In an emergency situation, it is desirable to estimate quickly which, if any, of the possible toxic elements are involved. In the development of any such rapid screen, compromises are made that result in conditions that are not optimal for all the elements included. Thus, the best detection limits are not obtained for all the elements. In spite of these obvious limitations, the method described here is capable of rapidly detecting abnormally high (i.e., toxic) levels of nine elements of interest. Once these have been identified,

TABLE 6

Detection limits for several elements

Element	Detection limits (ng ml^{-1})		
	This system[a]	Haas et al.[b]	Aqueous[c]
Se	47	80	75
As	81	12	76
Cr	12	1	6.1
Zn	—	—	1.8
Cd	2	5	2.5
Pb	37	15	42
Ni	42	4	15
Mn	6	—	1.4
Cu	24	—	5.4

[a]All elements except manganese were determined from measurements on the in-house base pool. Manganese was evaluated from the normal-level SRM. [b]Simultaneous i.c.p. system incorporating an ultrasonic nebulizer [1]. [c]From Winge et al. [11], calculated from $DL \simeq 0.03C/(I_n/I_b)$, where C is the concentration of analyte that yielded the net analyte intensity, I_n, and background intensity, I_b.

further investigation with a more sensitive technique, such as Zeeman graphite-furnace a.a.s. can be done to verify their presence. The detection limits of i.c.p./a.e.s., although not superior to those obtained by the graphite-furnace method, are satisfactory for screening suspect urine specimens for toxic levels of most of the elements investigated.

REFERENCES

1 W. J. Haas Jr., V. A. Fassel, F. Grabau IV, R. N. Knisely and W. L. Sutherland, Adv. Chem. Ser., 172 (Ultratrace Met. Anal. Biol. Sci. Environ.) (1979) 91.
2 R. M. Barnes and J. S. Genna, Anal. Chem., 51 (1976) 1065.
3 L. Friberg, G. F. Nordberg and V. B. Vouk, Handbook on the Toxicology of Metals, Elsevier/North-Holland/Biomedical Press, Amsterdam, 1979.
4 R. C. Baselt, Biological Monitoring Methods for Industrial Chemicals, Biomedical Publications, Davis, CA, 1980.
5 G. F. Wallace, V. V. Pirc and R. D. Ediger, Can. J. Spectrosc., 27 (1982) 46.
6 H. M. McNair, Trends Anal. Chem., 1 (1982) IV.
7 H. E. Wise Jr. and P. D. Fahrenthold, Environ. Sci. Technol., 15 (1981) 1292.
8 G. L. Schmidt and W. Slavin, Anal. Chem., 54 (1982) 2491.
9 S. A. Myers and D. H. Tracy, Spectrochim. Acta, Part B, 38 (1983) 1227.
10 G. F. Wallace, At. Spectrosc., 5 (1984) 5.
11 R. K. Winge, V. J. Peterson and V. A. Fassel, Appl. Spectrosc., 33 (1979) 206.
12 R. D. Ediger and F. J. Fernandez, Atomic Spectrosc., 1 (1980) 1.
13 G. F. Wallace, At. Spectrosc., 2 (1981) 93.
14 R. D. Ediger and D. W. Hoult, At. Spectrosc., 2 (1980) 41.
15 G. L. Long and J. D. Winefordner, Anal. Chem., 55 (1983) 712A.

Analytica Chimica Acta, 174 (1985) 211—223
Elsevier Science Publishers B.V., Amsterdam — Printed in The Netherlands

INSIGHTS INTO COAL STRUCTURE FROM DEGRADATION WITH RUTHENIUM TETROXIDE AND TANDEM MASS SPECTROMETRY

K. E. SINGLETON and R. G. COOKS

Department of Chemistry, Purdue University, West Lafayette, IN 47907 (U.S.A.)

K. V. WOOD*

Engine/Fuels Laboratory, Chemistry Building, Purdue University, West Lafayette, IN 47907 (U.S.A.)

K. T. TSE and L. STOCK

Department of Chemistry, University of Chicago, 5753 S. Ellis Ave., Chicago, IL 60637 (U.S.A.)

(Received 4th April 1985)

SUMMARY

The products of ruthenium tetroxide oxidation of coal (Illinois No. 2) at ambient temperature were examined by tandem mass spectrometry using positive and negative chemical ionization. The negative-ion mass spectrum of the coal sample displays seven homologous series of ions. Individual compounds were characterized by recording daughter spectra. In this way, the following types of compounds were identified: aliphatic dicarboxylic acids, aromatic dicarboxylic and tricarboxylic acids, anhydrides of the di- and tri-carboxylic acids, and dianhydrides corresponding to the tetracarboxylic aromatic acids. The positive-ion mass and daughter spectra provided additional confirmation. Two series of ions dominate the positive-ion mass spectrum, those from the aliphatic dicarboxylic acids, and the corresponding anhydrides. The fragmentation behavior of model compounds was examined to confirm these assignments. The carboxylic acids and anhydrides identified suggest the presence of particular structural features in the coal prior to oxidation. These include C_2—C_6 aliphatic bridges between aromatic units, fused ring aromatic structures, tetralin and indan structures.

Oxidative chemical reactions have frequently been used in attempts to characterize coal and coal-related materials [1—7]. If one utilizes a reaction which generates specific types of products, the structural units in the original coal can be inferred from product analysis. The extent of oxidation varies greatly with both the type of coal and the method of oxidation. Many common oxidizing agents are quite drastic, degrading both aliphatic and aromatic portions of a given compound [1]. Other methods oxidize only the aliphatic portion, leaving the aromatic structure intact in the form of aromatic carboxylic acids [1]. By using these oxidants, one obtains information on the number and types of aromatic rings in the original coal. Yet another class of oxidants will degrade the aromatic structure, leaving the connecting aliphatic portions intact. A common example of this last method is the use of a mixture

0003-2670/85/$03.30

of hydrogen peroxide/trifluoroacetic acid and sulfuric acid to yield dicarboxylic acids and their branched analogs [7].

The limitations of this procedure, as discussed by Liotta and Hoff [8] have encouraged the introduction of similar but milder oxidation procedures. Ruthenium tetroxide oxidizes aromatic nuclei to yield aromatic and heteroaromatic carboxylic acids, some with alkyl substituents [6]. Alkyl substituents are generally left inact, so that the procedure yields aliphatic dicarboxylic acids for tetralins, indans and alkyl-bridged structures. The results for model systems can then be used to predict the products of analogous reactions of more complex materials. Recent work here has illustrated the value of the ruthenium tetroxide oxidation procedure in structural studies on coal. Infrared spectroscopy and magnetic resonance spectra have suggested a greater number of methyl groups per carbon atom than accounted for by this oxidation procedure, suggesting the possible presence of methylated hydroaromatic structures. Dehydrogenation prior to oxidation was found to yield additional ethanoic acid, confirming the conclusion that methyl groups are relatively abundant in aliphatic fragments of the hydroaromatic skeleton of coal (unpublished results, L. M. Stock and S. H. Wang).

A particularly appropriate method for characterizing oxidative degradation products is tandem mass spectrometry (m.s./m.s.) [9, 10]. The use of two stages of mass spectrometry facilitates complex mixture analysis without the need for time-consuming separations prior to the introduction of the sample into the instrument. This is accomplished by setting the first mass analyzer to pass only one selected mass of interest, dissociating this ion by collision, and then mass-analyzing the fragments. The resulting daughter spectra permit identification of individual constituents in the mixture [11]. Mass spectra themselves are used to survey the degradation mixture for possible constituents of interest.

Tandem mass spectrometry has been used in conjunction with various methods of ionization [12], but several factors favored the use of negative-ion chemical ionization (n.i.c.i.) [13] in this study. First, oxidative degradation produces acids which should be readily ionized by n.i.c.i. Second, the value of n.i.c.i. lies in its selectivity for compounds having acidic protons, thereby enhancing their relative abundance in a complex mixture. Third, this soft ionization method minimizes the production of fragment ions which needlessly increase the complexity of the first mass spectrum in the m.s./m.s. method. Positive-ion chemical ionization was used to supplement the information obtained from n.i.c.i.

The use of chemical degradation to probe the structure of coal by the measurement of carboxylic acids, which can be associated with specific structural features, is a particular example of the combination of m.s./m.s. with chemical degradation in coal science. Another example has recently been reported in which organosulfur compounds are characterized [14].

EXPERIMENTAL

Illinois No. 2 coal was oxidized by using ruthenium tetroxide which was generated from ruthenium(III) trichloride hydrate in a mixture of water, acetonitrile and carbon tetrachloride at ambient temperature with excess of sodium bromate, sodium periodate, periodic acid or sodium hypochlorite [5, 6]. After removal of volatiles, the residue was methylated with diazomethane in ether. The methylated product was extracted into dichloromethane. Base-catalyzed hydrolysis of the soluble fraction yielded a sample, which was then acidified with hydrogen chloride in ether and partitioned by solubility in dichloromethane.

Tandem mass spectrometry was used to analyze the dichloromethane-soluble fraction for the oxidation products. A Finnigan triple quadrupole mass spectrometer [15] was available. Samples were introduced via a direct insertion probe and ionized by either positive- or negative-ion chemical ionization (c.i.). The reagent gas used for negative-ion spectra was a mixture of isobutane with a small amount of nitrous oxide (total pressure ca. 0.3 Torr). The negative ions result from either proton abstraction by OH^- yielding $(M-H)^-$ ions in the case of carboxylic acids or electron capture yielding $M^{-\bullet}$ in the case of the anhydrides. Isobutane (ca. 0.4 Torr) was selected as the reagent gas for the positive ion spectra. The ion source was maintained at ca. 460 K. Daughter spectra were obtained by selecting the ion of interest with the first quadrupole (Q1) and passing it into the second quadrupole (Q2) where it undergoes collision-induced dissociation. The resulting fragments are mass analyzed with the third quadrupole (Q3). Argon was used as the collision gas at a pressure of ca. 2×10^{-3} Torr which corresponds to multiple collision conditions. The axial kinetic energy of ions entering the collision quadrupole was 20 eV. The potential of Q3 relative to Q2 was ±2 eV; the potential of Q1 was set to optimize ion-beam intensity.

RESULTS AND DISCUSSION

The negative-ion c.i. mass spectrum of the oxidized coal sample (Fig. 1) shows several homologous series of ions. These series, with initial members 89^-, 148^-, 165^-, 192^-, 218^-, 250^- and 276^-, account for almost all the ion current in Fig. 1. Most of these series (Table 1) are short, showing just two or three ions of significant intensity. One series, that beginning with *m/z* 89, is almost interrupted at *m/z* 103 before continuing at *m/z* 117, 131, 145. Daughter scans were used to identify the compounds which belong to these homologous series, as discussed below.

The positive-ion c.i. mass spectrum (Fig. 2) is dominated by two series of ions, beginning at 91^+ and 101^+. There are also contributions from other series including that beginning at *m/z* 75.

The daughter ion spectra of the relevant ions obtained by negative-ion chemical ionization are presented in Table 2. The series of ions beginning at

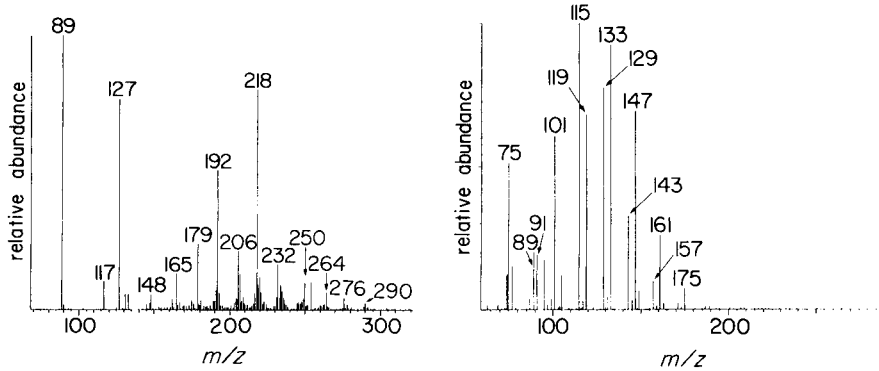

Fig. 1. Negative-ion chemical-ionization mass spectrum of the oxidized coal mixture. (*m/z* 127 is attributed to I^-.)

Fig. 2. Positive-ion chemical-ionization mass spectrum of the oxidized coal mixture.

TABLE 1

Series assignment of the dominant ions detected in a negative-ion chemical-ionization mass spectrum

Dibasic aliphatic acids	89^-, 117^-, 131^-, 145^-, 159^-, 173^-, 187^-, 201^-
Dibasic aromatic acids	165^-, 179^-, 193^-
Aromatic anhydrides	148^-, 162^-, 176^-
Aromatic anhydride with monobasic acid	192^-, 206^-, 220^-
Aromatic dianhydrides	232^-, 246^-

m/z 89 is due to dicarboxylic acids. The ions at 89^-, 117^-, 131^- and 145^- were identified as the conjugate bases of oxalic, succinic, glutaric and adipic acids, respectively. Figure 3 compares the daughter spectrum of the $(M-H)^-$ ion of oxalic acid with that of *m/z* 89 in the coal oxidation product. The spectra are dominated by fragments corresponding to CO and CO_2 loss. The spectrum of the coal-derived mixture shows only a few low abundance ions not present in that of the authentic compound. The oxalic acid behavior is typical of the negative-ion m.s./m.s. data taken in this study. Analogous data were obtained for other members of this (and other) homologous series. The major fragmentations of the higher dicarboxylic acids include combinations of losses of CO_2 and H_2O. Scheme 1 illustrates the fragmentation pattern of the succinic acid conjugate anion under collision-induced dissociation. The presence of higher members of this series which are not even distinguishable in the mass spectrum is evident when daughter spectra are recorded. The daughter spectra of *m/z* 159, 173, 187 and 201 each exhibit fragment ions expected for dicarboxylic acids. For example, the fragmentation of 187^- is characterized by losses of 18 (H_2O), 44 (CO_2), 62 (CO_2, H_2O), 72 (CO, CO_2) and 88 (2 CO_2). It is not known whether these higher members are linear or branched.

TABLE 2

Negative ion chemical ionization daughter spectra

Molecular weight	Selected ion[a]	Neutral fragment mass (abundance)									Additional neutral fragments[b]
		15	18	28	44	62	72	88	116	144	
60	59(100)		(16)								
74	73(100)			(3)	(4)						42(3), 38(32), 36(26), 32(7)
88	87(100)				(58)						
102	101(20)				(100)						60(15), 59(4), 58(3), 56(4), 17(4)
116	115(64)				(100)			(7)			
130	129(42)			(9)	(100)	(3)		(5)			94(10), 45(6), 37(4), 36(18)
90	89(100)			(11)	(75)						
104	103(11)			(3)	(100)	(3)	(18)				46(3)
118	117(38)		(11)		(100)						
132	131(11)		(4)		(100)	(6)					
146	145(32)		(11)		(100)	(15)					
160	159(100)		(9)		(77)	(58)					90(10), 76(20), 64(4), 46(16), 32(10)
174	173(14)		(10)		(14)	(100)	(6)	(10)			100(3), 90(3)
188	187(32)		(17)	(5)	(29)	(100)	(18)	(64)			132(3), 114(6), 106(7), 104(3), 100(3), 90(4), 74(8)
202	201(100)		(12)	(7)	(28)	(25)	(6)	(35)			120(14), 104(4), 102(6), 90(15), 80(4), 76(20), 60(3), 36(7), 32(6)
148	148(67)			(12)	(4)		(100)				111(9), 59(3)
162	162(100)			(3)	(11)	(6)	(3)				90(3), 45(7), 36(4), 1(64)
176	176(100)	(11)	(56)	(13)	(24)	(12)	(44)	(22)			106(5), 100(3), 96(3), 89(14), 63(6), 59(4), 56(4), 51(4), 45(4), 43(4), 17(8), 1(55)
166	165(16)				(100)			(94)			80(3), 36(8)
180	179(3)				(4)		(3)				90(100)
194	193(39)			(33)	(67)		(100)	(17)	(32)		117(4), 80(3), 73(13), 46(5), 45(7), 36(5), 30(3), 29(3), 1(3)
192	192(59)			(49)	(7)		(100)		(11)		45(6), 1(3)
206	206(100)	(39)		(5)	(7)		(8)				59(99)
220	220(100)	(11)		(6)	(14)		(10)	(3)	(3)		73(57), 59(44), 29(20)
232	232(94)						(100)			(3)	
246	246(100)	(7)		(3)	(4)		(21)				100(3)
250	250(21)	(9)			(3)		(4)	(4)	(4)		131(3), 117(3), 104(21), 103(100), 90(3), 73(5), 59(70), 32(18)
264	264(13)	(4)			(3)			(3)	(5)		131(6), 118(8), 117(100), 104(3), 103(16), 87(4), 73(46), 59(30), 46(8), 32(3), 29(8)
276	276(100)	(4)			(20)		(12)	(15)	(16)		160(3), 131(6), 117(7), 103(17), 76(4), 73(47), 59(85), 45(5), 30(3)
290	290(100)						(6)		(4)	(3)	145(4), 117(5), 73(70), 59(19)
218	218(74)				(5)		(100)				

[a]Relative abundance of the selected ion is in parentheses; only fragment ions of greater than 2% relative abundance are listed in the table. [b]Mass of the neutral fragment lost followed by the relative abundance in parentheses.

As already noted, the intensity of the ion at *m/z* 103, which corresponds to malonic acid, is very weak in the mass spectrum (Fig. 1). The daughter spectrum of 103^- may contain malonic acid but it is at most a minor component of the low abundance ion. The presence of an enolizable hydrogen

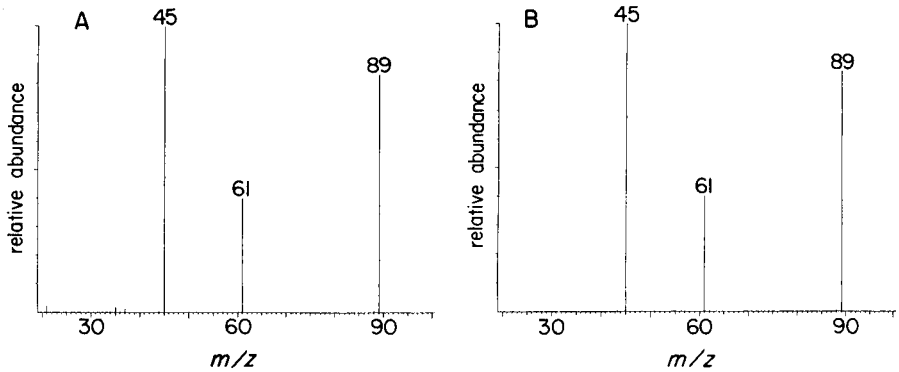

Fig. 3. Comparison of the daughter spectra of 89^- from (A) the oxidized coal mixture and (B) the oxalic acid conjugate anion.

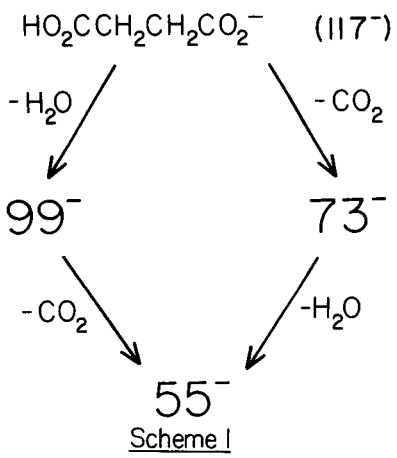

Scheme I

between the two carbonyls results in further oxidation in the ruthenium tetroxide oxidation procedure, thus explaining the low abundance of malonic acid in this sample (unpublished results, Stock and Wang).

Positive-ion c.i. was used to record daughter spectra of *m/z* 91 and 119 from the oxidized coal sample, and the spectra were compared to those of protonated oxalic and succinic acids, respectively. A good match was observed, supporting the conclusions drawn from the negative-ion data. Also consistent with the negative-ion mass spectrum is the fact that the relative abundance of protonated malonic acid is very low. The major components of the positive-ion mass spectrum at *m/z* 133 and 147 are protonated glutaric and adipic acids, respectively, as confirmed by comparison of their daughter spectra with those of standards. Similarly, *m/z* 161, 175, 189 and 203 all exhibit the fragmentations expected for dicarboxylic acids. For example, the fragmentation of 189^+ is distinguished by the losses of 18 (H_2O), 46 (HCO_2H), 64 (HCO_2H, H_2O), 74 (HCO_2H, CO) and 92 ($2\,HCO_2H$). Some of the fragment ions present in each of these spectra indicate contributions from

components other than the α,ω-dicarboxylic acids. This is expected because these ions are present at background levels in the c.i. mass spectrum (Fig. 2).

From the foregoing, there is abundant evidence in both the positive- and negative-ion data for a series of dicarboxylic acids stretching from C_2 to at least C_{10}. Judging from the positive-ion data, and allowing for the decreasing ion transmission and increased fragmentation at higher mass, one concludes that the amounts of the products drop sharply at adipic acid (*m/z* 147) which could result from oxidation of tetralin or its analogs. It is possible that the next higher homolog represents a branched chain dicarboxylic acid but evidence for this is inconclusive.

A second dominant series of ions is present in the positive-ion mass spectrum, beginning at *m/z* 101. The ions correspond to the anhydrides of the aliphatic dicarboxylic acids discussed previously. The fragmentation patterns correlate well with those of the acids from which they derive. For example, the daughter spectrum of *m/z* 101 is characterized by peaks at *m/z* 101, 73, 55, 45 and 29. These are the same peaks as are present in the daughter spectrum of protonated succinic acid. The anhydrides are easily formed in the ion source and therefore may not actually be present in the oxidized coal mixture.

The presence of monocarboxylic acids was investigated by means of daughter scans because this ion series was not evident in the n.i.c.i. spectrum. A homologous ion series begins at 59^-, although the first two members give ions of very low abundance. The dominant loss of 44 (CO_2) in the daughter spectra of 87^-, 101^-, 115^- and 129^- suggests that these ions are due to carboxylic acids, possibly keto acids. Keto acids might be expected to fragment to stable gaseous negative ions, in contrast to monocarboxylic acids. The presence of keto acids could also account for the dominant peak at *m/z* 43 (CH_3CO^+) in the positive-ion c.i. daughter spectra of 61^+, 75^+, 89^+, 103^+ and 117^+. The daughter spectrum of 61^+ indicates the presence of protonated acetic acid by comparison with an authentic sample, whereas that of 75^+ suggests that propionic acid is not present. However, the daughter spectrum of 89^+ indicates that pyruvic acid is present (Fig. 4). This is based on the

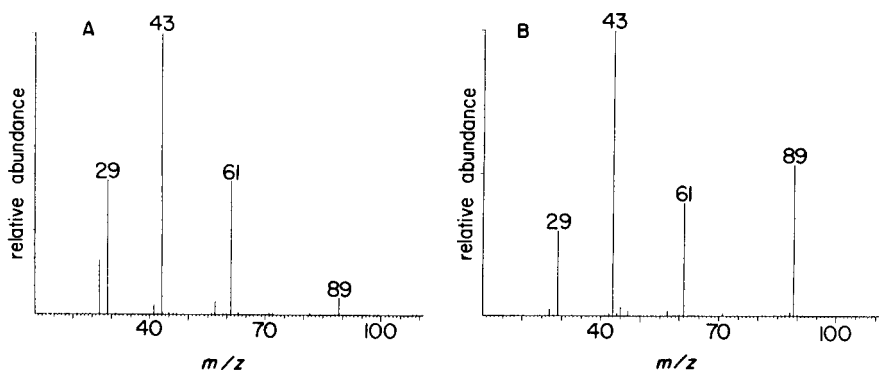

Fig. 4. Comparison of daughter spectra of 89^+ from (A) the oxidized coal mixture and (B) the protonated pyruvic acid cation.

presence of the ion at *m/z* 61, which occurs in both the protonated pyruvic acid and oxidized coal daughter spectra, but is absent in the daughter spectrum of protonated butyric acid. The weakness of the peaks in these spectra suggests a low abundance of these compounds. The remaining series of ions present in the negative-ion mass spectrum correspond to aromatic carboxylic acids and the related anhydrides. For convenience, Table 1 summarizes the masses of the ions and the assignments made. Each series is considered in turn below.

The primary component at *m/z* 148 is phthalic anhydride. The daughter spectrum, distinguished by a loss of 72 (CO, CO_2), matches the daughter spectrum of the authentic compound with some additional peaks that can be attributed to these losses in combination with the loss of water. (The primary fragment ions are *m/z* 148, 31%; *m/z* 120, 10%; *m/z* 89, 10%; *m/z* 86, 22%; *m/z* 76, 100% and *m/z* 37, 10%.) The daughter spectrum of 162^- is characterized by a dominant loss of $H^\bullet$, possibly a hydrogen atom from a methyl group on the ring. Additional losses of CO, CO_2 from both $M^{-\bullet}$ and $(M-1)^-$ suggest the anhydride structure. Although not the dominant component, less intense peaks corresponding to those observed in homophthalic anhydride are present. The daughter spectrum of 176^- is also characterized by a hydrogen atom loss. The other fragment ions observed are due to losses of 15 ($CH_3^\bullet$), 18 (H_2O), 28 (CO), 62 (CO_2, H_2O) and 72 (CO, CO_2).

The corresponding positive-ion spectra support these identifications. The positive-ion spectrum of 149^+ (Fig. 5) confirms the presence of the anhydride of phthalic acid. Fragmentation proceeds by three sequential losses of CO, with less abundant ions resulting from the losses of HCO_2H from the parent ion, and C_2H_2 from *m/z* 65 (ion resulting from the third CO loss). The daughter spectrum of 163^+ appears to correspond to that expected for the C_1 analog. The fragmentations seen in the parent anhydride are present, but the fragment ions are all fourteen daltons more massive, suggesting that the aromatic ring is methylated. Higher members of the anhydride series may be

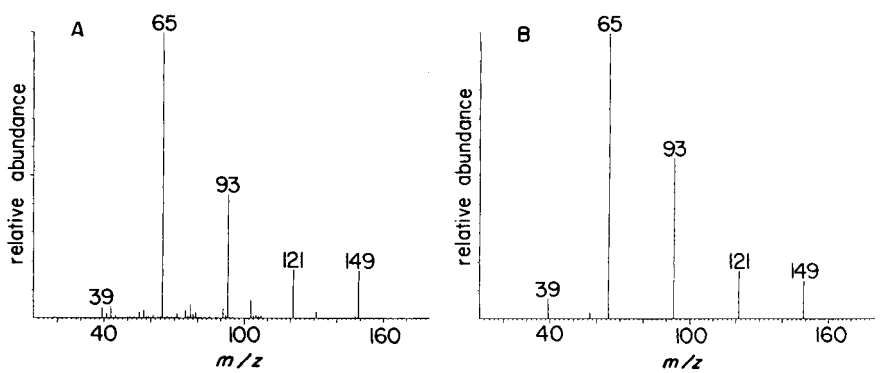

Fig. 5. Comparison of daughter spectra of 149^+ from (A) the oxidized coal mixture and (B) the protonated phthalic anhydride cation.

present in smaller amounts but they were not specifically sought by using daughter spectra.

The daughter spectrum of the first member of the next series, 165^-

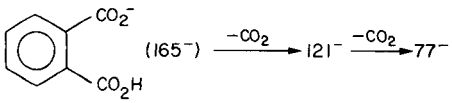

implies that these compounds are benzenedicarboxylic acids. Comparison with standards shows that terephthalic and phthalic acids can be differentiated (base peaks of 121^- and 77^-, respectively), while the spectrum of the conjugate base of isophthalic acid is identical to that of terephthalic acid. The coal sample appears to contain a mixture of the isomers, based on the approximately equal abundances of 121^- and 77^-. The daughter spectrum of the coal sample, like the authentic compounds, contains only 77^- and 121^- as major fragment ions. The daughter spectrum of 179^-, the next member of the series, contains the expected loss for the C_1 benzenedicarboxylic acid analog, loss of CO_2 to 135^-. However, 179^- is predominantly the proton-bound dimer of oxalic acid as indicated by an abundant ion at *m/z* 89 and low abundance ions at *m/z* 61 and 45. Furthermore, the absence of an abundant ion at *m/z* 91 suggests that the methyl group is ring-attached and not inserted between the ring and the acid moiety similar to homophthalic acid.

Positive-ion data provide corroboration for the assignment of the benzenedicarboxylic acid structure. The daughter spectrum of 167^+ appears to be comprised of a combination of the three isomeric acids. The spectrum of phthalic acid is dominated by four sequential losses of CO while the loss of water (to form the anhydride) is a relatively minor fragment. In contrast, the ions arising from CO loss are insignificant in the daughter spectra of protonated terephthalic and isophthalic acids, which are dominated by intense peaks at *m/z* 79 and *m/z* 77. The daughter spectrum of 181^+ is consistent with expectations for the C_1 analog. The same peaks as occur in the parent compound are present from *m/z* 43 to *m/z* 121, with additional peaks at *m/z* 135, 149 and 163 (losses of 46, 32 and 18, respectively). If the oxalic acid dimer (*m/z* 181) is present, it is a minor component in the positive-ion spectrum. The daughter spectrum of 195^+ corresponds to the C_2 analog, exhibiting essentially the same types of fragmentation as the daughter spectrum of 181^+.

The foregoing data establish the presence of several isomers of the benzenedicarboxylic acids and their methylated homologs. These compounds presumably give rise to the anhydrides which comprise the previous series and it may be that the anhydrides are generated in situ in the hot ion source of the mass spectrometer. The point is moot, however, because both compound types probably originate from fused ring aromatic compounds. Figure 6 illustrates some fused ring aromatic precursors, which might be oxidized by ruthenium tetroxide to produce aromatic acids.

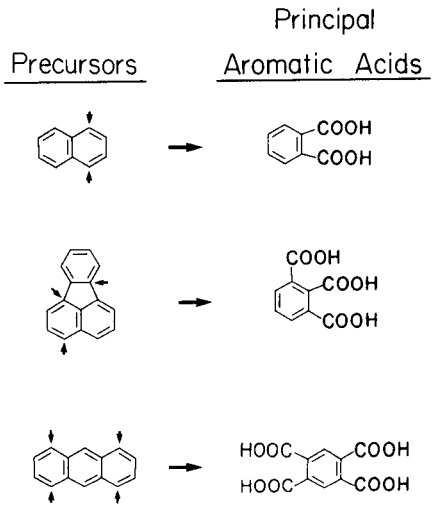

Fig. 6. Some fused ring aromatic precursors and the principal aromatic acids formed.

The next homologous series of ions of interest in the negative-ion chemical-ionization mass spectrum is the series, 192^-, 206^-, 220^-, ... The major component in the daughter spectrum of 192^- is the monocarboxy-substituted benzenedicarboxylic anhydride (Scheme 2). The spectrum is characterized by various combinations of losses of 28 and 44 [losses of 28 (CO), 44 (CO_2), 72 (CO, CO_2), 88 ($2CO_2$) and 116 (CO, $2CO_2$)]. The loss of CO in the oxidized coal mixture spectrum (50% relative abundance, m/z 120 is base

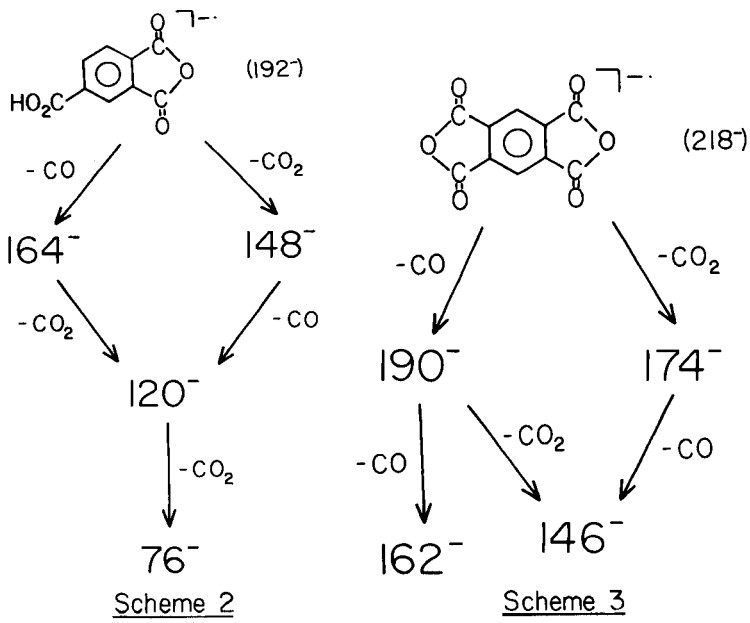

peak) is significantly greater than that in the 1,2,4-benzenetricarboxylic anhydride (trimellitic anhydride) spectrum, (5% relative abundance, *m/z* 120 is base peak), implying that the dominant component present is the 1,2,3-benzenetricarboxylic anhydride (hemimellitic anhydride). The ions 206^- and 220^- appear to contain the C_1 and C_2 analogs of the anhydride with losses of 28 (CO), 44 (CO_2), 72 (CO, CO_2), and 116 (CO, $2CO_2$). However, the dominant loss of 59, and a smaller loss of 15, in the daughter spectrum of 206^- strongly indicates the presence of a second very abundant component. The ion at 220^- appears to correspond to the C_2 analog, but also contains dominant losses of 59 and 73, again suggesting the presence of a second component.

The positive-ion spectrum from the oxidized coal exhibits low abundance fragment ions resulting from the losses of H_2O, CO and HCO_2H from $(M + H)^+$. These losses correspond to dominant fragment ions in the authentic spectrum of trimellitic anhydride. However, the dominant fragment ion in the oxidized coal spectrum (*m/z* 103) appears to result from the presence of a second component. The minor fragment ions in the 207^+ and 221^+ spectra correspond to the C_1 and C_2 analogs of protonated monocarboxy-substituted benzenedicarboxylic anhydrides. However, as observed in the negative-ion spectra, the C_1 and C_2 analog spectra are dominated by a second major constituent as evidenced by the dominant losses of CH_3OH (possibly arising from an OCH_3 substituent) and subsequent loss to *m/z* 103. The *m/z* 103 ion is the base peak in all three daughter spectra from oxidized coal.

Because the anhydride is easily formed in the ion source, the amount of benzenetricarboxylic acid present in the oxidized coal is expected to be small or absent. This is supported by the low abundance of 209^- in the mass spectrum. The daughter spectrum of 209^- (Fig. 7) confirms the presence of benzenetricarboxylic acid. The C_1 analog appears to be present at 223^-. The positive-ion daughter spectra are very complex, suggesting the presence of several compounds at each mass.

The benzenetetracarboxylic dianhydride is present at 218^-, indicated by a dominant loss of 72 (CO, CO_2), and small losses of 28 (CO), 44 (CO_2) and 56

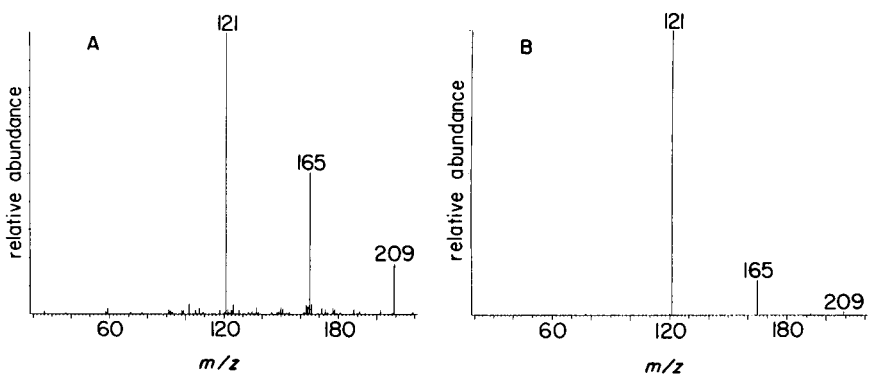

Fig. 7. Comparison of daughter spectra of 209^- from (A) the oxidized coal mixture and (B) the trimellitic acid conjugate anion.

(2 CO) (Scheme 3), and by comparison with the spectrum of authentic 1,2,4,5-benzenetetracarboxylic (pyromellitic) dianhydride. The daughter spectrum of 232^- is distinguished by intense peaks at *m/z* 232 and 160 (loss of CO, CO_2). The presence of these peaks, in addition to peaks of low intensity at *m/z* 217, 204, 188, 116 and 88 [losses of 15 ($CH_3^\bullet$), 28 (CO), 44 (CO_2), 116 (2 CO_2, CO) and 144 (2 CO_2, 2 CO)], are consistent with a C_1 analog of benzenetetracarboxylic dianhydride. The fragmentation pattern of 246^- (C_2 analog) also suggests that the alkyl group(s) is attached to the ring. The positive-ion spectra support these conclusions. In the daughter spectrum of 219^+, losses include 18 (H_2O), 46 (HCOOH), 72 (CO, CO_2), 90 (HCO_2H, CO_2), 100 (CO, 2 CO_2) and 144 (2 CO, 2 CO_2). The spectra of 233^+ and 247^+ appear to be the C_1 and C_2 analogs. In all three spectra, additional components are present. The presence of the dianhydride suggests that benzenetetracarboxylic acid is present in the oxidized coal mixture, although it is not evident in the mass or daughter spectra. This is based on the dominance of 218^- and the negligible amount of 253^- [$(M - H)^-$] in the mass spectrum of 1,2,4,5-benzenetetracarboxylic acid (pyromellitic acid).

The last two series in the n.i.c.i. mass spectrum begin at *m/z* 250 and 276. The daughter spectra of 250^-, 264^- and 278^- appear to be homologous, with losses suggesting alkyl and carboxyl substituents. Both alkyl and carboxyl substituents also appear to be present in the series beginning at *m/z* 276. The corresponding positive-ion spectra are relatively complex, but they suggest the presence of these substituents. Among the possibilities for the structures of the components in these last two series are alkyl-substituted anhydrides or dianhydrides.

CONCLUSIONS

It is possible to draw some conclusions about the structural components present in the unoxidized coal based on the observed products in the oxidized mixture. The presence of oxalic acid is indicative of a biaryl precursor, while succinic acid suggests aryls with two bridging methylene groups. Diacids of higher mass may also derive from the analogous bridging groups. Alternatively, additional precursors are possible, e.g., the oxidation of acenaphthene, indans and tetralins could yield succinic, glutaric and adipic acids, respectively.

The observed benzenecarboxylic acids may derive from naphthalene-type structures. For example, 1-hydroxynaphthalene is converted almost quantitatively to phthalic acid (unpublished results, L. M. Stock and S. H. Wang). Structures such as acenaphthene or naphthoic acid could both yield benzenetricarboxylic acids. Arylacetic acids also derive from aromatic compounds with bridging methylene groups [6]. The various alkyl-substituted benzoic acid compounds are probably products of oxidation of alkyl-substituted aromatics, in which side chain groups are preserved. The oxidation of 4-pentylbiphenyl yields benzoic acid, hexanoic acid and 4-pentylbenzoic acid with only trace pentanoic acid (unpublished results, Stock and Wang).

The alkyl- and carboxy-substituted mono- and di-anhydride analogs are of interest in that they may derive from highly substituted aromatics. Ring and heteroatom substitutions are also likely in the aryl structures.

In summary, this method is easily applied to the analysis of complex mixtures, allowing direct analysis without further sample workup. The results correspond well with those expected based on previous work with model compounds. The dominant components present in both the negative-ion and positive-ion c.i. mass spectra were dibasic aliphatic carboxylic acids, as well as carboxy- and alkylcarboxy-substituted benzenes. These results concur with work suggesting a relatively large abundance of methyl groups in the macromolecular structure of coal. These products were relatively easily identified based on the fragmentation patterns in the daughter spectra and/or comparison with spectra of the corresponding standards.

This work was supported by the Department of Energy (DE-FG22-PC50803).

REFERENCES

1 R. Hayatsu, R. G. Scott and R. E. Winans, in W. S. Trahanovsky (Ed.), Oxidation in Organic Chemistry, Part D, Academic Press, New York, 1982, Chap. 4.
2 N. C. Deno, K. W. Curry, B. A. Greigger, A. D. Jones, W. G. Rakitsky, K. A. Smith, K. Wagner and R. D. Minnard, Fuel, 59 (1980) 694.
3 R. K. Hessley, B. M. Benjamin and J. W. Larsen, Fuel, 61 (1982) 1085.
4 T. V. Verheyen and R. B. Johns, Anal. Chem., 55 (1983) 1564.
5 N. Mallya and R. A. Zingaro, Fuel, 63 (1984) 423.
6 L. M. Stock and K. T. Tse, Fuel, 62 (1983) 974.
7 N. C. Deno, B. A. Greigger and S. G. Stroud, Fuel, 57 (1978) 455.
8 R. Liotta and W. S. Hoff, J. Org. Chem., 45 (1980) 2887.
9 F. W. McLafferty (Ed.), Tandem Mass Spectrometry, John Wiley & Sons, New York, 1983.
10 R. A. Yost and D. D. Fetterolf, Mass Spectrom. Rev., 2 (1983) 1.
11 J. D. Ciupek, R. G. Cooks, K. V. Wood and C. R. Ferguson, Fuel, 62 (1983) 829.
12 R. G. Cooks, K. L. Busch and G. L. Glish, Science, 222 (1983) 273.
13 D. Zakett, J. D. Ciupek and R. G. Cooks, Anal. Chem., 53 (1981) 723.
14 K. V. Wood, R. G. Cooks, J. A. Laugal and R. A. Benkeser, Anal. Chem., 57 (1985) 692.
15 J. R. B. Slayback and M. S. Story, Ind. Res. Dev., (1981) 129.

Analytica Chimica Acta, 174 (1985) 225—235
Elsevier Science Publishers B.V., Amsterdam — Printed in The Netherlands

THERMOMETRIC AND OTHER TITRATIONS OF SPARINGLY SOLUBLE COMPOUNDS IN AQUEOUS MICELLAR MEDIA

SHYAM S. SHUKLA

Department of Chemistry, University of Connecticut, Storrs, CT 06268 (U.S.A.)

LOUIS MEITES*

Department of Chemistry, George Mason University, 4400 University Drive, Fairfax, VA 22030 (U.S.A.)

(Received 22nd March 1985)

SUMMARY

Several organic acids and bases that are very sparingly soluble in water have been determined by acid-base and redox titrimetry after solubilizing them in micellar suspensions of sodium dodecylsulfate or cetyltrimethylammonium bromide. Thermometric titrations are much more rapid, convenient, accurate, and precise than the corresponding potentiometric ones. Titrations in such media can effect some differentiations that cannot be made in water and are also much more economical than titrations in non-aqueous solvents.

Many organic compounds are too sparingly soluble in water to be determined titrimetrically in that medium, and they are therefore usually titrated in non-aqueous solutions. Underwood [1] and Pellizetti and Pramauro [2] showed that many such compounds can be titrated in aqueous solutions if they are solubilized by a micellar surfactant. However, these authors also showed that potentiometric titrations are unsatisfactory for this purpose, for the pH measured with a glass electrode is so unstable that it drifts for as much as half an hour after each addition of reagent, especially in the vicinity of the equivalence point.

The work described here was undertaken in the expectation that similar difficulties would not arise in thermometric titrimetry. Since they do not, thermometric titrations of micellar solutions provide an attractive alternative to non-aqueous titrimetry. This paper outlines the principles, scope, and limitations of these titrations.

EXPERIMENTAL

Reagents

Cetyltrimethylammonium bromide and sodium dodecylsulfate were obtained from the Aldrich Chemical Co. and from Dr. J. P. Kratohvil, respectively. A 0.1 M solution of the former was slightly alkaline, probably because it contained some free trimethylamine, but adding a drop or two of

0003-2670/85/$03.30

0.004 M hydrochloric acid to 50 cm^3 of it sufficed to lower the pH to a value well below 7. Similarly, although a 0.06 M solution of sodium dodecylsulfate was slightly acidic, a drop or two of 0.004 M sodium hydroxide sufficed to raise the pH of 50 cm^3 of it to a value well above 7. In the titrations reported below, the average amount of substance titrated was of the order of 0.5—1 mmol, and blank corrections for acidic and basic impurities in the surfactants would have been negligibly small.

The other chemicals were obtained from either Aldrich Chemical Co. or Eastman Kodak. They were of ordinary reagent grade and were used without purification. Standard solutions of hydrochloric acid and sodium hydroxide were prepared in conventional ways, with due care to avoid contamination by carbon dioxide, and were standardized by using potassium hydrogenphthalate as the primary standard.

Methods

The thermometric titrator, which has been described elsewhere [3], was of fairly conventional design but incorporated a trigger device connected to two electrodes, one in the solution being titrated and the other in the reagent-delivery line. A small bubble of air is drawn into the tip of that line to prevent interdiffusion of the solutions during thermal equilibration. On actuating the motor that drives the syringe-type buret, the bubble is slowly expelled from the tip. The actual addition of reagent begins at the instant when an electrical connection is established between the two solutions, and the trigger device produces a small spike on the recorded titration curve at that instant. The reagent-delivery system was recalibrated whenever any of its components was changed. The overall sensitivity of the (10^5 ohm) thermistor and Wheatstone bridge was always close to 32.0 K V^{-1}. Since the values of ΔH° for these reactions are generally between 40 and 50 kJ mol^{-1}, titrations of 0.005—0.01 M solutions were made without difficulty. Titration curves were recorded with a Sargent Model SRLG strip-chart recorder.

Corrections were applied for heat exchange, for heats of dilution, and for any difference between the temperatures of the reagent and the solution being titrated. Each titration was continued well beyond the end-point to obtain a portion of the curve on which changes of temperature were due to these three causes alone. The addition of reagent was then stopped, and recording was continued to obtain a portion on which they were due to heat exchange alone, and from which the Newtonian heat-exchange constant could be evaluated in the manner described elsewhere [3]. After the heats of dilution had been evaluated in a blank titration, the values of all three corrections were easily computed at each point on the curve.

A few potentiometric titrations were conducted to obtain estimates of pK_a in micellar systems. They were made with a Corning Model 112 pH meter and a combination electrode, and entailed drifts and variations of pH like those described by others [1, 2].

Most of the calculations reported here were made in BASIC with a Radio

Shack TRS-80 Model II microcomputer. The general program for effecting nonlinear regression has been described elsewhere [4].

RESULTS AND DISCUSSION

Titrations of organic bases

Figure 1 shows a typical thermometric titration curve, which was obtained by adding 0.400 M hydrochloric acid, at a rate of 1.106×10^{-2} cm^3 s^{-1}, to 50 cm^3 of a solution which was 8.69×10^{-3} M in α-naphthylamine and 0.10 M in sodium dodecylsulfate. Although α-naphthylamine is not only very sparingly soluble but also very weakly basic in water ($pK_a = 3.92$ for its conjugate acid [5]), the curve is well formed, and three titrations of 0.4—0.5 mmol of amine gave a mean error of +0.26% and a relative mean deviation of ±0.51%.

Reilley et al. [6] and Tyrrell [7] concluded that the product $c_b^0 K_t$ should have a value at least as large as 10^2 in order to yield an analytically useful end-point on a segmented titration curve based on an isovalent ion-association titration (i.e., one based on a reaction of the form $B^- + H^+ = BH(aq)$ or something equivalent to it): c_b^0 is the initial concentration of the substance titrated, K_t is the concentration equilibrium constant of the reaction under the conditions used, and the extent of dilution is assumed to be negligible. For the titration of Fig. 1, c_b^0 was 8.7×10^{-3} mol dm^{-3}, while the value of K_t would have been 8.3×10^3 mol^{-1} dm^3 in an aqueous solution of low ionic strength. Hence the product $c_b^0 K_t$ would have had a value of only 72 in such a solution, which is well below the accepted minimum.

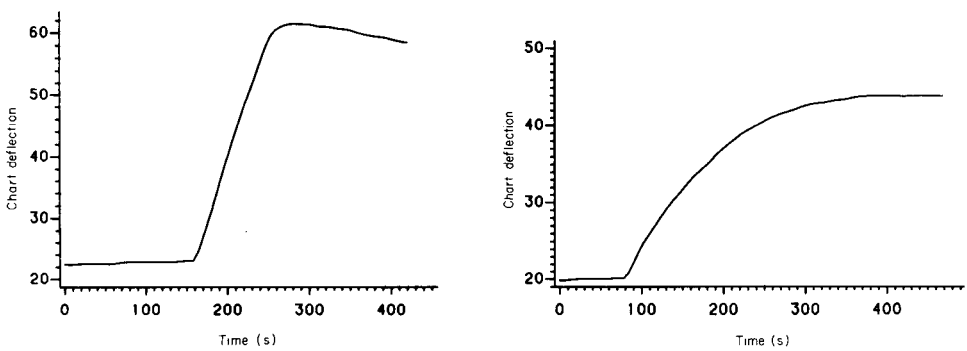

Fig. 1. Thermometric titration curve for the titration of α-naphthylamine with hydrochloric acid under the conditions described in the text. The reagent was added at a constant rate of 0.01106 cm^3 s^{-1}, and the sensitivities of the bridge and recorder were such that one chart division corresponds to 1.60 mK.

Fig. 2. Thermometric titration curve for the titration of 50 cm^3 of a 9.94×10^{-3} M solution of *p*-nitroaniline with 0.448 M hydrochloric acid, which was added at a constant rate of 0.01106 cm^3 s^{-1}. The sensitivities of the bridge and recorder were such that one chart division corresponds to 0.64 mK. The equivalence point occurs 100.3 s after the addition of reagent is begun.

In the presence of a micellar electrolyte, such calculations may be complicated by two phenomena. An uncharged species (such as α-naphthylamine) undergoes extraction into the hydrocarbon-like interior of the micelle, while a charged one (such as α-naphthylammonium ion) may undergo binding to oppositely charged groups concentrated at the surface of the micelle. Each of these processes decreases the activity of the substance in the aqueous phase, but they have opposite effects on the value of K_t. For α-naphthylamine in the presence of micelles of dodecylsulfate, the first process would lead to a decrease of the basicity of the amine and thus to a decrease of the value of K_t, while the second would lead to a decrease of the acidity of the ammonium ion and thus to an increase of the value of K_t. A potentiometric titration similar to the thermometric one shown in Fig. 1 gave $pK_a = 5.35$, which is 1.4 unit higher than in the absence of micelles. This indicates that binding of α-naphthylammonium ion to micellar sulfate groups is the more important of the two phenomena, even though the distribution coefficient that governs the extent of solubilization of the free amine is very large. The value of pK_a in the micellar solution corresponds to $c_b^0 K_t = 2 \times 10^3$, which is well above the limit of feasibility according to Reilley et al. [6] and Tyrrell [7]. The success of the titration reflects these considerations as well as the efficacy of the micelles in solubilizing the amine.

Similar behavior was observed in thermometric titrations of other sparingly soluble amines with hydrochloric acid in the presence of sodium dodecylsulfate. Graphical locations of the end-points in the customary way gave relative mean deviations less than ±0.2% in titrations of *n*-hexylamine and *o*-chloroaniline, for which the values of pK_a in water are 10.60 and 2.65, respectively [5]. For extremely weakly basic amines, however, the shifts of pK_a resulting from the interactions described above were too small to yield sharp end-points, as may be seen from the titration curve for *p*-nitroaniline (for which $pK_a = 1.0$ in water [5]), which is shown in Fig. 2.

Non-linear regression analysis has proved to be the method of choice for locating poorly defined, and even invisible, end-points on both sigmoidal [8, 9] and segmented [10, 11] titration curves, and also for evaluating the physicochemical parameters that characterize these curves. Applying it to data obtained in thermometric titrations of 0.027 M *o*-chloroaniline with 0.487 M hydrochloric acid, in a fashion generally similar to that of Christensen et al. [12—14], gave $K_t = 1.30 \times 10^3$ mol^{-1} dm^3 in a solution containing 0.10 M sodium dodecylsulfate. The corresponding value of pK_a for *o*-chloroanilinium ion in such a solution is 3.11, only 0.46 p*K* unit higher than in water. This is a much smaller effect than the corresponding one for α-naphthylammonium ion.

Similar treatment of data obtained in titrations of 0.00994 M *p*-nitroaniline (for which $pK_a = 1.0$ in water) with 0.448 M hydrochloric acid gave $K_t = 4.0 \times 10^2$ in the presence of 0.10 M sodium dodecylsulfate, corresponding to $pK_a = 2.61$. The effect of solubilization in micelles of dodecylsulfate is thus slightly larger for *p*-nitroaniline than for α-naphthylamine.

Although the accuracies and precisions of such titrations were poor (±20%) even when the concentration of the amine was evaluated by non-linear regression analysis, the value of $c_b^0 K_t$ is only about 4 even in the micellar solution (as against 0.1 in water), and this figure is far below the accepted limit of feasibility.

Titrations of organic acids

Table 1 summarizes the results that were obtained in thermometric titrations of a number of uncharged carboxylic acids and phenols with sodium hydroxide in solutions containing 0.04—0.06 M cetyltrimethylammonium bromide. In all these titrations, the end-points were sharp and could easily be located by the familiar graphical technique. In contrast, Forman and Hume [15] found benzoic acid (pK_a = 4.20 in water) to be the weakest acid that exhibited a distinct end-point when titrated thermometrically in acetonitrile; *p*-toluic and acetic acids, for which the values of pK_a are 4.37 and 4.76, respectively, were too weak to be titrated successfully.

The value of pK_a for the conjugate acid of an uncharged base is increased

TABLE 1

Thermometric titrations of uncharged carboxylic acids and phenols with sodium hydroxide in solutions containing micelles of cetyltrimethylammonium bromide (50 cm^3 of a solution containing 0.04—0.06 M cetyltrimethylammonium bromide in addition to the acid or phenol was titrated with approximately 0.4 M sodium hydroxide, which was added at a rate of 0.01106 cm^3 s^{-1})

Compound titrated	pK_a	Number of millimoles		Error (%)
		Taken	Found	
m-Nitrobenzoic acid	3.49	0.4357	0.4391	0.78
			0.4391	0.78
			0.4381	0.55
		0.2525	0.2514	−0.44
α-Naphthylacetic acid	4.24	0.2506	0.2498	−0.32
p-Toluic acid	4.37	0.4977	0.5019	0.84
			0.5008	0.62
			0.4997	0.40
		0.2545	0.2577	1.25
n-Hexanoic acid	4.88	0.3009	0.2999	−0.33
o-Nitrophenol	7.23, 5.94[b]	0.1869[a]	0.1865	−0.21
m-Nitrophenol	8.35	0.5061	0.5073	0.24
			0.5062	0.02
			0.5030	−0.61
		0.2545	0.2579	1.34
		Mean and mean deviation: 0.33 ± 0.53		

[a] Because the commercial product was grossly impure, this value was obtained from the result of an assay by potentiometric titration.

[b] This value of pK_a pertains to the micellar solution and was calculated from the data obtained in a potentiometric titration; the other values pertain to aqueous solutions [5].

by the presence of negatively charged micelles because the effect of binding of the positively charged acid to the micelles outweighs that of extraction of the base into their interior. The value of pK_a for an uncharged acid is decreased by the presence of positively charged micelles for a similar reason: extraction of the acid into the interior of the micelles lowers its activity in the aqueous phase and would tend to increase the value of pK_a, but this effect is outweighed by that of binding of the negatively charged conjugate anion to the micelles. Negatively charged micelles of dodecylsulfate decrease the value of pK_a for the conjugate acid of an uncharged base to an extent that varies from one base to another; for the bases studied in this work the average change was 1.15 ± 0.5 unit. From the single result for *o*-nitrophenol in the presence of cetyltrimethylammonium bromide, positively charged micelles appear to exert an effect of roughly equal magnitude, though of opposite sign, on the value of pK_a for an uncharged acid.

To elucidate these effects further, and also to investigate the feasibility of titrating mixtures of acids or bases in micellar solutions, two mixtures of benzoic and *n*-nonanoic acids were titrated potentiometrically with sodium hydroxide: one in the presence of 0.06 M sodium dodecylsulfate, and the other in the presence of 0.04 M cetyltrimethylammonium bromide. In water the values of pK_a for these acids are so nearly equal (4.20 and 4.96, respectively [5]) that there would not be an inflection at the equivalence point for the stronger acid even if both were sufficiently soluble to render the titration feasible. Figure 3 shows the titration curve obtained in the presence of dodecylsulfate. There is definitely a point of maximum slope at the first equivalence point, even though it is too poorly defined to be located with reasonable accuracy or precision by classical techniques. Analysis of these

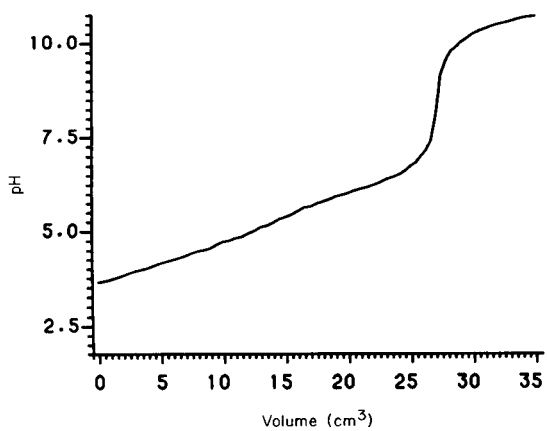

Fig. 3. Potentiometric titration curve for the titration of 50 cm^3 of a solution which contained 5.61×10^{-3} M *n*-nonanoic acid, 5.00×10^{-3} M benzoic acid, and 0.06 M sodium dodecylsulfate, with 0.0187 M sodium hydroxide.

data by non-linear regression entailed the evaluation of six parameters: the concentration and the dissociation constant of each acid, and the values of K_w and y_{H^+}, the apparent single-ion activity coefficient of hydrogen ion [10]. Strong interactions among the values of several of these parameters caused the fit to be ill-conditioned, and therefore excessively time-consuming. They were consequently replaced by six others: c_1^0 (the initial concentration of the stronger acid), c_2^0/c_1^0, $y_{H^+}K_{a1}$ (which is formally equivalent to $a_{H^+}[A_1^-]/[HA_1]$, where square brackets denote concentrations), $y_{H^+}K_{a2}$, $y_{H^+}K_w$ (which is equivalent to $a_{H^+}[OH^-]$), and y_{H^+}. This new set of parameters led to prompt and satisfactory convergence on the values c_1^0 = 0.00494 M (concentration of benzoic acid taken, 0.00500 M), c_2^0 = 0.00521 M (concentration of n-nonanoic acid taken, 0.00561 M), K_{a1} (the concentration dissociation constant of benzoic acid in the medium employed) = 2.10×10^{-4} mol dm^{-3}, K_{a2} (the corresponding constant for n-nonanoic acid) = 3.80×10^{-6}, K_w^0 (the thermodynamic ion-product constant of water, calculated on the assumption that $y_{H^+} = y_\pm$) = 9.82×10^{-15} mol^2 dm^{-6}, and y_{H^+} = 0.254. The mean of the relative errors in the initial concentrations is −4.2%, which is similar to the errors obtained by earlier workers [1, 2] from potentiometric titrimetry and is largely attributable to the drifts and uncertainties of the measured pH values. The difference, 1.74 unit, between the values of pK_a is more than twice as large as in water, and accounts for the appearance of a discernible inflection at the first equivalence point. The agreement of K_w^0 with the expected value (1.01×10^{-14} mol^2 dm^{-6}) serves to confirm the reliabilities of the other values. The value obtained for y_{H^+} is unexpectedly low, presumably because hydrogen ions are electrostatically or otherwise bound to the negatively charged micelles.

Similar analysis of the data obtained in a titration in the presence of cetyltrimethylammonium bromide gave c_1^0 = 0.00511 M (concentration of benzoic acid taken, 0.00516 M), c_2^0 = 0.00533 M (concentration of n-nonanoic acid taken, 0.00533 M), K_{a1} = 1.59×10^{-3} mol dm^{-3}, K_{a2} = 4.75×10^{-5} mol dm^{-3}, K_w^0 = 9.29×10^{-15} mol^2 dm^{-6}, and y_{H^+} = 0.524. Here the mean of the relative errors in the initial concentrations was only −0.5%, while the difference between the values of pK_a is 1.52 unit, just twice as large as in water. It appears likely that many differentiating titrations can be made more feasible and more precise by conducting them in micellar solutions. Of course, there are many mixtures that cannot be resolved even in a micellar medium, such as one of *o*- and *p*-nitrophenol in the presence of cetyltrimethylammonium bromide. In water, the pK_a values for these compounds are 7.23 and 7.16, respectively; in the micellar medium each changes to about 5.9, and differentiation is still impossible. As usual, each practical case must be judged on its own merits.

Application of non-linear regression analysis

Non-linear regression analysis has been used to interpret acid-base and other titration curves for about a decade, and has proved to give useful

results even in extremely unfavorable situations [9, 16]. An attempt was therefore made to apply it, together with the solubilization model of Yatsimirskii and co-workers [17, 18], to the data obtained in a number of the titrations described above. The titration of *o*-chloroaniline with hydrochloric acid in the presence of micelles of sodium dodecylsulfate provides a typical example.

The model assumes that the base being titrated is in equilibrium with its conjugate acid and hydrogen ion in each phase, and that each of these three substances can undergo partition between that phase and the micellar one. Partition coefficients are defined by equations of the form $P_i = a_{i,m}/a_{i,w}$, where the subscripts m and w denote the micellar and aqueous phases, respectively. The partition coefficients are interrelated [19] by the equation

$$K_{t,m} = K_{t,w} P_{RNH_3^+} / P_{RNH_2} P_{H^+} \quad (1)$$

where $K_{t,m}$ and $K_{t,w}$ are the equilibrium constants for the titration reaction in the two phases. The corresponding changes of enthalpy may be denoted by ΔH_m and ΔH_w, and the changes of enthalpy associated with the transfer of hydrogen ion and *o*-chloroaniline from the aqueous phase to the micellar one may be denoted by ΔH_{H^+} and ΔH_{RNH_2}, respectively. The molar volume V_m of the micellar phase constitutes a tenth adjustable parameter, and is needed in the equations so that the number of moles of each substance in each phase can be calculated. Values of the molar volumes of some surfactants are available in the literature [17—19] but are in very poor agreement.

After correction of the data for extraneous heat effects, the following results were obtained: $c^0_{RNH_2} = 0.02767$ M (concentration of *o*-chloroaniline taken = 0.02675 M), $P_{RNH_2} = 89$, $P_{RNH_3^+} = 0.48$, $P_{H^+} = 0.93$, $K_{t,w} = 118$ mol^{-1} dm^3, $\Delta H_{H^+} = 64$ J mol^{-1}, $\Delta H_{RNH_2} = 4.1$ kJ mol^{-1}, $\Delta H_w = -27$ kJ mol^{-1}, $\Delta H_m = -34$ kJ mol^{-1}, and $V_m = 0.11$ dm^3 mol^{-1}. These figures are clearly wrong in several respects, and they give a deviation plot with sharply defined features that are reproducible from one titration to another. Whether the error is due to the comparatively small (fourfold) excess of surfactant used in these experiments, a systematic drift of the errors associated with the measurements of pH, or some other phenomenon, the model is certainly useless for predicting and interpreting titration curves in media like these.

A second analysis was done by assuming that only three parameters were involved. Together with the results obtained in the same titration of *o*-chloroaniline in the presence of sodium dodecylsulfate, these were the initial concentration of the chloroaniline (0.02523 M), and the "overall" equilibrium constant (1.2×10^3 mol^{-1} dm^3) and change of enthalpy (—25.0 kJ mol^{-1}) for the titration reaction. The same parameters would be used to analyze a thermometric titration curve. What was surprising was that the standard deviation from regression was about an order of magnitude smaller than that for the fit with ten parameters, and that the amplitude of, and sharpness of the features on, a deviation plot were very much smaller.

Evidently this model provides a better description of the potentiometric titration curve than the more complicated one does, but the relative error in the initial concentration is still markedly inferior to those obtained from thermometric titrations, which are shown in Table 2 along with the results obtained for several other amines. It is interesting to note that the value of pK_a for *o*-chloroaniline in water is nearly a full unit below that for *m*-chloroaniline, which was the weakest base that Forman and Hume [15] were able to titrate successfully in acetonitrile.

Other titrations in micellar media

Other kinds of titrations can also be done in micellar media. For example although both *o*- and *p*-nitroaniline are so weakly basic (in water the value of pK_a for the former is 1.5 unit below that for *o*-chloroaniline, while that for the latter is even lower) that acidimetric titrations of both were unsuccessful in the presence of the surfactants employed in this work, both could be titrated with *N*-bromosuccinimide. In a typical experiment, a 10^{-3} M solution of a nitroaniline, solubilized in micelles of sodium dodecylsulfate, was titrated with a 0.08 M solution of the reagent, solubilized with the same surfactant. It is well known that *N*-bromosuccinimide is only very slowly soluble in water at room temperature, and some workers [20] have consequently resorted to heating to 80°C to effect its dissolution, but in the presence of sodium dodecylsulfate complete solution was readily achieved by stirring for a few minutes. The reaction with either nitroaniline was found to be too slow for thermometric or even visual titration, and titrations were made by adding about a 30% excess of the reagnet, allowing the mixture to

TABLE 2

Thermometric titrations of amines with hydrochloric acid in solutions containing micelles of sodium dodecylsulfate (50 cm^3 of a solution containing 0.10 M sodium dodecylsulfate in addition to amine was titrated with approximately 0.4 M hydrochloric acid, which was added at a rate of 0.01106 cm^3 s^{-1}.) Values of pK_a pertain to aqueous solutions and to the conjugate acids of the amines listed [5]

Compound titrated	pK_a	Number of millimoles		Error (%)
		Taken	Found	
n-Hexylamine	10.60	0.5500	0.5630	2.4
		0.5245	0.5350	2.0
α-Naphthylamine	3.92	0.4840	0.4816	−0.50
		0.4348	0.4386	0.87
		0.4087	0.4104	0.42
o-Chloroaniline	2.65	1.338	1.349	0.82
		1.204	1.216	1.04
		0.536	0.539	0.56
		Mean and mean deviation: 0.95 ± 0.65		

stand for a few minutes at room temperature, and determining the excess of reagent by iodimetric back-titration with standard sodium thiosulfate. This is the procedure that is generally used in titrations with this reagent [21, 22]. Four titrations of 0.3009 mmol of *p*-nitroaniline gave a mean relative error of −1.6 ± 0.3%, almost exactly half the error achieved by Tiwari et al. [22].

Conclusions

Much information about the behaviors of compounds of these and other classes will be needed in order to reduce these preliminary observations to routine analytical practice. There are, however, three reasons why the labor required to obtain that information will be worth while. One is that many substances too slowly or sparingly soluble in water to be titrated conveniently, if at all, are readily solubilized in micellar media. A second is that the properties of the solubilized substances differ from those in water in ways that will often render titrations feasible even though they are impossible in water. A third is that the cost of, say, 100 cm^3 of aqueous 0.1 M sodium dodecylsulfate is approximately 4% of the cost of an equal volume of glacial acetic acid, and 1.3% of the cost of an equal volume of acetonitrile.

This work was aided in part by grant number CHE-8106103 from the National Science Foundation. The paper is based in part on a thesis submitted by Shyam S. Shukla in partial fulfillment of the requirements for the Ph.D. degree at Clarkson College of Technology in July, 1983.

REFERENCES

1 A. L. Underwood, Anal. Chim. Acta, 93 (1977) 267.
2 E. Pellizetti and E. Pramauro, Anal. Chim. Acta, 117 (1980) 430.
3 E. J. Voll and L. Meites, Anal. Chim. Acta, 115 (1980) 249.
4 L. Meites, The General Non-Linear Regression Program CFT4A, The George Mason Institute, Fairfax, VA, 1984.
5 D. D. Perrin, Dissociation Constants of Organic Bases in Aqueous Solutions, Butterworths, London, 1965.
6 C. N. Reilley, R. W. Schmidt and F. S. Sadek, Anal. Chem., 30 (1958) 947; J. Chem. Educ., 36 (1959) 555.
7 H. J. V. Tyrrell, Talanta, 11 (1964) 843.
8 F. Ingman, A. Johansson, S. Johansson and R. Karlsson, Anal. Chim. Acta, 64 (1973) 113.
9 D. M. Barry and L. Meites, Anal. Chim. Acta, 68 (1974) 435.
10 L. Meites and J. G. McCullough, Anal. Chim. Acta, 76 (1975) 219.
11 J. G. McCullough and L. Meites, Anal. Chem., 47 (1975) 1081.
12 J. J. Christensen, J. Ruckman, D. J. Eatough and R. M. Izatt, Thermochim. Acta, 3 (1972) 203.
13 D. J. Eatough, J. J. Christensen and R. M. Izatt, Thermochim. Acta, 3 (1972) 219.
14 D. J. Eatough, R. M. Izatt and J. J. Christensen, Thermochim. Acta, 3 (1972) 233.
15 E. J. Forman and D. N. Hume, Talanta, 11 (1964) 129.
16 D. M. Barry, L. Meites and B. H. Campbell, Anal. Chim. Acta, 69 (1974) 143.

17 A. K. Yatsimirskii, K. Martinek and I. V. Berezin, Tetrahedron, 27 (1971) 2855.
18 I. V. Berezin, K. Martinek and A. K. Yatsimirskii, Russ. Chem. Rev., 42 (1973) 787.
19 K. Martinek, A. K. Yatsimirskii, A. P. Osipov and I. V. Berezin, Talanta, 29 (1973) 963.
20 L. S. Bark and P. Prachiabpaibul, Anal. Chim. Acta, 87 (1976) 505.
21 N. K. Mathur and C. K. Narang, Determination of Organic Compounds with *N*-Bromosuccinimide and Allied Reagents, Academic Press, London, 1975.
22 R. D. Tiwari, J. P. Sharma and I. C. Shukla, Talanta, 14 (1967) 853.

Analytica Chimica Acta, 174 (1985) 237—244
Elsevier Science Publishers B.V., Amsterdam — Printed in The Netherlands

GAS CHROMATOGRAPHIC BEHAVIOUR AND PHARMACOLOGICAL ACTIVITY OF NEUROLEPTICA

L. BUYDENS and D. L. MASSART*

Vrije Universiteit Brussel, Farmaceutisch Instituut, Laarbeeklaan 103, B-1090 Brussel (Belgium)

P. GEERLINGS

Vrije Universiteit Brussel, Algemene Chemie, Fakulteit Wetenschappen, Pleinlaan 2, B-1050 Brussel (Belgium)

(Received 9th February 1985)

SUMMARY

Biological activity in vitro, quantified as equilibrium inhibition constants to the dopamine receptor, of a series of neuroleptica are correlated with parameters describing polar and apolar interactions of these molecules with the receptor. Gas-chromatographic retention indices on stationary phases of different polarity are compared with parameters that are classically used in such quantitative structure/activity studies. To describe apolar interactions, a series of classical parameters such as several valence molecular indices and log k' in a reversed-phase h.p.l.c. system are included; retention indices on the apolar stationary phase, OV101, are used as the gas-chromatographic (g.c.) parameter. To take the more specific polar interactions into account, quantum-chemical charge parameters such as the dipole moment and the charge on atoms directly involved in the interaction were calculated. Retention indices on the more polar phase OV17 are taken as the g.c. parameter for polar interactions. It is shown that the retention indices on OV101 can replace classical parameters describing aspecific or apolar interactions. The retention indices of OV17 do not correlate with biological activity and are worse than the charge parameters.

The gas chromatographic behaviour of a compound on a given stationary phase, as reflected by the degree of retention of the compound, is governed by the interactions of the molecules with the stationary phase [1, 2]. Depending on the electronic properties of the molecules and of the stationary phase, or more precisely the presence of local or overall polarity in the interacting systems, the interactions between the stationary phase and the molecules may be classified as polar (e.g., dipole-dipole interactions, hydrogen bonding) or apolar (dispersion interactions) [3]. It has been shown earlier [4—9] that gas-chromatographic retention indices can be correlated with parameters describing the physical and chemical properties of the molecules. These parameters can be divided into two main classes, depending on their importance in describing apolar or polar interactions. In the rest of this article, "class 1" parameters relate to apolar interactions, and "class 2" parameters describe the polar interactions. Apolar interactions are described by the molar refractivity, the log P (octanol/water) and by topological

0003-2670/85/$03.30

parameters such as connectivity indices. Hammett's sigma and also various electronic parameters (calculated according to quantum mechanics) such as charges on atoms or atom groups or the dipole moment, all related to local or global molecular polarity, belong to "class 2".

Retention indices on apolar stationary phases can be correlated with parameters of "class 1". Very good correlations were obtained between retention indices on squalane, an apolar phase, and the molecular connectivity indices both in the case of molecules belonging to the same chemical family [4, 5, 7—9] as for a data set consisting of relatively small molecules belonging to different chemical classes such as alcohols and ketones [4—6]. To describe the retention behaviour on polar phases parameters of "class 2" are necessary. Good correlations were obtained between retention indices on DEGS, a polar phase, and Hammett's sigma or charge parameters calculated from quantum mechanics [6].

The pharmacological activity of drugs is governed mainly by the degree of interaction of the molecules with the receptor. These interactions are of the same type as described above [10]. Using QSAR (quantitative structure/activity relationships), one tries to explain or predict the pharmacological activity by means of the same molecular descriptor variables as described above [11—14]. Because both phenomena, chromatographic and pharmacological behaviour, can be related to the same parameters, one can think of the gas chromatographic behaviour either as a model system or as a predictor variable for the pharmacological behaviour. To investigate this, a group of pharmacologically active compounds, the neuroleptica, was chosen. The study was directed to establishing, for these drug molecules, the degree to which the classical molecular descriptor variables used in QSAR, can be replaced by parameters describing the gas chromatographic behaviour.

The pharmacological activity was quantified by means of the equilibrium inhibition constant, K_i (see below) [15]. Retention indices on OV101 and OV17 were evaluated as well as a number of classical descriptor parameters.

THEORY

The pharmacological activity of molecules can be quantified by means of the IC_{50} value. This is a measure of the relative binding affinity of the drug to the receptor. It is the concentration that inhibits 50% of the specific binding of a labelled ligand to the receptor. From the IC_{50} values, the equilibrium inhibition constants can be calculated [16] from

$$K_i = IC_{50}/(1 + C/K_d) \tag{1}$$

where C is the concentration of the labelled ligand, and K_d is the equilibrium constant of the labelled ligand with the receptor.

The K_i values of about 20 molecules, belonging to the series of neuroleptica were taken from the literature [15]. This group contains different chemical

classes such as phenothiazines, butyrophenones and others (see Table 1). In order to compare the capacity to describe the pharmacological behaviour, a series of the classical parameters and of chromatographic parameters were calculated. Table 2 shows how they can be subdivided in the two aforementioned classes.

In "class 1", the first series of parameters used are the different valence molecular connectivity indices, which are topological parameters and can be calculated from the molecular skeleton. A detailed survey of these connectivity indices is available [11]. It may be recalled that for all the path indices the bonds considered must be adjacent. For ^5X_p, for example, all atoms forming 5 adjacent bonds have to be taken into account, the corresponding pattern being "/\/\/", in the symbolism of Kier and Hall [11]. These path indices describe the overall bulkiness of the molecules. When the cluster and path-cluster terms are calculated, certain branching patterns are taken into account (e.g., $\begin{array}{c}|\\/\backslash/\\|\end{array}$ for ^5X_c). The cluster and path cluster (c and pc) indices describe a more specific branching in the molecules. Another parameter often used in QSAR studies is the logarithm of the partition coefficient between octanol and water (log $P_{o/w}$) [12—14]. This parameter is often replaced by the log k' value obtained in a reversed-phase high-performance liquid chromatography (h.p.l.c.) system [14]. Usually a C18 bonded phase is used in such studies. Barbato et al. [17] used it for the determination of the log $P_{o/w}$ for phenothiazines.

TABLE 1

Neuroleptica included in the study

PHENOTHIAZINES	*BUTYROPHENONES*
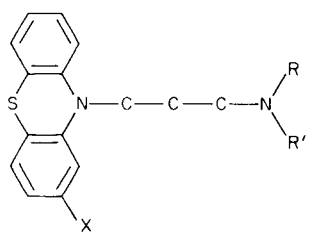	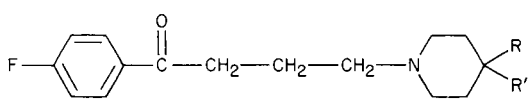
Chlorpromazine	Spiperone
Promazine	Benperidol
Alimemazine	Haloperidol
Thioridazine	
Levomepromazine	*OTHERS*
Propericiazine	Penfluridol
Prochlorperazine	Clothiapine
Trifluperazine	Clozapine
Perphenazine	Loxapine
Fluphenazine	
Chlorprothixene (Thioxanthene)	

TABLE 2

Parameters used in the regression equations

CLASS 1
Retention indices on OV101.
Valence molecular connectivity indices "X".
Path terms: ${}^0X$; ${}^1X$; ${}^2X_p$; ${}^3X_p$; ${}^4X_p$; ${}^5X_p$.
Cluster and path-cluster terms: ${}^3X_c$; ${}^4X_c$; ${}^5X_c$; ${}^5X_{pc}$.
Log k' h.p.l.c. (C18) (see text).

CLASS 2
Retention indices on OV17.
Charge parameters calculated from quantum chemistry.
qN.
qX (only for the phenothiazines.)
Molecular dipole moment: D.

For the parameters of "class 2", the choice was governed by previous knowledge about the drug/neuroleptic receptor interaction. As can be seen in Table 1, all molecules possess a tertiary aliphatic nitrogen atom. According to several authors, this nitrogen atom is very important in the drug/receptor interaction [18, 19]. Therefore the net charge on that nitrogen was chosen as a parameter to describe the polar interactions with the receptor. These charges were calculated by the CNDO/2 method [20]. This semi-empirical quantum-chemical method in which only the valence electrons are explicitly taken into account yields acceptable charge distributions [20] without demanding prohibitively large computer times for larger systems. The dipole moment was also calculated by the CNDO/2 method as a measure of overall polarity. For calculating dipole moments, the choice of molecular conformation is very important. Because the conformation of these molecules at the receptor site is unknown, crystallographic data [21] were taken for the rigid parts of the molecules while the flexible parts, where free rotation is possible, were fixed in their most extended conformation.

To represent the chromatographic behaviour, the retention indices on OV17 and OV101 were selected. These two phases show different polarity. In other work, which is reported elsewhere [22], it was shown that retention indices on OV101 correlate best with the connectivity indices while the retention behaviour on OV17 is best described by qN, the net charge on the nitrogen atom. Therefore, the capability of parameters of "class 1" will be compared to the retention indices on OV101 for describing apolar interactions. The retention behaviour on OV17 will be compared with the charge on the nitrogen atom for use in describing polar interactions.

EXPERIMENTAL

The gas-chromatographic retention indices were evaluated with a Varian 3700 gas chromatograph. (A complete list with the values of the g.c. retention

indices and of all the calculated molecular parameters is available from the authors upon request.) The columns (2 m long, 2 mm i.d.) were packed with 3% (w/w) OV17 or 3% OV101 on Gas-chrom Q (100/120 mesh; Altech). Column temperature was 260°C; detection was by flame ionization. Retention times were measured by means of a Varian Vista CDS-401.

Log k' values for h.p.l.c. were evaluated with a Varian 8500 liquid chromatograph. The column (250 mm long, 4.5 mm i.d.) was of LiChrosorb-RP18 (10 μm). The dead volume was measured by means of potassium dichromate. The mobile phase was acetonitrile/acetic acid/water/propylamine (90/5/10/0.01). Acetonitrile (h.p.l.c. quality), glacial acetic acid (p.a.) and propylamine (p.a.) were from Merck. Water was twice-distilled and further purified on a Gelman filter. The flow rate was 2.0 ml min^{-1} and the injection volume 50 μl. An ultraviolet detector (254 nm) was used. The retention times were measured by means of a Varian Vista CDS-401.

The connectivity indices were calculated from the formulae given by Kier and Hall [11] with a specially prepared FORTRAN program. The quantum-chemical parameters were computed with the QCPE CNINDO program [23], extended to 80 atoms and 200 atomic orbitals; 3*d* orbitals were not included in the atomic basis set for second row elements (chlorine, sulphur). In order to establish which parameters are most powerful in describing pharmacological activity, regression techniques were used. Equations of the following form were investigated:

$$-\log(K_i)_i = a_0 + a_1 X_{i,1} + \cdots + a_n X_{i,n} \qquad (2)$$

Here, $(K_i)_i$ is the equilibrium inhibition constant of compound i, and $X_{i,j}$ is one of the n molecular descriptor parameters as described above for compound i; a_0, a_1,... are the regression coefficients.

The multiple correlation coefficient (MR) is the correlation coefficient of the experimental value with the value predicted by Eqn. 2; MR is a measure of the quality of the regression equation. A stepwise regression technique was used: the variables are entered in the regression equation one by one. The first variable entered is the one that explains the greatest part of the variance in the dependent variable; this is the one that has the largest correlation coefficient (R) with the dependent variable. The second descriptor parameter entered is the one that explains the greatest part in the variance not yet explained by the variable already present in the regression equation. Variables are entered only if their contribution to the multiple correlation coefficient of the regression equation is significant. The regression equations were calculated by using the SPSS program [24].

RESULTS AND DISCUSSION

The results are summarized in Tables 3—7. As can be seen from Tables 3 and 4, the first parameter entered is the net charge on the nitrogen atom. This confirms the crucial nature of this atom in the drug/neuroleptic receptor

TABLE 3

Stepwise regression for all compounds (Parameters: OV101; $\log k'$; X_p; qN; OV17.)

Step	Variable	*MR*	*R*
1	qN	0.72	0.72
2	OV101	0.75	0.67

interaction. Once this effect is filtered out, the remaining variance is accounted for by differences in the apolar properties of the molecules. These apolar properties are related to descriptor variables of "class 1" in Table 2. This is reflected in the entry of these parameters in the regression equation after the net charge on the nitrogen atom in Tables 3 and 4. To compare the power of the individual parameters, regressions were constructed including the chromatographic behaviour on OV101 and the X_p indices (Table 3). In Table 4 the different X-indices are separately introduced in the regression equations to compare them individually. One observes that OV101 and the path-connectivity indices are equivalent in describing the apolar effects of the interaction once the effect of the nitrogen interaction has been filtered out of the total variance. If, however, the 5-cluster index is introduced in the stepwise regression, the results are superior to OV101 or the path-connectivity indices. This cluster term describes a specific branching pattern in the molecules, which is not the same for the different chemical classes in the data set. This may indicate some specific steric requirements for the interaction.

To confirm these results, the subgroup of phenothiazines was selected from the total data set. These phenothiazines belong to the same chemical class and are closely related structurally. They differ mainly in the branching on the nitrogen atom and in a substituent on the aromatic ring (Table 1). Therefore the net charge on this substituent is also included in the regression study. The results for this subgroup are summarized in Tables 5 and 6. Here, apolar effects account for the most important part of the variance. This can be explained by the fact that the specific interactions via the nitrogen atom are more constant within a group of structurally related substances. The difference in the interaction strength is then governed by those properties of

TABLE 4

Regressions for all compounds (Parameters: qN; X_p or X_c.)

Step	Variable	*MR*	*R*	Step	Variable	*MR*	*R*
1	qN	0.72	0.72	1	qN	0.72	0.72
2	^0X	0.72	0.57	2	^4X_p	0.72	0.60
1	qN	0.72	0.72	1	qN	0.72	0.72
2	^1X	0.72	0.72	2	^5X_c	0.81	0.26
1	qN	0.72	0.72				
2	^3X_p	0.72	0.60				

TABLE 5

Stepwise regression for phenothiazines only (Parameters: OV101; log k'; X_p; $X_{c,pc}$; qN; qX; D; OV17.)

Step	Variable	*MR*	*R*
1	OV101	0.75	0.75
2	qX	0.84	0.50
3	qN	0.86	0.53

the molecules which are not directly related to charge distribution in the neighbourhood of the nitrogen atom, approximated again by the descriptor parameters of "class 1" or the retention indices on OV101. A stepwise regression was done in which all descriptor parameters were included (Table 5). To compare the power of the connectivity indices with the retention indices on OV101, regressions, including the X-indices separately, were calculated (Table 6). The results in Tables 5 and 6 show that OV101 is equivalent to the path connectivity term while the cluster terms are worse. This means that within this group, not the specific branching but rather the overall size is important for the interaction. From these results, one can conclude that OV101 as an apolar phase is as good as the best classical parameter for describing apolar interactions related to, e.g., molecular size for this set of neuroleptica with their receptor. It is, however, less suitable for the description of specific steric requirements. At this stage it should be pointed out, however, that pharmacological activity is quantified here as a direct interaction with the receptor, whereas in vivo the drugs have to pass membranes before reaching the receptor site. Because these membranes are essentially lipid layers, the apolar effect will become more important in the overall pharmacological activity.

From the previous results, it emerges that the retention indices on OV17 are worse than the classical electronic parameters of "class 2". It is qN that enters the regression equation and not the retention indices on OV17 in Table 3. To compare the power of OV17 with the classical parameter, the regressions of Table 7 were calculated; OV17 is clearly worse than qN.

TABLE 6

Regressions for phenothiazines only (Parameters: X; qN; qX.)

Step	Variable	*MR*	*R*	Step	Variable	*MR*	*R*
1	^0X	0.76	0.76	1	^4X_p	0.72	0.72
2	qX	0.77	0.50	2	qX	0.73	0.50
1	^1X	0.76	0.76	1	qN	0.53	0.53
2	qX	0.76	0.50	2	qX	0.65	0.50
1	^3X_p	0.74	0.74	3	^5X_c	0.75	0.30
2	qX	0.74	0.50				

TABLE 7

Regressions for all compounds

Step	Variable	*MR*	*R*
1	OV101	0.67	0.67
2	OV17	0.67	0.61
1	OV17	0.61	0.61
2	^5X_c	0.63	0.30

This is reasonable because the polar interactions at the receptor are expected to be highly selective. To describe these interactions, one needs parameters which will only coincidentally also be the optimal parameters for describing the interactions on a polar stationary phase.

REFERENCES

1 B. L. Karger, L. R. Snyder and C. Eon, Anal. Chem., 50 (1978) 2126.
2 H. Declercq, J. Despontin, L. Kaufman and D. L. Massart, J. Chromatogr., 122 (1977) 535.
3 P. W. Atkins, Physical Chemistry, Oxford Univ. Press, Oxford, 1978.
4 L. Buydens and D. L. Massart, Anal. Chem., 53 (1981) 1990.
5 L. Buydens, D. Coomans, M. Vanbelle, D. L. Massart and R. Vanden Driessche, J. Pharm. Sci., 72, 11 (1983) 1327.
6 L. Buydens, P. Geerlings and D. L. Massart, Anal. Chem., 55 (1983) 738.
7 Y. Michotte and D. L. Massart, J. Pharm. Sci., 66 (1977) 1630.
8 B. L. Kier and L. H. Hall, J. Pharm. Sci., 68 (1979) 120.
9 J. S. Millership and A. D. Woolfson, J. Pharm. Pharmacol., 30 (1978) 483.
10 J. E. Gearien, in W. O. Foye (Ed.), Principles of Medicinal Chemistry, 2nd edn., Lea & Febiger, Philadelphia, 1981, Chap. 6.
11 L. B. Kier and L. H. Hall, Molecular Connectivity in Chemistry and Drug Research, Academic Press, New York, 1976.
12 C. Hansch, in E. J. Ariens (Ed.), Drug Design, Vol. 1, Academic Press, New York, 1971.
13 Y. C. Martin, Quantitative Drug Design, M. Dekker, New York, 1978.
14 M. S. Tute, in N. J. Harper and A. B. Simmonds (Eds.), Advances in Drug Research, Vol. 6, Academic Press, London, 1971, Chap. 1.
15 J. E. Leysen, in E. Usdin, S. Dahl, L. Gram and O. Lingsaerde (Eds.), Clinical Pharmacology in Psychiatry. Neutroleptic and Antidepressant Research, MacMillan Publishers, London, 1981, pp. 35–62.
16 Y. C. Cheng and W. H. Prusoff, Biochem. Pharmacol., 22 (1973) 3099.
17 F. Barbato, M. Recanatini, C. Silipo and A. Vittoria, Eur. J. Med. Chem. – Chem. Ther., 17 (1982) 229.
18 J. J. Kaufman and E. Kerman, Int. J. Quantum Chem.: Quantum Biology Symp., 1 (1974) 259.
19 J. P. Tollenaere, H. Moereels and L. A. Raymaekers, in E. J. Ariens (Ed.), Drug Design, Vol. 10, Academic Press, New York, 1980, Ch. 2.
20 J. A. Pople and D. L. Beveridge, Approximate Molecular Orbital Theory, McGraw-Hill, New York, 1970.
21 J. P. Tollenaere, H. Moereels and L. A. Raymaekers, Atlas of the Three-dimensional Structure of Drugs, Elsevier/North Holland Biomedical Press, Amsterdam, 1979.
22 L. Buydens, D. L. Massart and P. Geerlings, J. Chromatogr. Sci., 23 (1985) 304.
23 P. Dobosch, CNINDO, Q.C.P.E., Program No. 141, Indiana Univ., Bloomington.
24 N. H. Nie, C. H. Hull, J. G. Jenkins, K. Stenbrenner and D. H. Bent, SPSS Statistical Package for the Social Sciences, 2nd edn., McGraw Hill, New York, 1975.

Analytica Chimica Acta, 174 (1985) 245—258
Elsevier Science Publishers B.V., Amsterdam — Printed in The Netherlands

SUB-MICROLITRE PERMITTIVITY DETECTORS FOR HIGH-PERFORMANCE LIQUID CHROMATOGRAPHY

A. HOSSEINY, F. BENMAKROHA and J. F. ALDER*

Department of Instrumentation and Analytical Science, UMIST, Manchester M60 1QD (Great Britain)

(Received 8th February 1985)

SUMMARY

A theoretical model is developed for the response of permittivity detectors working at radiofrequency for h.p.l.c. applications. Three types of cell were tested: a coil cell, a parallel-ring cell and a two-wire intrusive cell. All offer small cell volumes (ca. 700 nl for the coil cell, 9 nl for the parallel-ring cell and 40 nl for the intrusive two-wire cell). The last cell, with a 20-MHz Franklin oscillator, is shown to be most useful for conventional and microbore h.p.l.c., offering low instrument noise and reasonable sensitivity. The model is shown qualitatively to describe the observed response well. The coil cell also offers the possibility of monitoring conductivity changes in electrolyte solutions through frequency-change measurements. The theoretical response function indicates that the oscillator frequency is proportional to the square root of the eluate conductivity.

The development of microbore and capillary high-performance liquid chromatography (h.p.l.c.) has generated a requirement for detectors with low dead-volumes. Knox and Gilbert [1] reasoned that the volume of a detector in capillary h.p.l.c. should be less than one-half the standard deviation of a typical peak volume, which dictates a detector volume of about 10 μl for an open microbore capillary of 10 μm internal diameter (i.d.). The minimum dead-volume requirement is somewhat less for packed microcapillaries and considerably less restrictive for microbore columns. Scott and Kucera [2] showed that 1-μl detection cells would be adequate for typical microbore columns, typically 1 mm i.d., whereas smaller columns and packed microcapillaries would require detectors of ca. 100 nl internal volume.

Miniaturization of existing detectors can provide a solution to the problems of microcolumn h.p.l.c. detection, although the small cell volumes have caused some engineering problems. Several common detectors have been miniaturized to this end, including u.v. spectrophotometric [3—5], fluorescence [6] and electrochemical devices [7].

Previous work in this laboratory [8—12] has shown that conductivity [9], permittivity [8, 10, 11] and permittivity simultaneously with conductivity [12] can provide very useful analytical information in the detection of polar materials containing no u.v. chromophore. Although the cell volume used in

0003-2670/85/$03.30

permittivity and conductivity measurements in that work could be as little as 1—2 μl, it was considered that a miniaturized detection cell would be useful for microcolumn h.p.l.c. Engineering a miniaturized cell in the volume range 10—100 nl becomes prohibitively expensive and the approach adopted in this work was to make a cell with a volume confined not mechanically but electrically by the sensor itself.

Three cell designs were tested: two non-intrusive and one intrusive. It was assumed that the eluting medium could be directed into narrow (0.15—1 mm i.d.) tubes made of PVC, PTFE or glass. The non-intrusive detectors comprising a coil or a parallel ring capacitor were fitted round this tube; for the intrusive cell, two wires were pushed through the side of a plastic tube in antiparallel configuration (Fig. 1).

The use of radiofrequency Q-meters with both capacitance and inductance cells is well known in the application of high-frequency titrations and oscillometry. Toyoda [13] outlined the theory of operation of these cells and investigated the inductively-coupled Q-meter technique, considering the Q changes provided by the axial flow of aqueous liquids through a coil. Johansson et al. [14] demonstrated the use of a high-frequency capacitance cell for the continuous monitoring of taurine- and glycine-conjugated bile acids separated by reverse-phase partition chromatography. Jackson [15] clamped two aluminium electrodes, 1 mm apart, around the end of a glass column of Sephadex. A 1—10 MHz r.f. coupling technique was used and a response to 1 ng of sodium chloride was claimed, although the noise level was apparently ten times this response.

THEORETICAL MODEL OF THE OSCILLATOR RESPONSE WITH RESPECT TO CONDUCTIVITY AND PERMITTIVITY CHANGES IN THE CELL

The three detection cells used were incorporated into the tank circuits of high-frequency oscillators. A change in the permittivity of the medium enclosed by the cell will result in a change in the cell capacitance and hence in the resonant frequency of the oscillator. A change in the conductivity of the

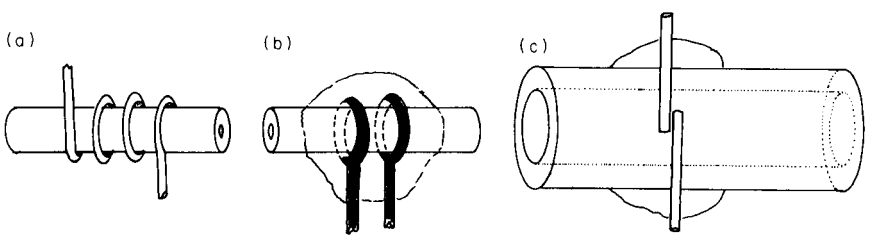

Fig. 1. (a) Coil cell made of PTFE tube (0.3 mm i.d., 1.5 mm o.d.) with 0.5 mm diameter silver-plated copper wire wrapped at 10-mm spacing. (b) Parallel-ring cell made of PTFE tube (0.15 mm i.d., 1.5 mm o.d.) with 0.4 mm diameter silver-plated copper wire rings, 0.5 mm apart, held by epoxy resin. (c) Intrusive two-wire cell made of PVC tubing (1.5 mm i.d., 2 mm o.d.) with 0.4 mm diameter silver-plated copper wire inserted as indicated and held by epoxy resin.

medium may also influence the oscillation frequency. In the coil capacitor (Fig. 1a), the coil acts both as the inductive element and the varying capacitive element in the oscillator circuit. In this respect it differs from the two-ring capacitor and two-wire capacitor, where the inductive element is a separate inductor, not influenced by either permittivity or conductivity alterations in the cell. Apart from this, the modelling of the circuits containing the three detector elements is similar.

Toyoda [13] modelled a circuit comprising a coil, inside which is a stream of conducting liquid (Fig. 2a). It is on this description that the present circuit is discussed. Lopatin [16] described a similar circuit but his goal was different. The findings of the present interpretation generally agree with and complement both the previous discussions.

In Toyoda's model [13] one can consider the tank circuit (Fig. 2b) as comprising an inductor L in parallel with the cell capacitance, ϵC, where C is the capacitance of the empty cell and ϵ is the permittivity of the medium contained within the cell; ϵ represents the permittivity of the entire medium and is the appropriate summation of the solvent, solute and cell body permittivities. Any series capacitance, C_1, is also in parallel with the inductor as is the total residual parallel capacitance in the resonance circuit. The cell capacitance is shunted by a resistance R which is the reciprocal of the conductivity σ of the medium within the capacitance. If one assumes that the cell body has infinite resistance, this represents the appropriate summation of the conductivities of the solvent and solute media.

For the coil capacitor, in parallel with the inductor L is a resistance of magnitude kLR where k is a constant said to be about 10^3 H^{-1} at h.f./v.h.f., which represents the induced resistance caused by eddy currents in the coil at high frequencies [13]; L and R are as defined above. For the two-ring and two-wire capacitors, the magnitude of R is the resistance of the air gap within the inductor, or that of the inductor former and tuning slug. In either case, it does not represent the conductance of the flow stream and thus is not involved in the circuit model. Indeed, the value kLR will be so high that it can

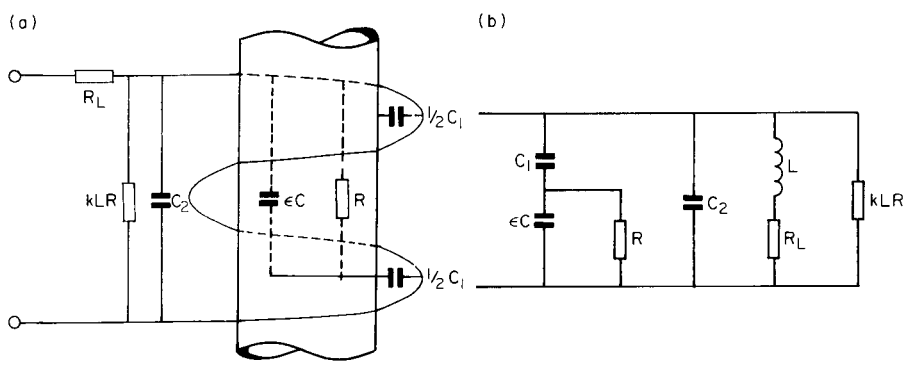

Fig. 2. (a) Toyoda's model for a coil cell [14]. (b) Equivalent circuit of Toyoda's model. For explanation, see text.

be represented by an open circuit and thus be neglected in considering the capacitor sensor circuits.

The aim of the circuit modelling, therefore, is to describe the relationship between the oscillation frequency (f) of the tank circuit represented by $\omega = 2\pi f$, as a function of permittivity ϵ of the medium in the detector cell, and as a function of the conductivity $\sigma = R^{-1}$, where R is the resistance of the liquid contained within the cell. One is therefore seeking to identify $\omega(\epsilon)$, $\omega(\sigma)$ and the response sensitivity $d\omega/d\epsilon$ and $d\omega/d\sigma$.

Rather than derive the relationship for the general case, which is complicated, certain assumptions will be made about the practical situation, i.e., $f \geqslant 15$ MHz ($\omega \geqslant 10^8$ rad s^{-1}) and $R_L < 1$ ohm, $L \approx 1$ μH, $C \approx C_1 \approx 1$ pF and $C_2 \approx 100$ pF. Two different cases are assumed in general: in case 1, ϵ is assumed to be changing, i.e., the detector is monitoring permittivity changes, with $2 < \epsilon < 80$ and $R > 10$ Mohm; in case 2, the detector is monitoring conductivity changes, and $R > 1000$ ohm and $\epsilon \approx 80$ and is constant.

The coil capacitor cell

Case 1. A non-conducting dielectric liquid in the cell volume. The admittance of the circuit, $1/Z$, shown in Fig. 2(b), is

$$\frac{1}{Z} = \frac{\omega^2 C_1^2 R}{1 + \omega^2(\epsilon C + C_1)^2 R^2} + \frac{R_L}{R_L^2 + (\omega L)^2} + \frac{1}{kLR}$$
$$+ j\left\{\frac{\omega C_1[1 + \omega^2 \epsilon C(\epsilon C + C_1)R^2]}{1 + \omega^2 R^2(\epsilon C + C_1)^2} + \omega C_2 - \frac{\omega L}{R_L^2 + (\omega L)^2}\right\} \quad (1)$$

All the terms are defined in Fig. 2(b) and in the text above. Equation 1 can be expressed as $1/Z = A + jB$. At resonance, the reactive component B becomes zero. Assuming that $\omega \geqslant 10^8$ and $R_L^2 \ll (\omega L)^2$, then from eqn. 1

$$\omega C_1\{[1 + \omega^2 \epsilon C(\epsilon C + C_1)R^2]/[1 + \omega^2(\epsilon C + C_1)^2 R^2]\} + \omega C_2 - 1/\omega L = 0 \quad (2)$$

Rearranging this equation and assembling terms in powers of ω yields

$$\omega^2[L(C_1 + C_2) - (\epsilon C + C_1)^2 R^2] + \omega^4 L R^2[C_2(\epsilon C + C_1)^2 + \epsilon C C_1(\epsilon C + C_1)]$$
$$- 1 = 0 \quad (3)$$

Equation 3 can be written as $D\omega^4 + E\omega^2 + F = 0$, where $D = LR^2[C_2(\epsilon C + C_1)^2 + \epsilon C C_1(\epsilon C + C_1)]$, $E = L(C_2 + C_1) - (\epsilon C + C_1)^2 R^2$ and $F = -1$. The roots of this equation are

$$\omega^2 = [-E \pm (E^2 - 4DF)^{1/2}]/2D \quad (4)$$

Setting $(E^2 - 4DF) = G$,

$$G = L^2(C_2 + C_1)^2 - 2L(C_2 + C_1)(\epsilon C + C_1)^2 R^2 + (\epsilon C + C_1)^4 R^4$$
$$+ 4LR^2 C_2(\epsilon C + C_1)^2 + 4LR^2 \epsilon C C_1(\epsilon C + C_1)$$

After extensive rearrangement and simplification by carefully expunging the less significant terms, bearing in mind the values of the component elements, one can identify $G \approx (\epsilon C + C_1)^4 R^4$ as the dominant expression.

Two roots of Eqn. 4 are mathematically possible, but one gives ω^2 as a negative quantity and so can be ignored. The real solution is

$$\omega^2 = [2(\epsilon C + C_1)^2 R^2 - L(C_1 + C_2)]/2LR^2[C_2(\epsilon C + C_1)^2 + \epsilon C C_1(\epsilon C + C_1)]$$

As $L(C_1 + C_2) \ll (\epsilon C + C_1)^2 R^2$ in the first term of Eqn. 3, ignoring the former term and rearranging gives

$$\omega = \{LC_2[1 + \epsilon C C_1/C_2(\epsilon C + C_1)]\}^{-1/2} \tag{5}$$

Differentiation of Eqn. 5 with respect to ϵ yields

$$d\omega/d\epsilon = -\omega^3 LCC_1^2/2(\epsilon C + C_1)^2$$

Equation 5 can be rearranged to give

$$\omega = [LC_2(1 + C_s/C_2)]^{-1/2} \tag{6}$$

where C_s is the series sum of C_1 and ϵC; i.e. $1/C_s = 1/C_1 + 1/\epsilon C$. The significance of the terms is now clear. Without C_1 and ϵC, the resonance circuit would have an oscillation frequency given by $(LC_2)^{-1/2}$. The parallel capacitance C_s perturbs the frequency of oscillation by an amount proportional to the ratio $(C_s/C_2)^{-1/2}$.

Differentiation of Eqn. 6 yields $d\omega/d\epsilon = (\omega^3 L/2)(dC_s/d\epsilon)$. Substituting for ω in this equation by using Eqn. 6 gives

$$d\omega/d\epsilon = -\{2L^{1/2}[C_2(1 + C_s/C_2)]^{3/2}\}^{-1}(dC_s/d\epsilon)$$

This gives a form which is relatively easy to comprehend. The ratio C_s/C_2 would normally be $\ll 1$, giving an equation of the form

$$d\omega/d\epsilon = -2C_2(LC_2)^{-1/2}(dC_s/d\epsilon) \tag{7}$$

The coefficient contains a term $(LC_2)^{-1/2}$ which is closely related to the resonance frequency of the oscillator circuit if $C_2 \gg C_s$. As the circuit frequency of the oscillator is increased, the value of C_2 would necessarily have to be decreased to maintain stable oscillation. One would have in practice, therefore, a sensitivity $d\omega/d\epsilon$ which should increase more than linearly with frequency.

This circuit modelling reveals a number of features of the use of a coil as a non-intrusive permittivity change sensor. The relation between the liquid permittivity and the circuit resonant frequency is non-linear, and the sensitivity $d\omega/d\epsilon$ is influenced by the ratio of the coil capacitance to the total capacitance in the circuit, to the Q of the circuit, and particularly to the ratio $\epsilon C/C_1$ through its influence on $dC_s/d\epsilon$. The sensitivity increases with frequency because the value of the parallel capacitance C_2 will need to decrease as the circuit oscillation frequency is increased. An advantage of v.h.f. operation is that the size of the coil is decreased to millimetre dimensions

and so becomes compatible with analytical requirements for h.p.l.c. detection. This, coupled with the low parallel capacitance, makes the v.h.f.-coil permittivity detector most attractive.

Case 2. A conducting liquid of constant dielectric constant in the cell volume. Equation 3 can be rearranged in terms of R

$$R^{-1} = \omega^2\{(\epsilon C + C_1)[LC_1\epsilon C + LC_2(\epsilon C + C_1)]\}^{1/2}$$

If ϵ is constant, as would effectively be the case for dilute conducting aqueous solutions, the expressions in ϵ can be considered as a constant M, where $M = \{(\epsilon C + C_1)[LC_1\epsilon C + LC_2(\epsilon C + C_1)]\}^{1/2}$, and thence $\omega = (RM)^{-1/2} = (\sigma/M)^{1/2}$. R is the resistance of the stream of liquid within the cell volume, if the reasonable assumption is made that the contribution from the containing tube is zero. Therefore $d\omega/d\sigma = (M\sigma)^{-1/2}/2 = 1/2M\omega$. Clearly, the sensitivity of the coil capacitor towards conductivity changes, $d\omega/d\sigma$, is inversely proportional to the circuit frequency. As will be shown later, however, the dimensions of the coil still need to be compatible with the cell volume, and hence higher-frequency operation is desirable.

Circuit analysis for the parallel-ring and two-wire cells

There are major differences between the equivalent circuit for the coil capacitor and the circuits for the parallel-ring and two-wire capacitors. Both can be represented diagrammatically by Fig. 2(b), but the components have different values and different significance. Primarily, for the latter circuits, the pure resistance kLR refers entirely to the inductor L, and the R in that expression refers to the core material of the inductor which is either air, a coil former or ferrite. In any case kLR can be considered as very large and can be approximated to an open circuit. The value of C_1 is of some significance. Whereas before it arose as a supposed capacitance in series with the cell, in the case of these purely capacitive cells it can have any value which is desired, as it can be introduced as a circuit component. Thus there is another possible difference between the coil and capacitor cells. Whereas the series element C_1 is always present in the coil cell, it can be absent in the capacitive cells. In this case (seen by drawing a short circuit through C_1 in Fig. 2(b) and expunging the element kLR) the admittance of the circuit at resonance is

$$1/Z = [R_L/R_L^2 + \omega^2L^2] + 1/R + j\omega\{\epsilon C + C_2 - [L/(R_L^2 + \omega^2L^2)]\}$$

(cf. Eqn. 1). Therefore, by analysing the circuit as before

$$\omega = [L(\epsilon C + C_2)]^{-1/2} \tag{8}$$

and

$$d\omega/d\epsilon = -C/2L^{1/2}(\epsilon C + C_2)^{3/2} \tag{9}$$

It is to be noted that R does not figure in the reactive part of the admittance, so the conductance of the eluent does not influence the resonance frequency of the circuit (but it will influence the Q).

Contribution of eluate permittivity to the overall value of the permittivity of the medium in the cell

The term ϵ referred to above is the permittivity of the medium sensed by the cell. For the two-wire capacitor this will be the permittivity of the eluent itself with a very minor contribution from the tube material where the wires pass through the tube wall. For the parallel-ring and the coil capacitors, the permittivity will be that of the eluent plus a major contribution from the cell walls.

To a first approximation, if one assumes the field within a coil to be uniform across a diameter and down the length of the coil, the proportion of the total permittivity contributed by the cell wall and eluent will be in proportion to their relative permittivities, (ϵ_t, ϵ_e) and volume fractions (v_t, v_e)

$$\epsilon = v_t\epsilon_t + v_e\epsilon_e \tag{10}$$

where $v_t + v_e = 1$. It is assumed that the liquid and tube walls are isotropically distributed within the entire cell, which is clearly not the case. The equation must be modified to account for the geometric position of each component with regard to changes in the electric field strength in the sensor cell. If this modification is denoted by functions P_t and P_e, which are defined for a known cell geometry and frequency, so that $\epsilon = P_t v_t \epsilon_t + P_e v_e \epsilon_e$, then the contribution of the analyte solute permittivity (ϵ_a) to the total permittivity of the medium within the cell will be a function of the product of its volume fraction, v_a, with its permittivity

$$\epsilon = P_t v_t \epsilon_t + P_e(v_s\epsilon_s + v_a\epsilon_a) \tag{11}$$

where v_s and ϵ_s are the volume fraction and permittivity of the solvent, respectively, and $v_s + v_a = 1$. Generally, for dilute solutions, $v_s \approx 1$ and the small effect from the solute can be represented as a product of dielectric increment, δ, and molar concentration of the species, m_a, in the solvent [17], i.e., $\delta m_a = v_a\epsilon_a$. In Eqn. 11, the product $P_t v_t \epsilon_t$ is a constant, t, for a given cell, and for dilute solutions the equation can be written as

$$\epsilon = t + P_e(\epsilon_s + \delta m_a) \tag{12}$$

Equation 12 makes clear the obvious conclusion that maximum sensitivity to changes of permittivity in the eluate will be achieved if both the tube walls and the solvent have small values of the product of volume fraction and permittivity. This emphasizes that an intrusive capacitive cell will be more sensitive than a non-intrusive cell, and that the permittivity of the cell wall and its volume are critical for a non-intrusive cell. All of these points are borne out by the results of this and previous work.

Shape of the theoretical curves of $\omega(\epsilon)$

It is clear from the preceding sections that in order to plot the theoretical curves of $\omega(\epsilon)$, it is necessary to know not only the true value of all the circuit components but also the values of the coefficients in Eqns. 10—12.

A programme of work to measure all these parameters is being undertaken in these laboratories. The nominal circuit component values of inductance, capacitance and resistance can readily be inserted, however, and the functions described in Eqns. 5 and 8 plotted. These are shown in Fig. 3. It must be emphasized that the scale on the ordinate axis has no significance in terms of measurable frequency change with the practical circuit, and is therefore omitted. The permittivity refers to ϵ as defined in Eqn. 12 and not to the permittivity of the eluate. Only the shapes of the curves are therefore significant in this context but nonetheless they give a guide as to whether or not the theory is a reasonable description of the practice. The results obtained with the coil and parallel-ring cells lie on curves which closely resemble the theoretical curves appropriate to the respective cells.

EXPERIMENTAL

Two different types of oscillator were designed and built. The results obtained were compared with the theoretical model described above.

290-MHz oscillator

A Colpitts-type oscillator was built to oscillate at about 290 MHz (Fig. 4). Frequency was largely dependent on capacitor C_1. By selecting the appropriate value of C_1, the frequency was set at 290 MHz. The oscillator was built on a copper ground plane with all leads kept as short as possible. An output buffer was added to the oscillator and it was housed in an aluminium die-cast box by using two plastic holders so that there was no electrical connection between the board and the box. This box was placed in another aluminium diecast box containing the battery. All the leads for power and output were connected directly to the oscillator circuit board to eliminate r.f. leakage. The coil and parallel-ring cells (Fig. 1a, b) were used in conjunction with this circuit.

Coil cell. The cell comprised a PTFE tube (0.3 mm i.d., 1.5 mm o.d.)

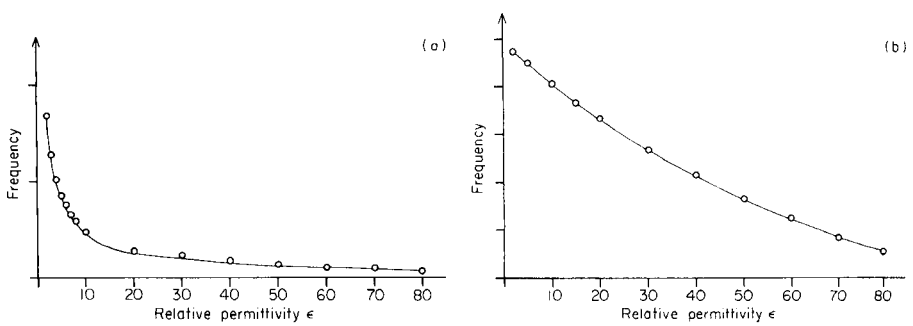

Fig. 3. Theoretical response curves: (a) for the coil cell plotted from Eqn. 5; (b) for the parallel-ring and two-wire cells plotted from Eqn. 8. (—) Theoretical curves based on selected constants; (○) experimental points.

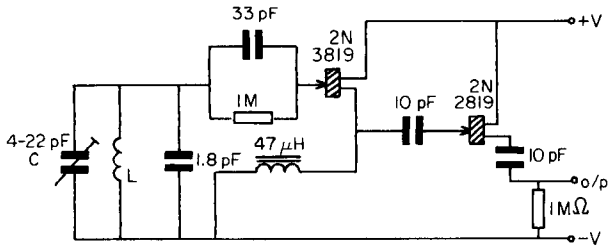

Fig. 4. Circuit diagram of the 290-MHz oscillator. (L is 2 turns of 0.5 mm diameter silver-plated copper wire. For the coil cell, the eluate was passed through the coil in a PTFE tube. For the parallel-ring and two-wire cells, the inductor was left empty and the cell was wired in parallel to C.)

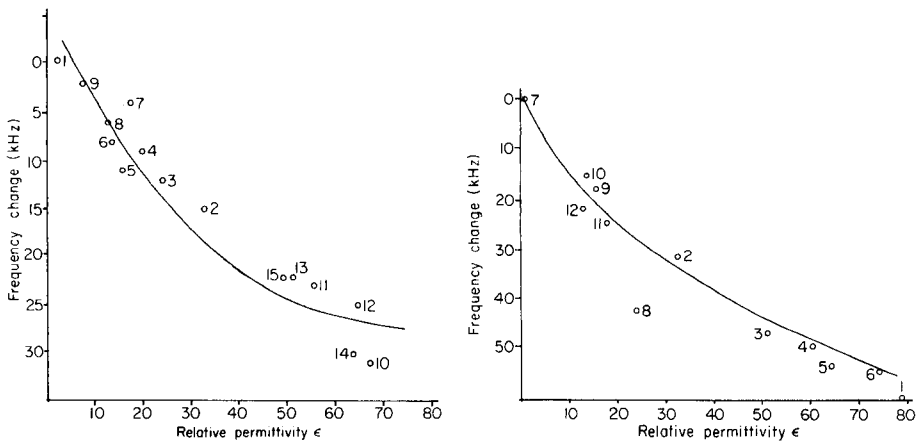

Fig. 5. Relationship between the frequency change (compared to hexane) and permittivity of samples for a coil cell at 290 MHz: (1) hexane; (2) methanol; (3) ethanol; (4) propan-1-ol; (5) butan-2-ol; (6) pentan-1-ol; (7) 2-methylpropan-1-ol; (8) benzyl alcohol; (9) 1,1,1-trichloroethane; (10) 25% methanol in water; (11) 50% methanol in water; (12) 25% ethanol in water; (13) 50% ethanol in water; (14) 25% propanol in water; (15) 50% propanol in water.

Fig. 6. Relationship between frequency change (compared to hexane) and permittivity of samples for a two-ring cell at 290 MHz. (1) water; (2) methanol; (3) 60% methanol in water; (4) 40% methanol in water; (5) 30% methanol in water; (6) 10% methanol in water; (7) hexane; (8) ethanol; (9) butan-2-ol; (10) pentan-1-ol; (11) 2-methylpropan-1-ol; (12) benzyl alcohol.

around which was wrapped two turns of 0.5-mm diameter silver-plated copper wire over a length of 1 cm. The coil was the frequency-determining element of the 290-MHz Colpitts oscillator and the cell volume was ca. 0.7 μl. The frequency response of the circuit with this cell was measured by passing liquids of known permittivity through the coil, via the PTFE tube. The response curve (Fig. 5) is of the same shape as the theoretical curve shown in Fig. 3(a), supporting the view that the theory is valid. The effect of flow rate over the range 0.1—10 μl min^{-1} was negligible.

Parallel-ring, non-intrusive capacitive cell. Two separate loops of silver-plated copper wire, 0.4 mm diameter, were wrapped 0.5 mm apart around a 1.5 mm o.d., 0.15 mm i.d. PTFE tube, and the assembly was set in epoxy resin. The response of the cell to liquids of different permittivity revealed a non-linear relationship between permittivity and the change in frequency (Fig. 6). The oscillator frequency dependence on permittivity measured as for the coil cell was found closely to resemble the predicted dependence shown in Fig. 3(b).

A 9-nl cell was constructed to this design and the response to various solvents was measured. The results are shown in Table 1. The oscillator was noisy when used with this cell (ca. 2 kHz peak-to-peak noise), so that overall the arrangement was unsatisfactory for low concentration measurements, although the small volume and non-intrusive nature of the cell were attractive.

The non-intrusive coil and two-ring cells coupled with the 290-MHz oscillator were clearly unable to provide the sensitivity required for h.p.l.c. This was due as much to the instability of the v.h.f. oscillator as to the relatively small contribution of the eluate permittivity to the permittivity sensed by the cell (Eqn. 12).

The 20-MHz Franklin oscillator and the intrusive two-wire cell

Franklin oscillators working up to 100 MHz offer remarkable stability over a wide bandwidth and are well suited to this work [8, 10—12]. A circuit operating at 20 MHz was built for this study (Fig. 7). It was constructed on a ground plane by using point-to-point wiring and comprised the oscillator based on Q_1 and Q_2, a buffer stage Q_3, three stages of voltage amplification Q_4, Q_5 and Q_6 and two further buffer stages, Q_7 and Q_8. The circuit was contained in a die-cast box and the h.p.l.c. eluate was passed through the cell, via small openings in the box wall. It was clear that the decrease in oscillator frequency would lead to a decrease in absolute frequency change for a given permittivity change, as a consequence of the increase in circuit component values at the lower frequency. To compensate for this, the two-wire intrusive cell was adopted, as the contribution of cell-wall permittivity and the cell

TABLE 1

Data for frequency changes compared to air for samples with different permittivities when a non-contacting capacitive cell is used [18]

Sample	Change in frequency (kHz)	ϵ at 25°C	Sample	Change in frequency (kHz)	ϵ at 25°C
Distilled water	1055.1	78.54	Butan-2-ol	479.7	17.8
Methanol	698.5	32.63	Pentan-1-ol	462.0	13.9
Ethanol	631.2	24.3	Acetone	441.6	20.7
Propan-1-ol	591.4	20.1	Hexane	195.4	1.89
2-Methylpropan-1-ol	556.0	17.7	Air	0.0	1.00

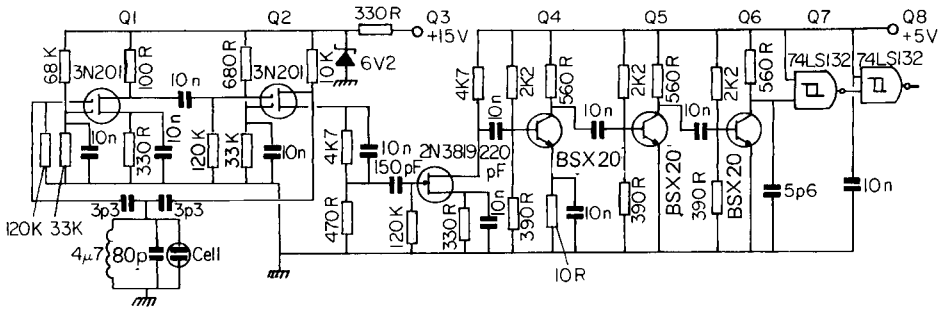

Fig. 7. Circuit diagram of the 20-MHz Franklin oscillator (for explanation, see text).

volume/eluent volume ratio were clearly decreased. It was recognized that the intrusive cell was less attractive in two respects. First, the intrusion would cause flow turbulence; the effect of this would be negligible, however, as the detector was the last part of the chromatographic system and the turbulence would be most apparent downstream. Secondly, the wires could be fouled and corroded by the eluate, this is inevitable with an intrusive design and the advantages of high sensitivity and low cell volume must be weighed against this disadvantage.

The two-wire cell comprised two 0.4-mm diameter silver-plated copper wires mounted in an anti-parallel configuration (Fig. 1c) with 0.1-mm overlap spaced about 0.5 mm apart across a PVC tube (1.5 mm i.d.). The cell volume was estimated to be 40 nl.

Experiments with this cell and the 20-MHz Franklin oscillator gave the results shown in Fig. 8. The general shape of the frequency vs. permittivity response based on literature values [18] was as predicted by Eqn. 8 over the range $\epsilon = 10$—40. The relationship is almost linear over this range.

Evaluation for detection in h.p.l.c.

Both the 290-MHz and the 20-MHz two-wire cell detectors were used in conventional and microbore h.p.l.c. with a variety of eluents, to compare their performance. Primary alcohols and n-alkyl acetates were chosen because they offer a wide range of permittivities, are miscible in methanol/water mixtures and are not easily detected by u.v. absorption.

290-MHz Detector. Solutions in methanol/water (70:30 and 60:40) of the first six primary alcohols were prepared and injected as 20-µl samples onto a 30 cm long, 5 mm i.d. ODS Ultrasphere-endcapped C18 column (5 µm particle diameter). Figure 9 is the resulting chromatogram of 10 µl of the C_1—C_5 mixture in 60:40 methanol/water. A mixture of methyl, ethyl, propyl and amyl acetates was separated on this column in 60:40 methanol/water at 0.9 ml min^{-1}. All the acetates were readily detected.

To calibrate the detector, solutions of methanol, acetone and toluene were made up in methanol/water, injected onto the column, and eluted with

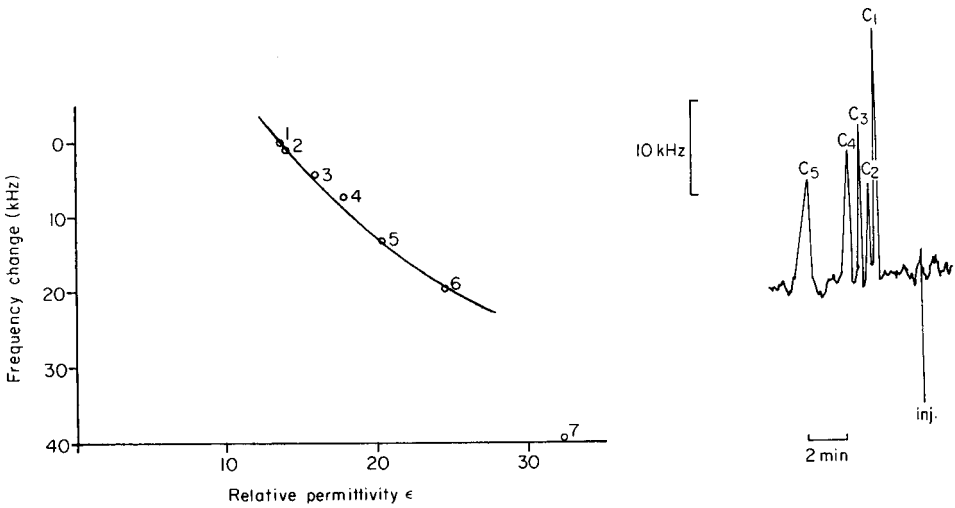

Fig. 8. Relationship between frequency change (compared to benzyl alcohol) and permittivity using the intrusive two-wire cell at 20 MHz: (1) benzyl alcohol; (2) pentan-1-ol; (3) butan-2-ol; (4) 2-methylpropan-1-ol; (5) propan-1-ol; (6) ethanol; (7) methanol.

Fig. 9. Chromatogram of C_1—C_5 primary alcohols (10 μl equivolume mixture, mobile phase 60:40 methanol/water, 290 MHz oscillator, two-wire cell.

the methanol/water mixture. It was found that the detector response was linear for 1—20 μl of injected sample, with gradients of 2.3 Hz nl^{-1} for toluene, 1.9 Hz nl^{-1} for methanol and 1.4 Hz nl^{-1} for acetone. Background noise was typically ±1 kHz, so the overall detection limit of the system was inadequate for low concentration work.

20-MHz Detector. Similar experiments to the above were done with mixtures of primary alcohols and alkyl acetates. Figure 10 shows a chromatogram of the first six primary alcohols. The detector response was linear over the range 0—2.5 μl of injected material. The gradients (Hz nl^{-1}) of the calibration plots were: methyl acetate, 1.13; ethyl acetate, 1.56; propyl acetate, 1.17; amyl acetate, 0.68; methanol, 3.52; ethanol, 1.50; butan-2-ol, 1.49; pentan-1-ol, 0.97. The considerably decreased background noise level is particularly noticeable compared with the 290-MHz oscillator, being typically ±50 Hz. This makes the overall sensitivity adequate for h.p.l.c.

A series of experiments was done with a microbore h.p.l.c. The detector cell was connected to the system in series with a u.v. detector. Figure 11 shows the chromatogram obtained from a solution of 43 μg ml^{-1} of toluene in methanol injected into a 70:30 methanol/water eluent. The column used (10 cm long, 2 mm i.d.) was of Spherisorb 5.5 ODS2 (5 μm particle diameter). It can be seen that the u.v. detector does not indicate the presence of methanol, whereas the permittivity detector shows methanol and toluene. The response to methanol and toluene was linear up to 5 μl of sample

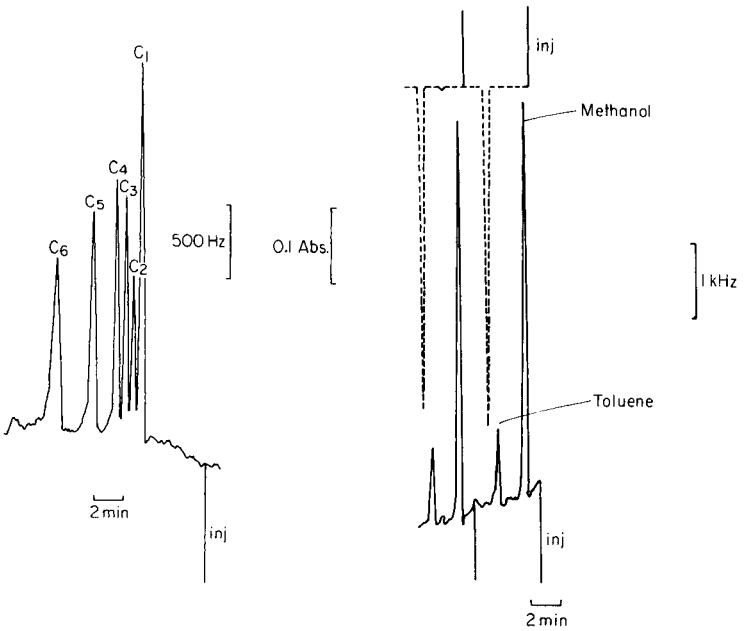

Fig. 10. Chromatogram of C_1—C_6 primary alcohols (10 μl equivolume mixture, mobile phase 70:30 methanol/water, 20-MHz oscillator, two-wire cell).

Fig. 11. Chromatograms of 10 μl of 43 μg ml^{-1} toluene in methanol with 70:30 methanol/water eluent at 1 ml min^{-1}; (—) permittivity detector; (---) u.v. detector.

injected. The toluene response (frequency change in Hz) over this range was given by 4.6 X ng of toluene.

CONCLUSIONS

Different designs of cells and two oscillator types and frequencies have been tested. Overall, operation of an intrusive, two-wire capacitive cell as part of a 20-MHz Franklin oscillator is the best combination for microbore h.p.l.c., giving a higher signal/noise ratio and a cell volume of ca. 40 nl. Although theory predicts an increase in sensitivity with rise in frequency (Eqns. 7 and 9), this is not achieved in practice. Increased circuit noise and instability causes a degradation in signal/background ratio at higher frequencies. This and other work [12] suggest that the region 20—30 MHz may offer the best signal/noise ratio at present. Of the other two cell designs, the parallel loop offers the more attractive compromise between cell volume and sensitivity. The coil-capacitive cell may well find useful application in monitoring of flow streams on a larger scale and has the unique property of being able to sense conductivity changes directly related to frequency.

The theoretical model developed to describe the detector response was

found to be in good qualitative agreement with the practical results. Work is now in progress to relate quantitatively circuit component values and cell geometry to both theoretical and observed detector response. It is believed that optimization of cell design and circuit construction will decrease background noise and drift to yield improvements in sensitivity. This will result from semiconductors with lower noise, temperature-compensated circuit elements and optimized layouts.

This work shows that measurements of permittivity change offer an attractive method of detection for microbore and conventional h.p.l.c., offering reasonable sensitivity with small cell volume and general response characteristics. When combined with the conductivity and temperature-correction systems developed earlier [11, 12], the general approach offers a versatile detection system for liquid chromatography.

A. H. was supported by the S.E.R.C., and F. B. by the Algerian Government. We are grateful to Shell Biosciences Ltd., Sittingbourne, for the loan of equipment and laboratory facilities.

REFERENCES

1 J. H. Knox and M. J. Gilbert, J. Chromatogr., 186 (1979) 405.
2 R. P. W. Scott and P. Kucera, J. Chromatogr., 169 (1979) 51.
3 T. Tsuda and M. Novotny, Anal. Chem., 50 (1978) 632.
4 T. Tsuda, K. Hibi, T. Nakanishi, T. Takenchi and D. Ishii, J. Chromatogr., 158 (1978) 227.
5 Y. Hirata, M. Novotny, T. Tsuda and D. Ishii, Anal. Chem., 51 (1979) 1807.
6 Y. Hirata and M. Novotny, J. Chromatogr., 186 (1979) 521.
7 Y. Hirata, P. T. Lim, M. Novotny and R. M. Wightman, J. Chromatogr., 181 (1980) 287.
8 J. F. Alder and A. Thoër, J. Chromatogr., 178 (1979) 15.
9 J. F. Alder and P. K. P. Drew, Anal. Chim. Acta, 110 (1979) 325.
10 J. F. Alder, P. K. P. Drew and P. R. Fielden, J. Chromatogr., 212 (1981) 167.
11 J. F. Alder, P. K. P. Drew and P. R. Fielden, Anal. Chem., 55 (1983) 256.
12 J. F. Alder, P. R. Fielden and A. J. Clarke, Anal. Chem., 56 (1984) 985.
13 S. Toyoda, Bull. Chem. Soc. Jpn., 33 (1960) 504; 34 (1961) 944.
14 G. Johansson, K. J. Karrman and A. Norman, Anal. Chem., 30 (1958) 1397.
15 A. Jackson, J. Chem. Educ., 42 (1961) 447.
16 B. A. Lopatin, Conductivity and Oscillometry, Israel Programme for Scientific Translation, Jerusalem, 1971.
17 G. Oster, J. Am. Chem. Soc., 68 (1946) 2036.
18 A. A. Maryott and E. R. Smith, National Bureau of Standards Circular 514, August 10, 1951.

Analytica Chimica Acta, 174 (1985) 259—268
Elsevier Science Publishers B.V., Amsterdam — Printed in The Netherlands

DETERMINATION OF TRACES OF LEAD AND COPPER AFTER PRECONCENTRATION ON IMINODIACETIC ACID-CELLULOSE FILTERS
An Approach to Lead and Copper Speciation

M. C. GENNARO*, E. MENTASTI, C. SARZANINI and C. BAIOCCHI

Dipartimento di Chimica Analitica, Università di Torino, Via P. Giuria 5, 10125 Torino (Italy)

(Received 15th November 1984)

SUMMARY

The effects of some organic acids with different complexing ability (oxalic, malic, citric, iminodiacetic and ethylenediaminetetraacetic acids) on the preconcentration and determination of lead(II) and copper(II) were investigated. A chelating material consisting of iminodiacetic acid chemically bound to a cellulose substrate was found effective for the preconcentration and determination of traces of Pb(II) and Cu(II) in the presence of organic material, and overcame various interference effects. The metal uptakes on the treated filter are strictly related to the competing effects (concentration and chelating strength) of the different ligands investigated. The results can be arranged in different classes which may be useful in studies of trace metal speciation.

When metals at trace levels are determined in liquid samples, the presence of organic components is generally indicated as being responsible for important interference effects. For example, when anodic stripping voltametry is used to evaluate metal contents in natural waters, the organic matter can adsorb on the electrode, giving rise to unpredictable effects on the peak current [1, 2]. When absorption or emission spectrometric techniques are used, fluctuating results can be obtained for metal contents that are neither reproducible nor accurate.

With plasma spectrometry, interference effects may arise during sample nebulization, thermal decomposition and atomization processes in the flame, because matrix components produce variations in the physical properties of the sample solution or in the excitation conditions in the plasma. Metal atoms can be involved, at high flame temperatures, in the formation of oxides, sulphides, carbides, etc. and in volatile complexes that can be stable at the temperature of the flame. Interferences deriving from organic components can be very serious and their effect on measurements is not predictable, owing to the great variety of possible collateral reactions, which may cause poor accuracy and/or reproducibility [3—5]. The organic components in the sample itself often also behave as ligands towards metals, giving rise to different complexation equilibria.

0003-2670/85/$03.30

In determinations of trace metals, the preconcentration techniques necessary to raise the metal concentrations to easily measurable levels must be regarded as essential to the analysis. High preconcentration factors are generally achieved by the use of chelating materials which fix metal ions from their dilute solutions. However, when this procedure is used, competitive equilibria between complexation with the chelating materials and complexation with ligands in the sample must be taken into account.

In this paper, the effects of organic acids with different complexing abilities on the preconcentration and determination of traces of lead(II) and copper(II) ions are reported. Lead and copper(II) were considered, not only because of their interest from a toxic point of view but also because these metals are generally less labile in real samples [6—9]. The ligands considered were oxalic, malic, citric, iminodiacetic and ethylenediaminetetraacetic acids at concentrations ranging between 10^{-6} and 10^{-2} M; the mole ratios of metal to ligand were between 0.5 and 1000, at different pH values. The interference effects on plasma emission spectrometric measurements are described, as well as competitive equilibria in the preconcentration step when metals are fixed on a chelating material consisting of iminodiacetate groups chemically bonded on a cellulose substrate. This material was reported previously and characterized with reference to a large series of metal ions [10].

EXPERIMENTAL

Materials and apparatus

The supporting material for the chelating iminodiacetic groups was commercial Whatman-41 cellulose filter discs, cut to a suitable size (47-mm diameter) for a Millipore filtration system. The preparation, described in detail previously [10], involves chlorination of cellulose with phosphorus oxytrichloride in dimethylformamide (DMF) as solvent, and subsequent replacement of the chlorine groups with iminodiacetate groups, through reaction at 105—110°C for ca. 150 min in a saturated solution of disodium iminodiacetate in DMF.

Metal stock standard solutions for atomic absorption (1000 mg l^{-1}; C. Erba) were diluted as required. All chemicals were analytical-grade reagents. Water was double-distilled in quartz. All glassware and polyethylene and polypropylene vessels were thoroughly cleaned by soaking in 6 M nitric acid and repeatedly rinsing with twice-distilled water.

A d.c. plasma Spectraspan IV (SMI, Andover, MA) was used for the emission measurements. Two-point calibrations (high and low standards) were used. The most suitable wavelengths were chosen for measurements of each metal in mixtures; accuracy and reproducibility of measurements were evaluated. The pH was measured with an Orion 811 pH meter, equipped with glass and calomel electrodes. Adjustable Eppendorf pipettes and Micrometric Instrument precision syringes were used for solution preparation.

Calculations

All calculations for distribution of the complex species in solutions containing the metal and the ligands, as well as the competitive equilibria for metal complexation between the ligands in solution and the iminodiacetic acid (IDA) bound to the cellulose substrate, were done on an SEL 32/27 computer, connected to a Teleray-100 terminal and an OKI-84 printer. A program called BASECO [11] was used; this can process equilibrium calculations for up to fifty complexes formed by up to twenty components. The original program was modified in order to obtain a plot of the complex species concentrations as a function of pH for each system.

RESULTS AND DISCUSSION

In order to evaluate the type and extent of interferences produced by organic ligands on the copper and lead measurements by plasma emission spectroscopy, solutions containing each metal (5.00 mg l^{-1}) and each of the considered ligands at concentrations up to 8.0×10^{-2} M were prepared at different pH values. The metals were quantified at the appropriate wavelength against standard solutions containing only the metals at the same pH values.

In agreement with the literature, the emission signals were unstable and the metal contents were higher than expected when the organic acid was present at concentrations higher than 10^{-4} M. This situation was observed to practically the same extent for all the ligands investigated for both lead and copper. Emission at the relevant wavelength by the ligand itself was checked by examining solutions containing only the ligands at concentrations of $>10^{-4}$ M; the signal intensity did not increase proportionally with increasing ligand concentration. Roughly, positive errors as great as 50% and precision no better than 10% were obtained from all the measurements. This effect could be overcome only when the metal standard solutions, against which the metal in the sample was measured, contained the same ligand at the same concentration as in the sample solution. The standard additions method was therefore tested. Solutions containing 0.50 mg l^{-1} copper and 7.87×10^{-2} M citric acid were prepared, with four additions of standard copper up to 5.00 mg l^{-1}, and adjusted to pH values of 2.6 or 7.0 prior to measurement of copper. The data obtained did not depend on pH, so that all data were introduced in the least-squares regression, which gave a result of 0.54 mg l^{-1} copper, i.e., an error of about 8%, against a 20% error obtained by direct measurement. Thus, although the standard additions method improves matters, a technique for removing organic compounds from the matrix would be preferable.

For this purpose, the cellulose filter modified with IDA groups seems suitable, provided that conditions can be found in which the metals can be quantitatively fixed and removed from any complexes formed with the organic components of the matrix. The technique is simple, consisting only of passing the sample through the filter and then eluting the metal with a suitable

reagent. It should not be necessary to know the matrix composition previously, because the metal is measured in a solution containing only the metal ion and the eluent. Further, preconcentration of the metal will also be possible.

The technique was applied to solutions containing lead(II) or copper(II) and oxalic, malic, citric, iminodiacetic (IDA) or ethylenediaminetetraacetic (EDTA) acid. These acids show different complexing ability towards the metals. Concentrations were up to 8.0×10^{-2} M, in molar metal-to-ligand ratios from 1:0.5 to 1:1000, at different pH values; the filters were conditioned at the same pH value. For the systems investigated, release was always obtained with 10.00 ml of 1.0 M hydrochloric acid; release efficiency was checked by measuring the metal both on the eluted acid solution and on the filtering solution; the latter results were calculated from calibrations obtained with metal standard solutions containing the appropriate ligand. The large collection of data showed the competition for the metal which takes place between the immobilized IDA and the ligand in the solution.

As examples, some typical results for metal uptake are reported; the solutions examined contained molar concentration ratios (L being the ligand) $C_L/C_{Pb} = 1$ or 1000 (Table 1) or $C_L/C_{Cu} = 1$ (Table 2). It can be seen (Table 1) that lead is quantitatively retained on the filter from solutions containing a ligand-to-metal ratio of 1, when the ligand is malic, oxalic, citric and/or IDA; but with EDTA, which has a much higher complexing ability, competition occurs even at a ligand-to-metal ratio of 0.5. Under the same conditions (Table 2), the copper uptake is lower than that of lead and EDTA is again the most competitive of the ligands.

As expected, lead retention on the filter is generally lower when the competing ligand is present at 1000-fold concentrations with respect to the metal

TABLE 1

Uptake of lead(II) on IDA-filters from solutions containing malic acid, oxalic acid, citric acid, IDA or EDTA ($C_{Pb} = 2.41 \times 10^{-5}$ M)

pH	Lead uptake (%)				
	Malic acid	Oxalic acid	Citric acid	IDA	EDTA
$C_L/C_{Pb} = 1$					
3.00	100 ± 1	100 ± 1	100 ± 2	100 ± 1	85 ± 2[a]
5.00	100 ± 1	100 ± 1	100 ± 2	100 ± 1	68 ± 2[a]
7.00	100 ± 1	100 ± 2	100 ± 2	100 ± 1	45 ± 2[a]
$C_L/C_{Pb} = 1000$					
3.00	93 ± 3	50 ± 2	100 ± 4	100 ± 2	0
5.00	71 ± 2		63 ± 3	100 ± 2	0
7.00	62 ± 2	80 ± 2	60 ± 3	87 ± 2	0

[a] $C_L/C_{Pb} = 0.5$.

TABLE 2

Uptake of copper(II) on IDA-filters from solutions containing a ligand (C_L/C_{Cu} = 1; C_{Cu} = 7.87 × 10^{-5} M)

pH	Copper uptake (%)			
	Malic acid	Oxalic acid	Citric acid	EDTA
3.00	100 ± 1	86 ± 1	92 ± 1	5 ± 1
5.00	100 ± 1	96 ± 1	97 ± 1	5 ± 1
7.00	100 ± 1	93 ± 1	93 ± 1	4 ± 1

(Table 1). But retention always exceeds 50% in these systems, and is quantitative when the competing ligand is citric acid (pH 3.0) and, surprisingly, IDA itself (pH 3.0 or 5.0). At first glance, the behaviour of lead with oxalic acid (C_L/C_{Pb} = 1000, Table 1) seems anomalous because the formation constant for the complex is very similar to the values for the malic and citric acid complexes. However, the stability order is maintained when the data are compared via the conditional formation constants. In general, all the uptakes are lower for Cu(II) than for Pb(II); this is surely related to the generally larger formation constants of the copper complexes in the solution.

In order to estimate better the relationship between the percentage uptake on the filter and the stability of the preformed complexes, the species distribution was computed as a function of pH for the same metal/ligand systems. For this purpose, the literature constants [12, 13] of protonation, hydrolysis and complex formation were corrected for ionic strength and the above-mentioned computer program was used to calculate the species distribution, taking into account all the equilibria possible in the solutions to be passed through the modified filter. The comparison between experimental and calculated data confirmed that the more stable the complex species in solution, the lower is the metal uptake on the filter itself. This general picture agrees with literature uptake data obtained on Chelex-100 resin [14, 15]. It is worth emphasizing, however, that high metal uptakes are obtainable even from solutions containing stable complexes. As an example, Table 3 and Fig. 1(b) show the calculated data (charges are omitted and only species present at concentrations $\geq$0.1% are reported) for a solution of 2.41 × 10^{-5} M lead(II) and 2.41 × 10^{-3} M citric acid. Under these conditions (e.g., at pH 7.0), the lead is nearly all complexed as hydroxocitrate, yet the IDA-filter can fix 96% of the total lead present (Fig. 1a), breaking down this complex.

An attempt was then made to calculate the competing equilibria possible between the IDA immobilized on the filter and the various ligands present in the solution. It was assumed as a first approximation that the immobilized IDA acts in the same way as in aqueous solution, producing the same metal complex species with the same stability as in solution. It was also necessary

TABLE 3

Comparison between experimental lead(III) uptake on the IDA-filter from citric acid solution and calculated species distribution in the absence or presence of IDA[a]

pH	Experimental Pb(II) uptake (%)	Calculated species concentrations (%)			
		Citric acid		Citric acid and IDA[b]	
3.00	100 ± 3	Pb	96.5	Pb	96.5
		PbA	0.2	PbA	0.2
		PbHA	2.2	PbHA	2.2
		PbH_2A	1.1	PbH_2A	1.1
				PbIDA	0.2
				PbHIDA	0.2
5.00	100 ± 3	Pb	10.8	Pb	10.5
		PbA	49.0	PbA	47.4
		PbA_2	1.8	PbA_2	1.7
		PbHA	5.8	PbHA	5.6
		$Pb(HA)_2$	0.1	$Pb(HA)_2$	0.1
		$Pb(OH)_2A$	32.4	$Pb(OH)_2A$	31.3
				PbIDA	3.4
7.00	96 ± 3	PbA	1.5	PbA	1.5
		PbA_2	0.3	PbA_2	0.3
		Pb(OH)A	97.9	Pb(OH)A	96.2
		$Pb(OH)_2A$	0.3	$Pb(OH)_2A$	0.3
				PbIDA	1.7

[a] $C_{Pb} = 2.41 \times 10^{-5}$ M and $C_A = 2.41 \times 10^{-3}$ M (A = citric acid) in all cases. [b] $C_{IDA} = 3.49 \times 10^{-4}$ M.

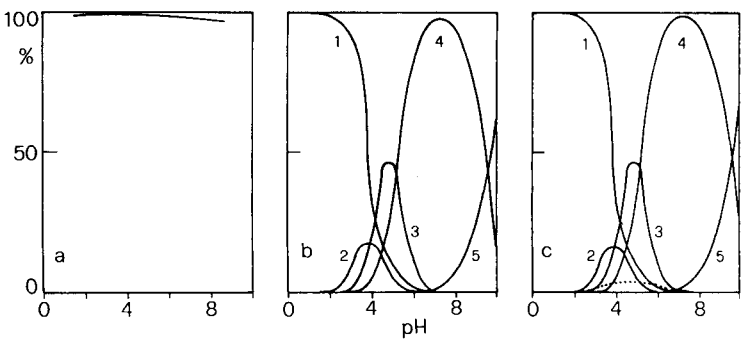

Fig. 1. Comparison between experimental Pb(II) uptake on the IDA-filter (a) and calculated species distribution in absence (b) and in presence (c) of IDA. Curves: (1) Pb; (2) PbHA; (3) PbA; (4) Pb(OH)A; (5) $Pb(OH)_2A$; (···) PbIDA. The concentrations are the same as in Table 3 ($C_L/C_{Pb} = 100$).

to assign a molar concentration to the ligand bound on the cellulose. The amount of IDA fixed on the filter cannot be measured directly and it was assumed to correspond to the number of micromoles of the metal for which the filter showed the highest capacity (i.e., lead, 34.9 μmol of which can be

fixed on a filter). This amount was then referred to the total volume of the solution passed. Comparison of the data so calculated with the experimental uptakes showed that the latter were greater than would be expected if one compares the stability of the IDA-filter complexes with that of the preformed complexes in the various solutions of metal and ligand. Table 3 and Fig. 1(c) report the calculated data for a solution containing lead and citric acid as before, but with IDA present at the concentration evaluated for the filter. For pH 7.0, at which the experimental lead uptake is 96% of the total lead, the calculated data indicate that only 1.7% of the total lead should be present in solution as the IDA complex. The possibility was considered that the hypothetical assignment of the concentration of IDA bound on the filter might not be valid. Therefore, this IDA concentration was calculated by successive approximations to the value which best fitted the experimental uptake data. This calculation suggested that it would be necessary to consider an IDA concentration of about 2 M in the case of lead uptake and of 0.02 M for copper. Because the same value is obviously to be expected, regardless of the metal, another interpretation is suggested in order to explain the greater chelating ability shown by IDA bound to cellulose. The fixation equilibria are established in a heterogeneous phase, thus it should be possible to assign greater formation constants to such complexes than those relevant to solutions. Accordingly, concentrations and other conditions were kept constant and the values of constants of the 1:1 complex were progressively varied to fit the experimental shapes.

Figures 2 and 3 indicate that, by imposing formation constants of 5×10^{12} for the PbIDA complex and 1×10^{12} for the CuIDA complex, the calculated shapes fit the experimental ones. These values, which may be named "observed constants", are also valid when the distribution of complex

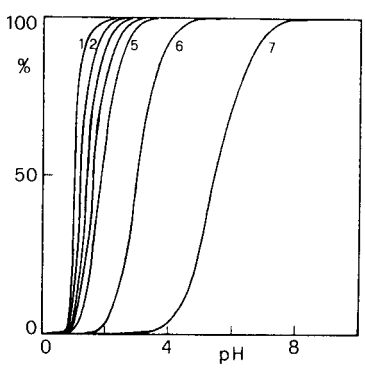

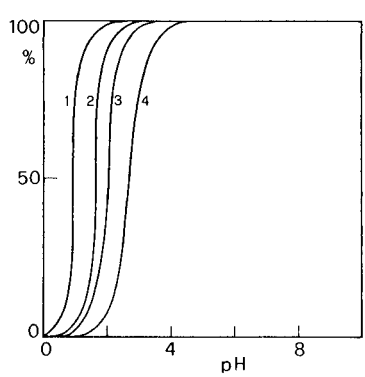

Fig. 2. Distribution of free and bound lead in the presence of IDA for different formation constants: (1) $\log \beta = 14.0$; (2) $\log \beta = 13.0$; (3) $\log \beta = 12.7$; (4) $\log \beta = 12.5$; (5) $\log \beta = 12.0$; (6) $\log \beta = 10.0$; (7) $\log \beta = 7.3$. $C_{Pb} = 2.41 \times 10^{-5}$ M; $C_{IDA} = 3.49 \times 10^{-4}$ M.

Fig. 3. Distribution of free and bound copper in the presence of IDA for different formation constants: (1) $\log \beta = 15.0$; (2) $\log \beta = 13.0$; (3) $\log \beta = 12.0$; (4) $\log \beta = 10.6$. $C_{Cu} = 7.87 \times 10^{-5}$ M; $C_{IDA} = 3.49 \times 10^{-4}$ M.

species in the presence of competing ligands is calculated. As these values are intermediate between those evaluated in solution for the IDA and EDTA complexes, it may be that the IDA groups bound on cellulose assume a structure resembling that of EDTA. The more rigid structure assumed when the IDA groups are immobilized should favour chelation, possibly with formation of a 1:2 complex predominating, two bound IDA groups acting analogously to an EDTA molecule. It is worth noting that both Pb(II) and Cu(II) show formation constants of similar strength for EDTA.

Application to the analysis of real samples

By means of a high-performance liquid chromatographic technique for the separation and determination of organic acids in wines and beverages [16], the content of citric acid in a commercial orangeade was shown to be 2.30 g l^{-1} and that of malic acid 0.20 g l^{-1} (the main acid components). In these conditions, the direct measurement of lead on the orangeade is affected by an intolerable positive error. The use of the IDA-filter was therefore tested. Model solutions containing citric and malic acids as before and 0.200 mg l^{-1} lead were prepared and passed through the filter. After release of lead with 1.0 M hydrochloric acid at a volume ratio of 1:20 to the sample solution, the spectrometric measurement showed a lead recovery of 100.0 ± 0.5%. Results of the same order were obtained when the treatment was repeated on orangeade previously ultracentrifuged, filtered and adjusted to pH 3. The results, which make it possible to exclude the presence of lead at low trace levels in such drinks, confirm that the proposed method can be used to determine traces of lead with good precision and accuracy even in complex matrices.

An approach to speciation

Information regarding metal speciation in natural waters is of great current interest. Experimental procedures, modelling and calculation have been used to estimate the distribution of all the possible complex species in which a metal may be present in a real sample. Experimental data are often based on anodic stripping voltametric (a.s.v.) measurements [6, 15, 17]; the metals are grouped into operational classifications, based on their a.s.v. lability, when measured without any treatment or after uptake on chelating materials (filtration and batch) or acid digestion. Another proposed method [18] of collecting information on the strength of the complexes present in a real sample, and of evaluating apparent formation constants, is to titrate metals with ligands showing different complexing ability.

The results described above concerning metal uptakes from different solutions could be useful in this field of investigation. Tables 4 and 5 list all the experimental results for uptake for lead(II) and copper(II) from the ligand solutions studied. The data are grouped in classes covering different percentage uptake ranges. The inverse relationship between the percentage uptake and the affinity of the ligand for the metal is clear.

TABLE 4

Ranges of percentage uptake of Pb(II) on IDA-filters from solutions containing the indicated metal-to-ligand mole ratios[a]

pH	Lead uptake (%)							
	0	40—50	50—80	80—95	>95			
3.00	PbEDTA 1:10 1:50 1:1000	PbOx 1:1000		PbEDTA 1:0.5 PbMal 1:1000	PbCit 1:1 1:100 1:1000	PbMal 1:1 1:2 1:10 1:50 1:100	PbIDA 1:1 1:100 1:1000	PbOx 1:1
5.00	PbEDTA 1:10 1:50 1:1000		PbCit 1:1000 PbMal 1:1000 PbEDTA 1:0.5		PbCit 1:1 1:100	PbMal 1:1 1:2 1:10 1:50 1:100	PbIDA 1:1 1:100 1:1000	PbOx 1:1
7.00	PbEDTA 1:10 1:50 1:1000	PbEDTA 1:0.5	PbCit 1:1000 PbMal 1:1000	PbOx 1:1000 PbIDA 1:1000	PbCit 1:1 1:100	PbMal 1:1 1:2 1:10 1:50 1:100	PbIDA 1:1 1:100	PbOx 1:1

[a] $C_{Pb} = 2.41 \times 10^{-5}$ M; Ox = oxalic acid, Mal = malic acid, Cit = citric acid.

TABLE 5

Ranges of percentage uptake of Cu(II) on IDA-filters from solutions containing the indicated metal-to-ligand mole ratios[a]

pH	Copper uptake (%)								
	0	<25	25—50	50—75	75—90	90—95	>95		
3.00	CuEDTA 1:300	CuOx 1:1000 CuEDTA 1:1	CuIDA 1:300 CuEDTA 1:0.5	CuCit 1:30 1:300 1:1000	CuIDA 1:30 CuOx 1:1 CuMal 1:30 CuMal 1:300	CuCit 1:1 1:10	CuMal 1:0.3 1:0.6 1:1 1:15		
5.00	CuEDTA 1:300	CuEDTA 1:1 CuCit 1:1000	CuOx 1:1000 CuCit: 1:300 CuEDTA 1:0.5 CuIDA 1:300	CuIDA 1:30	CuMal 1:300		CuMal 1:0.3 1:0.6 1:1 1:15 1:30	CuCit 1:1 1:10 1:30	CuOx 1:1
7.00	CuEDTA 1:300	CuEDTA 1:1 CuCit 1:300 1:1000	CuOx 1:1000 CuIDA 1:300 CuEDTA 1:0.5 CuCit 1:30	CuCit 1:10 CuMal 1:30 1:300	CuIDA 1:30	CuOx 1:1 CuCit 1:1	CuMal 1:0.3 1:0.6 1:1 1:15		

[a] $C_{Cu} = 7.87 \times 10^{-5}$ M; abbreviations as for Table 4.

If a real sample of known total metal concentration is passed through the IDA-filter and the filtrate and eluate are subjected to emission spectrometry, then the retained and unretained fractions of metal may be evaluated with the sensitivity and selectivity offered by the spectrometric process. The relative amounts of metal fixed and unretained are a function of the stability of the pre-existing complexes formed between the metal and the organic material in the sample. By comparing the percentage uptakes with data such as those listed in Tables 4 and 5, it becomes possible to obtain information, if not for a specific ligand, at least for the coordinating ability of the organic substances in the sample, i.e., the combined effect of the conditional formation constant of the complex formed and the concentration of the ligand. Under favourable conditions, e.g., a choice between two ligands of different chelating strength, it might be possible to identify the ligand itself. In the procedure suggested, there is no pH adjustment, and sample solutions having pH within the range 3—7 are treated directly. Speciation equilibria in real samples would obviously be upset by any pH adjustment.

The preparation of other chelating materials with different capacities and selectivities towards metals would enable other classifications to be identified, each perhaps being characterized by narrower ranges of apparent constants.

REFERENCES

1 T. M. Florence and G. E. Batley, Crit. Rev. Anal. Chem., 9 (1980) 219.
2 T. M. Florence, Talanta, 29 (1982) 345.
3 J. Komarex and L. Sommer, Talanta, 29 (1982) 159.
4 M. Thompson, M. H. Ramsey and B. J. Coles, Analyst, 107 (1982) 1286.
5 M. W. Blades and G. Horlick, Spectrochim. Acta, Part B, 36 (1981) 881.
6 P. Figura and B. McDuffie, Anal. Chem., 52 (1980) 1433.
7 R. N. Sylva, Water Res., 10 (1976) 789.
8 J. C. Duinker and C. J. Kramer, Mar. Chem., 5 (1977) 207.
9 M. S. Shuman and L. C. Michael, Environ. Sci. Technol., 12 (1978) 1069.
10 M. C. Gennaro, C. Baiocchi, E. Campi, E. Mentasti and R. Aruga, Anal. Chim. Acta, 151 (1983) 339.
11 S. Sammartano and C. Rigano, personal communication.
12 L. G. Sillen and A. E. Martell, Stability Constants of Metal Ion Complexes, Spec. Publications No. 17, 25, The Chem. Soc. (London) 1964, 1971; D. D. Perrin, Stability Constants of Metal Ion Complexes, Part B, Pergamon Press, Oxford, 1979.
13 A. E. Martell and R. M. Smith, Critical Stability Constants, Vol. 1, Plenum Press, New York, 1976.
14 P. Figura and B. McDuffie, Anal. Chem., 51 (1979) 129.
15 T. M. Florence and G. E. Batley, Talanta, 23 (1976) 179.
16 E. Mentasti, M. C. Gennaro, C. Sarzanini, C. Baiocchi and M. Savigliano, J. Chromatogr., 322 (1985) 177.
17 T. M. Florence, Anal. Chim. Acta, 141 (1982) 73.
18 J. Lee, Water Res., 17 (1983) 501.

Analytica Chimica Acta, 174 (1985) 269—277
Elsevier Science Publishers B.V., Amsterdam — Printed in The Netherlands

SPECIATION OF BOUND AND FREE METALS EVALUATED FOR LOBSTER DIGESTIVE GLAND EXTRACTS

R. D. GUY*

Department of Chemistry, Dalhousie University, Halifax, Nova Scotia, B3H 4J1 (Canada)

C. L. CHOU and J. F. UTHE

Fisheries and Environmental Sciences, Department of Fisheries and Oceans, Halifax Laboratory, Halifax, Nova Scotia B3J 2S7 (Canada)

(Received 20th March 1985)

SUMMARY

A simple method is described for the speciation of metal ions in biological extracts with a short desalting gel-filtration column. The system was optimized for the eluent and gel type to provide accurate free metal ion levels and minimum processing times. The four separation media studied were Sephadex G25, Bio-Gel P-6DG, controlled pore glass CPG40, and Fractogel HW40F. The best medium was the Fractogel HW40F because it was not compressible and allowed a pump to be used to obtain uniform flow rates. The eluent was 0.10 M ammonium acetate/0.01 M citric acid adjusted to pH 7.0. This eluent minimized ion/gel interactions and gave a lower salt content relative to other possible eluents. The separation time was 10 min per sample per metal ion of interest. The detection limits relative to the mass of wet tissue for the column/flame spectrometer system were 0.80 $\mu g\ g^{-1}$, 0.80 $\mu g\ g^{-1}$, and 1.6 $\mu g\ g^{-1}$ for zinc, cadmium and copper, respectively. The method is evaluated for a lobster digestive gland extract; the methodology should be applicable to other systems containing nonlabile metal species.

Divalent metal ions in biological material can be found in complexes with both high and low molecular weights. Rabenstein and Isab [1], for example, used nuclear magnetic resonance (n.m.r.) techniques to show that zinc in human erythrocytes is bound to both the peptide glutathione and the protein hemoglobin. Many animal species have been shown to produce a cadmium-binding protein when exposed to cadmium. This low-molecular-weight cytoplasmic protein (6000—10,000 daltons) with high sulphydryl and metal content was first isolated by Margoshes and Vallee [2]. The speciation of metal ions in biological systems is important because the distribution of metal ions in biological extracts can be used to estimate the status of exposure of an animal to chemical toxins. It has been suggested [3], for example, that the toxic effects of cadmium may occur only when a specific cadmium-binding protein is saturated and the cadmium enters the other protein pools. A second reason for the speciation of metal ions in biological samples is the relationship between chemical form and bioavailability [4, 5]. A rapid method for the speciation of metal ions in biological samples would aid in

0003-2670/85/$03.30

bioavailability studies. The speciation method should at least permit differentiation between protein-bound species and free or low-molecular-weight complexes.

Several speciation methods for biological samples have been reported in the literature. These include differential pulse polarography [6], gel-filtration chromatography coupled to a graphite-furnace atomic absorption spectrometer [7], and high-performance gel-permeation chromatography with atomic absorption spectrometry [8].

The procedure described here was developed to differentiate between free and protein-bound cadmium in lobster digestive gland extracts. The aim was to develop a rapid speciation procedure that could be used as a semi-routine monitor of metal distribution in biological extracts with a minimum of sample cleanup. The high-performance gels are relatively expensive and can be contaminated with real extracts so the low-pressure classical gels were studied as a means of doing a simple desalting-type experiment. This desalting experiment can differentiate between free ions and ions bound to medium and high-molecular-weight proteins. The cadmium levels in lobster digestive glands can range from 2 mg kg^{-1} (w/w) to over 500 mg kg^{-1} [9]. This range of cadmium levels suggested that a simple coupling of the column to a flame atomic absorption spectrometer would provide sufficient sensitivity for the determination.

EXPERIMENTAL

Apparatus and materials

The chromatographic system consisted of an Eldex 120S single-piston pump, a Rheodyne Model 50 low-pressure sample injection valve fitted with a 1.0-ml sample loop, a Pharmacia column with C16/40 endpieces and AC-16 flow adapter, and a LKB Uvicord II detector. The chromatographic system was coupled to a Perkin-Elmer model 403 atomic absorption spectrometer fitted with a deuterium arc background corrector and a Perkin-Elmer air/acetylene burner. All connections were made with teflon tubing of 0.8-mm i.d. and 0.5-mm o.d.

Four types of separation media were tested: Sephadex G-25 (medium grade, Pharmacia), Bio-Gel P-6DG (Bio-Rad), Fractogel HW40F (EM Science), and controlled pore glass CPG40 (glycophase, Pierce Chemical Co.).

Procedures

Lobsters (*Homarus americanus*) with high cadmium levels were captured within Belledune Harbour, New Brunswick, a site associated with a lead smelter [9]. The lobsters were transported live to the Halifax Fisheries Research Laboratory, individually packed in open polyethylene bags over wet ice. They were held alive in a sea-water aquarium until use. The intact digestive gland was removed and weighed. A portion (3 g) of fresh digestive gland was immediately transferred to a glass Potter-Elvehjem homogenizer

fitted with a motorized teflon pestle and the rest of the tissue was stored at −90°C. The digestive gland was homogenized with approximately 10 ml of 1.0 M ammonium acetate at pH 7.0 for 30—60 s at the slowest speed. The homogenate was transferred to a 50-ml Nalgene polycarbonate centrifuge tube with 10 ml of fresh acetate and centrifuged three times at 30 000 g for 30 min at 4°C. After each centrifugation, the supernatant liquid and pellet were separated and the liquid was recentrifuged. The final supernatant liquid was filtered through a Millipore fritted disc (Millipore XX-10-025-14) overlaid with one layer of flow adaptor nylon screen (Pharmacia). Systematic studies with this procedure indicated that sample decomposition occurred with time, i.e., the free cadmium content increased and the bound cadmium decreased. This was attributed to degradation of the proteins by proteases present in the lobster digestive gland extract, and was prevented by making the sample 0.01 mM in toluenesulfonyl fluoride, a known protease inhibitor [10].

The filtrates were analyzed for the total metal content by flame atomic absorption spectrometry [9]. Aliquots (1 ml) were injected into the chromatographic system for the speciation experiments. The gel bed was 1.6 × 9.5 cm for each gel. The soft gels (Sephadex G-25 and Bio-Gel P-6DG) were used with gravity flow augmented by the pull of the flame nebulizer. The combination of gravity flow and nebulizer gave a flow rate of 3.5 ml min^{-1}. The Fractogel and controlled-pore glass were used with the single piston pump at a flow rate of 3.5 ml min^{-1}.

RESULTS AND DISCUSSION

Rapid differentiation of free and bound metals in the biological extracts has two requirements. They are complete elution of each metal ion and a reproducible retention time for each metallic species. Complete elution of all added metal is necessary to prevent cross-contamination between standards and samples. Initial studies with Sephadex G25 and an eluent composed of 0.01 M tris(hydroxymethyl)aminomethane (Tris) and 0.10 M ammonium acetate gave complete recovery of copper species but incomplete recovery of cadmium and zinc species. Removal of the Tris and increasing the ammonium acetate to 1.0 M gave complete recovery of cadmium and zinc. A preliminary experiment with the Bio-Gel P-6DG and 1.0 M ammonium acetate gave >95% recovery of cadmium and zinc but the apparent recovery of copper varied from 107 to 145% over a series of injections. In this experiment, a copper and cadmium standard was injected between each lobster extract to serve as calibration. The high recovery for copper was attributed to the lobster extract desorbing copper adsorbed by the gel from the standard copper solutions. The 1.0 M ammonium acetate eluent was not sufficient to elute the free copper(II) ion completely from the gels and cross-contamination of samples would result unless a new eluent was formulated.

Gel-filtration matrices have trace amounts (3—5 μmol g^{-1}) of ion-exchange

groups [11]. The interaction of metal ions with these groups will have two effects in the speciation experiment. The separation will be a combination of two mechanisms, a size separation based upon the pore size of the gel and an ion-exchange separation based on the relative competition between divalent ions and the eluent for the exchange sites. The ion-exchange mechanism will be characterized by an increase in elution volume (relative to the total inclusion volume) and/or tailing of the peaks. A second effect of the groups is the removal of free ions from a finite sample causing a decrease in the free metal ion peak height or area. Figure 1 shows the effect of changing the ionic strength on the elution of free copper from Bio-Gel P-6DG. The shapes of the peaks should be compared with that of free cadmium in the 1.0 M ammonium acetate eluent. The peak shape of the free copper(II) ion improved with an increase of the eluent ionic strength. The effect of chemical form of the ion on the elution of copper(II) ion in 2.0 M ammonium acetate is shown in Fig. 2. Chromatogram A is for copper(II) ion present as the anionic EDTA complex and chromatogram C was the blank determined by injecting 0.16 μmol of EDTA. Chromatogram B, however, is the blank determined by injecting 0.16 μmol of EDTA after the injection of 0.16 μmol of copper(II) ion in the ammonium acetate eluent. Chromatogram B shows a significant blank and suggests that the 2.0 M ammonium acetate eluent does not prevent binding of free copper(II) ion to the gel matrix. Copper bound to strong ligands, however, was completely eluted. To prevent cross-contamination one would need to clean the column after each run. An injection of EDTA after each sample would allow one to prevent cross-contamination and obtain a complete mass balance. A possible problem with this procedure, however, would be shifts in the chemical speciation of real samples induced by the Cu^{2+}/gel interaction.

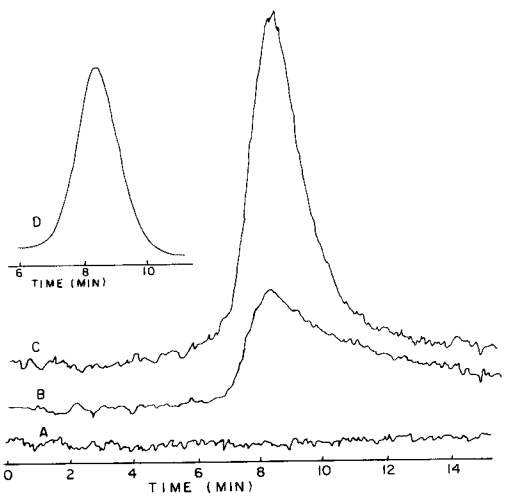

Fig. 1. Chromatograms of 0.157 μmol of free copper(II) ion on Bio-Gel P-6DG: (A) blank injection; (B) 1.0 M ammonium acetate eluent; (C) 2.0 M ammonium acetate eluent; (D) cadmium in 1.0 M ammonium acetate eluent.

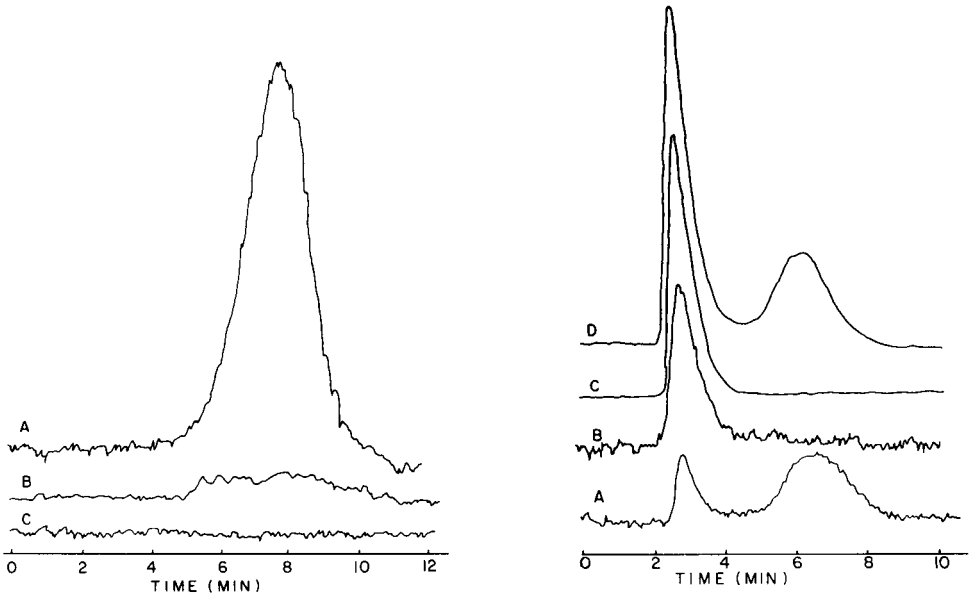

Fig. 2. Effect of chemical form on the copper(II) ion recovery with Bio-gel P-6DG and 2.0 M ammonium acetate eluent: (A) 0.157 μmol of copper(II) ion and 0.314 μmol of EDTA; (B) EDTA washing after 0.157 μmol of free copper(II) ion; (C) EDTA washing after chromatogram A.

Fig. 3. Chromatograms for lobster extracts on Bio-gel P-6DG with citric acid/ammonium acetate eluent: (A) zinc; (B) copper; (C) cadmium; (D) extract with 23 nmol of cadmium as spike.

The washing step would also increase the analysis time for each sample. The adsorption of copper(II) ion onto the gel in the 1.0 M ammonium acetate eluent was also noted for the Sephadex, Fractogel, and controlled pore glass.

The complete recovery of copper(II) ion in the presence of EDTA and the complexing agent Tris and the recovery of cadmium and zinc in eluents of higher ionic strength lends support to the argument that anionic sites on the gel matrix may play an important role in the elution of free ions. The retention of a metal ion in an ion-exchange system is controlled by the solution ionic strength and the chemical form of the metal ion. This is best described by the formulation proposed by Ringbom [12]:

$$D = [NH_4^+]_R K_{NH_4}^{Cu} [NH_4^+]_w \alpha_{Cu}$$

where R represents the resin and w the aqueous phase, K is the exchange constant, and α takes into account the complexation of copper in the aqueous phase. The effect of the ion-exchange groups can be controlled either by an increase in the ionic strength (i.e., $[NH_4^+]_w$) or by the addition of a metal complexation agent to the eluent to increase α. As Tris was not strong enough to prevent the binding of cadmium or zinc to the gel, citric and tartaric acids were studied as possible eluents.

The citric and tartaric acids were tested using 0.157 μmol of free copper-(II) ion injected onto the column in eluent and the recovery was estimated by injection of 0.35 μmol of EDTA after the copper chromatogram. The eluent was formulated with either 0.01 M citric acid or 0.10 M tartaric acid in ammonium acetate at pH 7. Both eluents gave complete recovery of copper, cadmium and zinc if the ammonium acetate concentration was 0.10 M. The citrate eluent (0.01 M citric acid and 0.10 M ammonium acetate adjusted to pH 7) was selected for the analysis of the lobster extracts because it minimized the salt content of the eluent and gave complete recovery. A low salt content in the eluent will minimize problems in clogging of the burner. This eluent was found to be suitable for the complete recovery of copper, zinc and cadmium from the Sephadex G-25, Bio-Gel P-6DG, and Fractogel HW40F gels but was not suitable for the controlled pore glass system. The controlled pore glass gave poor recovery in this eluent and was not studied further.

A potential problem with gel-filtration procedures for metal speciation in protein systems is the lability of the metal protein complex. A metal ion and protein system in equilibrium will tend to dissociate on the column because the larger metal protein species will be separated from the smaller free ion. The degree of dissociation will depend on the lability of the complex and the length of time to complete the separation. Evans et al. [13] studied the separation of labile zinc-binding ligands in milk using Sephadex gels. They noted that the Sephadex gel bound significant amounts of zinc and, to prevent dissociation of the labile complexes, they used zinc-equilibrated buffers to minimize shifts in chemical equilibria. This procedure would not work in the present speciation procedure because one of the aims was to determine the free metal ion in the biological extracts and the added cation would compete with sample cations for protein-binding sites and alter the chemical speciation. The citric acid added to the eluent to prevent ion/gel interactions would alter the speciation if the binding proteins were labile. The specific binding proteins for cadmium, copper, and zinc in mammalian liver and kidney extracts contain a high component of sulphydryl groups and often have a cadmium/cysteine ratio of 1:3. A preliminary characterization of the cadmium-binding protein in the lobster extract also showed a cadmium/cysteine ratio of 1:3. One may expect, therefore, that these extracts would show a chemistry similar to the metallothioneins isolated from mammals. Li et al. [14] have shown that cadmium thioneins have a half-life of about 60 h for the removal of cadmium from the thionein complex by EDTA. Zinc thioneins, however, were found to have a considerably shorter half-life for the removal of zinc by EDTA (about 0.6 h). This suggests that, if the lobster binding protein is similar to the metal thioneins, then there should be no significant shifts in the speciation with time but the zinc may give poorer results. A Sephadex G25 column was used to study the distribution of cadmium and copper in a lobster sample in the presence of 0 and 75-fold excess of EDTA. A comparison of the chromatograms at 0 and

60 min indicated that less than 20% of the metal was present as the EDTA complex after 60 min. These results suggest that the citric acid will not change the speciation of copper and cadmium bound to the lobster proteins if the separation step is done rapidly. A second check of this assumption was done by comparing the copper, zinc, and cadmium speciation in a lobster digestive gland extract using a Sephadex G25 column and either 2.0 M ammonium acetate or the citrate eluent. There was no significant difference between the two sets of results.

Figure 3 shows the chromatogram for the three metals in a lobster extract using Bio-Gel P-6DG. A comparison of the shape of the protein-bound cadmium and the free cadmium peaks indicated that peak-area measurements are necessary to obtain quantitative results because a calibration curve would be prepared by injecting free metal ion standards. An accurate peak area requires a uniform eluent flow rate. The flow rate for the gravity systems was controlled by the aspiration rate of the nebulizer. A comparison of fine- and medium-sized gels showed that it was not possible to match the flow rates satisfactorily with a fine gel because channelling occurred at a flow rate of 3.5 ml min^{-1}. The Sephadex and Bio-Rad gels are compressible and it was not possible to include a pump in the system to improve the flow rate.

The Fractogel bead uses a semi-rigid, spherical gel made from a hydrophilic vinyl polymer. The mechanical strength of the gel is such that low-pressure pumps can be used to increase the flow rates. A 1.6 × 9.5-cm bed of a fine-sized gel allowed a pump and aspirator flow rate of 3.5 ml min^{-1} without noticeable channelling. Figure 4 shows a chromatogram for a lobster extract spiked with free cadmium. The elution volumes of blue dextran and sodium ions are also indicated for comparison. The binding substance for cadmium ions in the lobster extract was retained relative to blue dextran and the free cadmium in the lobster extract was retained relative to blue dextran and the free cadmium eluted slightly earlier than the sodium ions. Fractogel HW40F has a protein fractionation range of 10 000–100 daltons. A series of studies comparing the elution times of cadmium in 1.0 M ammonium acetate eluent on the Fractogel column showed that NTA, EDTA, and citric acid complexes of cadmium eluted earlier than the "free" cadmium. The short column bed provides sufficient resolution to distinguish free and bound metal with a separation time of 10 min for each metal of interest.

Chromatograms of lobster extracts and free ions near the detection limits for cadmium, zinc, and copper are shown in Fig. 5. The detection limits were found to be 0.10, 0.10, and 0.20 μg for bound zinc, cadmium, and copper, respectively. Because of band broadening, the detection limits for the free metal ions with the Fractogel system were 0.20, 0.20, and 0.5 μg for zinc, cadmium, and copper, respectively. These detection limits are absolute amounts for a 1.0-ml sample loop. The detection limits for the extraction procedure and the desalting separation were 0.8, 0.8, and 1.6 $\mu g\ g^{-1}$ of wet tissue for bound zinc, cadmium and copper, respectively.

Table 1 shows the recovery and reproducibility for cadmium, copper, and zinc in the lobster digestive glands. A short desalting-type separation with

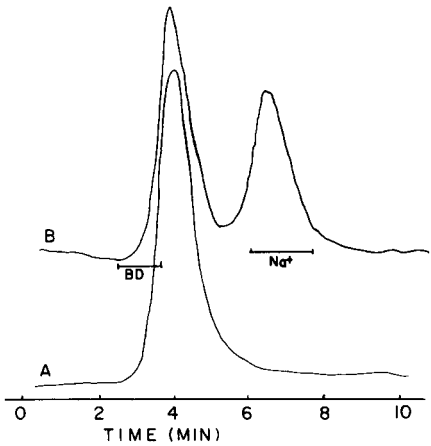

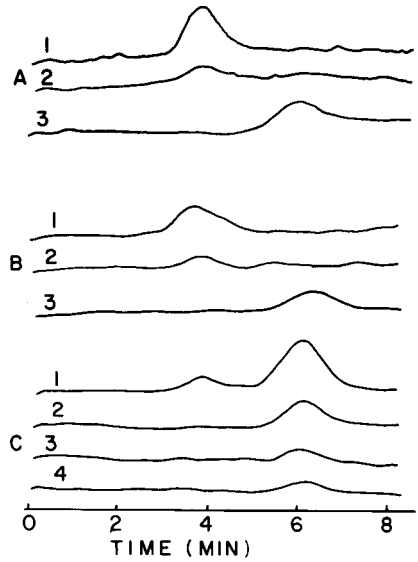

Fig. 4. Chromatograms for lobster extract on Fractogel HW40F with the citric acid eluent: (A) extract; (B) extract + 23 nmol of cadmium spike (BD, blue dextran).

Fig. 5. Chromatograms near the detection limit for lobster extracts on Fractogel HW40F citric acid eluent. (A) Cadmium: (1) 0.38 μg in extract; (2) 0.10 μg in extract; (3) 0.20 μg in eluent. (B) Copper: (1) 0.38 μg in extract; (2) 0.10 μg in extract; (3) 0.50 μg in eluent. (C) Zinc: (1) 0.467 μg in extract; (2) 0.2 μg in eluent; (3) 0.1 μg in eluent; (4) 0.05 μg in eluent.

TABLE 1

Typical lobster extract data[a]

Sample	Amount (μg)	Peak area	Recovery (μg)	
			Bound	Free
Cd standard	5.00	160 ± 2.4	—	—
Lobster 1	2.00	45.0	1.41	—
		19.6	—	0.62
Lobster 2	6.75	138 ± 5	4.32	—
		80 ± 0	—	2.50
Cu standard	10.0	390 ± 6	—	—
Lobster 1	1.89	81 ± 2	2.08	—
Lobster 2 + 2.5 μg spike	5.69	122	3.13	—
		97	—	2.49
Zn standards	1.25	101 ± 1	—	—
	2.50	197 ± 1.5	—	—
	3.75	297 ± 3.5	—	—
Lobster 1	2.64	55 ± 3	0.69	—
		159 ± 1.5	—	2.00

[a]The total amounts were measured by flame atomic absorption spectrometry. Areas were measured using a planimeter. Uncertainties are the standard deviation of six injections.

the Fractogel HW40F bead was suitable for differentiating between "free" and "bound" metal in the extracts. The gel used in this study, however, does not provide sufficient resolution to differentiate between metal bound to metallothionein-sized proteins and metal bound to proteins of higher molecular weight.

The lobster digestive gland was selected as a typical sample for metal speciation in biological samples. The procedure, as described in this paper, should be applicable to other systems in which free vs. bound speciation is desired, provided that the bound metal species is not labile.

This research was supported in part by a grant from the Natural Sciences and Engineering Research Council of Canada.

REFERENCES

1 D. L. Rabenstein and A. A. Isab, FEBS Lett., 121 (1980) 61.
2 M. Margoshes and B. L. Vallee, J. Am. Chem. Soc., 79 (1957) 4813.
3 D. A. Brown and K. W. Chatel, Chem. Biol. Interact., 22 (1978) 271.
4 J. F. Uthe and C. L. Chou, J. Environ. Sci. Health, A, 15 (1980) 101.
5 H. M. Crews, J. A. Burrell and D. J. McWeeney, Proc. Heavy Metals in the Environment Conference, Heidelberg CEP Consultants Ltd., Edinburgh, 1 (1983) 278.
6 C. L. Chou, J. F. Uthe and E. G. Zook, J. Fish. Res. Bd. Can., 35 (1978) 409.
7 P. E. Gardiner, J. M. Ottaway, G. S. Fell and R. R. Burns, Anal. Chim. Acta, 124 (1981) 281.
8 K. T. Suzuki, J. Pharmobiodynamics, 3 (1980) 518.
9 J. F. Uthe, C. L. Chou and D. Robinson, Can. Tech. Rep. Fish. Aquatic Sci., 963 (1980) 165.
10 W. F. Prouty and A. L. Goldberg, J. Biol. Chem., 247 (1971) 3341.
11 B. Gelotte, J. Chromatogr., 3 (1960) 330.
12 A. Ringbom, Complexation in Analytical Chemistry, R. E. Krieger, Huntington, New York, 1979, p. 207.
13 G. W. Evans, P. E. Johnson, J. G. Brushmiller and R. W. Adams, Anal. Chem., 51 (1979) 839.
14 T. Y. Li, A. J. Kraker, C. F. Shaw and D. H. Petering, Proc. Natl. Acad. Sci. USA, 77 (1980) 6334.

Analytica Chimica Acta, 174 (1985) 279—285
Elsevier Science Publishers B.V., Amsterdam — Printed in The Netherlands

THE SEPARATION OF IRIDIUM AND RUTHENIUM BY ION FLOTATION

DANIEL M. DOWNEY* and SCOTT A. CLIPPER

Department of Chemistry, West Virginia University, P.O. Box 6045, Morgantown, WV 26506 (U.S.A.)

(Received 14th March 1985)

SUMMARY

Mixtures of iridium(IV) and ruthenium(III) as $IrCl_6^{2-}$ and $RuCl_6^{3-}$ are separated by ion flotation. Iridium (IV) is selectively floated from mixtures of the metal complexes in aqueous 1.0 M hydrochloric acid with hexadecylpyridinium bromide (HPB) and nitrogen. Ruthenium(III) does not float under the same conditions. In order to assess the usefulness of this procedure, the separation was also investigated with hexadecyltrimethylammonium bromide and hexadecyltripropylammonium bromide, from solutions of varying concentrations of sodium chloride, sodium nitrite and hydrochloric acid. Under optimal conditions at the 5×10^{-5} M level, 78% of the iridium is recovered free of ruthenium, provided that excess of HPB and >1 M chloride are present.

In recent years, separation and recovery processes for the platinum group metals have seen marked improvements. Berg and Downey [1, 2] examined the use of ion flotation for the separation of several binary systems of these metals. Improvements have also been noted using ion exchange [3] and liquid-liquid extraction [4]. Because of the increase in demand for these metals [5] and new uses that have arisen with new technology [6], it is still of interest to continue work on the refinement and purification of these metals.

It is the purpose of this paper to present a novel ion-flotation separation for the binary system of iridium and ruthenium. The separation involves the selective flotation of the hexachloro complexes of Ir(IV), $IrCl_6^{2-}$, and Ru(III), $RuCl_6^{3-}$, with a surfactant such as hexadecylpyridinium bromide (HPB) or hexadecyltrimethylammonium bromide (HTMAB). The separation is based on charge and steric factors. The divalent $IrCl_6^{2-}$ forms readily floatable products, known as sublates, of the empirical formula MS_2, where M represents the metal and S the surfactant. The trivalent $RuCl_6^{3-}$, however, requires three surfactant molecules per ion for flotation, which is sterically unfavorable and thus produces little or no flotation [2].

0003-2670/85/$03.30

EXPERIMENTAL

Reagents and apparatus

High-purity sodium hexachloroiridate(IV) (Alfa Chemical Co.) was dissolved in aqua regia. The solution was fumed to dryness twice with hydrochloric acid and the residue was dissolved in 2 M hydrochloric acid. High-purity sodium hexachlororuthenate(III) (Alfa Chemical Co.) was dissolved in 2 M hydrochloric acid. The stock solutions were prepared as 0.0100 M metal in 2 M hydrochloric acid and were spiked with the radioactive tracers, ^{192}Ir and ^{106}Ru (New England Nuclear Corp.).

The surfactants HTMAB and HPB (Fisher Scientific) were recrystallized once from absolute ethanol. Hexadecyltripropylammonium bromide (HTPAB) was prepared by reacting 1-bromohexadecane (Aldrich Chemical Co.) with tripropylamine (Aldrich) and was recrystallized twice from absolute ethanol. The stock solutions (0.100 M) were prepared in absolute ethanol.

All other chemicals used were of analytical-reagent grade.

Ion-flotation experiments were done in a glass column made by lengthening to 30 cm an ordinary glass, 60-ml Buchner funnel containing a fine glass fritted disc (4—5.5 μm nominal porosity) and fitted with a stopcock for drainage just above the frit. Nitrogen, which was humidified with water, was bubbled through the frit at a flow rate of 12 cm^3 min^{-1}. Further details of the system can be found elsewhere [7].

Spectrophotometric data were obtained with a Bausch and Lomb Spectronic 2000; the scanning range was 250—650 nm.

Procedures

The flotation was monitored by measuring the activity of 5.00-ml aliquots of sample solution removed from the flotation cell at appropriate intervals. In the initial studies, only one isotope was present. The concentration of iridium or ruthenium remaining in solution was determined by counting the activity of the aliquots with a 2 × 2-in. NaI(Tl) crystal, examining the 468.1-keV peak of ^{192}Ir and the 511.9-keV peak of ^{106}Ru decay during the preliminary studies. In subsequent flotations involving mixtures of iridium and ruthenium, a high-purity germanium detector was used to resolve the two peaks.

Plots of C_t/C_0 vs. time were prepared to monitor rates of removal; C_t is the concentration of solute in solution at time t, and C_0 is the original concentration. Also, the percentage of metal floated at any time was calculated as $\%F_t = (1 - C_t/C_0)(100)$.

Flotation procedure. Sample solutions were prepared in 100-ml volumetric flasks by adding enough metal chloro-complex solution to give a final metal concentration of 5.00×10^{-5} M. Enough hydrochloric acid was added to give a final concentration of 1.0 M. The solution was diluted to approximately 95 ml with distilled water and then 0.200 ml of 0.100 M surfactant was

added to give an initial surfactant concentration of 2.00×10^{-4} M. Absolute ethanol was added to give a final ethanol concentration of 1.0 ml per 100 ml of solution. The solution was then diluted to volume with distilled water, allowed to mix for 10 min, and then transferred to the flotation cell. A 5.00-ml aliquot was removed via pipet to establish the exact initial metal concentration by radiation counting. Nitrogen was then passed through the column for 30 min, at which time the separation was complete. The solution was drained and another 5.00-ml aliquot was removed and counted to establish the final metal concentration. The froth was collapsed with ethanol and collected with a final volume of less than 5.00 ml.

In addition to the above procedure, certain sample solutions were prepared with hydrochloric acid or sodium hydroxide solution to vary the hydrogen ion concentration from pH 4.0 up to a concentration of 8 M. Certain samples were also prepared with sodium chloride or nitrite to study the effect of neutral salts on the flotation.

RESULTS AND DISCUSSION

The efficiency of ion flotation depends on several factors [9]; to establish optimum separation conditions, several factors were investigated.

Choice of surfactant

It has been shown [1] that cationic surfactants with a primary chain length of 16 methyl units resulted in the maximum removal of iridium(IV) from solution; thus the surfactants used for this study were hexadecyltrimethylammonium bromide (HTMAB), hexadecyltriethylammonium bromide (HTEAB), hexadecyltripropylammonium bromide (HTPAB), and hexadecylpyridinium bromide (HPB). As can be seen from Table 1, the percentage of Ir(IV) floated increases and the percentage of Ru(III) floated decreases as the substituents on the quaternary ammonium function group increase in chain length from methyl to propyl, reaching a relative maximum and minimum, respectively, with the pyridinium complex. Apparently, the crowding of three bulky groups around the Ru(III) chloro complex

TABLE 1

Flotation of Ir(IV) and Ru(III) with various surfactants[a]

Surfactant	Ir(IV) floated (%)		Ru(III) floated (%)	
	0.01 M HCl	1 M HCl	0.01 M HCl	1 M HCl
HTEAB	59 ± 2	62 ± 3	8 ± 3	13 ± 2
HTMAB	64 ± 2	64 ± 2	3 ± 2	7 ± 2
HTPAB	68 ± 2	74 ± 2	1 ± 2	4 ± 2
HPB	69 ± 3	78 ± 2	0 ± 2	0 ± 2

[a]Conditions as recommended in the Procedure.

required for flotation is sterically unfavorable, which is in agreement with earlier findings [1]. Table 1 indicates that the most selective flotation of Ir(IV) from Ru(III) was obtained with HPB. Therefore all subsequent flotation studies were directed to optimizing solution conditions to enhance the removal of iridium while depressing the flotation of ruthenium.

Influences of neutral salt concentration

It has been shown [9] that the flotation process is affected by the ionic strength of the solution, which is dependent on the neutral salt concentration. Neutral salts can often influence the ion to be collected by forming complexes, which may be a precipitate, a neutral species, or an oppositely charged species, all of which could change the flotation behavior. Figure 1 gives rate-of-removal curves for iridium and ruthenium in HPB solutions of 0.5—3.0 M chloride as sodium chloride or hydrochloric acid. Figure 2 shows similar curves obtained in the presence of sodium nitrite. In these studies, the initial pH was 2.50. As the neutral salt concentration was gradually increased, a maximum was reached with a steady decrease after that point. Amounts of Ir(IV) removed varied from 64% to 78% to 32% for HCl concentrations of 0.01, 1, and 8 M, respectively, and from 45% to 64% to 28% for the same concentration of NaCl. Amounts of Ru(III) removed were in the range of 0—10% (at 8 M HCl) for the same concentrations of HCl and 3—15% (at 1 M NaCl) for the same concentrations of NaCl. For nitrite concentrations between 0.05 and 3 M, removal of Ir(IV) decreased from 56 to 0% and removal of Ru(III) changed from 42% to a maximum of 70% at 0.6 M and a minimum of 0% at 3 M.

For solutions up to 4 M HCl and NaCl, colloidal precipitates were observed in the bulk solution when Ir(IV) was mixed with the surfactant HPB. This was not observed when nitrite was present.

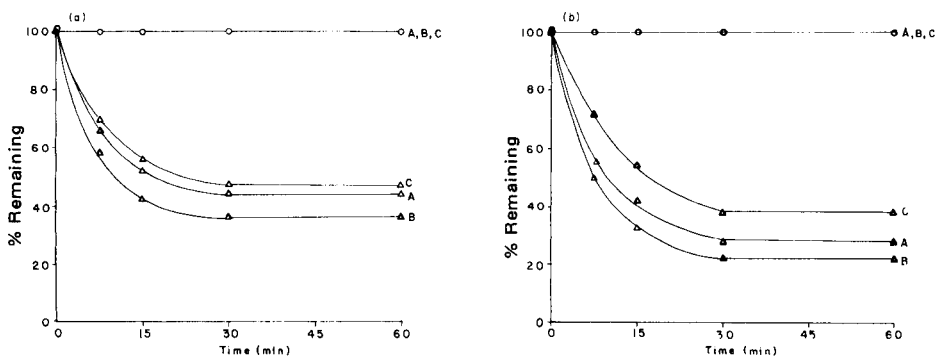

Fig. 1. Flotation of mixtures of Ir(IV) (△) and Ru(III) (○) with HPB. (a) From solutions of various NaCl concentrations: (A) 0.5 M; (B) 1.0 M; (C) 3 M. (b) From solutions of various HCl concentrations: (A) 0.5 M; (B) 1 M; (C) 3 M. Initial conditions: 5×10^{-5} M Ru(III), 5.00×10^{-5} M Ir(IV), 2.00×10^{-5} HPB, pH 2.0, nitrogen at 12 cm^3 min^{-1}.

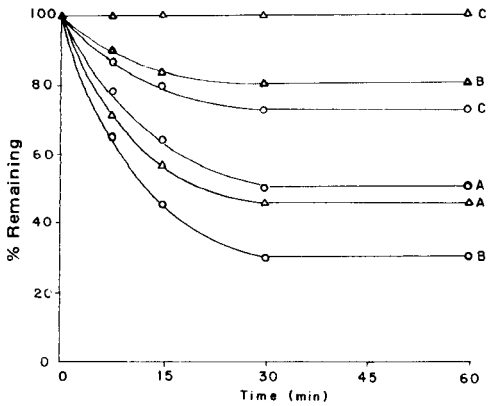

Fig. 2. Flotation of mixtures of Ir(IV) (△) and Ru(III) (○) with HPB from solutions of various sodium nitrite concentrations: (A) 0.1 M; (B) 0.5 M; (C) 1.0 M. Conditions as in Fig. 1.

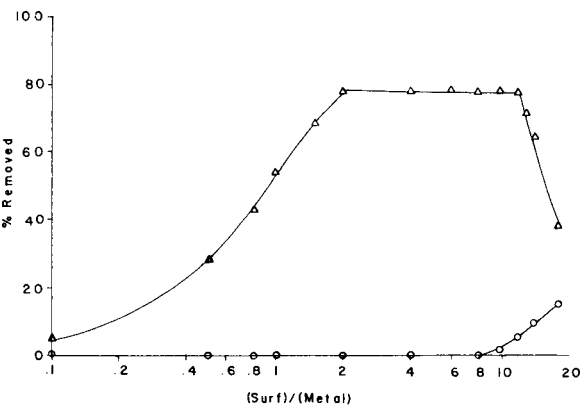

Fig. 3. Effect of varying surfactant/metal concentration on percentage floated for mixtures of Ir(IV) (△) and Ru(III (○) from solution. Initial conditions: 1.00 M [H^+], nitrogen at 12 cm^3 min^{-1}.

An earlier study by Berman and McBryde [8] indicated that quaternary ammonium functional groups partially reduce the Ir(IV) to Ir(III). Because Ir(III) exhibits flotation behavior similar to that of Ru(III) [2], an oxidizing agent was used to convert any reduced iridium back to Ir(IV). This, however, also resulted in the oxidation of a portion of the ruthenium to Ru(IV) and the consequent flotation of the Ru(IV). The oxidants tested were cerium(IV) and iron(III). Because of the similarities of the oxidation potentials of Ir(III) and Ru(III), it was noted that anything that oxidized the Ir(III) to Ir(IV) would also partially oxidize the Ru(III) to Ru(IV). As the results presented in Table 2 indicate, separation is not possible with strong oxidants present.

TABLE 2

Influence of oxidants on flotation[a]

Surfactant	Ir(IV) floated (%)		Ru(III) floated (%)	
	Ce(IV)	Fe(III)	Ce(IV)	Fe(III)
HTMAB	85 ± 2	—	30 ± 2	—
HTEAB	91 ± 2	—	27 ± 2	—
HTPAB	97 ± 2	—	13 ± 2	—
HPB	90 ± 2	52 ± 2	24 ± 2	14 ± 2

[a]Conditions as recommended in Procedure except for added oxidant.

Influence of ratio of surfactant to metal chloro complex

Depending on the source and type of the ore from which the iridium and ruthenium are to be obtained, variations in the percentage of the metals present can arise; therefore, it was important to know if variations in the initial ratio of surfactant-to-metal concentrations would result in significant differences in the percentage of metal floated. The metal concentration was held constant at 5.00×10^{-5} M and the surfactant concentration was varied to establish the optimum surfactant/metal ratio. The percentage of metal chloro complex floated vs. the log of the ratio of surfactant to metal concentration is plotted in Fig. 3. These data indicate that careful control of the initial concentration of the surfactant is not critical as long as there is an excess of surfactant present and that Ir(IV) can be selectively floated from Ru(III) below a ratio of 10. An excess of surfactant is necessary to provide a foam support, which prevents redispersion of the sublate into solution. It is interesting to note that after a certain point, the percentage of ion floated decreases. This is attributed to the critical micelle concentration (c.m.c.) being exceeded. It has been shown [9] that the presence of micelles is detrimental in ion flotation. The use of the surfactant is based on its physical properties, namely the hydrophobic group at one end and a charge at the other. When the surfactant molecules are grouped in a micelle, this configuration is lost, and no flotation is obtained. It has also been suggested that this phenomenon could be caused by the peptization of precipitate with excess of surfactant, and also by the competition for bubble interfaces with surfactant having chloride as its counter-ion.

It was also of interest to see if a change in the initial metal concentration would result in a significant change in the percentage floated of the metal chloro complex. This was investigated by maintaining a surfactant/metal concentration ratio of 4 while the metal chloro complex concentration was varied. For metal ion and HPB concentrations between 5×10^{-6} and 5×10^{-4} and 2×10^{-5} and 2×10^{-3} M, respectively, the percentages removed were essentially constant at 77% for Ir(IV) and 0% for Ru(III).

Stability of the chloro complexes

The chloro complexes are probably in equilibrium with various aqua/chloro and hydroxo/chloro complexes, depending upon the chloride ion concentration [6]. Spectrophotometric data for Ir(IV) complex ions were obtained to establish the extent of hydration and, by comparison to spectra presented earlier [10], it was found that solutions of $\geqslant 1$ M chloride contained the fully substituted $IrCl_6^{2-}$ complex ion. In solutions with <1 M chloride, there was some hydration resulting in the formation of $IrCl_5(H_2O)^-$, $IrCl_4(H_2O)_2$ and other complex ions, as indicated by peak shifts. However, the extent of hydration could not be determined. The literature [6] indicates that ruthenium(III) complexes exhibit similar behavior in solutions of various chloride ion concentrations.

Conclusion

The above results indicate that up to 78% of the iridium can be recovered free of ruthenium in the optimum flotation experiment. The separation is not affected by the mole ratio of the metal ions nor by surfactant concentration so long as an excess is present. Although the separation is not quantitative for a material with a mole ratio of 1:10 (Ir:Ru), the unfloated ruthenium can be enriched nearly 50-fold. Up to 90% of the ruthenium can be recovered free of iridium by adding strong oxidants to ensure complete removal of iridium.

Acknowledgement is made to the Donors of the Petroleum Research Fund, administered by the American Chemical Society, for support of this work. One of the authors (S. A. C.) also thanks the Petroleum Research Fund for a summer undergraduate fellowship.

REFERENCES

1 E. W. Berg and D. M. Downey, Anal. Chim. Acta, 120 (1980) 237; 123 (1981) 1; 134 (1982) 313.
2 E. W. Berg and D. M. Downey, Anal. Chim. Acta, 121 (1980) 239.
3 A. P. Evers, R. I. Edwards and M. M. Fieberg, U.S. Patent, 4,130,625, Dec. 19, 1978.
4 A. Diamantatos, Anal. Chim. Acta, 67 (1973) 317.
5 F. E. Beamish, The Analytical Chemistry of the Noble Metals, Pergamon Press, Oxford, 1966.
6 S. I. Ginzburg, Analytical Chemistry of the Elements: Platinum Metals, Wiley, New York, 1975.
7 D. M. Downey and C. McLaughlin, Radiochim. Acta, 33 (1983) 91.
8 S. S. Berman and W. A. E. McBryde, Can. J. Chem., 36 (1958) 835.
9 F. Sebba, Ion Flotation, Elsevier, New York, 1980.
10 J. C. Chang and C. S. Garner, Inorg. Chem., 4 (1965) 209.

Analytica Chimica Acta, 174 (1985) 287—291
Elsevier Science Publishers B.V., Amsterdam — Printed in The Netherlands

Short Communication

APPLICATION OF A SWEPT-POTENTIAL ELECTROCHEMICAL DETECTOR IN THE LIQUID-CHROMATOGRAPHIC DETERMINATION OF NITROSAMINES

MICHAEL B. THOMAS, HUGGINS MSIMANGA and PETER E. STURROCK*

School of Chemistry, Georgia Institute of Technology, Atlanta, Georgia 30332-0400 (U.S.A.)

(Received 11th January 1985)

Summary. A swept-potential detector, operating in the square-wave voltammetric mode, is used in the liquid-chromatographic determination of a mixture of eight nitrosamines. Only three compounds were completely separated by the C-18 column. Three more were resolved by educing constant-potential chromatograms from the computer buffer. Mathematical deconvolution via fast-Fourier transform was applied to the remaining components.

In recent years, several publications have reported on the determination of nitrosamines [1—9]. The interest in nitrosamines stems from their carcinogenic nature and wide distribution as discussed by Samuelsson and Osteryoung [1] and by Vohra [2]. Several papers have dealt with the polarographic determination of nitrosamines [3—7]. Unfortunately, although modern polarographic methods are quite sensitive, they are not capable of the determination of most mixtures without a prior separation step, and the usual polarographic procedures are not suitable for volatile compounds because of the necessity for the removal of oxygen from the system. Analytical methods need to be applicable to mixtures of volatile and involatile nitrosamines, and to this end, several papers have advocated high-performance liquid chromatography (h.p.l.c.) with electrochemical detection [1, 2, 8, 9].

Most applications of h.p.l.c. entail the complete resolution of the components of the mixture by the column while the detector serves only to quantify each component. However, newer techniques rely on the detector to help identify the components and even to help resolve two or more components that are not completely resolved by the column. Outstanding examples are the multiwavelength ultraviolet (u.v.) detector [10] and the use of a mass spectrometer as a detector [11]. An analogous detector is the swept-potential electrochemical detector, first reported and applied to a mixture of two nitrosamines by Samuelsson et al. [12]. Reardon et al. [13] recently described improved instrumentation for swept-potential detection, and this communication describes the application of this new instrument to a mixture of nitrosamines in which the chromatographic peaks of several components overlap.

0003-2670/85/$03.30

Experimental

The h.p.l.c. system and swept-potential detector used in this study have been described [13—15]. The only significant changes from the previous work were the use of a Zorbax-ODS 4.6 × 150-mm column (DuPont Instruments) and the use of a methanol bubbler between the helium tank and the gas-dispersion tube in the mobile-phase reservoir to minimize changes of mobile-phase composition during a series of chromatograms.

The nitrosamines studied are listed in Table 1. These compounds (Sigma Chemical Company) were used without further purification. Because of the possible carcinogenic effects of *N*-nitroso compounds, they were ordered in serum bottles with septum caps. Stock solutions were prepared by injecting 50.0 ml of h.p.l.c.-grade methanol into the serum bottles. These stock solutions were diluted further in volumetric flasks to obtain sample solutions suitable for injection. All sample solutions were stored in the dark.

Mobile phases consisted of 0.20 M acetate buffers of various pH values, h.p.l.c.-grade methanol (Fisher), and 1-heptane sulfonic acid sodium salt (Eastman Kodak) as ion-pairing agent. The mobile phases were prepared as before [15] except for the addition of the ion-pairing agent.

Results and discussion

Figure 1 is a chromatogram of the eight nitrosamines listed in Table 1. This chromatogram was produced by summing the 21 difference measurements obtained in each square-wave voltammetric sweep and is similar to what would be observed with a d.c. electrochemical detector set to the potential of the negative limit of the sweep. The peaks for NDIPLA and NDM are not completely separated. In addition, the peaks for NMA, NDP, and NBE are fused into one asymmetric peak. The peaks for NDE, NBP, and

TABLE 1

Voltammetric peak potentials and chromatographic capacity factors

Compound	Abbreviated name	Peak potential[a]	Capacity factor[b]
N-Nitrosodiisopropanolamine	NDIPLA	−1.06	0.31
N-Nitrosodimethylamine	NDM	−1.14	0.41
N-Nitrosodiethylamine	NDE	−1.06	1.13
N-Nitroso-*N*-methylaniline	NMA	−0.84	3.68
N-Nitroso-di-n-propylamine	NDP	−1.04	3.87
N-Nitroso-*N*-ethylbutylamine	NBE	−1.04	4.15
N-Nitroso-*N*-butylpropylamine	NBP	−1.04	7.63
N-Nitrosodibutylamine	NDB	−1.02	15.58
Oxygen		−1.08	1.73

[a]Potentials were measured vs. Ag/AgCl in equal-volume mixtures of methanol and 0.02 M acetate buffer. Final pH was 5.55. [b]Capacity factors on Zorbax-ODS 4.6 × 150 mm column with mobile phase (note a) at 1.1 ml min^{-1}.

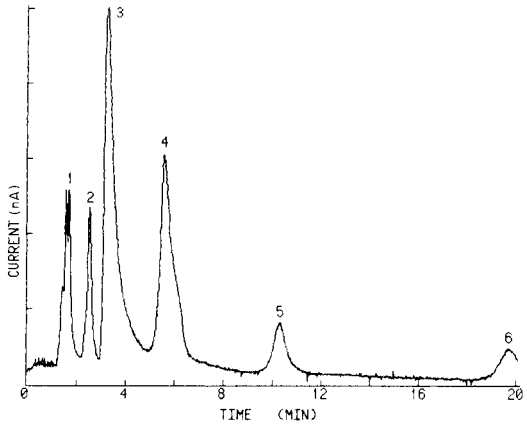

Fig. 1. Chromatogram of a mixture of nitrosamines. Peaks: (1) NDIPLA and NDM; (2) NDE; (3) oxygen; (4) NMA, NDP, and NBE; (5) NBP; (6) NDB. Currents summed over potential range of −0.80 to −1.22 V vs. Ag/AgCl. Injection of 10 μl containing 174 ng of each nitrosamine. See notes to Table 1 for composition of mobile phase. Voltammetric parameters: pulse, −50 mV; step, −20 mV; frequency, 30 Hz. Voltammograms of 21 points repeated once each second.

NDB are well separated. At lower percentages of methanol in the mobile phase, the peak from oxygen in the injected sample overlaps with the peak of NDE because the capacity factor for oxygen increases less than that for NDE. It was decided not to purge the sample solution with helium to remove the oxygen because of the volatility of the lower-molecular-weight nitrosamines. No significant changes in selectivity factors resulted from moderate changes in mobile-phase pH or from the addition of heptane sulfonic acid up to 2 mm in the mobile phase.

Figure 2 is a 3-D representation of a section of the complete run. The variations of reduction potentials are obvious and suggest approaches to resolving the two areas of overlapping peaks. The resolution of the NDIPLA/NDM doublet is greatly enhanced by the use of constant-potential chromatograms as shown in Fig. 3. Such chromatograms are constructed by educing one difference-current measurement from each sweep with each measurement corresponding to the same base potential. Figure 3 also shows clearly two unknown impurities which follow the solvent front very closely.

The use of constant-potential chromatograms also allows the complete resolution of the peak of NMA from the overlapping peaks of NDP and NBE as seen in Fig. 4, curve D. Unfortunately, NDP and NBE are so similar in reduction potential that constant-potential chromatograms cannot resolve them.

Mathematical deconvolution was applied to the NMA/NDP/NBE triplet starting with the raw data of Fig. 4, curve B, using the same microprocessor as for instrument control and data acquisition. An interpolated baseline was subtracted to produce the data of Fig. 5, curve A. Next, the data were

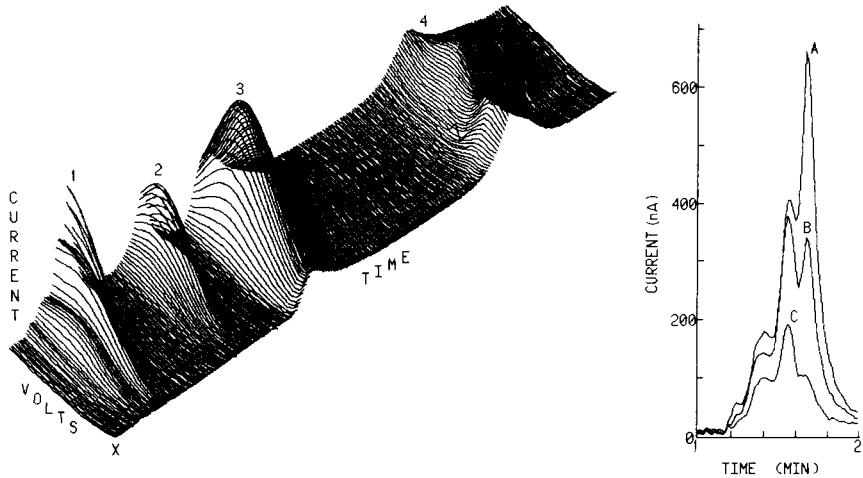

Fig. 2. 3-D chromatogram of a section of experiment depicted in Fig. 1. The time axis shows retention times from 1.0 to 6.7 min. Potential axis is from —0.80 to —1.22 V vs. Ag/AgCl. Origin (X) is 1.0 min and —0.80 V.

Fig. 3. Chromatograms at constant base potentials. Data are from the same experiment as Figs. 1 and 2, peak 1. Potentials of curves vs. Ag/AgCl: (A) —1.22 V; (B) —1.10 V; (C) —0.98 V.

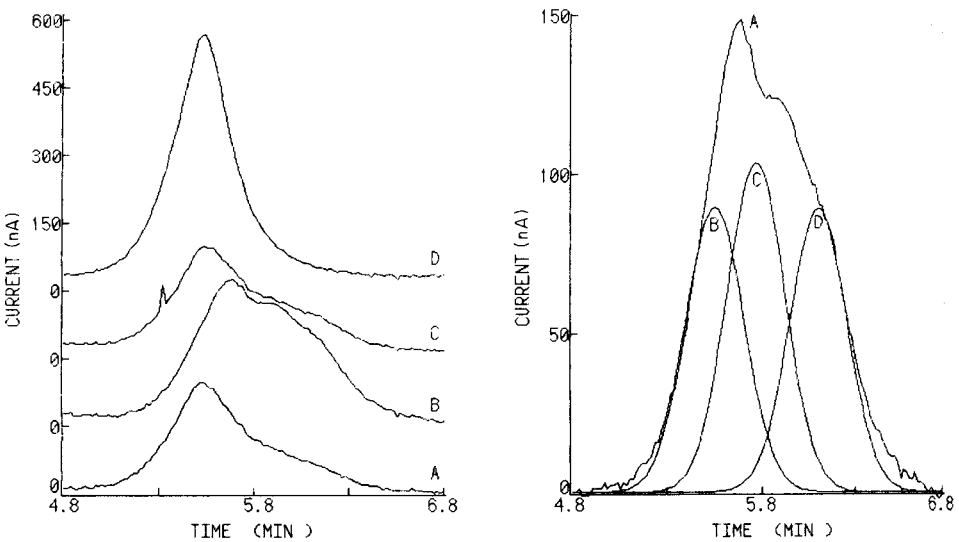

Fig. 4. Chromatograms at constant base potentials. Data are from the same experiment as Figs. 1 and 2, peak 4. Potentials of curves vs. Ag/AgCl: (A) —1.22 V; (B) —1.10 V; (C) —0.98 V; (D) —0.86 V.

Fig. 5. Deconvolution of curve B, Fig. 4. Curve A, baseline-subtracted experimental data. Curves B—D, deconvoluted peaks for NMA, NDP, and NBE, respectively. See text for details.

digitally filtered to remove high-frequency noise. A cutoff criterion described by Isenhour and Lam [16] was used for the fast Fourier-transform smoothing. Finally, an extension of the parameter estimation analysis of Binkley and Dessy [17] was used to perform the curve deconvolution on the assumption of three Gaussian peaks with the same half-height width. The linear parameter estimation was performed in the spatial frequency domain, by the least-squares method, after input of preliminary estimates of peak positions, peak width, and peak heights. The iterative calculation first optimizes the peak positions and then the peak width, using the minimum of residuals as the criterion of best fit. Finally, the peak heights are calculated in a similar manner. The resulting components are illustrated in Fig. 5, curves B—D. The retention time for curve B (NMA) is within one second of the retention time measured from Fig. 4, curve D.

This work was supported by Cooperative Agreement CR-808565 between the School of Chemistry of the Georgia Institute of Technology and the Analytical Chemistry Branch of the Environmental Research Laboratory, United States Environmental Protection Agency.

REFERENCES

1 R. Samuelsson and J. Osteryoung, Anal. Chim. Acta, 123 (1981) 97.
2 S. Vohra, Trends Anal. Chem., 1 (1982) 145.
3 H. Lund, Acta Chem. Scand., 11 (1957) 990.
4 K. Hasebe and J. Osteryoung, Anal. Chem., 47 (1975) 2412.
5 S. Chang and G. Harrington, Anal. Chem., 47 (1975) 1857.
6 H. Pylyplw, Jr. and G. Harrington, Anal. Chem., 53 (1981) 2365.
7 R. Samuelsson, Anal. Chim. Acta, 102 (1978) 133; 108 (1979) 213.
8 S. Vohra and G. Harrington, J. Chromatogr. Sci., 18 (1980) 379.
9 G. Harrington, S. Vorha and J. Wang, Banbury Report, 12 (1982) 175.
10 A. McDowell and H. Pardue, Anal. Chem., 49 (1977) 1171.
11 R. Willoughby and R. Browner, J. Lawrence (Ed.), Trace Analysis, Vol. 2, Academic Press, New York, 1982.
12 R. Samuelsson, J. O'Dea and J. Osteryoung, Anal. Chem., 52 (1980) 2215.
13 P. Reardon, G. O'Brien and P. Sturrock, Anal. Chim. Acta, 162 (1984) 175.
14 P. Sturrock and K. Williams, Anal. Chem., 54 (1982) 2629.
15 J. Scanlon, P. Flaquer, G. Robinson, G. O'Brien and P. Sturrock, Anal. Chim. Acta, 158 (1984) 169.
16 H. Lam and T. Isenhour, Anal. Chem., 53 (1981) 1179.
17 D. Binkley and R. Dessy, Anal. Chem., 52 (1980) 1335.

Analytica Chimica Acta, 174 (1985) 293—297
Elsevier Science Publishers B.V., Amsterdam — Printed in The Netherlands

Short Communication

DETERMINATION OF CHOLESTEROL BY FLOW INJECTION ANALYSIS WITH IMMOBILIZED CHOLESTEROL OXIDASE

M. MASOOM and ALAN TOWNSHEND*
Department of Chemistry, University of Hull, Hull HU6 7RX (Great Britain)
(Received 7th January 1985)

Summary. The injected sample passes through a column of enzyme immobilized on controlled pore glass, at pH 7.0, and the hydrogen peroxide produced is detected amperometrically. As little as 0.2 μg of cholesterol can be detected. The method is applied to blood serum, wax-wool alcohol and an extract of butter.

Cholesterol, a steroid alcohol, is the precursor of bile acids, steroid hormones and provitamin D_3. Although food provides substantial amounts of total body cholesterol, most of the cholesterol needed for normal body functions is endogenously synthesized. Despite its usefulness, cholesterol has been identified as a risk factor in the occurrence of heart disease [1], and there is a connection between elevated blood cholesterol levels and atherosclerosis. Such cholesterol is partly present in an esterified form, the proportion by weight of esterified to free cholesterol in the body being 60:40. Apart from its importance as a metabolite for various clinical investigations, cholesterol determination in food products and cosmetics is also very important.

A variety of methods including spectrophotometry [2, 3], gas—liquid chromatography [4, 5] and high-performance liquid chromatography [6], is available for cholesterol determination in foods. For blood cholesterol determination, these methods have been replaced mainly by enzymatic procedures [7, 8] because of their rapidity, selectivity, sensitivity and greater accuracy. The enzymatic methods for total cholesterol are based on the hydrolysis of cholesterol esters to free cholesterol, which is oxidized by using cholesterol oxidase (COD) to 4-cholestene-3-one and hydrogen peroxide. The methods that have been proposed differ mainly in the coupled indicator reaction used to measure the hydrogen peroxide by a spectrophotometric [7] or fluorimetric [9] procedure, or it may be determined amperometrically [10].

With the advent of immobilized enzyme technology and fast flow systems, a highly selective and rapid analytical method for determination of cholesterol in foods as well as blood can be developed. This communication describes a system for flow injection analysis (f.i.a.) based on an immobilized COD reactor and an amperometric flow-cell detector [11].

0003-2670/85/$03.30

Experimental

Materials and reagents. Cholesterol oxidase (cholesterol:oxygen oxidoreductase EC.1.1.3.6; ca. 10 U mg^{-1}), sitosterol, stigmasterol and cholesterol were obtained from the Sigma Chemical Co. Wax-wool alcohol was a gift from Croda Chemicals Ltd., Goole, North Humberside. All other chemicals were analytical grade.

Solutions of cholesterol containing sodium chloride and a surfactant were prepared as follows. To a 100-ml volumetric flask containing a known amount of cholesterol (10—100 mg) was added 5 ml of isopropanol. The solid dissolved and 4 ml of Triton X-100 and 0.87 g of sodium chloride were added. The flask was shaken well, placed in hot water for 1 min and made up to volume with deionized water to give clear 0—100 mg dl^{-1} cholesterol solutions. At higher concentrations, the solution was somewhat turbid. The solutions of stigmasterol, sitosterol and wax-wool alcohol were prepared by the same procedure.

Immobilization of cholesterol oxidase. Cholesterol oxidase was immobilized on controlled porosity glass (CPG) by cross-linking with glutaraldehyde as described previously for glucose oxidase [11], except that 50 U was immobilized on 200 mg of glass.

Extraction of cholesterol from butter [12]. English butter (5 g) was refluxed while stirring with 50 ml of freshly prepared methanolic 2 M potassium hydroxide. The mixture, while still warm, was transferred to a 200-ml separating funnel. After cooling to room temperature, 100 ml of (1 + 1) ether/petroleum ether was added and shaken very well. The phases were allowed to separate for 15 min. The clearly separated lower organic phase was drained off and the extraction process was repeated. The combined organic layers were evaporated on a rotary evaporator. The residue obtained was dissolved by the same procedure as was used to prepare the standard cholesterol solutions.

Apparatus and procedure. The simple flow-injection manifold for cholesterol determination is shown in Fig. 1. The immobilized enzyme was packed in a glass column (25 × 2.5 mm i.d.) and incorporated into the flow system. The pump, injection valve and detector were as reported earlier [11].

Results and discussion

Optimization. Non-ionic surfactants such as Triton X-100 are effective as lipid solubilizing agents. When a surfactant is used to solubilize lipids, the surfactant/lipid ratio must be carefully adjusted, because the solubility of the lipid and the activity of the enzyme may be affected by the amount of the surfactant present. Because of the important role played by Triton X-100, its effect on the immobilized enzyme activity was examined, by measuring the responses of cholesterol solutions containing various concentrations of surfactant. The immobilized enzyme showed an increase in response with increasing surfactant concentration, the peak being highest at 4 ml dl^{-1} Triton X-100 (Fig. 2); subsequent measurements were therefore made with this concentration.

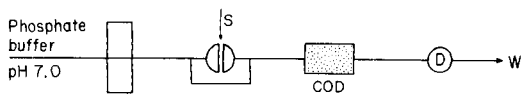

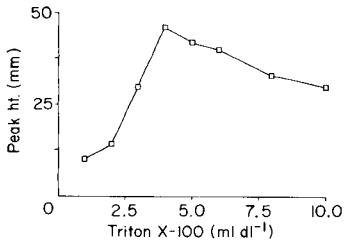

Fig. 1. Manifold for cholesterol determination.

Fig. 2. Effect of Triton X-100 concentration on the activity of immobilized cholesterol oxidase (20 mg dl^{-1} cholesterol solution at pH 7.0).

The effect of pH on the activity of immobilized COD was studied over the range 5.0—8.0 by using phosphate buffers (0.1 M) as the carrier stream. The peak height for 50 mg dl^{-1} cholesterol reached a maximum at pH 7.0 but dropped sharply at pH 7.5. The immobilized enzyme therefore had the same optimum pH as the soluble enzyme [13].

Soluble enzymes are often very sensitive to temperature, and at elevated temperatures denaturation occurs. The peak height for 10 mg dl^{-1} cholesterol (at pH 7.0) obtained with the immobilized enzyme increased almost linearly with increasing temperature from 25°C up to 50°C but then decreased at 55°C. In comparison the soluble enzyme is not very stable even at room temperature. However, to increase the lifetime of the enzyme, subsequent experiments were done at 30°C, at which temperature the immobilized enzyme showed good activity.

Calibration. The manifold for cholesterol determination is shown in Fig. 1. Cholesterol standard solutions were injected into the system and the peak height responses gave a linear calibration graph for 0—80 mg dl^{-1} cholesterol (Fig. 3) with a r.s.d. of 1.0—3.0%. The sample throughput was 80 h^{-1}. As little as 0.2 μg of cholesterol could be detected.

Cholesterol oxidase catalyzes the oxidation of cholesterol and other 3-β-hydroxysterols but the rate of oxidation decreases in the order cholesterol > *p*-sitosterol > camphosterol > stigmasterol [14]. Therefore the response to phytosterols such as sitosterol and stigmasterol was also measured. The calibration graphs obtained are also shown in Fig. 3. The enzyme shows significant sensitivity to these sterols. This suggests that when cholesterol is determined, all β-hydroxysterols will contribute to the response. The levels of these other sterols in serum is negligible, so that the determination of cholesterol in blood should be specific, but their presence in food products is significant, and they will therefore interfere.

Determination of free cholesterol in blood. Two control sera, Versatol Hi (with an elevated cholesterol level) and Versatol Lo (with a lower cholesterol level than normal) were reconstituted and diluted three-fold with the diluent supplied and an amount of Triton X-100 equivalent to that present in the

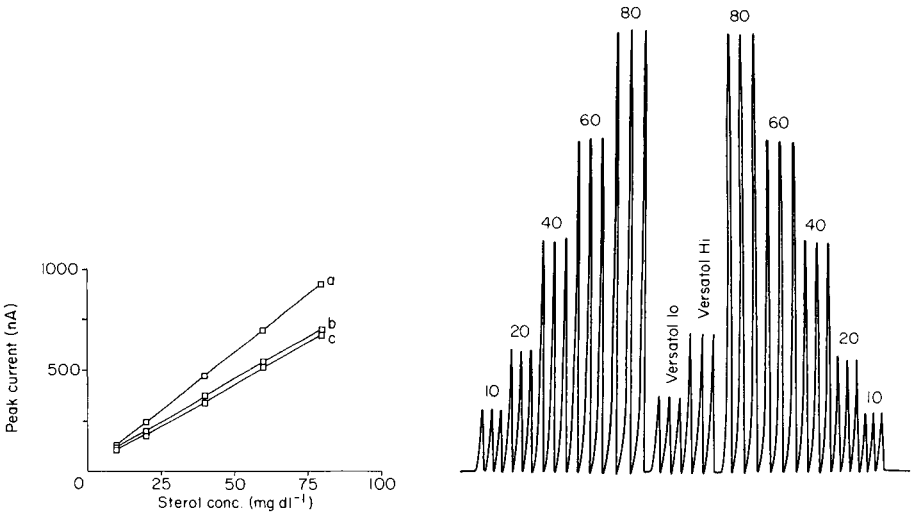

Fig. 3. Calibration graphs for: (a) cholesterol; (b) sitosterol; (c) stigmasterol.

Fig. 4. Calibration and control sera responses.

standard cholesterol solutions. Figure 4 shows a typical recorder output for a series of cholesterol standards and the two control sera. The results are summarized in Table 1.

The concentration of free cholesterol in blood is 38—40% of the total cholesterol present, and 60—62% of it is in an esterified form, which is not a substrate for COD. The total cholesterol values assigned to the control sera used are 186 and 96 mg dl^{-1} with a consensus range of ±9 mg dl^{-1}, as determined by the classical enzymatic procedure [7]. Therefore 38—40% of the totals for free cholesterol are 71—74 and 36—38 mg dl^{-1}, respectively. The values of 72 and 40.5 mg dl^{-1} obtained by the present procedure show good agreement, indicating the validity of the procedure for free cholesterol determination in blood.

Analysis of wax-wool alcohol and butter for sterols. Wax-wool alcohol is extracted from saponified wool grease for use in cosmetic preparations. Its cholesterol content is determined routinely by using a tedious chemical method. A pre-analysed sample of this wax-wool alcohol was obtained and analysed by the present method. Six solutions of 0—100 mg dl^{-1} wax-wool alcohol were injected into the system which was calibrated with pure cholesterol solutions. The cholesterol concentration obtained was 30.0 ± 4.3% (standard deviation) as compared to the expected 32%.

The Libermann-Burchard colour reaction [15] and g.l.c. [16] have mainly been used in the analysis of butter for cholesterol. Results obtained by the present procedure were 2.40 ± 0.02 g kg^{-1} (for 6 separate determinations) are well within the range obtained for butter by g.l.c. (2.27 g kg^{-1}) and the Libermann-Burchard reaction (2.70 g kg^{-1}).

TABLE 1

Calibration data for standard cholesterol solutions and control sera

	Standards					Control sera	
Cholesterol (mg dl^{-1})	10	20	40	60	80	V.Hi[a]	V.Lo[b]
Peak height[c] (nA)	129	244	482	696	925	293	161
S.d. (nA)	3.1	7.8	5.9	4.3	7.5	2.9	2.3
R.s.d. (%)	2.4	3.2	1.2	0.6	0.8	1.0	1.4

[a] 71—74 mg dl^{-1} (see text). [b] 36—38 mg dl^{-1} (see text). [c] Mean of 6 readings.

Stability of cholesterol oxidase. Cholesterol oxidase immobilized on CPG by cross-linking with glutaraldehyde showed very high stability. The same enzyme column has been used at room temperature for over 3 months, without observing any loss in activity.

The authors thank Mr. S. J. Leigh of Croda Chemicals, Goole, for providing the pre-analysed wax-wool alcohol sample.

REFERENCES

1 R. I. Levy, Clin. Chem., 27 (1981) 653.
2 J. Sweeney and J. L. Weihrauch, Crit. Rev. Food. Sci. Nutr., 8 (1976) 131.
3 B. Zak, Clin. Chem., 23 (1977) 1201.
4 C. Tu, W. D. Powrie and O. Fennema, J. Food Sci., 35 (1970) 601.
5 A. J. Sheppard, D. R. Newkirk, W. D. Hubbard and T. Osgood, J. Assoc. Off. Anal. Chem., 60 (1977) 1302.
6 D. R. Newkirk and A. J. Sheppard, J. Assoc. Off. Anal. Chem., 64 (1981) 54.
7 C. C. Allain, L. S. Poon, C. S. G. Cham, W. Richmond and P. C. Fu, Clin. Chem, 20 (1974) 470.
8 I. Karube, K. Hara, H. Matsuoka and S. Suzuki, Anal. Chim. Acta, 139 (1982) 127.
9 H. S. Huang, J. W. Kuan and G. G. Guilbault, Clin. Chem., 21 (1975) 1605.
10 H. S. Huang, S. S. Kuan and G. G. Guilbault, Clin. Chem., 23 (1977) 671.
11 M. Masoom and A. Townshend, Anal. Chim. Acta, 166 (1984) 111.
12 Methods of Enzymatic Food Analysis, Boehringer, Mannheim, W. Germany, 1984.
13 A. Noma and K. Nakayama, Clin. Chem. N.Y., 22 (1976) 336.
14 J. Reitsch and B. Entressangles, Rev. Fr. Corps Gras, 27 (1980) 185.
15 D. E. Lacroix, W. A. Mattingly, N. P. Wong and J. A. Alford, J. Am. Diet. Assoc., 62 (1973) 275.
16 L. M. Lampert, Ind. Eng. Chem. Anal. Ed., 2 (1930) 159.

Analytica Chimica Acta, 174 (1985) 299—303
Elsevier Science Publishers B.V., Amsterdam — Printed in The Netherlands

Short Communication

A CHLOROQUINE MEMBRANE ELECTRODE WITH LOW DETECTION LIMIT

VASILE V. COŞOFREŢ

Institute of Chemical and Pharmaceutical Research Bucharest, 74351-Sos. Vitan 112, Bucharest-3 (Romania)

RICHARD P. BUCK*

Department of Chemistry, University of North Carolina, Chapel Hill, NC 27514 (U.S.A.)

(Received 11th December 1984)

Summary. A PVC membrane electrode for chloroquine [7-chloro-4-(4-diethylamine-1-methylbutylamino)-quinoline] based on a chloroquine/dinonylnaphthalene sulphonic acid ion-pair is described. The electrode shows near-Nernstian response in the 10^{-2}—10^{-6} M range and a detection limit of 2×10^{-7} M. Its selectivity relative to various inorganic ions, amino acids, neurotransmitters, drugs, and some excipients is reported. Direct potentiometry is used to determine chloroquine in pharmaceutical preparations with good results.

Several antimalarial compounds of the aminoquinoline class possess significant activity against hepatic amoebiasis in hamsters and in man. The most important are chloroquine, hydroxychloroquine and quinacrine. However, only chloroquine (I) has found acceptance in the treatment of amoebiasis. It is active against hepatic amoebiasis in hamsters but has little or no activity when tested against intestinal infections in animals. Chloroquine is used for

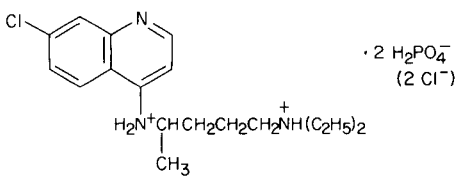

(I)

the treatment of extra-intestinal amoebiasis in man, but has poor activity against the intestinal form, presumably because it is so readily absorbed that it does not reach effective concentrations [1]. The U.S. Pharmacopeia [2] recommends that chloroquine in pharmaceutical preparations be determined by extraction with chloroform followed by spectrophotometry at 343 nm.

Many ion-selective membrane electrodes sensitive to various drugs have been reported [3, 4], but not many of them provide acceptable detection limits and selectivity. The use of dinonylnaphthalene sulphonic acid (DNNS) as a counter ion in poly(vinyl chloride) (PVC) membranes, plasticized with dioctylphthalate, has led to coated-wire electrodes with good selectivity for

0003-2670/85/$03.30

organic cations over common inorganic cations [5]. Important results were obtained by Freiser and co-workers [6—8], who developed membrane electrodes selective to many drugs of abuse, β-adrenergic and calcium blockers and other pharmaceuticals. DNNS has also been used in phenothiazine PVC membrane electrodes [9] which were useful in pharmaceutical analysis.

This communication describes a sensitive and selective PVC-membrane electrode based on chloroquine/DNNS as the electroactive material and *o*-nitrophenyloctyl ether (*o*-NPOE) as plasticizer. This electrode is useful for the assay of chloroquine in ranges down to 1 μg ml^{-1} with good precision. The low detection limit (64 ng ml^{-1}) makes it suitable for the analysis of biological samples without preconcentration because the therapeutic concentration range is about 120 ng ml^{-1} [10]. The principal interferences in the determination are the metabolites of chloroquine. Among them *N*-desetylchloroquine, which represents the major metabolic pathway (about 23% of the detectable urinary excretion) as well as bis(desetyl)chloroquine, 4′-hydrochloroquine, 4′-carboxychloroquine and 4-amino-7-chloroquine (all of which account for less than 3% of the total dose) are under investigation.

Experimental

Reagents and materials. All reagents were of analytical-reagent grade, used as received. Chloroquine diphosphate (Sigma), *o*-nitrophenyloctyl ether (Fluka), PVC of high molecular mass (Aldrich) and DNNS (Pfaltz and Bauer) were used. Pharmaceutical preparations (USP quality) were obtained from local drug stores. All solutions were prepared with distilled water in a 0.05 M potassium hydrogenphthalate/sodium hydroxide buffer of pH 4.2. Ionic strength was maintained in all cases at 0.05 M.

Electrode preparation and handling. The PVC membrane and the electrode were prepared as described elsewhere [9], except that the membrane composition was 4.0% (w/w) DNNS, 32.0% (w/w) PVC and 64.0% (w/w) *o*-NPOE. The DNNS in the polymer membrane was converted to the chloroquine-form by soaking the electrode in a solution of 10^{-2} M chloroquine diphosphate for 24 h after electrode preparation. The electrode, containing 10^{-3} M chloroquine diphosphate solution at pH 4.2 as internal solution, was stored between measurements in the same solution.

E.m.f. measurements and electrode calibration. Potentiometric measurements were made with a digital pH/mV meter (Orion Model 701A or Pracitronic Model MV 870). The $(chloroquine)^{2+}$-selective membrane eletrode was used with an Orion double-junction silver/silver chloride reference electrode (Model 91-01) with 10% (w/v) potassium nitrate in the outer compartment. The pH was measured with an Orion 91-02 glass combination electrode or with a Radiometer G202B glass electrode in conjunction with a Radiometer calomel electrode (K401). Electrode calibration was done in the usual way.

Direct potentiometric measurement of chloroquine in the microgram range. The electrode pair was placed in the aqueous solution of chloroquine (25.0 ml) buffered at pH 4.2. After equilibration by stirring, the e.m.f. was

recorded and compared with the calibration graph. The value obtained was checked by a standard addition. For this purpose, 1.0 ml of standard 10^{-4} M chloroquine diphosphate was added.

Potentiometric assay of chloroquine hydrochloride in injectable solutions. The contents of five ampules of chloroquine hydrochloride injections (5 ml each; 1 ml is equivalent to 40 mg of base) were mixed in a 100-ml beaker. An aliquot (1.0 ml) was diluted to the mark with distilled water in a 100-ml volumetric flask (solution A); 1.0 ml of this solution was pipetted into a 250-ml volumetric flask and the volume was adjusted to the mark with the hydrogenphthalate pH 4.2 buffer (solution B). An aliquot (25.0 ml) of solution B was pipetted into a 100-ml beaker and both indicator and reference electrodes were immersed. After electrode equilibration by stirring and recording of the e.m.f., 1.0 ml of standard 10^{-3} M chloroquine diphosphate at pH 4.2 was added and the change in e.m.f. was recorded and used to calculate the chloroquine hydrochloride content of the ampules.

Potentiometric assay of chloroquine diphosphate in tablets. Five tablets from the same lot were finely powdered. A portion of the powder, equivalent to about 100 mg of chloroquine diphosphate, was dissolved in distilled water in a 100-ml volumetric flask and the solution was diluted to the mark (solution A). An aliquot (1.0 ml) of solution A was pipetted into a 250-ml volumetric flask and the volume was adjusted to the mark with the hydrogenphthalate pH 4.2 buffer (solution B). An aliquot (25.0 ml) of solution B was used for the chloroquine assay as described above.

Results and discussion

Membrane material. Chloroquine reacts with DNNS to form a stable water-insoluble ion-pair which is very soluble in the membrane phase. The ion-pair was obtained in situ by soaking the DNNS/PVC membrane in the chloroquine diphosphate solution. Of the plasticizers tested, *o*-nitrophenyloctyl ether, dioctylphthalate and di-isobutylphthalate, the first showed the best response times and reproducibility.

Electrode characteristics. The critical response characteristics of the electrode membrane are summarized in Table 1. Calibrations were done at pH 4.2 and a constant ionic strength of 0.05 M, provided by using the specified hydrogenphthalate pH 4.2 buffer. The calibration curves for a set of five chloroquine membrane electrodes were found to be similar and reproducible from day to day.

The effect of pH on the potential readings was studied by recording the e.m.f. obtained for 10^{-3} and 10^{-4} M chloroquine solutions which had been adjusted to different pH values by addition of very small volumes of sodium hydroxide and/or hydrochloric acid solutions. The potential/pH plots indicated that the potentials were almost independent of pH in the range 2—8. At higher pH values, the e.m.f. decreased because of the gradual increase in the concentration of unprotonated chloroquine and so the precipitation of chloroquine base.

TABLE 1

Response characteristics for the chloroquine membrane electrode

Parameter	Value
Slope[a] (mV/log a)	28.6 ± 0.42[b]
Intercept (mV)	301 ± 2.1[c]
Linear range (M)	10^{-2}—10^{-6}
Useable range (M)	10^{-2}—5×10^{-7}
Detection limit	2×10^{-7} M (64 ng ml^{-1})

[a]Average value calculated for 10^{-3}—10^{-5} M range. [b]Standard deviation of average slope value for multiple calibrations (153 values). [c]Standard deviation of values recorded during one month.

The selectivity of the chloroquine-membrane electrode is related to the free energy of transfer of the doubly-charged chloroquine cation between the aqueous and organic phases. As a check on possible cationic interferences, the electrode was calibrated in chloroquine diphosphate solutions containing a fixed amount (10^{-2} M) of various possible interfering substances [11]. The data in Table 2 show that the electrode exhibits negligible interference from various drugs, amino acids, and lower quaternary ammonium compounds. There is essentially no response to the inorganic cations commonly present in pharmaceutical or biological samples. Many lipophilic amines (alkaloids, phenothiazines, phencyclidine, amitriptyline and similar compounds, chlorpheniramine, diphenhydramine, methadone, propranolol, higher quaternary ammonium compounds, etc.) interfere. As far as is known, chloroquine is never present together with such compounds, either in pharmaceuticals or in clinical samples; therefore, relevant selectivity coefficients were not evaluated.

The chloroquine membrane electrodes provided stable e.m.f. readings within 30 s in the 10^{-2}—10^{-5} M range. In very dilute solutions ($\leqslant 10^{-6}$ M),

TABLE 2

Selectivity coefficients for the chloroquine membrane electrode[a]

Interfering species	$K_{i,j}^{Pot}$	Interfering species	$K_{i,j}^{Pot}$
K^+, Na^+, Ca^{2+}, Mg^{2+}	$<10^{-4}$	Choline	9.3×10^{-4}
L-Arginine	1.1×10^{-4}	Acetylcholine	1.0×10^{-3}
L-Histidine	1.1×10^{-4}	Arecoline	2.3×10^{-2}
L-Glycine	1.1×10^{-4}	Carbachol[b]	1.5×10^{-4}
Isoniazid	1.2×10^{-4}	Succinylcholine	1.4×10^{-4}
γ-Aminobutyric acid	1.1×10^{-4}	$(CH_3)_4N^+$	7.6×10^{-3}
Dopamine	1.2×10^{-4}	$(C_2H_5)_4N^+$	6.8×10^{-1}

[a]The chloroquine cation is indicated as i, the interference as j. [b]Carbamylcholine.

TABLE 3

Determination of chloroquine in ARALEN preparations (Winthrop) with the chloroquine membrane electrode and standard addition[a]

Product	Sample	Result (% of nominal)	Product	Sample	Result (% of nominal
ARALEN hydrochloride	1	98.7 (1.10)	ARALEN phosphate	1	101.2 (0.87)
(injectable solutions;	2	100.8 (1.22)	(500 mg/tablet)	2	99.9 (1.26)
5 ml/vial: 1 ml = 50 mg $CHQ^{2+}2Cl^-$)	3	99.3 (1.25)		3	96.7 (0.81)
	4	101.3 (1.60)		4	102.0 (0.72)

[a] V_x = 25.0 ml; V_s = 1.0 ml; C_s = 10^{-3} M. Values are the mean of five determinations with relative standard deviation (%) in parentheses.

response times were 1—2 min. Reproducibilities of e.m.f. readings were acceptable in both these ranges.

Applications. The chloroquine membrane electrode proved useful for quantifying chloroquine (chloride or phosphate form) by the standard addition method. The analysis of pure chloroquine diphosphate solutions (<2.0 μg ml^{-1}) provided an average recovery of 100.2% with a relative standard deviation of 1.7% (n = 10).

The determination of chloroquine in two pharmaceutical preparations gave good results (Table 3).

REFERENCES

1 W. J. Ross, in M. E. Wolff (Ed.), Burger's Medicinal Chemistry, 4th edn. Part II, Wiley, New York, 1981, Ch. 19.
2 United States Pharmacopeia, XX Rev., U.S. Pharmacopeial Convention, Rockville, MD (1980).
3 V. V. Coşofreţ, Membrane Electrodes in Drugs Analysis, Pergamon Press, Oxford, 1982.
4 V. V. Coşofreţ and R. P. Buck, Ion-Selective Electrode Rev., 6 (1984) 59.
5 C. R. Martin and H. Freiser, Anal. Chem., 52 (1980) 562.
6 T. Yamada and H. Freiser, Anal. Chim. Acta, 125 (1981) 179.
7 L. Cunningham and H. Freiser, Anal. Chim. Acta, 139 (1982) 97.
8 L. Cunningham and H. Freiser, Anal. Chim. Acta, 157 (1984) 157.
9 V. V. Coşofreţ and R. P. Buck, Analyst, 109 (1984) 1321.
10 W. Sadeé and G. C. M. Beelen, Drug Level Monitoring, Wiley, New York, 1980.
11 P. Bailey, Analysis with Ion-Selective Electrodes, 2nd Edn., Heyden, London, 1980.

Analytica Chimica Acta, 174 (1985) 305—311
Elsevier Science Publishers B.V., Amsterdam — Printed in The Netherlands

Short Communication

PRECONCENTRATION OF TRACE METALS IN NATURAL WATERS WITH 2,2'-DIPYRIDYL-4-AMINO-3-HYDRAZINO-5-MERCAPTO-1,2,4-TRIAZOLEHYDRAZONE SUPPORTED ON SILICA GEL

C. SAMARA and TH. A. KOUIMTZIS*
Laboratory of Analytical Chemistry, University of Thessaloniki, Thessaloniki (Greece)
(Received 23rd January 1985)

Summary. The new hydrazone, supported on silica gel, is used to preconcentrate traces of copper, zinc, lead, nickel, cobalt and cadmium from tap, lake and sea water. Conditions for quantitative retention are established. Copper, zinc, lead, cadmium and nickel are quantitatively eluted with 0.1 M EDTA, and cobalt with 2 M perchloric acid. The metals are measured by atomic absorption spectrometry.

Direct determination is possible for only a restricted number of trace elements in natural waters. Preconcentration prior to quantifying the element is needed in most cases. Various methods are used to preconcentrate metals from natural waters. Complexation with organic reagents supported or immobilized on various supports is becoming increasingly popular, on account of high selectivity, simplicity and effectiveness [1—7]. The purpose of this communication is to introduce a new hydrazone, 2,2'-dipyridyl-4-amino-3-hydrazino-5-mercapto-1,2,4-triazolehydrazone (DPTH), as a selective reagent for preconcentration of certain metal ions. This hydrazone is insoluble in water and its solubility in common organic solvents is very low. It dissolves in dimethylformamide. It is shown below that this reagent, supported on silica gel, is useful for the preconcentration of copper, lead, nickel, zinc, cadmium and cobalt.

Experimental

Reagents. 2,2'-Dipyridyl-4-amino-3-hydrazino-5-mercapto-1,2,4-triazolehydrazone was prepared by heating together, in ethanol, di-2-pyridyl ketone and 4-amino-3-hydrazino-5-mercapto-1,2,4-triazole. The hydrazine, which has a low solubility in ethanol, remained as a solid when the ketone was added in small excess. The mixture was refluxed until all the hydrazine had dissolved, at which time the yellow hydrazone began to deposit. The crude product was recrystallized twice from ethanol (m.p. 274—277°C). The hydrazone was identified by elemental analysis and i.r. and mass spectral characteristics.

A 2×10^{-4} M solution of DPTH was prepared in ethanol. Concentrated solutions of DPTH were prepared in dimethylformamide. Metal ion solutions

0003-2670/85/$03.30

were prepared from their nitrates; their concentrations were determined by EDTA titration. Buffer solutions were passed through a column of DPTH on silica gel prior to use. Analytical-reagent grade chemicals were used throughout.

Apparatus. Perkin-Elmer 403 and Pye-Unicam SP190 atomic absorption spectrometers were used for all trace metal measurements.

Preparation of DPTH on silica gel. Silica gel of chromatographic grade (Merck, Kieselgel-40, 35—70 mesh ASTM) was soaked with twice its volume of (1 + 1) hydrochloric acid for a day and washed with deionized water until free from chloride. It was then soaked with twice its volume of (1 + 2) nitric acid for 24 h, washed with deionized water and dried at 120°C for 24 h. About 100 g of treated silica gel was stirred with 100 ml of dimethylformamide containing 1.5 g of DPTH. After standing for 24 h, the silica gel impregnated with DPTH was heated at ca. 80°C under reduced pressure to remove all dimethylformamide. The dried material was washed repeatedly with deionized water to dislodge any unadsorbed reagent until the washings appeared clear. Finally, the yellow product was dried at ca. 80°C under reduced pressure and stored in a dark glass bottle.

Batch experiments. A 10-ml sample solution containing a known amount of the studied metal ion was adjusted to the appropriate pH and shaken with 0.5 g of DPTH on silica gel in a 100-ml glass-stoppered flask. The supernatant liquid was filtered through a dry filter paper. The metal ion concentration was determined in aliquots of the filtrate by atomic absorption spectrometry (a.a.s.). The pH of the filtrate was also measured.

Column experiments. A glass column (10 mm i.d., 140 mm long), with a coarse sintered-glass disc and a stopcock at the bottom, was filled with 2—4 g of DPTH on silica gel to give a bed height of 6—12 cm. A given volume of aqueous sample containing the individual metal ions was adjusted to a suitable pH, and percolated through the column at 1—4 l h^{-1}, under mild suction. After passage of the sample, the column was washed with 20 ml of deionized water, and an eluting solution (see below) was passed through at 1—3 ml min^{-1}. The effluent was collected in a volumetric flask and diluted to volume, and the metal ion was quantified by a.a.s. In all cases, reagent blanks were measured, and standard solutions were used for calibration.

Analysis of tap, lake and sea water. Adjust 1—2 l of water sample to pH 7. Add sodium fluoride (ca. 1 g l^{-1}) followed by 10 ml of 1 M sodium acetate, and stir for a few minutes. Pass the solution through the column at 1 l h^{-1}. Wash the column with deionized water, and pass 25 ml of 0.1 M EDTA at 1 ml min^{-1}. Collect the effluent in a 25-ml volumetric flask, and determine the metal ion concentration by a.a.s. (only a small part of the calcium fluoride retained on the column is dissolved by the EDTA, but this has not any significant effect on the results). To re-use the column, wash it with 1.0 M EDTA and with deionized water.

Results and discussion

The DPTH reagent, like most hydrazones, forms chelates with various metal ions, especially those of the transition series; DPTH supported on silica gel also forms chelates, and as a result the metal ions are concentrated from dilute solutions.

The amount of DPTH which could be supported on silica gel was determined spectrophotometrically after its elution with dimethylformamide; it was found to be 4 ± 1 mg g^{-1}. The chelating capacity of DPTH on silica gel is sufficient (e.g., ca. 13 μmol Cu^{2+} at pH 5) to collect metals from large volumes of natural waters. The solid material showed no change in its capacity after a storage period of several months. Another advantage of this material is that elution of DPTH from silica gel with aqueous solutions in the pH range 1—9 is negligible. The adsorbent could be re-used several times.

Effect of pH on recovery of metal ions. The recovery of each metal ion from an aqueous solution at various pH values was examined by batch experiments; 10 ml of solution containing 100 μg of metal and 0.5 g of the chelating material were used. The results for DPTH on silica gel and silica gel alone are illustrated in Fig. 1. The pH values were measured after equilibration. A significant difference in retention between DPTH on silica and untreated silica gel is observed for copper, cobalt, nickel and cadmium. It is known, however, that silica gel itself can bind various multicharged metal ions [8].

The retention of metal ions from aqueous solutions was also examined after various shaking times. The results showed that the metal ions were collected very rapidly on the chelating material. Thus, copper, zinc, cadmium

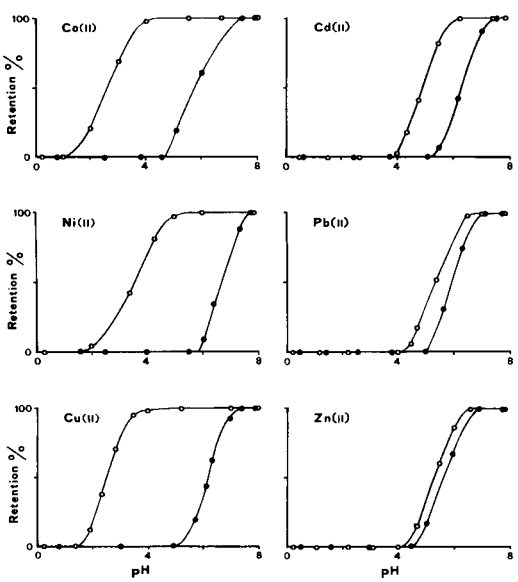

Fig. 1. Effect of pH on retention of metal ions from aqueous solution: (○) DPTH on silica gel; (●) untreated silica gel.

and lead were collected quantitatively in 3 min, while cobalt and nickel required 6 min.

Elution of metal ions. The elution of metal ions from DPTH on silica gel was examined by batch equilibration and column operation. Several solutions were tested first by the batch method. The results obtained showed that ca. 10 μg of copper, zinc, cadmium, nickel and lead were quantitatively eluted with 0.1 M EDTA or DPTA while cobalt remained on the gel. It was also found that copper, zinc, cadmium and nickel were quantitatively eluted with 0.1 M potassium cyanide. About 85% of the cobalt was eluted with this cyanide solution but lead remained on the column. Cobalt was quantitatively eluted from the column by $\geqslant$1.5 M perchloric acid, but elution of DPTH from the gel was also observed.

Similar results were obtained when the above eluting solutions were applied to column operation. Results obtained for the elution of 25 μg of copper with EDTA and cyanide are given in Fig. 2. Therefore, EDTA was used to elute copper, zinc, cadmium, nickel and lead, while perchloric acid was used for elution of cobalt.

Retention of metal ions on the column. The retention of the studied metal ions on the column was examined under various experimental conditions. Various volumes of deionized, tap, lake or sea water, containing metal ions at various concentrations, were passed through the column at different flow rates. The amount of retained metal ion was determined after elution with 0.1 M EDTA. For cobalt the elution was done with 2 M perchloric acid. The results obtained for deionized water solutions at pH 7, 0.01 M in acetate, are summarized in Table 1. They show that the retention of the metal ions is quantitative.

Interferences. The effect of various substances on the retention of metal ions on the column was examined. For this purpose, 1 l of a test solution containing 10 μg l^{-1} of the studied metal ion, and other ions at various concentrations, was passed through the column. The amount of metal ion

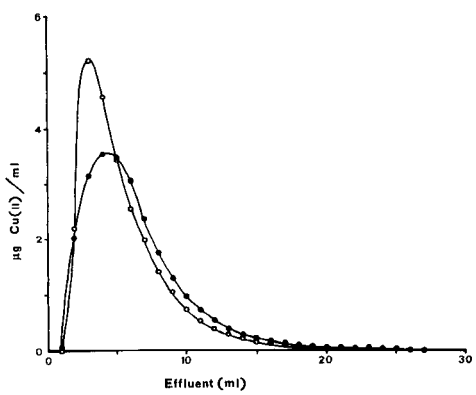

Fig. 2. Elution of copper(II) retained on the DPTH column with: (○) 0.1 M potassium cyanide; (●) 0.1 M EDTA.

TABLE 1

Recovery of metal ions from 3 g of DPTH on silica gel, with column operation

Metal ion	Sample vol. (l)	Flow rate ($l\ h^{-1}$)	Metal ion conc. ($\mu g\ l^{-1}$)	Recovery[a] (%)
Cu^{2+}	0.5	1.0	12	100 ± 2
	1.0	2.0	5	98 ± 3
	2.0	3.0	3	94 ± 3
Zn^{2+}	0.5	1.0	10	100 ± 2
	1.0	2.0	4	100 ± 2
	2.0	3.0	2	99 ± 3
Cd^{2+}	0.5	1.0	10	100 ± 3
	1.0	2.0	4	98 ± 3
	2.0	3.0	2	95 ± 4
Ni^{2+}	0.5	1.0	12	100 ± 2
	1.0	2.0	5	99 ± 2
	2.0	3.0	3	96 ± 3
Pb^{2+}	0.5	1.0	12	100 ± 2
	1.0	2.0	5	99 ± 3
	2.0	3.0	3	97 ± 5
Co^{2+}	0.5	1.0	12	100 ± 2
	1.0	2.0	10	100 ± 3
	2.0	3.0	10	97 ± 4

[a]Mean of 5 determinations ± standard deviation.

TABLE 2

Effect of ions on the recovery of metal ions from the DPTH column

Ion	Concentration	Recovery (%)				
		Cu	Ni	Cd	Pb	Zn
Fe^{3+}	1 mg l^{-1}	100	100	100	100	100
	2 mg l^{-1}	90	88	85	85	90
Ca^{2+}	1 mg l^{-1}	100	100	100	100	100
	2 mg l^{-1}	100	100	90	88	100
	3 mg l^{-1}	80	85	60	50	88
PO_4^{3-}	10^{-4} M	70	89	70	45	100
	10^{-5} M	100	100	100	100	
Citrate	10^{-4} M	66	45	55	40	100
	10^{-5} M	100	100	100	100	
	10^{-5} M	100	100	100	100	
Tartrate	10^{-4} M	100	88	60	40	100
	10^{-5} M		100	100	100	
Oxalate	10^{-4} M	100	47	20	80	100
	10^{-5} M		100	100	100	

retained was determined after elution. The results obtained showed that the presence of each of the studied metal ions had no effect on the retention of the others at concentrations up to 1 mg l^{-1}. Common ions such as Na^+, K^+, Cl^-, sulphate, nitrate and acetate did not interfere. The presence of acetate ions was found to be favourable for the retention of the metal ions, probably because the monoacetate complexes of cations exchange more rapidly than the hydroxo complexes which are formed at pH 6—7 [9].

The effects of various other ions and substances are given in Table 2. These results show that large amounts of calcium affect the retention of the metal ions. Thus, when the recovery of metal ions from laboratory tap water (hardness about 270 mg l^{-1} $CaCO_3$) and sea water was examined, it was found to be much less than quantitative. This interference was overcome by treating the samples with sodium fluoride, which precipitated most of the calcium. The efficiency of recovery of spikes added to both tap and sea water with and without addition of sodium fluoride at pH 7 in 0.01 M acetate, are given in Table 3. The recovery was measured by the standard addition method.

Analysis of water samples. Tap, lake and sea waters were analysed for

TABLE 3

Recovery of metal ion spikes from tap and sea water

Metal added	Conc. ($\mu g\ l^{-1}$)	Tap water[a]		Sea water[a]	
		No NaF	NaF	No NaF	NaF
Cu	5.0	75 ± 5	98 ± 3	70 ± 6	93 ± 3
Zn	80.0	83 ± 3	98 ± 2	75 ± 5	98 ± 4
Cd	5.0	65 ± 6	95 ± 4	55 ± 7	90 ± 5
Pb	10.0	65 ± 6	94 ± 5	55 ± 8	90 ± 6
Ni	5.0	67 ± 4	94 ∓ 3	57 ± 5	92 ± 4

[a]Mean of 5 determinations ± standard deviation.

TABLE 4

Analytical results for tap, lake and sea water samples

Metal	Concentration ($\mu g\ l^{-1}$)					
	Tap water		Lake water		Sea water	
	a	b	a	b	a	b
Cu	3.3	3.5	3.7	3.9	5.0	5.3
Zn	220.0	231.0	34.0	35.5	42.5	41.0
Cd	—	—	1.7	1.8	3.2	4.3
Ni	3.0	3.1	3.8	4.0	7.8	8.2
Pb	15.8	17.3	12.0	13.4	16.8	18.9

[a]Present method. [b]Standard addition a.a.s. procedures [10, 11].

copper, nickel, zinc, cadmium and lead by the recommended procedure. The results are summarized in Table 4, and are in good accordance with these found by independent methods. Samples of sea water (near-shore at Agia Triada Thermaikos gulf) and lake water (lake of Agiou Vasiliou) were filtered during collection and acidified to pH 1.5 with nitric acid for storage purposes.

REFERENCES

1 K. Terada, K. Matsumoto and H. Kimura, Anal. Chim. Acta, 153 (1983) 237.
2 J. Jezorek and H. Freiser, Anal. Chem., 51 (1979) 366.
3 S. Willie, R. Sturgeon and S. Berman, Anal. Chim. Acta, 149 (1983) 59.
4 L. Saari and W. Seitz, Anal. Chem., 56 (1984) 813.
5 K. Terada and K. Nakamura, Talanta, 28 (1981) 123.
6 K. Terada, K. Morimoto and T. Kiba, Anal. Chim. Acta, 116 (1980) 127.
7 K. Terada, K. Matsumoto and Y. Taniguchi, Anal. Chim. Acta, 147 (1983) 411.
8 O. Wolfbeis and H. Offenbacher, Fresenius Z. Anal. Chem., 319 (1984) 282.
9 P. Burba, K. Lieser, V. Neitzert and H. Röber, Fresenius Z. Anal. Chem., 291 (1978) 273.
10 Standard Methods for the Examination of Water and Wastewater, 13th edn., 1971, p. 417.
11 Manual of Methods in Aquatic Environment Research, FAO, Rome 1975, Part 1, p. 202.

Analytica Chimica Acta, 174 (1985) 313—316
Elsevier Science Publishers B.V., Amsterdam — Printed in The Netherlands

Short Communication

DETERMINATION OF UREA BY ION CHROMATOGRAPHY WITH AN IMMOBILIZED UREASE REACTOR

SHUNICHI UCHIYAMA*, YOSHINOBU TOHFUKU, SHUICHI SUZUKI and GIICHI MUTO

Department of Environmental Engineering, The Saitama Institute of Technology, 1690, Fusaiji, Okabe, Saitama 369-02 (Japan)

(Received 7th December 1984)

Summary. An immobilized urease reactor can be used with ion chromatography for the simultaneous determination of urea, and sodium, potassium and ammonium ions. The conversion of urea to ammonium ion was found to be 76.5%. The calibration graph for urea was linear over the range 1×10^{-5}—1×10^{-3} M (RSD 3%). The method was applied to human urine and a chemical fertilizer.

Ion chromatography is a powerful technique for the determination of low levels of inorganic ions in various aqueous solutions [1, 2]. In general, however, it is difficult to determine neutral species because they have little affinity for ion-exchange resins and are not separated from each other. It is well known that some enzyme reactions convert neutral species to determinable ionic species such as ammonium or phosphate ions. Therefore, in this study, an immobilized enzyme column was used in conjunction with ion chromatography in order to increase the variety of species that can be determined. Simultaneous determination of ionic and neutral species is possible. In the proposed system, the immobilized enzyme column is attached between the injection loop and sample syringe, to convert neutral species to ions before the sample is introduced into the eluent. Only the pH-adjusted sample solution passes through the immobilized enzyme so that the activity of enzyme should be maintained for a long time.

The enzymatic hydrolysis of urea catalysed by urease was chosen to illustrate the method. Simultaneous determinations of sodium, ammonium and potassium ions and urea in human urine and chemical fertilizer were done successfully.

Experimental

A Dionex 2000i ion chromatograph with a conductivity detector was used. The eluent and regenerating solution were 0.005 M nitric acid and 0.02 M potassium hydroxide, respectively. Urease (E.C.3.6.1.1; Wako

0003-2670/85/$03.30

Chemicals) was immobilized on porous glass beads (pore size 70—150 μm) as described by Johansson and Ögren [3]. The treated beads (0.6 g) were filled into a glass column (5 mm i.d., 50 mm long), which was connected between the injection loop and sample syringe (Fig.1). The activity of the immobilized urease in this column was 0.70 unit (one unit liberates 1 mg of ammoniacal nitrogen from urea in 5 min at pH 7.0 at 30° C). The sample volume for each injection was chosen as 2 ml in order to eliminate any memory effect in the enzyme column. This volume is much larger than the dead space in the column. The sample was injected through the urease reactor into the sample loop during about 3 s. All chemicals used were reagent grade and all chromatographic experiments were done at room temperature (20°C).

Human urine was diluted 100 times with distilled water and this diluted solution was analysed in the above system. A chemical fertilizer containing urea (Seibu Kagaku S-500), 0.1 g, was dissolved in 1 l of distilled water, and the chromatograms of this solution were measured.

Results and discussion

Figure 2 shows the chromatograms for the determination of 1×10^{-3} M Na^+, K^+ and urea. The peak of urea appears clearly in the chromatogram obtained with the immobilized urease column. It should be emphasized that the sodium and potassium peaks were unaffected in shape and height when the sample had passed through the enzyme column. The precision of the peak height of urea was about 2.5%, which was about the same as that for Na^+ and K^+. No errors were caused by the manual injection of sample solution, and it is considered that the enzyme reaction rate is so fast that manual injection does not influence the conversion ratio of urea to ammonium ion.

The calibration graph for urea was linear over the concentration range from 1×10^{-5} M to 1×10^{-3} M (RSD 3%). The percentage conversion of urea to ammonium ion was calculated from the equation: conversion (%) = $100(h_{urea}/2h_{NH_4^+})$ where h is peak height; 2 mol of NH_4^+ is produced from 1 mol of urea by urease. From this equation and the calibration graphs for

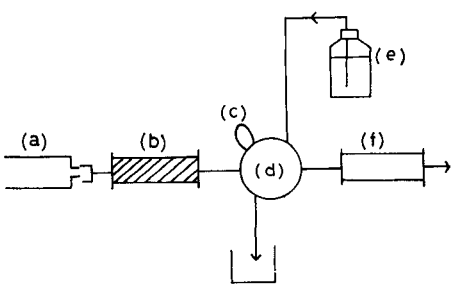

Fig. 1. Immobilized urease column reactor in ion chromatography. (a) Sample syringe; (b) immobilized urease reactor; (c) injection loop; (d) injection valve; (e) eluent; (f) guard column leading to separator column.

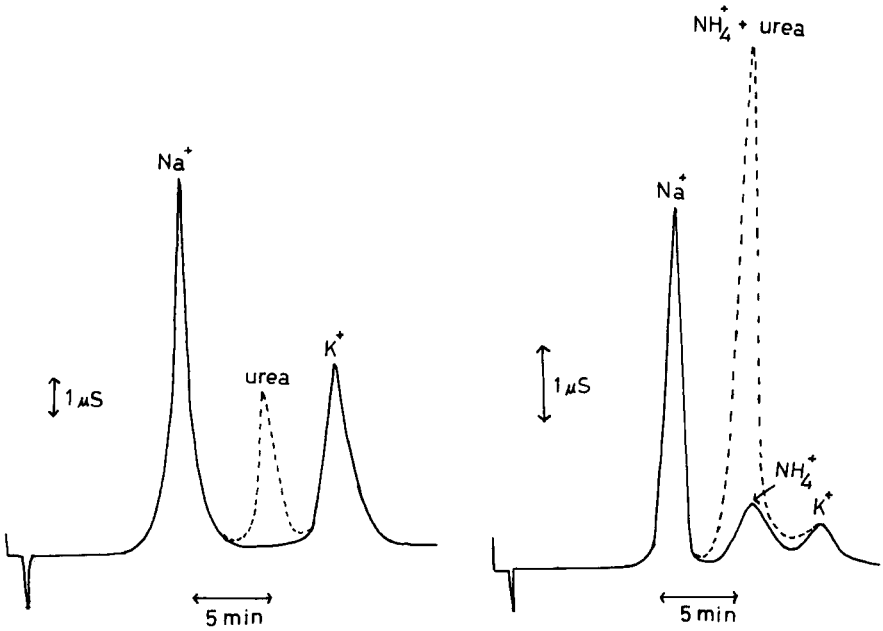

Fig. 2. Chromatograms for 1×10^{-3} M Na^+, urea and K^+: (---) with the immobilized urease reactor; (—) without the reactor.

Fig.3. Chromatograms for the determination of Na^+, NH_4^+, urea and K^+ in human urine: (---) with the immobilized urease reactor; (—) without the reactor.

urea and ammonium ion, the conversion was found to be 76.5%. This value did not decrease over three months, during which time about 10 chromatograms were run with the same urease reactor.

Figure 3 shows the chromatograms for the determination of Na^+, NH_4^+, K^+ and urea in human urine. The chromatogram obtained without the urease column has the same pattern as that reported by Anderson [4]. The ammonium peak is, of course, greatly increased when the sample is first passed through the enzyme reactor, and the difference in peak heights enables urea to be quantified. Chromatograms of the chemical fertilizer solution were obtained by the same method as for human urine, and urea and the cations were again determined. In chromatograms of human urine and chemical fertilizer, the concentrations of urea were calculated from a calibration graph for pure urea solutions. The results obtained for the urine and fertilizer are shown in Table 1.

From the results and discussion described above, ion chromatography with an immobilized enzyme reactor included should be effective for the simultaneous determination of neutral and ionic species. It is expected that this procedure could be applied with appropriate enzymes to many other neutral species.

TABLE 1

Results for human urine and chemical fertilizer (mean values of five determinations are given)

	Human urine ($\times 10^{-3}$ M)	RSD (%)	Chemical fertilizer (%)	RSD (%)
Na^+	52.3	2.1	0.582	2.2
	52.3[a]	2.0	0.582[a]	2.3
K^+	8.03	2.3	9.85	2.4
	8.03[a]	2.2	9.83[a]	2.2
NH_4^+	31.9	1.6	13.5	1.5
$CO(NH_2)_2$	315[a]	2.5	10.1[a]	2.4

[a]Results obtained with the immobilized urease column in position. Other results were calculated from calibration plots for Na^+, K^+ and NH_4^+ obtained by conventional ion chromatography without the urease reactor.

We thank Mr. T. Fijihira, T. Hara and S. Ohsawa for their experimental assistance.

REFERENCES

1 H. Small, T. S. Stevens and W. C. Bauman, Anal. Chem., 47 (1975) 1801.
2 H. Small, Anal. Chem., 55 (1983) 235A.
3 G. Johansson and L. Ögren, Anal. Chim. Acta, 84 (1976) 23.
4 C. Anderson, Clin. Chem., 22 (1976) 1424.

Analytica Chimica Acta, 174 (1985) 317—322
Elsevier Science Publishers B.V., Amsterdam — Printed in The Netherlands

Short Communication

IDENTIFICATION OF THE DECOMPOSITION PRODUCTS OF NITROBENZANTHRACENES IN SOLUTION

BERIT IVERSEN and TYGE GREIBROKK*

Department of Chemistry, University of Oslo, P.O.B. 1033, Blindern, 0315 Oslo 3 (Norway)

(Received 27th February 1985)

Summary. Air oxidation products of nitrobenzanthracenes and nitrodibenzanthracenes were separated with high-performance liquid chromatography. The major products were identified as quinones, and the bulk of the minor products were identified as nitroquinones. Tentative structures are assigned on the basis of mass spectrometry.

Based on their mutagenic features in the Salmonella/microsome tests, nitro-substituted polynuclear aromatic hydrocarbons (nitro-PAH) and oxygenated derivatives of PAH and nitro-PAH are believed to account for a significant part of the "excess mutagenicity" of samples of airborne particulate matter [1, 2]. However, despite the fact that thousands of determinations of PAH and derivatives of PAH have been done around the world, the main contributors to this mutagenicity have still not been identified, and few nitro compounds have actually been found in such samples. Because the major methods of purification and separation in this area have been developed for determinations of PAH, and because later modifications have not necessarily improved the ability to purify and detect trace amounts of relatively polar PAH derivatives, it seems not unreasonable to state that the use of certain methods would need to be reconsidered. Supporting this statement is the reported fact that nitropyrene-3,6-diones could not be eluted by capillary gas chromatography [3].

Despite the indications that nitro compounds may be involved, few studies of the possible decomposition of nitro-PAH have been made. Pitts et al. [4] found that nitroanthracene was oxidized to anthraquinone and suggested that similar reactions could represent the fate of other nitro-PAH. Yasuhara and Fuwa [5] found that 1-nitropyrene-2-ol was produced by photolysis of 1-nitropyrene in the presence of air. Unlike many nitro-PAH, 1-nitropyrene-2-ol was not mutagenic in the absence of mammalian activation, but gave a mutagenic response similar to benzo(a)pyrene with a preparation containing rat liver microsome [2].

During the purification of nitrobenzanthracenes and nitrodibenzanthracenes [6], several compounds were found to be unstable in solution. This communication describes the main decomposition products in

0003-2670/85/$03.30

acetonitrile solution in the presence of air under normal laboratory lighting conditions. The products were purified by high-performance liquid chromatography (h.p.l.c.) and the structures were examined by mass spectrometry.

Experimental

Solvents and standards. All the solvents were h.p.l.c. grade S (Rathburn Chemicals, Walkerburn, G.B.). The nitro-PAH (see Table 1) were synthesized in this laboratory [6]. Benzanthraquinone was obtained from Aldrich.

Instrumentation. The h.p.l.c. fractionations were obtained with Waters Model 6000-A pumps, a U-6K injector and a Model 440 u.v. detector at 280 nm. The 70-eV electron impact mass spectra were obtained on a Jeol JMS-DX-303 mass spectrometer with the JMA-DA-5000 data system.

Procedure. Each nitro-PAH (0.1 mg) in 0.5 ml of acetonitrile was stirred magnetically in open vials at room temperature on the bench. Evaporated solvent was replaced at intervals. The gradual disappearance of the nitro-PAH and the formation of new products was followed by injecting 5-μl aliquots onto a 4.6 × 200-mm column of Brownlee MPLC-C18 which was eluted with methanol/water in ratios of 80:20 to 90:10. The ratios between the quinones and nitroquinones formed were evaluated from peak-height measurements after detection at 280 nm; approximately equal molar absorptivity was assumed. After a major part of the starting materials had disappeared, each solution was concentrated and fractionated on Hypersil 3-μm silica (9 × 250 mm) with dichloromethane/hexane (1:1). The chromatograms presented below were obtained on a 4.6 × 200-mm Brownlee MPLC silica column. The quinone and the nitroquinone fractions were collected, the solvent was evaporated, the residue was dissolved in 25—50 μl of acetone, and 0.5—1-μl aliquots were taken for direct probe introduction in the mass spectrometer. The fragmentation was examined at ion-source temperatures of 165°C and 200°C. The mass spectra given were obtained at 165°C.

Results and discussion

7-Nitrobenz(a)anthracene was oxidized more rapidly than 12-nitrobenz(a)-anthracene (Table 1), but both compounds gave the same main product, benz(a)anthracene-7,12-dione (Fig. 1). The quinone was identified by mass

TABLE 1

Half-lives of nitroanthracenes by stirring in acetonitrile solution open to air under normal laboratory lighting conditions

Compound	Half-life (days)
7-Nitrobenz(a)anthracene	10
12-Nitrobenz(a)anthracene	20
7-Nitrodibenz(a,h)anthracene	30
9-Nitrodibenz(a,c)anthracene	20

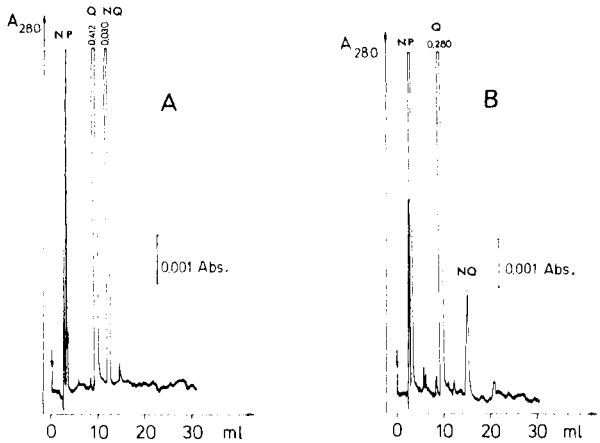

Fig. 1. H.p.l.c. separation of the oxidized products of 7-nitrobenz(a)anthracene (A) and 12-nitrobenz(a)anthracene (B) on 5-μm silica with dichloromethane/hexane (50:50) with detection at 280 nm. Peaks: Q, quinones; NQ, nitroquinones; NP, unreacted nitro-PAH.

spectrometric [7] and chromatographic comparison with an authentic sample. The loss of the nitro group and the formation of the quinone is thought to proceed through a radical reaction similar to the formation of anthraquinone from 9-nitroanthracene [8]. Both nitrobenzanthracenes produced small amounts of nitroquinones in addition (Fig. 1). The nitroquinones may have been formed by photochemical decomposition of peroxides from 1,4-addition of singlet oxygen [9] to the positions of high electron density, or more probably by radical reactions in the processes leading to the formation of the quinones because no peroxides were found. The quinone/nitroquinone ratios were estimated to be about 15:1 (7-nitro) and 100:1 (12-nitro). Based on the mass spectral fragmentation patterns (Fig. 2), the nitroquinones were tentatively identified as the 1,4-diones. The complete lack of M—OH and M—HNO fragments [6, 10] in the 12-nitroquinone showed the absence of an abstractable proton in the 1-position. In addition to the molecular ions (*m/z* 303), the M—NO (*m/z* 273), M—NO_2 (*m/z* 257), M—NOCO (*m/z* 245), M—NO_2CO (*m/z* 229) and M—NOCOCO (*m/z* 217) ions were the most abundant fragments. Fragments corresponding to loss of NO were significantly less abundant in the 12-nitroquinone than in the 7-nitroquinone (Fig. 2); this probably reflects the spatial requirements for rearrangement of the nitro group leading to the loss of NO [11]. Because of the small amounts available, the tentative structures of the nitroquinones have not yet been verified by n.m.r.

Adding another benzene ring, as in 7-nitrodibenz(a,h)anthracene, would not be expected to have a major effect on the oxidation pattern. In complete agreement with the findings above, a quinone and a nitroquinone were found in a ratio of approximately 15:1 (Fig. 3A). The mass spectra (Fig. 4A, C) suggested the structures to be dibenz(a,h)anthracene-7,14-dione and

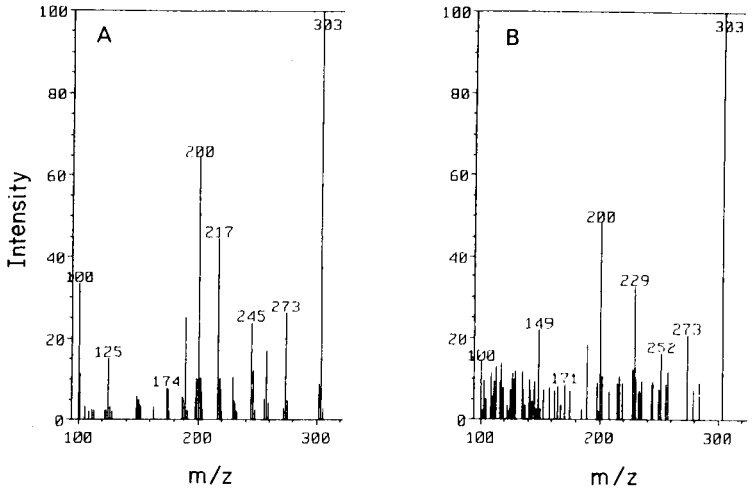

Fig. 2. Mass spectra of the minor oxidation products tentatively identified as 7-nitrobenz(a)anthracene-1,4-dione (A) and 12-nitrobenz(a)anthracene-1,4-dione (B).

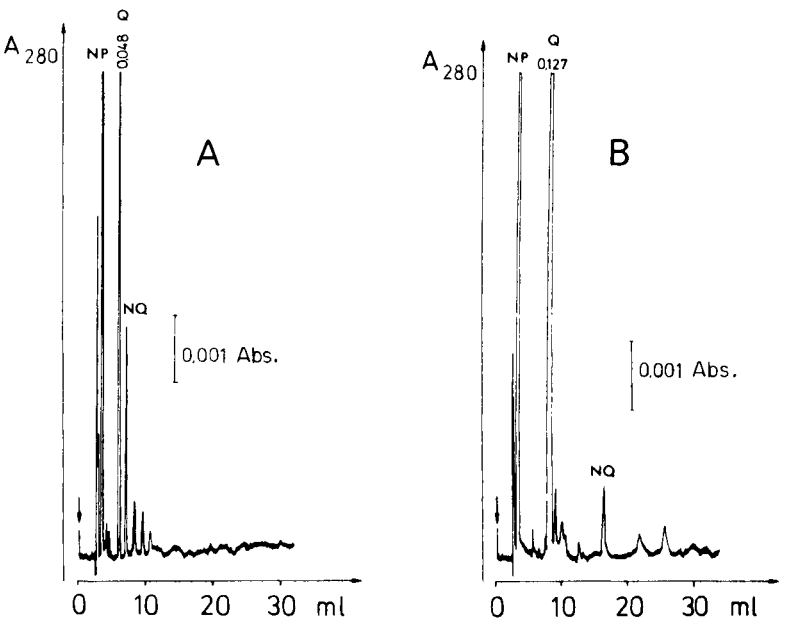

Fig. 3. H.p.l.c. separation of the oxidized products of 7-nitrodibenz(a,h)anthracene (A) and 9-nitrodibenz(a,c)anthracene (B). Conditions and peak notation as in Fig. 1.

7-nitrodibenz(a,h)anthracene-8,11-dione. The quinone had the typical abundant M—CO and M—2CO fragments [12] and the nitroquinone lacked the M—OH and M—HNO fragments, indicating the 8,11-dione.

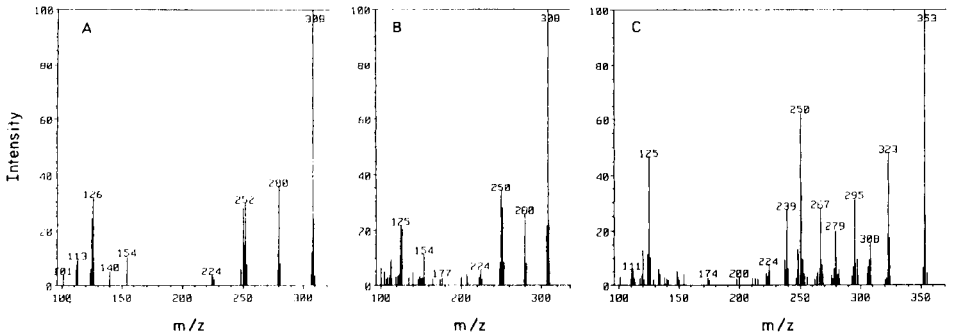

Fig. 4. Mass spectra of the quinones tentatively identified as dibenz(a,h)anthracene-7,14-dione (A) and dibenz(a,c)anthracene-9,14-dione (B), and mass spectrum of the minor oxidation product tentatively identified as 7-nitrodibenz(a,h)anthracene-8,11-dione (C).

The decomposition of 9-nitrodibenz(a,c)anthracene resulted in a quinone and a minor product in a ratio of approximately 100:1 (Fig. 3B). The quinone, with the characteristic fragmentation pattern (Fig. 4B), is difficult to attribute to any structure other than dibenz(a,c)anthracene-9,14-dione. The structure of the minor product, which appeared to be a tetraoxo derivative (*m/z* 340), has not yet been solved. 10-Nitrodibenz(a,c)anthracene gave only one soluble oxidation product, which was identified as the same quinone that was obtained from 9-nitrodibenz(a,c)anthracene. Formation of dibenz(a,c)anthracene-9,14-dione from 10-nitrodibenz(a,c)anthracene supports the notion of a radical-based oxidation mechanism. The structure of an insoluble product which precipitated from the solution has not been identified.

The formation of quinones and nitroquinones from nitrobenzanthracenes and nitrodibenzanthracenes in solutions open to the air under normal lighting conditions suggests that similar processes can take place also on airborne particulate matter in the environment. The possible fate of other nitro-PAH in solution and on particulates appear to deserve further study.

REFERENCES

1 C. Y. Wang, M. S. Lee, C. M. King and P. O. Warner, Chemosphere, 9 (1980) 83.
2 G. Löfroth, L. Nilsson, E. Agurell and A. Yasuhara, Z. Naturforsch., Teil C, 39 (1984) 193.
3 M. C. Paputa-Peck, R. S. Marano, D. Schuetzle, T. L. Riley, C. V. Hampton, T. J. Prater, L. M. Skewes, T. E. Jensen, P. H. Ruehle, L. C. Bosch and W. P. Duncan, Anal. Chem., 55 (1983) 1946.
4 J. N. Pitts, Jr., K. A. Cauwenberghe, D. Grosjean, J. T. Schmid, D. R. Fitz, W. L. Belser, Jr., G. B. Knudson and P. M. Hynds, Science, 202 (1978) 515.
5 A. Yasuhara and K. Fuwa, Chem. Lett., (1983) 347.
6 B. Iversen, L. K. Sydnes and T. Greibrokk, Acta Chem. Scand., in press.
7 J. König, E. Balfanz, W. Funcke and T. Romanowski, Anal. Chem., 55 (1983) 599.
8 D. L. Chapman, D. C. Heckert, J. W. Reasoner and S. P. Thackaberry, J. Am. Chem. Soc., 88 (1966) 5550.

9 D. R. Kearns, Chem. Rev., 71 (1971) 395.
10 H. Svendsen, H.-P. Rönningsen, L. K. Sydnes and T. Greibrokk, Acta Chem. Scand., Ser. B, 37 (1983) 833.
11 J. H. Beynon, M. Bertrand and G. R. Cooks, J. Am. Chem. Soc., 95 (1973) 1739.
12 C. J. Proctor, B. Kralj, E. A. Larka, C. J. Porter, A. Maquestian and J. H. Beynon, Org. Mass Spectrom., 16 (1981) 312.

Analytica Chimica Acta, 174 (1985) 323—326
Elsevier Science Publishers B.V., Amsterdam — Printed in The Netherlands

Short Communication

PARTITION OF EUROPIUM(III) WITH β—DIKETONES AND NEUTRAL ADDITIVES BETWEEN MICELLAR AND BULK PHASES IN AQUEOUS NONIONIC SURFACTANT SOLUTIONS

TOMITSUGU TAKETATSU

College of General Education, Kyushu University, Ropponmatsu, Chuo-Ku, Fukuoka 810 (Japan)

(Received 15th January 1985)

Summary. The distribution ratio of europium(III) with a β-diketone and a neutral adduct between micellar and bulk phases in aqueous nonionic surfactant solution was measured by a spectrofluorimetric method as a function of hydrogen ion concentration. The synergic effect of trioctylphosphine oxide for the various β-diketone chelates is much greater than that of tributyl phosphate.

Metal chelates solubilized into a micellar solution of a nonionic surfactant have been applied in various analytical methods such as spectrophotometry [1, 2], spectrofluorimetry [3, 4] and titrimetry [5]. Estimation of the distribution ratios of metals with chelate formation between micellar and bulk phases is significant for analytical applications. In the present communication, the distribution ratios are given for europium(III) with furoyltrifluoroacetone (FTA), pivaloyltrifluoroacetone (PTA), thenoyltrifluoroacetone (TTA), benzoyltrifluoroacetone (BFA) and heptafluorobutanoylpivaloylmethane (HFBPM) in the presence and absence of tributyl phosphate (TBP) and trioctylphosphine oxide (TOPO) adducts in aqueous nona(oxyethylene) dodecyl ether (BL-9EX) solution. The ratios were measured spectrofluorimetrically as a function of hydrogen ion concentration. The variation of the distribution ratio for the Eu/TTA, Eu/TTA/TBP and Eu/TTA/TOPO systems with temperature is also reported.

Experimental

Stock solution. The concentrations in the mixed stock solution (pH 4.5—5.5) used were 1×10^{-5} mol dm^{-3} europium(III) chloride, 1×10^{-3} mol dm^{-3} β-diketone, 1×10^{-2} mol dm^{-3} acetic acid, 0.2 mol dm^{-3} sodium chloride and 1.0% (w/v) BL-9EX. The concentration of TBP or TOPO was 1×10^{-3} mol dm^{-3}.

Procedure. A portion (10 ml) of the above stock solution was adjusted to approximately the desired pH value with dilute hydrochloric acid, transferred to a 20-ml volumetric flask and made up to volume with water. The solution was poured into a 25-ml stoppered flask and shaken mechanically in a

0003-2670/85/$03.30

thermostat for at least 1 h. The fluorescence was measured at an emission wavelength of 610 nm in a 1-cm quartz cell with apparent excitation wavelengths of 370 (FTA), 305 (PTA), 355 (TTA), 345 (BFA) and 320 nm (HFBPM), respectively, in the presence and absence of TBP or TOPO.

Results and discussion

If the equilibrium equations introduced for the Eu(III)/TTA and Eu(III)/TTA/TOPO systems [6] can be applied to systems containing the other β-diketones (HA) and neutral adducts (S), then the EuA_3 and EuA_3S_2 complexes will be formed by the following reactions:

$$Eu^{3+}_{(b)} + 3HA_{(b)} \rightleftharpoons EuA_{3(m)} + 3H^+_{(b)} \quad (1)$$

and

$$Eu^{3+}_{(b)} + 3HA_{(b)} + 2S_{(m)} \rightleftharpoons EuA_3S_{2(m)} + 3H^+_{(b)} \quad (2)$$

Subscripts (b) and (m) refer to the mutually equilibrated bulk and micellar phases, respectively. The equilibrium constants $k_1 = [EuA_3]_{(m)}[H^+]^3_{(b)}/[Eu^{3+}]_{(b)}[HA]^3_{(b)}$ and $k_2 = [EuA_3S_2]_{(m)}[H^+]^3_{(b)}/[Eu^{3+}]_{(b)}[HA]^3_{(b)}[S]^2_{(m)}$ are expanded as follows:

$$\log k_1 = \log D_1 + 3 \log [H^+]_{(b)} - 3 \log [HA]_{(b)} \quad (3)$$

$$\log k_2 = \log D_2 + 3 \log [H^+]_{(b)} - 3 \log [HA]_{(b)} - 2 \log [S]_{(m)} \quad (4)$$

where $D_1 = [EuA_3]_{(m)}/[Eu^{3+}]_{(b)}$ and $D_2 = [EuA_3S_2]_{(m)}/[Eu^{3+}]_{(b)}$, respectively. When Eqns. 3 and 4 are differentiated with respect to $\log [H^+]_{(b)}$, then $d\log D_1/d\log [H^+]_{(b)} = -3$ and $d\log D_2/d\log [H^+]_{(b)} = -3$ are obtained; here, the concentrations of HA and S can be assumed to be constant because they are in large excess relative to europium(III).

If it can be assumed that the concentration of europium(III) in the micellar phase is linearly proportional to the fluorescence intensity, and that almost all the europium(III) species exist in the micellar phase, then in the pH range for which the intensity is constant and maximal, the values of D_1 and D_2 can be calculated by using the fluorimetric data.

The equilibrium constant β_{ad} for the adduct formation in the micellar phase

$$EuA_{3(m)} + 2S_{(m)} \rightleftharpoons EuA_3S_{2(m)}$$

is derived from the values of k_1 and k_2:

$$\beta_{ad} = [EuA_3S_2]_{(m)}/[EuA_3]_{(m)}[S]^2_{(m)} = k_2/k_1 \quad (5)$$

Figure 1 shows that all the plots of $\log D_1$ vs. $\log [H^+]_{(b)}$ and $\log D_2$ vs. $\log [H^+]_{(b)}$ are almost linear (about −3). The values of $\log k_1$, $\log k_2$ and $\log \beta_{ad}$ can be estimated by using the equations described above. These values are given in Table 1. The apparent equilibrium constants for the EuA_3 chelate formation increase in the order FTA < PTA < TTA < BFA < HFBPM and the synergic effect of TOPO on the EuA_3S_2 adduct formation in the micellar phase is much greater than that of TBP.

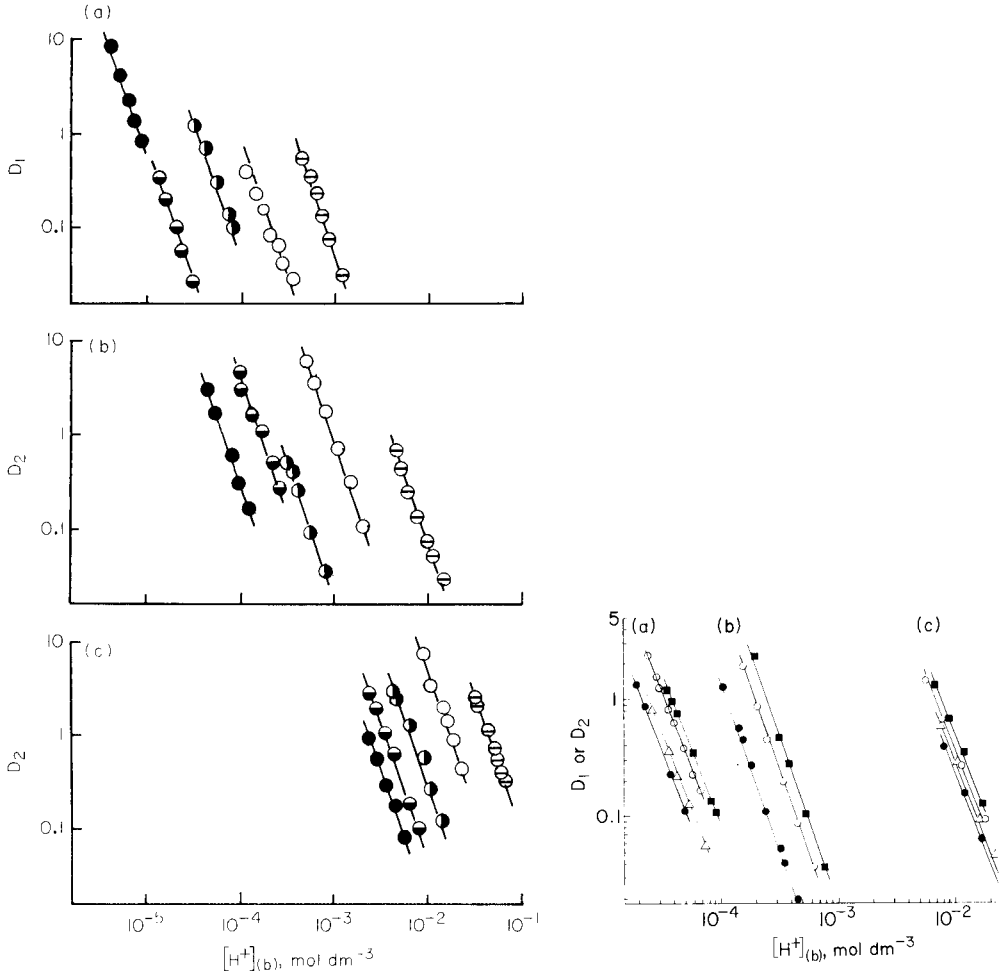

Fig. 1. Variation of the distribution ratio in the different systems as a function of hydrogen ion concentration. (a) Eu/HA; (b) Eu/HA/TBP; (c) Eu/HA/TOPO. (●) FTA; (⊖) PTA; (◑) TTA; (○) BFA; (⊖) HFBPM.

Fig. 2. Variation of distribution ratio in Eu/TTA, Eu/TTA/TBP and Eu/TTA/TOPO systems as a function of hydrogen ion concentration at various temperatures: (a—c) as in Fig. 1; (●) 10° C; (△) 15° C; (○) 20° C; (■) 25° C.

Figure 2 shows that the graphs of log D_1 vs. log $[H^+]_{(b)}$ and log D_2 vs. log $[H^+]_{(b)}$ for the Eu/TTA, Eu/TTA/TBP and Eu/TTA/TOPO systems are almost linear (about −3), irrespective of temperature used. The Eu/TTA chelating reaction is endothermic and enthalpy change ΔH was estimated to be about 75 kJ mol^{-1} by van't Hoff equation. The enthalpy changes on the adduct formation in the micellar phase were ca. 30 and −34 kJ mol^{-1} for the Eu/TTA/TBP and Eu/TTA/TOPO systems, respectively.

TABLE 1

Apparent equilibrium constants for Eu/HA, Eu/TTA/TBP and Eu/TTA/TOPO systems at 298 K

β-Diketone	EuA_3	$EuA_3(TBP)_2$		$EuA_3(TOPO)_2$	
	$\log k_1$	$\log k_2$	$\log \beta_{ad}$	$\log k_2$	$\log \beta_{ad}$
FTA	−5.1	3.9	9.0	8.5	13.6
PTA	−4.0	5.1	9.1	9.0	13.0
TTA	−3.4	5.7	9.1	10.1	13.5
BFA	−2.4	7.4	9.8	11.2	13.6
HFBPM	−0.3	9.2	9.5	13.5	13.8

REFERENCES

1 T. Taketatsu and A. Sato, Bull. Chem. Soc. Jpn., 53 (1980) 3713.
2 T. Taketatsu, M. Aihara and Y. Kimoto, Bunseki Kagaku, 30 (1981) 328.
3 T. Taketatsu and A. Sato, Anal. Chim. Acta, 108 (1979) 429.
4 T. Taketatsu, Talanta, 29 (1982) 397.
5 S. Okawa, B. Kominami and A. Kawase, Bunseki Kagaku, 29 (1980)267.
6 T. Taketatsu, Chem. Lett., (1981) 1057.

Analytica Chimica Acta, 174 (1985) 327—330
Elsevier Science Publishers B.V., Amsterdam — Printed in The Netherlands

Short Communication

IDENTIFICATION OF A MAJOR NEW INVOLATILE *N*-NITROSO COMPOUND IN SMOKED BACON

ROBERT C. MASSEY*, COLIN CREWS, M. JOHN DENNIS, DAVID J. McWEENY, JAMES R. STARTIN and MICHAEL E. KNOWLES

Ministry of Agriculture, Fisheries and Food, Food Science Laboratory, Queen Street, Norwich, NR2 4SX (Great Britain)

(Received 8th March 1985)

Summary. The new *N*-nitroso compound identified in smoked bacon is 2-(hydroxymethyl)-3-nitrosothiazolidine-4-carboxylic acid. Identification was based on comparison of data from liquid chromatography, capillary gas chromatography and mass spectrometry with those for the authentic compound, the synthesis of which is described.

The occurrence of *N*-nitroso compounds in foodstuffs and the environment is of concern because of the carcinogenicity exhibited by many of them in animal feeding studies [1]. The heterocyclic involatile compound *N*-nitroso-thiazolidine-4-carboxylic acid (NTCA) has recently been reported in smoked cured meats [2, 3] and in the urine of smokers [4]. It has been suggested [2] that NTCA formation results from nitrosation of thiazolidine-4-carboxylic acid formed by reaction of cysteine with formaldehyde present in smoke. The presence of an additional unknown *N*-nitroso compound in smoked cured meats in amounts up to 1—2 mg kg^{-1} was recently observed [3]. The identification of this compound is now reported.

Experimental

Synthesis of 2-(hydroxymethyl)-3-nitrosothiazolidine-4-carboxylic acid. L-Cysteine (5.0 g, 40 mmol) was dissolved in water (50 ml) and added to an aqueous solution (50 ml) of glycolaldehyde (5.0 g, 85 mmol), and the pH was adjusted to 7.0 with aqueous potassium hydroxide. After 15 min, the solution was adjusted to pH 3.0 with dilute sulphuric acid and treated with sodium nitrite (2.85 g, 40 mmol) in 25 ml of dilute sulphuric acid at pH 3.0. The solution was kept at room temperature for 1 h, treated with sulphamic acid (5 g) and sodium sulphate (50 g), and extracted with ethyl acetate (4 × 200 ml). The combined extracts were dried over anhydrous sodium sulphate (50 g), filtered and concentrated to dryness on a rotary evaporator. The resulting yellow oil comprised a mixture of isomers (**a** + **b**) and was purified by preparative high-performance liquid chromatography to yield a colourless oil. The "**b**" isomer was obtained by washing the oil with toluene followed by

cold ethyl acetate. The resulting precipitate was recrystallized from acetone to give the pure "**b**" isomer as a white crystalline solid. [Yield 0.8 g, 10%; m.p. 116—117°C; peaks at 238 nm (ϵ = 6400) and 358 nm (ϵ = 85 l mol^{-1} cm^{-1}); ^{1}H-n.m.r., AMX (3.16—5.14 ppm), AA^{1}X (4.13—5.86 ppm) (carboxylic and hydroxy protons were not observed presumably because of rapid inter/intramolecular exchange); 31.4% C, 4.1% H, 14.4% N, 16.7% S found; calculated for $C_5H_8N_2O_4S$, 31.25% C, 4.2% H, 14.6% N, 16.7% S.]

Bacon extract preparation. An acidified aqueous slurry of bacon was prepared and extracted with ethyl acetate and the extract was concentrated to dryness and re-dissolved in acetone as described previously [3].

Chromatography. Analytical high-performance liquid chromatography (h.p.l.c.) was done on a Zorbax CN (25 × 0.5 cm i.d.) column with a thermal energy analyzer (t.e.a.) as detector (Thermo Electron Corp., Waltham, MA). For bacon extracts (20 μl), the mobile phase was hexane/acetone/acetic acid (74:25:1) at 4 ml min^{-1}. A 5-μm Apex CN column (25 × 1.0 cm i.d.) was used for preparative h.p.l.c.; the eluent was the same as that just described but at a flow rate of 8 ml min^{-1}. Bacon extracts (200 μl) were injected and the fraction eluting at 4.2—5.2 min was collected, concentrated to dryness and treated with bis(trimethylsilyl)trifluoracetamide (BSTFA). Aliquots (1 μl) of this solution were injected onto a CP-Sil-8CB column (10 m × 0.32 mm i.d.) for capillary g.c./t.e.a.; the temperature-programming was 60°C (1 min), 25°C min^{-1}, 90°C (1 min), 3°C min^{-1} to 200°C.

Results and discussion

A typical liquid chromatogram of a smoked bacon extract is shown in Fig. 1. The chromatogram was obtained by using the *N*-nitroso-selective t.e.a. detector and shows the presence of NTCA and the unknown compound. The unknown compound was isolated by preparative h.p.l.c. and treated with BSTFA to form a volatile trimethylsilyl (TMS) derivative. Capillary g.c./t.e.a. of the derivatized fraction revealed the presence of two peaks (Fig. 2). Electron-impact mass spectrometry (e.i.m.s.) indicated that the peaks were isomeric and studies with deuterated TMS derivatives showed the presence of two derivatized functional groups. The mass spectra of the two peaks were essentially identical; that of the "**a**" isomer is shown in Fig. 3. Comparison

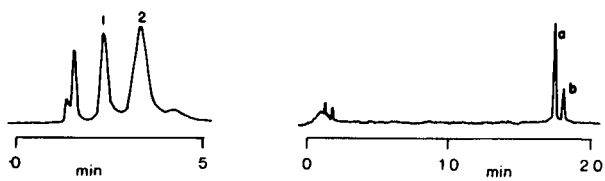

Fig. 1. Liquid chromatogram of smoked bacon extract. Peaks: (1) NTCA; (2) new *N*-nitroso compound.

Fig. 2. Gas chromatogram of new *N*-nitroso compound isolated from smoked bacon; peaks **a** and **b** relate to isomeric forms.

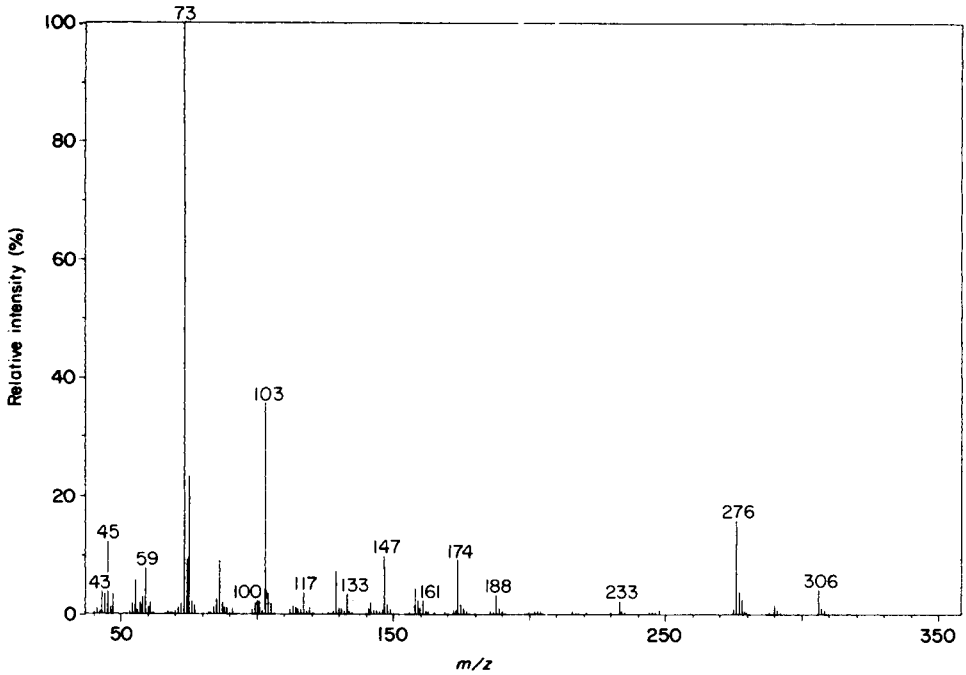

Fig. 3. Capillary g.c./electron-impact mass spectrum (VG 12000 quadrupole) of *N*-nitroso compound isolated from smoked bacon.

of the relative intensities of the *m/z* 306 and 276 signals with spectra of a series of model *N*-nitroso compounds showed that the *m/z* 306 species was unusually stable and unlikely to be the molecular ion. This was confirmed after identification of the compound as 2-(hydroxymethyl)-3-nitrosothiazolidine-4-carboxylic acid (I). The unambiguous identification of the smoked

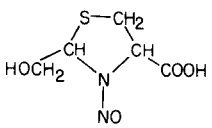

(I)

bacon *N*-nitroso compound as compound I was based on the following features: coincident capillary g.c. retention times of the smoked bacon isomers with the *syn* and *anti* isomers of compound I; identical g.c./e.i.m. spectra of the smoked bacon isomers with those of compound I; coincident h.p.l.c./t.e.a. retention times of the smoked bacon isomers and isomers of compound I under conditions that resolved the *syn* and *anti* isomers (Spherisorb 5-μm Phenyl, 25 X 0.5 cm, 4 ml min^{-1} hexane/acetone/acetic acid (81:18:1), retention times 4.1 and 4.8 min). The g.c./e.i.m. spectrum in Fig. 3 may reasonably be interpreted in terms of two successive losses of 30 absolute mass units from the unobserved molecular ion (M = 336) of the derivatized

compound I. The m/z species at 306 corresponds to loss of NO and the m/z 276 signal to an intramolecular transfer of the TMS group from the ring-CH_2OTMS moiety to N followed by loss of the CH_2O fragment.

Compound I was prepared by reaction of L-cysteine and glycolaldehyde at neutral pH followed by nitrosation under mildly acidic conditions. The product structure was confirmed by ^{1}H-n.m.r., u.v. spectroscopy, elemental analysis and mass spectrometry ($M + 1 = 193$ observed by desorption chemical ionization with ammonia as reagent gas).

A literature search has failed to reveal any previous report on either the preparation of compound I or its presence in foodstuffs. The reasons for the occurrence of this compound in smoked cured meats are being investigated and will be reported elsewhere together with a survey of the extent of its presence in retail products.

REFERENCES

1 P. M. Magee and J. M. Barnes, Adv. Cancer Res., 10 (1967) 163.

2 T. Helgason, S. W. B. Ewen, B. Jaffray, J. M. Stowers, J. R. Outram and J. R. A. Pollock, *N*-Nitrosamines in smoked meats and their relation to diabetes. In: I. K. O'Neill, R. C. von Borstel, C. T. Miller, J. Long and H. Bartsch (Editors), *N*-nitroso compounds: Occurrence, Biological Effects and Relevance to Human Cancer, IARC Scientific Publications No. 57, International Agency for Research on Cancer, Lyon, 1984, pp. 911—920.

3 A. R. Tricker, M. J. Perkins, R. C. Massey, C. Bishop, P. E. Key and D. J. McWeeny, Food Additives and Contaminants, 1 (1984) 245.

4 H. Ohshima, M. Friesman, I. O'Neill and H. Bartsch, Cancer Lett., 20 (1983) 183.

Analytica Chimica Acta, 174 (1985) 331—337
Elsevier Science Publishers B.V., Amsterdam — Printed in The Netherlands

Short Communication

REFERENCE VALUE STANDARDS FOR pH MEASUREMENTS IN 5, 15 AND 30% (w/w) ACETONITRILE/WATER SOLVENT MIXTURES AT TEMPERATURES FROM 288.15 TO 308.15 K

TORQUATO MUSSINI*, PAOLO LONGHI, SANDRA RONDININI and MICHELE TETTAMANTI

Department of Physical Chemistry and Electrochemistry, University of Milan, Via Golgi 19, I-20133 Milano (Italy)

ARTHUR K. COVINGTON

Electrochemistry Research Laboratories, Department of Physical Chemistry, The University, Newcastle-upon-Tyne NE1 7RU (Great Britain)

(Received 7th January 1985)

Summary. Reference value standards, pH (RVS), for 0.05 mol kg^{-1} potassium hydrogenphthalate (KHPh) reference buffer solutions in 5, 15 and 30% (w/w) acetonitrile/water mixed solvents at temperatures from 288.15 to 308.15 K are determined from reversible e.m.f. measurements of the cell $Pt|H_2|KHPh + KCl|AgCl|Ag|Pt$. Values of the first ionisation constant of *o*-phthalic acid (H_2Ph; benzene-1,2-dicarboxylic acid) in these mixed solvents are also determined from analogous measurements. The consistency of the results is analysed by multilinear regression of the quantity $p(a_H\gamma_{Cl})$ as a function of both solution composition and temperature. The standard pH (RVS) values determined are given by the equation $pH\ (RVS) = 4.0080 + 6.330x + 16.177x^2 - 115.3x^3 + 0.3089u - 201.0ux^2 + 909ux^3 + 13.04v$, where x is the mole fraction of acetonitrile in the mixed solvent, $u = z/(1 + z)$, $v = [\ln(1 + z) - u]$, $z = (T - \theta)/\theta$, and $\theta = 298.15$ K.

The context of the recently approved IUPAC criteria for standardisation of pH measurements in aqueous [1] and aqueous-organic media [2], reference value standards (RVS) for a 0.05 mol kg^{-1} (molal) solution of potassium hydrogenphthalate (KHPh) have been determined over ranges of temperature and solvent composition for water and such co-solvents as methanol (dipolar amphiprotic) [3] and 1,4-dioxane (nonpolar aprotic) [4]. Three pH (RVS) values (one of which is at −12°C) are also available with the co-solvent dimethylsulphoxide [5]. The present determination of RVS data for water and the popular, dipolar aprotic, co-solvent, acetonitrile, contributes to knowledge of the behaviour of co-solvents. To this end, the reversible e.m.f., E_A, of the cell

$$\underline{Pt|H_2\ (1\ atm)|KHPh\ (m = 0.05\ mol\ kg^{-1}) + KCl\ (m_1)|AgCl|Ag|Pt} \qquad (A)$$
$$\text{in acetonitrile/water mixtures}$$

was measured at temperatures from 288.15 to 308.15 K at various molalities m_1 of potassium chloride (0.005—0.1 mol kg^{-1}) in acetonitrile/water mix-

0003-2670/85/$03.30

tures at 5, 15 and 30% (w/w) acetonitrile (see Table 1). These solvent mixtures have relative permittivities (dielectric constants) of 77, 73 and 65, respectively; thus, for the present purpose, ionic association can safely be neglected. To obtain essential values of the first ionisation constant, K_1, of *o*-phthalic acid (H_2Ph; benzene-1,2-dicarboxylic acid) within the same range of temperature and solvent composition, the above e.m.f. measurements of cell A were supplemented by reversible e.m.f. measurements of the cell

$$\underline{\text{Pt}|\text{H}_2\ (1\ \text{atm})|\text{H}_2\text{Ph}\ (m_2) + \text{KHPh}\ (m_3) + \text{KCl}\ (m_4)|\text{AgCl}|\text{Ag}|\text{Pt}} \qquad \text{(B)}$$
$$\text{in acetonitrile/water mixtures}$$

at various molalities of the mixed electrolyte ($0.008 < m_2 = m_3 = m_4 < 0.05$ mol kg^{-1}) (see Table 2). Ancillary density values for the above solvent mixtures were also determined.

Experimental

The hydrogen electrodes and the silver/silver chloride electrodes in cells A and B were prepared as described previously [4, 6, 7]. The potentiometric and the thermostatted apparatus were also described earlier [8]. The measured e.m.f. values were corrected to 1 atm (101 325 Pa) pressure of hydrogen by using vapour-pressure values interpolated from data available in the literature [9]. The solutions were made up by weight from triply-distilled water and reagent-grade Carlo Erba chemicals (acetonitrile, potassium chloride, potassium hydrogenphthalate and *o*-phthalic acid); before use, potassium chloride and potassium hydrogenphthalate were dried at 110°C [1]. The densities of the acetonitrile/water solvent mixtures, required for the calculation of the A and B constants in Eqn. 3, were measured at each temperature by means of a Type 40 Paar DMA microdensimeter equipped with a Type D3 Haake thermostat. The relative permittivities of each solvent mixture, also required for the above A and B constants, were interpolated from data available in the literature [10].

Results and discussion

The first step in the approach to the pH (RVS), as implied by the Nernst expression of E_A for cell A, is evaluation of the quantity

$$\text{p}(a_{\text{H}}\gamma_{\text{Cl}}) = -\log(a_{\text{H}}\gamma_{\text{Cl}}) = \text{pH} + \text{p}\gamma_{\text{Cl}} = (E_A - E^\circ)/k + \log m_1 \qquad (1)$$

where $k = RT\ (\ln 10)/F$, E° is the standard e.m.f. of the cell (values of which are available [6, 11]), a and γ are the ionic activities and activity coefficients (the ions involved are denoted by the subscripts without charge numbers). $\text{p}(a_{\text{H}}\gamma_{\text{Cl}})$ is a thermodynamic quantity, unlike the two non-thermodynamic quantities, pH and $\text{p}\gamma_{\text{Cl}}$, into which it is eventually split: thus, $\text{p}\gamma_{\text{Cl}}$ must be calculated on non-thermodynamic grounds, by the Debye-Hückel equation:

$$\text{p}\gamma_{\text{Cl}} = AI^{1/2}/(1 + a_0BI^{1/2}) \qquad (2)$$

TABLE 1

Values of e.m.f. E_A (given in mV) of cell A at various molalities m_1 (given as mmol kg^{-1}) of KCl in 0.05 m potassium hydrogenphthalate for various acetonitrile/water solvent mixtures at different temperatures (K) with relevant standard e.m.f.s E°, densities ρ, relative permittivities ϵ, and Debye-Hückel constants A and B

m_1	5% (w/w) acetonitrile			m_1	15% (w/w) acetonitrile			m_1	30% (w/w) acetonitrile		
	288.15	298.15	308.15		288.15	298.15	308.15		288.15	298.15	308.15
	E_A	E_A	E_A		E_A	E_A	E_A		E_A	E_A	E_A
—	—	—	—	5.025	613.45	620.23	626.31	5.007	630.13	636.24	641.61
—	—	—	—	5.025	612.99	620.07	625.91	5.007	628.80	634.80	640.60
8.008	587.47	593.80	600.43	—	—	—	—	—	—	—	—
10.005	581.31	588.14	595.25	10.009	596.52	600.05	607.97	9.942	612.43	617.36	622.06
10.005	581.18	587.97	594.94	10.009	594.17	600.65	606.84	9.942	—	615.93	—
19.991	—	—	574.24	20.007	579.84	584.17	589.69	20.020	595.49	599.89	603.83
—	—	—	—	20.007	580.04	585.57	590.59	20.020	595.63	600.00	604.28
—	—	—	—	30.015	569.24	573.09	578.58	29.997	585.59	589.41	592.39
—	—	—	—	30.015	—	573.14	579.13	29.997	586.29	589.65	594.21
49.975	—	544.65	550.67	49.938	556.07	559.27	563.65	50.026	572.08	574.78	579.00
49.975	—	545.50	550.88	—	—	—	—	50.026	572.59	575.63	579.47
69.993	531.97	535.69	541.13	69.989	546.77	550.88	554.37	69.998	—	—	568.50
69.993	532.10	537.13	541.73	69.989	546.83	551.24	555.42	—	—	—	—
99.981	522.65	527.04	531.40	99.996	537.65	541.41	544.68	100.02	552.97	555.37	558.35
99.981	523.02	527.51	531.65	99.996	537.61	541.68	544.98	100.02	552.72	555.73	558.17
E°(mV)[a]	224.16	217.92	211.28		216.44	209.94	203.03		204.94	198.04	190.73
ρ[b]	0.9920	0.9890	0.9847		0.9753	0.9703	0.9646		0.9455	0.9389	0.9320
ϵ[c]	80.80	77.00	73.40		76.80	73.10	69.80		68.96	65.56	62.84
A[d]	0.5139	0.5247	0.5332		0.5496	0.5628	0.5712		0.6340	0.6481	0.6542
a_0B[d,e]	1.5059	1.5080	1.5073		1.5320	1.5349	1.5327		1.5902	1.5919	1.5854

[a]From Ref. [6]. [b]In kg dm^{-3}. [c]Interpolated from data in Ref. [9]. [d]In $mol^{-1/2}$ $kg^{1/2}$. [e]From Eqn. 4.

TABLE 2

Values of e.m.f. E_B (in mV) of cell B at various molalities of the mixed electrolyte H_2Ph (m_2) + KHPh (m_3) + KCl (m_4), with $m_2 = m_3 = m_4$ (mmol kg^{-1}) in different acetonitrile/water solvent mixtures at various temperatures (K)

m_2	15% (w/w) acetonitrile			m_2	30% (w/w) acetonitrile		
	288.15	298.15	308.15		288.15	298.15	308.15
	E_B	E_B	E_B		E_B	E_B	E_B
8.002	535.32	536.63	539.64	8.001	537.13	537.70	538.23
8.002	535.03	538.02	539.90	8.001	—	537.50	538.31
9.997	527.39	529.80	531.48	10.001	531.36	531.29	532.00
9.997	527.27	529.99	531.46	10.001	531.49	532.08	532.58
14.888	517.47	519.56	521.20	—	—	—	—
14.888	517.23	519.45	521.20	—	—	—	—
20.000	510.09	511.90	512.62	20.000	513.83	513.15	512.92
20.000	509.68	511.59	513.15	20.000	513.20	513.93	513.54
30.000	499.46	500.71	501.65	30.002	504.53	504.08	503.13
30.000	499.21	500.54	501.90	30.002	504.44	503.60	500.96
39.998	491.81	494.88	496.32	39.998	496.05	495.60	494.18
39.998	491.67	492.74	493.64	39.998	—	495.58	494.36
50.000	486.80	487.65	487.90	—	—	—	—
50.000	486.62	487.52	488.04	—	—	—	—

to obtain pH from $p(a_H \gamma_{Cl})$:

$$pH = (E_A - E^\circ)/k - pm_1 - AI^{1/2}/(1 + a_0 BI^{1/2}) \quad (3)$$

In Eqn. 3, I is the actual ionic strength of the 0.05 m KHPh buffer in potassium chloride at m_1, and the ion-size parameter a_0 is given the same value [12] fixed by the Bates-Guggenheim convention [13] and internationally endorsed for aqueous standard buffers. This implies that

$$(a_0 B)_T = 1.5\ [(\epsilon^w \rho^s)/(\epsilon^s \rho^w)]_T^{1/2} \quad (4)$$

where ϵ^w, ϵ^s, ρ^s and ρ^w are the relative permittivities and the densities of water (^{w}) and acetonitrile/water mixture (^{s}), respectively. The molality m_H of H^+, on which depends the ionic strength $I = (0.05 + 2m_1 + m_{HPh} + 4m_{Ph} + m_H)/2$ of the KHPh/KCl electrolyte, can be calculated from I as $pm_H = p(a_H \gamma_{Cl}) - 2AI^{1/2}/(1 + a_0 BI^{1/2})$. Because of this interrelation of I with m_H, the calculation must proceed by successive iterations (for each m_1 at which E_A was measured) involving the molalities m_{HPh} and m_{Ph} for the hydrogenphthalate and phthalate ions, respectively, in terms of the first acidity constant K_{a1} of *o*-phthalic acid H_2Ph; the iteration steps with related equations have been described [3, 4, 14, 15]. Once convergence has been obtained, the I value found is inserted into Eqn. 3 and pH is then plotted against m_1. The intercept at $m_1 = 0$ gives the sought standard pH (RVS) value for 0.05 mol kg^{-1} KHPh.

These pH (RVS) values are quoted in Table 3 together with the relevant

TABLE 3

Standard pH (RVS) values of 0.05 *m* potassium hydrogenphthalate buffers (with corresponding standard errors), as obtained starting from Eqn. 3 or from the multilinear regression (Eqn. 8), in various acetonitrile/water solvent mixtures at various temperatures T, together with the relevant values of $p(a_H\gamma_{Cl})^\circ$, of the first acidity constant K_{a1} of phthalic acid, and of the actual ionic strength I of the buffers

Acetonitrile (% w/w)	0	5	15	30
T = 288.15 K				
pH (RVS)[a]	3.998 ± 0.001[c]	4.162 ± 0.004	4.550 ± 0.007	5.031 ± 0.006
pH (RVS)[b]	4.005 ± 0.003	4.158 ± 0.006	4.525 ± 0.010	5.005 ± 0.018
$p(a_H\gamma_{Cl})^\circ$	4.091 ± 0.003	4.245 ± 0.006	4.619 ± 0.010	5.111 ± 0.018
pK_{a1}	2.936 ± 0.001[d]	3.110 ± 0.009[e]	3.411 ± 0.009	3.684 ± 0.009
I (mol kg^{-1})	0.05306	0.05319	0.05276	0.05174
T = 298.15 K				
pH (RVS)[a]	4.005 ± 0.001[c]	4.163 ± 0.007	4.527 ± 0.007	4.985 ± 0.006
pH (RVS)[b]	4.008 ± 0.002	4.158 ± 0.006	4.504 ± 0.010	4.958 ± 0.018
$p(a_H\gamma_{Cl})^\circ$	4.096 ± 0.002	4.247 ± 0.006	4.599 ± 0.010	5.067 ± 0.018
pK_{a1}	2.950 ± 0.001[d]	3.104 ± 0.006[e]	3.371 ± 0.006	3.607 ± 0.007
I (mol kg^{-1})	0.05312	0.05314	0.05264	0.05162
T = 308.15 K				
pH (RVS)[a]	4.019 ± 0.001[c]	4.176 ± 0.007	4.521 ± 0.005	4.950 ± 0.005
pH (RVS)[b]	4.025 ± 0.003	4.172 ± 0.006	4.498 ± 0.010	4.929 ± 0.018
$p(a_H\gamma_{Cl})^\circ$	4.114 ± 0.003	4.263 ± 0.006	4.595 ± 0.010	5.039 ± 0.018
pK_{a1}	2.967 ± 0.001[d]	3.102 ± 0.009[e]	3.336 ± 0.009	3.551 ± 0.002
I (mol kg^{-1})	0.05311	0.05303	0.05248	0.05153

[a]From Eqn. 3. [b]From Eqn. 8. [c]From Ref. [14]. [d]From Refs. [15, 16]. [e]Interpolated from Eqns. 6.

pK_{a1} values for the various solvent mixtures and temperatures investigated, including pure water [14—16] to facilitate comparison. The K_{a1} values were separately determined from the e.m.f., E_B, of the cell B (see Table 2). By combining the expressions for E_B and K_{a1}, the extrapolation function ϕ can be defined, where

$$\phi = [(E_B - E^\circ)/k] + \log[(m_2 - m_H)m_4/(m_3 + m_H)] = pK_{a1} - (b_{Cl} - b_{HPh})I \quad (5)$$

and the standard e.m.f., E°, is the same as for cell A; b_{Cl} and b_{HPh} are the specific interaction parameters in the extended Debye-Hückel equations for $p\gamma_{Cl} = AI^{1/2}/(1 + a_0BI^{1/2}) - b_{Cl}I$ and for $p\gamma_{HPh} = AI^{1/2}/(1 + a_0BI^{1/2}) - b_{HPh}I$. Neglecting the small contribution of the second acidity constant of H_2Ph, for the mixed electrolyte in cell B, one can write $m_{Cl} = m_4$, $m_{HPh} = m_3 + m_H$, and, for ionic strength, $I = m_3 + m_4 + m_H$. Again m_H and I are interrelated, thus another iterative calculation cycle, as described previously

[3, 4, 14, 15], is necessary to obtain the appropriate I values for each concentration of the mixed electrolyte at which E_B was measured, at each temperature and solvent composition. The intercept at $I = 0$ of the ϕ vs. I plot gives pK_{a1}. The pK_{a1} values at 5% (w/w) acetonitrile in Table 3 were interpolated from the present results at 15 and 30% (w/w) and those at 0% (pure water) [16], by the following least-squares polynomials at the respective temperatures:

$$\begin{aligned} pK_{a1} &= 2.9360 + 8.1745x - 21.7893x^2 \quad \text{(at 288.15 K)} \\ pK_{a1} &= 2.9500 + 7.2765x - 19.7482x^2 \quad \text{(at 298.15 K)} \\ pK_{a1} &= 2.9670 + 6.3349x - 16.7132x^2 \quad \text{(at 308.15 K)} \end{aligned} \tag{6}$$

where x is the mole fraction of acetonitrile in the solvent mixture. Here, $p(a_H \gamma_{Cl})$ is the essential basis for critical interpretation, and analysis of internal consistency, of results by means of a single-stage multilinear regression method [3, 4, 17]. This method yields thermodynamic functions and their estimated standard errors and has mole fraction x of co-solvent (acetonitrile), temperature T and molality m_1 of KCl as independent variables. This scheme leads to the regression equation

$$\begin{aligned} p(a_H \gamma_{Cl}) = {} & C_0 + C_1 x + C_2 x^2 + C_3 x^3 + C_4 m_1^{1/2} x + C_5 m_1^{1/2} x^2 + C_6 m_1 \\ & + C_7 m_1 x + C_8 m_1 x^2 + C_9 m_1^2 + C_{10} m_1^2 x^3 + C_{11} u + C_{12} u x^2 \\ & + C_{13} u x^3 + C_{14} v \end{aligned} \tag{7}$$

where $u = z/(1 + z)$, $v = [\ln (1 + z) - u]$, $z = (T - \theta)/\theta$ and $\theta = 298.15$ K.

Calculation with the BMPD package [18] in conjunction with the MULTIREG program [6] resulted in the following parameters (with corresponding estimated standard errors, $n = 159$): $C_0 = 4.0958 \pm 0.0024$, $C_1 = 6.38 \pm 0.35$, $C_2 = 17.1 \pm 4.5$, $C_3 = -118 \pm 17$, $C_4 = 9.6 \pm 4.0$, $C_5 = -47 \pm 32$, $C_6 = -0.97 \pm 0.16$, $C_7 = -24 \pm 12$, $C_8 = 144 \pm 120$, $C_9 = 6.2 \pm 1.9$, $C_{10} = -1916 \pm 1623$, $C_{11} = 0.355 \pm 0.041$, $C_{12} = -200 \pm 23$, $C_{13} = 906 \pm 145$, $C_{14} = 12.5 \pm 2.6$. The above C_0 value is of course that for $p(a_H \gamma_{Cl})$ at $m_1 = 0$, $T = 298.15$ K and $x = 0$, i.e., $p(a_H \gamma_{Cl})^\circ$ for pure water. Values of $p(a_H \gamma_{Cl})^\circ$ for the solvent compositions and temperatures investigated are quoted with the corresponding standard errors in Table 3. Provided that the ionic strength I° of the 0.05 m KHPh buffer free of potassium chloride is known (through iterative calculation of the type outlined above), it can be inserted in Eqn. 2 to obtain $p\gamma^\circ_{Cl} = A(I^\circ)^{1/2}/[1 + a_0 B(I^\circ)^{1/2}]$, which finally allows the pH (RVS) value to be evaluated as pH (RVS) $= pa^\circ_H = p(a_H \gamma_{Cl})^\circ - p\gamma^\circ_{Cl}$. These pH (RVS) values based on Eqn. 7 can, for interpolation, be expressed by

$$\begin{aligned} \text{pH (RVS)} = {} & 4.0080 + 6.330x + 16.177x^2 - 115.3x^3 + 0.3089u \\ & -201.0ux^2 + 909ux^3 + 13.04v \end{aligned} \tag{8}$$

and are quoted in Table 3 alongside the parallel set of values obtained by extrapolating to $m_1 = 0$ the pH values from Eqn. 3. The maximum and

mean deviations are 0.027 and 0.014 respectively, which complies well with the general requirements of pH standard measurements. Although inspection of the results in Table 3 shows that both $p(a_H \gamma_{Cl})^\circ$ and pH (RVS) are continuous and smooth functions of solvent composition and temperature, it is worthwhile emphasising again, as explained recently [4], that each pH (RVS) quoted in Table 3 is valid only for the pH scale in the solvent of composition considered.

The financial support granted by the National Research Council of Italy (CNR) is gratefully acknowledged.

REFERENCES

1 A. K. Covington, Pure Appl. Chem., 55 (1983) 1467.
2 T. Mussini, A. K. Covington, P. Longhi and S. Rondinini, Criteria for Standardisation of pH Measurements in Aqueous Organic Solvent Mixtures, Pure Appl. Chem., 57 (1985) 865.
3 T. Mussini, A. K. Covington, F. Dal Pozzo, P. Longhi, S. Rondinini and Z. -Y. Zou, Electrochim. Acta., 28 (1983) 1593.
4 T. Mussini, A. K. Covington, M. Cicognini, P. Longhi and S. Rondinini, Anal. Chim. Acta, 162 (1984) 103.
5 M. J. Taylor, J. Chem. Eng. Data, 24 (1979) 230.
6 P. Longhi, T. Mussini, F. Penotti and S. Rondinini, J. Chem. Thermodyn., 17 (1985) 355.
7 P. Giammario, P. Longhi and T. Mussini, Chim. Ind. Milan, 53 (1971) 347.
8 T. Mussini and A. Pagella, J. Chem. Eng. Data, 16 (1971) 49.
9 D. F. Othmer and S. Josefowitz, Ind. Eng. Chem., 39 (1947) 1176.
10 C. Moreau and G. Douhéret, J. Chem. Thermodyn., 8 (1976) 403.
11 T. Mussini, P. Longhi and P. Giammario, Chim. Ind. Milan, 53 (1971) 1124.
12 R. G. Bates, Determination of pH. Theory and Practice, 2nd edn., Wiley, New York, 1973, pp. 243–253.
13 R. G. Bates and E. A. Guggenheim, Pure Appl. Chem., 1 (1960) 1163.
14 H. P. Bütikofer and A. K. Covington, Anal. Chim. Acta, 108 (1979) 179.
15 W. J. Hamer, G. D. Pinching and S. F. Acree, J. Res. Natl. Bur. Stand., 35 (1945) 539.
16 R. A. Robinson and R. H. Stokes, Electrolyte Solutions, 2nd rev. edn., Butterworths, London, 1965, pp. 520, 529.
17 A. K. Covington and Z. -Y. Zou, Electrochim. Acta, 28 (1983) 1587.
18 BMPD Statistical Software, Department of Biomathematics, University of California, LA, 1976.

Analytica Chimica Acta, 174 (1985) 339—341
Elsevier Science Publishers B.V., Amsterdam — Printed in The Netherlands

Short Communication

DETERMINATION OF LEAD IN NICKEL-BASE ALLOYS BY ATOMIC ABSORPTION SPECTROMETRY WITH INTRODUCTION OF SOLID SAMPLES INTO AN INDUCTION FURNACE

I. S. BUSHEINA and J. B. HEADRIDGE*
Department of Chemistry, The University, Sheffield S3 7HF (Great Britain)
(Received 12th February 1985)

Summary. Lead (0.2—26 $\mu g\ g^{-1}$) is determined in 1—9 mg samples of alloys dropped into the furnace. Standardized alloys were used for calibration. Data on accuracy and precision are presented for 23 nickel-base alloys.

Atomic absorption spectrometry (a.a.s.) with introduction of solid samples into an induction furnace has been used for the determination of bismuth [1], silver and thallium [2], cadmium, indium and zinc [3], and tellurium [4] in nickel-base alloys. Lead is also a deleterious trace element in these alloys and in British Standard 375:1977 it is stated that the maximum permitted concentration in Grade R-99.95B refined nickel is 1 $\mu g\ g^{-1}$. There is obviously a need to determine very low concentrations of lead in nickel and nickel-base alloys by a convenient method such as a.a.s. with a furnace but this has not been done in the past with an induction furnace because of large lead blanks resulting from traces of lead in the graphite material used to construct the cores of the induction furnaces. The problem has now been overcome by using graphite cores and side-arms constructed from UF4S-grade graphite (Ultra Carbon) baked under vacuum for 15 h at ca. 1700°C before use. Results are presented for 23 nickel-base alloys.

Experimental

Most of the nickel-base alloys were the same as those used in the work on cadmium, indium and zinc [3]. The procedures with the induction furnace were similar to those already described [3]. The experimental conditions for the determination of lead are shown in Table 1. A lead hollow-cathode lamp (Activion) was used at 283.3 nm. Calibration graphs of peak area vs. mass of lead for concentrations of lead $\leqslant 10\ \mu g\ g^{-1}$ and $>10\ \mu g\ g^{-1}$ were constructed from alloys R-3385 (1.2 μg Pb g^{-1}) and R-3387 (8.4 μg Pb g^{-1}) respectively.

Results and discussion

When damping position 1 was used, the calibration graphs were straight lines passing through the origin. The characteristic mass was 65 pg at 2230°C.

TABLE 1

Experimental conditions for the determination of lead with the induction furnace

Concn. range for Pb ($\mu g\ g^{-1}$)	Sample mass range (mg)	Flow rate of stir gas ($cm^3\ min^{-1}$)	Core temp. (°C)	Damping position[a]
<1	3—9	100	2200—2300	1
1—10	1—6	150	2100—2250	1
10—26	1—5	200	2100—2250	3

[a]Positions 1 and 3 correspond to time constants of 0.2 and 3 s, respectively.

At damping position 3, the calibration graphs also passed through the origin but were curved towards the mass axis because of the damping applied to the amplifier signal. This damping was necessary to keep the peak absorbances below 1.0. A higher stir flow rate was also used for the same reason.

TABLE 2

Results for the determination of lead in nickel-base alloys

Alloy	Supplier's result ($\mu g\ g^{-1}$)	Pb found ($\mu g\ g^{-1}$)	R.s.d. ($n < 6$) (%)
R-3386	2.2	2.1	8
R-3387	8.2	8.4	16
R-3388	4.7	4.4	17
R-4743	8.1	7.5	9
R-4750	0.9	1.1	6
R-6285	4.4	4.2	12
R-6286	10	9.5	10
R-6287	2.6	2.3	18
RRF-1	2.5	2.6	9
RRF-2	8.7	8.5	5
R-7247[a]	2.2	2.1	8
R-7248[a]	8.2	8.4	8
DTA	0.25	0.31	21
DTB	6.9	7.1	9
DTC	16	12	19
DTD	20	20	9
DTE	26	24	8
DTF	26	25	8
ST-1	1.1	0.9	10
ST-2	1.9	1.7	3
ST-3	3.4	3.2	6
BCS 345	0.2	0.25	11
BCS 346	21	20	9

[a]Iron-base alloy containing ca. 30% of nickel.

Results for the determination of lead in 23 nickel-base alloys are shown in Table 2. Good agreement between the results in the second and third columns shows that the accuracy of the method is good. The precision (average relative standard deviation = 10%) is that to be expected for this method. The limit of detection calculated as twice the standard deviation for BCS 345 is 0.06 $\mu g\ g^{-1}$ but this would be lower if calculations were made on nickel-base alloys which contained less than 0.25 $\mu g\ g^{-1}$ lead. The estimated limit of detection calculated from a published formula [3] is 0.02 $\mu g\ g^{-1}$. This communication completes the study on the determination of trace elements in nickel-base alloys by a.a.s. with addition of solid samples to an induction furnace. The advantages and disadvantages of using an induction furnace rather than a resistively heated furnace were outlined earlier [3].

We thank the University of El-Fateh, Libya, for a studentship for I. S. B. We are indebted to the S.E.R.C. and Rolls-Royce Ltd. (Derby) for financial assistance and to Wiggin Alloys Ltd., M.Q.A.D., Rolls-Royce Ltd. (Derby and Filton), Ross and Catherall Ltd. and the Bureau of Analysed Samples Ltd. for analysed samples.

REFERENCES

1 J. B. Headridge and R. Thompson, Anal. Chim. Acta, 102 (1978) 33.
2 A. A. Baker, J. B. Headridge and R. A. Nicholson, Anal. Chim. Acta, 113 (1980) 47.
3 I. S. Busheina and J. B. Headridge, Anal. Chim. Acta, 142 (1982) 197.
4 J. B. Headridge and R. A. Nicholson, Analyst (London), 107 (1982) 1200.

Analytica Chimica Acta, 174 (1985) 343—346
Elsevier Science Publishers B.V., Amsterdam — Printed in The Netherlands

Short Communication

USE OF CYANIDE TO REMOVE INTERFERENCES IN THE DETERMINATION OF COPPER, ZINC AND CADMIUM BY ATOMIC ABSORPTION SPECTROMETRY

M. M. EL-DEFRAWY, A. M. ABDALLAH* and A. F. EL-ASMY
Department of Chemistry, Faculty of Science, University of Mansoura (Egypt)
(Received 7th January 1985)

Summary. A variety of ligands affects the absorbance of copper, zinc and cadmium in the air/acetylene flame. This effect is removed by the addition of 0.1 M potassium cyanide.

The origins of interferences in flame atomic absorption spectrometry (a.a.s.) are numerous [1—3]. The composition of the dry aerosol particles varies in the presence of concomitant species so that their properties vary particularly with respect to their size and rate of vaporization, which govern the magnitude of the analytical signal [4]. When these properties differ between sample and calibration solutions, interferences may result. The type of interference studied here is that which originates from the presence of organic ligands in the sample solutions. Such substances seriously affect the atomic absorption determination of copper, zinc and cadmium, which are known to be free from condensed-phase interference.

Experimental

A Unicam SP-90A series 2 atomic absorption spectrometer was used which incorporated a HTA photomultiplier tube, Unicam hollow-cathode lamps for copper, zinc and cadmium, and a 10-cm slot burner head for the air/acetylene flame. The optimum instrumental parameters are listed in Table 1. All the stock solutions of cations and anions were prepared from reagent-grade chemicals or diluted from spectrochemical solutions for a.a.s. (BDH Chemicals). The complexes investigated were prepared as recommended [5, 6]. The concentration of copper or zinc in each studied complex solution was 10 μg ml^{-1} and of cadmium, 3 μg ml^{-1}.

Results and discussion

Because the absorbance is directly proportional to the free analyte atom population in the flame, the relationship between absorbance and the height of measurement above the burner top is an adequate criterion for evaluating interference effects when the analyte is present in different matrices.

0003-2670/85/$03.30

TABLE 1

Optimum conditions for the determination of copper, zinc and cadmium by a.a.s.

	Copper	Zinc	Cadmium
Wavelength (nm)	324.8	213.9	228.8
Slit-width (mm)	0.1	0.1	0.15
Lamp current (mA)	5	6	6
Acetylene flow rate (l min^{-1})	1.0	1.3	1.5
Air flow rate (l min^{-1})	5.0	5.0	5.0

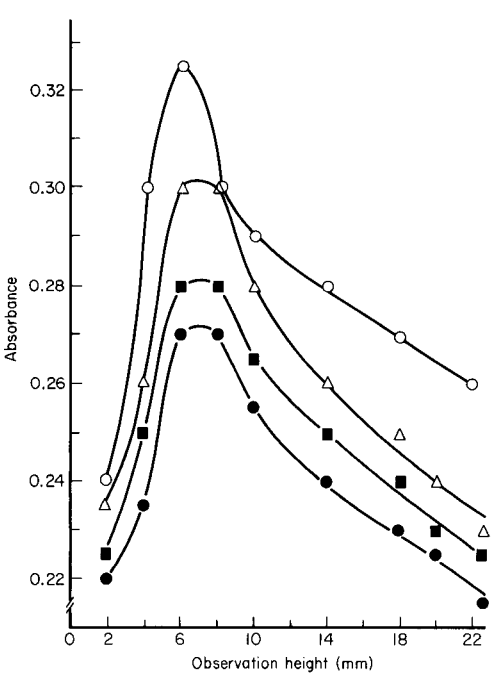

Fig. 1. Zinc absorbance as a function of observation height for zinc complexes (10 μg ml^{-1} zinc in each solution): (○) zinc chloride; (■) dichloro(4-phenyl-1-acetyltri-methylammoniumthiosemicarbazide)zinc(II) chloride dihydrate; (●) chloroaquo(4-phenyl-1-cyanoacylthiosemicarbazide)zinc(II); (△) dichlorodiaquo(4-phenyl-1-isobutyroylthiosemicarbazide)zinc(II) dihydrate.

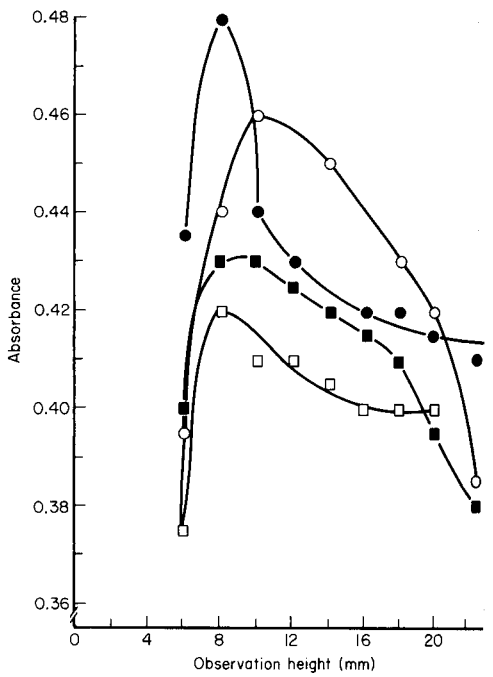

Fig. 2. Cadmium absorbance as a function of observation height for cadmium complexes (3 μg ml^{-1} cadmium in each solution): (○) cadmium nitrate; (●) bis(4-phenyl-1-benzoylthiosemicarbazide)cadmium(II) monohydrate; (■) dichloro(4-phenyl-1-acetylpyridiniumthiosemicarbazide)cadmium(II) chloride; (□) dibromo(4-phenyl-1-acetylpyridiniumthiosemicarbazide)cadmium(II) chloride.

Figures 1 and 2 indicate the absorbances obtained for zinc and cadmium in different complexes and at various heights above the burner head. They show serious variations in the free atom population of the two analytes with

changes in observation height and ligand. Attempts to produce similar graphs for some copper complexes gave results that were unsatisfactory.

Figures 3 and 4 show the behaviour of copper, zinc and cadmium when their complexes were aspirated after making their solutions 0.1 M in potassium cyanide, essentially under the same experimental conditions. Obviously, the distribution graphs almost coincide. This indicates that cyanide has converted copper, zinc and cadmium to a common form, i.e., their cyano complexes, and has eliminated the interfering effects of the other ligands.

The presence of 2000 μg ml^{-1} chloride, bromide, phosphate, silicate, nitrate, sulphate, peroxodisulphate, borate, chromate, hydrogenphthalate, tartrate, succinate, glycine, 8-quinolinol, EDTA, pyrogallol, catechol or ethanolamine in the presence of 0.1 M cyanide does not affect the atomic absorbance of 10 μg ml^{-1} copper or zinc or 3 μg ml^{-1} cadmium.

An attractive feature of cyanide addition is that there is no need to use

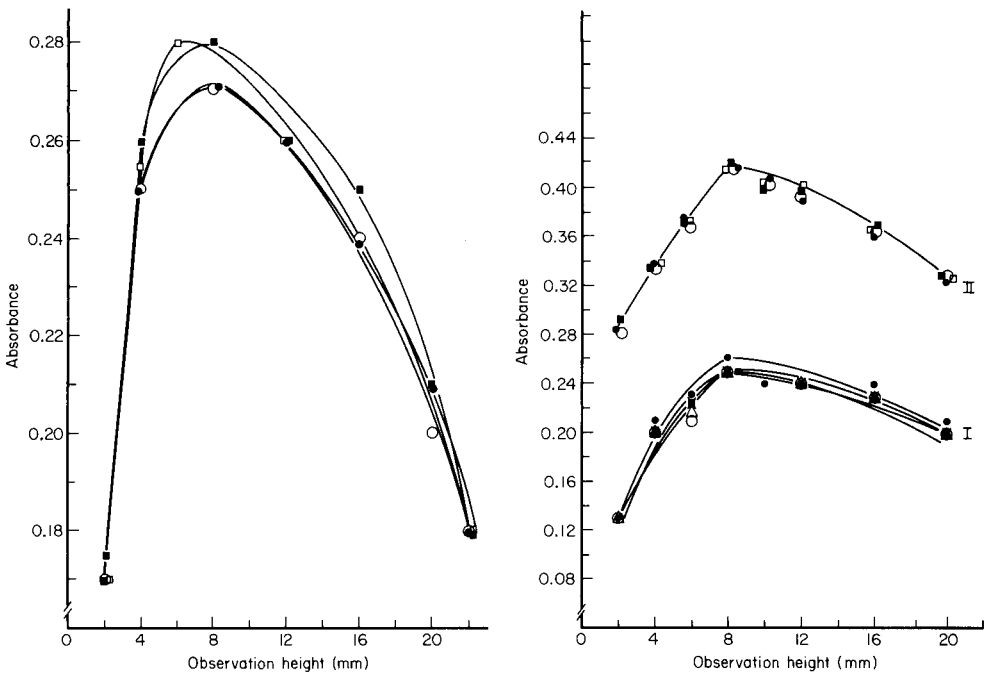

Fig. 3. Copper absorbance as a function of observation height for copper complexes (10 μg ml^{-1} copper in each solution) in the presence of 0.1 M potassium cyanide. (○) copper chloride; (▪) acetato(1,4-diphenylthiosemicarbazide)copper(II); (●) dichloro-(4-phenyl-1-isobutyroylthiosemicarbazide)copper(II) monohydrate; (○) bis[4-phenyl(2,4-dinitrophenyl)thiosemicarbazide]copper(II); (□) chloro(4-phenyl-1-cyanoacylthiosemicarbazide)copper(II) tetrahydrate.

Fig. 4. Absorbance as a function of observation height for (I) zinc complexes and (II) cadmium complexes in the presence of 0.1 M potassium cyanide (symbols and conditions as in Figs. 1 and 2).

additional steps to get rid of such undesirable matrix effects. Cyanide addition has similarly been shown to eliminate interfering effects in the determination of ruthenium [7], cobalt [8], molybdenum [9], iron [10] and chromium [11].

REFERENCES

1 J. C. Van Loon, Analytical Atomic Absorption Spectroscopy, Academic Press, London, 1980.
2 J. Ruběska, Can. J. Spectrosc., 20(6) (1975) 156.
3 E. M. Bulewicz and P. J. Padley, Spectrochim. Acta, Part B, 28 (1973) 125.
4 C. B. Boss and G. M. Hieftje, Anal. Chem., 51(7) (1979) 895.
5 M. M. Mostafa, A. M. Shallaby and A. F. El-Asmy, J. Inorg. Nucl. Chem., 43 (1981) 2992.
6 M. M. Mostafa, A. M. Shallaby and A. F. El-Asmy, Trans. Met. Chem., 6 (1981) 303.
7 M. M. El-Defrawy, J. Posta and M. T. Beck, Anal. Chim. Acta, 102 (1978) 185.
8 M. M. El-Defrawy, J. Posta and M. T. Beck, Anal. Chim. Acta, 115 (1980) 155.
9 A. M. Abdallah, M. M. El-Defrawy, M. A. Mostafa and A. B. Sakla, Anal. Chim. Acta, 174 (1985) 347.
10 A. M. Abdallah, M. M. El-Defrawy, M. A. Mostafa and A. B. Sakla, Talanta, 32(1) (1985) 19.
11 A. M. Abdallah, M. M. El-Defrawy and M. A. Mostafa, Anal. Chim. Acta, 165 (1984) 105.

Analytica Chimica Acta, 174 (1985) 347—352
Elsevier Science Publishers B.V., Amsterdam — Printed in The Netherlands

Short Communication

CHARACTERIZATION OF INTERFERING EFFECTS IN THE DETERMINATION OF MOLYBDENUM BY ATOMIC ABSORPTION SPECTROMETRY

A. M. ABDALLAH, M. M. EL-DEFRAWY and M. A. MOSTAFA
Department of Chemistry, Faculty of Science, University of Mansoura (Egypt)
A. B. SAKLA*
Microanalytical Center, Faculty of Science, University of Cairo, Dokki, Giza (Egypt)
(Received 7th January 1985)

Summary. The effect of anions on molybdenum absorbance depends on the pH; low pH causes the formation of iso- or heteropoly anions which change the atomization process in the flame. Organic ligands also depress the release of molybdenum atoms but cyanide radicals in the flame scavenge, e.g., OH radicals from such ligands and prevent their depressive effect. Certain cations (La, Ce, Mg, Ca, Sr and Ba) appear to form spinels; boric acid minimizes this effect.

The sensitivity of determination of molybdenum by atomic absorption spectrometry (a.a.s.) has been reported to be higher if fuel-rich flames are used [1, 2]. Many papers [3—7] have given procedures for overcoming various interferences in the determination of molybdenum in a variety of samples. Studies have been made [8, 9] of the effect of several elements on the absorbance of molybdenum. David [1] has used aluminium as a releasing agent for the determination of molybdenum in stainless steel and Pollock [10] used the same technique for the analysis of slags. Mostyn and Cunningham [11] recommended ammonium chloride as an interference suppressor. Kirkbright et al. [12] determined molybdenum in alloy steels by using a nitrous oxide/acetylene flame and recommended the addition of iron to the standards to compensate for its depressive effect on molybdenum absorbance. Similar procedures have been employed by others [13, 14]. Knight and Pyzyna [15] claimed that it is necessary to match the composition of sample and standards for the accurate determination of molybdenum in tool steels. A procedure for the determination of molybdenum in liquid fertilizers [16] used addition of phosphoric acid to eliminate many interferences.

The aim of this investigation was to characterize the molybdenum compounds formed with interfering species, and to find means of preventing their formation.

Experimental

A Unicam SP-90A series 2 atomic absorption spectrometer, fitted with a new HTA photomultiplier tube (EMI), and a PM-8251 single-pen recorder were used. A continuous titration device [17] was attached to the instrument and the results were processed with a programmable pocket calculator. The instrumental parameters used were: wavelength, 313.9 nm; slit-width, 0.15 mm (monochromator dispersion 1.56 nm mm^{-1} at 310 nm); observation height, 0.4—0.5 cm above the burner top; air flow rate, 5 l min^{-1}; acetylene flow rate, 1.8 l min^{-1}.

Results and discussion

Effect of anions. A series of almost neutral solutions was prepared containing 100 μg Mo ml^{-1} (added as molybdate) plus the interfering anion in increasing concentrations. The ions tested were Br^-, I^-, NO_2^-, NO_3^-, ClO_4^-, Cl^-, SO_4^{2-} and PO_4^{3-}, added as their sodium or potassium salts. The results obtained revealed no interference from $\leqslant$1000 μg ml^{-1} of any of these ions. However, phosphoric, hydrochloric and sulphuric acids interfered when present at this concentration, giving changes in absorbance of −10, +10 and −40%, respectively. Molybdate is likely to polymerize as the pH is decreased to give a series of isopoly species or, in the presence of anions such as phosphate, heteropoly species [18]. A structural relationship is to be expected between the dry aerosol products and their precursors, the polymeric species in solution. Such products have different particle sizes and stabilities during evaporation and disintegration in the flame, and must account for the changes in molybdenum absorbance.

Effect of complexing agents. Reactions in hydrocarbon flames are complicated, and the composition of the flame is made more complex when the sample contains combustible components [19]. Figure 1 shows the effect of some ligands on the absorbance for 100 μg Mo ml^{-1}. Five of the six ligands have depressive effects of between 63 and 15%, but there is no indication of stoichiometric complexation.

Organic ligands enrich the flame with oxidizing entities such as OH, O, O_2 and NO, which preclude complete atomization of molybdate in the flame. A decrease in the concentration of such oxidizing species in the flame should help in producing molybdenum atoms. To investigate the validity of this concept, potassium cyanide solutions of increasing concentration were sprayed into the flame and the OH and CO emission intensities were recorded. Figure 2 shows the simultaneous decrease of the OH concentration and increase of the CO concentration. The following radical reactions can take place in the vapour phase:

$$CN + OH \rightarrow CO + N + H$$

$$CN + NO \rightarrow CO + N_2$$

Figure 3 shows support for this concept, the scavenging action of CN on OH and NO produced from the thermal decomposition of the ligands nullifying the effect of these ligands on the molybdenum absorbance.

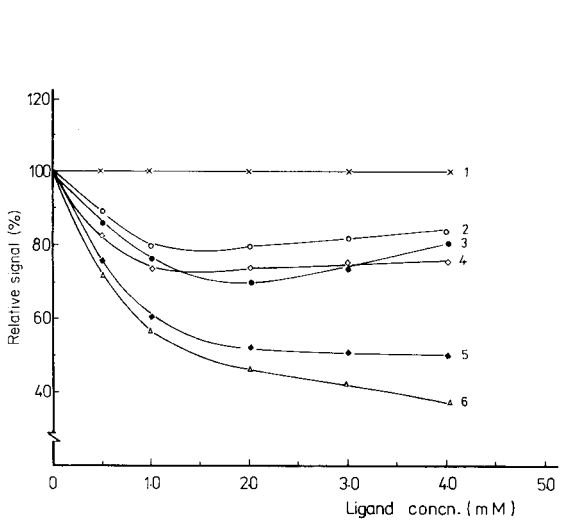

Fig. 1. Molybdenum absorbance as a function of ligand concentration: (1) KCN; (2) DCTA; (3) NTA; (4) EDTA; (5) sulphosalicylic acid; (6) glycine. Ligand added to 100 μg Mo ml^{-1}.

Fig. 2. Effect of potassium cyanide on: (1) CO emission intensity at 219 nm, (2) OH emission intensity at 281.1 nm. (Intensity of CO or OH already present in the flame is assumed to be 100; all other readings are referred to this value.)

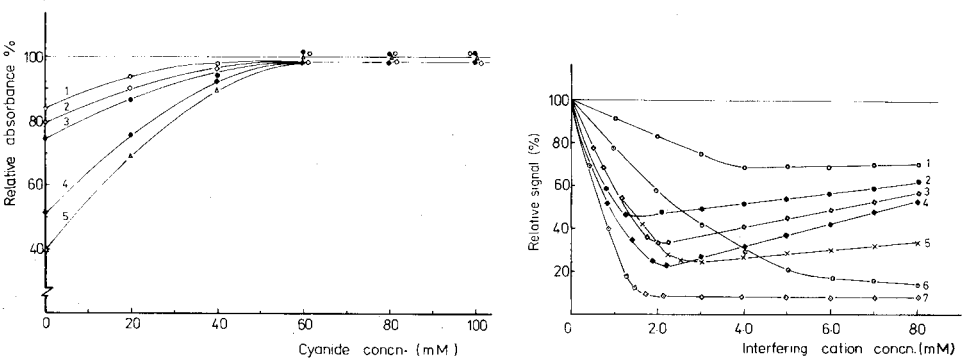

Fig. 3. Effect of potassium cyanide on the absorbance from 100 μg Mo ml^{-1} in presence of 4 × 10^{-3} M: (1) DCTA; (2) NTA; (3) EDTA; (4) sulphosalicylic acid; (5) glycine. (Absorbance of 100 μg ml^{-1} molybdenum alone = 100. Organic ligand at 4 × 10^{-3} M.)

Fig. 4. Effects of cations on the absorbance from 200 μg Mo ml^{-1} at pH 7: (1) Mg; (2) Ce; (3) Sr; (4) Ba; (5) Ca; (6) Mn; (7) La.

Effect of cations. Figure 4 shows the effect of some metal ions on molybdenum absorbance. The more or less abrupt changes of slope on the curves all indicate a stoichiometric relation between the interferent and molybdenum compatible with spinel formation [20, 21] (Table 1). The

TABLE 1

The structural formulae and melting points of some spinels [20, 21]

Interfering metal, M	Stoichiometry obtained Mo:M	Structural formulae	Melting point (°C)
La	3:2	$La_2O_3 . 3MoO_3$	1181
Ce	3:2	$Ce_2O_3 . MoO_3$	973
Ca	1:1	$CaO . MoO_3$	1250
Sr	1:1	$SrO . MoO_3$	≅ 1600
Ba	1:1	$BaO . MoO_3$	1480
Mn	3:1	$Mn_3O_4 . MoO_3$	—
Mg	2:1	$2MgO . MoO_3$	—

spinels, which contain molybdenum, the metal cation and oxygen [18], dissociate only slowly, so that the severity of the interference is not much decreased by measuring the absorbance higher in the flame (i.e., after a longer residence time). The relative depression of the absorbance by the interfering cations is smaller at lower interferent concentrations.

Figure 5 shows the effect of boric acid on molybdenum absorbance in the presence of some metal ions. Boric acid removes most of the metal ion

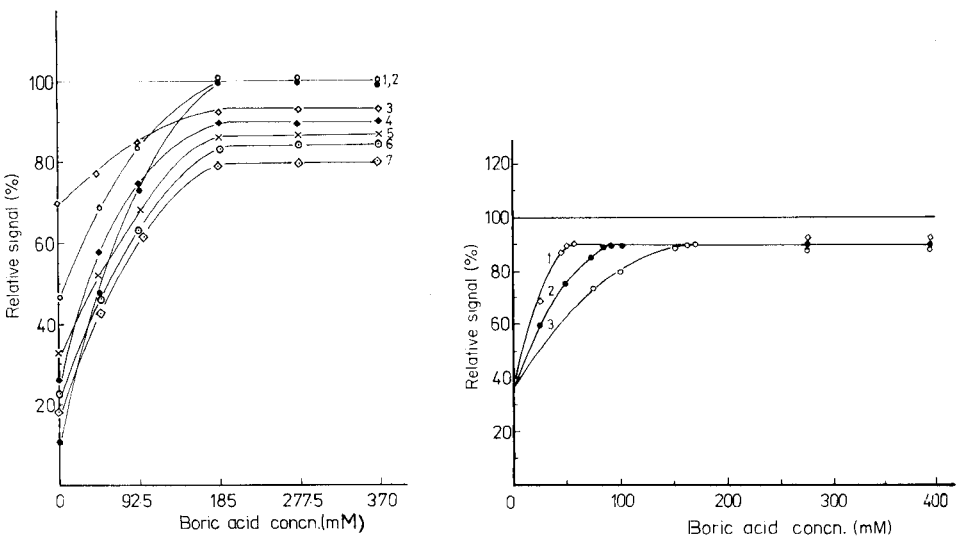

Fig. 5. Effect of boric acid on the absorbance from 100 μg Mo ml^{-1} in solutions containing: (1) 2:3 La:Mo; (2) 2:3 Ce:Mo; (3) 2:1 Mg:Mo; (4) 1:1 Ca:Mo; (5) 1:1 Sr:Mo; (6) 1:1 Ba:Mo; (7) 3:1 Mn:Mo.

Fig. 6. Effect of boric acid on signal for 2.08×10^{-3} M Mo in presence of calcium: (1) 7.5; (2) 12.5; (3) 25×10^{-3} M Ca.

depressions although not as effectively as cyanide. No change in the OH emission intensity at 281.1 nm was found when boric acid was present, therefore its effect is not to provide a more reducing environment, unlike cyanide.

The effect of borate is probably to react preferentially with the metal ions to prevent spinel formation. The lower molybdenum absorbance in the presence of excess of borate and the alkaline earth metal ions, however, may be due to an increase in oxygen content of the flame owing to some metal borate decomposition to metal boride and oxygen. The use of a reducing flame should minimize this effect. Lanthanum and cerium borates, however, are much more stable and therefore this effect will be less. Figure 6 shows the effect of boric acid on the molybdenum absorbance in the presence of different concentrations of calcium. The curves indicate that an increase in borate concentration commensurate with the increase in calcium concentration is needed to restore the absorbance to the plateau region.

Figure 7 shows how the absorbance of magnesium, calcium and strontium vary with the concentration of boric acid. The interference increases linearly with boric acid concentration up to a certain mole ratio of borate to metal, above which there is no further increase in suppression. The values of the critical ratios are 6:1 for calcium and strontium, and 12:1 for magnesium. These observations show that compounds are formed by these elements with boron in the flame.

For accurate determination of molybdenum by a.a.s. in a fuel-rich air/acetylene flame, addition of boric acid should be made to the sample solutions and standards to overcome cationic interferences. The presence of organic substances in the sample solutions necessitates addition of potassium cyanide to samples and standards.

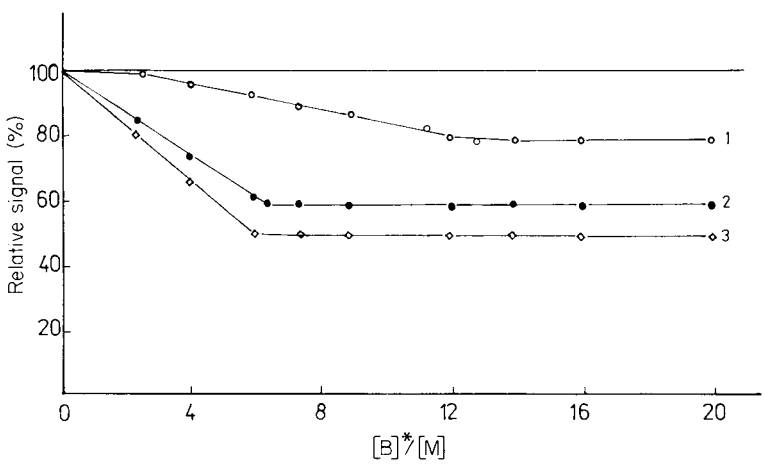

Fig. 7. Effect of boric acid on absorbance of 2.08×10^{-3} M Mo in presence of: (1) Mg; (2) Ca; (3) Sr, all at 1×10^{-3} M.

REFERENCES

1 D. J. David, Analyst, 86 (1961) 730.
2 G. F. Kirkbright, M. K. Peters and T. S. West, Analyst, 91 (1966) 705.
3 T. Nakahara and C. L. Chakrabarti, Anal. Chim. Acta, 104 (1979) 99.
4 Y. Chau and K. Lum-Shue-Chan, Anal. Chim. Acta, 48 (1969) 205.
5 J. O. Pierce and J. Cholak, Arch. Environ. Health, 13 (1966) 208.
6 L. R. P. Butler and P. M. Mathews, Anal. Chim. Acta, 36 (1966) 319.
7 S. R. Koirtyohann and M. Hamilton, J. Assoc. Off. Anal. Chem., 54 (1971) 787.
8 R. Caboi, Period. Mineral., 37 (1968) 717.
9 J. D. Kerbyson and C. Ratzkowski, Can. J. Spectrosc., 15 (1970) 43.
10 E. N. Pollock, At. Absorpt. Newsl., 9 (1970) 47.
11 R. A. Mostyn and A. F. Cunningham, Anal. Chem., 38 (1966) 121.
12 G. F. Kirkbright, A. M. Smith and T. S. West, Analyst, 91 (1966) 200.
13 Y. Endo, T. Hata and Y. Nakahara, Jpn. Anal., 18 (1969) 878.
14 D. R. Thomerson and W. J. Price, Analyst, 96 (1971) 321.
15 D. M. Knight and M. K. Pyzyna, At. Absorpt. Newsl., 8 (1969) 129.
16 N. S. Romanova and T. N. Viadimirskaya, Khim. Promst., Moscow, Ser. Metody Anal. Kontrolya Kach. Prod. Khim. Prom-Sti., 11 (1979) 18.
17 J. Posta and J. Lakatos, Magy. Kém. Foly., 68 (1980) 284.
18 H. J. Emeléus and A. G. Sharpe, Modern Aspects of Inorganic Chemistry, 4th edn., ELBS and Routledge & Kegan Paul, London, 1978.
19 E. Pungor, Flame Photometry, Van Nostrand, London, 1968.
20 R. C. Weast (Ed.), Handbook of Chemistry and Physics, 60th edn., CRC Press, Boca Raton, FL, 1981.
21 G. V. Samsonov, Poroshk. Metall., Akad. Nauk Ukr. SSR 3, 2 (1963) 65; Izv. Akad. Nauk SSSR, Neorg. Mater., 1 (1965) 1803.

Analytica Chimica Acta, 174 (1985) 353—357
Elsevier Science Publishers B.V., Amsterdam — Printed in The Netherlands

Short Communication

ATOMIC ABSORPTION SPECTROMETRIC DETERMINATION OF MOLYBDENUM IN LUBRICATING OILS WITH USE OF EMULSIONS

J. B. BEFERULL BLASCO and M. DE LA GUARDIA CIRUGEDA*

Departmento de Química Analítica, Facultad de Ciencias Químicas, Universidad de Valencia, Burjasot, Valencia (Spain)

A. SALVADOR CARREÑO

Seminario de Física y Química, Escuela de Magisterio de Valencia, Universidad de Valencia, Valencia (Spain)

(Received 7th December 1984)

Summary. Samples (0.1 g) containing molybdenum disulphide are digested with aqua regia or with a (1 + 1) hydrofluoric/nitric acid mixture, without complete destruction of the matrix, and the molybdenum is determined in an air/acetylene flame, after emulsification with a non-ionic surfactant (Nemol K-39). The detection limit is ca. 30 μg Mo g^{-1}, and the r.s.d. is 2.9% for 6 analyses of a sample containing 6.5 mg Mo g^{-1}.

Determination of metals in lubricating oils is of interest for both the control of additives and the study of motor wear [1]. Flame atomic absorption spectrometry (a.a.s.) is the most useful technique for such determinations [2]. Recently, the use of emulsions for introduction of samples and standards in flame a.a.s. has allowed the rapid determination of additives containing calcium [3], barium [4], zinc [5], dissolved lead [6] and total iron [7] in used oils without the need for organometallic standards. Nevertheless, this technique has not been applied to the determination of metals in solid, oil-insoluble additives.

At present, molybdenum disulphide is widely used as an additive for motor oils. The fine particles suspended in the oil improve its rheological features and allow wear to be repaired by accumulation in hollows and damaged zones [8]. Visible emission spectrometry [9] and x-ray fluorescence spectrometry [10] have been used for the determination of molybdenum in oils, though a.a.s. is most widely applied. For the analysis of used oils by a.a.s., Merryfield [11] diluted the oil with xylene and determined the molybdenum directly, although molybdenum metal in suspension is not recovered in this way [12]. For this reason, prior to dilution with an organic solvent, Brown et al. [13] and Kauffman et al. [14] attacked the samples with a mixture of acids, and used organometallic standards.

In the present communication, a method is proposed for determining molybdenum in oils containing molybdenum disulphide by flame a.a.s. with use of emulsions. The results obtained are compared with those found by flame a.a.s. after sample ashing and acid dissolution of the residue.

0003-2670/85/$03.30

Experimental

Apparatus. A Perkin-Elmer model 5000 or a Pye-Unicam SP-1900 atomic absorption spectrometer was used. The optimal instrumental settings were the same for both oil/methyl isobutyl ketone (MIBK) emulsions in water and aqueous molybdenum solutions. For sample attack, 100-ml Pyrex flasks with bakelite stoppers, and 50-ml polyethylene flasks with polyethylene stoppers were used.

Reagents. An aqueous 1000 μg ml^{-1} molybdenum solution was prepared from ammonium heptamolybdate. An aqueous 20% (v/v) solution of Nemol K-39 (nonylphenol/ethylene oxide condensate, average molecular weight 710, average degree of condensation 10.7) was obtained from Hoechst. All mineral acids were analytical-reagent grade.

General procedure. Weigh exactly 0.1—1 g of oil into a pyrex flask, add 4 ml of aqua regia and heat at 150°C for 30 min. Acid attack may also be done in polyethylene flasks with 2.5 ml of (1 + 1) hydrofluoric/nitric acid, with heating at 60°C for 60 min. After the acid treatment, add 3 ml of MIBK to dissolve the oil residues and emulsify with 10 ml of the 20% Nemol K-39 solution, with manual shaking. Add 25 ml of distilled water. Prepare standards in a similar way, but from a molybdenum sulphide-free oil. Dilute with 3 ml of MIBK, add the same amount of acid as for the samples and emulsify with 10 ml of Nemol K-39 solution as above. Introduce molybdenum as an aqueous solution.

The wavelength was 313.26 nm, and the hollow-cathode lamp current was 10 mA. For the Perkin-Elmer 5000, the slit-width was 0.15 mm, and the burner height was 8 mm; the gas flows were 4.5 l min^{-1} nitrous oxide, 4.2 l min^{-1} acetylene. For the SP-1900, the slit-width was 0.7 nm, the burner height was 6 mm, and the gas flow settings were air = 40 and acetylene = 25.

Results and discussion

Sample emulsification. Owing to the problems caused by the physical state of the additive in sample atomization, and because direct determination of molybdenum in emulsified samples was impossible, chemical attack on the samples was necessary prior to their emulsification and nebulization. The use of 10 ml of aqueous 20% Nemol K-39 solution allowed transparent, highly stable emulsions of any residual oil to be obtained from 0.1—0.5 g of oil sample diluted with 3 ml of MIBK. For larger (0.5—1.0 g) amounts of oil, milky emulsions were obtained, but their stability was adequate for flame a.a.s. The original presence of 1—4 ml of aqua regia did not affect either the stability of the emulsions or the absorbance of emulsified standards.

Sample digestion. Three types of acid were investigated: concentrated nitric acid, aqua regia and a (1 + 1) nitric/hydrofluoric acid mixture. A synthetic sample of 10 mg ml^{-1} molybdenum was prepared from molybdenum sulphide and a molybdenum-free oil. A 0.1-g sample was digested in a tightly stoppered flask with nitric acid or aqua regia for 2 h at 100°C. With 2—4 ml of nitric acid a recovery of $\leqslant$80% was attained,

whereas the same volume of aqua regia gave complete recovery of molybdenum. To decrease the time required, the temperature was varied. For 4 ml of aqua regia, increasing the temperature decreased the time of digestion (Table 1); complete recovery was achieved at 150°C for 30 min. Increasing the amount of aqua regia also decreased the digestion time needed (Table 1).

The nitric/hydrofluoric acid system was also investigated. Table 2 shows that the time of shaking for emulsification after digestion had no influence above 5 min, and that digestion for 60—90 min at 60°C was needed to ensure complete recovery of molybdenum (Table 2). Variation in the amount of acid mixture from 1.0 to 2.5 ml gave recoveries of 96.5—100.0%.

Consequently, digestion of the oil samples prior to their emulsification

TABLE 1

Effect of temperature and volume of aqua regia on digestion time[a]

Temp. (0°C)	Vol. of aqua regia (ml)	Digestion time[b] (min)	Recovery (%)
100	4	210	103
120	4	120	102
140	4	40	102
150	4	30	103
150	1	45	101
150	2	55	104
150	3	45	105
150	5	20	104

[a]0.1 g samples; 9.94 mg g^{-1} molybdenum. [b]The time needed for total disappearance of colour.

TABLE 2

Influence of temperature, digestion time and shaking time for the hydrofluoric/nitric acid mixture (2.5 ml)[a]

Temperature (0°C)	Digestion time[b] (min)	Shaking time (min)	Recovery (%)
Room	—	5	33
50	45	5	90
50	45	10	86
50	90	5	102
50	90	10	101
60	45	5	94
60	60	5	103
60	90	5[c]	104
60	90	5	98

[a,b]See Table 1. [c]With ultrasonic treatment.

can be done with either 4 ml of aqua regia at 150°C for 30 min or 2.5 ml of the nitric/hydrofluoric acid mixture at 60°C for at least 60 min. Both digestion procedures guarantee complete recovery of molybdenum. The use of aqua regia requires a higher temperature, which is compensated by the shorter digestion time and by the use of ordinary glassware.

Analytical features. The a.a.s. measurements were done with both air/acetylene and nitrous oxide/acetylene flames. In general, the results obtained indicated that under the present experimental conditions more stable readings were obtained with the former flame, but the nitrous oxide flame is more interference-free.

The calibration graphs obtained with aqueous standards were compared with those obtained with emulsified standards. Their slopes (Table 3) are very similar. The detection limit (the molybdenum concentration in the oil giving an absorbance equal to that of the blank plus three times its standard deviation) is somewhat higher for the aqua regia-containing emulsions than for the nitric/hydrofluoric acid emulsions (Table 3).

Four commercial samples of lubricating oils were analyzed by digestion

TABLE 3

Analytical features of the methods used

Medium	Calibration equation[a]	Detection limit (μg ml^{-1})		Sample wt. (g)
		In final soln.	In oil	
Aqua regia emulsion	$A = 0.0092C + 0.014$	0.14	60	0.1
HF/HNO_3 emulsion	$A = 0.0092C + 0.009$	0.08	33	0.1
Aqueous solution	$A = 0.0094C + 0.000$	0.16	53	0.3[b]

[a] A, absorbance; C, concentration in μg ml^{-1}. [b] Sample weight necessary for analysis by flame a.a.s. after complete ashing of samples.

TABLE 4

Accuracy and precision of the proposed method

Sample	Reference method[a]			Emulsion method			
	Mean Mo conc. (mg g^{-1})	n[b]	R.s.d. (%)	Mean Mo conc. (mg g^{-1})	n[b]	R.s.d. (%)	Error (%)
A	9.09	18	4.4	9.17	7	6.8	0.9
B	6.66	5	2.5	6.51	6	2.9	2.1
C	6.61	5	0.8	7.02	5	2.5	6.2
D	8.23	9	1.8	8.29	9	2.4	0.5

[a] See text. [b] Number of samples analyzed.

with aqua regia. Table 4 shows the results obtained, compared with those obtained by a reference procedure consisting of ashing previously burner-dried oil samples (0.3—3.0 g) at 450°C in a muffle furnace for 150 min, dissolving the residue in 25 ml of concentrated nitric acid and 2 ml of 60% perchloric acid, heating to dryness, dissolving the residue in 5 ml of (1 + 1) hydrochloric acid and diluting to 100 ml. Samples so prepared were nebulized into the flame and their absorbance measured. Aqueous molybdenum standards containing the same amount of hydrochloric acid as the sample solutions were used for calibration. Mineralization with a mixture of nitric, sulphuric and perchloric acid suffered from interference of sulphuric acid on the molybdenum signal. The results obtained show that the method proposed is accurate and has adequate precision. Because the sample weight is only one third of that required for the reference method, the precision of the latter is usually better.

Conclusions

The method proposed, based on the formation of emulsions, has advantages over methods involving total decomposition of oil samples, in that the sample preparation time and sample manipulation are much less. The method also allows the use of aqueous solutions in the preparation of standards for determining total molybdenum in oil samples.

REFERENCES

1 A. D. King, D. R. Hilligoss and G. F. Wallace, At. Spectrosc., 5 (1984) 189.
2 M. de la Guardia and A. Salvador, At. Spectrosc., 5 (1984) 150.
3 M. de la Guardia, A. Salvador and V. Berenguer, Analusis, 8 (1980) 448.
4 M. de la Guardia, A. Salvador and V. Berenguer, Analusis, 9 (1981) 74.
5 V. Berenguer and J. Hernández, Quím. Anal., 31 (1977) 81.
6 J. Hernández, L. Polo and A. Bernal, Anal. Chim. Acta, 108 (1977) 39.
7 A. Salvador, M. de la Guardia and V. Berenguer, Talanta, 30 (1983) 986.
8 D. Pérez Parra, Lubricantes: su Empleo y Selección, C.E.A.C., Madrid, 1963.
9 D. Blanco, Ión (Madrid), 408 (1975) 507.
10 D. Jovanovic, Anal. Chem., 42 (1970) 775.
11 R. N. Merryfield, Anal. Chem., 51 (1979) 1965.
12 C. S. Saba and K. J. Eisentraut, Anal. Chem., 51 (1979) 1927.
13 J. R. Brown, C. S. Saba, W. E. Rhine and K. J. Eisentraut, Anal. Chem., 52 (1980) 2365.
14 R. E. Kauffman, C. S. Saba, W. E. Rhine and K. J. Eisentraut, Anal. Chem., 54 (1982) 975.

Analytica Chimica Acta, 174 (1985) 359—363
Elsevier Science Publishers B.V., Amsterdam — Printed in The Netherlands

Short Communication

DETERMINATION OF TRACES OF HYDROGENSULFITE BY CHEMILUMINESCENCE WITH CERIUM(IV) SULFATE AS THE REAGENT

KOJI TAKEUCHI* and TAKASHI IBUSUKI

Department of Air Pollution Control, National Research Institute for Pollution and Resources, 16-3 Onogawa, Yatabe, Ibaraki 305 (Japan)

(Received 30th October 1984)

Summary. Trace amounts of hydrogensulfite in aqueous solution (0.19—50 ng ml^{-1} SO_2) are determined continuously with a chemiluminescence method based on a cerium(IV) sulfate reagent at pH 1.8. The intensity per unit SO_2 concentration is about 5 times that obtained with a permanganate reagent. The inhibitory effects of nitrite, transition metal ions and formaldehyde are also reduced.

Measurements of traces of sulfur dioxide or sulfurous acid in the environment are becoming more important in order to understand acid precipitation and the global sulfur cycle. However, few sensitive methods are available for determining sulfur dioxide in solution except for some spectrophotometric methods. Chemiluminescence, obtained by oxidation of hydrogensulfite [1], has been applied to the measurement of atmospheric background concentrations of sulfur dioxide [2].

The continuous determination of trace amounts of hydrogensulfite by using an acidic potassium permanganate solution was reported recently [3]. Small amounts of sodium formate added to the aqueous sample solutions satisfactorily stabilized the sulfite species. However, the method had some limitations. The concentration of potassium permanganate in the reagent solution should be as low as possible, because the absorption band of permanganate overlaps the emission band; this made it difficult to obtain more intense chemiluminescence. Further, some substances such as nitrite seriously quenched the luminescence. Addition of some fluorescers to the permanganate/sulfite system was examined in attempts to intensify the luminescence [4], but the detection limit was not improved because the fluorescers also increased the dark current.

Other oxidizing agents were tested to try to remove these disadvantages. Neither hydrogen peroxide nor potassium peroxodisulfate gave any chemiluminescence, despite their high redox potentials. Stauff and Jaeschke [1] concluded that cerium(IV) sulfate was less useful for the determination of sulfite because of the weak chemiluminescence. But, it was unexpectedly found that cerium(IV) sulfate is a more efficient reagent than potassium permanganate.

0003-2670/85/$03.30

Experimental

The flow-type chemiluminescent analyzer described before [3] was used with a Pyrex glass discoid reaction cell (12.6 mm i.d., 4.8 mm wide, 0.7 ml capacity). Flow rates of reagent and sample solutions were 1.2 and 2.0 ml min^{-1}, respectively. The applied high voltage of the photomultiplier was —710 V and the photon counting period was 100 s or 10 s depending on the light intensity. A Hitachi 330 spectrophotometer and an Orion 601 pH meter were also used.

A standard stock solution (0.5 g l^{-1} SO_2) was prepared daily by dissolving sodium metabisulfite ($Na_2S_2O_5$) to purified water deoxygenated by nitrogen bubbling, and was standardized spectrophotometrically against iodine solutions [5]. Sample solutions containing 0—100 ng ml^{-1} sulfur dioxide were prepared as follows: ca. 450 ml of purified water (without deoxygenation) was fed into a 500-ml volumetric flask; 1-ml aliquots of both 0.05 M (M = mol dm^{-3}) sodium hydroxide and 1 mM sodium formate solutions were added. After addition of 0—100 μl of the stock solution with a micropipette, the flask was filled up to the mark with purified water.

A sulfuric acid (0.01 M) solution of 0.3 mM cerium(IV) sulfate was used as the reagent solution. All reagents were of analytical grade. Purified water (18 MΩ cm) was supplied from a Millipore Milli-Q system.

Results and discussion

Sample solutions. Sulfurous acid species in sample solutions were well stabilized by raising the pH of the solution to slightly alkaline (ca. 9.5) and by adding small amounts of sodium formate (1—2 μM). It was found that formate protected sulfite species from oxidation even in the presence of dissolved oxygen at least for one day after preparation. The concentration of oxygen dissolved in water at atmospheric pressure (0.29 mM at 25° C) is much higher than that of sodium formate added (up to 2 μM), thus formate may act as a radical scavenger in the autoxidation of sulfite.

Reagent solution. The dependence of the chemiluminescence intensity on the pH of a reagent solution containing 0.3 mM cerium(IV) sulfate was examined over the pH range 1.4—2.8 for 20 ng ml^{-1} SO_2 standards. Maximum intensity was obtained at pH 1.8—2.1; the intensity decreased at both the lower and the higher pH regions. Therefore, the pH of the reagent solution was adjusted to 1.8 with sulfuric acid (0.01 M) in all later work. The decrease in the chemiluminescence intensity at the higher pH is attributed to the remarkable decrease in cerium(IV) concentration owing to the small solubility product of cerium(IV) hydroxide (2×10^{-51}, [6]). The decrease in the intensity at lower pH is attributed to the decrease in the fraction of hydrogensulfite. Maximum and constant chemiluminescence was obtained over the range of 10^{-4}—3×10^{-3} M cerium(IV) sulfate at pH 1.8.

The absorption band of cerium(IV) in the reagent solution lies in the ultraviolet region at 270 nm ($\epsilon \approx 3900$ l mol^{-1} cm^{-1}); the cerium(III) ion which will be formed absorbs u.v. radiation of shorter wavelength than

cerium(IV). Therefore, absorption of emitted radiation by the reagent was assumed to be negligible. It became possible to use 10—300 times greater equivalents of cerium(IV) reagent for hydrogensulfite than those of the permanganate reagent and the chemiluminescence efficiency thus became independent of the concentration of the oxidizing agent. Furthermore, the cerium(IV) reagent solution was much more stable than the potassium permanganate solution, maintaining its titer for several weeks. Consequently, all of the problems associated with the permanganate reagent were overcome by the use of cerium(IV) sulfate.

Calibration curve. The chemiluminescence intensity increased linearly with hydrogensulfite concentration up to ca. 50 ng ml^{-1} SO_2 as shown in Fig. 1. In this range, the intensity was represented by 1.50 $[SO_2]$ + 0.99 (r = 0.9986). The slope was more than 5 times greater than that obtained with the permanganate reagent. The average background current was 0.994 count s^{-1} with a standard deviation of 0.096 from repeated measurements (each for 100 s) of a blank sample solution (containing sodium hydroxide and sodium formate but no hydrogensulfite). The detection limit was thus calculated as 0.19 ng ml^{-1} SO_2. The relative standard deviation was within 5% for samples of 10—50 ng ml^{-1} SO_2.

Interferences. Table 1 summarizes the effects of interfering species. The chemiluminescence intensities were compared to that obtained for a 20 ng ml^{-1} SO_2 sample free from foreign species. In the last column, typical

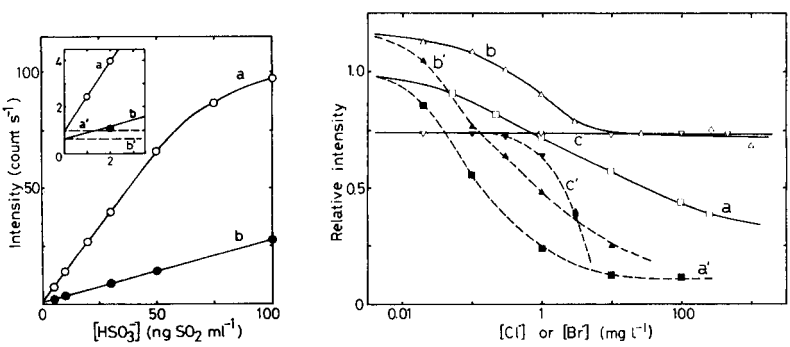

Fig. 1. Chemiluminescence intensity vs. hydrogensulfite concentration. The lower end of the curves, expanded × 10, are shown in the inset. Reagent solution: (a) 0.3 mM cerium(IV) sulfate/0.01 M sulfuric acid; (b) 2 μM potassium permanganate/1.5 mM sulfuric acid (obtained previously [3]). Curves a′ and b′ are the background luminescences for the cerium(IV) and permanganate systems, respectively.

Fig. 2. Change of chemiluminescence intensity with the concentrations of chloride (a—c) and bromide (a′—c′) in sample solutions. Reagent solution: 0.3 mM cerium sulfate/0.01 M sulfuric acid. (a, a′) Samples containing only 20 ng ml^{-1} SO_2; (b, b′) sodium sulfate (8 mM) added to the samples beforehand; (c, c′) sodium chloride (1.4 mM) and sodium sulfate (7.7 mM) added to the samples beforehand (the value of the abscissa does not include this additional chloride).

TABLE 1

Influences of interfering species on chemiluminescence intensity[a]

Species	Added as	Relative intensities at foreign species concn. (mg l^{-1})					$C_{90\%}$[b] (mg l^{-1})	$C_{50\%}$[b] (mg l^{-1})	C_{rain} (mg l^{-1})
		0.02	0.1	1	10	100			
CO_2	$NaHCO_3$	1.00	1.00	1.00	1.00	0.92	120	280	0.60[c]
PO_4^{3-}	Na_2HPO_4	1.00	1.00	1.00	0.84	0.26	6	50	0.06[d]
NO_2^-	$NaNO_2$	0.87	0.60	0.08	0	0	0.008	0.14	<0.05[e]
Cl^-	NaCl	0.98	0.88	0.73	0.64	0.44	0.07	50	0.20[d]
Br^-	NaBr	0.85	0.55	0.23	0.12	0.12	0.016	0.13	—
I^-	KI	0.47	0.15	0	0	0	0.002	0.022	<0.003[f]
Fe^{2+}	$FeSO_4$	1.00	1.00	0.92	0	0	1.1	1.7	0.436[g]
Mn^{2+}	$MnSO_4$	0.99	0.75	0.15	0	0	0.045	0.26	0.024[g]
HCHO	formalin[i]	0.99	0.93	0.51	0.07	0	0.15	1.1	—
CH_3CHO	—	0.97	0.84	0.66	1.01	1.02	0 057	—	—
H_2O_2	—	0.91	0.68	0.08	0	0	0.025	0.18	0.001–0.16[h]

[a]Response for 20 ng SO_2 ml^{-1} = 1.00. [b]Concentrations of interfering species which decreased the chemiluminescence intensities to 90% and 50%, respectively. [c]Calculated from the Henry's law constant at 20° C. [d—h]See [7—11]. [i]Contained ca. 10% methanol.

concentrations of the foreign species observed in rainwater are given. It was found that ammonium, magnesium, potassium, sodium, nitrate and sulfate ions did not interfere even at 100 mg l^{-1} levels.

Comparison of the values of $C_{90\%}$ and C_{rain} shows that for rainwater samples the species listed in Table 1, except for chloride and hydrogen peroxide, will not interfere with the measurement. It should be noted that $C_{90\%}$ for nitrite, Fe(II), Mn(II) and formaldehyde became 8, 2.8, 1.5 and 3.8 times greater, respectively, than those obtained with the permanganate reagent.

The effect of chloride ion on the chemiluminescence is shown by curve (a) in Fig. 2. When an appropriate electrolyte such as sodium sulfate was added to the sample solution, the chemiluminescence intensity became independent of the chloride concentration over a wide range (10—1000 mg l^{-1}) as shown by curve (b). Large amounts of neutral salts were found to enhance the intensity. Therefore, the interference from chloride was successfully eliminated by adding certain amounts of chloride and another salt to sample solutions although the absolute chemiluminescence intensity decreased to 60%. For example, curve (c) in Fig. 2 was obtained for sample solutions to which extra sodium chloride (1.4 mM) and sodium sulfate (7.7 mM) were added (i.e., 50 mg l^{-1} chloride and an ionic strength equal to that of the reagent solution). This treatment was also useful for reducing the bromide interference. The $C_{90\%}$ of bromide became 50 times greater (0.8 mg l^{-1}, curve c′) than that without the treatment (curve a′). Large amounts of chloride seemed to mask the effect of bromide.

Hydrogen peroxide was considered to act not as an oxidizing agent but simply as a quencher because the chemiluminescence response was independent of the time after hydrogen peroxide was introduced. Formate seemed to protect hydrogensulfite from oxidation by hydrogen peroxide. Therefore, it is possible to make corrections for the interference, if the concentration of hydrogen peroxide in the sample is measured independently.

Conclusion

Cerium sulfate(IV) as the reagent in the chemiluminescence method makes it possible to determine continuously $\mu g\ l^{-1}$ levels of hydrogensulfite. The intensity obtained with cerium(IV) sulfate became more than 5 times greater than that obtained with potassium permanganate and the detection limit was also remarkably lowered. The advantages of cerium(IV) sulfate over the permanganate reagent are that a sufficiently high concentration of reagent can be used, the chemiluminescence intensity is independent of cerium(IV) concentration over a wide range, and the reagent solution is stable. In addition, interferences from nitrite, transition metal ions and formaldehyde are greatly reduced. Therefore, trace amounts of hydrogensulfite ion in rainwater can easily be determined by the present method without pretreatment. Data for rainwater are being collected.

REFERENCES

1 J. Stauff and W. Jaeschke, Z. Naturforsch., Teil B, 33 (1978) 293.
2 F. X. Meixner and W. A. Jaeschke, Int. J. Environ. Anal. Chem., 10 (1981) 51.
3 K. Takeuchi and T. Ibusuki, Bunseki Kagaku, 33 (1984) E107.
4 M. Yamada, T. Nakada and S. Suzuki, Anal. Chim. Acta, 147 (1983) 401.
5 T. Ozawa, Nippon Kagaku Zasshi, 87 (1966) 573.
6 L. G. Sillen and A. E. Martell (Eds.), Stability Constants of Metal-Ion Complexes, The Chemical Society, London, 1964, p. 44.
7 W. A. Scheider, W. R. Snyder and B. Clark, Water Air Soil Pollut., 12 (1979) 171.
8 J. M. Hales and M. T. Dana, J. Appl. Meteorol., 18 (1979) 294.
9 S. Utsumi, M. Shiota, N. Yonehara and I. Iwasaki, Nippon Kagaku Zasshi, 85 (1964) 32.
10 N. J. Pattenden, J. R. Branson and E. M. R. Fisher, in H.-W. Georgii and J. Pankrath (Eds.), Deposition of Atmospheric Pollutants, Reidel, Dordrecht, 1982, p. 173.
11 G. L. Kok, Atmos. Environ., 14 (1980) 653.

Analytica Chimica Acta, 174 (1985) 365—368
Elsevier Science Publishers B.V., Amsterdam — Printed in The Netherlands

Short Communication

SPECTROPHOTOMETRIC DETERMINATION OF HYDROXYLAMINE ALONE AND IN THE PRESENCE OF MONOCHLORAMINE

MICHEL FERRIOL* and JOSETTE GAZET

Laboratoire de Physico-chimie minérale II (Associé au C.N.R.S. no. 116), Université Lyon I, 43 Bd. du 11 novembre 1918, 69622 Villeurbanne Cedex (France)

(Received 4th January 1985)

Summary. Hydroxylamine ($< 3 \times 10^{-3}$ mol l^{-1}) is quantified by ultraviolet spectrophotometry after reaction with an excess of formaldehyde in buffered solution at pH 12.2. The absorbance of the formaldoxime produced is measured at 218 nm (ϵ = 5480 l mol^{-1} cm^{-1}) when hydroxylamine is alone but at 230 nm (ϵ = 3230 l mol^{-1} cm^{-1}) when monochloramine is present.

During a study of the degradation of monochloramine in water, a problem arose in examining the kinetics of the reaction between chloramine and hydroxylamine. The main procedures [1—7] available for the determination of hydroxylamine were unsuitable because there was no way to stop the reaction with chloramine. A more convenient method, based on the reactivity of hydroxylamine with aldehydes and especially formaldehyde in alkaline medium [8], was therefore developed.

The reaction produced formaldoxime which absorbs in the ultraviolet range

$$NH_2OH + HCHO \rightleftharpoons CH_2{=}N{-}OH + H_2O$$

To ensure complete formation of the oxime, a large excess of formaldehyde is needed. In the presence of monochloramine, another reaction takes place between chloramine and formaldehyde. The fast rate of this reaction in alkaline medium enables the reaction between chloramine and hydroxylamine to be stopped instantaneously [9].

Figure 1 shows the ultraviolet spectrum of a mixture prepared from hydroxylamine and formaldehyde at pH 12.2. The absorbance is maximal at 218 nm. When hydroxylamine is alone, the absorbance is measured at this wavelength. In mixtures with monochloramine, hydroxylamine is determined at 230 nm because there is then negligible interference between the spectra of the products of the formaldehyde/hydroxylamine and formaldehyde/chloramine reactions.

Experimental

A Cary 15 double-beam spectrophotometer was used for absorbance measurements.

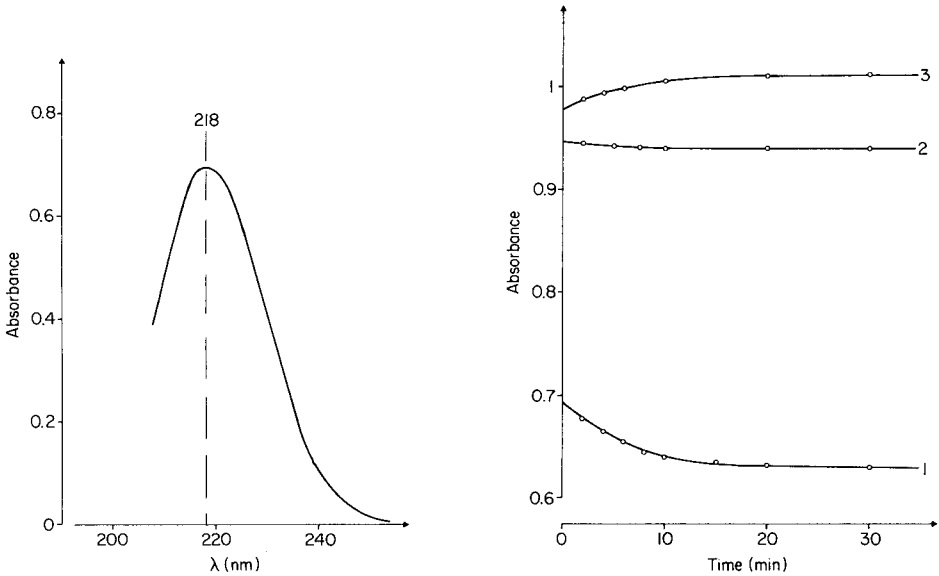

Fig. 1. Ultraviolet spectrum of a formaldehyde/hydroxylamine mixture at pH 12.2. Conditions: 1.30×10^{-4} mol l^{-1} NH_2OH, 1.84×10^{-2} mol l^{-1} HCHO, ca. 20°C.

Fig. 2. Evolution of maximum absorbance as a function of time for several sodium hydroxide concentrations: (1) 0.002, (2) 0.01, (3) 0.1 mol l^{-1} NaOH. Conditions: 1.73×10^{-4} mol l^{-1} NH_2OH, 1.84×10^{-2} mol l^{-1} formaldehyde; measurement at 218 nm.

Solutions. Formaldehyde solutions were obtained by diluting the reagent-grade commercial product (30% w/w). Hydroxylamine solutions were prepared from reagent-grade hydroxylammonium chloride. Monochloramine is unstable in water. Solutions were prepared just before use by reacting sodium hypochlorite and ammonia as described previously [10]. The monochloramine concentration was determined by ultraviolet spectrophotometry at 243 nm (ϵ = 458 l mol^{-1} cm^{-1}).

Procedure. The hydroxylamine solution (5 ml) of concentration less than 3×10^{-3} mol l^{-1} was added to a 50-ml volumetric flask containing 5 ml of a ca. 0.2 mol l^{-1} formaldehyde solution and the mixture was diluted to volume with buffer solution at pH 12.2 (0.042 mol l^{-1} sodium hydroxide/0.029 mol l^{-1} disodium hydrogenphosphate). After 20 min, the absorbance was measured at 218 nm.

Results

Influence of pH. The evolution of maximum absorbance with time was studied for sodium hydroxide concentrations of 0.002, 0.001 and 0.1 mol l^{-1} with constant concentrations of hydroxylamine and formaldehyde. Figure 2 shows the experimental graphs. The minimum time for recording the spectra was 2 min after the reagents had been mixed, thus

the curves were extrapolated to zero time. As can be seen, the absorbance at zero time increases with the sodium hydroxide concentration, and the trends of the curves differ according to the pH. With 0.002 mol l^{-1} sodium hydroxide, the absorbance decreases as a function of time; with 0.01 mol l^{-1} sodium hydroxide, the trend is much less pronounced and with 0.1 mol l^{-1} sodium hydroxide, the absorbance increases with time. In all three cases, the absorbance stabilizes after 20—30 min, but then decreases slightly (0.5—0.7%) after 90 min. Thus measurements must be made under strictly defined pH conditions to obtain reproducible results. A buffered medium at pH 12.2, in which equilibrium is attained in about 20 min, was selected for routine purposes.

The procedure described above was used for establishment of the calibration graph and for the determination of unknown solutions. The calibration was linear for hydroxylamine concentrations in the range 0.4×10^{-4}—2.3×10^{-4} mol l^{-1}. The molar absorptivity was 5480 ± 40 l mol^{-1} cm^{-1}; the intercept was -2.09×10^{-3}. These data were calculated by the least-squares method from the results of 15 independent measurements.

Determination of hydroxylamine in the presence of monochloramine. As indicated above, absorbances were measured at 230 nm in this case. At this wavelength, the least-squares method gave a straight-line plot for the measured absorbance as a function of hydroxylamine concentration in the range 0.4×10^{-4}—2.3×10^{-4} mol l^{-1}. The molar absorptivity was 3230 ± 80 l mol^{-1} cm^{-1} and the intercept was -8.83×10^{-3}. These results were obtained from 10 independent measurements.

The method was tested by determining hydroxylamine in the presence of monochloramine in alkaline medium. For this purpose, standard solutions of hydroxylamine were mixed with different volumes of 6.00×10^{-3} mol l^{-1} monochloramine. Then, 5 ml of the mixtures were treated by the procedure described above, except that after 20 min the absorbance was measured at 230 nm. Table 1 gives the results obtained. There is very good concordance between the experimental and standard values for the hydroxylamine concentration.

TABLE 1

Influence of monochloramine on the determination of hydroxylamine

Concentrations taken (10^{-3} mol l^{-1})		A_{230}	NH_2OH found (10^{-3} mol l^{-1})
NH_2Cl	NH_2OH		
5.29	0.51	0.170	0.53
4.80	0.86	0.290	0.90
3.00	1.09	0.355	1.10
4.00	1.45	0.465	1.44
3.00	2.18	0.695	2.15

Discussion

Results obtained by Jencks [11] show that the formation of oximes proceeds in two steps with formation of an intermediate carbinolamine:

$$R_1R_2C{=}O + NH_2OH \rightleftharpoons R_1R_2HC{-}NHOH \rightleftharpoons R_1R_2C{=}N - OH + H_2O$$

The reaction is catalyzed by acids and bases, each step reaching equilibrium. The mechanism of the acid catalysis was studied extensively but that of the base catalysis was given less attention. It seems that it is the dehydration step of carbinolamine which is catalyzed [11].

The evolution of the curves in Fig. 2 can be explained by assuming that the intermediate carbinolamine absorbs in the ultraviolet range with a molar absorptivity higher than that of the oxime. Thus, the recorded spectra would represent the sum of those of the oxime and carbinolamine. Their different courses as a function of time and pH would be due to different rates of the two steps in the reaction until equilibrium is reached.

REFERENCES

1 N. P. Komar, T. G. Shapavalova and A. N. Zots, Zh. Anal. Khim., 29 (1974) 829.
2 P. Pitta, A. Calatroni and C. Zio, Analyst (London), 107 (1982) 341.
3 G. C. M. Bourke, G. Stedman and A. P. Wade, Anal. Chim. Acta, 153 (1983) 277.
4 T. K. Korpela and M. J. Makela, Anal. Biochem., 110 (1981) 251.
5 D. P. Johnson, Anal. Chem., 40 (1968) 646.
6 S. Shahine and R. Mahmoud, Mikrochim. Acta, (II) (1978) 431.
7 F. Dias, A. S. Olojola and B. Jaselkis, Talanta, 26 (1976) 47.
8 V. Grignard, Traité de Chimie Organique, Tome XV, Masson & Cie, Paris, 1958.
9 H. Delalu, Thèse de Doctorat d'Etat ès-Sciences, no. 77-29, Lyon, France, 1977.
10 H. Delalu and R. Cohen-Adad, J. Chim. Phys., 76 (1979) 465.
11 W. P. Jencks, J. Am. Chem. Soc., 81 (1959) 475.

Analytica Chimica Acta, 174 (1985) 369—373
Elsevier Science Publishers B.V., Amsterdam — Printed in The Netherlands

Short Communication

SPECTROPHOTOMETRIC DETERMINATION OF MICRO AMOUNTS OF CATIONIC POLYMERIC FLOCCULANTS BY FLOW INJECTION ANALYSIS

KYOJI TÔEI* and TAKAHISA ZAITSU

Department of Chemistry, Faculty of Science, Okayama University, Tsushimanaka, Okayama-shi 700 (Japan)

CHIAKI IGARASHI

Ebara Research Co., Ltd., Fujisawa-shi 251 (Japan)

(Received 4th January 1985)

Summary. Cationic polymeric flocculants in water are determined spectrophotometrically with the anionic compound 3-(2-hydroxy-3-carboxyanilide-1-azonaphthalene)-4-hydroxybenzenesulfonic acid at pH 10 by flow injection analysis. The calibration graph at 680 nm is rectilinear from 0 to 20 mg l^{-1} under optimal conditions. The relative standard deviation for 20 injections of Cat-Floc (10 mg l^{-1}) was 1.2%; the sample throughput was 60 h^{-1}.

Cationic polymeric flocculants are usually determined by colloid titration with potassium poly(vinyl sulfate) as titrant and toluidine blue as indicator. For determination of trace amounts of the polymer, spectrophotometry is more sensitive and accurate than the colloid titration. The reagent 3-(2-hydroxy-3-carboxyanilide-1-azonaphthalene)-4-hydroxybenzenesulfonic acid (HCAHB) was synthesized previously as an indicator for the colloid titration [1]. Here the cationic polymer is determined spectrophotometrically with this reagent and the method is adapted to flow injection analysis (f.i.a.).

Experimental

Chemicals. For the HCAHB solution, the sodium salt of the reagent (0.267 g) is dissolved in 250 ml of distilled water to give a 2.2×10^{-3} M solution. This solution (10 ml), 0.2 ml of 0.1 M EDTA and 10 ml of 0.1% PVA-217EE, a poly(vinyl alcohol), are mixed and diluted with distilled water to give 250 ml of solution, which is 8.8×10^{-5} M in HCAHB and 8×10^{-5} M in EDTA.

The cationic flocculants used were Cat-Floc (Calgon Corp., U.S.A.) which is a 15% poly(dimethyldiallylammonium chloride) solution, and Eba-Growth C-104G (Ebara Research Co., Japan) which is mainly composed of poly(2-methacryloxyethyltrimethylammonium chloride) and has a molecular weight of about 2×10^6. The titer of the flocculant solutions was determined by

0003-2670/85/$03.30

colloid titration with standard 1.25×10^{-3} M potassium poly(vinyl sulfate) solution.

Other reagents used were of analytical-reagent grade.

Apparatus. Spectra were measured with a Shimadzu UV-300 recording spectrophotometer and absorbances with a Shimadzu UV-140-02 spectrophotometer. The pH was measured with a Hitachi-Horiba M-5 pH meter.

General procedure. Mix 5 ml of sample solution, 10 ml of 1.1×10^{-4} M HCAHB solution and 4 ml of ammonia/ammonium chloride buffer solution (pH 9.8, 0.1 M) in a 25-ml volumetric flask, dilute to the mark with distilled water, and shake thoroughly. Measure the absorbance at 680 nm in a 10-mm cell.

Flow injection procedure. A schematic diagram is shown in Fig. 1. A double-plunger pump (Kyowa Seimitsu KHU-W-52) is used to drive reagent solution and distilled water each at a rate of 0.6 ml min^{-1}. Absorbances are measured in a flow cell (18 μl, 10-mm path length), and recorded by Toa Dempa FBR-252A recorder. The concentrations in the reagent solution are twice those used in the general procedure; thus the volumes of HCAHB, EDTA and PVA-217EE specified above are diluted with 80 ml of the ammonia buffer solution and diluted to 250 ml with distilled water. This solution was used for Eba-Growth C-104G. For the determination of Cat-Floc, 100 ml of 2 M potassium nitrate was added instead of the same volume of distilled water. The sample solution (120 μl) was injected from a 6-way valve (Kyowa Seimitsu KMH-6V) into the carrier stream.

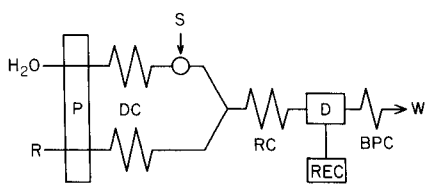

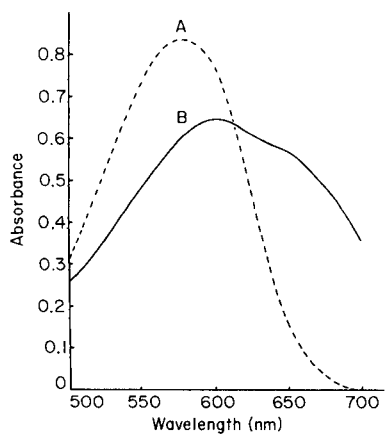

Fig. 1. Manifold: R, reagent flow; P, double-plunger pump (0.6 ml min^{-1}); DC, damping coil (1.0 mm i.d., 7 m); S, sample injector; RC, reaction coil (0.5 mm i.d., 1 m); D, spectrophotometer (λ = 680 nm) with flow cell; REC, recorder; BPC, back-pressure coil (0.25 mm i.d., 1 m); W, waste.

Fig. 2. Absorption spectra obtained with HCAHB (4.4×10^{-5} M) at pH 9.8: A, reagent blank; B, 10 mg l^{-1} Cat-Floc.

Results

The absorption spectra obtained by the general procedure are shown in Fig. 2. The maximum wavelengths of the reagent and of the same solution containing 10 mg l^{-1} Cat-Floc are 575 nm and 600 nm, respectively. The absorbance at 680 nm was used because the reagent blank is small (0.02) and the absorbance difference is large. The pH was adjusted by mixing 0.1 M ammonia and 0.1 M ammonium chloride in various ratios covering the pH range 9—10.8. Blanks were unaffected over this range; solutions containing 10 mg l^{-1} Cat-Floc taken through the general procedure gave constant absorbance between pH 9.3 and 10.1 with a steep decrease below pH 9.3 and a gradual decrease above pH 10.1; pH 9.8 was therefore selected.

The calibration graphs obtained in the general procedure are shown in Fig. 3. The curve for Cat-Floc (0—10 mg l^{-1}) is concave; when 5 ml of 2 M potassium nitrate is added, the curve becomes straight, but the sensitivity decreases. In contrast, the calibration plot for Eba-Growth C-104G is straight without potassium nitrate. Obviously it is necessary to select the most appropriate ionic strength for the particular flocculant being determined.

With the flow-injection manifold outlined in Fig. 1, sample throughput is 60 h^{-1}. The responses to Cat-Floc (0—10 mg l^{-1}) are shown in Fig. 4; the relative standard deviation for 20 injections of Cat-Floc (10 mg l^{-1}) was 1.2%.

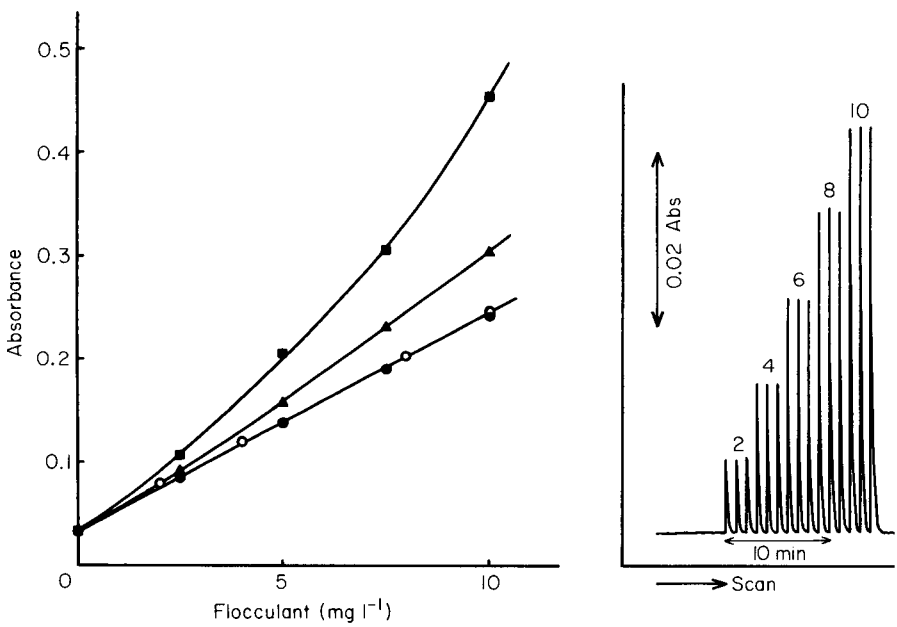

Fig. 3. Effect of potassium nitrate on calibration curves. Flocculant: (■, ▲, ●) Cat-Floc; (○) Eba-Growth C-104G. Volume of 2 M KNO_3 added: (■) none; (▲) 1 ml; (●) 5 ml; (○) none.

Fig. 4. Signals for Cat-Floc (2—10 mg l^{-1}) in the flow-injection manifold.

The effect of ions co-existing with Eba-Growth C-104G (20 mg l^{-1}) was examined. The results are shown in Table 1. The HCAHB reagent reacts with calcium and magnesium ions, but these ions are masked with EDTA in the recommended procedure.

Application to treated waste water. Waste water was treated with Eba-Growth C-104G to form coagulum and filtered. The residual flocculant in the filtered water was determined by the above flow-injection method. If the turbidity was high, the solution was diluted. At the same time, the samples were determined by colloid titration [2]. The results are shown in Table 2. If a sample is highly turbid and does not clear on dilution, it cannot be determined by this method.

TABLE 1

Effect of diverse ions on the determination of Eba-Growth C-104G (20 mg l^{-1})

Ion	Conc. added (M)	Recovery of flocculant (%)	Maximum conc.[a] (M)
Na^+	4×10^{-2}	103	9.6×10^{-3}
K^+	3×10^{-3}	98	4.7×10^{-3}
Ca^{2+}	2×10^{-3}	100	1.0×10^{-3}
Mg^{2+}	1×10^{-3}	100	9.3×10^{-4}
Fe^{3+}	2×10^{-4}	98	$< 1.8 \times 10^{-6}$
Cl^-	6×10^{-3}	97	1.0×10^{-2}
SO_4^{2-}	4×10^{-4}	98	3.6×10^{-4}
HPO_4^{2-}	2×10^{-2}	103	1.1×10^{-2}
NO_3^-	4×10^{-3}	100	$< 8.1 \times 10^{-6}$

[a]Maximum concentrations found in samples of treated waste waters by Analytical Division of Ebara General Institute.

TABLE 2

Determination of cationic polymeric flocculant in treated waste water

Sample[a]	Dilution[b]	Found (mg l^{-1})	Reference[c] (mg l^{-1})
A	—	11.5	10.4 ± 2
B	—	21.0	20.8 ± 2
C	1/2	20.0	20.8 ± 2

[a]Sample A: night-soil is diluted by water, aerated by an activated sludge process and settled (waste-activated sludge). The overflow water is precipitated by aluminum sulfate (alum sludge). The combined sludge is treated with Eba-Growth C-104G and filtered by a dehydrator; the filtrate is A. Sample B: municipal sewage is settled, aerated and settled again. The sludge is digested by an activated sludge process and mixed with Eba-Growth C-104G; the filtrate is B. Sample C: domestic sewage is aerated, mixed with Eba-Growth C-104G and gravity-settled; the supernatant fluid is C. [b]The sample was diluted with redistilled water. [c]Obtained by colloid titration.

Conclusion. Micro amounts of two cationic polymeric flocculants can be determined spectrophotometrically by using the azo compound, HCAHB. The method was applied successfully to f.i.a. This method is very useful for the control of water treatment by cationic polymeric flocculant.

REFERENCES

1 K. Tôei, H. Miyata and T. Ono, Bunseki Kagaku (Japan Analyst), 26 (1977) 268.
2 K. Tôei and K. Kawada, Bunseki Kagaku (Japan Analyst), 21 (1972) 1510.

Analytica Chimica Acta, 174 (1985) 375—378
Elsevier Science Publishers B.V., Amsterdam — Printed in The Netherlands

Short Communication

DETERMINATION OF TOTAL CHROMIUM BY FLOW INJECTION ANALYSIS

M. J. WHITAKER
Conoco Inc., P.O. Box 1267, 346 RDE, Ponca City, OK 74603 (U.S.A.)
(Received 20th March 1985)

Summary. The determination of total chromium by flow injection analysis is described. Cerium(IV) and nitric acid are used to convert chromium(III) to chromium(VI); the oxidation rate is enhanced by placing the reaction coil in an 80°C oil bath. 1,5-Diphenylcarbazide is used to form a colored complex with chromium(VI) that is measured at 540 nm. For both chromium(III) and chromium(VI), relative standard deviation of less than 1% is achieved with a sampling rate of 40 per hour. Linear response is obtained for 0.5—10 mg l^{-1} chromium.

The development of an automated total chromium method without the need for a preliminary digestion step was the aim of this study. In the standard methods [1], to determine total chromium, the sample was digested with a sulfuric/nitric acid solution and then oxidized with potassium permanganate to convert all chromium to chromium(VI). The digested sample was then treated with 1,5-diphenylcarbazide and the red-violet product was measured spectrophotometrically at 540 nm.

The determination of chromium(VI) with diphenylcarbazide by flow injection analysis (f.i.a.) has been previously investigated [2, 3]. These studies dealt only with chromium(VI) present in the samples. In the investigation described here, chromium ions are oxidized in the flowing stream to chromium(VI) and then reacted with diphenylcarbazide. The reaction product is measured spectrophotometrically in a 5-mm flow cell at 540 nm. The analog signal from the spectrophotometer is monitored by a laboratory computer system. The procedure has several advantages over other methodologies. Some advantages are elimination of the time-consuming digestion, high sample throughput (40 per hour), and good precision for both Cr(VI) and Cr(III) standards at low mg l^{-1} levels.

Experimental

Reagents. All chemicals used were of analytical-reagent grade. The carrier stream was the oxidizing reagent which is 0.35 mM cerium(IV) and 1.0 M nitric acid. This solution was prepared by dissolving 0.9996 g of cerium(IV) ammonium sulfate monohydrate in 64.10 ml of concentrated nitric acid and dilution to 1 l with deionized water. The merging stream solution was

0003-2670/85/$03.30

2.1 mM 1,5-diphenylcarbazide, which was prepared by dissolving 0.5 g of diphenylcarbazide in 50 ml of acetone and then diluting to 1 l with deionized water.

Standards. A 1000 mg l^{-1} chromium(III) stock standard solution was prepared by dissolving 5.1250 g of chromium(III) chloride hexahydrate in 1 l of deionized water. To use as a comparison standard, a 1000 mg l^{-1} chromium(VI) stock primary standard solution was prepared by dissolving 2.8290 g of potassium dichromate in 1 l of deionized water.

Apparatus. The flow-injection manifold used is shown in Fig. 1. A 140-μl sample is injected into the carrier stream (oxidizing reagent) which flows through a 3-m 0.5-mm i.d. Teflon coil immersed in an oil bath at 80°C. The flow-injection instrument used was a Fiatron SHS-200 (Fiatron, Milwaukee, Wisconsin) equipped with an RCA Cosmac microboard computer. The microprocessor controls a six-channel, ten-speed, forward-and-reverse peristaltic pump; a dual-channel, four-way solenoid Teflon sample injector; and the functional and operational modes of the SHS-200. The programmable sample volume mode (mode-20) was selected for these experiments, and the optimal sample volume injection was found to be 140 μl. The flow rate used for the sample, carrier and reagent stream was 1.20 ml min^{-1}. These flow rates were obtained when the pump speed was 90% and the pump tubing was 0.056-in. i.d. Tygon.

The absorbance of the chromium(VI)/diphenylcarbazide complex was measured at 540 nm with an Isco V^4 variable-wavelength detector (Isco; Lincoln, Nebraska). The flow-through cell had a 5-mm path length and a total volume capacity of 10 μl. The attenuation was set at 0.5-absorbance full scale, and the absorbance measurements were recorded on a strip chart recorder.

The standards and samples were poured into 4-ml sample cups and placed in an Alpkem AS-175 auto-sampler, which was interfaced to the SHS-200, and all sampling, injection, and wash times were controlled by the microprocessor.

A Hewlett-Packard 8450A u.v.-visible spectrophotometer was used for spectral scans as required.

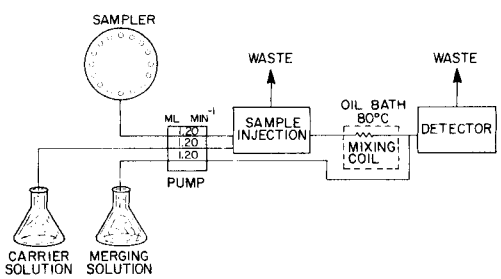

Fig. 1. Merging-stream f.i.a. manifold for the determination of total chromium.

Results and discussion

Spectral scan. Figure 2 shows spectral scans of cerium(IV), chromium(VI) and chromium(III), and of chromium(VI) complexed with diphenylcarbazide. The chromium(III) solution (peaks 406 and 574 nm) was taken through the total chromium procedure and then a spectral scan was done on the colored product (peak 540 nm). The chromium(III) peaks did not appear in this scan, showing that all the chromium(III) was oxidized to chromium(VI).

Effects of cerium(IV) concentration. Figure 3 is a plot of voltage change (ΔV) vs. cerium(IV) concentration (mM) for a 7 mg l^{-1} chromium(III) standard. The concentration of cerium(IV) was varied from 0.02 to 1.4 mM, while the concentration of nitric acid was held constant at 1.0 M. The diphenylcarbazide reagent was also held constant at 4.1 mM. The curve rises very quickly from zero ΔV at 0.02 mM cerium(IV) to the maximum ΔV of 0.682 at 0.35 mM cerium(IV). As can be seen from Fig. 3, 0.35 mM is the most effective oxidizing concentration of cerium(IV) in a 1.0 M nitric acid solution.

Effects of nitric acid concentration. The effect of nitric acid concentration was studied for an 8 mg l^{-1} chromium(III) standard. The concentration of nitric acid was varied from 0.50 to 2.00 M, while the concentrations of cerium(IV) and diphenylcarbazide were held constant at 0.35 mM and 4.1 mM, respectively. The curve rose and fell gently as the acid concentration was increased, with the peak maximum at 1.00 M nitric acid, the maximum response being $\Delta V = 0.830$.

Effects of temperature. Figure 4 is a plot of peak height versus temperature (°C) of the oil bath. A 6 mg l^{-1} chromium standard was processed in the manifold while the temperature was varied from 25 to 95°C. The maxi-

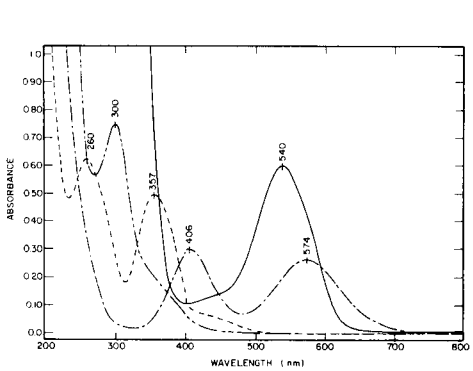

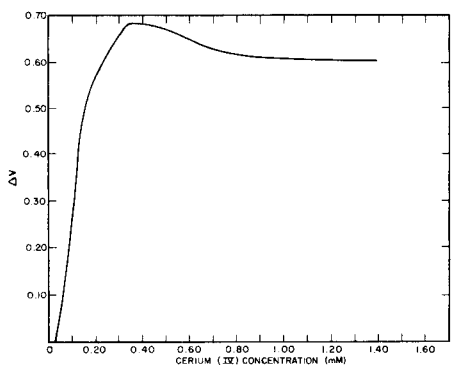

Fig. 2. Spectral scans: (—··—) cerium (IV); (- - -) chromium(VI); (—·—) chromium(III); (—) chromium(VI) complexed with diphenylcarbazide.

Fig. 3. Curve of ΔV vs. cerium(IV) concentration (mM) for a 7-mg l^{-1} chromium(III) standard. Ten concentrations were used to define the curve.

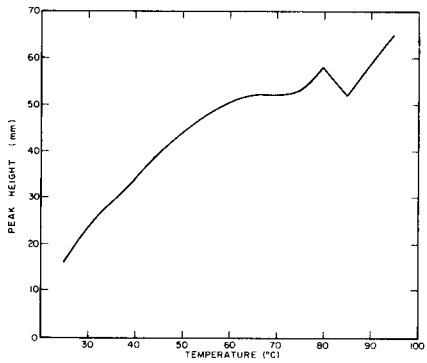

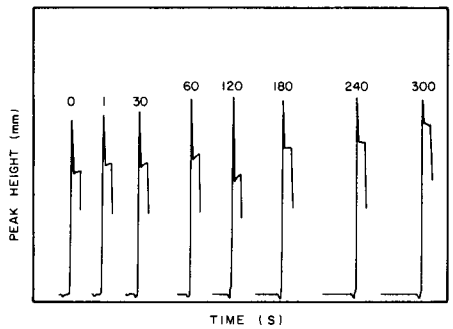

Fig. 4. Curve of peak height (mm) vs. temperature (°C) of the heated oil bath.

Fig. 5. Graph of peak height (mm) vs. time (s) that the sample was stopped in the 80°C oil bath. Times are indicated by the number above each peak.

mum peak height was achieved at 95°C but at 90 and 95°C small air bubbles developed. Air bubbles did not develop at 80°C, which was chosen for subsequent studies.

Effects of stopped flow. Figure 5 is a graph of peak height (mm) versus the time (s) that the sample and oxidant were stopped in the 80°C bath. At the end of the designated time, the system was restarted, and the oxidized sample was reacted with diphenylcarbazide. The system stopped again in the flow cell on the decreasing side of each response peaks to establish when the color-forming reaction reached completion. The last five standards in Fig. 5 had the same peak height response. However, the color-forming reaction does not appear to have reached completion until 240 s. The peaks indicate that total oxidation does not occur until some time between 30 and 60 s. However, the gain in peak height response from 0 to 60 s is not sufficient to warrant utilizing the stopped-flow technique because it would decrease the sampling rate.

Determination of chromium(III) and (VI). Studies with standards showed that peak height varied linearly with chromium concentration between 0.5 and 10 mg l^{-1}. The mean value for ten 5 mg l^{-1} chromium(III) standards was 4.96 mg l^{-1} with a relative standard deviation of 0.80%; the mean value for ten 5 mg l^{-1} chromium(VI) standards was 4.94 mg l^{-1} with RSD of 0.61%. For twenty 1 mg l^{-1} chromium(III) standards, the RSD was 2.9%.

REFERENCES

1 Standard Methods for the Examination of Water and Wastewater, 15th edn., American Public Health Association, New York, 1981, p. 187.
2 S. S. Jorgensen and M. A. B. Regitano, Analyst, 105 (1980) 292.
3 J. C. deAndrade, J. C. Rocha, C. Pasquini and N. Baccan, Analyst, 108 (1983) 621.

ANALYTICA CHIMICA ACTA, VOL. 174 (1985)

AUTHOR INDEX

(continued from inside backcover)

(continued from outside back cover)

(continued on facing page)

CONTENTS

(Abstracted, Indexed in: Anal. Abstr.; Biol. Abstr.; Chem. Abstr.; Curr. Contents Phys. Chem. Earth Sci.; Life Sci.; Index Med.; Mass Spectrom. Bull.; Sci. Citation Index; Excerpta Med.)

(continued on inside back cover)